TESIS DE LA UNIVERSIDAD DE ZARAGOZA

2024 244

Martha Isabel Minjarez Saenz

Flavoenzymes in Microbial Systems: Analysis of Structure-Function Relationships

Director/es
Medina Trullenque, María Milagros
Martínez Júlvez, Marta María

ISSN 2254-7606

Prensas de la Universidad
Universidad Zaragoza

Universidad de Zaragoza
Servicio de Publicaciones

ISSN 2254-7606

Universidad Zaragoza
1542

Tesis Doctoral

FLAVOENZYMES IN MICROBIAL SYSTEMS: ANALYSIS OF STRUCTURE-FUNCTION RELATIONSHIPS

Autor

Martha Isabel Minjarez Saenz

Director/es

Medina Trullenque, María Milagros
Martínez Júlvez, Marta María

UNIVERSIDAD DE ZARAGOZA
Escuela de Doctorado

Programa de Doctorado en Bioquímica y Biología Molecular

2024

Universidad Zaragoza
1542

Tesis Doctoral

Flavoenzymes in Microbial Systems: Analysis of Structure-Function Relationships

Autor

Martha Minjárez Sáenz

Director/es

Milagros Medina Trullenque
Marta Martínez Júlvez

FACULTAD DE CIENCIAS

2023

Dña. MILAGROS MEDINA TRULLENQUE, Catedrática del Departamento de Bioquímica y Biología Molecular y Celular de la Universidad de Zaragoza,

Dña. MARTA Mª MARTÍNEZ JÚLVEZ, Profesora Titular del Departamento de Bioquímica y Biología Molecular y Celular de la Universidad de Zaragoza,

CERTIFICAN:

Que la Tesis Doctoral "**Flavoenzymes in Microbial Systems: Analysis of Structure-Function Relationships"** ha sido realizada por la licenciada MARTHA MINJÁREZ SÁENZ en el Departamento de Bioquímica y Biología Molecular y Celular (Facultad de Ciencias) y en el Instituto de Biocomputación y Física de Sistemas Complejos (BIFI), de la Universidad de Zaragoza bajo su dirección, y que reúne, a su juicio, las condiciones requeridas para optar al Grado de Doctor por la Universidad de Zaragoza**.**

En Zaragoza, noviembre de 2023

Fdo.: Milagros Medina Trullenque

Fdo.: Marta Mª Martínez Júlvez

AGRADECIMIENTOS

Agradezco sinceramente a todos quienes contribuyeron a hacer posible este logro significativo. Este trabajo marca el cierre de un capítulo y el inicio de nuevas travesías y desafíos.

En primer lugar, mi profundo agradecimiento al Consejo Nacional de Humanidades, Ciencias y Tecnologías (CONAHCYT) de México, con el programa de Becas de Doctorado en el Extranjero, por su generoso respaldo financiero, esencial para llevar a cabo este proyecto.

A mis padres José Luis y Rosa María, a mi hermana Rossy, a mi gata Fernanda María, y familia entera, les agradezco por su amor incondicional. A mi esposo Javier y a sus padres, que se convirtieron también en mis padres.

Quiero expresar mi gratitud hacia mis directoras de tesis, la Dra. Milagros Medina y la Dra. Marta Martínez, cuya paciencia, sabiduría y guía constante han sido fundamentales a lo largo de este viaje académico.

Mis más sinceros agradecimientos al Dr. Alberto Ramírez Mata, a la Dra. Beatriz Eugenia Baca, y a mi querida María Luisa Xiqui, quienes me motivaron para continuar mi formación y cultivar mi amor por la ciencia.

No hay suficiente papel y tinta para nombrar a todos aquellos amigos que, a pesar de la distancia, estuvieron ahí para darme su aliento y apoyo inquebrantable. Con especial dedicación a Sandra, Elayne, Pamela y Eduardo. A las nuevas amistades forjadas en España: Ana Esteban y Ana Díaz con las que compartí mi vida y el encierro del Covid. A mis hermanas de investigación y compañeras de parranda, Paty, Ruth, Raquel, Sonia y Evelyn. A Jorge y nuestras mañanas de café. A los amigos y compañeros del Bifi, por aquellas noches de malas difracciones y comida chatarra. A mis Axolotitas mexicanas, Laura, Chely, Loly, MaJo, Cynthia, Mayte y Antonio. A los profesores Javier Sancho y Marta Martínez, por sus consejos sobre el arte, la vida y el amor.

Asimismo, extiendo mi agradecimiento a mis colegas y compañeros de investigación por su colaboración invaluable en los experimentos y análisis de datos.

Gracias por ser parte fundamental de este viaje académico y personal.

"Do. Or do not. There is no try."
Yoda
The Empire Strikes Back

Index

INDEX

RESUMEN:

Esta Tesis Doctoral se planteó con objeto de mejorar nuestra comprensión de los mecanismos de acción específicos de especie en sistemas dependientes de flavoenzimas como parte de redes metabólicas complejas. Las flavoproteínas y flavoenzimas son biomoléculas versátiles involucradas en procesos celulares como la transducción de señales, síntesis de nucleótidos y defensa contra el estrés oxidativo. Utilizan derivados de riboflavina como cofactores (FMN y/o FAD), los cuales les otorgan propiedades de óxido-reducción únicas. Los sistemas dependientes de flavoenzimas son esenciales en todo tipo de organismos, y algunas se han revelado como interesantes dianas terapéuticas o herramientas biotecnológicas. Como primer objetivo, se planteó la descripción del contenido del flavoproteoma de la bacteria patógena *Brucella ovis*, agente causal de la brucelosis ovina, Este estudio, permitió identificar un total de 78 flavoproteínas, casi todas flavoenzimas, para las que se prevé una alta diversidad funcional. El 55% de ellas forman parte del proteoma central del género Brucella, y la mayoría de ellas intervienen en procesos como el mantenimiento celular, la supervivencia, la respuesta al estrés, la virulencia y la infectividad. Curiosamente, se observó también una alta divergencia en algunas de estas flavoproteínas con respecto a homólogos cercanos en otras especies, sugiriendo posibles actividades catalíticas modificadas o aún no identificadas. Por tanto, este estudio permitió identificar algunas flavoenzimas que pueden resultar en la identificación de dianas para la búsqueda de antimicrobianos y/o nuevas herramientas biotecnológicas. Adicionalmente, se planteó la caracterización funcional y estructural de tres enzimas que componen un sistema multienzimático y que están involucradas de forma secuencial en las etapas iniciales de la biosíntesis de los componentes del peptidoglicano en el citosol de *B. ovis*: en particular, la enzima UDP-N-acetilglucosamina enolpiruvil transferasa (MurA), la flavoenzima UDP-N-acetilglucosamina enolpiruvato reductasa (MurB) y la enzima UDP-N-acetilmuramoil-L-alanina ligasa (MurC) de *B. ovis*. En este trabajo, estas tres enzimas se han sobreexpresado de forma heterológa y purificado a homogeneidad, lo que ha permitido estandarizar metodologías para su caracterización bioquímica, biofísica y estructural. En particular, disponer de estas enzimas ha permitido profundizar en sus propiedades especie-específicas en *Brucella*, proponer la actividad enzimática de MurA de *B. ovis* como diana para la búsqueda de antimicrobianos, y establecer las bases que permitirán una mejor comprensión de este sistema, así como posibles intervenciones futuras en él. Finalmente, este estudio se planteó también profundizar en el mecanismo de acción de la Flavina-Ferredoxina

Tioredoxina Reductasa (FFTR) de la cianobacteria *Gloeobacter violaceus* durante el proceso de transferencia de electrones desde su potencial donador fisiológico, la ferredoxina Fdx1. Esta FFTR es una enzima homodimérica, que presenta como centros redox una molécula de FAD y un grupo disulfuro, y que se propone juega un papel clave en la reducción de la tiorredoxina utilizando los electrones procedentes de Fdx1. En particular, en este estudio, se han evaluado las propiedades de óxido-reducción de FFTR frente a distintos donadores de electrones tanto en la proteína nativa como en diversas variantes en el entorno de sus dos centros redox, el FAD y el grupo disulfuro. Los resultados obtenidos muestran como el entorno del FAD contribuye a modular significativamente sus propiedades de óxido-reducción, y ponen de manifiesto la complejidad de los mecanismos de transferencia de electrones en este sistema. En conclusión, esta Tesis Doctoral contribuye a mejorar nuestra comprensión en cuanto a la variabilidad y versatilidad de los sistemas dependientes de flavoenzimas aquí estudiados.

1. Introduction

1. INTRODUCTION

1.1 Flavins and Flavoproteins: historical overview

Flavins were described for the first time in 1879, when the English chemist Wynter Blyth isolated a bright yellow pigment from cow's milk, which he called lactochrome (Blyth, 1879). Later, several reports described it as a water-soluble substance with green fluorescence present in several foods like milk, malt, eggs, liver, and pig heart (Warburg & Christian, 1933). Subsequently, in early 1930s, a significant amount of research in the vitamins area was undertaken. In these years, Paul Karrer and Richard Kuhn received the Nobel Prize in Chemistry for their studies with vitamins and carotenoids. In particular, their most symbolic achievement was the characterization of riboflavin (RF, vitamin B2), which was described as "a yellow pigment that is part of the vitamin B complex and that plays a vital role in living beings", also making its artificial synthesis and production possible (Karrer et al., 1935; Kuhn et al., 1935). The name RF was given to replace the variety of names previously used (lactoflavin, ovoflavin, hepatoflavin), which were related to the source from which the pigment was isolated. RF represents the D-ribityl derivative of the isoalloxazine heterocycle (Figure 1.1 and 1.2), whose yellow color gives the second part of the name (from Latin: Flavus = yellow). Several groups contributed to the identification of the first flavin cofactor present in proteins, flavin mononucleotide (FMN), and Kuhn and co-workers also synthesized it. Almost at the same time, Warburg and Christian isolated a yellow protein from yeast that catalyzed the oxidation of nicotinamide adenine dinucleotide phosphate (NADPH) by molecular oxygen, being this the first flavoprotein discovered and known as "Old Yellow Enzyme" (Warburg & Christian, 1933). Using ammonium sulfate at pH 2.0, Hugo Theorell precipitated the yellow protein, separating the white protein precipitate from the yellow supernatant that, separately, did not catalyze the reaction. The second identified flavin cofactor, flavin adenine dinucleotide (FAD), was isolated as the cofactor of D-amino acid oxidase (Warburg & Christian, 1933) and was synthesized in 1954 (Christie et al., 1954). Due to the role as cofactors in enzymatic catalysis of RF derivatives, all these studies demonstrated the biochemical basis for the need of RF as a vitamin in mammals (Theorell, 1935).

Flavoproteins have either FMN or FAD as a prosthetic group or as a cofactor, and are involved in a large number of biological processes, many of them related to their oxido-reduction properties (Figure 1.1). Most of them are enzymes that actively participate in aerobic metabolism by catalyzing the two-electron dehydrogenation of various substrates and are responsible for one-electron transfer to different metal centers via their semi-reduced

semiquinone radical state (Walsh & Wencewicz, 2013). Flavoproteins also play a significant role in soil detoxification processes via the hydroxylation of aromatic compounds, forming parts of multi-redox-center enzymes, such as nicotinamide adenine dinucleotide (NADH) dehydrogenase, xanthine oxidase/dehydrogenase, and cytochrome P450 reductase (Fraaije & Mattevi, 2000; Iyanagi et al., 2012). Flavin-dependent light-responsive proteins and enzymes, such as DNA photolyases, cryptochromes, as well as light-oxygen-voltage (LOV) and blue-light sensors using FAD (BLUF) domains participate in many critical biological processes, including DNA repair, photoregulation of circadian rhythms, and gene expression (Swartz et al., 2001; Edwards, 2006; Mattevi, 2006; Joosten & Berkel, 2007).

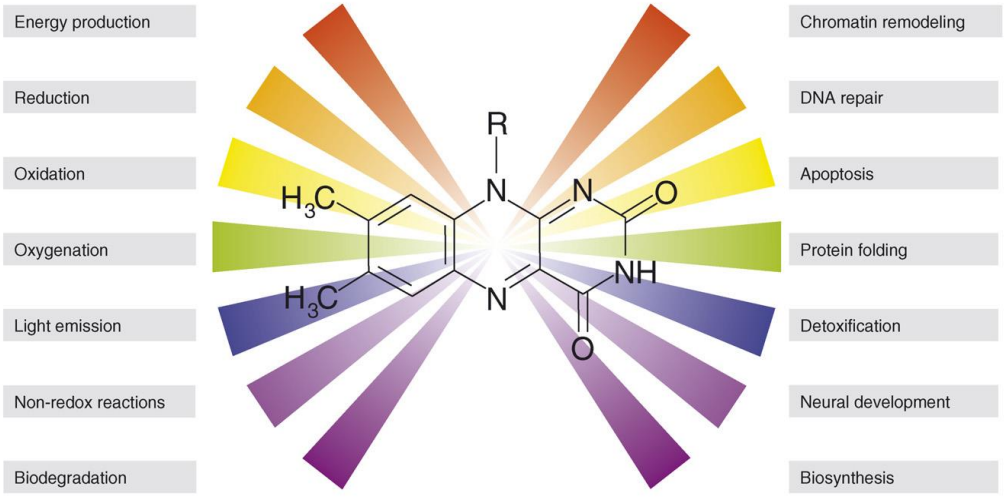

Figure 1.1. Summary of main biological functions of flavoenzymes (Joosten & Berkel, 2007).

Other reactions catalyzed by flavoenzymes include the oxidation of alcohols (Romero & Gadda, 2014), oxidations and reductions of aldehydes and lactols (Dijkman & Fraaije, 2014; Martin et al., 2020), as well as (cyclic) alkane hydroxylation and aromatic hydroxylation (Li et al., 2008; Chakraborty et al., 2010), Baeyer-Villiger oxidation, epoxidation, sulfoxidation, phosphite ester, selenide, organoboron, and amine oxidations (Walsh & Chen, 1988), dehalogenation, halogenation, decarboxylation (Lan & Chen, 2016; van Pée & Unversucht, 2003), and bioluminescence (Brodl et al., 2018).

1.2. The isoalloxazine ring and the flavin cofactors

Flavins are compounds that derivate from the 7,8-dimethyl-10-alkylisoalloxazine, also referred as lumichrome, with various modifications on the isoalloxazine ring substituents, frequently at N10 (Edwards, 2014). The isoalloxazine ring is one of the most versatile redox-active groups in the cell, capable of one- and two-electron transfers when bound to proteins. Because of this, flavoproteins and flavoenzymes often serve as intermediaries between obligate

one and two electron donors and acceptors. The isoalloxazine ring is formed by the fusion of the hydrophobic ring of dimethylbenzene with the hydrophilic ring of pteridine, a compound made up of pyrazine and thymine rings (derived from pyrimidine). Furthermore, the redox potential of the isoalloxazine ring is suitable for the metabolism of a wide range of biological molecules through the interconversion of single and double bonds (Fraaije & Mattevi, 2000; Kodali & Thorpe, 2010). The flavin family is extended to all compounds containing an isoalloxazine nucleus that derivates from the heterocyclic structure of benzo[g]pteridine. Their 2,4-dioxo derivatives are the alloxazines with the most relevant representatives being lumichrome, 5-deazaflavins, and their corresponding N-oxides and flavinium salts. Nonetheless, the biologically most relevant molecules are the isoalloxazine derivates: lumiflavin, RF, FMN and FAD (Sikorska et al., 2004) (Figure 1.2).

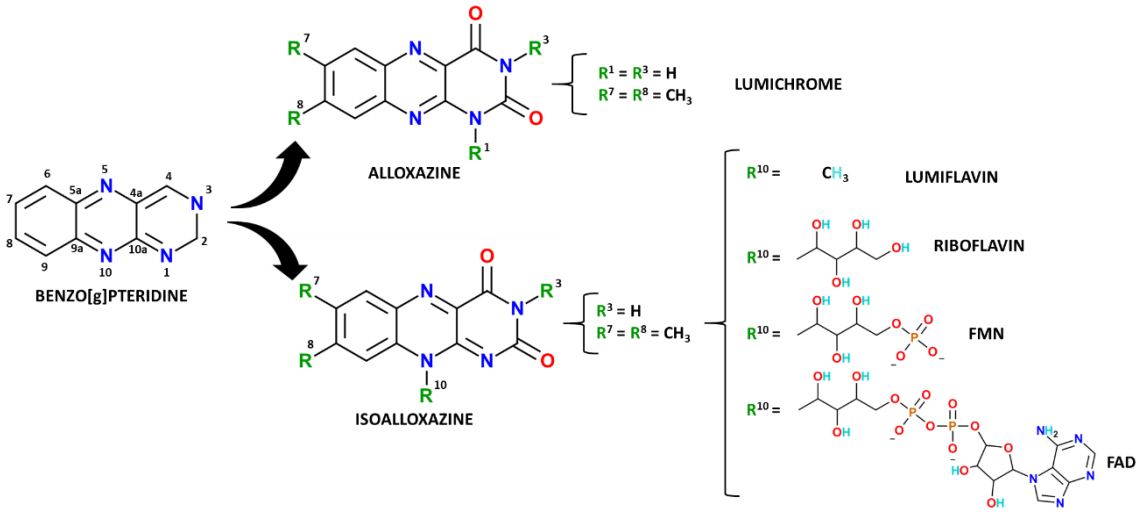

Figure 1.2. Structure of benzo[g]pteridine, alloxazine, isoalloxazine and its biologically relevant derivatives: RF, FMN and FAD.

RF is formed by the fusion of N10 of the isoalloxazine ring to one ribitol molecule through a carbon-nitrogen bond (C-N10). If a phosphate group is then bound to the terminal ribose carbon, FMN is formed (Metzler et al., 2003). The FAD consists of two nucleotides, adenine nucleotide (adenosine monophosphate) and FMN, bridged together through a pyrophosphate group. Another non-technical, but widely extended terminology, is the designation of the two faces of the isoalloxazine ring, *si* and *re*. If the isoalloxazine ring is oriented with the N10 in the lower part of the molecule, the *re* face is the one in which the benzene is located at the left side (Fig 1.3).

In vivo, the biosynthesis of FMN and FAD occurs through the sequential action of two ubiquitous activities: riboflavinkinase (RFK) that phosphorylates the RF precursor to FMN, and FMN:adenylyltransferase (FMNAT) that catalyzes the transformation of FMN into FAD.

In most mammals, two different monofunctional enzymes have each of these activities, but in prokaryotes a single bifunctional enzyme, known as FAD synthase (FADS), holds both activities (Moreno et al., 2022). Moreover, while most bacteria and plants are able to biosynthesize the RF precursor, mammals cannot produce it and have to incorporate it from the diet as a vitamin (Serrano et al., 2013).

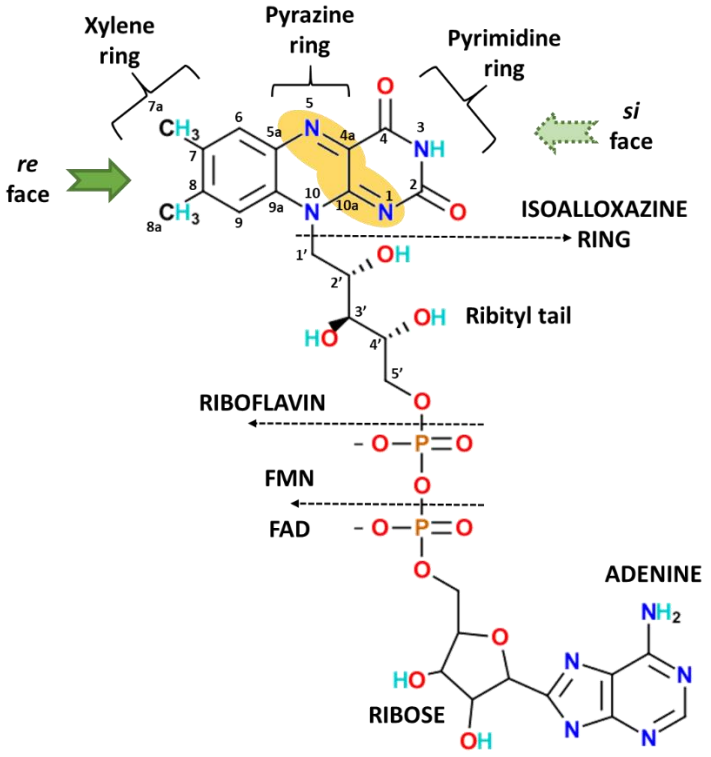

Figure 1.3. Structure of biological relevant flavin cofactors. The catalytic core structure of flavin cofactors is the 7,8-dimethylisoalloxazine ring, which comprises an electron-rich xylene ring, an electron-deficient pyrimidine ring, and a bridging electrophilic pyrazine ring. The catalytically relevant N5–C4a–C10a–N1 locus is shadowed in yellow. RF, FMN and FAD have a ribityl unit fused to the 7,8-dimethylisoalloxazine moiety at N10. FMN is in addition decorated with a 5-phosphoryl group at the ribityl end, while FAD is further extended by an adenosine monophosphate.

1.3 Flavoproteins and flavoenzymes: oxido-reduction and spectroscopic properties

Within flavoproteins, flavins are capable to underway oxido-reduction processes, to stabilize different redox states and to react with other redox centers. Moreover, changes in the redox state of the flavin cofactor within flavoproteins is widely used for signaling and detection in biological processes (Hill et al., 1996; Swartz et al., 2001), which are not exclusively characteristic of redox processes. The part of the molecule that actively participates in these processes is the isoalloxazine ring, particularly its N5–C4a–C10a–N1 locus (Figure 1.3), while the ribityl side chain, the phosphates, and the adenine nucleotide mainly contribute to its anchoring to the protein (Murthy & Massey, 1997). The isoalloxazine ring can exist in three

different redox states: flavoquinone or oxidized (Flv_{ox}), flavosemiquinone or one-electron reduced (Flv_{sq}), and flavohydroquinone or two-electron reduced (Flv_{rd}). Noticeably, while free flavins hardly stabilize the semiquinone, the protein environment in some flavoproteins contributes to its stabilization (Edmondson & Tollin, 1983). This confers some flavoenzymes the versatility to catalyze two electrons (in the form of a hydride ion) as well as one electron transfer processes (Figure 1.4) (Palfey & McDonald, 2010). Moreover, under physiological conditions, the semiquinone and hydroquinone states can be present in either their neutral or anionic forms (Kao et al., 2008) (Figure 1.4). This is due to the fact that each redox state of the isoalloxazine undergoes acid-base equilibria depending on the pH and on the interaction network among the ring atoms and the protein environment (Pavlovska & Cibulka, 2021). In that way, flavins can act as intermediates, hitching reactions where one of the substrates can only accept or transfer one electron, and the other one needs to interchange two electrons at a time (Mulo & Medina, 2017).

The different FMN and FAD redox states presented by these cofactors relate to different electronic states with characteristic spectroscopic features (Kao et al., 2008; B. Liu et al., 2010). All oxidized flavins exhibit high absorption in the UV and visible regions with three maxima at wavelengths close to 265, 370 (band II) and 450 (band I) nm, the last two bands conferring them a yellow-orange color (Massey, 2000). The spectral shape is practically the same for RF and FMN, but shows little wavelength displacement and lower intensity for FAD due to the formation of an internal coupling between the isoalloxazine ring and the adenine of the molecule (van den Berg et al., 2002). In the visible region, FAD and FMN present two absorption maxima: 375 and 450 nm for FAD (ε_{375} = 9.3 $mM^{-1}cm^{-1}$ and ε_{450} =11.3 $mM^{-1}cm^{-1}$, respectively) and 373 and 445 nm for FMN (ε_{373} =10.4 $mM^{-1}cm^{-1}$ and ε_{445} =12.02 $mM^{-1}cm^{-1}$, respectively) (Munro & Noble, 1999). The oxidized absorption spectra of flavins when forming part of flavoproteins resemble those of free flavins, but the interactions of the flavin ring with the protein environment usually induce small displacements in the position and intensity of maxima, as well as the apparition of spectral shoulders (Figure 1.4). This makes the spectra of each flavoprotein unique. The enzyme-bound neutral semiquinone has a characteristic blue to green color and typically has a broad absorption 500–650 nm band peaking around 580-600 nm. The anionic semiquinone exhibits a red color and has two dominant peaks around 380 and 490 nm, being its spectrum particularly influenced by the polarity of the solvent (Massey & Palmer, 1966; Henriques et al., 2010; Pimviriyakul & Chaiyen, 2020). Reduced species have a pale yellow color due to the bleaching of bands I and II, which differs from the bright yellow of the oxidized state (Weber, 1950).

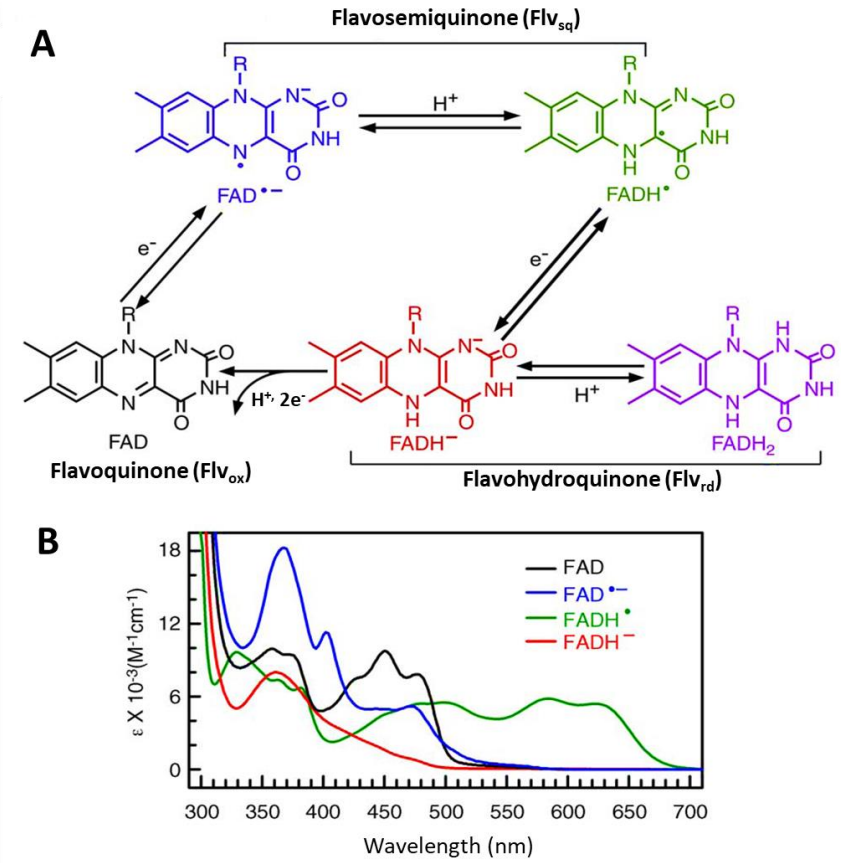

Figure 1.4. Oxido-reduction of flavins. (A) Redox forms of the isoalloxazine ring usually found within flavoproteins: oxidized (black), anionic (blue) and neutral (green) semiquinone, and anionic (red) and neutral (purple) fully reduced. **(B)** Typical features of absorption spectra found in the visible spectra of oxidized, anionic semiquinone, neutral semiquinone reduced forms as found in various FAD-containing enzymes. Adapted from (Liu et al., 2010).

Together with aromatic amino-acids, flavins are the most important fluorophores in proteins. Their oxidized state exhibits a high fluorescence quantum yield, being the maxima of excitation and emission around 440-450 and 525-530 nm, respectively (Figure 1.5A) (Sun et al., 1972). The fluorescence quantum yield for RF and FMN at pH 7.0 is ten times higher than that of FAD. Once again, this effect results from the stacking of the isoalloxazine ring and the adenine group of the nucleotide that quenches the flavin fluorescence. In aqueous solution such conformation is in equilibrium with the open fluorescent one (Figure 1.5A) (van den Berg et al., 2002; Weber, 1950). Nevertheless, when FMN and FAD become part of flavoproteins their fluorescence can be moderately altered, completely disappear (Keilin & Hartree, 1946) or stay unaltered (Straub, 1939), depending on the manner in which the isoalloxazine ring gets allocated within the protein (Weber, 1950). Regarding the semiquinone states, the study of their fluorescence is usually scarce because they are transient short-lived species in many catalytic cycles and are not stable in solution (Su et al., 2019). The hydroquinone usually displays weak

fluorescence in solution as consequence of its low absorption, but at low temperature or into a rigid protein environment it can show enhanced fluorescence (Ghisla & Massey, 1989).

Figure 1.5 shows a comparative summary of different absorption and emission spectra produced by the different redox states or media conditions for flavin cofactors either when free or within the protein environment. Figure 1.5A shows typical spectra for oxidized FAD in solution, with peaks at 375 (band II) and 450 (band I) nm, while FMN enclosed in a flavodoxin mutant (W60F/Y98F Fld, from *Desulfovibrio vulgaris*) shows bands at 384 and 454 nm and some shoulders at 432, and 476 nm. The fluorescence emission maximum of Flv_{ox} around 530 nm in solution shifts to the blue within the hydrophobic flavodoxin environment. Figure 1.5B shows the absorption and emission spectra of semiquinones in two flavoproteins. Absorption of the neutral $FMNH^{\bullet}$ in flavodoxin extends up to 700 nm, and for it a broad emission spectrum peaking at 700 nm can be observed. On its side, the anionic $FAD^{\bullet-}$ semiquinone of a type 1 cryptochrome shows a weak emission spectrum peaking at 513 nm. In addition, Figure 1.5C shows the absorption and emission spectra of fully reduced anionic and neutral flavins ($FADH^-$ and $FADH_2$) in solution and within photolyase. Upon excitation at 360 nm, weak fluorescence emissions peaking at 455 nm for anionic hydroquinone ($FADH^-$) and at 480 nm for neutral hydroquinone ($FADH_2$) are observed. However, $FADH^-$ in photolyase shows an absorption band at 360 nm, with fluorescence emission peaks at 515 and 545 nm. In general, the fluorescence intensity of fully reduced flavins in solution is much weaker than that within the protein, suggesting very different quenching and dynamic factor associated with a bending motion of the isoalloxazine ring. Thus, enzymes can use geometric constraints and electrostatic interactions to manipulate the configuration of the flavin cofactor, planar or bent, to achieve various biological functions. In this same figure, it is shown how the flavin ring is nearly planar in fully reduced photolyase, allowing excited flavin molecules to exist long enough to react with substrates to repair damaged DNA. In the case of cryptochrome semiquinone anionic state, the protein is more flexible and results in complex deactivation dynamics of a few to hundreds of picoseconds (Kao et al., 2008).

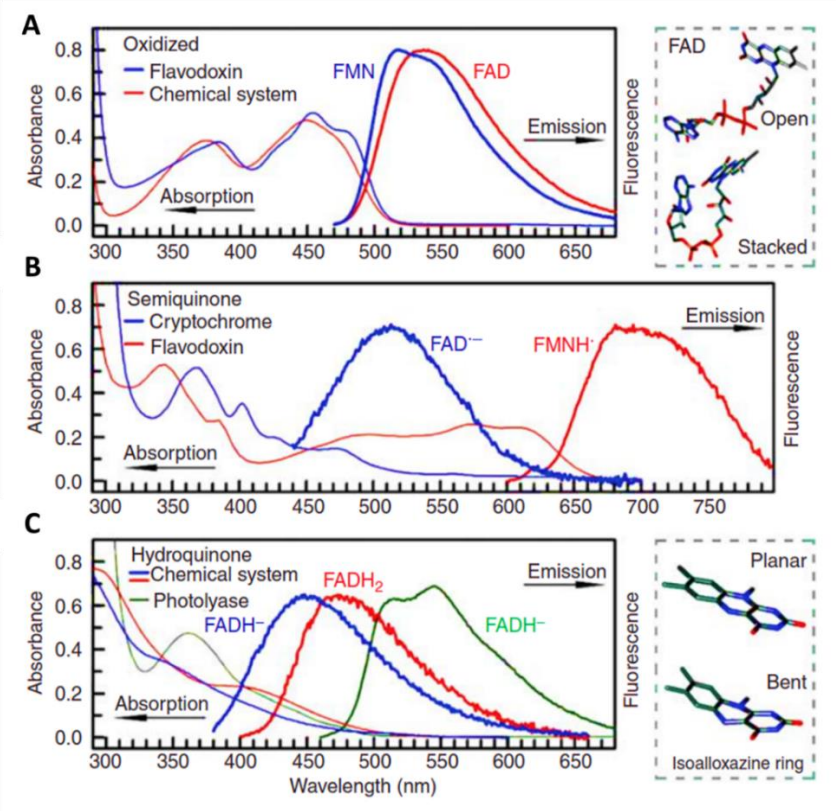

Figure 1.5. Absorption and emission spectra of model flavins and flavoproteins in different redox states. (A) Oxidized state of free FAD and of FMN within flavodoxin. **(B)** Anionic semiquinone state of FAD ($FAD^{\cdot-}$) in cryptochrome and neutral semiquinone state of FMN ($FMNH^{\cdot}$) in flavodoxin. **(C)** Hydroquinone of free FAD in anionic ($FADH^{-}$) and neutral ($FADH_2$) states, and of $FADH^{-}$ within photolyase. The excitation wavelengths are 400 nm for FAD and FMN, 420 nm for $FAD^{\cdot-}$, 580 nm for $FMNH^{\cdot}$, and 360 nm for $FADH^{-}$ and $FADH_2$. The fluorescence emissions of $FAD^{\cdot-}$ in cryptochrome and $FADH^{-}$ and $FADH_2$ in solution are very weak. *Upper right frame*: Schematic representation of FAD in open and stacked conformations. The stacked conformation was adapted from U-shaped FAD in photolyase. *Lower right frame*: Schematic representation of the isoalloxazine ring in planar and "butterfly" bent conformations. Figure taken from (Kao et al., 2008).

At pH 7.0, the midpoint reduction potential for the two-electron electron exchange of the free flavin is around -200 mV ($E_{ox/rd}$ -219 mV for FAD, -205 mV for FMN, and -200 mV for RF). The high thermodynamical instability of the semiquinone in free flavins is reflected in the midpoint reduction potential of the two half-reactions: $E_{ox/sq}$ is more negative than $E_{sq/rd}$ (Lowe & Clark, 1956). Thus, midpoint reduction potentials for FMN at pH 7.0 and 20 °C are $E_{ox/sq}$=-313 mV and $E_{sq/rd}$ = -101 mV (Mayhew, 1999). Nonetheless, the versatility in terms of catalysis of flavoproteins is due to the wide range of oxidation-reduction potentials that their flavin cofactors can acquire within each particular protein environment, which extend from -495 to +80 mV (Ghisla & Massey, 1989a; Walsh et al., 1978). Thus, when flavins are part of flavoproteins, their midpoint reduction potentials can be modified as a consequence of their isoalloxazine ring interaction with the protein (Ghisla & Massey, 1986). For this reason, and depending on the relative modulation of $E_{ox/sq}$ and $E_{sq/rd}$ values, some flavoproteins reach the

stabilization of near 100% of the semiquinone state. In addition, to all above mentioned forms, electronic states where partial charge of the flavin ring is transferred from or to one of the states to a neighboring molecule can be found and they are known as charge-transfer states (Mayhew, 1999).

A large variety of flavoenzymes use equivalents of pyridine nucleotides, nicotinamide adenine dinucleotide (NAD^+/H) and nicotinamide adenine dinucleotide phosphate ($NADP^+$/H) (Figure 1.6), to oxidize/reduce the FAD cofactor; for example, reductases, oxygenases and dehydrogenases. $NAD(P)^+$/H coenzymes usually form a transient complex with the enzyme, where a specific chemical hydride transfer (HT) reaction occurs. Then, the oxidized/reduced coenzyme is released from the flavoenzyme, and a second substrate restores the reduced/oxidized flavin redox state and closes the catalytic cycle (Cao et al., 2020; Nivière et al., 1998). The biosynthetic precursors of $NAD(P)^+$/H coenzymes come from the vitamin B3 or niacin (Makarov et al., 2018). NAD^+ consists of an adenine nucleoside and a nicotinamide nucleoside joined by a pyrophosphate bridge. $NADP^+$ is similar to NAD^+ with the additional presence of a phosphate group on the 2' position of the ribose ring that carries the adenine moiety (Kawai & Murata, 2008). The reactivity of these molecules is limited to their nicotinamide ring, while the remaining part of the coenzyme molecule participates exclusively in the recognition and binding to the protein. $NAD(P)^+$/H nucleotides can thus be considered as a storage for hydride ions, the equivalent of two electrons and a proton, as well as to the related amount of energy or reducing powder (Kyte, 1995). NADH and NADPH present similar spectroscopic properties, exhibiting absorption maxima at 259 and 338 nm (Figure 1.6), with molar extinction coefficient values of 14.3 and 6.2 $mM^{-1}cm^{-1}$, respectively. When oxidized, $NAD(P)^+$ coenzymes have virtually no absorbance at 340 mm but keep the maximum peak at 259 nm with a molar extinction coefficient of 17.9 $mM^{-1}cm^{-1}$ (Bernofsky & Wanda, 1982). NADH and NADPH are fluorescent, but their oxidized states show no appreciable fluorescence. In aqueous solution, when the nicotinamide of NADPH is excited at ~335 nm, a fluorescence emission band at 445-460 nm (violet to blue fluorescence) is observed (Blacker et al., 2014).

In general, during the metabolism, $NADP^+$/H is used for anabolic redox reactions, whereas NAD^+/H is used for catabolic processes. This is possible because the $NADP^+$/NADPH ratio is generally displaced to the reduced state while the NAD^+/NADH in displaced towards the oxidized one. Finally, the midpoint reduction potential of the $NADP^+$/NADPH pair is identical to that of NAD^+/NADH: E'_0: -320 mV (Spaans et al., 2015).

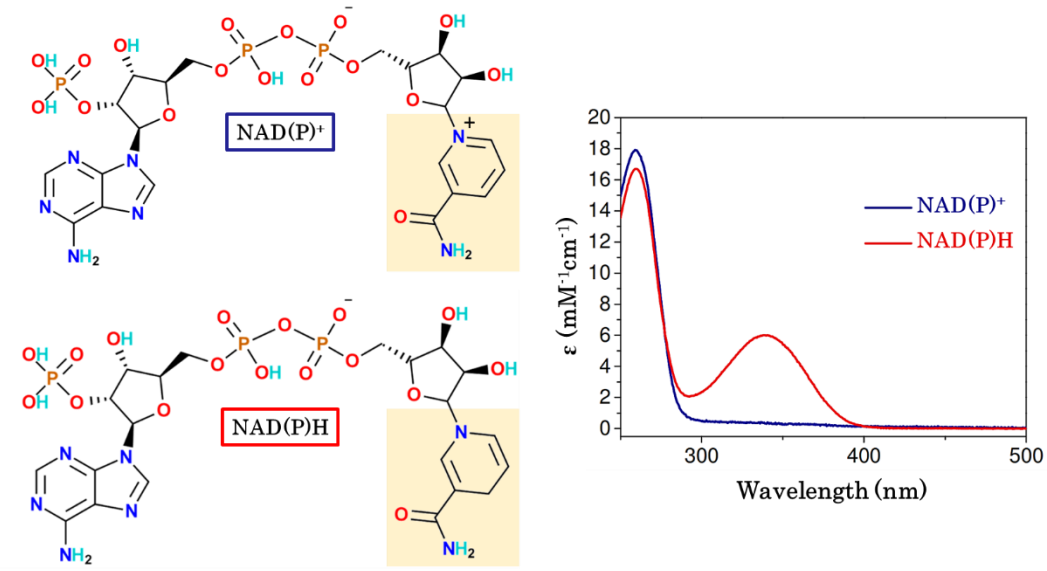

Figure 1.6. $NAD(P)^+$ and NAD(P)H structures and their absorption spectra.

1.4 Current knowledge of flavoprotein content in different species

The partial study of 22 genomes of different species, including archaea, eubacteria, protozoa and eukaryotes, revealed that the universe of flavin-dependent proteins contains around 380 different proteins, with the number of genes encoding flavin-dependent proteins varying widely and covering a range of 0.1 to 3.5% of the predicted genes. Thus, it appears that some species are highly dependent on flavin-dependent oxidoreductases for degradation or biosynthesis, while others have minimized their flavoprotein arsenal. More than 80% of the identified flavoenzymes in this study were oxidoreductases, while the remaining enzymes were classified as transferases (4.3%), lyases (2.9%), isomerases (1.4%) and ligases (0.4%). 75% of these enzymes used FAD and 25% FMN, and most of them bind the cofactor non-covalently (90%) (Macheroux et al., 2011).

The *Homo sapiens* flavoproteome was first detailed in 2013, discovering 90 genes that coded for 77 different flavin-dependent proteins, of which 84% required FAD, 16% FMN and five both (Lienhart et al., 2013). Most of them catalyze redox processes in primary metabolic pathways such as the citric acid cycle, β-oxidation, and amino acid degradation (Figure 1.7). Ten occur as isoenzymes that play special functions in the human body. Some others participate in the biosynthesis of other essential cofactors and hormones, such as coenzyme A, coenzyme Q, haem, pyridoxal 5´-phosphate, steroids and thyroxine, and are important for the regulation of folate and different metabolites through the use of tetrahydrofolate. Thus, RF plays a very important role in the human metabolism, but, as above mentioned, it is only biosynthesized by bacteria, fungi and plants, being an essential compound for man and animals that must be

acquired through the diet (Merrill & McCormick, 2020). Once internalized into cells, RF is phosphorylated by a RFK activity to produce FMN, and, if necessary, further converted to FAD by a FMNAT activity (Giancaspero et al., 2015). Later, the cofactors are integrated to the flavoproteins that play essential roles in various processes; including the mitochondrial respiratory chain oxidative phosphorylation, β-oxidation, amino acid metabolism and choline degradation, the conversion and recycling of niacin, folate, and vitamin B6, the synthesis of all hemoproteins, including hemoglobin, nitric oxide synthase, P450 enzymes, electron transfer and transport, oxygen storage, the metabolism of essential fatty acids in brain lipids, the absorption and utilization of iron, the regulation of thyroid hormones, cell development, among many others (Lemieux & Blier, 2022). Therefore, RF deficiency would have negative consequences for many bodily functions, including brain functions (Kennedy, 2016). In *H. sapiens*, more than 50 flavoproteins are associated with disorders caused by allelic variants that affect their function and health (Lienhart et al., 2013).

The search for flavoproteins in the yeast *Saccharomyces cerevisiae* genome identified 68 genes encoding flavin-dependent proteins with 47 different biochemical functions, 35 requiring FAD (74%), 15 FMN (26%) and 3 being diflavin enzymes harboring FMN and FAD (Gudipati et al., 2014). Some of these flavoproteins participate in redox processes around the electron transport chain, the iron metabolism (such as iron absorption, biogenesis of iron and sulfur stores, and insertion of the haem cofactor into apocytochromes) or in tRNA modification reactions (Gudipati et al., 2014) (Fig 1.7). *S. cerevisiae* has been used as a model organism to studying fundamental biological processes, since~ 30% of human genes implicated in human diseases have a yeast homologue and the majority of disease-related human flavoproteins operate in the mitochondrion. Therefore, owing to the similarity of mitochondrial processes in eukaryotes, yeast homologs located in mitochondria appear particularly suitable models to improve our understanding of human mitochondrial diseases (Foury, 1997; Lienhart et al., 2013).

In plants, in addition to the general metabolic functions described above, flavoproteins also act as photoreceptors that mediate the perception of blue light (Christie et al., 2015), as well as in the regulation of the cell cycle and tolerance to salt stress (Espinosa-Ruiz et al., 1999), CO_2 assimilation, stomatal conductance, regulation of photosynthesis in the dark phase (Fuentes et al., 2011), and nitrate utilization (Crawford et al., 1988). Most of these studies have been carried out in *Arabidopsis thaliana*, a plant of the mustard family that has become an essential model for scientists since the 1980s (Meinke et al., 1998; Hayashi & Nishimura, 2006). *A. thaliana*, uses many flavoenzymes for specific plant purposes and fundamental

metabolic activities during development and for signal transduction pathways in response to biotic and abiotic stresses. Its flavoproteome content was described in 2020 (Schall et al., 2020), reporting up to 249 genes that encode possible flavoproteins, equivalent to 0.91% of its total genome. It is therefore larger than the human and yeast flavoproteomes. Out of these 249 flavoproteins, 211 and 32 exclusively bind FAD and FMN, respectively, while 3 bind both cofactors. Regarding their classification, 88.3% are oxidoreductases, 3.2% are lyases and 1.2% are transferases and for 6.83% of its flavoproteins the enzymatic activity has not yet been classified (Lienhart et al., 2013; Schall et al., 2020; Eggers et al., 2021).

As a result of these few sets of reported flavoproteomes, the main observation is the high percentage of oxidoreductases versus other flavoenzymes and flavoproteins (Figure 1.7). Oxidoreductases are a broad group of enzymes that catalyze electron transfer (ET) from one molecule, the reductant or electron donor, to another, the oxidant or electron acceptor. They often need coenzymes such as $NAD(P)^+/H$ and cofactors such as flavins. In fact, $NAD(P)^+/H$ coenzymes are required by about 80% of oxidoreductases (Paul et al., 2019), including peroxidases, reductases, dehydrogenases, oxidases, oxygenase, and hydroxylases. Noticeably, despite their potential interest, there were no reports about the full flavoproteome content of any pathogenic bacteria at the beginning of this study.

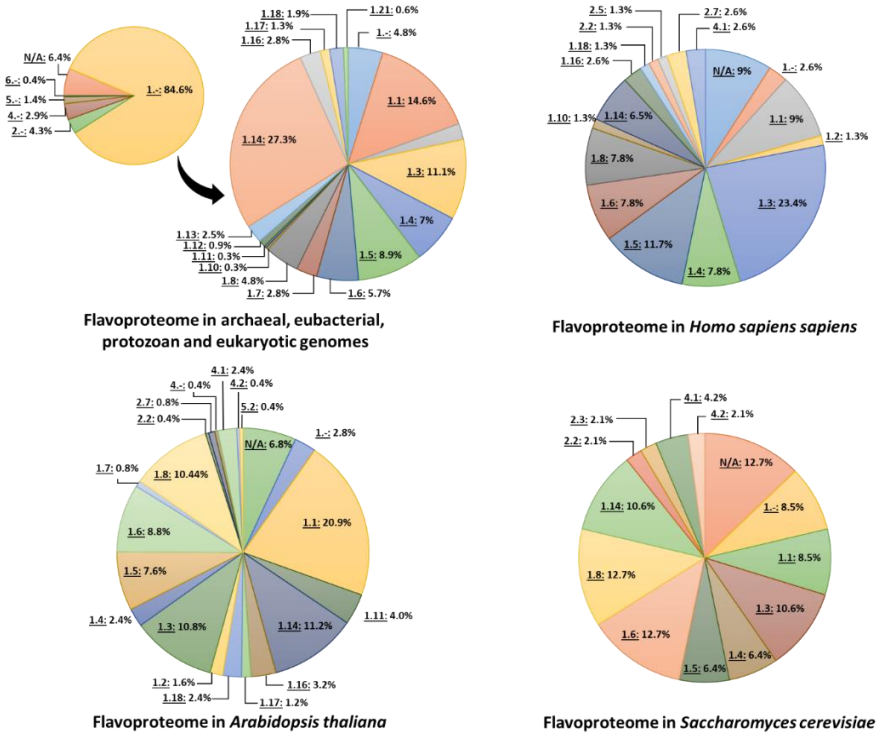

Figure 1.7. Distribution of flavoenzyme functions from reported studies in different species. Pie charts were generated by the enzyme classification according to the Enzyme Commission numbers (EC number): Class 1. oxidoreductases; 2. transferases; 4. lyases; 5. isomerases; 6. ligases; N/A: Not available.

1.5 The biosynthesis of peptidoglycan building blocks: the UDP-N-acetylglucosamine enolpyruvate reductase system

1.5.1 The peptydoglycan

The peptidoglycan (PG), also called murein, is a unique and essential structural element in the cell wall of most bacteria. Made of glycan strands cross-linked by short peptides, the sacculus forms a closed bag-shaped structure surrounding the cytoplasmic membrane (Vollmer et al., 2008). The PG involves the thickness of the layers surrounding the plasma membrane, a single membrane for Gram-positive bacteria and two membranes for Gram-negative bacteria, which is decorated with other glycopolymers, such as teichoic acids (TA) or polysaccharides (PSs), and proteins (Figure 1.8). In Gram-negative bacteria the PG is only a few nanometers thick, representing one to a few layers, the saccule accounts for about 10% of the cell wall, while in Gram-positive bacteria the peptidoglycan is 30-100 nm thick and contains many layers and is equivalent to almost 90% of the cell wall (Silhavy et al., 2010).

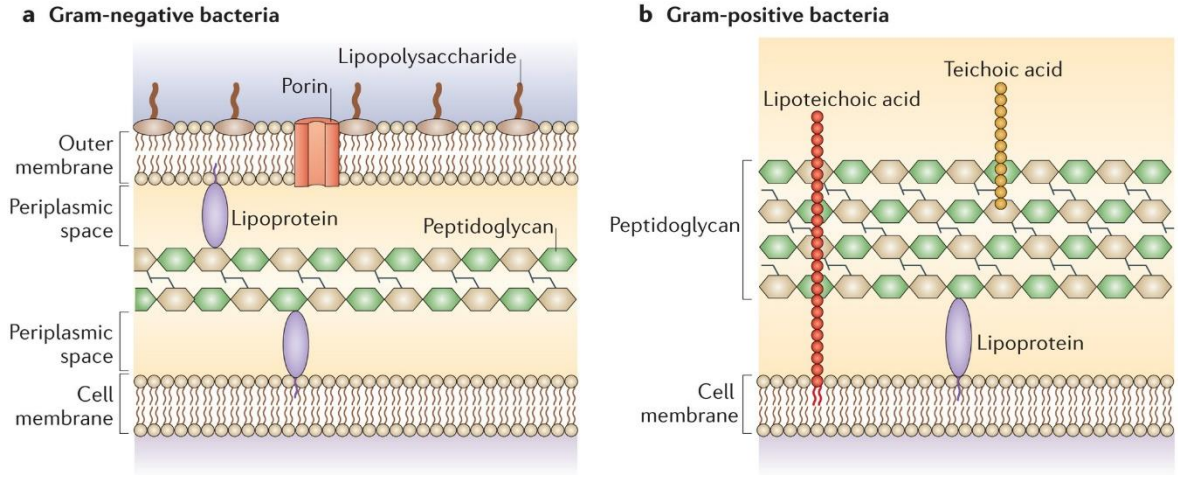

Figure 1.8. Cell walls of Gram-negative and Gram-positive bacteria. (A) The cell wall of Gram-negative bacteria consists of a thin layer of PG in the periplasmic space between the inner and outer lipid membranes. The outer membrane contains lipopolysaccharides on its outer leaflet and facilitates non-vesicle-mediated transport through channels such as porins or specialized transporters. **(B)** Gram-positive bacteria have a single lipid membrane surrounded by a cell wall composed of a thick layer of PG and lipoteichoic acid that is anchored to the cell membrane by diacylglycerol (Brown et al., 2015).

The cell wall has multiple functions: it protects cell integrity by supporting internal osmotic pressure, maintains cell morphology, provides protection against environmental changes, gives structural support for the components of the lipid membrane, and regulates cell growth and division. The wall also mediates bacterial interactions with abiotic surfaces, infecting bacteriophages or eukaryotic host cells (Chapot-Charter & Kulakauskas, 2014; Scheffers & Pinho, 2005).

1.5.2 The biosynthesis of the peptidoglycan

The PG biosynthesis includes more than twenty reactions that take place at three different locations in the cell (Zoeiby et al., 2003; Barreteau, 2008; Pazos & Peters, 2019). First, the synthesis of precursors of the Uridine-N-acetylglucosamine diphosphate (UNAG) occurs in the cytoplasm and requires four successive enzymatic activities (Figure 1.9):

1. A molecule of *D*-fructose-6-phosphate (F6P) is transformed into *D*-glucosamine-6-phosphate (G6P) by the action of dimeric glucosamine-6-phosphate synthase (GlmS), using *L*-glutamine as a nitrogen source.
2. Phosphoglucosamine mutase (GlmM) catalyzes the interconversion of the G6P to glucosamine-1-phosphate (Glc1P).
3. Glucosamine-1-phosphate acetyltransferase (GlmU) catalyzes then the transfer of an acetyl group from acetyl-CoA to Glc1P to produce N-acetylglucosamine-1-phosphate (GlcNAc1P).
4. GlmU, a bifunctional enzyme that also acts as a N-acetylglucosamine-1-phosphate uridyltransferase, finally catalyzes the transfer of uridine 5'-monophosphate from uridine 5'-triphosphate (UTP) to GlcNAc1P, in the presence of Mg^{2+} ions, yielding inorganic pyrophosphate and UNAG. UNAG is also present in eukaryotes because N-acetylglucosamine (GlcNAc) is an important component of large biomolecules such as chitin and glycoproteins. However, the eukaryotic pathway of UNAG biosynthesis differs from the prokaryotic pathway.

Subsequently, on the inner face of the cytoplasmic membrane, formation of the monomeric PG building block N-acetylglucosamine-N-acetylmuramylpentapeptide takes place. This occurs via a six-step process catalyzed by the enzymes known as MurA, MurB, MurC, MurD, MurE and MurF:

5. UDP-N-acetylglucosamine enolpyruvyl transferase (MurA) catalyzes the transfer of the enolpyruvate moiety from phosphoenolpyruvate (PEP) to position 3'-hydroxyl of UNAG to produce enolpyruvil-UDP-N-acetylglucosamine (UNAGEP) with the release of inorganic phosphate (Pi).
6. UNAGEP is then reduced by the flavoenzyme UDP-N-acetylglucosamine-enolpyruvate reductase (MurB) using one equivalent of NADPH and a solvent-derived proton. This two-electron reduction creates the lactyl ether substituent at the C3 position of UDP-N-acetylmuramic acid (UNAM).

7. UDP-N-acetylmuramate-alanine ligase (MurC) is a non-ribosomal peptide ligase that catalyzes the addition of *L*-alanine to the UNAM. This reaction requires ATP and produces ADP, Pi and UDP-N-acetylmuramoyl-L-alanine (UNAM-A).
8. UDP-N-acetylmuramoyl-*L*-Alanine-*D*-Glutamate ligase (MurD) catalyzes the addition of *D*-glutamate to UNAM-A and forms UNAM-A-E.
9. UDP-N-acetylmuramoylalanyl-*D*-glutamate-2,6-diaminopimelate ligase (MurE) is an ATP-dependent ligase that incorporates the third amino acid of the peptide system, generally either *meso*-A2pm (most Gram-negative bacteria and bacilli) or *L*-lysine (most Gram-positive bacteria). Nonetheless, in certain species, other amino acids are encountered, for example, *L*-ornithine, LL-A_2pm, *meso*-lanthionine, *L*-diaminobutyric acid and *L*-homoserine (Basavannacharya et al., 2010; Munshi et al., 2013).
10. UDP-N-acetylmuramoylalanyl-*D*-glutamyl-2,6-diaminopimelate-*D*-alanyl-*D*-alanyl ligase (MurF) catalyzes the addition of the *D*-Ala-*D*-Ala dipeptide to the UNAM-A-E-K molecule.

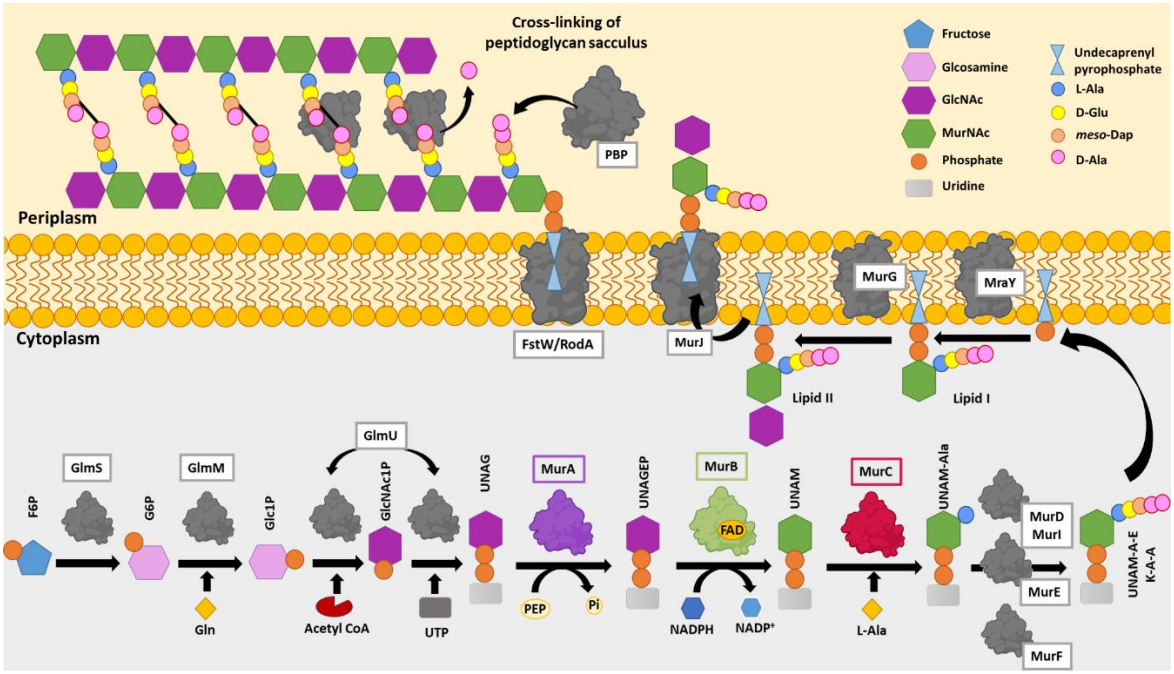

Figure 1.9. Overall view of the peptidoglycan biosynthesis path. Scheme of the steps in the biosynthesis and attachment of a new PG strand to an existing sacculus, with particular emphasis on the different synthetic and degrading enzymes. Boxes with colored edges highlight MurA, MurB, and MurC.

Finally, the polymerization reaction of the PG building blocks takes place in the periplasm, but before, a series of modifications carried out by the proteins anchored to the membrane occur:

11. The integral membrane protein MraY translocase catalyzes the first membrane-associated step, transferring UNAM-A-E-K-A-A from the cytoplasm to bactoprenol (C_{55}-P), a transporter associated with the cytoplasmic side of the inner membrane. This molecule is called lipid I.
12. One molecule of UNAG binds to lipid I by the MurG transferase, converting it into lipid II, the subunit that will be incorporated into the macromolecular PG (UNAG-UNAM-A-E-K-A-A) (Goffin & Ghuysen, 2002; Bouhss et al., 2004; Typas et al., 2011).
13. The transport of lipid II from the internal face to the external face of the cytoplasmic membrane is the last step in the biosynthesis of PG, being catalyzed by the flipases MurJ-like (Sham et al., 2015).
14. Elongation of the murein saccule takes place in the periplasm using the FtsW-RodA synthases that catalyze the incorporation of lipid II into pre-existing murein together with the enzymes "penicillin binding proteins" (PBP), as they have the ability to covalently bind penicillin and other β-lactams. This binding is produced by the structural similarity between the terminal D-Ala-D-Ala of the pentapeptide chain and the β-lactam antibiotics (Sauvage et al., 2008). The peptides are cut with DD-, LD- and DL-carboxypeptidases (CPases) and the crosslinkings are cleaved by DD- and LD-endopeptidases (EPases). The amidases remove the peptides from the glycan chains, while the specific exo- or endo-lytic transglycosylases (LT) cleave them to form 1,6-anhydro-N-acetylmuramic acid residues (anhMurNAc). LD-TPases are responsible for the formation of LD crosslinkings, the binding of the main outer membrane lipoprotein (Lpp), which is anchored to the outer membrane, and the binding of unusual D-amino acids (Typas et al., 2011).

1.5.3 The peptidoglycan biosynthesis and the development of antimicrobials

Gram-negative bacteria have a thin cell wall that is surrounded by an outer membrane, and this additional protective layer prevents many substances from entering the bacteria. However, this membrane contains channels called porins, which allow the entry of various molecules into the components of the PG wall. These molecules include drugs such as β-lactam antibiotics that can attack PBPs by forming links among them, and, glycopeptide antibiotics, like vancomycin, that bind to the D-Ala-D-Ala portion in lipid II and prevent the addition of new units to the PG. This leads to the lysis of the bacteria (Kapoor et al., 2017). The antibiotic resistance among bacteria that causes life-threatening infections has led to the need to find new

drugs that inhibit bacterial cell wall biosynthesis. While antibacterial drug development has primarily focused on Gram-positive pathogens, such as methicillin-resistant *Staphylococcus aureus* (MRSA) and *Streptococcus pneumoniae*, the emergence of highly resistant strains of Gram-negative bacteria, particularly *Pseudomonas aeruginosa*, *Klebsiella pneumoniae*, *Mycotobacter baumannii*, and *Escherichia coli*, highlights the need to focus more on targets in Gram-negative organisms. Therefore, PG biosynthesis is an attractive target for the development of broad-spectrum antimicrobial agents (Bugg et al., 2011).

1.6 The *Brucella* genus: model system to evaluate the flavoproteome content of a pathogenic bacteria and the enzymes involved in PG biosynthesis

Noticeably, at the beginning of this study the flavoproteome content had not yet been reported for any pathogenic bacteria, reason why it was of interest to initiate the evaluation of the flavin content in the *Brucella* genus. Human brucellosis was first described in 1859 as Malta fever or Mediterranean fever and was later isolated by Sir David Bruce from British soldiers in 1887 (Freer et al., 1996). Brucellosis is a zoonosis with cosmopolitan distribution that has become a serious economic and public health problem, especially in countries whose economies depend on cattle production (bovine, sheep, goats or pigs) (Christie, 1980). *Brucella* sp. are Gram-negative bacilli measuring 0.6-1.5 x 0.5-07 µm. They are strictly aerobic, non-spore forming, non-motile and their cell envelope is similar in structure to Enterobacteria. However, they differentiate from other Gram-negative bacteria by its PG being strongly associated with the outer membrane, and by the optimal growth requiring the addition of CO_2 (5-10%) at 37 °C in a pH of 6.6-7.4 (Alton et al., 1988; Alton & Forsyth, 1996). Infected animals are the main source of bacterial dispersion, being the genital or breast secretions the main pollution vehicle (Sbriglio et al., 2007). Sexually mature or pregnant mammals are more susceptible because *Brucella* has affinity for the tissues of the reproductive organs (Matope et al., 2011). *Brucella* bacteria adhere and penetrate the conjunctivae or damaged skin of the host. Then they are phagocytosed by neutrophils and monocytes, surviving intracellularly. Thus, the bacterium ensures a transport mechanism within phagocytes, spreading to different organs. Once inside the cell, it establishes itself in the plasmatic reticulum where it lives and multiplies (Detilleux et al., 1990). This eventually produces severe placentitis with infection of the fetus and abortion in females, and loss of fertility due to orchitis and epididymitis in males (Frenchick et al., 1985; Khan & Zahoor, 2018).

For many years, six species of the *Brucella* genus have been described as the most common cause of infections. Frequently, each *Brucella* species is associated with specific

hosts. *B. abortus* usually causes brucellosis in cattle, mink and buffalo, *B. melitensis* is the most relevant species causing infections in sheep and goats (and causes the majority of human brucellosis worldwide), and *B. ovis* causes infertility in rams and abortions in sheeps. *B. canis* causes disease in dogs, and *B. neotomae* in rodents. *B. suis*, presenting a large diversity of strains compared to other *Brucella* species, mainly affects pigs, European hares, reindeer and caribou (Corbel, 2006). Subsequently, additional species have been described to cause diseases in other organisms, including *B. pinnipediae* in marine mammals (seals, marine elephants and walrus), *B. ceti* in cetacea (whales, marsoundpas and dolphins), *B. microti* in voles, *B. vulpis* in foxes and *B. papionis* in baboons (Foster et al., 2007; Scholz et al., 2008; Guzmán-Verri et al., 2012; Whatmore et al., 2014). In addition, several new atypical strains causing diseases in humans and other mammalian hosts have been described. In many cases, these isolates were initially misidentified as *Ochrobactrum*, being later relabeled within the *Brucella* genus (Hördt et al., 2020; Oren & Garrity, 2020).

1.7 The Ferredoxin flavin-thioredoxin reductase in thioredoxin systems responsible for the reduction of disulfide bonds in *Gloeobacter violaceus*

Reactive oxygen species (ROS) are natural byproducts of cellular oxidative metabolism that play important roles in the modulation of cell survival, cell death, differentiation, cell signaling, and inflammation-related factors production (Dayem et al., 2017). During aerobic respiration and cellular metabolism, oxygen is converted into water and carbon dioxide, respectively, contributing to the production of energy in the form of ATP in cells (Babcock & Wikström, 1992). In these processes, oxygen is partially reduced to reactive radical and non-radical oxygen species. Superoxide is generated by transfer of one electron to O_2 either from the electron transport chain or by NADPH oxidase enzymes. Superoxide is known to damage the iron–sulfur clusters of proteins (Fe–S) by causing the release of Fe(II) into the extracellular matrix (Fridovich, 1983; Imlay, 2013). Superoxide species undergo dismutation to hydrogen peroxide that is reactive towards a variety of functional groups in biomolecules; for example, the thiols of the cysteine-containing proteins are oxidized to form sulfenic acids. Thus, disulfide bonds formed by oxidation of thiols in proteins, peptides, and glutathione are found during reaction with ROS or in the process of attenuating them (Winterbourn, 2008). The major ubiquitous disulfide reductase system responsible for maintaining proteins in their reduced state is the thioredoxin reductase/thioredoxin system (Figure 1.10) (Dharmaraja, 2017). This system is responsible for the reduction of disulfide bonds in target proteins under physiological conditions. It is widely distributed in almost all types of cells and constitutes one of the main antioxidant systems (Balsera & Buchanan, 2019). It is composed of a reduced substrate, a

thioredoxin reductase (TrxR), and a thioredoxin (Trx). Trxs are highly conserved proteins that contain an invariant WCGPC motif with the two Cys forming a redox-active intramolecular disulfide bridge (Eklund et al., 1991). TrxR catalyzes the reduction of the disulfide bond of Trx using electrons derived from a reduced substrate, which can usually be in the form of NAD(P)H or ferredoxin (Fdx) (Arnér & Holmgren, 2000). Thus, Trx reduces a disulfide in selected proteins via dithiol-disulfide exchange reactions, modulating the activity and/or structure of the targets and, accordingly, numerous cellular specific pathways (Figure 1.10) (Cheng et al., 2011; Lu & Holmgren, 2014).

Based on their active sites TrxR enzymes can be divided into two groups which are not phylogenetically related:

- Ferredoxin-thioredoxin reductases (FTR), which are well-characterized Fe-S enzymes in oxygenic photosynthetic organisms and catalyze the transfer of reducing equivalents from photochemically reduced Fdx to Trx (Dai et al., 2000).
- Flavin-thioredoxin reductases, which comprise a diverse group of enzymes, with the most prominent members being NADPH-thioredoxin reductases (NTR) that receive reducing equivalents from NADPH (Arscott et al., 1997;Williams et al., 2000). Other members include Fdx-flavin-thioredoxin reductase (FFTR, formerly known as DTR) originally described in fermentative bacteria (Hammel et al., 1983), and deazaflavin-dependent thioredoxin reductase found in methanogenic archaea (Susanti et al., 2016). These three types of enzymes (NTR, FFTR, and deazaflavin thioredoxin reductase) form a homologous group of enzymes that connect metabolism, fermentation, and methanogenesis, respectively, with the reduction of Trx targets as needed by the cell (OR that the cell requires).

Some cyanobacteria, as in the thylakoid-less *Gloeobacter* genus and the ocean-dwelling green oxyphotobacterium *Prochlorococcus* genus, lack NTR and FTR but contain a TrxR flavoenzyme (formerly named as deeplyrooted thioredoxin reductase or DTR) (Buey et al., 2017). Recent studies have shown that some Fdx might reduce these enzymes and have reported the crystallographic structure of the transient complex between the plant-type Fdx1 and TrxR from *Gloeobacter violaceus*. All these data suggest that this cyanobacterial enzyme belongs to the Fdx-flavin-thioredoxin reductase (FFTR) family, originally described in the anaerobic bacterium *Clostridium pasteurianum* (Buey et al., 2018; Hammel et al., 1983). Accordingly, the enzyme termed DTR was renamed as FFTR (Buey et al., 2021).

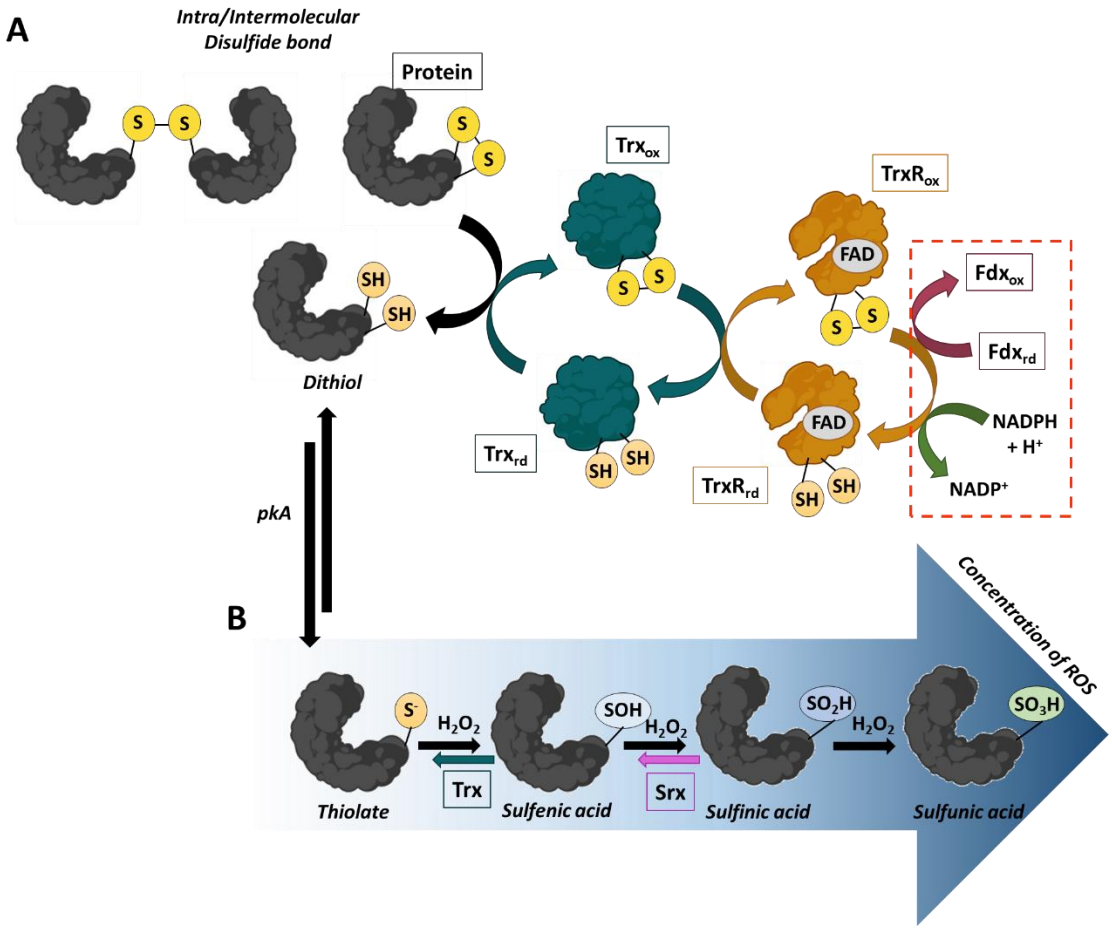

Figure 1.10. General representation of a TrxR/Trx systems. (A) Thioredoxin reductases (TrxRs, orange) reduce Trxs (in blue), which in turn, reduce target proteins via a dithiol/disulfide exchange reaction. The system may be dependent on either NADPH or Fdx (in red dash box) as primary electron donor to the FAD cofactor of TrxR. **(B)** As a result of an increased concentration of ROS (peroxides), cysteine thiol/thiolate (SH/S^-) groups of a protein are oxidized yielding sulfenic acid (SOH), which can then react either with another thiol to form intra- or inter-molecular disulfide bonds (S–S), or to suffer a second oxidation to sulfonic acid (SO_2H) by sulferredoxin (Srx) (pink arrow). Any furher oxidation to sulfonic acid (SO_3H) is generally irreversible *in vivo*.

2. Objectives

2. OBJECTIVES

This Doctoral thesis aims to contribute to our understanding of species-specific action mechanisms of enzymes and, particularly, flavoenzymes as part of complex metabolic networks. The aimed to characterize the flavoprotein content of one pathogenic bacterium, choosing *Brucella ovis* as a model, and in particular its flavoenzyme-dependent system that is involved in the PG biosynthesis. In addition, this study also aimed to better understand the catalytic mechanism of FFTR of *Gloeobacter violaceus*. Understanding the variability and versatility of all these studied flavoenzymes dependent systems is a first step to broaden their potential biotechnological and therapeutic applicability.

In summary, the following specific objectives were established for this PhD Thesis:

1. To describe the flavoproteome content of the pathogenic bacteria *B. ovis*, and to identify and investigate those flavoprotein candidates as being targets in the search for antimicrobials and/or new biotechnological tools.
2. To overproduce, and functionally and structurally characterize the enzymes involved in the three initial cytoplasmic steps of the PG biosynthesis in *B. ovis:* MurA, MurB and MurC.
3. To understand how FFTR from *G. violaceus* works in the ET with its potential Fdx1 donor, comparing its wild type state to FFTR mutants at the Fdx1 binding site and sulfhydryl reducing motif. This will give us insight into its mechanism of action.

3. Materials & Methods

3. MATERIALS AND METHODS

3.1 Biological Material

3.1.1 The enzymes of *B. ovis* involved in the PG biosynthesis

Genes encoding for the UDP-N-acetylglucosamine enolpyruvyl transferase (BoHTMurA) (BOV_RS01375), the UDP-N-acetylglucosamine-enolpyruvate reductase (BoHTMurB) (BOV_RS06850), and the UDP-N-acetylmuramoyl:L-alanine ligase (BoHTMurC) (BOV_RS06855) from *B. ovis* were synthetized with an 70bp elongation at 5´end that encoded for a 6-His tagged tail, the PreScission protease cleavage site, and a NdeI restriction site. These sequences were codon optimized for expression in *E. coli* and then cloned between NcoI/BamHI sites of the plasmid pET28a(+) (Figure 3.1) (GenScript). The BOV_RS06850 gene was also cloned between NcoI/BamHI sites without the 70 bp sequence and therefore lacking the 6-His tagged tail (BoMurB).

3.1.2 Bacteria strains

The *E. coli* bacterial strains used in this work to maintain and amplify plasmid DNAs, as well as to overexpress the products encoded by the corresponding genes cloned in pET-28a(+) are described in Table 3.1.

Table 3.1. Characteristics of basic *E. coli* strains used in this work.

Strain	Genotype	Applications	Proteins	Supplier
BL21 (DE3)	B F- *fhuA2 ompT gal dcm lon hsdSB (rB-mB-) gal* [*mal*B+]K-12(λS) λ(DE3 [*lac*I *lacUV5-T7 gene1 ind1 sam7 nin5*])	Sobreexpression of recombinant proteins	BoMurB	Invitrogen
C41(DE3)	derives from the BL21 (DE3) strain, F – *omp*T *hsdSB (rB-mB-) gal dcm* (DE3)		BoHTMurA BoHTMurB BoHTMurC	
DH5α	F-ϕ80*lacZ*ΔM15 Δ(*lacZ*YA-argF) U169 *rec*A1 *end*A1 *hsd*R17 (rK-, mK+) *pho*A *sup*E44 λ- *thi*-1 *gyr*A96 *rel*A1	Conserved plasmids	All constructions	

3.1.3 Proteins of *Gloeobacter violaceus*

FFTR_WT, FFTR_Δtail, FFTR_W315A, FFTR_C135S and Fdx1 from *G. violaceus* were provided by PhD. Mónica Balsera from the Instituto de Recursos Naturales y Agrobiología de Salamanca (IRNASA-CSIC), Spain (Buey et al., 2021).

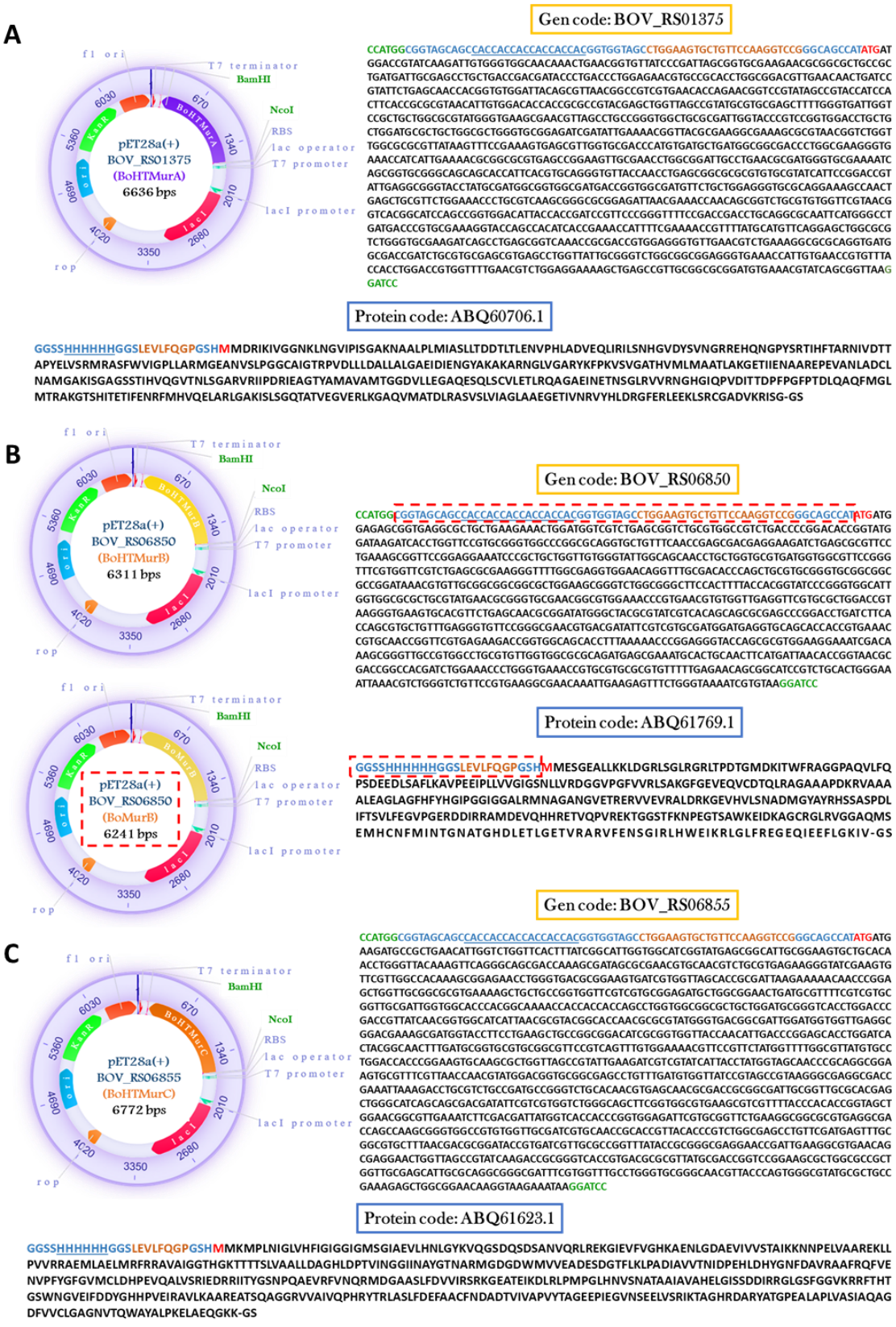

Figure 3.1. Mur genes cloned in the pET28a(+) plasmid. (A) Construct of BOV_RS01375 for BoHTMurA. **(B)** construct of BOV_RS06850 for BoHTMurB and BoMurB (without the sequence in red dashed box). **(C)** Construct of BOV_RS06855 for BoHTMurC. Sequences of NcoI/BamHI sites are shown in green at 5'and 3'ends, respectively, the NdeI restriction site and the sequence encoding the 6-His tagged are in blue, the PreScission protease cleavage site is in orange, protein sequence is in bold black and the initial codon for Methionine is in red.

3.2 Molecular biology techniques

3.2.1 Competent Cells

A single colony of *E. coli* (BL21(DE3), C41(DE3) or DH5α) from LB agar plates was grown in 10 mL of Luria–Bertani (LB) medium (10 g/L NaCl, 10 g/L tryptone, 5 g/L yeast extract), without antibiotic, at 37 °C overnight under constant shaking at 180 r.p.m. Next day, 5 mL of culture were transferred to 200 mL of LB medium and grown under the same conditions until the exponential phase was reached (optical density at 600 nm between 0.3 and 0.5). Growth was stopped by incubating the culture on ice for 20 min. Cells were transferred to pre-chilled falcon tubes and centrifuged for 10 min at 2,500 g at 4 °C. The cell pellet was re-suspended in 1 mL of pre-chilled grinding buffer (100 mM $CaCl_2$, 70 mM $MgCl_2$, 40 mM NaAc, pH 5.5) and shaken gently, subsequently adding 19 mL of the same buffer. Sample was then centrifuged for 10 min at 1,800 g at 4 ºC, removing the supernatant. The cells in the pellet were re-suspended in 4 mL of pre-chilled storage buffer (100 mM $CaCl_2$, glycerol 15%). Competent cells were pooled in 200 µL aliquots, immediately frozen under liquid nitrogen and stored at -80 ºC until use.

3.2.2 Transformation

Transformation of *E. coli* strains with the generated constructs, was carried out by heat shock at 42 ºC. Competent cells were slowly thawed upon incubation on ice for ~20 min. 1 µL of purified plasmid DNA (40-100 ng), and appropriate negative and positive controls (sterile mili-Q water and empty plasmid pET28a(+), respectively), was added to 100 µL of competent cells, and the mixture was kept on ice for 15 min. Then, cells were subjected to heat shock at 42 °C for 50 s in a dry bath, followed by 2 min on ice. 900 µL of LB medium without antibiotic were added to the transformed cells, and incubated at 37 °C and 180 r.p.m. for 1:30 h. Each transformation was then seeded on two 30 µg/mL kanamycin LB agar plates: one with 100 µL, and another with the remaining 900 µL previously centrifuged and re-suspended in a minimum volume. Plates were incubated at 37 °C overnight. Glycerol stocks were made up by combining 900 µL of culture grown from positive transformants with 100 µL of glycerol. Glycerol stocks were then stored at -80 °C.

3.2.3 Purification of plasmidic DNA and restriction endonuclease digestion

To assess the cell transformation process, plasmidic DNA was extracted using the alkaline lysis method for low number copy of plasmids (Birnboim & Doly, 1979). Cells were cultured in 25 mL of LB with antibiotic at 37 ºC overnight. Next day, 5 mL of the culture were centrifuged at 11,300 g for 3 min in 1 mL eppendorf tubes. The supernatant was discarded and

300 µL of cold P1 solution (50 mM Tris/HCl pH 8.0, 10 mM EDTA, 4 mg/mL lysozyme) were added to re-suspend the pellet. Then, 400 µL of P2 solution (200 mM NaOH, 1% sodium dodecyl sulfate (SDS)) were added and mixed at room temperature by gently inversion. 350 µL of cold P3 solution (3 M potassium acetate) were mixed at the same way, observing the appearance of a white precipitate, and incubated for 10 min on ice. After centrifugation at 11,300 g for 15 min at 4 ºC, the supernatant was taken and transferred to another eppendorf tube. It was washed with 200 µL phenol and 200 µL chloroform-isoamyl alcohol and centrifuged 8 min at 11,300 g. Two phases were formed. The aqueous one was selected and treated twice with chloroform-isoamyl alcohol. After centrifuging at 11,300 g 8 min again, the aqueous phase was transferred to an eppendorf tube adding 0.7 vol of 2-propanol, mixing gently. After 10 min at room temperature, the mixture was centrifuged at 16,300 g for 20 min and the supernatant was discarded. The pellet was washed with 1 mL of cold ethanol (70%) three times. Traces of ethanol were carefully removed and DNA was let to dry with the eppendorf tube open. Precipitated DNA was then re-suspended in 50 µL of water (mili-Q with 1:100 RNseA) and incubated at 37 ºC for 30 min. The procedure for double digestions with restriction endonucleases (NcoI-BamHI) followed the protocols provided by New England BioLabs$_{Inc}$. In a 50 µL reaction, 1 µg of DNA, 5 µL of NEBuffer r3.1 buffer (10X), 1 µL (10 U) of NcoI, 1 µL (20 U) of BamHI, and 50 µL of nuclease-free water were combined. The mixture was incubated at 37 °C for 5-15 min. After the specified incubation time, the reaction was terminated by incubating the mixture at 80 °C for 20 min.

3.2.4 Agarose gel electrophoresis

The results of DNA extraction or restriction enzyme digestion were verified by electrophoresis. Agarose gels (0.8-1.5%) were used in 1x TAE buffer (comprising 4.8 g Tris base, 1 mL acetic acid, and 2 mL of 500 mM EDTA in 1000 mL water), supplemented with 20 µL of a 0.025% ethidium bromide solution for every 100 mL of gel. Electrophoresis was conducted at a consistent voltage (60-110 V) and separation time (60-100 min). The size of DNA fragments was gauged by comparing signals to the GeneRuler™ Plus DNA Ladder (Thermo Fisher). Subsequently, the gels were illuminated under UV light to visualize the results.

3.3 Production and purification of recombinant proteins

All working buffers used during protein purifications are listed in table 3.2.:

Table 3.2. Working Buffers for protein extraction and purification.

Buffer Type	Composition	Enzymes Purification
Buffer A	50 mM Bis-Tris Propane, pH 7.6, 250 mM KCl, 1 mM DTT and 10 mM imidazole	BoHTMurA BoHTMurB BoHTMurC
Buffer B	50 mM Bis-Tris Propane, pH 8.0, 100 mM KCl and 1 mM DTT	
Lysis Buffer	50 mM Tris/HCl, pH 8.0, 0.5 mM DTT and 0.3 mg/mL lysozyme	BoMurB
Buffer C	50 mM Tris/HCl, pH 8.0, 0.5 mM DTT	
Buffer D	50 mM Tris/HCl pH 8.0, 0.5 mM DTT and 30% $(NH_4)_2SO_4$	
Buffer E	50 mM Tris/HCl pH 8.0, 100 mM KCl, 0.5 mM DTT	

Equipment used were: Centrifuge GYROZEN, High-Speed 2236R with rotors: Fixed Angel, Cat. No. GRF-L-1000-6, with max velocity 7,000 r.p.m. (10,825 g); GRF-L-250-6, 10,000 r.p.m. (17,664 g); GRF-L-50-6, 22,000 r.p.m. (54,111 g). Refrigerated Eppendorf™ Centrifuge 5427 R. ÄKTA™ Pure System and ÄKTA™ UPC 900 System.

3.3.1 Small-scale protein expression and SDS-PAGE

Protein overexpression tests were carried out in 10 mL LB medium to verify the optimal growth and induction conditions, varying the temperature, induction time and/or IPTG concentration. The results were analyzed using SDS-PAGE electrophoresis. For this, 1 mL of medium was centrifuged for 5 min at 12,000 g and the bacterial pellet was then re-suspended in 100 µL of 50 mM Tris/HCl pH 7.6. From this volume 16 µL were taken, to which 4 µL of 5x loading buffer (10% SDS, 5% β-Mercaptoethanol, 30% Glycerol, 250 mM Tris/HCl pH 6.8, and 0.5% bromophenol blue dye) were added, and the mixture was heated at 95 °C for 5 min. In all the analyzed cases for Mur proteins production, the optimal levels of overexpression were achieved with 1 mM IPTG and induction times of 5-12 h adjusting the temperature (18-30 ºC).

3.3.2 Medium-scale protein expression

Cultures for the expression of the *B. ovis* proteins were carried out in LB medium (Figure 3.3). A colony containing the corresponding construct was inoculated into a falcon with 10 mL of LB with kanamycin (30 µg/mL). The growth culture was then transferred to a bottle with 250 mL of LB and kanamycin and incubated for 10 h overnight at 37 ºC and 180 r.p.m. Then, several 2 L Erlenmeyer flasks containing 1 L of LB each and supplemented with kanamycin (30 µg/mL) were inoculated with the overnight culture and incubated under the selected conditions until the optical density at 600 nm reached the optimum value for each protein (0.5-0.6). Expression was induced by adding 1 mM IPTG to each flask. Induction times and temperatures were different depending on the protein; BoHTMurA cultures grew at 20 ºC for 16 h, BoHTMurB and BoMurB at 30 ºC for 5 h and BoHTMurC at 18 ºC for 12 h. Cells

were harvested by centrifugation at 3,500 g for 10 min at 4 ºC, washed with 0.15 M NaCl and stored at -20 ºC.

Cells grown in LB medium containing *B. ovis* protein were resuspended in a volume (2 mL per gram of cell pellet) of either Buffer A or Lysis Buffer (depending on the protein, see Table 3.2) on ice, adding ½ tablet of cOmplete™, EDTA-free protease inhibitor cocktail (Roche). The obtained solution was sonicated (DRH UP200 DR Hielser sonicator) for 10 cycles of 30 s at 80% amplitude each followed by rest periods of 1 min, in an ice bath. The resulting homogenate was centrifuged at 44,800 g for 1 h and 4 °C and the supernatant was collected.

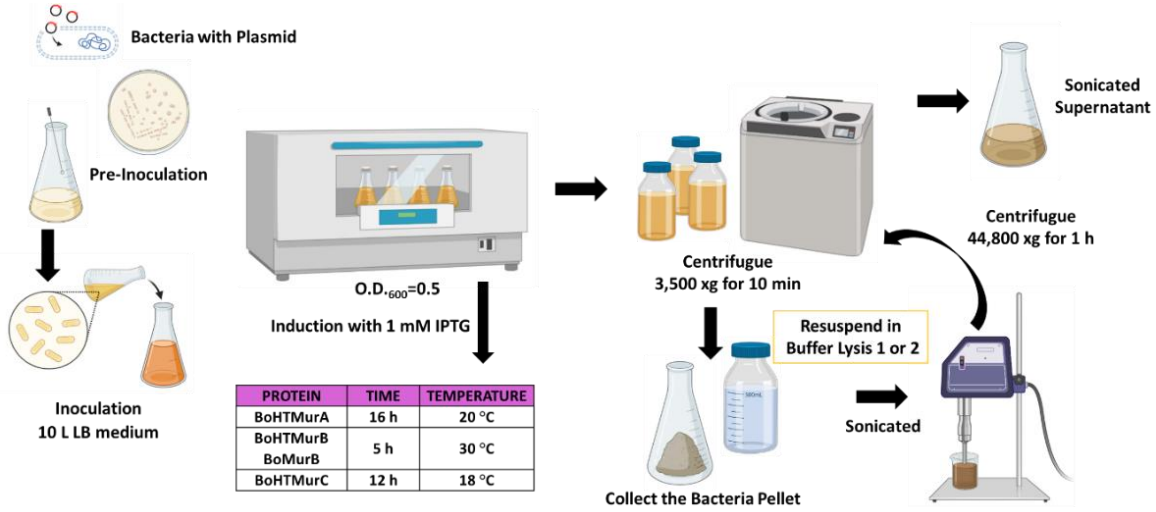

Figure 3.3 Steps for medium-scale protein overexpression and extraction from cell culture.

3.3.3 Purification of recombinant proteins by His-Trap Affinity chromatography

Affinity chromatography was used as the first step for BoMurs purification, using a 5 mL His-Trap Ni^{2+} affinity column (His-Trap™ HP, Cytiva). This column was equilibrated with 3 column volumes (CV), of Buffer A or Lysis Buffer. The crude extract was filtered with CHROMAFIL®Xtra 0.45 µm, then loaded onto it. The column was washed with an additional 3 CV to remove the non-bound proteins and other stuff. Elution of the target protein from the column was achieved with 80 mL of a 10-500 mM gradient of imidazole in Buffer B. Imidazole competes with the His-Tag for binding to the metal-charged resin and thus it is used for elution of the protein from the IMAC column. 3 mL fractions were collected after registering their absorbance at 280 nm on the ÄKTA™ system (Cytiva). Later, its purity and integrity were analyzed by 12% SDS/PAGE. The fractions containing the protein were pooled and concentrated using 10 kDa Merck Amicon™ ultrafiltration devices (Millipore), removing the imidazole by washing with Buffer B.

3.3.4 His_6-Tags Removing

When required, the His_6-tags fused to the N-terminal of recombinant proteins were removed by proteolytic cleavage by using the PreScission protease, which cleaves the polypeptide at the target site incorporated in the construct between the His-tail and the protein sequence. 10 mg of His-tag protein were incubated with 2 mg of protease for 48 h at 4 ºC. The protease and His-tag were eliminated from the mixture by coupling a 5 mL GSTrap™ HP (Cytiva), where the protease binds as it is merged to a Gluthatione S-transferase, with a 5 mL His-Trap Ni^{2+} (Cytiva), which interacts with the free His-tag. Protein without the His_6-tag eluted using Buffer B and was collected in 2 mL fractions.

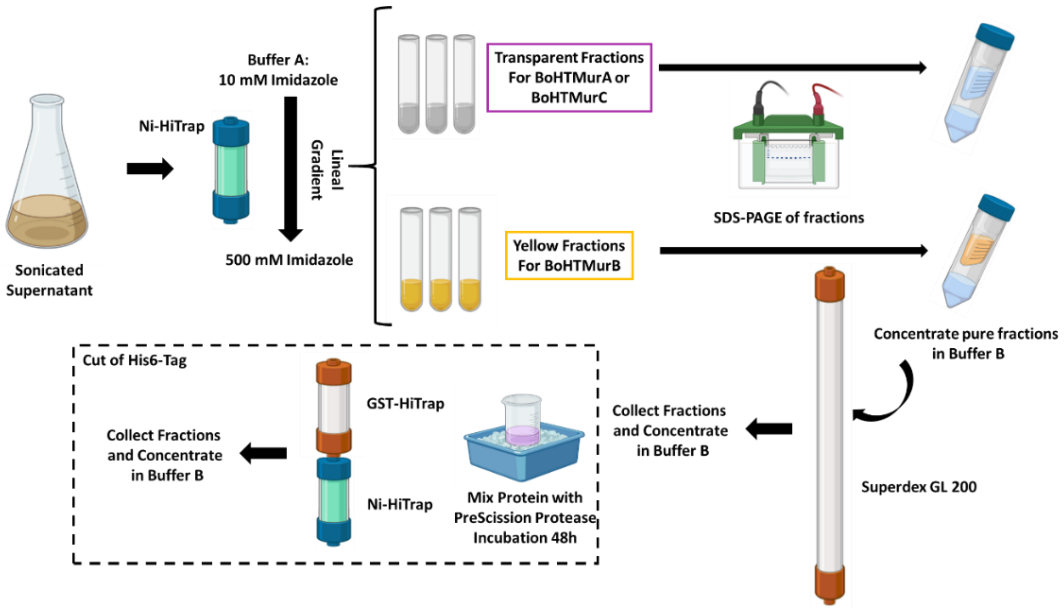

Figure 3.4 Steps for the purification of proteins with a His_6-tag (BoHTMurA, BoHTMurB and BoHTMurC).

3.3.5 BoMurB purification by ammonium sulfate precipitation

Purification of BoMurB without the His_6-tag required a different protocol. After sonication and centrifugation, the supernatant was adjusted to 30% of $(NH_4)_2SO_4$ (Wingfield, 1998), stirred on ice for 1 h, and centrifuged at 44,800 g for 10 min and 4 °C. The supernatant was collected, and the process repeated with 60% and 80% of $(NH_4)_2SO_4$. In the last step, the yellow precipitate was collected and dissolved in Buffer D, loaded onto a DEAE-Sepharose column pre-equilibrated with Buffer D, and eluted with a reverse gradient from 30% to 0% of $(NH_4)_2SO_4$ (Buffer C). The yellow fractions were pooled and dialyzed in Buffer C. Then, the protein was loaded onto a DEAE-Sepharose column, pre-equilibrated with Buffer C, and eluted with a linear gradient from 0 to 500 mM KCl. The new yellow fractions were pooled and dialyzed in Buffer C, and then loaded onto another anionic exchange column, a 5 mL HiTrap™ Q FF (Cytiva), and eluted with a linear gradient from 0 to 500 mM KCl again. Finally, the

fractions were pooled and concentrated on 10 kDa Merck Amicon™ ultrafiltration devices (Millipore) and washed with Buffer E.

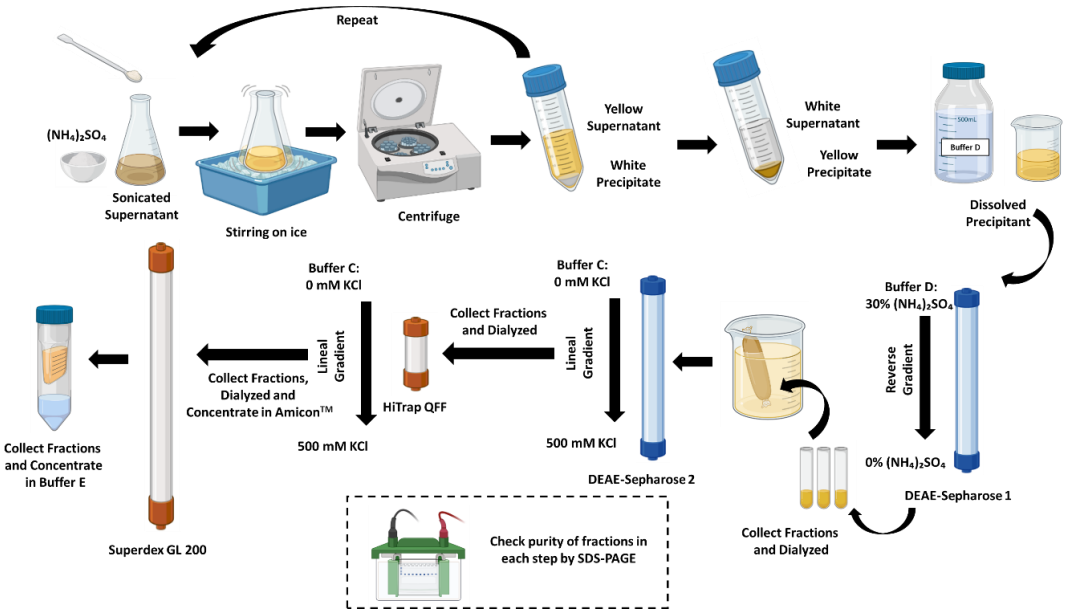

Figure 3.5. Scheme for the steps of purification of BoMurB by precipitation with $(NH_4)_2SO_4$ followed by two consecutive anionic exchange columns. The final step involves a gel fitration chromatography.

3.3.6 Size-exclusion chromatography (SEC)

BoHTMurB and BoMurB were subjected to further purification by SEC using a Superdex 200 10/300 GL column (Cytiva), pre-equilibrated with Buffer B or E (depending on the protein, see Table 3.2). SDS-PAGE was used to assess protein purity. The pure fractions were pooled and concentrated by 10 kDa Merck Amicon™ ultrafiltration devices (Millipore) and stored at -80 °C.

3.3.7 Clear Native PAGE (CN-PAGE)

Once the working proteins were obtained and purified to homogeneity, CN-PAGE gels were run to evaluate potential quaternary organization of native proteins. Proteins were prepared in a non-reducing, non-denaturing sample buffer, which maintained their structure and native charge density. The gel was prepared in the same way as an SDS-PAGE, but did not contain SDS in the recipe. In the same way, the electrophoresis buffer lacked a denaturing agent.

3.3.8 MALDI-TOF

Proteomic analyses were performed in the Proteomics Platform of Servicios Científico Técnicos del CIBA (IACS-Universidad de Zaragoza), a member of ProteoRed ISCIII. Protein identification involves analyzing the peptide fingerprint (MS) and fragmentation spectra (MS/MS) of peptides generated after trypsin digestion. To achieve this, a pure sample of

BoHTMurB in 50 mM Bis-Tris Propane pH 8.0 was denatured in an SDS-PAGE gel. Following staining and destaining, the gel was thoroughly washed with Milli-Q water, and the blue-stained bands were excised. These gel bands were then transferred to an Eppendorf tube containing 100 µL of water. The gel bands were subjected to an automated digestion process (Intavis, Bioanalytical Instruments, Cologne, Germany). Gel pieces were washed sequentially with water, ammonium bicarbonate (100 mM), and acetonitrile (ACN). Subsequently, the samples were reduced by incubation with DTT (10 mM) at 60°C for 45 min and alkylated by incubation with iodoacetamide (50 mM) at room temperature for 30 min in darkness. Eventually, the proteins were digested with trypsin overnight at 37 °C (5 ng/µl, Trypsin Gold, Promega, WI, USA). Digestion was terminated by adding 0.5% trifluoroacetic acid (TFA), and trypsin-digested peptides were sequentially extracted using increasing concentrations of ACN in water. The samples were then evaporated in a concentrator and reconstituted in 2% ACN 0.1% formic acid (FA) solution.

Protein identification was carried out using a hybrid triple quadrupole/linear ion trap mass spectrometer (6500QTRAP+, Sciex, Foster City, CA, USA) coupled with a nano/micro-HPLC (Eksigent LC425, Sciex). Online preconcentration and desalting of samples were performed using a C18 precolumn (Luna® 0.3 mm ID, 20 mm, 5 µm particle size, Phenomenex, CA, USA) at a flow rate of 10 µL/min for 3 min. Peptide separation was accomplished using a C18 column (Luna® 0.3 mm ID, 150 mm, 3 µm particle size, Phenomenex, CA, USA) at a flow rate of 5 µL/min. The column temperature was maintained at 40 °C. The elution gradient ranged from 5% to 30% ACN (0.1% FA) over 30 min.

The mass spectrometer was coupled to an ESI source (Turbo V™) using a 25 µm ID hybrid electrode and operated in positive mode. Source parameters were set as follows: capillary voltage 5000 V, declustering potential 85 V, and curtain and ion source gases (nitrogen) at 15 psi. Analyses were conducted using an information-dependent acquisition method with the following steps: initially, a survey scan of unique and enhanced mass spectra (EMS, 400-1400 m/z) was performed, from which the five most intense peaks underwent enhanced product ion scanning [EPI (MS/MS)]. The MASCOT search engine (MatrixScience, UK) was employed, utilizing publicly available protein sequence databases (Swissprot, NCBI, etc.) according to the taxonomy specified in the request. The search parameters included two missed cleavages, fixed modification of carbamidomethyl (cysteines), and peptide and fragment mass tolerance of 0.5 Da.

3.4 Spectroscopic characterization of proteins

3.4.1. UV-Vis Absorption Spectroscopy

UV-Vis absorption spectrophotometry is a technique that uses a beam of light to assess the light absorption by compounds in a solution at specific wavelengths. Spectrophotometers, which consist of a light source, monochromator, and photometer, measure these spectra. The absorbed energy prompts electrons to transition from ground to excited states. Spectra are generated by tracking light absorption relative to wavelength. Molecules with electrons in delocalized aromatic systems or with metals tend to absorb light in the near UV (250-400 nm) or visible (400-800 nm) range.

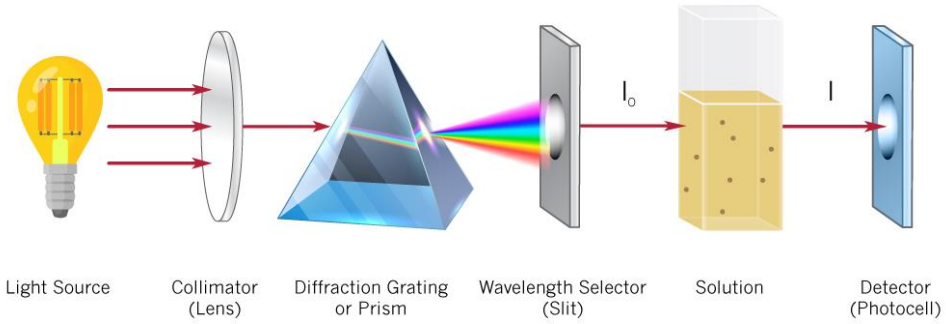

Figure 3.6. Schematic drawing of the optical setup of a monochromatic UV-Vis spectrophotometer. A sample in solution is placed in a cuvette of known dimensions. The light beam from the radiation source passes through a monochromator that selects a specific wavelength. The radiation passes through the sample and the unabsorbed, or transmitted, light is collected by a detector that generates the signal expressed in optical density (absorbance units). The two parameters that characterize a particular band are the position at the maximum (λ_{max}) and its intensity (Figure taken from (https://www.implen.de/uv-vis-spectrophotometer/).

The concentration (c) of any sample in solution can be determined by intrinsic absorbance measurements at a particular wavelength in combination with the Lambert-Beer law,

Eq 3.1. $$A = \varepsilon c l$$

where ε is the molar extinction coefficient at the evaluated wavelength, l is the path length of the cuvette and A the measured absorbance.

Proteins typically exhibit distinct absorption bands in their near-UV spectrum attributed to the presence of aromatic amino acid side chains. While most biomolecules lack visible absorption, certain proteins with prosthetic groups like haem, copper, iron metal clusters, or flavin cofactors such as FAD and FMN, exhibit absorption in the visible range of 400-800 nm. Furthermore, the absorbance ratio at 280/460 nm is used to assess the purity of proteins containing FAD.

3.4.1.1 Determination of molar extinction coefficients

The molar extinction coefficient has units of $M^{-1}cm^{-1}$ and is a proportional constant that relates the absorption of molar solutions. Since the absorbance of a molecule is a function of the wavelength, the extinction coefficient must also refer to each specific wavelength. To quantify the concentration of the protein of interest, without resorting to a colorimetric method (such as Bradford's), determination of ε was determined for each protein.

3.4.1.1.1 Extinction coefficients in the UV region of proteins lacking cofactors. Precipitation with guanidine-HCl method

Tyr, Trp, Phe and Cys side-chains contribute to the protein absorption in the UV region, and therefore to its extinction coefficient. For the samples of BoHTMurA and BoHTMurC, which have no prosthetic group, this method was used to determine their ε in the aromatic band around 280 nm (Pace et al., 1995). The theoretical extinction coefficient of the protein in its unfolded state (ε_{TU}) was estimated using the ProtParam by Expasy tool. A 6 M solution of guanidinium chloride (Gdn HCl) was prepared in the working buffer (50 mM Bis-Tris propane 100 mM KCl, pH 8.0 for BoHTMurA and 50 mM Tris/HCl, 100 mM KCl, pH 8.0 for BoHTMurC). A concentrated solution (5-10 mg/ml) of the protein was prepared and 2 aliquots of 10 µL were taken. The first aliquot was placed in an Eppendorf tube with 990 µL of working buffer and the second in another tube with 990 µL of 6 M Gdn HCl solution. The UV-Vis absorbance spectra of both samples, corresponding to the native and unfolded states of the protein, were measured in a quartz cuvette with an optical path length of 10 mm on a Specord 200 Plus spectrophotometer (Analytikjena) and their absorptions, respectively A_N and A_U, at the corresponding maximum wavelengths were noted. Finally, considering that the two solutions of the protein (native and unfolded) must have the same concentration, equation 3.2 can be applied to determine $\varepsilon_{N(\lambda)}$.

Eq 3.2 $$\frac{A_N}{\varepsilon N(\lambda)} = \frac{A_U}{\varepsilon TU(\lambda)}$$

3.4.1.1.2 Extinction coefficient of the bound Flavin or Extinction coefficients in the visible.

The protocol to calculate the molar extinction coefficient for flavoproteins was described by (Mayhew & Massey, 1969). The spectrum of a flavoprotein solution was recorded by taking the maximum absorbance value in the flavin band I in the Specord 200 Plus spectrophotometer (Analytikjena), using a quartz cuvette with an optical path of 1 cm. The sample was then thermally denatured at 90 °C and kept in the dark. After centrifugation, the spectrum of the supernatant, containing the flavin released from the protein, was measured. Applying the Lambert-Beer law to the BoHTMurB or BoMurB solutions before release of the

FAD cofactor, and to the released FAD, both having the same concentration, the relationship shown in equation. 3.3 allows to determine the extinction coefficient of BoMurB enzymes at the maximum of the band I of its flavin, $\varepsilon_{\text{Band Imax,BoMurB}}$.

$$\textbf{Eq 3.3} \qquad \frac{A_{\lambda Band\ Imax,BoMurB}}{\varepsilon_{Band\ Imax,BoMurB}} = \frac{A_{\lambda Band\ Imax,free\ FAD}}{\varepsilon_{Band\ Imax,free\ FAD}}$$

where A are the absorbances at the band I maximum of free FAD (450 nm) and of the flavoprotein (usually in the 445-465 nm range), $\varepsilon_{\text{Band I,free FAD}}$ is the extinction coefficient of free FAD at the band I maximun (ε_{450} is 11.3 $mM^{-1}cm^{-1}$ (Whitby, 1953)) and $\varepsilon_{\text{Band Imax,BoMurB}}$ is the unknown extinction coefficient of the flavoprotein at its band I maximun.

3.4.1.2 Protein quantification

The absorption spectra in the UV-vis region (250 to 700 nm) of the different Mur enzymes were recorded on either a Specord 200 Plus (Analytikjena) or a CARY 3500 (Agilent Technologies) spectrophotometers, using quartz cuvettes with a light path of 1 cm and with a scanning speed of 0.5 nm min^{-1}. Protein quantification was based on these spectra and the ε values calculated as above indicated.

These molar absorption coefficients were used for the quantification of *G. violaceus* proteins: ε_{458nm}=10.1±1.3 $mM^{-1}cm^{-1}$ for and ε_{450nm}=13.9±1.1 $mM^{-1}cm^{-1}$ for GvFFTR_Δtail, both taken from (Buey et al., 2021), the value for GvFdx1 was taken from that of *Anabaena* Ferredoxin (ε_{423nm} = 9.4 $mM^{-1}cm^{-1}$) (Pueyo & Gómez-Moreno, 1991) and those of GvFFTR_W315A (ε_{453nm} = 13.1 ± 0.7 $mM^{-1}cm^{-1}$ and GvFFTR_C135S (ε_{459nm} = 10.6 ± 0.8 $mM^{-1}cm^{-1}$) were spectrophotometrically determined in this work by thermal denaturation for 10 min at 90°C, followed by centrifugation, separation of the precipitated apoprotein, and spectroscopic quantification of the FAD released as previously described (Macheroux, 1999).

3.4.2 Fluorescence Spectroscopy

Fluorescence spectroscopy, also known as fluorimetry or spectrofluorometry, is a form of electromagnetic spectroscopy used to analyze the fluorescence exhibited by a given sample. This technique utilizes a beam of light, often in the ultraviolet range, to energize the electrons within the molecules of specific compounds, inducing them to emit light, typically within the visible spectrum, though not exclusively so. One key distinction between UV-visible spectroscopy and fluorescence spectroscopy lies in their respective purposes: UV-visible spectroscopy gauges the absorption of light within the UV-visible range, while fluorescence spectroscopy evaluates the light emitted by a sample within the fluorescence range subsequent to the absorption of higher-energy light compared to the energy levels of the emitted photons. The fluorescence spectrum quantifies the intensity of emission across different wavelengths,

which is directly connected to the energy difference between the excited and ground states during the process of photon excitation and emission. In this process, the emitted photons possess lower energy levels, resulting in longer emitted wavelengths (Ladokhin, 2000). The protein UV fluorescence spectra are mainly shaped by Trp and Tyr residues, reflecting environment polarity and interactions within different protein environments (Hellmann & Schneider, 2019). Similarly, flavin cofactor are important fluorophores, which when found within flavoproteins might show their fluorescence often quenched by the environment, enabling active site dynamics studies via their fluorescence changes, and making them relevant fluorescence proves to follow protein conformational changes and unfolding processes.

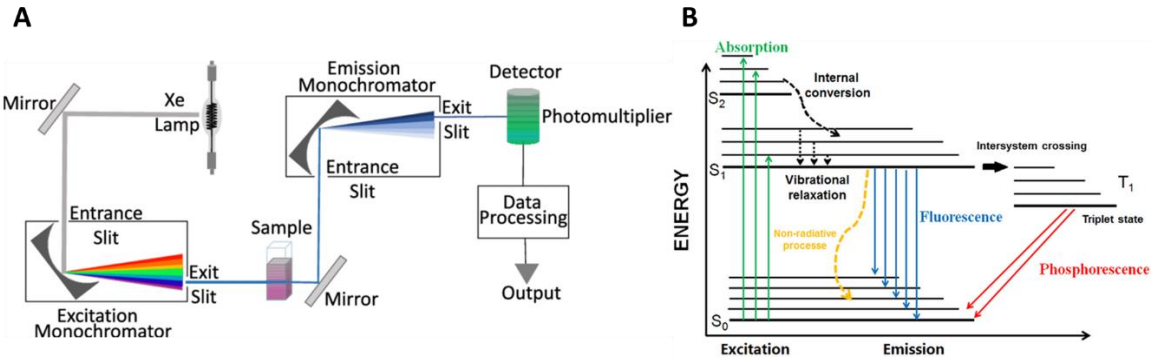

Figure 3.7. (A) Major components of a fluorescence spectrophotometer. The basic instrument includes a light source, two monochromators that select the excitation and emission wavelengths and a detector (Gomes et al., 2019). **(B) Jablonski diagram including vibrational levels for absorbance and fluorescence.** For certain molecules, fluorescence can result from a three-step process. In the first step the light energy of a photon is absorbed; an excited electron state S_2 occurs (excitation). In the excited state, which is limited in time, there are conformational changes in the molecule and a large number of possible interactions with its environment. Due to energy dissipation, the fluorescence energy level S_1 is below the excitation energy level. This energy level can be emptied by further processes, which reduces the quantum yield of the fluorescence radiation. In the third step, the molecule returns to its ground state S_0, releasing photons (emission). S denotes singlet states (spin paired), T denotes triplet states (unpaired spins), thus paramagnetic states. Solid lines represent radiative processes, dashed lines non-radiative processes (Schweizer et al., 2021).

Fluorescence emission spectra of aromatic residues were obtained by scanning from 300 to 400 nm upon sample excitation at 280 nm. The corresponding excitation spectra were obtained between 200 and 300 nm while recording the emission at the maximum of the emission spectra. The flavin emission spectra of BoHTMurB, BoMurB, GvFFTR, GvFFTR_W315A, GvFFTR_Δtail and GvFFTR_C135S, were taken by scanning from 480 to 600 nm upon excitation at 450 nm (FAD absorption maxima). Once the emission maximum was recorded, this value was fixed to collect the excitation spectra between 300-500 nm. Spectra were recorded in a Varian CARY Eclipse fluorimeter (Agilent technologies) with a scanning speed of 5 nm/s, using quartz cells with an optical path length of 1 cm, at 10 °C.

Typical working buffer for protein samples was 10 mM potassium phosphate, pH 8.0, while for BoHTMurA it was 50 mM Bis-Tris propane, 150 mM NaCl, pH 8.0.

3.4.3 Circular Dichroism

Circular Dichroism (CD) is one of the most useful techniques for measuring conformational changes in the secondary and the tertiary structure of proteins that correlate with different processes, such as aggregation, thermal or chemical unfolding, or ligand binding. This technique uses circularly polarized light in which the electric field rotates around the propagation axis at a constant magnitude. Optically active compounds like proteins present differential absorption of those components producing an elliptically polarized light. As a result, the differential spectrum is obtained. As a differential absorption spectroscopy, CD can be interpreted using the Lambert Beer law. CD is usually reported in terms of ellipticity (θ). In the case of proteins, the CD spectra are normalized by the following equations:

$$\textbf{Eq. 3.4} \qquad [\theta](\deg cm^2 dmol^{-1}) = \frac{\theta(\deg)*100}{c(M)*l(cm)}$$

$$\textbf{Eq. 3.5} \qquad [\theta](\deg cm^2 dmol^{-1}) = \frac{\theta*100}{c(M)*l(cm)*(N-1)}$$

where *[θ]* is the mean molar ellipticity in degree cm^2/dmol, *c* is the concentration in molar, *l* is the path length in cm, and *N* is the number of residues of the protein in case the signal comes from multiple chromophores in the sample (as is the case of the peptide bond in proteins).

There are two central regions to study protein signals by CD, the Far-UV and the Near-UV regions. In the first, the amide bonds are the chromophores, whereas in the second, the CD signal comes from the side chains of aromatic residues. In the Far-UV region, the observed bands inform about the secondary structure composition of the studied protein or peptide. For example, the α-helix presents two characteristic negative bands at 208 and 222 nm and a positive one near 193 nm. For the β structure, a broad negative band around 215–225 nm and a significant positive band at 195 nm are usually observed. Specifically, CD in the Far-UV provides information about the secondary structure of proteins. On its side, the Near-UV/Vis region, mainly contributed by Trp residues as well as cofactors, as flavins, in an asymmetrical environment, informs about the tertiary structure being present and changes in its conformation.

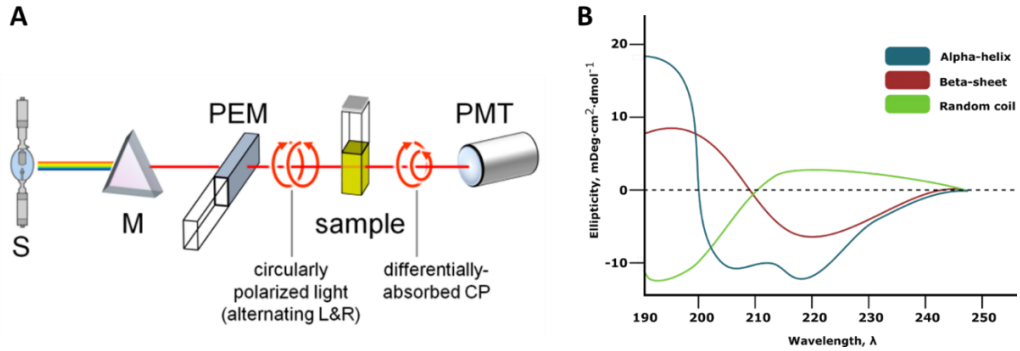

Figure 3.8. CD as a tool for the study of protein secondary and tertiary structure. **(A)** Schematic representation of a CD instrument configuration (Figure taken from (https://encyclopedia.pub/entry/67). **(B)** Representative Far-UV CD spectra of the characteristic secondary structure motifs detected in proteins and peptides: random-coil (green), α-helix (blue) and β-sheet (red) (Figure credit: Thomas Warwick, https://bitesizebio.com/59809/circular-dichroism-sample-preparation/).

CD spectra were recorded here to evaluate the secondary structure, folding, and thermal stability of different proteins. Spectra were recorded using a Chirascan spectropolarimeter (Applied Photophysics) with constant nitrogen flow at 10 ºC, with steps of 0.5 nm/s and 8 s of measurement time per point. Far-UV CD spectra (200-260 nm) were recorded using a 0.1 cm pathlength cell and 5 µM of each protein, and near-UV CD spectra (260-300 nm for BoHTMurA and BoHTMurC, and 260-700 nm for BoHTMurB and BoMurB) were recorded using a 1 cm path length cell and 20 µM of protein. The working buffer for BoHTMurA was 50 mM Bis-Tris Propane, pH 8.0, while for the other proteins it was 10 mM potassium phosphate, pH 8.0. The corresponding spectrum of the working buffer was subtracted in all cases.

3.5 Characterization of protein conformational stability

3.5.1 Thermal stability shift assay

Measurements of thermal denaturation temperatures were used to assess the stability of the proteins alone and in the presence of substrates. Denaturation curves were followed by changes in fluorescence emission of the aromatic residues for BoHTMurA and the flavin cofactor for BoHTMurB, as well as by changes in Far-UV and Near-UV-Vis CD signals. Curves were recorded from 283.15 to 363.15 K with scan rates of 1 and 1.5 °C/min for CD and fluorescence assays, respectively. Protein concentrations were 5 µM for Far-UV CD assays, and 10 µM for the fluorescence and the Near-UV CD assays. The working buffer was 50 mM Bis-Tris Propane, pH 8.0 for BoHTMurA, and 10 mM potassium phosphate, pH 8.0 for the other proteins. Concentrations of the substrates UNAG and UNAGEP were in 10-fold excess, and that of $NADP^+$ in 20-fold excess.

The individual experimental data sets were globally analyzed as one-transition process (i.e., two-step process, native ↔ unfolded, N ↔ U), two-transition processes (i.e. three-state process, native ↔ intermediate ↔ unfolded, N ↔ I ↔ U) or three-transition processes (i.e. four-state process, native ↔ intermediate1↔ intermediate2 ↔ unfolded, N ↔ I1↔ I2 ↔ U) by applying the following equations:

$$\textbf{Eq. 3.6} \quad S_{obs} = \frac{S_N + m_N T + (S_U + m_U T) e^{-(\Delta G/RT)}}{1 + e^{-(\Delta G/RT)}}$$

$$\textbf{Eq. 3.7} \quad S_{obs} = \frac{S_N + m_N T + (S_I + m_I T)\, e^{-(\Delta G_1/RT)} + (S_U + m_U T) e^{-((\Delta G_1 + \Delta G_2)/RT)}}{1 + e^{-(\Delta G_1/RT)} + e^{-((\Delta G_1 + \Delta G_2)/RT)}}$$

$$\textbf{Eq. 3.8} \quad S_{obs} = \frac{S_N + m_N T + (S_{I1} + m_{I1} T)\, e^{-(\Delta G_1/RT)} + (S_{I2} + m_{I2} T) e^{-((\Delta G_1 + \Delta G_2)/RT)} + (S_U + m_U T) e^{-((\Delta G_1 + \Delta G_2 + \Delta G_3)/RT)}}{1 + e^{-(\Delta G_1/RT)} + e^{-((\Delta G_1 + \Delta G_2)/RT)} + e^{-((\Delta G_1 + \Delta G_2 + \Delta G_3)/RT)}}$$

where S_{obs} is the measured protein signal at a given temperature (T), S_N, S_{I1}, S_{I2}, and S_U are the signals (origin intercept) of native, intermediate1, intermediate2 and unfolded protein conformations at 0 K, respectively and m_N, m_{I1}, m_{I2}, and m_U are the slopes of the linear temperature dependence of those signals, respectively. On the other hand, the free energy difference in Eq. 3.6, 3.7 or 3.8 follows,

$$\textbf{Eq. 3.9} \quad \Delta G_i = \Delta H_i \left(1 - \frac{1}{T_{mi}}\right) + \Delta C_{Pi} \left(T - T_{mi} - T \ln \frac{T}{T_{mi}}\right)$$

where ΔH_i is the Van't Hoff enthalpy for each unfolding transition, T_{mi} is the midtransition temperature for each unfolding transition, ΔC_{Pi} is the heat capacity change for each unfolding transition, and R is the ideal gas constant (8.314 $Jmol^{-1}K^{-1}$).

3.5.2 Differential Scanning Calorimetry (DSC)

Differential Scanning Calorimetry (DSC) is used to characterize the stability of proteins, or other biomolecules, by measuring the heat change associated with the molecule's thermal denaturation when heating at a constant rate. DSC measurement of 20 µM BoHTMurC in 50 mM Bis-Tris Propane, 100 mM KCl, 1 mM DTT, pH 8.0 was performed with a MicroCal PEAQ-DSC high-sensitivity scanner Microcalorimeter (Malvern Panalytical) at a heating rate of 1 ºC/min. The specific heat capacity curves were deconvoluted in integrated functions. The area of integration of the curve corresponds to the calorimetric enthalpy change (ΔH), while its maximum in x axis is the transition temperature (T_m) and in y axis is C_p. With these data, the ΔH Van't Hoff (ΔH_{VH}) is calculated using Eq. 3.10.

$$\textbf{Eq. 3.10} \quad \Delta H_{VH} = \frac{4RT_m^2 \; C_{p\,max}}{\Delta H_{cal}}$$

where T_m is in K (273+T_m), R is 1.9872 cal/mol K, and ΔH_{cal} is the total area. If $\Delta H_{VH}/\Delta H_{cal}$ =1, it corresponds to a single unfolding transition, while values lower than the unity point to the presence of oligomers and indicate more than one transition occurred in the process.

3.6 Methods to work under anaerobic conditions

Some processes involving reduced states of proteins are very sensitive to the presence of molecular oxygen, and they must be performed under strict anaerobic conditions to avoid protein re-oxidation. For stopped-flow (SF) experiments, for photoreductions and for measurement of midpoint reduction potentials, protein samples were tested under anaerobic conditions, performed by successive cycles of air removal (vacuum) and replacement by Argon (Ar) (Figure 3.9 and 3.10).

3.6.1 Glass tonometers and closed cuvettes to work under anaerobic conditions

The glass tonometers and closed cuvettes used in this study are homemade and designed to create anaerobic conditions inside and keep the samples oxygen-free (Figure 3.9). In the cases of glass tonometers, each has two vacuum stopcocks at each end. The upper valve ends in a glass tube of a fixed diameter to be coupled through a butyl rubber tube to the anaerobic train system (Figure 3.10). While the part of the lower end is of a smaller diameter according to the Luer-lock connection in the inlet valves of the SF drive syringes.

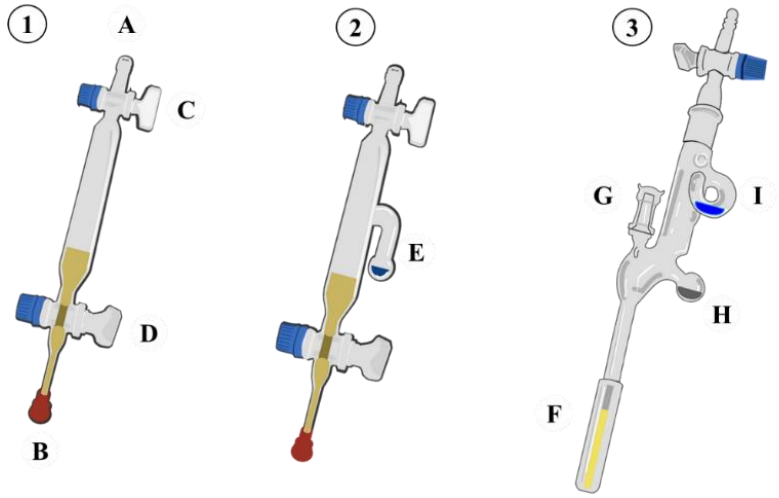

Figure 3.9. Anaerobic containers: 1 and 2 are glass tonometers and 3 is an anaerobic cuvette. **(A)** Glass end to connect through butyl rubber tubing to the Schlenk line. **(B)** Tonometer end cone with the exact dimensions to fit in the female Luer-lock fitting at the entrance valves of the SF drive syringes and to which the Suba-Seal rubber septum will be attached. **(C)** Vacuum stopcock valve to open/close the connection of the tonometer content to the anaerobic system. **(D)** Vacuum stopcock valve to flush sample from the tonometer chamber to the SF system. **(E)**, **(H)** and **(I)** Side-arms to place reagent solutions (shown in blue and grey) separated from the main sample solution (in yellow), in order to mix them after both have been made anaerobic. In general, (I) and (E) will contain a methyl viologen solution as an indicator of anaerobiosis. **(F)** Glass cuvette. **(G)** Capped tube for pouring solutions into the cuvette.

3.6.2 The schlenk line to prepare anaerobic solutions

Schlenk lines are anaerobic glass systems that allow alternate cycles for the evacuation of gases from a liquid sample contained in tonometer or closed cuvette using a vacuum pump, with those of refilling them with oxygen-free Ar/Nitrogen gas. The system consists of a glass

collection column ending at one side in a glass tube connected to a three-way vacuum stopcock (1). This stopcock is used to fill the cylinder with Ar gas at overpressure or to connect it to the vacuum pump that allows the gases to be evacuated from the system. This collector has 5 outlet tubes with stopcocks to connect several tonometers or closed cuvettes at the same time (2). Before reaching the three-way vacuum stopcock, the anaerobic gas from the gas cylinder enters into the system through a pressure regulator outlet (3). The copper tubing coming out from the pressure regulator outlet then fills in the terminal tube (sealed with epoxy resin) of a glass column two/thirds filled with BASF PuriStar® catalyst (R3–11 or R3–11G) used for the removal of oxygen impurities from gases and heated to 110–130 ºC with a heating tape. The Ar leaves this column using a second copper tubing sealed with epoxy to two in tandem 250 mL wash-bottles filled with a methyl viologen solution (1 mM methyl viologen, 10 mM EDTA, and 5 µM 5-deazariboflavin (5-dRf, in a 200 mM Tris/HCl pH 8.0 buffer) and whose exit is fussed by a glass tube to the three-way vacuum stopcock (1) that forms the gateway to the schlenk line system. Thus, the Ar gas reaches the sample free of oxygen.

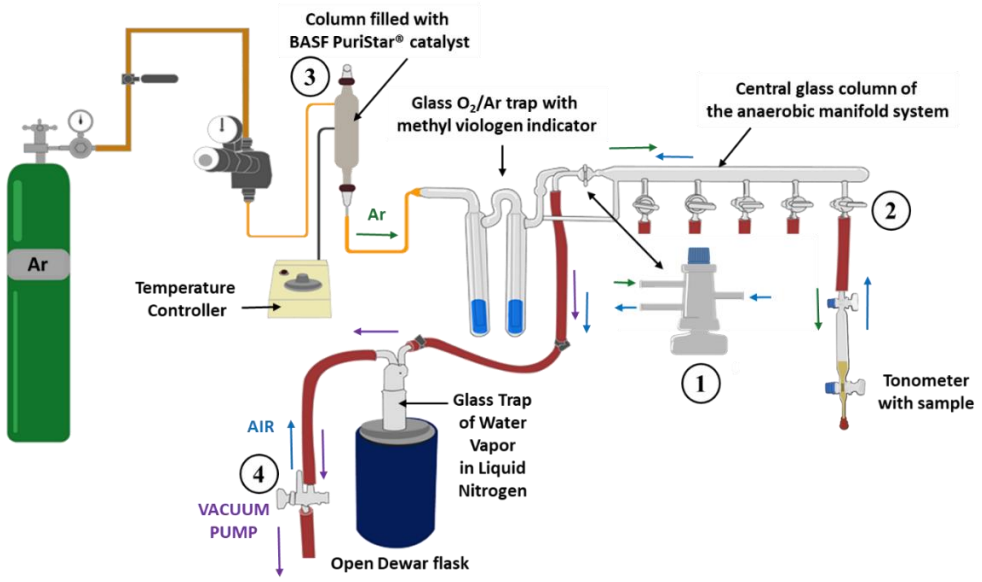

Figure 3.10. Schematic representation of the gas flow and the vacuum line in the schlenk line system. Valves: (1) three-way vacuum stopcock valve connecting either Ar or vacuum to the manifold system, (2) stopcock vacuum valves connecting the anaerobic manifold system to the tonometers through butyl rubber (in red), (3) pressure regulator outlet valve, and (4) three-way vacuum stopcock valve connecting vacuum either to the schlenk line or to the atmospheric air.

The third connection of stopcock valve (1) connects the system to the vacuum pump. The vacuum pump is connected by butyl rubber tube to the stopcock through a cold trap designed with an open Dewar flask with liquid nitrogen that serves to condense water vapor. A second stopcock valve (4) between the vacuum pump and the cold trap, allows the vacuum pump to the air atmosphere when turning it on and off, thus preventing the liquid from the

trapping flask from reaching the pump or the oil from the pump moving towards the schlenk line when vacuum is released (Ferreira & Medina, 2021).

3.7 Steady-state Enzymatic assays

3.7.1 Standard Malachite Green Assay for BoHTMurA Activity.

The bacterial MurA assay is based on the measurement of Pi generated by the MurA reaction. Free Pi can form a complex with the malachite green reagent, which absorbs at 620 nm, changing the solution color from yellow to green (Figure 3.11). The experiment started with 1 vol of 4.2% ammonium molybdate tetrahydrate in 4 N HCl, adding 3 vol of 0.045% malachite Green carbinol hydrochloride, shaking the solution for 30 min, filtering with CHROMAFIL®Xtra 0.45 µm and storing at 4 °C in an amber flask. Tween 20 was added at 0.01% to the reagent prior to use and the solution was stored on ice (Sherwood et al., 2014).

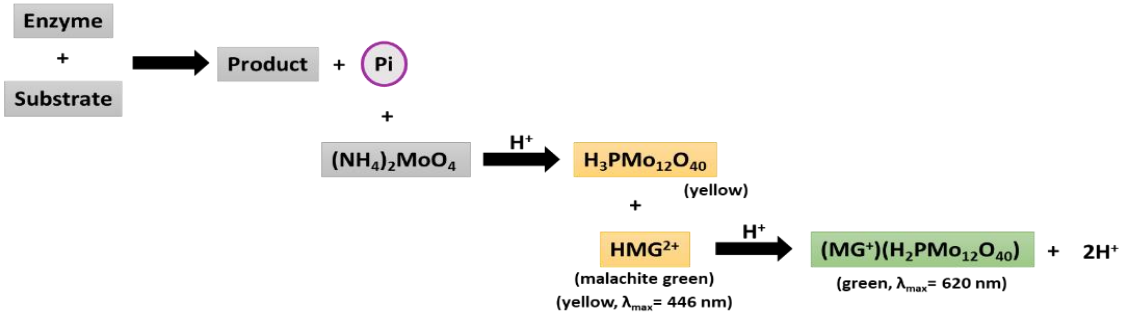

Figure 3.11. Reaction produced by the interaction of Pi and malachite green solution. The green complex formed is detected by absorbance at 640 nm.

The calibration plot was prepared with 100 mM stock of KH_2PO_4 and diluted to make a working stock of 1 mM. The working stock was diluted several times in assay buffer to give a concentration range from 100 µM to 2 µM in a total volume of 1 mL. A sample of 350 µl was taken from each solution and combined with 700 µl of the Malachite Green Reactive-Tween 20. The mixture was allowed to stand for 30 min and the absorbance was measured at 620 nm. The standard solutions were prepared in duplicate. The resulting data were plotted in an Excel shett and the standard calibration curve was generated.

The BoHTMurA activity assay was carried out by pre-incubating the enzyme with 200 µM of the UNAG (Sigma) substrate for 10 min at 37 °C. Then, 200 µM of PEP (Roche) was added to the mixture and the incubation was continued for another 20-40 min (Eniyan et al., 2016). Several buffers and pHs were tested to identify the appropriate assay conditions. (Table 3.3).

In addition, it was evaluated whether the presence of KCl, in the range of 0-100 mM in the reaction mixture increased the production of Pi in 50 mM Bis-Tris Propane pH 7.0 (Chang

et al., 2015; McCoy et al., 2003; Shahab et al., 2014; Xu et al., 2014). When the BoHTMurA reaction finished, a sample containing 350 µL of the reaction mixture was added to 700 µL of the malachite green reagent and the incubation continued for an additional 30 min at room temperature in the dark. The absorbance of the samples was read at 620 nm in conventional plastic cuvettes. Blanks consisted of the whole mix without the enzyme.

Table 3.3. Buffers with their ionic strength and pKa values, used to assay BoHTMurA activity.

Buffer	pH	Ionic strength (mM)	pKa	Apparent pKa
25 mM MES	6.0	12	6.21	6.02
	6.4	17		6.01
	6.8	21		
50 mM MES	6.0	24		5.99
	6.4	35		
	6.8	43		
100 mM MES	6.0	5		5.98
	6.4	75		5.97
	6.8	87		5.96
50 mM HEPES	6.0	NA	NA	NA
	6.4			
	6.8	9	7.66	7.44
25 mM Bis-Tris Propano	7.0	3	6.46	6.24
	7.4	1		
	7.8	NA	NA	NA
50 mM Bis-Tris Propano	7.0	7	6.46	6.26
	7.4	3		6.24
	7.8	NA	NA	NA
50 mM Tris/HCl	7.0			
	7.4	35	8.06	7.8
	7.8	24		7.79

3.7.1.1 Synthesis, purification and analysis of UNAGEP

Reactions for UNAGEP production contained in a total volume of 1 mL of 50 mM Bis-Tris Propane pH 7.0, 200 µM UNAG (Sigma), 200 µM PEP (Roche) and 50 nM of BoHTMurA. The reaction was allowed to stand for 30 min at 37 °C. BoHTMurA was removed using 10 kDa centricon (Amicon). UNAGEP was concentrated by removing the excess of water with a Savant SpeedVac (Thermo Scientific) and quantified by measuring the absorbance at 262 nm using $\varepsilon_{262\ nm}$= 9.8 $mM^{-1}cm^{-1}$ for UDP (Esposito et al., 2018).

3.7.1.2 Reaction product analysis by High Performance Liquid Chromatography (HPLC) and Nuclear Magnetic Resonance (NMR)

Reverse-phase HPLC using an Alliance Waters 2707 autosampler/2996, a photodiode array (PDA) detector (Waters) and a Waters HSST3 C18 column (4.6 x 50 mm, 3.5 mm) preceded by a pre-column (4.6 x 20 mm, 3.5 mm) of the same material, was used to separate and analyze reaction components and products. Samples of 10 µL were injected into the column with 1 mL/min flow rate. Experiments were performed at 25 ºC for 10 min following the

absorbance at 262 nm. Several isocratic mobile phases were analyzed in order to look for the conditions to separate reactants and products (Table 3.4).

Table 3.4. Buffers tested for UNAG and UNAGEP separation by HPLC.

Buffer	pH	Solvent	vol/vol	Reference
5 mM ammonium acetate	6.0	Methanol	1:1	This study
5 mM ammonium acetate	6.0	Methanol	6:4	(Serrano et al., 2012)
50 mM ammonium formate	3.5			(Raymond et al., 2003)
100 mM ammonium acetate	4.7	Methanol	3:7	(Mengin-Lecreulx et al., 1983)
		Methanol	3:2	
50 mM ammonium formate	4.3			(Bouhss et al., 1997)
water		Acetonitrile	85:15	(Montoya-Peleaz et al., 2005)
10 mM ammonium acetate		Acetonitrile	95:5	(Tan et al., 2021)

NMR can allow to identify the structure of organic and organometallic compounds, providing with the stereochemistry of the carbon skeleton as well as with information about other magnetically active nuclei. To verify that the reaction product was UNAGEP, the external NMR service provided of the iSQCH laboratory of the University of Zaragoza was used. Four vials containing the compounds Bis-Tris Propane, PEP, UNAG and UNAGEP at a concentration of ~20 mg/mL in 600 µL of deuterated water were analyzed by recording ^{1}H and ^{13}C NMR spectra.

3.7.2 BoHTMurB and BoMurB Activity

MurB enzymes are described to reduce the enolpyruvate moiety of UNAGEP to a lactyl group to form UNAM by using NADPH as hydride donor. The ability of BoHTMurB and BoMurB to catalyze this reaction was analyzed using a continuous assay monitoring the oxidation and reduction of NADPH and FAD, respectively, following changes in absorbance at 340 and 462 nm in a CARY 3500 spectrophotometer (Agilent Technologies). The following scheme summarizes the conditions chosen for the different experiments performed, starting with (1) several working buffers at a given (2) pH and (3) salt concentration. The first assays were performed only in the presence of (4) NADPH and (5) BoHTMurB/BoMurB in a range from 60 nM to 10 µM final concentration of the protein, at different temperatures and under both aerobic and anaerobic conditions (for assays performed above 32 ºC it was necessary to add 20% glycerol to avoid protein aggregation) (Benson et al., 1993; Sylvester et al., 2001). The same measurements were also repeated in the presence of different concentrations of UNAG/UNAGEP (6) (Anwar & Vlaovic, 1979; Benson et al., 1997; Nishida et al., 2006). Likewise, assays with coupled reactions (7) were carried out starting with BoHTMurA and BoHTMurB and the corresponding substrates (8) in the proportions described in section 3.7.1.1. Finally, BoHTMurC and its substrates (1 mM ATP; 0.2-2 mM L-Ala; 2-20 mM Mg_2Cl)

were also added to the reaction mix (Eniyan et al., 2016; Naqvi et al., 2016). Assays were performed at each purification step, starting with the crude extracts of the bacterium until a solution of the protein is in its purest state.

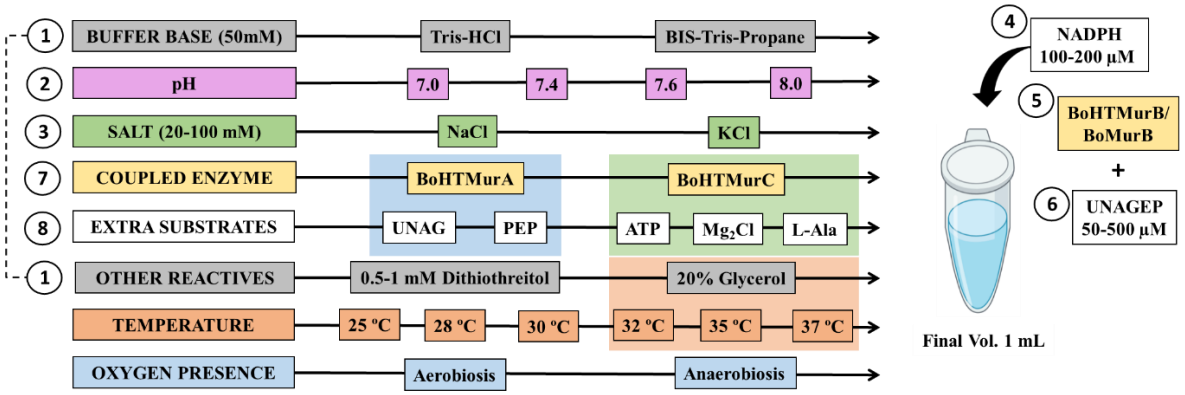

Figure 3.12. Summary of trials performed for evaluating the presence of activity in BoHTMurB and BoMurB.

3.8 Characterization of oxido-reduction processes

3.8.1 Photoreduction

Flavins are thermostable compounds but at the same time are photosensitive. In the absence of an external reductant, the isoalloxazine ring system can undergo photoreduction by light irradiation. Nonetheless, for their photoreduction, a sacrificial electron donor (e.g. typically trimethylamine, ethylenediaminetetraacetate (EDTA) and deprotonated amines) is needed (König et al., 2018). Typically, to assess the photoreduction of flavoproteins, a photo-catalyst such as free 5-dRF is employed, along with a sacrificial electron donor, often EDTA (van Schie et al., 2018).

3.8.1.1 Photoreduction by 5-deazariboflavin

The 5-dRf/EDTA system is used here to reduce flavins by means of controlled lighting. The energy of the electromagnetic radiation is capable of exciting 5-dRf to its triplet state (^{3}5-dRf) (Figure 3.12), which is quenched by EDTA, and in less than 1 µs, the reduced state of a single electron (semiquinone) of 5-dRf (5-dRfH•**)** and one radical specie (EDTA•) are produced. The EDTA• is unstable and undergoes a series of reactions in less than 1 ms, including decarboxylation and fragmentation, generating stable products that do not affect the reaction. The 5-dRfH• can be dismutated to the oxidized (5-dRf) and reduced (5-dRfH_2) states. Alternatively, in the presence of an electron acceptor, such as a flavoprotein, this radical species can also act as an electron donor and transfer its unpaired electron to the oxidized flavin (Flv_{ox}) or to the semiquinone flavin cofactor (Flv_{sq}) (Figure 3.12C).

The photoreduction of GvFFTR_W315A, GvFFTR_C135S and GvFdx1 was evaluated in mixtures containing approximately 20 µM final concentration of protein, 3 mM of EDTA, 4 µM of 5-dRF, 10 mM glucose and 10 UI/mL glucose oxidase in 20 mM Tris/HCl pH 7.6 and 150 mM NaCl. Anaerobic conditions were achieved by several cycles of evacuation and bubbling with O_2-free argon (Ferreira & Medina, 2021). The sample was then illuminated with blue light and spectra were recorded every 5 s using a CARY 3500 spectrophotometer (Agilent Technologies), scanning from 250 to 700 nm with an optical path length of 1 cm.

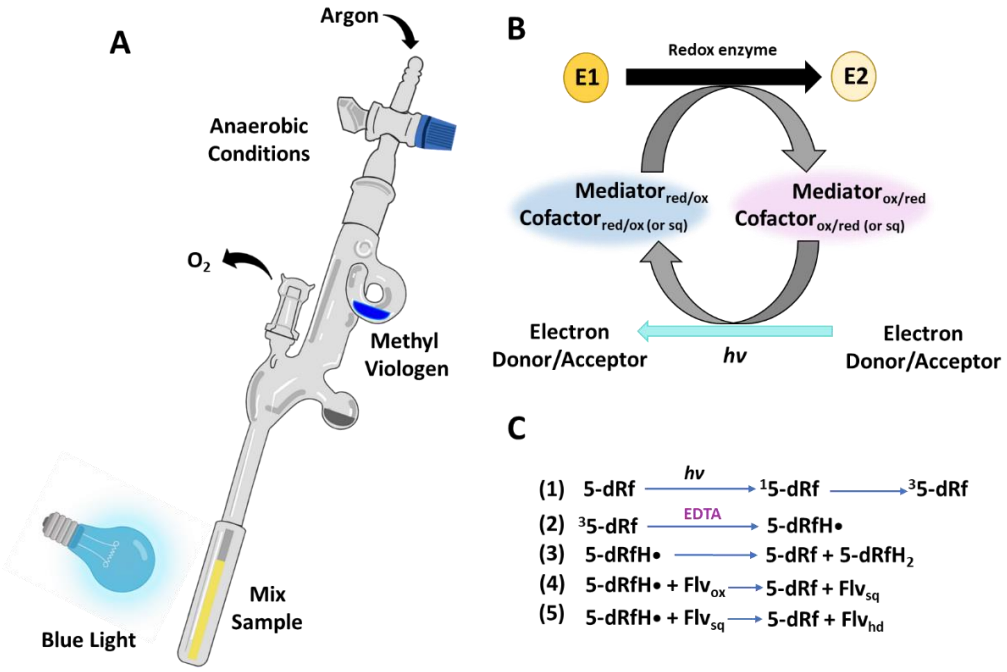

Figure 3.12. Flavoprotein photoreduction set. (A) Central scheme of the photoreduction experiment in a closed cuvette system, with a mix of protein, EDTA and 5-dRF. The cell is illuminated with blue light so that the different flavin-reducing species are produced. Methyl viologen is present to check the anaerobic conditions **(B)** Catalytic cycle of flavin redox reactions. **(C)** Redox steps underwent by 5-dRF upon photoirradiation in the presence of EDTA and either Flv_{ox} or Flv_{sq}.

3.8.1.2 Photoreduction by protonated buffers

Recently, it has been shown that certain buffers, as Bis-Tris Propane, can support photoexcitation of flavoproteins as well as serve as electron donors, without the need for 5-dRF/EDTA. Furthermore, the use of blue light during the process helps prevent photodegradation of reduced flavins and flavoproteins (Duan et al., 2021). Thus, the photoreduction of BoHTMurB and BoMurB was evaluated at around 20 µM final concentration of protein in 50 mM Bis-Tris Propane, 100 mM KCl, 1 mM DTT pH 8.0, 20% glycerol and 50 mM EDTA. Anaerobic conditions were obtained by several cycles of evacuation and bubbling with O_2-free argon in the Schlenk line system (Ferreira & Medina,

2021). The sample was then illuminated with blue light and spectra were recorded every 5 s using a CARY 3500 spectrophotometer (Agilent Technologies) scanning from 250 to 700 nm with an optical path length of 1 cm.

3.8.2 Determination of midpoint reduction potentials

3.8.2.1 Xanthine/Xanthine Oxidase Method

The midpoint reduction potentials (E_m) of BoHTMurB and the different GvFFTR variants were determined by making use of the xanthine/xanthine oxidase (XO) system (Maklashina & Cecchini, 2020). This method provides a slow continuous reduction of an indicator dye and the flavin in the presence of benzyl viologen (BV) or methyl viologen (MV), which ensures the rapid equilibration of reducing equivalents. This allows slow changes in equilibrium of the reduced and oxidized forms of the flavoprotein and dye, until both are completely reduced (Figure 3.13) (Massey, 1991). A series of spectra recorded over the course of the reaction is used to calculate the ratio of the oxidized and reduced forms of flavin and dye (Maklashina & Cecchini, 2020).

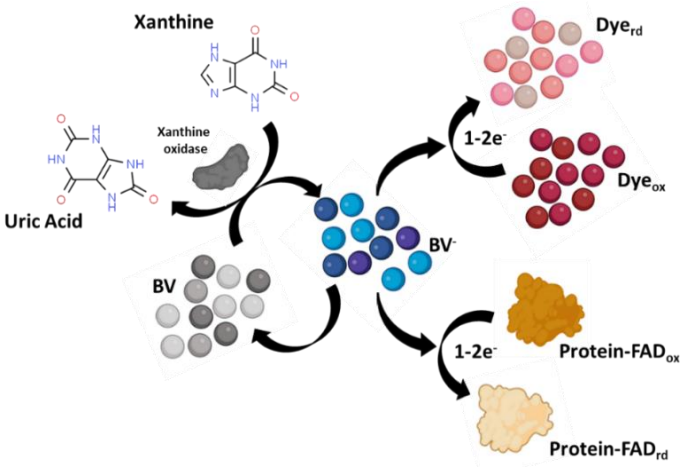

Figure 3.13. The xanthine/XO method. This is a slow continuous reduction of the protein-dye mixture using small amounts of reduced XO while scanning the UV–Vis spectrum at regular time intervals during reduction.

A typical experiment was carried out in a closed anaerobic cuvette with a final concentration around 10 µM of protein, 2 µM benzyl viologen, 500 µM xanthine, 5 µM dye, 10 mM glucose and 10 U/mL glucose oxidase under anaerobic conditions obtained by several cycles of vacuum application and bubbling with O_2 free argon. Then, 7.8 µg/mL of bovine milk XO (Sigma-Aldrich) was added to the mixture. Spectra were recorded every 5 min for up to 2 h, at 25 °C in a CARY 3500 spectrophotometer (Agilent Technologies), scanning from 250 to 700 nm.

For BoHTMurB, the phenosafranine dye (E_m=-252 mV) was chosen, assaying in 50 mM Bis-Tris propane, 100 mM KCl, 1 mM DTT, pH 8.0. For GvFFTR variants, concentration

of xanthine was increased up to 2 mM using the buffer 20 mM Tris/HCl, 150 mM NaCl, pH 8.0. Methyl viologen (E_m=-252 mV) was used as dye at 21 µM for FFTR_WT and FFTR_C135S, whereas for GvFFTR_W315A and GvFFTR_Δtail, phenosafranine (E_m=-252 mV) was the chosen dye.

The difference in E_m potential of the protein and the dye was calculated from a plot where the [oxidized]/[reduced] ratio for sample and dye of each spectrum is plotted against each other. The data were then fitted to the Nernst plot (Efimov et al., 2014). The reduction potentials of the flavin containing protein (P) and dye (D) are determined by their corresponding Nernst equations:

Eq. 3.11 $E_P = E_{m,P} + \frac{RT}{nF} ln\left(\frac{[P_{ox}]}{[P_{rd}]}\right)$ **Eq. 3.12** $E_D = E_{m,D} + \frac{RT}{nF} ln\left(\frac{[D_{ox}]}{[D_{rd}]}\right)$

Slow rates of electron input by XO ensure the equilibrium of the oxidized and reduced forms of the protein and dye at any given time point of the process. Thus, their electrochemical potentials are assumed to be equal:

Eq. 3.13 $E_{m,P} + \frac{RT}{nF} ln\left(\frac{[P_{ox}]}{[P_{rd}]}\right) = E_{m,D} + \frac{RT}{nF} ln\left(\frac{[D_{ox}]}{[D_{rd}]}\right)$

Defining "*x*" as a Nernst concentration term for the protein, and "*y*" as a Nernst concentration term for the dye,

Eq. 3.14 $x = \frac{RT}{nF} ln\left(\frac{[P_{ox}]}{[P_{rd}]}\right)$ **Eq. 3.15** $y = \frac{RT}{nF} ln\left(\frac{[D_{ox}]}{[D_{rd}]}\right)$

Eq. 3.16 $E_{m,P} + x = E_{m,D} + y$

When the protein is in redox equilibrium $[P_{ox}] = [P_{rd}]$, $x = 0$ and y is defined as ΔE, the difference in midpoint potentials of the protein and the dye.

Eq. 3.17 $E_{m,P} = E_{m,D} + \Delta E$

The ratio of [oxidized]/[reduced] for the protein and the dye is determined using the wavelengths designated for each component.

Eq. 3.18 $\frac{[oxidized]}{[reduced]} = \frac{A - A_{min}}{A_{max} - A}$

where A_{max} is the absorbance of the oxidized forms, A_{min} is the absorbance of the reduced forms, and A is the absorbance taken from each intermediate state spectrum. Now using the values of the thermodynamic constants, RT/nF equal to 12.5 when n = 2 and 25 when n=1; (R, the gas constant (8.314 $Jmol^{-1}K^{-1}$); T, the temperature in Kelvin; F, Faraday's constant (96,485 $Jmol^{-1}V^{-1}$); n, number of electrons for FAD and the dye reduction (1 or 2)), the final equations for x and y can be written as:

Eq. 3.19 $x = \frac{25}{n} * ln\left(\frac{A - A_{min}}{A_{max} - A}\right)$ **Eq. 3.20** $y = \frac{25}{n} * ln\left(\frac{A - A_{min}}{A_{max} - A}\right)$

The values of x (Eq. 3.19) and y (Eq. 3.20) were then plotted on a graph to later adjust it to the equation of the line with a slope of one and an intercept equal to y, or ΔE, a shift in the midpoint potentials between the protein FAD and the dye. Finally, the intercept value was added to or subtracted from the dye value.

3.8.2.2 Cyclic Voltammetry

Cyclic voltammetry (CVol) tests were performed by Prof. Sheila Sadeghi at the Department of Life Sciences and Systems Biology, Università Di Torino, using an Autolab PGSTAT12 potentiostat controlled by the GPES3 software (Ecochemie, The Netherlands). The glass electrochemical cell with a total volume of 1 mL was equipped with a platinum wire counter electrode, an Ag/AgCl (3 M NaCl, E_m= +220 mV) reference electrode and a 3 mm diameter glassy carbon working electrode (BASi, USA). The glassy carbon electrode was modified with a mixture of the protein and poly (diallyldimethylammonium chloride) polymer (PDDA) as follows: 5 µL of PDDA was mixed with 5 µL of BoHTMurB (147 µM) and drop coated onto the electrode (Dodhia et al., 2008). The modified bioelectrode was stored overnight at 4 °C. CVol of BoHTMurB protein was carried out at 25 °C under anaerobic conditions using a glove box with nitrogen saturated atmosphere (Belle Technologies, UK). CVol was performed by applying a potential between 0 and -700 mV at a scan rate of 120 mV/sec. A control experiment was carried out in the absence of the protein. The supporting electrolyte was 50 mM phosphate buffer pH 7.4 containing 100 mM KCl.

3.8.3 Stopped-flow kinetic measurements

SF is a spectroscopic technique used, among others, to study the kinetics and mechanisms of fast chemical reactions in solution. The instrument (Figure 3.14) is a rapid mixing device in which two solutions are quickly injected into a mixing chamber from two independent drive syringes. The mixed solution rapidly fills the optical observation cell displacing the previous contents with freshly mixed reactants. The system is typically controlled by a computer and the corresponding software, and it is usually coupled to either single wavelength absorption/fluorescence detectors or to a PDA detector. The PDA detector enables to record multiple-wavelength time-resolved measurements from a single SF drive.

In general, this instrument is used to follow fast reactions occurring on the milisecond to second time scale, but longer time measurements are also possible. At the beginning of the experiment, four tonometers were prepared. The first pair contained highly concentrated sodium dithionite solutions, while the second pair contained a working buffer solution Anaerobic conditions were generated for both solutions by several cycles of evacuation and bubbling with the O_2-free Ar using the system of the figure 3.10.

Tonometers with sodium dithionite were connected to the SF drive syringe at the loading position. The syringes were filled with the tonometer solution by slowly pulling down the bottom piston. Several shots were made to clean the system with anaerobic dithionite solution. These were then replaced with tonometers containing anaerobic working buffer and the procedure was repeated. The measurements with the working buffer were used to establish the baseline in the whole-absorption range allowed by the PDA detector. The data were saved and checked for stability over the selected measurement times. When the system was ready, the working tonometers were prepared with the required samples.

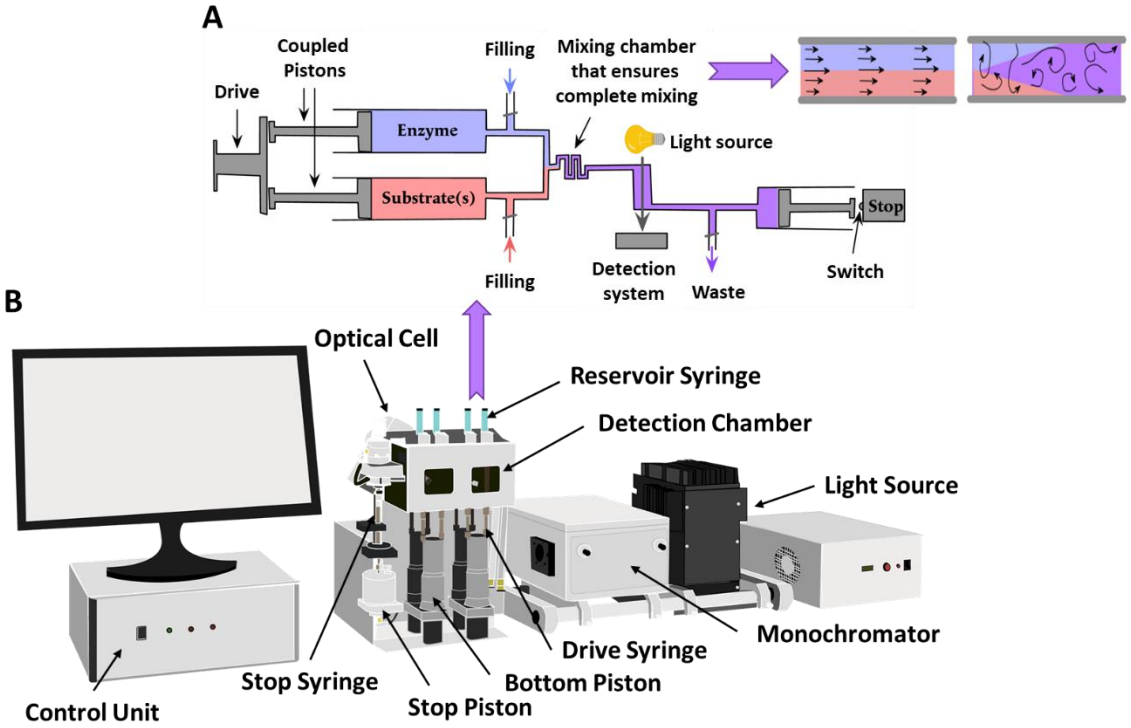

Figure 3.14. Components of Applied Photophysics stopped-flow instrument. PDA or single-wavelength absorption detectors are situated in line with the excitation lamp, while the fluorescence detector is placed perpendicular to the excitation lamp. The measurement starts when an impulse of the stop syringe piston by compressed air empties a fixed volume from this syringe to the waste. The stop valve quickly moves to connect the observation chamber with the stop-syringe while the drive syringes piston is pushed by compressed air. This makes the two drive syringes to release the same volume that was emptied to the waste in the stop syringe. Thus, flow from the drive syringes mixes in the mixing chamber, filling up the pipeline to the observation chamber, and displacing the older solution towards the stop-syringe. When this syringe fills in, its plunger moves back and triggers data acquisition in the observation cell. As both solutions mix in the mixing chamber, reaction starts and it is followed in the observation cell using the adequate detector coupled to the computer.

For the reduction of BoHTMurB by sodium dithionite, one tonometer contained the BoHTMurB sample (10 µM) and the second contained sodium dithionite (300 µM) in working buffer, 50 mM BIS-Tris Propane, 100 mM KCl, 1 mM DTT pH 8.0 at 25 ºC. After anaerobic cycles, the tonometers were connected to the SF syringes. Previously, the valve of the first syringe was opened and the content emptied by pushing the piston up to transfer the volume

back into the tonometer containing buffer. The valve was closed and the tonometer with anaerobic BoHTMurB connected, the valve was opened and the syringe loaded with the protein solution. The second drive syringe was reloaded with, and then the trigger system was activated to start a cycle by mixing the solutions and the PDA detector collected full-range absorption data for the indicated measurement time (collection of 100-400 spectra in 0.1-1 s). This provided a set of spectra along the reaction time, which were identical, as no reaction is expected to occur, and the initial spectrum of $BoHTMurB_{ox}$ was depicted. Subsequently, the buffer in the second drive syringe was replaced with the solution of the reducing agent. In the mixing chamber, 200 µL of each solution were combined per intervals from 0.1 to 2 s. For the photoreduction of BoHTMurB by SF, an anaerobic solution of protein BoHTMurB (20 µM) was prepared in 50 mM Bis-Tris Propane, 100 mM KCl, 1 mM DTT pH 8.0, 20% glycerol and 50 mM EDTA (tonometer 1) was mixed with anaerobic buffer (tonometer 2). In the reaction chamber, the mixture was exposed to lamp light (150 W xenon) for long periods of time (up to 8000 s), resulting in photoreduction of the FAD.

Potential electron transfer from reduced GvFdx1 to several oxidized GvFFTR variants was assayed in 20 mM Tris/HCl, 150 mM NaCl, pH 8.0, at 25 °C by SF. The first tonometer was prepared with the anaerobic flavoprotein. The second tonometer, containing anaerobic GvFdx1 in the working buffer in the presence of EDTA (3 mM) and 5-dRf (4 µM), was photoreduced by illumination with blue light. When GvFdx1 lost its red color, it was considered to be in the reduced state, and the tonometer was connected to the SF drive syringe. In this assay, both tonometers contained 10 mM glucose and 10 UI/mL glucose oxidase. Molar ratios of $GvFFTR_{ox}$:$GvFdx1_{rd}$ of 1:0.5, 1:1, and 1:4 were assayed for the reduction of the different $GvFFTR_{ox}$ variants by $GvFdx1_{rd}$, with final $GvFFTR_{ox}$ concentration being either in the 5 or 10 µM ranges. All reactions were followed by evolution of the absorption spectra (400-800 nm) using an Applied Photophysics SX17.MV stopped-flow and a PDA detector.

3.8.4 SF Data Processing

Analysis of time dependent spectral changes was performed by global analysis and numerical integration methods using Pro-Kineticist (App. Photo. Ltd.). Spectral intermediate species formed during reactions were resolved by singular value decomposition (SVD) using Pro-Kineticist (App. Photo. Ltd.). Data collected were deconvoluted considering sequential and irreversible reaction steps in the context of two (A → B → C), three (A → B → C → D) or four (A → B → C → D→ E) step mechanisms, were A-E are spectral species (not necessarily a given state), and allowed to determine their corresponding observed rate constants for these ($k_{A\rightarrow B}$, $k_{B\rightarrow C}$, $k_{C\rightarrow D}$, $k_{D\rightarrow E}$) as well as spectroscopic properties of intermediate species (Ferreira

& Medina, 2021). The estimated error of the determined rate constant values was ±15%. It should be emphasized that SVD analysis of PDA spectra over a selected time domain resolves the spectra into the minimum number of spectral intermediate species that are formed during the evaluated process, reflecting a distribution of protein intermediates (reactants, complexes, products...) at a given point along the reaction time course, and not discrete enzyme intermediates. Moreover, none of them represents individual species and, their spectra cannot be included as fixed values in the global-fitting. Consequently, a spectral intermediate, in particular one that is formed in the middle of a reaction sequence, is an equilibrium distribution of protein species that are formed in a resolvable kinetic phase. The validity of the model was assessed by the absence of systematic deviation from the residual plot at different wavelengths, inspection of the calculated spectra and consistence among the number of significant singular values with the fitted model. Simulations using Pro-Kineticist (App. Photo. Ltd.) were also performed to validate the determined ET kinetic constants and processes.

3.9 Protein Crystallization and X-Ray Diffraction

Protein crystallization is the process of obtaining protein crystals by addition of precipitating agents under controlled conditions, like temperature, ionic strength, and pH of the solution. This produces a supersaturated solution of the protein in which its natural conformation is maintained. One of the most important applications of protein crystallization is for X-ray diffraction analysis, since the obtained X-ray diffraction patterns can be used as raw data to allow the direct visualization of the 3D structure.

To obtain a protein structure using X-ray crystallography the following actions must be carried out (Figure 3.15):

1. Get a crystal of appropriate quality and size for the experiment.
2. Obtain a collection of diffraction patterns at the appropriate wavelength.
3. Process the X-ray diffraction data to get the lattice parameters (unit cell), symmetry (space group), and diffraction intensities.
4. Solve the electron density function, obtaining any information about the phases of the diffracted rays. For protein crystals, the phase problem (phase data lost in the experiment) can be successfully solved by three main methods:
    a. By introducing atoms with high scattering power into the crystal. This method, known as Multiple Isomorphous Replacement (MIR), is based on the Patterson method.

b. By introducing atoms that scatter X-rays anomalously, also known as Multi-Wavelength Anomalous Diffraction (MAD).
c. By Molecular Replacement (MR), which uses the previously known structure of a similar protein.

5. Build an initial structural model to explain the values of the electron density function and complete the model by locating the remaining atomic positions.
6. Refine the model byadjusting all atomic positions to get the calculated diffraction pattern as similar as possible to the experimental diffraction pattern, and finally validate and present the overall structural model obtained.

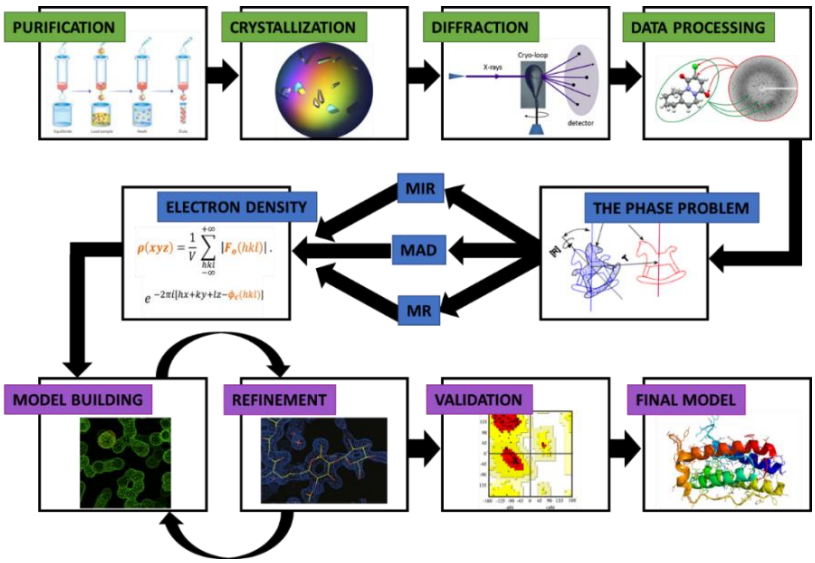

Figure 3.15. General diagram illustrating the process of resolving of molecular and crystal structures by X-ray diffraction.

3.9.1 Basic principles of protein crystallization.

The crystallization process consists of two major events: nucleation and crystal growth. Nucleation is the step where the molecules dispersed in the solvent start to gather into clusters, on the nanometer scale (increasing the solute concentration in a small region), that become stable under the current operating conditions. These stable clusters form the nuclei. The clusters must reach a critical size in order to become stable nuclei. Such critical size is dictated by the operating conditions (temperature, supersaturation, etc.). It is at the nucleation stage, where the atoms arrange themselves in a defined and periodic manner, that defines the crystal structure. Figure 3.16 shows the phase diagram of a common protein-crystallizing process, where, among others, the nucleation and crystal growth zones are illustrated as a function of the protein and precipitant concentration. The crystallization process also depends on the purity and homogeneity, of the protein, pH, temperature, ionic strength, etc.

In the vapor diffusion technique, a protein solution is mixed with a crystallization cocktail solution containing the precipitant to form the final crystallization drop. In the hanging drop setup a few microliters (usually 0.1–5 µL) of both the protein and the crystallization cocktail solution are placed on a siliconized cover slide, which then covers a well containing only the crystallization cocktail (0.05–1 mL), called reservoir liquor. In the sitting drop setup, the protein and the crystallization cocktail solution (also called mother liquor) are mixed in a depression of a small elevated post, which is placed within the crystallization cocktail containing reservoir. In both cases the wells are closed with siliconized cover slides that are sealed with grease to avoid evaporation and external influences. The reservoir contains a higher concentration of the precipitant than the crystallization drop, so water vapor diffusion from the crystallization drop into the reservoir is triggered to achieve a chemical equilibrium between the two liquids. As a result, the crystallization drop shrinks and the concentration of both protein and precipitant slowly increases until the solubility limit of the protein is exceeded resulting in a supersaturated solution. This is where phase separation, nucleation, and crystal growth occur (Bijelic & Rompel, 2018).

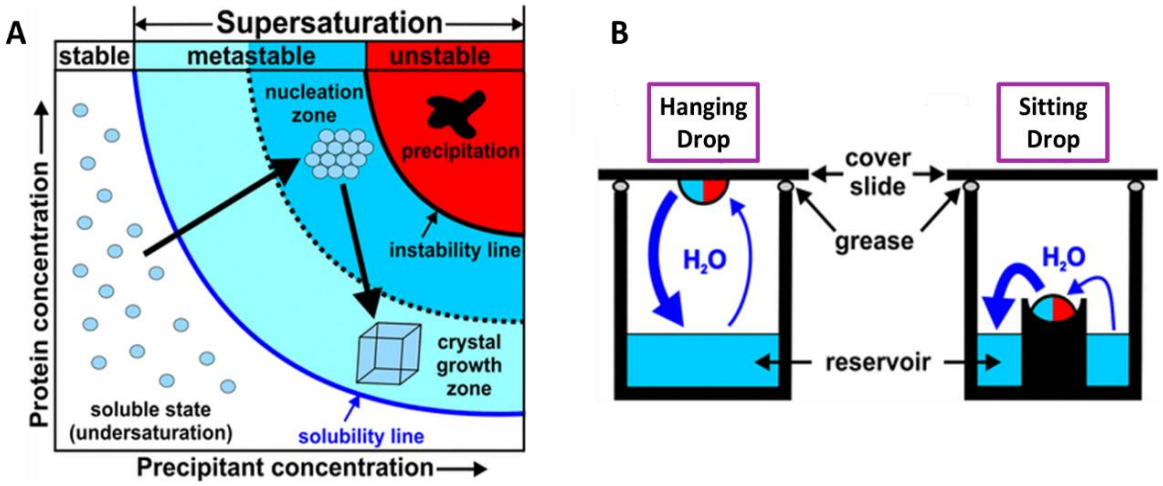

Figure 3.16. (A) Phase diagram of protein crystallization: The solubility line (dark blue line) divides the diagram into undersaturated (white background) and supersaturated (light blue, blue and red background) zones. The protein (blue bubbles) in solution in a single phase migrates to metastable region when the saturation increases. In this zone, transient nuclei are formed but do not reach the critical size. If the supersaturation proceeds (black arrow), the nucleation zone is reached, where nuclei can achieve a critical size and become stable. As the nuclei become larger and crystals start to appear, the protein concentration in the solution decreases and the system reaches the crystal growth zone again. In this zone, crystals continue to grow at lower supersaturation. At too high supersaturation, the unstable zone (red background) is reached, where proteins precipitate. **(B) Vapor diffusion crystallization technique** in two ways: Hanging drop and sitting drop. Precipitant solution is represented in blue color and protein solution in red (Bijelic & Rompel, 2018).

3.9.2 Crystallization of BoMur enzymes and complexes

The search for crystallization conditions of BoMurs started with sitting drops in 96 well plates using 0.3 µL of mother liquor and 0.3 µL of protein that were equilibrated against 60 µl

of mother liquor from the commercial kits JBScreen Classic I, Basic, JCSG++, PEG/Salt (Jena Bioscience) and MIDASplus, ProPlex, Structure Screen 1 & 2 and MORPHEUS (Molecular Dimensions). The best conditions for crystal formation were replicated in hanging drops in 24-well plates using different ratios of protein/reagent solutions (v/v) in drops, to optimize crystal size and quality. Adequate crystals were collected in nylon loops, soaked in a cryoprotectant solution (reagent solution plus 20-30% glycerol or ethylene glycol), and frozen in liquid nitrogen in a Dewar, where they were stored. Eventually, they were sent to the ALBA synchrotron in Barcelona, Spain (beamline 13, XALOC) for diffraction.

3.9.3 X-ray diffraction

X-ray diffraction is caused by the interaction of electromagnetic waves with the matter inside the crystals, and particularly with the electrons. These waves get scattered by the electrons, or each electron becomes a small X-ray source by its own. Scattered waves from all the electrons within each atom are added to each other, giving diffracted waves from each atom, etc. When the scattered waves are added, they may either get stronger or cancel each other. Those which get stronger are registered by the X-ray detector (Mayer, 2017).

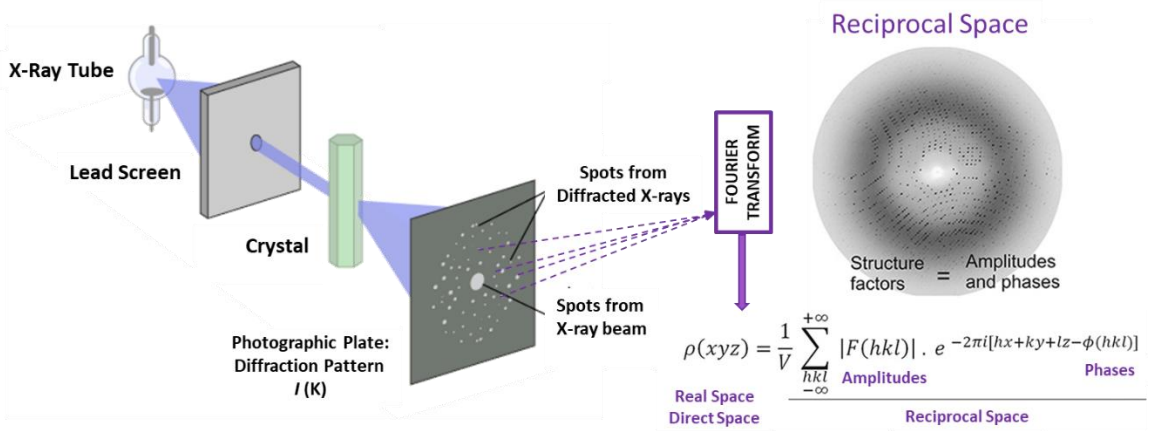

Figure 3.17. **Graphical representation of the single crystal X-ray diffraction technique.** A monochromatic X-ray beam bombards a crystal frozen that rotates on itself. The observed diffraction spots are the result of the impact on the detector of the wave diffracted by the electrons in the crystal (Imagine resource: University of California Museum of Paleontology, Understanding Science).

When a crystal is illuminated with radiation with about the same wavelength as the unit cell dimensions, the crystal acts as a diffraction grating and the scattered radiation will interfere constructively in a few directions but destructively in most. The resulting diffraction images have regularly spaced spots (of different intensities) superimposed on a low background.

3.9.4 Data collection and processing

Data processing itself consists of two basic stages, “integration” and “scaling and merging”. Integration may be sub-divided into four steps, while scaling and merging is usually

considered as a single step. The four steps involved in integration are: 1) spot finding, 2) indexing, 3) parameter refinement and 4) integration itself. Once the diffraction data has been collected, the next step is to calculate an electron density map from which the molecular model is built. The electron density map is a Fourier transform (Equation 3.21) of structure factors, which are comprised of amplitudes and phases.

Eq. 3.21 $$p(xyz) = \frac{1}{V}\sum_{-\infty}^{+\infty}|F_{obs}(hkl)| \cdot e^{-2\pi i[hx+ky+lz-\Phi_{cal}(hkl)]}$$

The amplitudes are calculated from the intensities of reflections recorded during data collection. The phase information, on the other hand, is not recorded and has to be determined (Taylor, 2003). This is termed the "phase problem" in crystallography and structure determination is the calculation of phase information needed to generate the electron density map. The methods MIR, MAD or MR provide knowledge about approximate phases which must be upgraded. In this work, the phase problem was solved by using the MR method (Figure 3.18). The calculated initial phases, Φ_{cal}(hkl), together with the observed experimental amplitudes, $|F_{obs}$(hkl)|, allow us to calculate an electron density map, over which we can build the structural model.

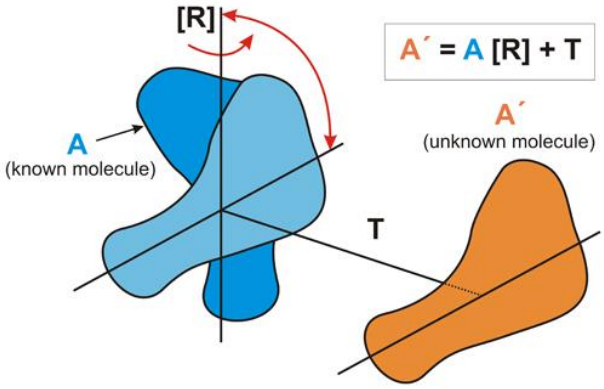

Figure 3.18. Scheme of the molecular replacement (MR) method. The molecule with known structure (A) is rotated through the [R] operation and shifted through T to bring it over the position of the unknown molecule (A'). (Imagine resource: https://www.xtal.iqfr.csic.es/Cristalografia/parte_07-en.html).

3.9.5 Model building, refinement and validation

The MR solutions were obtained with Molrep (Vagin & Teplyakov, 1997) which used as templates, protein structures with high sequence identity with that of the target protein. BLAST from ExPASy was used to search for these proteins, whose structures were known and deposited in the PDB database (Berman et al. 2000). The electron density map generation and automatic refinement were performed by Refmac5 (Murshudov et al., 1997) from the CCP4 package (Winn et al., 2011) and alternating manual model building by WinCOOT (Emsley et

al., 2010) and PROCHECK (Laskowski et al., 1993) was used to assess the final structure quality.

3.10 Bioinformatics Tools

3.10.1 Sequence searching

3.10.1.1 Flavoproteins in *B. ovis* ATCC 25840

Sequences for potential flavin-dependent proteins in *B. ovis*, were retrieved from the National Center for Biotechnology Information (NCBI) (https://www.ncbi.nlm.nih.gov/) and UniProtKB (https://www.uniprot.org/) databases, and the genome and proteome ensembles of the bacteria. We searched for proteins binding RF, FMN and FAD as ligands (Benson et al., 2012; Bateman et al., 2021). Sequences annotated in other species as consensus motifs for FMN- and FAD-binding were also used as query to retrieve putative *B. ovis* flavoproteins using BLASTp (https://blast.ncbi.nlm.nih.gov/Blast.cgi?PAGE= Proteins) online tools (Gish & States, 1993; Dym & Eisenberg, 2001; Macheroux et al., 2011). The identified putative *B. ovis* flavoproteins were analyzed in the context of homologous flavin-dependent proteins reported in bacteria, archaea, eukaryotes, fungi, plants and mammals.

3.10.1.2 BoMurA, BoMurB and BoMurC sequences

The NCBI database was used to analyze the genetic context of the *BomurA*, *B* and *C* genes. BLASTp and UniprotKB were used to find amino acid sequences related to the three Murs in various species of bacteria as well as within *Brucella* genus. In addition, all the structures deposited in the Protein Data Bank (PDB) (https://www.rcsb.org/) were analyzed. The Logo sequence was generated with WebLogo (https://weblogo.berkeley.edu/), where the probability of each amino acid is represented by the height of the letter and is scaled by how many sequences contributed to that position (4.3 bits is the maximum and shorter letters were generated from fewer sequences) (Crooks et al., 2004).

3.10.2 Flavoprotein classification

The Pfam database (https://pfam.xfam.org/) was used to classify the retrieved flavoproteins in domains and clans (El-Gebali et al., 2019). Enzyme Commission numbers (EC numbers), protein names, or metabolic functions were assigned after examining each protein for their information in homologues from different organisms using several databases. These included the BRENDA database (Jeske et al., 2019), the Enzyme Structures database (http://www.ebi.ac.uk/thornton-srv/databases/enzymes/), the KEGG PATHWAY database (https://www.genome.jp/kegg/pathway.html), the MetaCyc database collection (https://metacyc.org/), and the Pathogen-Host Interaction Data Integration Analysis System

(Phidias), particularly the *Brucella* Bioinformatics Portal (BBP) containing 17 *Brucella* genomes (Xiang et al., 2006, 2007). Potential virulent protein sequences were predicted using the pipelines of the servers VirulentPred (http://203.92.44.117/virulent/), a bi-layer cascade Support Vector Machine (SVM) methods developed for bacterial pathogens (Garg & Gupta, 2008) and VICMpred (https://bio.tools/vicmpred), specifically designed for Gram-negative bacterial proteins and also predicting general functional class (Waseem et al., 2017).

3.10.3 Sequence alignments and evolutionary analysis

3.10.3.1 Flavoproteins

For phylogeny, multiple sequence aligments (MSA) of sequences were produced using Clustal Omega (https://www.ebi.ac.uk/Tools/msa/clustalo/) (Becana et al., 2020; Sievers et al., 2011; Yruela et al., 2021). MSAs were then trimmed following the protocol of the TRIMAL software (Capella-Gutierrez et al., 2009). A maximum likelihood phylogenetic tree using the Subtree Pruning and Regrafting method was constructed with PHYML (https://ngphylogeny.fr) (Lemoine et al., 2019). The tree and cladogram were midpoint-rooted and plotted with FigTree (http://tree.bio.ed.ac.uk/software/%ef%ac%81gtree/). The approximate Likelihood-Ratio Test (aLRT) with a seed value of 123456 and bootstrap analysis with a value of 100 were performed. aLRT statistics: 0.022 proportion of invariant.

3.10.3.2 Murs proteins

Brucella and bacteria MSAs of Mur proteins were also aligned using ClustalW within MEGA11 software (Tamura et al., 2021). For constructing phylogenetic trees the Maximum Likelihood (ML) method and JTT matrix-based model (Kishino & Hasegawa, 1989) were used within MEGA11. 500 bootstrap replicates were conducted during the construction of each phylogenetic tree to test the confidence or reliability of the branches. Initial tree(s) for the heuristic search were obtained automatically by applying Neighbor-Join and BioNJ algorithms to a matrix of pairwise distances estimated using the JTT model, and then selecting the topology with superior log likelihood value. The trees and cladograms were midpoint-rooted and plotted with FigTree.

3.10.4 Structural modelling and representation

The BLASTp server was used to obtain identities and to search for the sequences of the most similar proteins with structures in the PDB, and for available 3D structures of flavin-dependent proteins of the *Brucella* genus. 3D structural homology models were built based on templates having at least 35% sequence identity using the Swiss-Model (Biasini et al., 2014) and/or RaptorX (Källberg et al., 2012) servers. Confidence scores calculated to indicate the

quality of predicted 3D models were P value for the relative global quality, global distance test (GDT), and un-normalized GDT (uGDT) for the absolute global quality.

Structural models for BoMurA were generated using the free software I-TASSER (https://zhanggroup.org/I-TASSER/) (Yang & Zhang, 2015; Zheng et al., 2021; Zhou et al., 2022) and the AlphaFold database (https://alphafold.ebi.ac.uk/) (Evans et al., 2021; Jumper et al., 2021). The validation of I-TASSER results relies on the assessment of the C-score, which serves as a confidence metric for evaluating the accuracy of the predicted models. This score is determined by considering the significance of threading template alignments and the convergence parameters of the structure assembly simulations. The C-score is typically in the range of [-5 to 2], where a C-score of a higher value signifies a model with high confidence and vice-versa. AlphaFold provides a confidence metric called the predicted local distance difference test (pLDDT) for each residue ranging from 0 to 100: pLDDT > 90 indicates very high and reliable confidence levels for the modeled structure, pLDDT > 70 indicates confident level, 70 > pLDDT > 50 indicates a low confidence level and pLDDT < 50 indicates very low confidence level.

The AlphaFold database retains generated models by combining amino acid sequence information, multiple sequence alignments, and homologous structures to predict the structure of individual protein chains. However, for predicting models in complex interactions, third-party versions of Google Colab AlphaFold2.ipynb (ColabFold v1.5.2-patch: AlphaFold2 using MMseqs2) were used, which link to a system capable of predicting the structure of multiple chains during training and inference, with native support for multiple characterization and symmetry handling (AlphaFold-Multimer) (Mirdita et al., 2022). This tool was instrumental in generating interaction models between BoMurB and BoMurC. PyMol software was used to visualize and makes the figures of the structures (DeLano, 2002).

3.10.5 Protein-protein docking

Protein-protein interactions play a central role in most cellular functions, making it crucial to understand the molecular details of how proteins associate with one another. Protein-protein docking tools are designed to identify the natural binding mode between two proteins. These predictions are essential to complement experimental techniques, especially since current technical limitations often prevent the acquisition of structural information at a proteomics scale. PyDockWeb (https://life.bsc.es/pid/pydock/) is a rigid-body docking method that employs FTDock for sampling and utilizes an efficient empirical potential for scoring. This potential includes terms related to electrostatics and desolvation, with a limited contribution from Van der Waals energy (Jiménez-García et al., 2013).

The experimental procedure was carried out using the crystallographically obtained structures of BoMurB and BoMurC. BoMurC, being the larger protein, acted as the "receptor" molecule, while BoMurB served as the "ligand." Constraints were applied to refine the complexes based on the potential surface amino acids in close proximity to the active sites of both proteins, allowing for conformations that enable the matching of domains, facilitating the exchange of product-substrate between BoMurB → BoMurC.

The obtained results are compiled in a file containing the top 100 solutions in the ranking, considering that it works with hundreds or even thousands of different poses. These conformations are accompanied by a table displaying the predicted energies at the interface of each conformation, including electrostatic energy, desolvation energy, Van der Waals energy, and the total energy, which is the sum of the three aforementioned energies. Additionally, there is an extra column called "relRST," which simplifies the percentage of satisfied constraints for each conformation.

3.10.6 Structural conservation analysis

The ConSurf server (https://consurf.tau.ac.il/consurf_index.php) (Glaser et al., 2003; Landau et al., 2005; Ashkenazy et al., 2016) is a bioinformatics tool used to determine the conservation of amino acids in proteins or protein sequences based on phylogenetic relationships between homologous sequences and plotting them on the 3D structure. The evolutionary rate was estimated based on the evolutionary relationship between the protein and its homologs and considering the similarity between the residues, as reflected in the substitution matrix. This information is valuable for research in structural biology and bioinformatics as it provides information on important functional and structural regions in proteins.

The main applications of the ConSurf Server are: (i) prediction of active sites and functional regions: highly conserved residues are usually associated with active sites, while less conserved regions may be involved in specific protein interactions or adaptation to different functions; (ii) identification of binding regions: ConSurf can help identify regions in a protein that are prone to interact with other proteins or ligands. This is useful in drug design and understanding protein-protein interactions; (iii) characterization of structure and function: by determining the conservation of amino acids in a protein, aspects of its structure and function can be inferred. Highly conserved regions are usually involved in structural stability, while less conserved regions may be related to specific functions or variations in function in different species. (iv) Design of experiments: ConSurf can help guide the selection of residues for site-directed mutagenesis, allowing the importance of certain amino acids in the function of a protein to be studied experimentally. ConSurf in comparison to other methods is the accurate

computation of the evolutionary rate by using either an empirical Bayesian method (Mayrose et al., 2004) or a ML method (Pupko et al., 2002). The continuous conservation scores are partitioned into a scale of 9 bins for visualization, such that bin 9 contains the most conserved positions and bin 1 contains the most variable positions.

3.10.7 General Software for data analysis

The data analysis as well as the construction of the graphs generated in this thesis were carried out with the scientific software Origin Pro 2021 (OriginLab). ProtParam tool by Expasy (https://web.expasy.org/protparam/) was used for computing physical and chemical parameters for the different protein sequences. The computed parameters include the molecular weight (Mw), theoretical isoelectric point (pI), amino acid composition, atomic composition, extinction coefficient, estimated half-life, instability index, aliphatic index and grand average of hydropathicity (GRAVY) (Gasteiger et al., 2005).

To compare the structural models generated by I-TASSER and AlphaFold, the TM-align tool (https://seq2fun.dcmb.med.umich.edu//TM-align/) was used. TM-align is an algorithm for sequence independent protein structure comparisons. For two protein structures of unknown equivalence, TM-align first generates optimized residue-to-residue alignment based on structural similarity using heuristic dynamic programming iterations. An optimal superposition of the two structures built on the detected alignment, as well as the TM-score value which scales the structural similarity, will be returned. TM-score ranges from 0 to 1, where 1 indicates a perfect match between the two structures. Following strict statistics of structures in the PDB, scores below 0.2 correspond to randomly chosen unrelated proteins while those higher than 0.5 assume generally the same fold in SCOP/CATH (Zhang & Skolnick, 2005).

4.

Mining the Flavoproteome of Brucella ovis, the Brucellosis Causing Agent in Ovis aries

4.1 SUMMARY

Flavoproteins are a diverse class of proteins that are mostly enzymes and contain as cofactors flavin mononucleotide (FMN) and/or flavin adenine dinucleotide (FAD), which enable them to participate in a wide range of physiological reactions. We have compiled 78 potential proteins building the flavoproteome of *B. ovis*, the causative agent of ovine brucellosis. The curated list of flavoproteins here reported is based on: i) the analysis of sequence, structure and function of homologous proteins, and their classification according to their structural domains, clans and expected enzymatic functions; ii) the constructed phylogenetic trees of enzyme functional classes using 19 *Brucella* strains and 26 pathogenic and/or biotechnological relevant alpha-proteobacteria together with *B. ovis*; and iii) the evaluation of the genetic context for each entry. Candidates account for ~2.7% of the *B. ovis* proteome and 75% of them use FAD as cofactor. Only 55% of these flavoproteins belong to the core proteome of *Brucella* and contribute to *B. ovis* processes involved in maintenance activities, survival and response to stress, virulence and/or infectivity. Several of the predicted flavoproteins are highly divergent in *Brucella* genus from revised proteins and for them it is difficult to envisage a clear function. This might indicate modified catalytic activities or even divergent processes and mechanisms still not identified. We have also detected the lack of some functional flavoenzymes in *B. ovis*, which might contribute to it being non-zoonotic. Finally, potentiality of *B. ovis* flavoproteome as source of antimicrobial targets or biocatalyst is discussed.

4.2 INTRODUCTION

Flavoproteins contain as cofactors the riboflavin (RF) derivatives flavin mononucleotide (FMN) and/or flavin adenine dinucleotide (FAD), and participate in a wide range of physiological reactions and metabolic pathways (Fraaije & Mattevi, 2000; Massey, 2000; Leys & Scrutton, 2016; Walsh & Wencewicz, 2013). Most of them are essential mediators in oxido-reduction processes, where they can either exchange one or two electrons whereas other cofactors or coenzymes exclusively catalyze one- (iron-sulphur clusters, haem groups, …) or two- (nicotinamide adenine nucleotides) electron transfer processes. This makes flavoenzymes to exhibit their redox versatility in a large number of metabolic redox processes. Moreover, among the around 500 different flavin-dependent proteins so far identified ~10% catalyze non-redox reactions or act as signaling and sensing molecules (Macheroux et al., 2011; Lienhart et al., 2013; Schall et al., 2020). Examples would include signal transduction in programmed cell death, embryonic development, chromatin remodeling, nucleotide synthesis, tRNA methylation, protein folding, and defense against oxidative stress (Murty & Adiga, 1982; Susin et al., 1999; Myllykallio et al., 2002; Gross et al., 2004; Nishimasu et al., 2009; Becker & Natarajan, 2012; Ferreira et al., 2014; Novo et al., 2021;), among others. Some flavoproteins are also involved in the xenobiotic metabolism of aromatic compounds, pathogens virulence and in light-dependent processes in which flavin receives photons; as luciferase light-emission, DNA reparation, plant phototropism and cellular clocks (Spellerberg et al., 1996; Briggs, 2007; Tsolis et al., 2009; McNeil et al., 2014; Zhang et al., 2017). Many flavoenzymes are also suitable biocatalysts due to their selectivity, control, and efficiency of the reactions they catalyze (Walsh & Wencewicz, 2013; Hall, 2020), as well therapeutic targets both in the treatment of infectious diseases and in mammalian pathological situations (Cremades et al., 2009; Martínez-Júlvez et al., 2017; Sebastián et al., 2018; Leone et al., 2018, 2019; Villanueva et al., 2019; Anoz-Carbonell et al., 2020; Lans et al., 2020). Despite their potential, only a few flavoproteins are widely exploited (Jortzik et al., 2014a). To expand their applicability, it is essential to investigate the flavoprotein content and diversity in different organisms. So far, detailed information of flavoproteomes has only been reported in *H. sapiens*, *S. cerevisiae* and *A. thaliana* (Lienhart et al., 2013; Gudipati et al., 2014; Schall et al., 2020; Eggers et al., 2021), to which has to be added a comparative analysis in a bunch of archaeal, eubacterial, protozoan and eukaryotic genomes (Macheroux et al., 2011). These studies indicate that whereas some organisms depend heavily on flavin-dependent activities, other maintain a minimum of flavoproteins. A better knowledge about content of flavoproteomes would surely help in the

understanding of metabolic requirements in different organisms, and benefit either industry or health.

Table 4.1. List of *Brucella* and alpha-proteobacteria evaluated in the context of *B. ovis* flavoproteins.

Brucellae species/strains	Pathogenic and Disease (host)	Alpha-proteobacteria (Williams et al., 2007)	Function / Disease
***Brucella abortus* 2308**	Yes / ovine brucellosis (zoonosis, veal, camel, buffalo)	***Agrobacterium tumefaciens* now *Rhizobium radiobacter***	biotechnological applications
***Brucella canis* ATCC 23365**	Yes / brucellosis (zoonosis, dog)	***Anaplasma phagocytophilum***	causative agent of granulocytic anaplasmosis
Brucella ceti	Yes /brucellosis (zoonosis, cetaceans, seals)	***Azorhizobium caulinodans***	nitrogen-fixing symbiotic bacteria in plants (*Sesbania* species)
Brucella inopinata	Yes / brucellosis	***Azotobacter vinelandii***	nitrogen-fixing symbiotic bacteria -biotechnology application: produces alginate)
Brucella intermedia or Ochrobactrum intermedium* (Velasco et al., 1998) *or* *Brucella ciceri	Yes / brucellosis	***Bartonella quintana***	causative agent of louse-born trench fever during World War I, causing deer ked dermatitis in humans
***Brucella melitensis* bv. 1 str. 16M**	Yes / ovine brucellosis (zoonosis, sheep, goats)	***Bartonella schoenbuchensis***	causative agent of bacteraemia in ruminants
***Brucella microti* CCM 4915**	Yes / brucellosis (red fox)	***Bradyrhizobium diazoefficiens***	nitrogen-fixing symbiotic bacteria -biotechnology application: produces alginate)
Brucella neotomae	Yes / brucellosis (rodents)	***Candidatus pelagibacter***	marine bacterium dominant in ocean surface waters (possibly the most numerous bacteria in the world)
***Brucella ovis* ATCC 25840**	Yes / ovine brucellosis (sheep)	***Caulobacter crescentus***	model for regulation of cell cycle and cellular differentiation (Farr Zuend et al., 2019)
Brucella_pinnipedialis		***Ehrlichia chaffeensis***	Human Monocytic Ehrlichiosis
***Brucella* sp. NVSL 07-0026**		***Gluconobacter oxydans***	biotechnological applications
***Brucella* sp. 10RB9215**		***Mesorhizobium loti***	nitrogen-fixing symbiotic bacteria in plants (*Lotus* species)
***Brucella* sp. BO3**		***Paracoccus yeei***	peritonitis - opportunistic bacterium in ambulatory peritoneal dialysis
***Brucella* sp. 6810**		***Phenylobacterium zucineum***	associated to human leukaemia
***Brucella* sp. 2280**		***Rhizobium etli***	nitrogen-fixing symbiotic bacteria in plants (*Phaseolus vulgaris*)
***Brucella* sp. 09RB8471**		***Rhizobium leguminosarum***	nitrogen-fixing symbiotic bacteria in plants (*Fabae* family)
***Brucella* sp. 09RB8910**		***Rhodobacter capsulatus***	model purple photosynthetic bacteria, biotechnological applications
***Brucella* sp. 2002734562**		***Rhodobacter sphaeroides* now *Cereibacter sphaeroides***	model purple photosynthetic bacteria, biotechnological applications
***Brucella suis* bv. 4 str. 40**	Yes / brucellosis (zoonosis, hare, pork, reindeer)	***Rhodopseudomonas palustris***	purple non-sulphur bacteria - switch between four different modes of metabolism
Brucella vulpis	Yes / brucellosis (red fox)	***Rickettsia rickettsii***	causative agent of Rocky Mountain Spotted Fever
		Rickettsia typhi	causative agent of murine typhus
		Ruegeria pomeroyi	model marine bacteria
		Sinorhizobium meliloti	nitrogen-fixing symbiotic bacteria in plants (*Medicago sativa, Medicago truncatula*)
		Sphingomonas paucimobilis	human infections
		Wolbachia pipientis	causative agent of Dengue
		Xanthobacter autotrophicus	biotreatment in wastewater (dichloroethane and toluene biodegradation)

In this context, we aimed to trace flavin-binding proteins in *B. ovis* (Jortzik et al., 2014), a gram-negative bacteria that provokes placentitis in sheep and genital lesions in rams that affect the quality of the semen and the fertility, and causes major economic impacts in countries and regions with sheep (*Ovis aries*) breeding activity (Picard-Hagen et al., 2015). The virulence of each particular *Brucella* species depends on enzymes and cell envelope proteins that act as virulence factors, and on the ability to fight against the host response (Mirnejad et al., 2017). Nonetheless, which genes and proteins are essential in these processes, as well as how they

interact during intracellular virulence, still remain unclear. Here, we have identified 78 candidates to constitute the *B. ovis* flavoproteome. We envisage a metabolic function for many of them upon evaluation of their presence in *Brucella* and pathogenic and biotechnological relevant alpha-proteobacteria (Table 4.1), as well as of their evolutionary fingerprint and genetic context. Our studies point to a list of flavoproteins with high probability to contribute to the *B. ovis* survival, virulence and/or infectivity, some of which have not yet been characterized in any homologue. This list is also discussed as a tool in the search for candidates as new biocatalyst or antimicrobial targets.

4.3 RESULTS

4.3.1 Overall features of the *Brucella ovis* flavoproteome

The *B. ovis* ATCC 25840 genome contains 2,890 genes organized in two chromosomes, CI (2.10 Mb, 1,928 genes) and CII (1.15 Mb, 962 genes) (Tsolis et al., 2009). Among them, we identified 78 flavoproteins encoded by 49 genes of CI (2.4 %) and 37 genes of CII (3.5 %). They constitute the curated flavoproteome of *B. ovis* (Tables 4.2 and 4.3) and represent ~2.7% of the *B. ovis* proteome. This percentage agrees with average estimations from the study of other flavoproteomes (Lienhart et al., 2013; Macheroux et al., 2011; Schall et al., 2020).

Fifty (64%) and twenty-two (28%) of these flavoproteins are predicted to bind, respectively, FAD and FMN as cofactor (Tables 4.2 and 4.3). Four (5%) would bind both: the NADH dependent dihydropyrimidine dehydrogenase, binding FMN and FAD respectively at its PreA and PreT subunits; the sarcosine oxidase beta subunit; the glutamate synthase, binding FMN and FAD respectively at the large and short subunits; and the assimilatory sulphite reductase (NADPH) alpha component cluster where FMN and FAD bind respectively at two of its subunits. The bifunctional riboflavin kinase/FAD synthase would bind RF, FMN and FAD, and the riboflavin synthase alpha subunit would bind RF as product. Despite the lower content of proteins binding FMN, the *B. ovis* flavoproteome is slightly biased towards FMN when considering overall kingdoms, where the majority of flavoenzymes bind FAD (75%) (Gudipati et al., 2014), or some eukaryotic flavoproteomes, as the *H. sapiens* one (with 84% FAD-dependent proteins) (Lienhart et al., 2013; Wegrzyn et al., 2019). Thirty-three of the identified flavoproteins in *B. ovis* are expected to use $NAD(P)^+/H$ as coenzyme, whereas a few would bind haem, iron-sulphur clusters, quinones, CTP or thiamine phosphate.

Table 4.2. Predicted flavoproteins encoded in the chromosome I of *Brucella ovis* ATCC 25840

	EC	Protein	Pfam Domain [a]	Locus Tag	Protein Code	Flavin	Coenzyme or Ligand	More similar PDB (% identity)
1	1.1.5.3	Glycerol-3-phosphate dehydrogenase	DAO (PF01266) 19-347 DAO_C (PF16901) 399-508	BOV_RS00950 (glpD)	ABQ60174.1	FAD	Quinone	2QCU (50)
2	1.1.99.1	Choline dehydrogenase (Glucose-methanol-choline GMC family)	GMC_oxred_N (PF00732) 4-292 GMC_oxred_C (PF05199) 384-521	BOV_RS02765 (betA)	ABQ61350.1	FAD		2JBV (35)
3	1.1.99.1	Choline dehydrogenase (GMC family)	GMC_oxred_N (PF00732) 4-295 GMC_oxred_C (PF05199) 388-524	BOV_RS07775	ABQ60630.1	FAD		4HA6 (31)
4	1.1.-.-[b]	***Potential FAD-binding oxygen oxidoreductase (glcE?)*** [c]	FAD_binding_4 (PF01565) 54-187 FAD-oxidase_C (PF02913) 223-463	BOV_RS06750	ABQ60928.1	FAD		3PM9 (29)
5	1.1.-.-[b]	***Potential FAD-binding oxygen oxidoreductase (glcE?)***	FAD_binding_4 (PF01565) 43-180 FAD-oxidase_C (PF02913) 219-469	BOV_RS02095	ABQ61939.1	FAD		3PM9 (60)
6	1.3.1.1	NADH dependent Dihydropyrimidine dehydrogenase subunit PreA	DHO_dh (PF01180) 4-307 Fer4_21 (PF14697) 340-400	BOV_RS01510 (preA)	ABQ60560.1	FMN	 2x(4Fe-4S)	2B4G (24) 1GTE (37)
		NADH dependent Dihydropyrimidine dehydrogenase subunit PreT	Fer4_20 (PF14691) 31-139 Pyr_redox_2 (PF07992) 153-441	BOV_RS01515 (preT)	ABQ61103.1	 FAD	4Fe-4S NAD(P)H	5JCA_L (32) 5VJ7_A (35)
7	1.3.1.88	tRNA dihydrouridine synthase B	Dus (PF01207) 22-316	BOV_RS05355 (DusB)	ABQ61416.1	FMN	NAD(P)H	6EI9 (41)
8	1.3.1.91	tRNA dihydrouridine20/20a synthase	Dus (PF01207) 21-320	BOV_RS04255 (dusA)	ABQ61966.1	FMN	NAD(P)H	3B0P (46)
9	1.3.1.98	UDP-N-acetylmuramate dehydrogenase	FAD_binding_4 (PF01565) 42-172 murB_C (PF02873) 206-304	BOV_RS06850 (MurB)	ABQ61769.1	FAD	NADPH	3TX1 (35)
10	1.3.5.1	Succinate dehydrogenase flavoprotein subunit	FAD_binding_2 (PF00890) 24-419 Succ_DH_flav_C (PF02910) 474-613	BOV_RS08985 (sdhA)	ABQ61077.1	FAD		2H88_A (63)
11	1.3.5.2	PyrD dihydroorotate dehydrogenase 2 (quinone)	DHO_dh (PF01180) 44-336	BOV_RS01655 (pyrD)	ABQ61413.1	FMN	Quinone	4ORI (48)
12	1.3.8.1	Short Chain Acyl-CoA dehydrogenase	Acyl-CoA_dh_N (PF02771) 37-155 Acyl-CoA_dh_M (PF02770) 160-268 Acyl-CoA_dh_1 (PF00441) 288-457 Acyl-CoA_dh_C (PF12806) 470-585	BOV_RS02120	ABQ60180.1	FAD		1BUC (29)
13	1.3.8.4	Isovaleryl-CoA dehydrogenase	Acyl-CoA_dh_N (PF02771) 7-118 Acyl-CoA_dh_M (PF02770) 122-217 Acyl-CoA_dh_1 (PF00441) 229-377	BOV_RS00090 (ivd)	ABQ60382.1	FAD		4KTO (83) 4O5M (100)
14	1.3.8.-[b]	Acyl-CoA dehydrogenase	Acyl-CoA_dh_N (PF02771) 12-123 Acyl-CoA_dh_M (PF02770) 127-221 Acyl-CoA_dh_1 (PF00441) 235-382	BOV_RS06310	ABQ61585.1	FAD		1RX0 (57)
15	1.4.3.5	Pyridoxamine 5'-phosphate oxidase	Putative_PNPOx (PF01243) 29-113 PNP_phzG_C (PF10590) 166-208	BOV_RS02140 (pdxH)	ABQ60142.1	FMN		1NDL (45)
16	1.4.3.19	Glycine oxidase ThiO	DAO (PF01266) 3-313	BOV_RS01020 (thiO)	ABQ60316.1	FAD		4YSH (27)
17	1.4.3.-[b]	***Potential Aminoacetone oxidase family FAD-binding enzyme/ NAD(P)/FAD-dependent dehydrogenase***	HI0933_like (PF03486) 5-391	BOV_RS06670	ABQ60616.1	FAD		3V76 (67)
18	1.4.3.-[b]	***Potential Aminoacetone oxidase family FAD-binding enzyme/ NAD(P)/FAD-dependent dehydrogenase***	HI0933_like (PF03486) 5-391	BOV_RS04985	ABQ60524.1	FAD		2I0Z (24)
19	1.4.99.-[b]	Predicted D-amino acid dehydrogenase small subunit	DAO (PF01266) 10-400	BOV_RS08480	ABQ61937.1	FAD		6J38 (23)
20	1.4.-.-[b]	***Pyridoxamine 5'-phosphate oxidase family protein***	Pyridox_ox_2 (PF12900) 10-141	BOV_RS06575	ABQ61684.1	FMN		3U0I (99) 2HQ9 (30)
21	1.5.1.20	Methylenetetra-hydrofolate reductase	MTHFR (PF02219) 14-291	BOV_RS06945 (metF)	ABQ60279.1	FAD	NAD(P)H	3FST (48)
22	1.5.1.-[b]	***Flavin reductase domain containing protein***	Flavin_Reduct (PF01613) 22-172	BOV_RS05125	ABQ60228.1	FMN	NAD(P)H	1EJE (29)
23	1.5.3.1	Sarcosine oxidase beta subunit	DAO (PF01266) 36-161	BOV_RS01075 (soxB_1)	ABQ60177.1	FAD & FMN		2GAG_B (64)

			DAO (PF01266) 8-222	BOV_RS01090 (soxB_2)	ABQ61310.1			2GAG_B (58)
		Sarcosine oxidase alpha subunit	Fer2_4 (PF13510) 16-102 FAD_oxidored (PF12831) 171-218 GCV_T (PF01571) 526-790 GCV_T_C (PF08669) 815-901	BOV_RS01100	ABQ61036.1	FMN	NADH 4Fe-4S	2GAG_A (47)
24	1.5.5.1	Electron transferring flavoprotein-ubiquinone oxidoreductase (ETF-QO)	Thi4 (PF01946) 12-52 ETF_QO (PF05187) 451-560	BOV_RS03100	ABQ61337.1	FAD	4Fe-4S quinone	2GMH (49)
25	1.6.5.2	WrpA type FMN-dependent NADH:quinone oxidoreductase	FMN_red (PF03358) 13-145	BOV_RS05025	ABQ60884.1	FMN	NAD(P)H quinone	5F4B (98)
26	1.7.-.-[b]	***Predicted NAD(P)H nitroreductase***	Nitroreductase (PF00881) 23-167	BOV_RS05130	ABQ60834.1	FMN	NAD(P)H	3K6H (43)
27	1.8.1.4	Dihydrolipoyl dehydrogenase (lpdA-2)	Pyr_redox_2 (PF07992) 57-399 Pyr_redox_dim (PF02852) 420-528	BOV_RS05390 (lpdA-2)	ABQ60398.1	FAD	NADH	2A8X (43)
28	1.8.1.4	Dihydrolipoyl dehydrogenase (lpdA-3)	Pyr_redox_2 (PF07992) 3-329 Pyr_redox_dim (PF02852) 348-456	BOV_RS09065 (lpdA-3)	ABQ61458.1	FAD	NADH	3URH (78)
29	1.8.1.7	Glutathione-disulphide reductase	Pyr_redox_2 (PF07992) 6-321 Pyr_redox_dim (PF02852) 341-449	BOV_RS04850 (gor)	ABQ61016.1	FAD	NADPH	4DNA (69)
30	1.8.1.9	Thioredoxin-disulphide reductase	Pyr_redox_2 (PF07992) 8-302	BOV_RS07155 (trxB)	ABQ60123.1	FAD	NAD(P)H	4JNQ (100)
31	1.8.1.9	Predicted thioredoxin-disulphide reductase	Pyr_redox_2 (PF07992) 9-171	BOV_RS04925	ABQ61134.1	FAD	NADP(H)	5YGQ (49) [d] 1NHS (30) 5VJ7 (34)
32	1.14.13.1	Predicted Salicylate hydroxylase	FAD_binding_3 (PF01494) 6-349	BOV_RS03690	ABQ60137.1	FAD	NAD(P)H	4BJZ (32)
33	1.14.13.1	Predicted Salicylate hydroxylase	FAD_binding_3 (PF01494) 2-328	BOV_RS04715	ABQ60978.1	FAD	NAD(P)H	3RP8 (27)
34	1.14.13.-[b]	Predicted UbiH/COQ6 monooxygenase family	FAD_binding_3 (PF01494) 14-322	BOV_RS08970	ABQ60166.1	FAD	NAD(P)H	4K22 (37)
35	1.14.14.3	Bacterial luciferase	Bac_luciferase (PF00296) 8-255	BOV_RS09695	ABQ60348.1	FMN		3FGC (20)
36	1.16.1.4	Cob (II)alamin reductase	Flavin_Reduct (PF01613) 60-208	BOV_RS06210	ABQ60249.1	FMN		3CB0 (99)
37	1.17.1.4	Xanthine dehydrogenase, small subunit	Fer2 (PF00111) 13-59 Fer2_2 (PF01799) 88-161 FAD_binding_5 (PF00941) 204-367 CO_deh_flav_C (PF03450) 376-476	BOV_RS01845 (xdhA)	ABQ61298.1	 FAD	NADH 2(2Fe-2S)	2W3S_A (48)
38	1.18.1.2	Ferredoxin-NADP$^+$ reductase	FAD_binding_6 (PF00970) 19-102 NAD_binding_1 (PF00175) 113-230	BOV_RS01770 (fpr)	ABQ61707.1	FAD	NADPH	6RRA (100)
39	2.1.1.74	Methylenetetrahydrofolate-tRNA-(uracil54-C5-)-methyltransferase NAD(P)H oxidase	GIDA (PF01134) 10-378	BOV_RS04425 (trmFO)	ABQ61275.1	FAD	NADH	3G5S (46)
40	2.1.1.229	tRNA (carboxymethyluridine34-5-O)-methyltransferase	GIDA (PF01134) 10-399 GIDA_assoc (PF13932) 402-612	BOV_RS09735 (mnmG)	ABQ60378.1	FAD	NADH	2ZXI (50)
41	2.2.1.6	Acetolactate synthase 3 catalytic subunit	TPP_enzyme_N (PF02776) 1-165 TPP_enzyme_M (PF00205) 191-327 TPP_enzyme_C (PF02775) 393-540	BOV_RS06655 (ilvB)	ABQ60081.1	FAD	Thiamine diPP	6DEN (46)
42	2.5.1.9	Riboflavin synthase alpha subunit	Lum_binding (PF00677) 20-258	BOV_RS03790 (ribE)	ABQ60518	RF		4E0F (98)
43	4.2.3.5	Chorismate synthase	Chorismate_synt (PF01264) 10-355	BOV_RS02190 (aroC)	ABQ60200.1	FMN		1UM0 (42)
44	7.1.1.2	NADH-quinone oxidoreductase subunit F (H$^+$ translocating)	Complex1_51K (PF01512) 47-216 SLBB (PF10531) 242-292 NADH_4Fe-4S (PF10589) 332-414	BOV_RS04000 (nuoF)	ABQ60521.1	 FMN	NADH 4Fe-4S	6Q9C_D (46)
45	--	Electron transferring flavoprotein alpha subunit (ETFa)	ETF (PF01012) 44-210 ETF_alpha (PF00766) 229-312	BOV_RS09295(etfA)	ABQ61011.1	 FAD		1EFP_A (69)
		Electron transferring flavoprotein beta subunit (ETFb)	ETF (PF01012) 29-206	BOV_RS09300 (etfB)	ABQ60428.1		AMP	1EFP_B (72)

[a] Pfam domains include name, code and residues in the *B. ovis* flavoprotein making the domain.
[b] Identified as flavoenzyme, but available information does not allow to fully predict its activity.
[c] Shown in black and italics those candidates for which a clear function cannot be depicted.
[d] More than one structure to represent the different regions of the protein.

Table 4.3. Predicted flavoproteins encoded in the chromosome II of *Brucella ovis* ATCC 25840

	EC	Protein	Pfam Domains [a]	Locus Tag	Protein Code	Flavin	Coenzyme or Ligand	More similar PDB (% identity)
46	1.1.2.3	L-lactate dehydrogenase (cytochrome c o b2)	FMN_dh (PF01070) 14-377	BOV_RS14715 (lldD)	ABQ62635.1	FMN		5ZBM (40)
47	1.1.-.-[b]	***Potential L-gulonolactone oxidase FAD-binding oxygen oxidoreductase*** [c]	FAD_binding_4 (PF01565) 22-149 nothing up to 444	BOV_RS14405	ABQ62001.1	FAD		4AUT (34)
48	1.1.1.402	D-erythritol 1-phosphate dehydrogenase	DAO (PF01266) 8-333 DAO_C (PF16901) 386-482	BOV_RS14450 (eryB)	ABQ62056.1	FAD	Quinone	2QCU (51)
49	1.1.99.1	Choline dehydrogenase (GMC family, membrane bound)	GMC_oxred_N (PF00732) 5-295 GMC_oxred_C (PF05199) 387-523	BOV_RS14905	ABQ62100.1	FAD		4HA6 (34)
50	1.1.99.2	Predicted L-2-hydroxyglutarate dehydrogenase	DAO (PF01266) 5-392	BOV_RS15155 (lhgO)	ABQ62911.1	FAD	NADH	3DME (37)
51	1.1.99.14	Glycolate dehydrogenase GlcD subunit	FAD_binding_4 (PF01565) 55-193 FAD-oxidase_C (PF02913) 229-470	BOV_RS11160 (glcD)	ABQ62237.1	FAD		3PM9(29)
52	1.3.1.-[b]/1.7..B1	Predicted alkene reductase: N-ethylmaleimide reductase, glycerol trinitrate reductase or xenobiotic reductase B	Oxidored_FMN (PF00724) 3-349	BOV_RS14625	ABQ62490.1	FMN	NAD(P)H	5N6G (69)
53	1.3.8.-[b]	Acyl-CoA dehydrogenase	AidB_N (PF18158) 17-173 Acyl-CoA_dh_M (PF02770) 188-282 Acyl-CoA_dh_1 (PF00441) 292-447	BOV_RS13205	ABQ62576.1	FAD		5EZ3 (100)
54	1.3.8.-[b]	Acyl-CoA dehydrogenase	Acyl-CoA_dh_N (PF02771) 4-116 Acyl-CoA_dh_M (PF02770) 120-214 Acyl-CoA_dh_1 (PF00441) 227-375	BOV_RS12330	ABQ62784.1	FAD		4N5F (63)
55	1.3.8.-[b]	Acyl-CoA dehydrogenase	Acyl-CoA_dh_N (PF02771) 9-115 Acyl-CoA_dh_M (PF02770) 120-218 Acyl-CoA_dh_1 (PF00441) 231-378	BOV_RS14135	ABQ62889.1	FAD		5LNX (36)
56	1.3.8.-[b]	Acyl-CoA dehydrogenase	Acyl-CoA_dh_N (PF02771) 3-157 Acyl-CoA_dh_M (PF02770) 163-271 Acyl-CoA_dh_1 (PF00441) 282-451 Acyl-CoA_dh_C (PF12806) 467-593	BOV_RS14115	ABQ62082.1	FAD		6IJC (61)
57	1.3.99.-[b]	Predicted KsdD-like steroid dehydrogenase	FAD_binding_2 (PF00890) 5-533	BOV_RS13530	ABQ62061.1	FAD		1D4D (25)
58	1.4.1.13	Glutamate synthase large subunit (alpha subunit)	GATase_2 (PF00310) 56-480 Glu_syn_central (PF04898) 508-794 Glu_synthase (PF01645) 856-1230 GXGXG (PF01493) 1309-1498	BOV_RS10585 (gltB)	ABQ61996.1	FMN	3Fe-4S	1EA0 (45)
		Glutamate synthase small subunit (beta subunit)	Fer4_20 (PF14691) 24-131 Pyr_redox_2 (PF07992) 148-465	BOV_RS10590 (gltD)	ABQ62546.1	FAD	NADPH 4Fe-4S	6S6U_G (37)
59	1.4.99.-[b]	D-amino acid dehydrogenase	DAO (PF01266) 3-397	BOV_RS14735 (dadA)	ABQ62278.1	FAD		4YSH (26)
60	1.4.-.-[b]	Predicted D-amino acid dehydrogenase	DAO (PF01266) 7-397	BOV_RS13345	ABQ62519.1	FAD		4YSH (26)
61	1.4.-.-[b]	Predicted D-amino acid dehydrogenase	DAO (PF01266) 34-384	BOV_RS13970	ABQ62405.1	FAD		4YSH (24)
62	1.5.3.1	Predicted monomeric Sarcosine oxidase	DAO (PF01266) 31-383	BOV_RS13970	ABQ62932.1	FAD		1ZOV (22)

63	1.6.99.1	***NADPH dehydrogenase (Old yellow enzyme)***	Oxidored_FMN (PF00724) 2-340	BOV_RS11390	ABQ62422.1	FMN	NADPH	3GR7 (34)
64	1.6.-.-[b]	***NADH dehydrogenase***	Pyr_redox_2 (PF07992) 8-325	BOV_RS12460	ABQ62704.1	FAD	NADH	4NWZ (31)
65	1.8.1.2	Assimilatory sulphite reductase (NADPH) alpha component cluster	PepSY_TM (PF03929) (3-149)	BOV_RS11420	WP_006015252.1			
			Hypothetical protein (81aa)	BOV_RS11425	WP_006015255.1			
			PepSY_TM (PF03929) (2-128)	BOV_RS11430	WP_006015257.1			
			Flavodoxin_1 (PF00258) (74-147)			FMN		6EFV (~30 *B. melitensis*)
			FAD_binding_6 (PF00970) (80-171)	BOV_RS11435	WP_006015259.1	FAD		
			NAD_binding_1 (PF00175) (189-291)				NADPH	
66	1.8.1.4	Dihydrolipoyl dehydrogenase (lpdA-1)	Pyr_redox_2 (PF07992) 7-326	BOV_RS12670 (lpdA-1)	ABQ62466.1	FAD	NAD(P)H	6CMZ (60)
			Pyr_redox_dim (PF02852) 345-453					
67	1.8.5.B1	Peptide-methionine (S)-S-oxide reductase (quinone) (Msr). MsrP catalytic subunit. MsrQ heme-binding subunit	Ferric_reduct (PF01794) 55-166	BOV_RS15075 (msrQ)	ABQ62365.1	FMN	heme b	6HCY_A (17)
			Oxidored_molyb (PF00174) 98-252	BOV_RS15070 (msrP)	ABQ62343	Molybdopterin	Quinone	1XDY (54)
68	1.13.11.32	Nitronate monooxygenase (formerly 2-nitropropane dioxygenase NPD)	NMO (PF03060) 124-342 (formerly NPD)	BOV_RS14290	ABQ62537.1	FMN		3BW2 (26)
69	1.13.11.79	Predicted aerobic 5,6-dimethylbenzimidazole synthase (BluB)	Nitroreductase (PF00881) 74-240	BOV_RS15390 (bluB)	ABQ62404.1	FMN	NADH	2ISK (36)
70	1.14.13.-[b]	UbiH/UbiF family hydroxylase	FAD_binding_3 (PF01494) 49-377	BOV_RS13080	ABQ62553.1	FAD	NAD(P)	5KOX_A (20)
71	1.14.13.2	4-hydroxybenzoate 3-monooxygenase	FAD_binding_3 (PF01494) 2-342	BOV_RS13400 (pobA)	ABQ62030.1	FAD	NAD(P)H	1PBE (63)
72	1.18.1.3/5	Predicted Ferredoxin/rubredoxin/ putidaredoxin NAD^+ Reductase	1: Pyr_redox_2 (PF07992) 4-301	BOV_RS13795	ABQ62051.1	FAD	NADH	3FG2 (45)
			2: Reductase_C (PF14759) 320-404					
73	1.-.-.- [b]	***Predicted nitroreductase family protein***	Nitroreductase (PF00881) 48-216	BOV_RS12545	ABQ62091.1	FMN		2IFA (55)
74	2.7.7.2	Bifunctional riboflavin kinase/FAD synthase	FAD_syn (PF06574) 18-172	BOV_RS11255 (ribF)	ABQ62831.1	FMN & FAD		2X0K (36)
	2.7.1.26		Flavokinase (PF01687) 190-313			RF & FMN		
75	2.7.1.180	FAD:protein FMN transferase	ApbE (PF02424) 18-296	BOV_RS11440	ABQ62066.1	FAD		5MGY (38) 6NXI (36)
76	2.7.13.3	Blue-light-activated histidine kinase	PAS_9 (PF13426) 34-136	BOV_RS13160	ABQ62113	FMN		6PPS (100)
			PAS_3 (PF08447) 184-259					
			HWE_HK (PF07536) 285-367					
77	4.1.1.36	Coenzyme A biosynthesis bifunctional protein: Phosphopantothenoyl-cysteine decarboxylase/Phosphopantothenate--cysteine ligase (CTP)	Flavoprotein (PF02441) 7-180	BOV_RS15430 (coaBC)	ABQ62036.1	FMN		1E20 (34)
	6.3.2.5		DFP (PF04127) 189-375				CTP	4QJI (42)
78	--	Protein NrdI	Flavodoxin_NdrI (PF07972) 5-122	BOV_RS11810 (nrdI)	ABQ62891.1	FMN		2XOD (36)

[a] Pfam domains include name, code and residues in the *B. ovis* flavoprotein making the domain.
[b] Identified as flavoenzyme, but available information does not allow to fully predict its activity.

It is worth mentioning that currently many of these proteins are only computationally annotated and, in many cases, with vague confidence regarding ligands (searching motifs for FAD also find NAD(P)H binding proteins), nature of the protein and metabolic function.

4.3.2 The structure conformational space in the *B. ovis* flavoproteome

3D structures of proteins from *B. ovis* are scarce; ten different proteins in fourteen PDB entries (Table 4.4). Only one corresponds to a flavoprotein that is also $NADP^+$/H dependent, Ferredoxin-$NADP^+$ reductase (FPR) (Pérez-Amigot et al., 2019), and three more correspond to structures, or subunits, of $NAD(P)^+$/H dependent proteins (Table 4.4). The PDB contains also eleven structures of potential flavoproteins from other *Brucella* (Table 4.5 and Figure 4.1). Ten correspond to nine *B. ovis* homologues sharing more than 98.5% identity, and two are also $NAD(P)^+$/H-dependent. For the remaining structure, the best match in *B. ovis* ATCC 25840 only shares 33% identity, but an identical sequence is found in *B. ovis* IntaBari-2002-82-58. Five of these flavoproteins are FAD-dependent (only two show FAD in the structure), three are FMN-dependent, and one might bind either RF, FMN or FAD (Table 4.5). Regarding function, seven are oxidoreductases with $NAD(P)^+$/H (quinone) dehydrogenase, acyl-CoA dehydrogenase, thioredoxin reductase or monooxygenase activities. Three are transferases; one is riboflavin synthase and two relate to the LOV domain of sensory histidine kinase. Noticeably, the PDB entry 3U0I from *Brucella melitensis*, identified as a pyridoxamine 5'-phosphate oxidase family protein of unknown function, shares nearly 100% identity with *B. ovis* ABQ61684.1. Most of these structures come from structural genomic projects on *B. melitensis, Brucella abortus* and *Brucella suis*, and their functions are not experimentally curated. Tables 1 and 2 show that in 66 (85%) and 39 (50%) of the candidates there are structures of homologues with more than 30% and 45% sequence identity, respectively, providing good structural models for at least ~50% of the *B. ovis* flavoproteins.

B. ovis flavoproteins use up to 26 Pfam clans and 73 domain families (Tables 4.2 and 4.3, Figures 4.2 and 4.3), and in 80% of the cases they fold using more than one domain. Nonetheless, only thirteen clans, plus six domains not assigned to any clan, are implicated in flavin binding (Figure 4.3), in agreement with the diversity in structural topologies for the interaction of these cofactors.

Table 4.4. PDB entries available for *Brucella ovis* ATCC 25840 proteins. Equally colored PDB lines correspond to different entries of the same protein.

PDB ID	Protein Name (potential function)	Gene	Flavin	NAD(P)$^+$/H-binding /ligand in structure	Functional Classification
6RR3	Ferredoxin-NADP$^+$reductase	BOV_RS01770	FAD	Yes/-	oxidoreductase
6RRA	Ferredoxin-NADP$^+$reductase:NADP$^+$ complex	BOV_RS01770	FAD	Yes/NADP$^+$	oxidoreductase
4X54	Putative short chain dehydrogenase/reductase	BOV_RS00560	-	Yes/-	oxidoreductase
5EL0	Putative short chain dehydrogenase/reductase:NAD$^+$ complex	BOV_RS00560	-	Yes/NAD$^+$	oxidoreductase
5ER6	Putative short chain dehydrogenase/reductase	BOV_RS10490	-	Yes/-	oxidoreductase
4Z0T	Putative oxoacyl-(acyl carrier protein) reductase	BOV_RS02275	-	Yes/-	oxidoreductase
5HA5[a]	Putative NAD-dependent oxidoreductase	ENT92748.1	-	Yes/NAD$^+$	oxidoreductase
5DWM	Phosphinothricin N-acetyltransferase	BOV_RS00430	-	No/-	Transferase
5DWN	Phosphinothricin N-acetyltransferase:AcetylCoA complex	BOV_RS00430	-	No/AcetylCoA	Transferase
5VM1	Xyloylose kinase	xylB	-	No/-	Transferase
4WOK	UDP-glucose 4-epimerase:NAD$^+$ complex	galE	-	Yes/NAD$^+$	Isomerase
7JFN	Leucine-, isoleucine-, valine-, threonine-, and alanine- ABC transporter/periplasmic (closed conformation)	BOV_RS10455	-	No/-	Transport protein
4XFK	Leucine-, isoleucine-, valine-, threonine-, and alanine- ABC transporter/periplasmic	BOV_RS10455	-	No/-	Transport protein
4Z9N	ABC transporter/periplasmic binding protein:Glutathione complex	BOV_RS03670	-	No/glutathione	Transport protein

[a]This PDB corresponds to a protein from *B. ovis* IntaBari-2002-82-58 that shares 100% identity with the reference strain here used.

Table 4.5. Summary of structures found in the PDB of proteins of the *Brucella* genus that putatively bind flavin cofactors.

PDB ID (Uniprot ID)	Protein	Flavin	$NAD(P)^+$/H- binding /ligands in structure	Species Strain	*B. ovis* ATCC 25840 gene	% Identity[a]	Functional Classification
5F4B (Q2YQ23)	$NAD(P)^+$/H (quinone) dehydrogenase	FMN	$NAD(P)^+$/-	*B. abortus* 2308	BOV_RS05025	98.49	oxidoreductase
4W9U (Q2YPZ4)	Acyl-CoA dehydrogenase	fad[b]	-	*B. abortus* 2308	ENT94890.1 4W9U[c]	100	oxidoreductase
4U83 (WP_076773354.1)	Putative Acyl-CoA dehydrogenase	fad[b]	-	*B. abortus* A13334	BOV_RS12330	99.20	oxidoreductase
4JNQ (Q8YID2)	Thioredoxin reductase	FADH2[d]	$NADP^+$/-	*B. melitensis* bv. 1 str. 16M	BOV_RS07155 (trxB)	99.69	oxidoreductase
5EZ3 (Q8YC61)	Acyl-CoA dehydrogenase	FAD	-	*B. melitensis* bv. 1 str. 16M	BOV_RS13205	99.64	oxidoreductase
4IRA/3CB0 (Q8YHT7)	Co(II)rrin reductase activity (CobR)	FAD/ FMN	-	*B. melitensis* bv. 1 str. 16M	BOV_RS06210	98.84	oxidoreductase
4O5M (A0A0H3G544)	Isovaleryl-CoA dehydrogenase	FAD	-	*B. suis* bv. 1, 1330	BOV_RS00090 (ivd)	99.74	oxidoreductase
4E0F (Q2YN92)	Riboflavin synthase	RF	-/RoSF, PyrM[e]	*B. abortus* 2308	BOV_RS03790 (ribE)	98.51	transferase
3T50 (Q8YC53)	LOV-PAS construct of sensory protein Blue-light-activated histidine kinase	FMN	-	*B. melitensis* bv. 1 str. 16M	BOV_RS13160	99.80	signalling protein (transferase)
6PPS (Q2YKK7)	LOV domain of sensory protein Blue-light-activated histidine kinase	FMN	-	*B. abortus* 2308	BOV_RS13160	99.80	signalling protein (transferase)
3U0I (Q2YQN9)	FAD-binding protein	fad[b]	-/NHE[f]	*B. abortus* 2308	BOV_RS06575	99.31	flavoprotein

[a] Identity versus *B. ovis* ATCC 25840 (reference strain).
[b] Lower cases indicate flavin cofactor binding is predicted, but no flavin is observed in the PDB structure.
[c] Not found in *B. ovis* ATCC 25840, but one of the domains is equivalent in *B. ovis* IntaBari-2002-82-58.
[d] FDH2, Dihydroflavine-adenine dinucleotide.
[e] RoSF, roseoflavine.
[f] NHE, 2-[N-cychlohexylamino]ethane sulfonic acid.

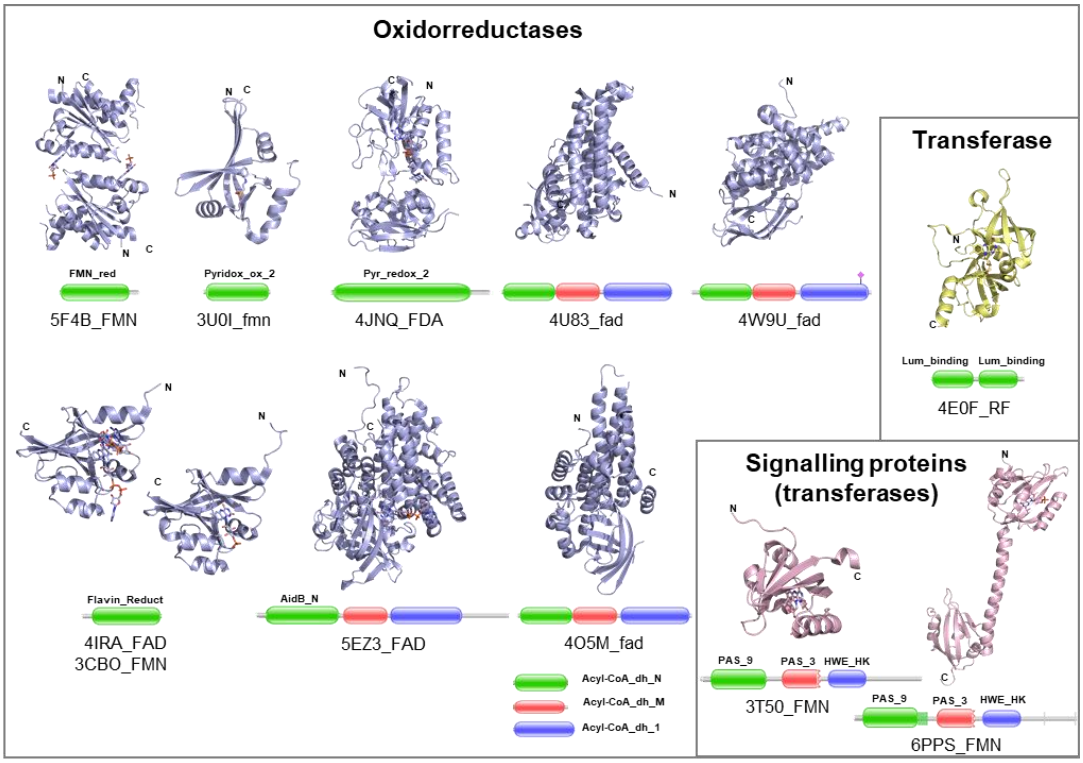

Figure 4.1. Cartoon representation of 3D structures of proteins of *Brucella* that putatively bind flavin cofactors. Cofactors, when present, are in sticks and written after the PDB code (see Table 4.4 for nomenclature). Below each structure its custom Pfam-style domain graphic is shown. Four oxidoreductases share the same legend for the assembly Acyl-CoA_dh_N, Acyl-CoA_dh_M and Acyl-CoA_dh_1 and it is placed under the main chart.

The NADP_Rossmann and TIM-barrel clans are the most widely represented and the preferred respectively for FAD and FMN binding in *B. ovis* flavoproteins, being highly spread in proteins and particularly within flavoproteins (Macheroux et al., 2011; Schall et al., 2020). The NADP_Rossmann fold appears in thirty-eight flavoproteins in *B. ovis*, but presumably it is not involved in flavin binding in domains FAD_oxidored of sarcosine oxidase alpha subunit and DFP of coenzyme A biosynthesis bifunctional protein, where it respectively binds NADH and CTP. From the thirty-six remaining flavoproteins, thirty-five bind FAD and riboflavin synthase binds RF (Lum_binding domain). NADP_Rossmann flavoproteins use mostly domains DAO (some completed by DAO_C domain caps) and Pyr_redox_2 (might contain also Pyr_redox_dim or Fer4_20 domains). Domain families FAD_binding_3, GMC_oxired_N (also having GMC_oxred_C), FAD_binding_2 (some completed with Succ_DH_flav_C), GIDA (holding also GIDA_assoc), HI0933_like and Thi4 are also represented. In this clan we want to notice a particular case: two proteins with DAO domains shorter than regular ones, ABQ60177.1 (BOV_RS01075, soxB_1) and ABQ61310.1 (BOV_RS01090, soxB_2), cover the primary sequence of the sarcosine oxidase beta subunit binding FAD in other *Brucella* orthologues (Table 4.2, Figure 4.4A).

On its side, the TIM_barrel clan is represented by nine flavoproteins that use up to seven different domains: Oxidored_FMN, Dus, DHO_dh, FMN_dh, Glu_syn_central+Glu-synthase and NMO.

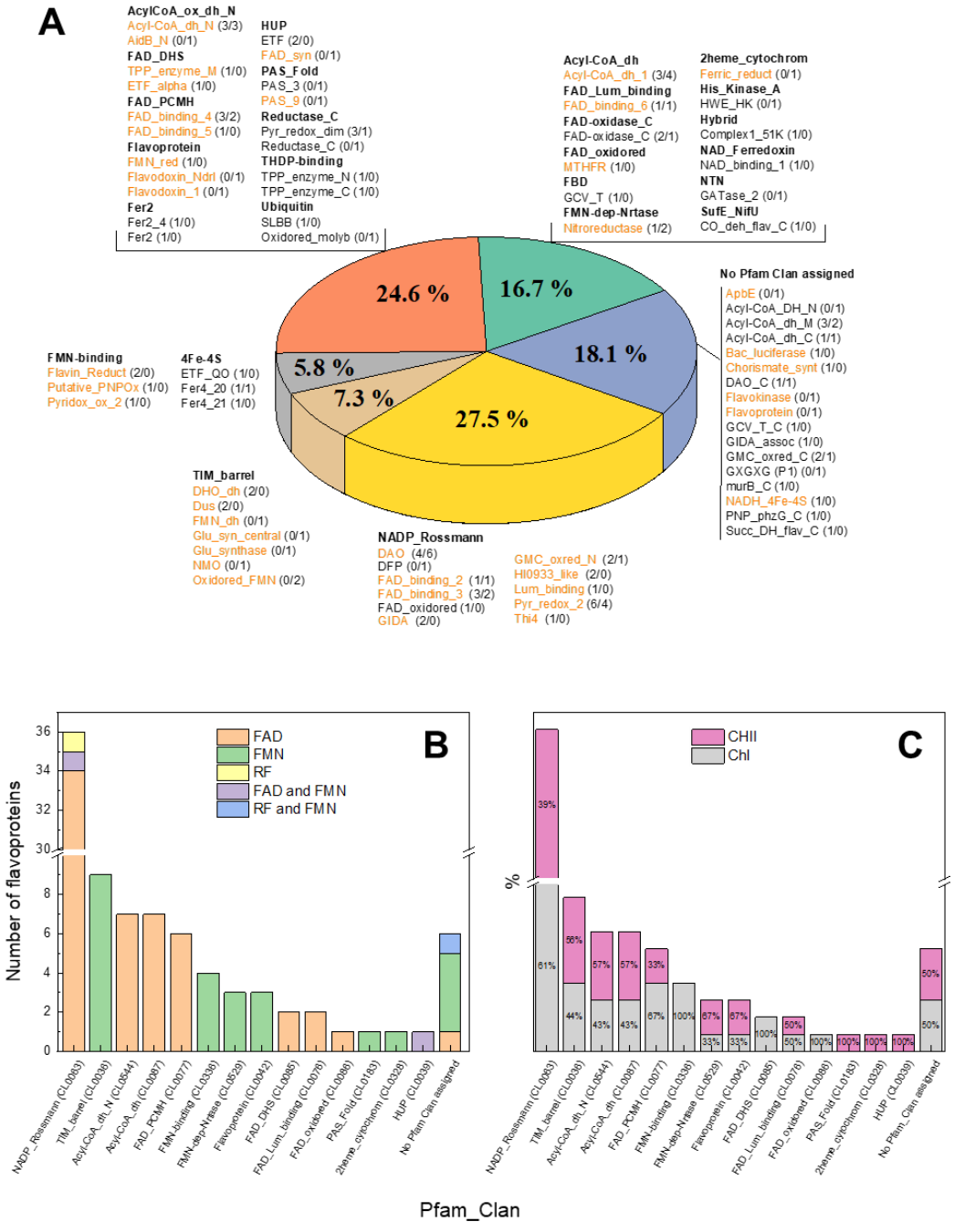

Figure 4.2. Distribution of *B. ovis* ATCC 25840 flavoproteins in structural Pfam clans and domain families. (A) Pie chart of the clans and domains found within the identified flavoproteins. Clan names are highlighted in bold. Names of domain families directly involved in flavin binding are colored in orange, whereas domains not involved in flavin binding but present in the flavoproteins are in black. Overall percentages are based on the number of domain families in each clan (including domains involved and not involved in flavin binding). Most populated clans concerning structural folding, NADP_Rossman and TIM_barrel, are shown individually, while the rest are grouped attending to the number of families found in each: three (grey), two (orange) or one (green). The blue portion includes domain families with no clan

assigned. The number for a particular domain presented in each chromosome is denoted in brackets, as (N/M) corresponding N and M respectively to CI and CII. Details for only flavin binding domains are shown in **Figure 4.3**. **(B)** Clans involved in flavin cofactor binding according to the flavin type. **(C)** Distribution of flavin binding clans by chromosomal location.

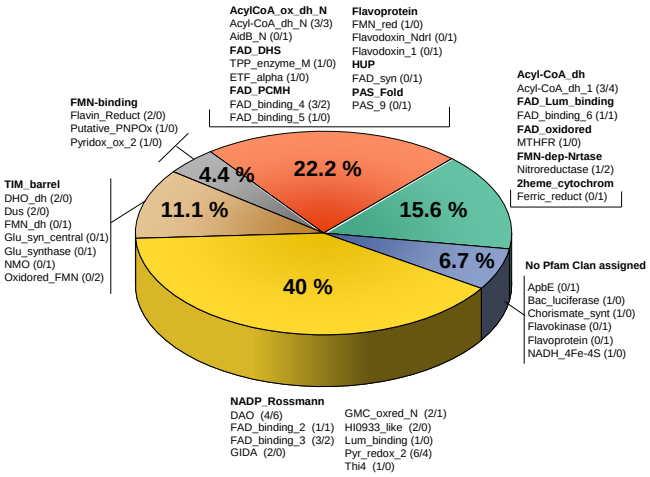

Figure 4.3: Pie chart of the clans and domains contributing to bind flavins in the *B. ovis* flavoproteome. Clan names are highlighted in bold. Overall percentages are calculated based on the number of domains directly contributing to bind flavins in each clan. NADP_Rossman, TIM_barrel and FMN-binding clans are shown individually, while the rest are grouped attending to the number of families found in each: two (orange) or one (green). The blue portion includes domain families with no clan assigned. The number for a particular domain presented in each chromosome is denoted in brackets, as (N/M) corresponding N and M respectively to CI and CII.

Clans AcylCoA_ox_dh_N and AcylCoA_dh appear in seven FAD dependent acyl-CoA dehydrogenases. Normally, they fold in Acyl-CoA_dh_N (in one case replaced by Aidb_N) and Acyl-CoA_dh_1 domains and use connecting Acyl-Coa_dh_M and/or ending Acyl-CoA_dh_C domains. The six flavoproteins of the FAD_PCMH clan bind FAD, five and one use respectively FAD_binding_4 and FAD_binding_5 domains (completed with FAD-oxidase_C, CO_deh_flav_C or murB_C domains).

The FMN-binding clan is predicted in four flavoproteins that bind FMN with Putative_PNPOx (with PNP_phzG_C domain), Flavin_Reduct and Pyridox_ox_2 domains. Three also FMN binding flavoproteins fall in each of the FMN-dep-Nrtase and Flavoprotein clans. The firsts have nitroreductase domains, presumably involved in reduction of nitrogen-containing compounds, whereas those in the second clan belong each to a different family: FMN_red (NAD(P)H-quinone dehydrogenase), Flavodoxin_NdrI (electron transport NrdI protein) and Flavodoxin_1 (assimilatory sulphite reductase alpha component). This subunit of assimilatory sulphite reductase contains also a FAD_binding_6 domain, of the

FAD_Lum_binding clan, that binds FAD. A FAD_binding_6 domain is also present in ferredoxin-$NADP^+$ reductase. The assimilatory sulphite reductase alpha component in *B. ovis* shows noticeable features (Figure 4.4B). In the current genome assembly, it is annotated as codified by four sequential genes (BOV_RS11420, BOV_RS11425, BOV_RS11430, and BOV_RS11435), which would make up to four protein subunits (WP_006015252.1, WP_006015255.1, WP_006015257.1 and WP_006015259.1), whereas in other *Brucella* all these components are encoded by either one or two genes (Figure 4.4B). Its central Flavodoxin_1 and FAD_binding_6 domains allocate FMN and FAD, respectively, whereas the additional domains will attach the protein to the membrane and bind the NADPH coenzyme. The functional protein will be complemented with a sulphite reductase (NADPH) haemoprotein beta-component (ABQ61351) codified in CI.

Only two *B. ovis* flavoproteins are members of the FADS_DHS clan. They adopt a Rossmann fold similar to clan NADP_Rossmann, but are distinguished since the FAD cofactor binds in the opposite direction. It is represented by the TPP_enzyme_M domain in the catalytic subunit of a synthase and ETF_alpha domain in the electron transferring flavoprotein alpha subunit (ETFa). Four clans are only found once in the *B. ovis* flavoproteome: the FAD_oxidored in the FAD dependent MTHFR domain of methylenetetrahydrofolate reductase; the PAS_Fold with the PAS_9 domain that binds FMN in the blue-light-activated histidine kinase; the HUP that binds FMN/FAD in the FAD_syn domain of bifunctional FAD synthase/flavokinase (FADS); and the 2heme_cytochrom binding FMN at the Ferric_reduct domain of MsrQ subunit of peptide-methionine (S)-S-oxide reductase (Msr).

Six domains not assigned to any clan also bind flavins in *B. ovis* flavoproteins: the Flavokinase domain binds RF/FMN in bifunctional FADS; the Bac_luciferase domain binds FMN in bacterial luciferase; the Chorismate_synt domain binds FMN in chorismate synthase; the NADH_4Fe_4S domain binds FMN at the NADH-quinone oxidoreductase subunit F; the ApbE domain binds FAD in the FAD:protein FMN transferase; and the Flavoprotein domain binds FMN in Coenzyme A biosynthesis bifunctional protein.

In agreement with the use of FAD-dependent enzymes for novel or unusual functions requiring the adaptation of already existing topologies or new structural designs (Macheroux et al., 2011), the less populated clans and domains in the *B. ovis* flavoproteome mainly contribute to FMN binding.

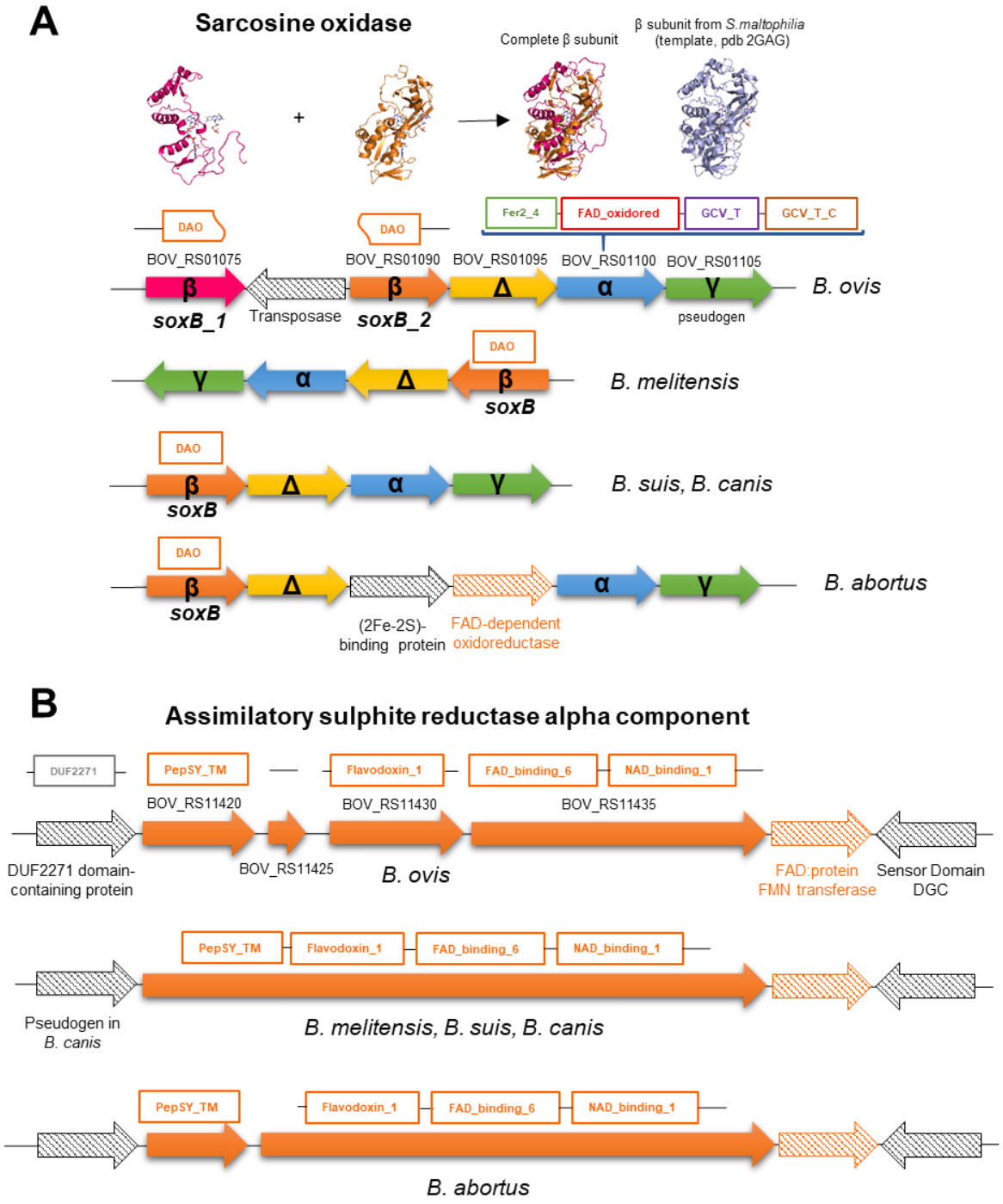

Figure 4.4. Genomic context for SoxB and sulphite reductase component genes in selected *Brucella* species. (A) Organisation of genes encoding different subunits of the membrane bound sarcosine oxidase subunit B (SoxB). In *B. ovis*, two genes soxB_1 and soxB_2, separated by a IS5 transposase gene, encode together the full length of the SoxB protein. On the top, the homology structural models of SoxB_1 and SoxB_2 proteins and their superposition on the SoxB from *Stenotrophomonas maltophilia* (2GAG_B) are shown. **(B)** Organisation of genes encoding for the assimilatory sulphite reductase alpha component. In both panels, gene senses are denoted by arrows and *B. ovis* gene codes are written next to the corresponding arrow. Structural Pfam domain families for subunits contributing to flavin binding are shown on the top of genes.

From the 78 identified candidates, only two flavoproteins are envisaged to bind flavins covalently. One is the succinate dehydrogenase flavoprotein subunit (SdhA), where

covalent binding through H60 (in the conserved FPTRSHTV motif) to the FAD isoalloxazine (C8M) is predicted, as observed for H45, H56 or H79 in *E. coli* (PDB 2WDQ), *Gallus gallus* (PDB 2H88) or *Ascaris suum* (PDB 4YSX) proteins (Figure 4.5A). Covalent attachment of FAD to SdhA is essential for Sdh function in other bacteria (McNeil et al., 2014). Covalent linking to FMN (C8M) is also predicted in the sarcosine oxidase beta subunit through H198 (H173 in the *Stenotrophomonas maltophilia* protein (PDB 2GAG)), sitting FMN at the alpha and beta subunits interface (Figure 4.5B). Sequence and structural modelling also point to blue-light-activated histidine kinase as undergoing photochemistry with cysteinyl-flavin adduct formation between C69 and the isoalloxazine C4a of FMN (Figure 4.5C). Altogether these observations point out that the cofactor is non-covalently bound in most *B. ovis* flavoproteins.

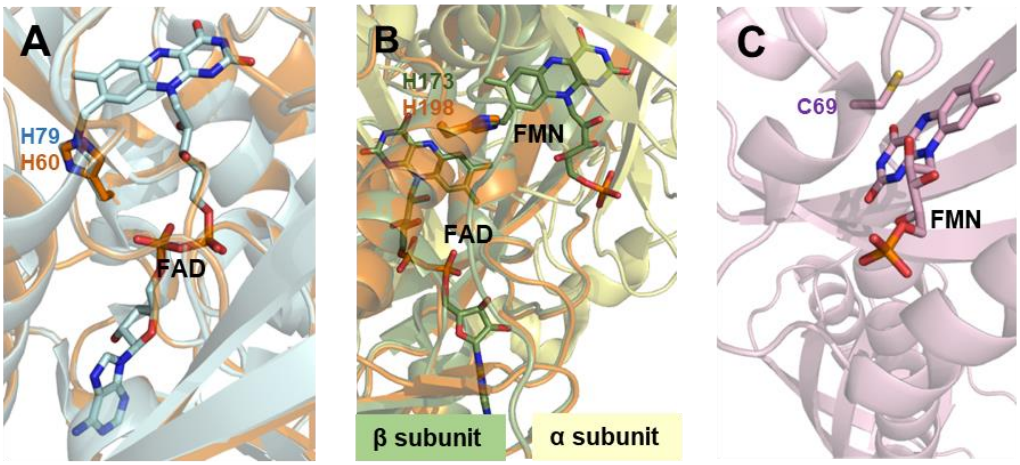

Template	p-value	Score	uGDT/GDT	uSeqID/SeqID
4YSX_A	$2.8e^{-16}$	560	519/85	373/61
2GAG_B	$2.4e^{-13}$	376	358/83	235/55

Figure 4.5. Structural models for *B. ovis* enzymes predicted to covalently bind the flavin cofactor. (A) succinate dehydrogenase flavoprotein subunit and **(B)** sarcosine oxidase beta subunit models (orange) for the covalent linking to C8M of flavins in *B. ovis*. Homology models were built using as templates the structures of *A. suum* (PDB 4YSX_A, light blue in (A)) and *S. maltophilia* (2GAG, green in (B)), respectively, and the RaptorX server. Parameters predicting models quality are summarized below the figure. **(C)** Structure of the blue-light-activated histidine kinase from *B. abortus* 2308 (6PPS), with 100% identity to the *B. ovis* enzyme. Relevant residues as well as cofactors belonging to the templates are shown in sticks. Images generated with PyMol (DeLano, 2002).

4.3.3 Enzymatic classification and metabolic functions of *B. ovis* flavoproteins

Most proteins of the *B. ovis* flavoproteome (76 out of 78) are flavoenzymes. We assigned enzymatic classes to all of them and full EC codes to nearly 70% (Table 4.6, Figures 4.6-4.8). The rest (30%) might have either divergent mechanisms from known flavoproteins

or still not reported full functions. Flavoenzymes fall into the oxidoreductases (EC 1.) (86%, 66 out of 76), transferases (EC 2.) (9.2%, 7 out of 76, one of them with two transferase activities), lyases (EC 4.) (2.6%, 2 out of 76), and translocases (EC 7.) (1.3%, 1 out of 76) classes (Tables 4.2, 4.3 and 4.7; Figure 4.9A). Therefore, most of *B. ovis* flavoenzymes participate in redox processes, in agreement with previous reported classifications (Macheroux et al., 2011; Schall et al., 2020).

Two flavoproteins are predicted not holding catalytic activity by themselves: ETFa and NrdI. The ETFa together with the beta subunit (ETFb) specifically transfer electrons from different dehydrogenases to the respiratory electron transfer chain (ETC) via the electron transferring flavoprotein-ubiquinone oxidoreductase (ETF-QO). Noticeably, etfA and etfB encoding genes in *B. ovis* sit next to a gene encoding for a $NADP^+$ dependent butyryl-CoA dehydrogenase (Table 4.8). This suggests that these three proteins might form a BCD bifurcating complex responsible for crotonyl-CoA reduction during butanol production. Homologues of *Clostridium acetobutylicum* have the same organization (Yoo et al., 2015), and ETF proteins are also pointed as potential targets for the treatment of some bacterial infections (Stietz et al., 2017). NrdI is a flavodoxin-like electron-transport protein with potential analogous functions to ferredoxins. It belongs to the core proteome of *Brucella* but is hardly populated in the evaluated alpha-proteobacteria (Table 4.7).

Table 4.6. Metabolic functions and virulence potential envisaged for flavoproteins and flavoenzymes from *B. ovis* ATCC 25840. Search for metabolic functions and virulence prediction carried out as indicated in the methods section.

EC	Protein	Protein Code	Metabolic Pathway	Pathway Category	VirulentPred[b]	VICMpred function[c]
1.1.5.3	Glycerol-3-phosphate dehydrogenase	ABQ60174.1	Degradation of sugar alcohols	Carbohydrate metabolism	Non-virulent	Metabolism
1.1.1.402	D-erythritol 1-phosphate dehydrogenase	ABQ62056.1	Degradation of sugar alcohols	Carbohydrate metabolism. **Virulence factor.**	Non-virulent	Metabolism
1.1.2.3	L-lactate dehydrogenase (cytochrome c o b2)	ABQ62635.1	Lactate fermentation	Fermentation and other catabolism	Non-virulent	Metabolism
1.1.3.8	***Potential L-gulonolactone oxidase FAD-binding oxygen oxidoreductase***	ABQ62001.1	Unclear function. Potentially involved in ascorbate metabolism	Potential role in nucleotide and cofactor metabolism	Non-virulent	Cellular Process
1.1.99.1	Choline dehydrogenase (Glucose-methanol-choline GMC family)	ABQ61350.1	Glycine betaine biosynthesis. Metabolism of disaccharides	Amino acid Metabolism. Carbohydrate metabolism	Non-virulent	**Virulence Factor**
1.1.99.1	Choline dehydrogenase (GMC family)	ABQ60630.1			**Virulent**	Cellular Process
1.1.99.1	Choline dehydrogenase (GMC family, membrane bound)	ABQ62100.1			Non-virulent	Metabolism / **Potential Virulence Factor**
1.1.99.2	Predicted L-2-hydroxyglutarate dehydrogenase	ABQ62911.1	Glutamate and glutamine metabolism	Amino acid metabolism	**Virulent**	Metabolism
1.1.99.14	Glycolate dehydrogenase GlcD subunit	ABQ62237.1	Glycolate and Glyoxylate degradation	Central and energy metabolism	Non-virulent	Metabolism
1.1.-.-	***Potential FAD-binding oxygen oxidoreductase (glcE?)***	ABQ60928.1	It might work with GlcD	Probably central and energy metabolism	Non-virulent	Metabolism
1.1-.-	***Potential FAD-binding oxygen oxidoreductase (glcE?)***	ABQ61939.1	It might work with GlcD	Probably central and energy metabolism	Non-virulent	Metabolism
1.3.1.1/2	NADH dependent Dihydropyrimidine dehydrogenase subunit PreA	ABQ60560.1	Pyrimidine and alanine metabolism	Nucleotide and cofactor metabolism. Amino acid metabolism	Non-virulent	Cellular Process / Metabolism
	NADH dependent Dihydropyrimidine dehydrogenase subunit PreT	ABQ61103.1			Non-virulent	Cellular Process / Metabolism
1.3.5.2	PyrD dihydroorotate dehydrogenase 2 (quinone)	ABQ61413.1	Pyrimidine Metabolism	Nucleotide and cofactor metabolism	Non-virulent	Metabolism
1.3.1.88	tRNA dihydrouridine synthase B	ABQ61416.1	Dihydrouridine modification of tRNA	Modification of cytoplasmic tRNAs	Non-virulent	Metabolism
1.3.1.91	tRNA dihydrouridine20/20a synthase	ABQ61966.1			Non-virulent	Metabolism
1.3.1.98	UDP-N-acetylmuramate dehydrogenase	ABQ61769.1	Peptidoglycan Biosynthesis. Cell wall biogenesis	Amino acid metabolism	**Virulent**	**Virulence Factor**
1.3.1.-/1.7.1.B1	Predicted alkene reductase: N-ethylmaleimide reductase, Glycerol trinitrate reductase or xenobiotic reductase B	ABQ62490.1	Degradation of toxic compounds	Xenobiotic metabolism and secondary metabolism	Non-virulent	Metabolism
1.3.5.1	Succinate dehydrogenase flavoprotein subunit	ABQ61077.1	Citric acid and methylaspartate cycles. Propionate fermentation	Fermentation and other catabolism. Central and energy metabolism. **Virulence factor**	Non-virulent	**Virulence Factor**
1.3.8.4	Isovaleryl-CoA dehydrogenase	ABQ60382.1	Leucine metabolism	Amino acid metabolism	**Virulent**	Cellular Process
1.3.8.-	Short Chain Acyl-CoA dehydrogenase	ABQ60180.1	Lipid metabolism. Butanone fermentation. Alanine, glutamate and glutamine metabolism. Ethylmalonyl-CoA pathway	Lipid metabolism. Fermentation and other catabolism. Amino acid metabolism. Central and energy metabolism	Non-virulent	Cellular Process
1.3.8.1	Acyl-CoA dehydrogenase	ABQ62576.1	Bacterial resistance during alkylation stress/Cell division/ AidB domains	Lipid and steroid metabolism. Resistance during alkylation stress. Defence from Host	**Virulent**	Metabolism
1.3.8.-	Acyl-CoA dehydrogenase	ABQ61585.1	Lipid metabolism. Butanone fermentation. Valine, alanine, tryptophan, glutamate and glutamine metabolisms. Ethylmalonyl-CoA pathway. Phenyl acetate degradation (aerobic). Cyclohexanol degradation. Adipate degradation	Lipid metabolism, Fermentation and other catabolism, Amino acid metabolism, Central and energy metabolism.	Non-virulent	Metabolism
1.3.8.-	Acyl-CoA dehydrogenase	ABQ62784.1			Non-virulent	**Virulence Factor**
1.3.8.-	Acyl-CoA dehydrogenase	ABQ62889.1			Non-virulent	**Virulence Factor**
1.3.8.-	Acyl-CoA dehydrogenase	ABQ62082.1			Non-virulent	Metabolism

1.3.99.-	Predicted KsdD-like steroid dehydrogenase	ABQ62061.1	Androgen and steroid metabolism	Lipid metabolism	Non-virulent	Metabolism
1.4.1.13	Glutamate synthase large subunit (alpha subunit)	ABQ61996.1	Glutamate and glutamine metabolism	Amino acid metabolism	Non-virulent	Metabolism
	Glutamate synthase small subunit (beta subunit)	ABQ62546.1				
1.4.3.5	Pyridoxamine 5'-phosphate oxidase	ABQ60142.1	Vitamin B6 metabolism	Nucleotide and cofactor metabolism	Non-virulent	Cellular Process / Metabolism
1.4.-.-	***Pyridoxamine 5'-phosphate oxidase family protein***	ABQ61684.1	Unclear function	Unclear function	**Virulent**	Cellular Process / Metabolism
1.4.3.19	Glycine oxidase ThiO	ABQ60316.1	Thiamine metabolism	Amino acid metabolism	Non-virulent	Metabolism
1.4.3.-	***Potential Aminoacetone oxidase family FAD-binding enzyme/ NAD(P)/FAD-dependent dehydrogenase***	ABQ60616.1	Potential role in amino acids and NAD metabolism	Amino acid metabolism. Nucleotide and cofactor metabolism	Non-virulent	**Virulence Factor**
1.4.3.-	***Potential Aminoacetone oxidase family FAD-binding enzyme/ NAD(P)/FAD-dependent dehydrogenase***	ABQ60524.1	Potential role in amino acids and NAD metabolism	Amino acid metabolism. Nucleotide and cofactor metabolism	Non-virulent	Metabolism
1.4.99.-	Predicted D-amino acid dehydrogenase small subunit	ABQ61937.1	Potential role in oxidative deamination of D-amino acids	Amino acid metabolism	Non-virulent	**Virulence Factor**
1.4.99.-	D-amino acid dehydrogenase	ABQ62278.1			**Virulent**	Metabolism / **Potential Virulence Factor**
1.4.-.-	Predicted D-amino acid dehydrogenase	ABQ62519.1			**Virulent**	Cellular Process
1.4.-.-	Predicted D-amino acid dehydrogenase	ABQ62405.1			Non-virulent	Metabolism
1.5.1.20	Methylenetetrahydrofolate reductase	ABQ60279.1	Tetrahydrofolate metabolism	Nucleotide and cofactor metabolism	Non-virulent	Cellular Process / Metabolism
1.5.1.-	***Flavin reductase domain containing protein***	ABQ60228.1	Flavin metabolism	Nucleotide and cofactor metabolism	**Virulent**	Cellular Process / Metabolism
1.5.3.1	Sarcosine oxidase beta subunit	ABQ60177.1	Creatine degradation	Fermentation and other catabolism	**Virulent**	Cellular Process / **Virulence Factor**
		ABQ61310.1				
	Sarcosine oxidase alpha subunit	ABQ61036.1				
1.5.3.1	Predicted monomeric Sarcosine oxidase	ABQ62932.1	Creatine degradation	Fermentation and other catabolism	Non-virulent	Cellular Process / Metabolism
1.5.5.1	Electron transferring flavoprotein-ubiquinone oxidoreductase (ETF-QO)	ABQ61337.1	Oxidative phosphorylation	Central and energy metabolism	Non-virulent	Metabolism
1.6.5.2	WrpA type FMN-dependent NADH:quinone oxidoreductase	ABQ60884.1	Potential role in protection from stress damage	Defence from Host	Non-virulent	Metabolism
1.6.99.1	***NADPH dehydrogenase (Old yellow enzyme)***	ABQ62422.1	Unclear function	Unclear function	Non-virulent	Cellular Process
1.6.-.-	***NADH dehydrogenase***	ABQ62704.1	Unclear function	Unclear function	Non-virulent	Metabolism
1.7.-.-	***Predicted NAD(P)H nitroreductase***	ABQ60834.1	Oxidation-reduction of diverse nitrogen containing compounds	Nitrogen metabolism	Non-virulent	Metabolism
1.8.1.2	Assimilatory sulphite reductase (NADPH) alpha component cluster	WP_006015252.1	Sulphate reduction	Amino acid metabolism	**Virulent**	Cellular Process / Metabolism
		WP_006015255.1				
		WP_006015257.1				
		WP_006015259.1				
1.8.1.4	Dihydrolipoyl dehydrogenase (lpdA-1)	ABQ62466.1	Oxidative decarboxylation of pyruvate. Citric acid cycle. Glycine metabolism. Acetyl-CoA biosynthesis	Central and energy metabolism. Amino acid metabolism	Non-virulent	Cellular Process
1.8.1.4	Dihydrolipoyl dehydrogenase (lpdA-2)	ABQ60398.1			Non-virulent	Metabolism
1.8.1.4	Dihydrolipoyl dehydrogenase (lpdA-3)	ABQ61458.1			Non-virulent	Metabolism
1.8.1.7	Glutathione-disulphide reductase	ABQ61016.1	Thiol redox pathway. Glutathione metabolism	Control the redox state of the cell	Non-virulent	Cellular Process
1.8.1.9	Thioredoxin-disulphide reductase	ABQ60123.1	Thiol thioredoxin related pathway. Reduction of cytoplasmic enzymes	Control the redox state of the cell	Non-virulent	Metabolism
1.8.1.9	Predicted thioredoxin-disulphide reductase	ABQ61134.1		Control the redox state of the cell	Non-virulent	Metabolism
1.8.5.B1	Peptide-methionine (S)-S-oxide reductase (quinone) (Msr). MsrP catalytic subunit. MsrQ heme-binding subunit	ABQ62365.1	Methionine reparation of periplasmic proteins	Protection from stress damage. Defence from host	**Virulent**	Cellular Process /Metabolism
		ABQ62343				
1.13.11.32	Nitronate monooxygenase (formerly 2-nitropropane dioxygenase NPD)	ABQ62537.1	Alkylnitronates degradation	Nitrogen metabolism	Non-virulent	Metabolism

1.13.11.79	Predicted aerobic 5,6-dimethylbenzimidazole synthase (BluB)	ABQ62404.1	Vitamin B12 metabolism	Nucleotide and cofactor metabolism	**Virulent**	Metabolism
1.14.13.1	Predicted Salicylate hydroxylase	ABQ60137.1	Phenol degradation	Xenobiotic metabolism and secondary metabolism	Non-virulent	Metabolism
1.14.13.1	Predicted Salicylate hydroxylase	ABQ60978.1	Phenol degradation	Xenobiotic metabolism and secondary metabolism	**Virulent**	**Virulence Factor**
1.14.13.-	Predicted UbiH/COQ6 monooxygenase family	ABQ60166.1	Ubiquinone biosynthesis	Central and energy metabolism	Non-virulent	**Virulence Factor**
1.14.13. -	UbiH/UbiF family hydroxylase	ABQ62553.1	Ubiquinone biosynthesis	Central and energy metabolism	Non-virulent	**Virulence Factor**
1.14.13.2	4-hydroxybenzoate 3-monooxygenase	ABQ62030.1	4-hydroxymandelate degradation	Fermentation and other catabolism	Non-virulent	Metabolism
1.14.14.3	Bacterial luciferase	ABQ60348.1	Bioluminescence	Bacterial luminescence	Non-virulent	Cellular Process
1.16.1.4	Cob(II)alamin reductase	ABQ60249.1	Vitamin B12 metabolism	Nucleotide and cofactor metabolism	**Virulent**	Metabolism
1.17.1.4	Xanthine dehydrogenase, small subunit	ABQ61298.1	Purine metabolism	Nucleotide and cofactor metabolism	Non-virulent	Cellular Process / **Potential Virulence factor**
1.18.1.3-5	Predicted Ferredoxin/rubredoxin/ putidaredoxin NAD^+ Reductase	ABQ62051.1	Protection from ROS stress damage	Defence from host	Non-virulent	**Virulence Factor**
1.18.1.2	Ferredoxin-$NADP^+$ reductase	ABQ61707.1	Protection from ROS stress damage	Defence from host	Non-virulent	Metabolism
1.-.-.-	***Predicted nitroreductase family protein***	ABQ62091.1	Reduction of nitrogen containing compounds.	Nitrogen metabolism	Non-virulent	Metabolism
2.1.1.74	Methylenetetrahydrofolate-tRNA-(uracil54-C5-)-methyltransferase NAD(P)H oxidase	ABQ61275.1	Post-translationally modification of tRNA	Modification of cytoplasmic tRNAs	Non-virulent	**Virulence Factor**
2.1.1.229	tRNA (carboxymethyluridine34-5-O)-methyltransferase	ABQ60378.1	Post-translationally modification of tRNA	Modification of cytoplasmic tRNAs	Non-virulent	**Virulence Factor**
2.2.1.6	Acetolactate synthase 3 catalytic subunit	ABQ60081.1	Acetoin degradation, valine and isoleucine metabolism	Fermentation and other catabolism. Amino acid metabolism	Non-virulent	Metabolism
2.5.1.9	Riboflavin synthase alpha subunit	ABQ60518	Flavin biosynthesis	Nucleotide and cofactor metabolism	Non-virulent	Cellular Process / Metabolism
2.7.7.2 2.7.1.26	Bifunctional riboflavin kinase/FAD synthase	ABQ62831.1	Flavin biosynthesis	Nucleotide and cofactor metabolism	Non-virulent	Metabolism
2.7.1.180	FAD:protein FMN transferase	ABQ62066.1	Flavin transfer	Maturation of other enzymes	Non-virulent	Metabolism
2.7.13.3	Blue-light-activated histidine kinase	ABQ62113	Light activated phosphorylation	Signal transduction. **Virulence factor**	Non-virulent	Cellular Process / **Potential Virulence Factor**
4.1.1.36 6.3.2.5	Coenzyme A biosynthesis bifunctional protein	ABQ62036.1	Coenzyme A metabolism	Nucleotide and cofactor metabolism	Non-virulent	Metabolism
4.2.3.5	Chorismate synthase	ABQ60200.1	Chorismate metabolism	Amino acid metabolism	Non-virulent	Cellular Process
7.1.1.2	NADH-quinone oxidoreductase subunit F (H^+ translocating)	ABQ60521.1	Oxidative phosphorylation	Central and energy metabolism	Non-virulent	Cellular Process
	Electron transferring flavoprotein alpha subunit (ETFa)	ABQ61011.1	Oxidative phosphorylation	Central and energy metabolism	Non-virulent	Cellular Process / Metabolism
	Electron transferring flavoprotein beta subunit (ETFb)	ABQ60428.1				
	Protein NrdI	ABQ62891.1	Electron exchange, nucleotide transport and metabolism	Nucleotide and cofactor metabolism	**Virulent**	Cellular Process

[a] Shown in bold black and italics those candidates for which a clear function cannot be depicted.

[b] VirulentPred was used to predict potential virulent proteins based on amino-acid compositions, similarity, position specific scoring matrix, dipeptide composition, higher order dipeptide composition and bi-layer cascade Support Vector Machine module. When one of these approaches produced a match, the protein was label as virulent. Positive virulence highlighted in bold.

[c] The pattern based score of VICMpred was used to classify potential functions for proteins among cellular process, metabolism, signalling or virulence factor. Positive virulence highlighted in bold.

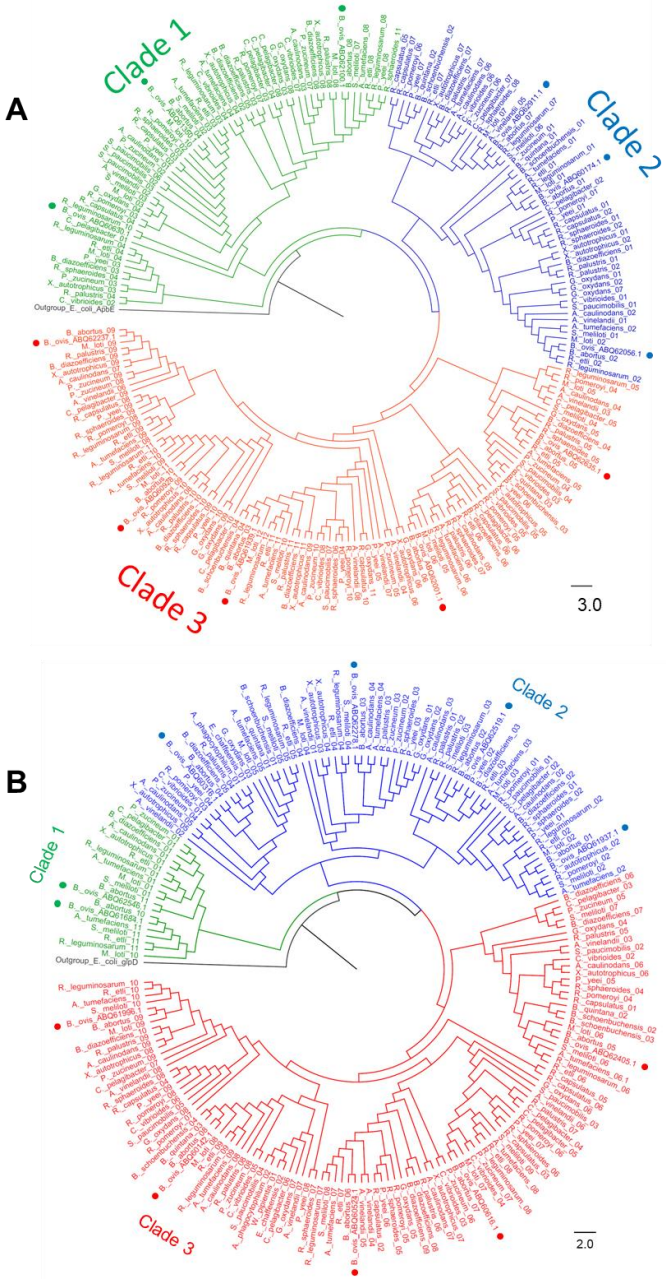

Figure 4.6. Phylogeny of *B. ovis* flavoproteins of subclasses (A) EC 1.1. and (B) EC 1.4. within alpha-proteobacteria. (A) Subclass EC 1.1. distributes in three phylogenetic clades (bootstrap > 92). Clade 1 clusters (bootstrap >90) three proteins of the GMC family, ABQ61350.1, ABQ60630.1 and ABQ62100.1 (EC. 1.1.99.1). Clade 2 groups (bootstrap >95) three proteins folding in DAO domains, ABQ60174.1, ABQ62056.1 and ABQ62911.1. Clade 3 clusters five proteins distributed in monophyletic branches ABQ61939.1, ABQ62001.1, ABQ62237.1, ABQ60928.1 and ABQ62635.1 with diverse functions (bootstrap >85). **(B)** Flavoenzymes of subclass EC 1.4. distribute in three clades (bootstrap > 90). Clade 1 includes ABQ61684.1 and ABQ62546.1, present in a reduced number of alpha-proteobacteria. Clade 2 comprises four proteins distributed in two subclades (bootstrap >88). ABQ60316.1 clusters separately (bootstrap >92), while ABQ62278.1, ABQ62519.1 and ABQ61937.1 are in the same subclade (bootstrap >77). Clade 3 clusters ABQ62405.1 in a divergent subclade (bootstrap >80), and ABQ60142.1, ABQ60524.1, ABQ60616.1 and ABQ61996.1, separately in four branches of other subclade (bootstrap > 80). Phylogenetic cladograms include 222 sequences of subclass EC 1.1. and 198 sequences of subclass EC 1.4. from *B. ovis* ATCC 25840, *B. abortus* 2308, and 26 alpha-proteobacteria related species. *E. coli* ApbE and *E. coli* GlpD were selected as outgroup in (A) and (B), respectively, to highlight the clear evolutionary separation between clusters. The likelihood aLRT (approximate likelihood-ratio test) statistical test and a bootstrap value of 100 were used.

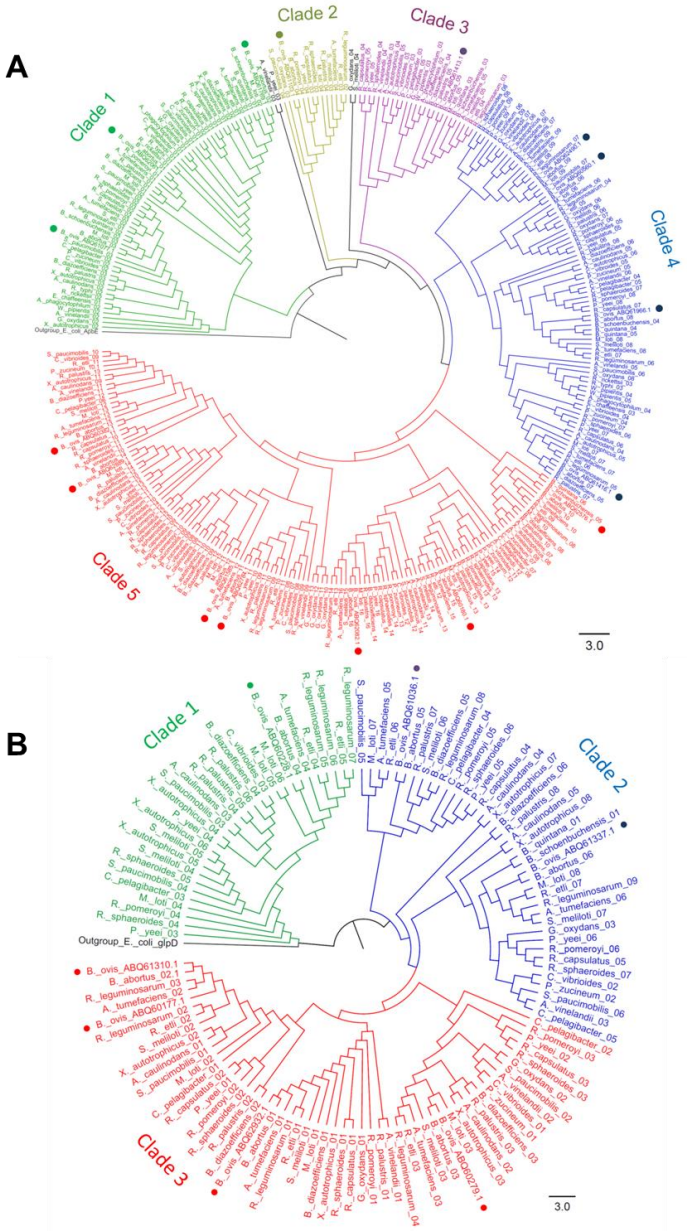

Figure 4.7. Phylogeny of *B. ovis* flavoproteins from subclasses (A) EC 1.3 and (B) EC 1.5. within alpha-proteobacteria. (A) Flavoenzymes of subclass EC 1.3. separate in five clades and are relatively conserved regarding evolution. Clade 1 groups ABQ62061.1 and ABQ61769.1 together and separately ABQ61077.1 (bootstrap >98). Clade 2 (bootstrap >73) and clade 3 (bootstrap >70) contain, respectively, ABQ61103.1 and ABQ61413.1, being these proteins the less conserved within studied species. Clade 4 distributes in four subgroups (bootstrap >95) including ABQ62490.1, ABQ60560.1, ABQ61416.1 and ABQ61966.1. Clade 5 includes seven ACAD homologues distributed in four subclades (bootstrap >90). The most divergent contains the entry ABQ62576.1 (bootstrap >98). **(B)** Flavoreductases of the subclass E.C 1.5 distribute in three clades (bootstrap >90). Clade 1 is the most divergent (bootstrap >98) and contains ABQ60228.1. Clade 2 separates in two branches (bootstrap >90) ABQ61036.1 and ABQ61337.1 homologues. Clade 3 distributes in two subclades (bootstrap >85). One subclade includes ABQ61310.1 and ABQ60177.1 grouped in the same branch and ABQ62932.1 in a separate branch, whereas the protein ABQ60279.1 clusters separately. Phylogenetic cladograms include 319 sequences of subclass EC 1.3. and 108 sequences of subclass EC 1.5. from *B. ovis* ATCC 25480, *B. abortus* 2308, and 26 alpha-proteobacteria related species. *E. coli* ApbE and *E. coli* GlpD were selected as outgroup in (A) and (B), respectively, to highlight the clear evolutionary separation between clusters. The likelihood aLRT (approximate likelihood-ratio test) statistical test and a bootstrap value of 100 were used.

4.3.4 *B. ovis* flavo-oxidoreductases participate in a large variety of metabolic pathways

Most *B. ovis* flavoenzymes are oxidoreductases and particularly belong to subclasses that use alcohols (EC 1.1.), CH-CH (EC 1.3.), CH-NH2 (EC 1.4.), CH-NH (EC 1.5.) or sulphur (EC 1.8.) groups as hydrogen or electron donors, as well as paired donors with incorporation or reduction of molecular oxygen (EC 1.14.). Some use as donors NAD(P)H (EC 1.6.), metals (EC 1.16) or nitrogenous compounds (various EC 1.- subclasses) (Tables 4.2, 4.3 and 4.6, Figure 4.9A).

The subclass alcohol flavo-oxidoreductase (Figure 4.6A) includes three enzymes of the GMC family (EC. 1.1.99.1). This large and diverse protein family shares structural fold and reaction mechanisms, with substrates ranging from sugars and alcohols to cholesterol and choline, and are usually related to the metabolism of methyl groups through betaine (Tables 4.2, 4.3 and 4.6). They are present in yeasts, bacteria, insects and filamentous fungi, being the latest use for biomass utilization, biosensors or food industry (Sützl et al., 2019). This subclass has also two alcohol oxidases that share 55% identity and phylogenetically cluster together (bootstrap >98) (Figure 4.6A). One is a canonical glycerol-3-phosphate dehydrogenase (GlpD) (EC 1.1.5.3, ABQ60174.1), and the other is envisaged erythritol oxidation activity (EC 1.1.1.402, ABQ62056.1) from gene context (BOV_RS14450, eryB) and phylogenetic analysis (Tables 4.2, 4.3 and 4.6, Figure 4.6A).

They likely supplement electrons for aerobic oxidative phosphorylation (OXPHOS) at the central junction of glycolysis, respiration and phospholipid biosynthesis, being essential for aerobic growth on glycerol-like molecules (Yeh et al., 2008). Noticeably, erythritol has a growth promoting effect on intracellular *Brucella* pathogens (Anderson & Smith, 1965; Meyer, 1967). GlpD is in the *Brucella* core proteome, but EryB lacks in some *Brucella* (Tables 4.7, Figure 4.6A). These observations highlight the importance of the shuttle of electrons in the *Brucella* metabolism. Other enzymes in this subclass are oxygen oxidoreductases. One is the GlcD subunit of glycolate dehydrogenase that catalyzes oxidation of glycolate and D-lactate, respectively, to glyoxylate and pyruvate (EC 1.1.99.2), a key function in microbial redox oxidative metabolisms. Glycolate dehydrogenase is usually built by several subunits, including a GlcE one. In *B. ovis* the gene upstream of glcD is a glcE pseudogene (Table 4.9). Nonetheless, the oxygen oxidoreductases ABQ60928.1 and ABQ61939.1 have similar features to GlcE and not precise function, so they might replace for the non-functional GlcE protein (Table 4.3 and 4.7). The protein ABQ62001.1 (EC 1.1.3.8) is also proposed as oxygen oxidoreductase. It has a non-classified long-C-

terminal (Table 4.3) and its closer available structural homologue is decaprenyl-phosphoryl-β-D-ribofuranose-2-oxidoreductase from *Mycobacterium smegmatis*, an essential enzyme in cell wall biosynthesis (Trefzer et al., 2012). This subclass also includes the hydroxyglutarate dehydrogenase (EC 1.1.99.2) and the FMN-dependent L-lactate dehydrogenase (EC 1.1.2.3), both in the core proteome of *Brucella* (Table 4.7). Altogether, alcohol flavo-oxidoreductases contribute to the energetic intake metabolism for *B. ovis* survival.

The subclass EC 1.3 includes seven acyl-CoA dehydrogenases (ACAD) (EC 1.3.8.-) widely represented in *Brucella* but not within alpha-proteobacteria (Figure 4.7A, Table 4.7). The most divergent ACAD (ABQ62576.1) has an AidB domain instead of an Acyl-CoA_dh_N one, and is 100% identical to a protein from *B. melitensis* whose 3D structure is available (PDB 5EZ3, Table 4.5, Figure 4.1). It has all features of *B. abortus* and *E. coli* homologues involved in the destruction of alkylating agents, suggesting it will provide resistance during alkylation stress as well as in cell division (Dotreppe et al., 2011). The ACAD annotated as isovaleryl-CoA dehydrogenase (ABQ60382.1) in UniProtKB might participate in the catabolism of branched chain amino acids. The other five ACADs could participate in fatty acid β-oxidation (Tables 4.2, 4.3 and 4.6), suggesting the use for *B. ovis* of lipids, probably recruited from host cells, as carbon sources (Macheroux et al., 2011). This subclass also includes the SdhA subunit of succinate dehydrogenase (Sdh) (EC 1.3.5.1) and the UDP-N-acetylmuramate dehydrogenase (MurB) (EC 1.3.1.98), two proteins that are in the core proteome of *Brucella* and conserved in all evaluated alpha-proteobacteria (Figure 4.7A, Table 4.7). The Sdh complex is built by different subunits (Table 4.8), localizes in the membrane of many bacteria, and catalyzes the oxidation of succinate to fumarate. It uses membrane quinone as electron acceptor and is the only enzyme linking the tricarboxylic acid cycle and the ETC (Kuo et al., 2018). MurB catalyzes the NADPH dependent reduction of UDP-N-acetylglucosamine-enolpyruvate to UDP-N-acetylmuramic acid (EC 1.3.1.98) and participates in the biosynthesis of peptidoglycan building blocks (Eniyan et al., 2018). Subclass EC 1.3 also includes two subunits of the dihydropyrimidine dehydrogenase (EC 1.3.1.1) involved in the β-alanine metabolism, the biosynthesis of pantothenate and CoA, and the pyrimidine nucleotide metabolism; two enzymes involved in the modification of cytoplasmic tRNAs (EC 1.3.1.88, 1.3.1.91); one PyrD dihydroorotate dehydrogenase (EC 1.3.5.2) involved in nucleotide metabolism; and finally one alkene reductase (EC 1.3.1.-/1.7.1.B1) and one KsdD-like steroid dehydrogenase (EC 1.3.99.-) that might, respectively, contribute to toxic compounds degradation and oxidation/dehydrogenation of ketosteroids.

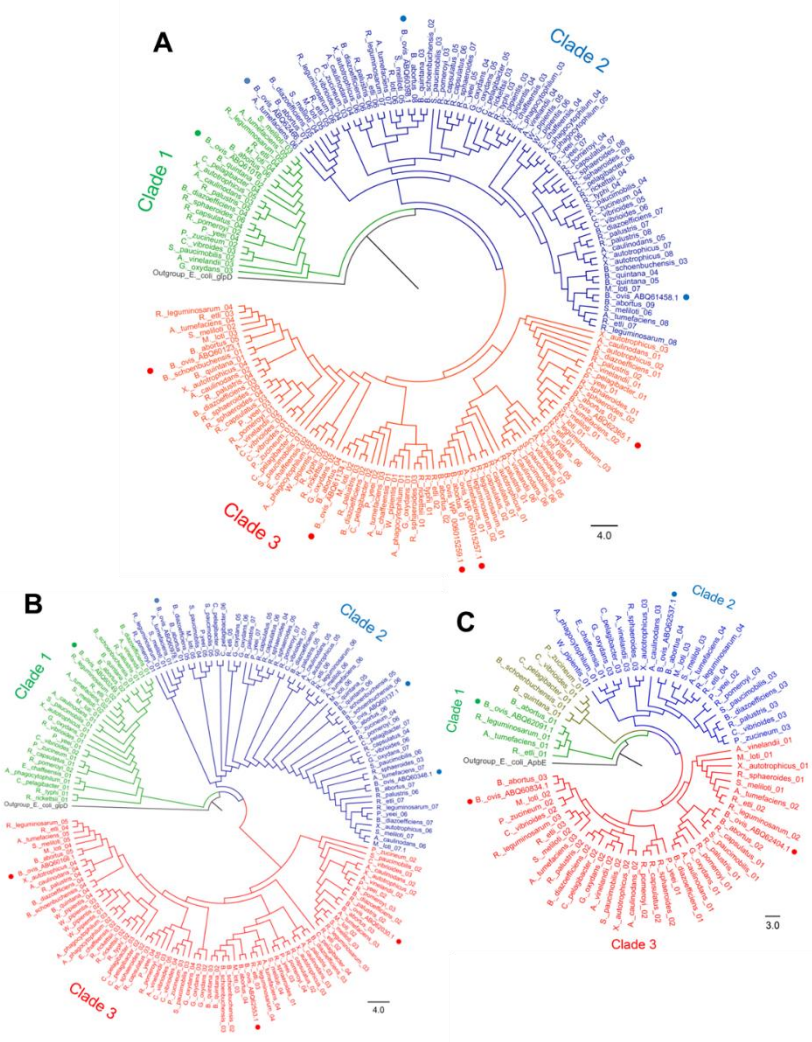

Figure 4.8. Phylogeny of *B. ovis* flavoproteins of subclasses (A) EC 1.8, (B) EC 1.14 and EC 1.16, and (C) related to nitrogen metabolism within alpha-proteobacteria. (A) Flavoenzymes of subclass EC 1.8. cluster in three clades (bootstrap > 90). Clade 1 contains ABQ61016.1. Clade 2 distributes in two subclades organised in different subgroups that contain ABQ62466.1, ABQ60398.1, and ABQ61458.1. Clade 3 clusters in two subclades (bootstrap >91). The first subclade separates in two branches WP_006015257.1 and WP_006015259.1 together and ABQ62365.1 separately. The second subclade clusters ABQ60123.1 and ABQ61134.1. **(B)** Flavoenzymes of subclass EC 1.14. and 1.16 distribute in three clades (bootstrap >80). Clade 1 includes the most divergent member, ABQ60249.1, that is the single member of the subclass 1.16. Clade 2 clusters ABQ60137.1, ABQ60978.1 and ABQ60348.1 (bootstrap >90). Clade 3 has three subclades and is more diverse. The most divergent subgroup includes ABQ62030.1 (bootstrap > 80), while ABQ60166.1 and ABQ62553.1 cluster in two branches of the other subclade (bootstrap > 96). **(C)** FMN dependent flavoreductases predicted to act on nitrogenous compounds separate in three clades. Clade 1 has ABQ62091.1 that is hardly conserved in alpha-proteobacteria. Clade 2 contains ABQ62537.1, and clade 3 separates in two branches ABQ62404.1 and ABQ60834.1 (bootstrap > 75). Phylogenetic cladograms include 177 sequences of class EC 1.8., 160 sequences of class EC 1.14./1.16. and 71 sequences of nitrogen metabolism from *B. ovis* ATCC 25840, *B. abortus* 2308, and 26 alphaproteobacteria related species. *E. coli* GlpD and *E. coli* ApbE were selected as outgroup in A and B, and C, respectively, to highlight the clear evolutionary separation between clusters. The likelihood aLRT (approximate likelihood-ratio test) statistical test and a bootstrap value of 100 were used.

Table 4.7. *Brucella ovis* ATCC 25840 flavoproteins and flavoenzymes found within the 20 *Brucella* and 26 alpha-proteobacteria of Table 4.1.

EC	Protein	Protein Code	*Brucella* content / 20 species	Alpha-proteobacteria content / 26 species [b]	Core protein in *Brucella* [c]
1.1.5.3	Glycerol-3-phosphate dehydrogenase	ABQ60174.1	20	12, 1-2x	Y
1.1.1.402	D-erythritol 1-phosphate dehydrogenase	ABQ62056.1	17	10, 2-2x, 1-3x	N
1.1.2.3	L-lactate dehydrogenase (cytochrome c o b2)	ABQ62635.1	20	21	Y
1.1.3.8	Potential L-gulonolactone oxidase FAD-binding oxygen oxidoreductase	ABQ62001.1	15	15	N
1.1.99.1	Choline dehydrogenase (Glucose-methanol-choline GMC family)	ABQ61350.1	18	18	N
1.1.99.1	Choline dehydrogenase (GMC family)	ABQ60630.1	14	10, 1-2x	N
1.1.99.1	Choline dehydrogenase (GMC family, membrane bound)	ABQ62100.1	14	16	N
1.1.99.2	Predicted L-2-hydroxyglutarate dehydrogenase	ABQ62911.1	16	14, 3-2x	N
1.1.99.14	Glycolate dehydrogenase GlcD subunit	ABQ62237.1	17	16, 4-2x	N
1.1.-.-[a]	Potential FAD-binding oxygen oxidoreductase (glcE?)	ABQ60928.1	19	17	N
1.1.-.-[a]	Potential FAD-binding oxygen oxidoreductase (glcE?)	ABQ61939.1	20	16	Y
1.3.1.1/2	NADH dependent Dihydropyrimidine dehydrogenase subunit PreA	ABQ60560.1	20	10 , 1-2x	Y
	NADH dependent Dihydropyrimidine dehydrogenase subunit PreT	ABQ61103.1	20	11	Y
1.3.5.2	PyrD dihydroorotate dehydrogenase 2 (quinone)	ABQ61413.1	20	24	Y
1.3.1.88	tRNA dihydrouridine synthase B	ABQ61416.1	20	22 , 1-2x	Y
1.3.1.91	tRNA dihydrouridine20/20a synthase	ABQ61966.1	20	17, 2-2x	Y
1.3.1.98	UDP-N-acetylmuramate dehydrogenase	ABQ61769.1	20	25	Y
1.3.1.-[a] /1.7.1.B1	Predicted alkene reductase: N-ethylmaleimide reductase, glycerol trinitrate reductase or xenobiotic reductase B	ABQ62490.1	15	18	N
1.3.5.1	Succinate dehydrogenase flavoprotein subunit	ABQ61077.1	20	**26**	Y
1.3.8.4	Isovaleryl-CoA dehydrogenase	ABQ60382.1	20	15, 2-2x, 1-3x	Y
1.3.8.-[a]	Acyl-CoA dehydrogenase	ABQ62576.1	19	13	N
1.3.8.1	Short Chain Acyl-CoA dehydrogenase	ABQ60180.1	19	14, 1-2x	N
1.3.8.-[a]	Acyl-CoA dehydrogenase	ABQ61585.1	18	14, 1-2x	N
1.3.8.-[a]	Acyl-CoA dehydrogenase	ABQ62784.1	19	9, 2-2x	N
1.3.8.-[a]	Acyl-CoA dehydrogenase	ABQ62889.1	18	12	N
1.3.8.-[a]	Acyl-CoA dehydrogenase	ABQ62082.1	18	17, 1-2x	N
1.3.99.-[a]	Predicted KsdD-like steroid dehydrogenase	ABQ62061.1	17	11	N
1.4.1.13	Glutamate synthase large subunit (alpha subunit)	ABQ61996.1	20	15, 1-2x	Y
	Glutamate synthase small subunit (beta subunit)	ABQ62546.1	11	11	N
1.4.3.5	Pyridoxamine 5'-phosphate oxidase	ABQ60142.1	20	20	Y
1.4.-.-[a]	Pyridoxamine 5'-phosphate oxidase family protein	ABQ61684.1	19	5	N
1.4.3.19	Glycine oxidase ThiO	ABQ60316.1	20	19	Y
1.4.3.-[a]	Potential Aminoacetone oxidase family FAD-binding enzyme/ NAD(P)/FAD-dependent dehydrogenase	ABQ60616.1	20	15, 1-2x	Y
1.4.3.-[a]	Potential Aminoacetone oxidase family FAD-binding enzyme/ NAD(P)/FAD-dependent dehydrogenase	ABQ60524.1	20	15, 1-2x	Y
1.4.99.-[a]	Predicted D-amino acid dehydrogenase small subunit	ABQ61937.1	20	11, 1-2x	Y
1.4.99.-[a]	D-amino acid dehydrogenase	ABQ62278.1	20	11, 3-2x	Y
1.4.-.-[a]	Predicted D-amino acid dehydrogenase	ABQ62519.1	19	8, 1-2x	N
1.4.-.-[a]	Predicted D-amino acid dehydrogenase	ABQ62405.1	20	20, 1-2x	Y
1.5.1.20	Methylenetetrahydrofolate reductase	ABQ60279.1	20	19	Y
1.5.1.-[a]	Flavin reductase domain containing protein	ABQ60228.1	20	7, 5-2x, 4-3x	Y
1.5.3.1	Sarcosine oxidase beta subunit	ABQ60177.1	0	0	N
		ABQ61310.1	20	14, 1-2x	Y
	Sarcosine oxidase alpha subunit	ABQ61036.1	20	15	Y
1.5.3.1	Predicted monomeric Sarcosine oxidase	ABQ62932.1	20	13	Y
1.5.5.1	Electron transferring flavoprotein-ubiquinone oxidoreductase (ETF-QO)	ABQ61337.1	20	21	Y
1.6.5.2	WrpA-type FMN-dependent NADH:quinone oxidoreductase	ABQ60884.1	20	13	Y
1.6.99.1	NADPH dehydrogenase (Old yellow enzyme)	ABQ62422.1	16	4	N
1.6.-.-	NADH dehydrogenase	ABQ62704.1	17	13	N
1.7.-.-[a]	Predicted NAD(P)H nitroreductase	ABQ60834.1	20	19	Y

1.8.1.2	Assimilatory sulphite reductase (NADPH) alpha component cluster	WP_006015252.1	This subunit does not bind flavin		
		WP_006015255.1	2	0	N
		WP_006015257.1	13	10	N
		WP_006015259.1	This subunit does not bind flavin		
1.8.1.4	Dihydrolipoyl dehydrogenase (lpdA-1)	ABQ62466.1	20	6	Y
1.8.1.4	Dihydrolipoyl dehydrogenase (lpdA-2)	ABQ60398.1	20	24, 2-2x	Y
1.8.1.4	Dihydrolipoyl dehydrogenase (lpdA-3)	ABQ61458.1	20	17, 8-2x	Y
1.8.1.7	Glutathione-disulphide reductase	ABQ61016.1	20	20	Y
1.8.1.9	Thioredoxin-disulphide reductase	ABQ60123.1	20	24, 2-2x	Y
1.8.1.9	Predicted thioredoxin-disulphide reductase	ABQ61134.1	19	11	N
1.8.5.B1	Peptide-methionine (S)-S-oxide reductase (quinone). MsrP catalytic subunit. MsrQ heme-binding subunit	ABQ62365.1	20	10, 1-2x	Y
		ABQ62343.1	This subunit does not bind flavin		
1.13.11.32	Nitronate monooxygenase (formerly 2-nitropropane dioxygenase NPD)	ABQ62537.1	15	21	N
1.13.11.79	Predicted aerobic 5,6-dimethylbenzimidazole synthase (BluB)	ABQ62404.1	18	15	N
1.14.13.1	Predicted Salicylate hydroxylase	ABQ60137.1	19	11, 8-2x	N
1.14.13.1	Predicted Salicylate hydroxylase	ABQ60978.1	17	4	N
1.14.13.-[a]	Predicted UbiH/COQ6 monooxygenase family	ABQ60166.1	20	20, 4-2x, 1-3x, 1-4x	Y
1.14.13. -[a]	UbiH/UbiF family hydroxylase	ABQ62553.1	19	15, 2-2x	N
1.14.13.2	4-hydroxybenzoate 3-monooxygenase	ABQ62030.1	18	15	N
1.14.14.3	Bacterial luciferase	ABQ60348.1	19	18	N
1.16.1.4	Cob(II)alamin reductase	ABQ60249.1	20	24	Y
1.17.1.4	Xanthine dehydrogenase, small subunit	ABQ61298.1	19	17	N
1.18.1.3-5	Predicted Ferredoxin/rubredoxin/ putidaredoxin NAD^+ Reductase	ABQ62051.1	17	16	N
1.18.1.2	Ferredoxin-$NADP^+$ reductase	ABQ61707.1	20	20	Y
1.-.-.-[a]	Predicted nitroreductase family protein	ABQ62091.1	20	7	Y
2.1.1.74	Methylenetetrahydrofolate-tRNA-(uracil54-C5-)-methyltransferase NAD(P)H oxidase	ABQ61275.1	18	18	N
2.1.1.229	tRNA (carboxymethyluridine34-5-O)-methyltransferase	ABQ60378.1	20	25	Y
2.2.1.6	Acetolactate synthase 3 catalytic subunit	ABQ60081.1	20	21	Y
2.5.1.9	Riboflavin synthase alpha subunit	ABQ60518.1	20	20	Y
2.7.7.2	Bifunctional riboflavin kinase/FAD synthase	ABQ62831.1	19	22	N
2.7.1.26					
2.7.1.180	FAD:protein FMN transferase	ABQ62066.1	16	4	N
2.7.13.3	Blue-light-activated histidine kinase	ABQ62113.1	19	2	N
4.1.1.36	Coenzyme A biosynthesis bifunctional protein: Phosphopantothenoylcysteine decarboxylase and Phosphopantothenate-cysteine ligase (CTP)	ABQ62036.1	17	23	N
6.3.2.5					
4.2.3.5	Chorismate synthase	ABQ60200.1	19	21	N
7.1.1.2	NADH-quinone oxidoreductase subunit F (H^+ translocating)	ABQ60521.1	20	23	Y
--	Electron transferring flavoprotein (ETF) alpha subunit	ABQ61011.1	20	21	Y
	Electron transferring flavoprotein (ETF) beta subunit	ABQ60428.1	20	21	Y
--	Protein NrdI	ABQ62891.1	20	7	Y

[a] Identified as flavoenzyme, but available information does not allow to fully predict its activity.

[b] "a-bx", indicates that in a number "a" of species there is a number "b" of isoforms of the protein. In red are highlighted those proteins found in all evaluated alpha-proteobacteria.

[c] Y, yes, conserved in the 20 *Brucella* species evaluated. N, no, not conserved in the 20 *Brucella* species evaluated

Table 4.8. Gene context for the genes encoding selected flavoproteins in the *Brucella ovis* ATCC 25840 at chromosome I. The table summarizes for each flavoprotein gene (highlighted in orange), the gene reading direction, the gene name and the name of expected produced protein. Similar data are also presented for upstream and downstream genes. Genes identified as transposases or pseudogenes are highlighted in grey and green respectively, and those codifying for tRNAs are shown in violet.

Up Stream		Flavoenzyme Gene Code		Down Stream	
5' ← 3' BOV_RS00080 Biotin carboxylase	**5' ← 3'** BOV_RS00085 Carboxyl transferase family protein	**5' ← 3'** BOV_RS00090 ivd: Isovaleryl-CoA dehydrogenase	**5' ← 3'** BOV_RS00095 Acetoacetate-CoA ligase	**5' ← 3'** BOV_RS00100 CHRD domain-containing protein	
5' → 3' BOV_RS00940 Response regulator transcription factor	**5' → 3'** BOV_RS00945 DeoR/GlpR transcriptional regulator	**5' → 3'** BOV_RS00950 glpD: Glycerol-3-phosphate dehydrogenase	**5' → 3'** BOV_RS00955 Sigma-54-dependent Fis family transcriptional regulator	**5' → 3'** BOV_RS00960 Aldehyde dehydrogenase family protein	
5' ← 3' BOV_RS01010 thiG: Thiazole synthase	**5' ← 3'** BOV_RS01015 thiS: Thiamine biosynthesis protein	**5' ← 3'** BOV_RS01020 thiO: Glycine oxidase	**5' ← 3'** BOV_RS01025 thiD: Phosphomethylpyrimidine kinase	**5' → 3'** BOV_RS01030 Sensory box/GGDEF domain/EAL domain protein	
5' → 3' BOV_RS01075 SoxB_1: Sarcosine oxidase beta subunit	**5' ← 3'** BOV_RS17650 IS5 family transposase	**5' → 3'** BOV_RS01090 SoxB_2: Sarcosine oxidase, beta subunit	**5' → 3'** BOV_RS01095 SoxD: Sarcosine oxidase, delta subunit	**5' → 3'** BOV_RS01100 SoxA: Sarcosine oxidase alpha subunit	
5' → 3' BOV_RS01505 MutT/nudix family protein	**5' ← 3'** BOV_RS01510 preA: NAD-dependent dihydropyrimidine dehydrogenase	**5' ← 3'** BOV_RS01515 preT: Putative pyridine nucleotide-disulphide oxidoreductase/ Dihydropyrimidine dehydrogenase	**5' ← 3'** BOV_RS01520 Uncharacterized protein	**5' → 3'** BOV_RS01525 pgi: Glucose-6-phosphate isomerase	
5' → 3' BOV_RS01645 SCP domain-containing protein	**5' → 3'** BOV_RS01650 Probable multidrug resistance protein NorM	**5' ← 3'** BOV_RS01655 PyrD: dihydroorotate dehydrogenase 2 (quinone)	**5' ← 3'** BOV_RS01660 DUF952 domain-containing protein	**5' ← 3'** BOV_RS17660 IS5-like element IS711 family transposase	
5' → 3' BOV_RS01760 panC: Pantothenate synthetase	**5' → 3'** BOV_RS01765 panB: 3-methyl-2-oxobutanoate hydroxymethyltransferase	**5' ← 3'** BOV_RS01770 fpr: Ferredoxin-NADP+ reductase	**5' ← 3'** BOV_RS01775 Fe-superoxide dismutase	**5' → 3'** BOV_RS01780 nspC: Carboxynorspermidine/ carboxyspermidine decarboxylase	
5' ← 3' BOV_RS01835 Chitooligosaccharide deacetylase	**5' → 3'** BOV_RS01840 Uncharacterized protein	**5' → 3'** BOV_RS01845 xdhA: Xanthine dehydrogenase, small subunit	**5' → 3'** BOV_RS01850 PSEUDOGEN xdhB	**5' → 3'** BOV_RS01855 xdhC: Xanthine dehydrogenase accessory protein	
5' → 3' BOV_RS02085 glyS: Glycine--tRNA ligase beta subunit	**5' → 3'** BOV_RS02090 Threonylcarbamoyl-AMP synthase	**5' → 3'** BOV_RS02095 Potential FAD-binding oxygen oxidoreductase (glcE?)	**5' ← 3'** BOV_RS02100 Uncharacterized protein	**5' ← 3'** BOV_RS02105 RHH_1 domain-containing protein	
5' ← 3' BOV_RS02110 Uncharacterized protein	**5' ← 3'** BOV_RS02115 Enoyl-CoA hydratase/isomerase family protein	**5' ← 3'** BOV_RS02120 Short Chain Acyl-CoA dehydrogenase	**5' → 3'** BOV_RS02125 Putative glyoxalase	**5' ← 3'** BOV_RS02130 purD: Phosphoribosylamine-glycine ligase	
5' ← 3' BOV_RS02130 purD: Phosphoribosylamine-glycine ligase	**5' → 3'** BOV_RS02135 ubiA: 4-hydroxybenzoate octaprenyltransferase	**5' ← 3'** BOV_RS02140 pdxH: Pyridoxamine 5'-phosphate oxidase	**5' → 3'** BOV_RS02145 17kDa_Anti_2 domain-containing protein	**5' → 3'** BOV_RS02150 Putative chaperone protein DnaJ	
5' → 3' BOV_RS02180 DUF374 domain-containing protein	**5' ← 3'** BOV_RS02185 Uncharacterized protein	**5' → 3'** BOV_RS02190 aroC: Chorismate synthase	**5' → 3'** BOV_RS02195 ribAB: 3,4-dihydroxy-2-butanone 4-phosphate synthase	**5' → 3'** BOV_RS02200 Histone deacetylase family protein	
5' ← 3' BOV_RS02755 Transcriptional regulator, AraC family	**5' ← 3'** BOV_RS02760 betB: Betaine aldehyde dehydrogenase	**5' ← 3'** BOV_RS02765 betA: Choline dehydrogenase (Glucose-methanol-choline GMC family)	**5' ← 3'** BOV_RS02770 betI: Transcriptional regulator	**5' → 3'** BOV_RS02775 Protein coding asparaginase	
5' ← 3' BOV_RS03090 Major facilitator family transporter	**5' ← 3'** BOV_RS03095 Type-4 uracil-DNA glycosylase	**5' → 3'** BOV_RS03100 Electron transferring flavoprotein-ubiquinone oxidoreductase (ETF-QO)	**5' ← 3'** BOV_RS03105 AP endonuclease family 1 domain protein	**5' ← 3'** BOV_RS03110 AMP nucleosidase	
5' → 3' BOV_RS03680 Amino acid ABC transporter, permease protein	**5' → 3'** BOV_RS03685 Amino acid ABC transporter, ATP-binding protein	**5' ← 3'** BOV_RS03690 Predicted Salicylate 1-monooxygenase	**5' ← 3'** BOV_RS03695 zf-CHCC domain-containing protein	**5' → 3'** BOV_RS03700 ppk: Polyphosphate kinase	
5' → 3' BOV_RS03780 Transcriptional repressor NrdR	**5' → 3'** BOV_RS03785 ribD: Riboflavin biosynthesis protein	**5' → 3'** BOV_RS03790 ribE: Riboflavin synthase alpha subunit	**5' → 3'** BOV_RS03795 ribH: 6,7-dimethyl-8-ribityllumazine synthase	**5' → 3'** BOV_RS03800 Transcription antitermination protein NusB	

5' → 3' BOV_RS03990 nuoD	**5' → 3'** BOV_RS03995 nuoE	**5' → 3'** BOV_RS04000 nuoF	**5' → 3'** BOV_RS04005 nuoG	**5' → 3'** BOV_RS04010 nuoH	
5' ← 3' BOV_RS04245 Amino acid ABC transporter, periplasmic amino acid-binding protein	**5' → 3'** BOV_RS04250 Uncharacterized protein	**5' → 3'** BOV_RS04255 dusA: tRNA dihydrouridine20/20a synthase	**5' ← 3'** BOV_RS04260 Uncharacterized protein	**5' ← 3'** BOV_RS04265 cosB: Adenosylcobinamide-GDP ribazoletransferase	
5' → 3' BOV_RS04415 Uncharacterized protein	**5' → 3'** BOV_RS04420 Uncharacterized protein	**5' ← 3'** BOV_RS04425 trmFO: Predicted Flavin-containing monooxygenase /Salicylate hydroxylase	**5' ← 3'** BOV_RS04430 Uncharacterized protein	**5' → 3'** BOV_RS04435 PSEUDOGEN	
5' ← 3' BOV_RS04713 moaA: GTP 3',8-cyclase	**5' → 3'** BOV_RS04714 GBBH-like_N domain-containing protein	**5' ← 3'** BOV_RS04715 Predicted Salicylate hydroxylase	**5' ← 3'** BOV_RS04720 fumB: Fumarate hydratase class I	**5' → 3'** BOV_RS04725 Cell wall degradation protein	
5' → 3' BOV_RS04840 ripA: Ribose-5-phosphate isomerase A	**5' → 3'** BOV_RS04845 DUF2059 domain-containing protein	**5' → 3'** BOV_RS04850 gor: Glutathione-disulphide reductase	**5' → 3'** BOV_RS04855 Phospho-2-dehydro-3-deoxyheptonate aldolase	**5' → 3'** BOV_RS04860 dgkA: Diacylglycerol kinase	
5' → 3' BOV_RS04915 BOV_0991 PSEUDOGENE	**5' → 3'** BOV_RS04920 BOV_0992 Ferredoxin, 2Fe-2S	**5' → 3'** BOV_RS04925 BOV_0993 Predicted thioredoxin-disulphide reductase	**5' ← 3'** BOV_RS04930 BOV_0994 Uncharacterized protein	**5' → 3'** BOV_RS04935 BOV_0995 folP: Dihydropteroate synthase	
5' ← 3' BOV_RS04975 Proline-rich region:Proline-rich extensin. FliO/MopB family protein	**5' → 3'** BOV_RS04980 PAS domain-containing hybrid sensor histidine kinase/response regulator	**5' → 3'** BOV_RS04985 Potential aminoacetone oxidase family FAD-binding enzyme / NAD(P)/FAD-dependent dehydrogenase	**5' → 3'** BOV_RS04990 Serine hydrolase	**5' ← 3'** BOV_RS17720 PSEUDOGENE	**5' ← 3'** BOV_RS05000 vitamin B12-dependent ribonucleotide reductase
5' ← 3' BOV_RS05015 Usp domain-containing protein	**5' ← 3'** BOV_RS05020 CinA-related protein	**5' → 3'** BOV_RS05025 wrpA: NAD(P)H dehydrogenase (quinone)	**5' → 3'** BOV_RS05030 tRNA-Leu	**5' → 3'** BOV_RS05040 PSEUDOGENE ilvA	
5' ← 3' BOV_RS05115 galE-2: UDP-glucose 4-epimerase	**5' → 3'** BOV_RS05120 MazG family protein	**5' ← 3'** BOV_RS05125 Flavin reductase domain containing protein	**5' ← 3'** BOV_RS05130 Putative NAD(P)H nitroreductase	**5' → 3'** BOV_RS05135 Uncharacterized protein	
5' ← 3' BOV_RS05345 ntrC: DNA-binding transcriptional regulator	**5' ← 3'** BOV_RS05350 ntrB: Histidine kinase	**5' ← 3'** BOV_RS05355 nifR3 or DusB: tRNA dihydrouridine synthase B	**5' → 3'** BOV_RS05360 Bifunctional enzyme IspD/IspF	**5' → 3'** BOV_RS05365 Competence/damage-inducible protein CinA	
5' ← 3' BOV_RS05380 lipA: Lipoyl synthase	**5' ← 3'** BOV_RS05385 Uncharacterized protein	**5' ← 3'** BOV_RS05390 IpdA-2: Dihydrolipoyl dehydrogenase	**5' ← 3'** BOV_RS05395 Acetyltransferase component of pyruvate dehydrogenase complex	**5' ← 3'** BOV_RS05400 pdhB: Pyruvate dehydrogenase E1 component subunit beta	
5' ← 3' BOV_RS06200 Putative lipoprotein	**5' ← 3'** BOV_RS06205 PSEUDOGEN	**5' ← 3'** BOV_RS06210 cobR: Cob(II)alamin reductase	**5' → 3'** BOV_RS06215 cobD-1: Cobalamin biosynthesis protein	**5' ← 3'** BOV_RS06220 Putative branched-chain amino acid ABC transporter, periplasmic amino acid-binding protein	
5' ← 3' BOV_RS06305 Uncharacterized protein	**5' ← 3'** BOV_RS16680 cobQ: Cobyric acid synthase	**5' → 3'** BOV_RS06310 Acyl-CoA dehydrogenase	**5' → 3'** BOV_RS06315 mmsB: 3-hydroxyisobutyrate dehydrogenase	**5' ← 3'** BOV_RS16685 Uncharacterized protein	
5' ← 3' BOV_RS06565 Fluoride efflux transporter CrcB	**5' → 3'** BOV_RS06570 Hypothetical protein	**5' ← 3'** BOV_RS06575 Pyridoxamine 5'-phosphate oxidase family protein	**5' → 3'** BOV_RS17790 IS5 family transposase	**5' ← 3'** BOV_RS06590 PhzF family phenazine biosynthesis protein	
5' ← 3' BOV_RS06645 Uncharacterized protein	**5' ← 3'** BOV_RS06650 ilvN: Acetolactate synthase	**5' ← 3'** BOV_RS06655 ilvB: Acetolactate synthase 3 catalytic subunit	**5' ← 3'** BOV_RS06660 miaA: tRNA dimethylallyltransferase	**5' → 3'** BOV_RS06665 serB: Phosphoserine phosphatase	
5' ← 3' BOV_RS06660 tRNA (adenosine(37)-N6)-dimethylallyltransferase MiaA	**5' → 3'** BOV_RS06665 Phosphoserine phosphatase SerB	**5' ← 3'** BOV_RS06670 Potential aminoacetone oxidase family FAD-binding enzyme / NAD(P)/FAD-dependent dehydrogenase	**5' ← 3'** BOV_RS06675 DegQ family serine endoprotease	**5' ← 3'** BOV_RS06680 DUF2065 domain-containing protein	

5' ← 3' BOV_RS06740 AsmA family protein	**5' ← 3'** BOV_RS17795 Hypothetical protein	**5' ← 3'** BOV_RS06750 Potential FAD-binding oxygen oxidoreductase (glcE?)	**5' ← 3'** BOV_RS06755 Heme-degrading domain-containing protein	**5' → 3'** BOV_RS06760 Serine/threonine protein kinase	
5' ← 3' BOV_RS06840 ftsQ: Cell division protein	**5' ← 3'** BOV_RS06845 ddlB: D-alanine-D-alanine ligase	**5' ← 3'** BOV_RS06850 murB: UDP-N-acetylmuramate dehydrogenase	**5' ← 3'** BOV_RS06855 murC: UDP-N-acetylmuramate-L-alanine ligase	**5' ← 3'** BOV_RS06860 murG: UDP-N-acetylglucosamine-N-acetylmuramyl-(pentapeptide) pyrophosphoryl-undecaprenol N-acetylglucosamine transferase	
5' → 3' BOV_RS06935 Putative peptidoglycan-binding protein	**5' → 3'** BOV_RS06940 Putative transporter	**5' ← 3'** BOV_RS06945 metF: Methylenetetrahydrofolate reductase	**5' ← 3'** BOV_RS06950 Transcriptional regulator, ArsR family	**5' ← 3'** BOV_RS06955 DUF2293 domain-containing protein	
5' → 3' BOV_RS16805 Uncharacterized protein	**5' ← 3'** BOV_RS07150 Transcriptional regulator, LysR family	**5' ← 3'** BOV_RS07155 trxB: Thioredoxin reductase	**5' → 3'** BOV_RS07160 Trk system potassium uptake protein	**5' → 3'** BOV_RS07165 lrp-1	
5' ← 3' BOV_RS07765 Sugar ABC transporter ATP-binding protein	**5' → 3'** BOV_RS07770 Hypothetical PepSY domain-containing protein	**5' → 3'** BOV_RS07775 Oxidoreductase GMC family Choline dehydrogenase	**5' ← 3'** BOV_RS07780 tRNA-Met	**5' ← 3'** BOV_RS07785 rRNA-5S ribosomal RNA	
5' ← 3' BOV_RS08470 Branched-chain amino acid ABC transporter, permease protein	**5' ← 3'** BOV_RS08475 4-hydroxyproline epimerase	**5' ← 3'** BOV_RS08480 D-amino acid dehydrogenase small subunit	**5' → 3'** BOV_RS08485 Transcriptional regulator, GntR family	**5' ← 3'** BOV_RS08490 Transcriptional regulator, MarR family	
5' ← 3' BOV_RS08960 Ammonium transporter	**5' ← 3'** BOV_RS08965 tesB	**5' → 3'** BOV_RS08970 Predicted UbiH/COQ6 monooxygenase family	**5' ← 3'** BOV_RS08975 Glyoxalase family protein	**5' ← 3'** BOV_RS08980 sdhB	
5' ← 3' BOV_RS08975 Glyoxalase family protein	**5' ← 3'** BOV_RS08980 sdhB: Succinate dehydrogenase iron-sulfur subunit	**5' ← 3'** BOV_RS08985 sdhA: Succinate dehydrogenase flavoprotein subunit	**5' ← 3'** BOV_RS08990 sdhD: Succinate dehydrogenase hydrophobic membrane anchor subunit	**5' ← 3'** BOV_RS08995 Succinate dehydrogenase cytochrome b556 subunit	
5' → 3' BOV_RS09055 xerC: Tyrosine recombinase	**5' → 3'** BOV_RS09060 Uncharacterized protein	**5' ← 3'** BOV_RS09065 IpdA-3: Dihydrolipoyl dehydrogenase	**5' ← 3'** BOV_RS09070 Uncharacterized protein	**5' ← 3'** BOV_RS09075 Transporter, LysE family	
5' → 3' BOV_RS09285 cysK: Cysteine synthase	**5' ← 3'** BOV_RS09290 3-hydroxybutyryl-CoA dehydrogenase	**5' ← 3'** BOV_RS09295 etfA: Electron transfer flavoprotein, alpha subunit	**5' ← 3'** BOV_RS09300 etfB: Electron transfer flavoprotein, beta subunit	**5' → 3'** BOV_RS09305 queC: 7-cyano-7-deazaguanine synthase	
5' ← 3' BOV_RS09685 Transcriptional regulator, LacI family	**5' → 3'** BOV_RS09690 Uncharacterized protein	**5' ← 3'** BOV_RS09695 Bacterial luciferase	**5' ← 3'** BOV_RS17075 Putative ABC transporter, periplasmic substrate-binding protein	**5' → 3'** BOV_RS09700 Branched-chain amino acid ABC transporter, permease protein	
5' ← 3' BOV_RS09725 parA: Chromosome partitioning protein	**5' ← 3'** BOV_RS09730 rsmG: Ribosomal RNA small subunit methyltransferase G	**5' ← 3'** BOV_RS09735 mnmG: tRNA uridine 5-carboxymethylaminomethyl modification enzyme	**5' → 3'** BOV_RS09736 mnmE: tRNA modification GTPase	**5' ← 3'** BOV_RS09737 Thioredox_DsbH domain-containing protein	

Flavoenzymes of subclass EC 1.4 are highly conserved within *Brucella*, but some are hardly present in alpha-proteobacteria (Figure 4.6B, Table 4.7). They particularly include a pyridoxamine 5'-phosphate oxidase family protein of unclear function present in the *Brucella* core proteome but only in five of the symbiotic alpha-proteobacteria evaluated (*Agrobacterium tumefaciens*, *Mesorhizobium loti*, *Rhizobium etli*, *Rhizobium leguminosarum*, *Sinorhizobium meliloti*). This suggests that it might be involved in nitrogen metabolism (Tables 4.5 and 4.7). Its crystal structure, solved for *B. melitensis*, predicts a dimer that might bind either FMN, FAD or F420 (8-hidroxi-5-deazaflavina) (Figure 4.5). Its genomic context, next to a PhzF family phenazine biosynthesis protein gene (downstream), is pretty similar in homologues. Moreover, in three *Brucella* (*B. melitensis*, *B. canis* and *B.*

microti) a gene for a Nudix hydrolase follows the phzF gene, and in the alpha-proteobacteria *Ochrobactrum anthropi* these genes are grouped together. Therefore, this protein might be somehow related to the hydrolysis of nucleoside diphosphates linked to other biomolecules. This subclass also includes glycine oxidase (ThiO, EC 1.4.3.19) involved in glycine oxidation to glyoxylate and in the thiamine metabolism; a potential D-amino acid oxidase (EC 1.4.99.-) with low similarity to other characterized enzymes of this type; pyridoxamine 5'-phosphate oxidase (EC 1.4.3.5) involved in the biosynthesis of pyridoxal 5'-phosphate (Di Salvo et al., 1998); the two flavoprotein subunits of a glutamate synthase that through three distinct active centres (EC 1.4.1.13) uses of L-glutamine as carbon and nitrogen source during cell growth, particularly within the host as shown by *B. abortus* (Hong et al., 2000); and two proteins folding in HI0933_like domains that are potential NAD(P)/FAD-dependent dehydrogenases of the aminoacetone oxidase family (EC 1.4.3.-). We cannot unambiguously provide a clear function for these two last proteins but they might have a particular role in *Brucella* because they are in its core proteome but poorly distributed in alpha-proteobacteria (Table 4.7).

Table 4.9. Gene context for the genes encoding selected flavoproteins in the *Brucella ovis* ATCC 25840 at chromosome II. The table summarizes for each flavoprotein gene (highlighted in orange) the gene reading direction, the gene name and the name of expected produced protein. Similar data are also presented for upstream and downstream genes. Genes identified as transposases or pseudogenes are highlighted in grey and green respectively and those codifying for tRNAs are shown in violet.

Upstream		Flavoenzyme Gene Code		Downstream	
5' → 3' BOV_RS10575 PSEUDOGENE	5' ← 3' BOV_RS10580 PSEUDOGENE	5' → 3' BOV_RS10585 gltB: Glutamate synthase large subunit	5' → 3' BOV_RS10590 gltD: Glutamate synthase, small subunit	5' ← 3' BOV_RS10595 Amino acid permease family protein	
5' ← 3' BOV_RS11145 Transcriptional regulator, LysR family	5' ← 3' BOV_RS17905 IS5-like element IS711 family transposase	5' → 3' BOV_RS11160 glcD: Glycolate oxidase, subunit	5' → 3' BOV_RS11165 PSEUDOGENE glcE	5' → 3' BOV_RS17195 PSEUDOGENE	
5' ← 3' BOV_RS11245 groES: Co-chaperone	5' → 3' BOV_RS11250 PSEUDOGENE	5' → 3' BOV_RS11255 ribF: Riboflavin biosynthesis protein	5' → 3' BOV_RS11260 ileS: Isoleucine--tRNA ligase	5' → 3' BOV_RS11265 Putative lipoprotein	
5' ← 3' BOV_RS11380 PSEUDOGENE	5' → 3' BOV_RS11385 CAIB/BAIF family protein	5' ← 3' BOV_RS11390 NADPH dehydrogenase (Old yellow enzyme)	5' → 3' BOV_RS11395 Bacterial regulatory protein, MerR family	5' ← 3' BOV_RS11400 Sensor protein QseC	
5' → 3' BOV_RS11420 PepSY domain-containing protein	5' → 3' BOV_RS11425 hypothetical protein	5' → 3' BOV_RS11430 flavodoxin domain-containing protein	5' → 3' BOV_RS11435 hypothetical protein	5' → 3' BOV_RS11440 FAD:protein FMN transferase	5' ← 3' BOV_RS11445 Sensor domain-containing diguanylate cyclase
5' → 3' BOV_RS11800 Putative transporter	5' → 3' BOV_RS11805 Protein NrdH	5' → 3' BOV_RS11810 Protein NrdI	5' → 3' BOV_RS11815 Protein NrdE	5' → 3' BOV_RS11820 Protein NrdF	
5' → 3' BOV_RS12320 PSEUDOGENE	5' → 3' BOV_RS12325 msrB: Peptide methionine sulfoxide reductase	5' ← 3' BOV_RS12330 Acyl-CoA dehydrogenase	5' ← 3' BOV_RS12335 Acetyl-CoA acetyltransferase	5' ← 3' BOV_RS12340 3-hydroxyacyl-CoA dehydrogenase type II	
5' → 3' BOV_RS12450 Uncharacterized protein	5' → 3' BOV_RS12455 Uncharacterized protein	5' ← 3' BOV_RS12460 NADH dehydrogenase	5' ← 3' BOV_RS12465 Bacterial regulatory protein, MarR family	5' ← 3' BOV_RS17935 Putative transposase for insertion sequence element IS6501	
5' ← 3' BOV_RS12535 Uncharacterized protein	5' → 3' BOV_RS12540 mogA: Molybdenum cofactor biosynthesis protein	5' ← 3' BOV_RS12545 Predicted nitroreductase family protein	5' → 3' BOV_RS17940 PSEUDOGENE	5' → 3' BOV_RS12555 Monovalent cation/proton antiporter, MnhA/PhaA subunit	

5' → 3' BOV_RS12660 Putative D-aminopeptidase	**5' → 3'** BOV_RS12665 Putative cell division protein FtsK	**5' → 3'** BOV_RS12670 lpdA-1: Dihydrolipoyl dehydrogenase	**5' ← 3'** BOV_RS12675 SURF1-like protein	**5' ← 3'** BOV_RS17325 Uncharacterized protein	
5' ← 3' BOV_RS13070 PSEUDOGENE	**5' ← 3'** BOV_RS13075 Phosphatidylcholine synthase	**5' → 3'** BOV_RS13080 UbiH/UbiF family hydroxylase	**5' ← 3'** BOV_RS13085 Hemimethylated DNA-binding region	**5' ← 3'** BOV_RS13090 Invasion associated locus B (IalB) protein	
5' ← 3' BOV_RS13150 tRNA	**5' ← 3'** BOV_RS13155 Lectin-like protein BA14k	**5' → 3'** BOV_RS13160 Blue-light-activated histidine kinase	**5' → 3'** BOV_RS13165 lipB: Octanoyltransferase	**5' ← 3'** BOV_RS13170 Putative membrane protein	
5' ← 3' BOV_RS13195 gatC: Aspartyl/glutamyl-tRNA(Asn/Gln) amidotransferase subunit C	**5' → 3'** BOV_RS13200 UPF0173 metal-dependent hydrolase	**5' ← 3'** BOV_RS13205 Acyl-CoA dehydrogenase	**5' → 3'** BOV_RS13210 Putative pre-16S rRNA nuclease	**5' → 3'** BOV_RS13215 pyrB: Aspartate carbamoyltransferase	
5' → 3' BOV_RS13335 Uncharacterized protein	**5' ← 3'** BOV_RS13340 Transcriptional regulator, AraC family	**5' ← 3'** BOV_RS13345 Predicted D-amino acid dehydrogenase	**5' ← 3'** BOV_RS13350 Amino acid ABC transporter, periplasmic amino acid-binding protein	**5' ← 3'** BOV_RS13355 Amino acid ABC transporter, periplasmic amino acid-binding protein	
5' → 3' BOV_RS13390 Putative transcriptional regulator PcaR	**5' ← 3'** BOV_RS13395 PSEUDOGENE	**5' → 3'** BOV_RS13400 pobA: 4-hydroxybenzoate 3-monooxygenase	**5' ← 3'** BOV_RS13405 Pca operon transcription factor PcaQ	**5' → 3'** BOV_RS13410 PSEUDOGENE	
5' → 3' BOV_RS13520 Probable branched-chain-amino-acid aminotransferase	**5' → 3'** BOV_RS13525 sulfite exporter TauE/SafE family protein. Transmembrane	**5' → 3'** BOV_RS13530 Predicted KsdD-like steroid dehydrogenase	**5' → 3'** BOV_RS13535 DUF3775 domain-containing protein	**5' → 3'** BOV_RS13540 aldehyde dehydrogenase family protein	
5' ← 3' BOV_RS13785 gcvT: Glycine cleavage system T protein	**5' → 3'** BOV_RS13790 Uncharacterized protein	**5' ← 3'** BOV_RS13795 Predicted Ferredoxin/rubedroxin/ putidaredoxin NAD+ Reductase	**5' ← 3'** BOV_RS13800 MurR/RpiR family transcriptional regulator	**5' → 3'** BOV_RS13805 N-formylglutamate amidohydrolase	
5' → 3' BOV_RS13960 Glutamine synthetase family protein	**5' → 3'** BOV_RS13965 Uncharacterized protein	**5' → 3'** BOV_RS13970 Predicted D-amino acid dehydrogenase	**5' ← 3'** BOV_RS18005 Transcriptional regulator, MarR family	**5' → 3'** BOV_RS18010 IS711 transposase orfA	
5' ← 3' BOV_RS14110 Putative fatty oxidation complex, beta subunit	**5' → 3'** BOV_RS14115 Acyl-CoA dehydrogenase	**5' ← 3'** BOV_RS14120 Uncharacterized protein	**5' → 3'** BOV_RS14130 Putative transcriptional regulator, LysR family	**5' → 3'** BOV_RS14135 Acyl-CoA dehydrogenase	**5' ← 3'** BOV_RS14140 nikE: Nickel import ATP-binding protein
5' ← 3' BOV_RS1475 PSEUDOGENE	**5' ← 3'** BOV_RS14280 Uncharacterized protein	**5' → 3'** BOV_RS14290 Nitronate monooxygenase (formerly 2-nitropropane dioxygenase NPD)	**5' → 3'** BOV_RS14295 tRNA	**5' → 3'** BOV_RS14300 SocA family protein	
5' ← 3' BOV_RS14395 PSEUDOGENE	**5' ← 3'** BOV_RS14400 EamA family transporter Transporter, DME family, Lipid Biosynthesis	**5' ← 3'** BOV_RS14405 Potential L-gulonolactone oxidase	**5' ← 3'** BOV_RS14415 UbiA prenyltransferase family. Transfer of alkyls different from methyl	**5' ← 3'** BOV_RS14415 DeoR/GlpR transcriptional regulator	
5' → 3' BOV_RS18245 Hypothetical protein	**5' → 3'** BOV_RS14445 Carbohydrate kinase/eryA	**5' → 3'** BOV_RS14450 eryB	**5' → 3'** BOV_RS14455 eryC Aminotransferase	**5' → 3'** BOV_RS14460 PSEUDOGENE	
5' → 3' BOV_RS14620 Transcriptional regulator, Lrp/AsnC family	**5' ← 3'** BOV_RS14625 Alkene reductase: N-ethylmaleimide reductase (Glycerol trinitrate reductase or xenobiotic reductase B)	**5' ← 3'** BOV_RS14630 Transcriptional regulator, ArsR family. Helix-turn-helix	**5' → 3'** BOV_RS14635 PSEUDOGENE	**5' ← 3'** BOV_RS14640 Predicted monomeric Sarcosine oxidase	**5' ← 3'** BOV_RS14645 PSEUDOGENE
5' ← 3' BOV_RS14705 Uncharacterized protein	**5' ← 3'** BOV_RS14710 PSEUDOGENE	**5' → 3'** BOV_RS14715 lldD: L-lactate dehydrogenase (cytochrome c o b2)	**5' → 3'** BOV_RS14720 Outer surface protein	**5' ← 3'** BOV_RS14725 Putative alanine catabolic operon transcriptional regulator	
5' ← 3' BOV_RS14725 Putative alanine catabolic operon transcriptional regulator	**5' → 3'** BOV_RS14730 alr: Alanine racemase	**5' → 3'** BOV_RS14735 dadA: D-amino acid dehydrogenase	**5' ← 3'** BOV_RS14740 Putative transcriptional regulator	**5' → 3'** BOV_RS14745 Putative omega-amino acid--pyruvate aminotransferase	
5' → 3' BOV_RS14900 Branched-chain amino acid ABC transporter, permease protein	**5' → 3'** BOV_RS14900 PSEUDOGENE	**5' → 3'** BOV_RS14905 Choline dehydrogenase (GMC family, membrane bound)	**5' → 3'** BOV_RS14910 MetQ/NlpA family ABC transporter substrate-binding protein	**5' → 3'** BOV_RS17565 PSEUDOGENE	
5' → 3' BOV_RS15060 G-protein beta WD-40 repeat:ATP/GTP-binding site motif A	**5' ← 3'** BOV_RS15065 Esterase/lipase/thioesterase, active site	**5' → 3'** BOV_RS15070 msrP: Protein-methionine-sulfoxide reductase catalytic subunit	**5' → 3'** BOV_RS15075 msrQ: Protein-methionine-sulfoxide reductase heme-binding subunit	**5' ← 3'** BOV_RS15080 Endoribonuclease L-PSP	
5' ← 3' BOV_RS15154 Uncharacterized protein	**5' ← 3'** BOV_RS15150 GGDEF domain protein	**5' ← 3'** BOV_RS15155 lhgO: L-2-hydroxyglutarate oxidase	**5' → 3'** BOV_RS15160 Putative exonuclease	**5' ← 3'** BOV_RS18050 Amidase	

5' → 3' BOV_RS15380 tRNA-Leu	**5' → 3'** BOV_RS15385 Amidohydro_3 domain-containing protein	**5' → 3'** BOV_RS15390 bluB: Predicted aerobic 5,6-dimethylbenzimidazole synthase	**5' → 3'** BOV_RS15395 Universal stress protein family	**5' → 3'** BOV_RS15400 Putative membrane protein	
5' → 3' BOV_RS15420 Uncharacterized protein	**5' → 3'** BOV_RS15425 prfC: Peptide chain release factor 3	**5' ← 3'** BOV_RS15430 coaBC: Coenzyme A biosynthesis bifunctional protein: Phosphopantothenoylcysteine decarboxylase / Phosphopantothenate-cysteine ligase (CTP)	**5' ← 3'** BOV_RS15435 ubiB: 2-polyprenylphenol 6-hydroxylase	**5' ← 3'** BOV_RS15440 ubiE: Ubiquinone/menaquinone biosynthesis C-methyltransferase	

The subclass EC 1.5 (Figure 4.8B) includes the methylenetetrahydrofolate reductase (EC 1.5.1.20), a central enzyme in the carbon fixation and tetrahydrofolate metabolisms; the iron-sulphur flavoprotein ETF-QO (EC 1.5.5.1) that accepts electrons from ETF proteins and contributes to the respiratory chain and OXPHOS pathways (Lee et al., 2009); the flavin reductase domain containing protein (EC. 1.5.1.-) that is the most divergent member and might have flavin reductase activity; and two sarcosine oxidase proteins (EC 1.5.3.1). One sarcosine oxidase (ABQ62932.1) relates to the monomeric soluble protein, whereas the other is composed by two subunits that bind flavins, alpha (ABQ61036.1) and beta (ABQ60177.1+ABQ61310.1), and is the membrane bound form. Sarcosine oxidases would catalyze demethylation of sarcosine as a way for *B. ovis* to grow with sarcosine, ensuring creatinine degradation and glycine, serine and threonine metabolism. All these flavoproteins of subclass EC 1.5 are in the core proteome of *Brucella*, but are not conserved in alpha-proteobacteria (Table 4.7).

The subclass EC 1.6 is represented by three flavoenzymes. The WrpA-type FMN-dependent NADH:quinone oxidoreductase (ABQ60884.1, EC 1.6.5.2) is present in all *Brucella* (Table 4.5 and 4.7). The *B. abortus* homologue structure (98.5% identity) relates it to NADH:quinone oxidoreductases, but in vitro its ability to bind redox cofactors and its oxidoreductase activity have not been proven. However, it modulates *B. abortus* interaction with the mammalian host and is suggested as a new functional class of WrpA/flavodoxin family proteins likely involved in cell survival under acute oxidative stress (Herrou et al., 2016). This subclass also includes the FMN-dependent NADPH dehydrogenase of the old yellow enzyme family (EC 1.6.99.1). It has not homologues in all *Brucella* and alpha-proteobacteria, and despite is highly studied in different species its acceptor and physiological function remain unclear. Finally, this subclass includes a FAD-dependent NADH dehydrogenase with unknown function (EC 1.6.-.-).

Up to eight flavoenzymes fall in the subclass EC 1.8. The sequence identity of the *B. ovis* FAD dependent glutathione-disulphide reductase (EC 1.8.1.7) with the *S. meliloti*

homologue indicates that it must contribute to maintain high levels of reduced glutathione to control redox homeostasis. This agrees with a recent report where disruptions in the gene encoding for it in *B. ovis* produce a significant disadvantage in bacterial growth (Tang et al., 2018; Varesio et al., 2021). The three predicted dihydrolipoyl dehydrogenases (ldpA-1, ldpA-2, ldpA-3, EC 1.8.1.4) are highly conserved in *Brucella* and alpha-proteobacteria, with the exception of ldpA-1 poorly represented in alpha-proteobacteria. Homologues in *B. suis* and *B. abortus* form part of complexes such as the alpha-ketoacid dehydrogenase, pyruvate dehydrogenase and glycine cleavage multienzyme, implicated in the biosynthesis of Acetyl-CoA and secondary metabolites, oxidative decarboxylation of pyruvate and glycine metabolism, which contribute to the bacteria pathogenicity (Table 4.10) (Rajashankar et al., 2005; Viadas et al., 2010; Abdou et al., 2017). The MsrQ subunit of peptide-methionine (S)-S-oxide reductase (quinone) (EC 1.8.5.B1) uses FMN and haem, and is complemented with molybdopterin and quinone at the MsrP subunit. Msr complex is essential for the maintenance of envelope integrity under bleach stress and protects proteins from oxidative-stress damage during host defense mechanisms (Gennaris et al., 2015). MrsQ is common to all *Brucella*, but not in alpha-proteobacteria. This subclass also has the two flavoprotein subunits of the assimilatory sulphite reductase (NADPH); the alpha component cluster that, together with a beta subunit, catalyzes the six-electron reduction of sulphite to sulphide (EC 1.8.1.2). This protein is usually involved in sulphate and sulphur assimilation, and in microbial metabolism in diverse environments. As above mentioned, it is singular in *B. ovis*, since in other *Brucella* a single protein contains the four components (Figure 4.4B). In addition, this subclass has two FAD-dependent thioredoxin-disulphide reductase like proteins (EC 1.8.1.9) with pyridine nucleotide-disulphide oxidoreductase activity potentially involved in the oxidation-reduction cycle of thioredoxin.

Most flavoenzymes of subclass EC 1.14 use NAD(P)H as donor and incorporate oxygen into the second substrate (Figure 4.9B). Two of them are related to salicylate hydroxylase activity (EC 1.14.13.1) contributing to the degradation of aromatic compounds and two are members of the UbiH/COQ6 monooxygenase and UbiH/UbiF hydroxylase families (EC 1.14.13.-) (Table 4.7). These later two enzymes are involved in the ubiquinone biosynthesis pathway (ARBA annotation: ARBA00004749, “ubiquinone biosynthesis”) and share moderate sequence similarity with well characterized flavoprotein monooxygenases, but close homologues have not been characterized yet (Young et al., 1973; Hajj Chehade et al., 2013; Liu et al., 2016). This subclass also has the 4-hydroxybenzoate 3-monooxygenase

(EC 1.14.13.2) that participates in the benzoate degradation and favours microbial metabolism in diverse environments (Wong et al., 1994; Westphal et al., 2018). Other member is the bacterial luciferase (EC 1.14.14.3) that incorporates oxygen into reduced FMN to form a peroxyflavin-adduct that upon interaction with aliphatic long-chain aldehydes produces highly fluorescent species. This luciferase is particularly common in symbiotic nitrogen-fixing alpha-proteobacteria (*A. tumefaciens*, *R. leguminosarum*, *S. meliloti*, except *R. pomeroyi*).

We have identified a single member of the subclass EC 1.16. This protein is assigned in UniProtKB as FMN-dependent 4-hydroxyphenylacetate 3-monooxygenase (EC 1.14.14.9, ABQ60249.1). However, it clearly diverges from subclass EC 1.14 (Figure 4.8B) and is identical to the Cob(II)alamin reductase (EC 1.16.1.4) of *B. melitensis* with structure and activity experimentally proven (Lawrence et al., 2008). Therefore, ABQ60249.1 must participate in the cobalamin (vitamin B12) biosynthetic pathway. The single member of subclass EC 1.17 is the small subunit of xanthine dehydrogenase (xdhA) (EC 1.17.1.4) that is present in most *Brucella* evaluated. This enzyme participates in the metabolism of purines and is made by several subunits.

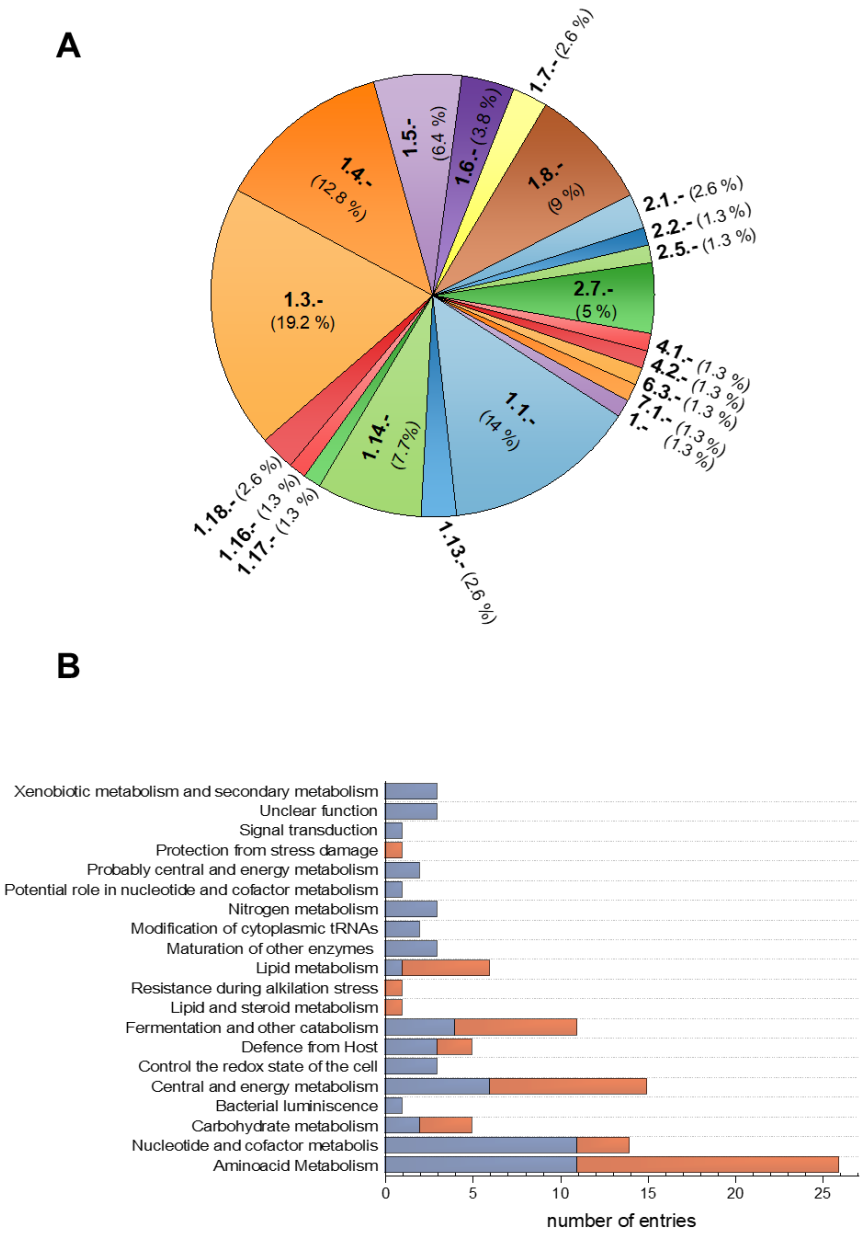

Figure 4.9. Metabolic functions for the *B. ovis* flavoproteins. (A) Pie chart distribution of ECs. **(B)** Number of flavoproteins involved in different metabolic pathways. Blue portions of bars relate to entries predicted to act in a single pathway, whereas orange ones represent entries acting in several pathways. No queda bien leyenda en otra página

The subclass EC 1.18. has two flavoenzymes that exchange electrons between pyridine nucleotides and iron-sulphur proteins. One is the bacterial type ferredoxin-$NADP^+$ reductase (EC 1.18.1.2), widely distributed in *Brucella* but not in alpha-proteobacteria, and for which 3D structure and mechanism of action as NADPH oxidoreductase are reported (Pérez-Amigot et al., 2019). It probably delivers electrons from NADPH to the redox-based metabolism. But considering that a superoxide dismutase is expressed downstream it might also oxidize NADPH to activate regulons that protect against oxidative damage (Krapp et

al., 2002) (Table 4.8). The other member is the ferredoxin/rubredoxin/putidaredoxin NAD^+ reductase (EC 1.18.1.3-5), with also potential role in cellular oxidative stress response or lipid metabolism.

Finally, four FMN dependent flavoreductases are predicted to act on nitrogenous compounds. The nitroreductase family protein (EC 1.-.-.-) has unknown precise function. The nitronate monooxygenase (EC 1.13.11.32) predicted to use molecular oxygen to oxidize alkyl nitronates, and to produce enzyme-bound nitronate radicals and peroxynitroethane species. The aerobic dimethylbenzimidazole synthase (BluB, EC 1.13.11.79) that putatively catalyzes the oxygen-dependent oxidative fragmentation of the reduced isoalloxazine of FMN to yield 5,6-dimethylbenzimidazole in the biosynthesis of cobalamin (Taga et al., 2007; Campbell et al., 2006). Finally, it is the NAD(P)H nitroreductase like protein (EC 1.7.-.-) that might oxidise diverse nitrogen-containing compounds (Hritz et al., 2006).

4.3.5 Flavoenzymes of the transferase class show varied activities in *B. ovis*

Flavotransferases (EC 2.) in *B. ovis* use different structural scaffolds and catalyze quite different reactions. Their distribution varies among *Brucella* and alpha-proteobacteria species (Table 4.7). Two of them fold in GIDA domains and act in the post-translationally modification of tRNAs (2.1) (Table 4.6). Three others participate in consecutive steps of the biosynthesis of flavin cofactors: the riboflavin synthase (EC 2.5.1.9), the bifunctional FADS with two independent transferase sites (EC 2.7.7.2, EC 2.7.1.26) that has recently been characterized showing species-specific traits in both of its activities (Moreno et al., 2022); and a FAD:protein FMN transferase (EC 2.7.1.180) potentially involved in the transfer of the FMN moiety from FAD to a target flavoprotein. This class includes also the acetolactate synthase 3 (EC 2.2.) that transfers acetaldehyde from one pyruvate to either another pyruvate or 2-oxobutanoate (EC 2.2.1.6) in the respective valine and isoleucine biosynthetic pathways (Audic et al., 2009); and the blue-light-activated histidine kinase (EC 2.7.13.3). This later enzyme undergoes photochemistry through its FMN chromophore by formation of a cysteinyl-flavin adduct that allosterically controls the enzymatic activity at its kinase protein domain (Figure 4.5C) (Swartz et al., 2007).

4.3.6 Lyases and translocases have a minor representation in the flavoproteome of *B. ovis*

Flavoproteins acting as lyases use the less common folding. One is chorismate synthase (EC. 4.2.3.5) that catalyzes the formation of chorismate, a starting substrate in the biosynthesis of aromatic amino acids (Foulongne et al., 2001). The other is a bifunctional enzyme that catalyzes two sequential steps in coenzyme A biosynthesis: the CTP dependent

conjugation of cysteine and 4'-phosphopantothenate to form 4-phosphopantothenoylcysteine (EC 6.3.2.5), followed by the FMN-dependent decarboxylation of this product to 4'-phosphopantotheine (EC 4.1.1.36) (Strauss et al., 2001).

Only one flavoprotein of the core proteome of *Brucella* (Table 4.7) is predicted as a translocase. The nuoF subunit of the complex I-like NADH quinone oxidoreductase that catalyzes the translocation of protons across membrane linked to a FMN dependent NADH dehydrogenase activity (EC 7.1.1.2) and contributes therefore to aerobic respiration and OXPHOS (Schulte et al., 2019).

4.3.7 The *B. ovis* flavoproteome in virulence and infectivity

In general, *Brucella* spp. do not show aggressive virulence mechanisms such as exotoxins, anti-phagocytic capsules, plasmids, fimbria, flagella or antigenic variation. Nonetheless, they are highly pathogenic for their preferred or accidental hosts and their silent capacity to adapt to the intracellular environment. They are considered as an evolutive virulence factor by itself (López-Goñi and Moriyón, 2004). In particular, *B. ovis* shows some peculiarities: (i) it does not produce H2S, does not hydrolyze urea, and does not reduce nitrate, contrary to most *Brucella* spp, (ii) its lipopolysaccharide protective envelope is naturally rough, (iii), it is the unique *Brucella* able to oxidize ribitol with the exception of *B. neotomae* (Ronneau et al., 2016; Tsolis et al., 2009). The flavoproteome partially contributes to these evolutionary abilities. An example is EryB, particularly present in species that cause abortions, as *B. ovis*, *B. melitensis* and *B. abortus* (Barbier et al., 2014; Petersen et al., 2013; Rodríguez et al., 2012; Sangari et al., 2000).

Thus the *B. ovis* flavoproteome can be a source of virulence, infectivity and survival factors, whose distribution varies among the close analyzed species (Tables 4.6 and 4.7). Two potential virulent candidates belong to the core proteome of alpha-proteobacteria: MurB and SdhA. Nonetheless, despite predictors indicate MurB as a potential virulent/infectivity factor there is no experimental evidence beyond its essential housekeeping role to maintain the peptidoglycan cell wall (Ragunathan et al., 2018). On the contrary, SdhA is a requirement for pathogenicity in *E. coli* (Kuo et al., 2018), to stabilize the vacuole integrity during replication in the intracellular pathogen (like *B. ovis*) *Legionella pneumophila* (Creasey & Isberg, 2012), and its reduction is detected early during infection in *B. abortus* (Lamontagne et al., 2009). Moreover, the SdhB gene is virulent in *L. pneumophila* (Brüggemann et al., 2006), and the SdhB subunit plays a role in filamentation and virulence in *Candida albicans* (Bi et al., 2018). The integrity of Sdh subunits is also

related with antibiotic resistance in *Salmonella enterica* and *Xanthomonas oryzae* pv. *Oryzae* (Karsi et al., 2009; Zhang et al., 2010). Up to seventeen of the flavoproteins predicted as potentially virulent factors in *B. ovis* belong to the core proteome of *Brucella* (or lack in a single species), and are already noticed as involved in the infection process of different pathogens (Tables 4.6, 4.7 and 4.10). Among them we can highlight the following: i) Msr that maintains bacterial membrane integrity and contributes to adhesion with eukaryotic cells (Gennaris et al., 2015; Sharma et al., 2017); ii) two D-amino acid dehydrogenases that could play a pleiotropic role in the production of important virulence factors and support pathobiological exclusive functions for different isoforms within an organism (Chang et al., 2015; Oliver & Silo-Suh, 2013); iii) one isovaleryl-CoA dehydrogenase involved in vegetative growth, conidiation and virulence of plant fungal pathogens (Li et al., 2019); iv) one glutamate synthase involved in chronic persistence of *B. abortus* infection in mice (Hong et al., 2000); v) one cob(II)alamin reductase conserved in most alpha-proteobacteria and whose deletion in *B. abortus* affects the pathogen survival (Shim et al., 2018); vi) two tRNA methyltransferases with role in virulence, stress response, growth and antibiotic susceptibility pathways (Farfán-López et al., 2020); and vii) NrdI, essential for the assembly of several subunits of class Ib ribonucleotide reductases expressed under oxidative stress and iron-limited growth conditions (Rhodes et al., 2014).

Other predicted virulent factors common in nearly all *Brucella* are: the membrane bound sarcosine oxidase, the blue-light-activated histidine kinase, and the pyridoxamine 5'-phosphate oxidase family protein. The blue-light-activated histidine kinase increases its own autophosphorylation to modulate the microorganism virulence in *B. abortus*, (Swartz et al., 2007; Rinaldi et al., 2016, 2021). The pyridoxamine 5'-phosphate oxidase family protein is very rare in other bacteria, but its conservation within *Brucella* suggests a particular still unclear function. In addition, *B. ovis* contains an important number of flavoproteins (some highly conserved in *Brucella*, but not all) whose homologues are required for the survival of different pathogens upon infection by acting in key metabolic pathways and suppressing host defenses (Table 4.10).

Table 4.10. Experimental data for flavoproteins found in *B. ovis* and reported in different pathogens as contributors to virulence, survival, biofilm formation and/or infection.

Protein	Brucella core	Protein Code	Representative Species	REFERENCE
Glycerol-3-phosphate dehydrogenase	Y	ABQ60174.1	*Pseudomonas aeruginosa, Mycoplasma* spp	(Blötz & Stülke, 2017; Daniels et al., 2014)
D-erythritol 1-phosphate dehydrogenase	N	ABQ62056.1	*Brucella* spp.	(Barbier et al., 2014)
Choline dehydrogenase (Glucose-methanol-choline GMC family)	N	ABQ61350.1	*E. coli, Acinetobacter baylyi, P. aeruginosa*	(Scholz et al., 2016; Wang et al., 2010; Wargo, 2013)
Choline dehydrogenase (GMC family)	N	ABQ60630.1		
Choline dehydrogenase (GMC family, membrane bound)	N	ABQ62100.1		
PyrD dihydroorotate dehydrogenase 2 (quinone)	Y	ABQ61413.1	*Pseudomonas aeruginosa*	(Guo et al., 2016)
Succinate dehydrogenase flavoprotein subunit	Y	ABQ61077.1	*E. coli, Salmonella enterica, Legionella pneumphila, Candida albicans, Xanthomonas oryzae pv. Oryzae*	(Bi et al., 2018; Brüggemann et al., 2006; Creasey & Isberg, 2012; Karsi et al., 2009; Kuo et al., 2018; Zhang et al., 2010)
Isovaleryl-CoA dehydrogenase	Y	ABQ60382.1	*Magnaporthe oryzae*	(Li et al., 2019)
Acyl-CoA dehydrogenase	N	ABQ62576.1	*Burkholderia cenocepacia, Mycobacterium spp*	(Hughes et al., 2007; Subramoni et al., 2011; Yang et al., 2015)
Acyl-CoA dehydrogenase	N	ABQ62784.1		
Acyl-CoA dehydrogenase	N	ABQ62889.1		
Glutamate synthase	Y	ABQ61996.1	*Brucella abortus, Xanthomonas oryzae pv. Oryzae*	(Hong et al., 2000; Pandey et al., 2014)
	N	ABQ62546.1		
Pyridoxamine 5'-phosphate oxidase	Y	ABQ60142.1	*Mycobacterium tuberculosis, Streptococcus pneumoniae*	(Ankisettypalli et al., 2016; El Qaidi et al., 2013)
Predicted D-amino acid dehydrogenase small subunit	Y	ABQ61937.1	*Pseudomonas aeruginosa, Cryptococcus neoformans, Cryptococcus gattii*	(Chang et al., 2015; Oliver & Silo-Suh, 2013)
D-amino acid dehydrogenase	Y	ABQ62278.1		
Predicted D-amino acid dehydrogenase	N	ABQ62519.1		
Flavin reductase domain containing protein	Y	ABQ60228.1	*Streptococcus pneumoniae*	(Morozov et al., 2018)
Sarcosine oxidase	Y	ABQ60177.1	*Pseudomonas aeruginosa PAO1*	(Gallagher & Manoil, 2001)
		ABQ61310.1		
		ABQ61036.1		
WrpA type FMN-dependent NADH:quinone oxidoreductase	Y	ABQ60884.1	*Brucella abortus*	(Herrou et al., 2016)
NADH dehydrogenase	N	ABQ62704.1	*Pseudomonas aeruginosa*	(Torres et al., 2019)
Assimilatory sulphite reductase (NADPH) alpha component cluster	N	WP_006015252.1	*Paracoccidioides brasiliensis, Salmonella enterica serovar Enteritidis*	(Liu et al., 2021; Menino et al., 2013)
		WP_006015255.1		
		WP_006015257.1		
		WP_006015259.1		
Dihydrolipoyl dehydrogenase (IpdA-1)	Y	ABQ62466.1	*Mycoplasma gallisepticum, Vibrio parahaemolyticu*	(He et al., 2015; Hudson et al., 2006)
Dihydrolipoyl dehydrogenase (IpdA-2)	Y	ABQ60398.1		
Dihydrolipoyl dehydrogenase (IpdA-3)	Y	ABQ61458.1		
	Y	ABQ62365.1		

Peptide-methionine (S)-S-oxide reductase (quinone) (Msr). MsrP catalytic subunit. MsrQ heme-binding subunit		ABQ62343.1	*Xanthomonas translucens pv. Undulosa, Staphylococcus Aureus, Helicobacter pylory*	(Gennaris et al., 2015; Sasindran et al., 2007; Sharma et al., 2017)
Predicted aerobic 5,6-dimethylbenzimidazole synthase (BluB)	N	ABQ62404.1	*Listeria monocytogenes, Mycobacterium spp, Brucella spp, Vibrio spp, Sinorhizobium meliloti*	(Anast et al., 2020; Campbell et al., 2006; Taga et al., 2007)
Predicted Salicylate hydroxylase	N	ABQ60978.1	*Verticillium dahliae, Peronospora parasítica, Ustilago maydis, Candidatus Liberibacter asiaticus*	(Donofrio & Delaney, 2001; Li et al., 2017; Luo et al., 2020; Rabe et al., 2013)
Cob(II)alamin reductase	Y	ABQ60249.1	*Listeria monocytogenes, Brucella ovis, Sinorhizobium meliloti*	(Anast et al., 2020; Lu et al., 1995; Shim et al., 2018)
Methylenetetrahydrofolate-tRNA-(uracil54-C5-)-methyltransferase NAD(P)H oxidase	N	ABQ61275.1	*Mycoplasma bovis, Pseudomonas aeruginosa, Salmonella enterica Serovar typhimurium, Streptococcus pyogenes*	(Cho & Caparon, 2008; Guo et al., 2017; Gupta et al., 2009; Shippy et al., 2012)
tRNA (carboxymethyluridine34-5-O)-methyltransferase	Y	ABQ60378.1	*Mycoplasma bovis, Pseudomonas aeruginosa, Salmonella enterica Serovar typhimurium, Streptococcus pyogenes,*	
Blue-light-activated histidine kinase	Only lacks in one	ABQ62113.1	*Brucella* spp., *Brucella abortus*	(Rinaldi et al., 2016, 2021; Swartz et al., 2007)
Chorismate synthase	N	ABQ60200.1	*Shigella flexneri, Burkholderia pseudomallei, Xanthomonas oryzae pathovar oryzae*	(Cersini et al., 1998; Song et al., 2012; Srilunchang et al., 2009)
Protein NrdI	Y	ABQ62891.1	*Streptococcus sanguinis, Mycobacterium tuberculosis*	(Rhodes et al., 2014; Zheng et al., 2008)

It is also interesting to note that the *B. ovis* genome contains a large amount of transposable recombinogenic elements and pseudogenes (up to 119 in CI and 125 in CII) that can contribute to its variability, adaptive and evolutionary capacities (Bartosik et al., 2003). Many of them sit next to or in flavoenzyme encoding genes (Tables 4.8 and 4.9). For example, one IS5 transposase is located between the gene encoding the pyridoxamine 5'-phosphate oxidase family protein and the gene encoding for the PhzF family phenazine biosynthesis protein. Other IS5 transposase interrupts the two SoxB genes (Figure 4.4A, Table 4.8), similarly to that reported in the *Pseudomonas aeruginosa* PAO1 and related to a reduction of pathogenicity (Gallagher & Manoil, 2001). Regarding pseudogenes, the *B. ovis*

xanthine dehydrogenase operon contains a pseudogene instead of a regular xdhB encoding region for the corresponding protein subunit (Table 4.8). This XdhB subunit is not expected to bind flavin, but its lack will make xanthine dehydrogenase not functional (Tsolis et al., 2009). The *B. ovis* BOV_RS11620 gene encoding for the NosR transcriptional regulator of the expression of the nitrous oxide reductase NosZ has also a deletion in its FMN_bind domain (PF04205). The nosX gene, necessary for NosR covalent flavinylation, is in addition a pseudogene (BOV_RS11650) (Zhang et al., 2017). These features introduce defects in the nitrogen metabolism of *B. ovis*, and contrary to other *Brucella* make it particularly unable for full denitrification and nitrous oxide respiration (Wunsch & Zumft, 2005). Thus, degradation of the *B. ovis* flavoproteome surely contributes to narrow its host range and to make it non-zoonotic (Tsolis et al., 2009).

4.3.8 The *B. ovis* flavoproteome as a source of antimicrobial targets and biocatalyst

Up to thirty-five *B. ovis* flavoproteins, most of them belonging to the *Brucella* core proteome, lack homologues in *O. aries* and other mammals (Table 4.11). This list could be potential targets for the search of antimicrobials. Some of them are already being explored as targets of inhibitors in other bacteria, as for example, UDP-N-acetylmuramate dehydrogenase (Hrast et al., 2018; Amera et al., 2020), riboflavin synthase (Serer et al., 2019), bifunctional riboflavin kinase/FAD synthase (Sebastián et al., 2018; Lans et al., 2020) or chorismate synthase (Bueno et al., 2019). In agreement, a comparative metabolomics study in *B. melitensis* also pointed chorismate synthase as an attractive target (Maskar & Meshram, 2013). Other of them with certain homology to the here identified thioredoxin-disulphide reductase (O'Loughlin et al., 2021) or FAD: protein FMN transferase are also being considered antimicrobial targets (Deka et al., 2022). Noticeably, Table 4.11 includes an important number of the *B. ovis* flavoproteins for which the exact physiological function is difficult to envisage. Among them are predicted alkene reductase and KsdD-like steroid dehydrogenase, the pyridoxamine 5'-phosphate oxidase family protein, two potential aminoacetone oxidase family FAD-binding dehydrogenases, two potential D-amino acid dehydrogenases, the predicted nitroreductase family protein and the NADPH dehydrogenase from the old yellow enzyme family. Of interest, the later enzyme has been reported to participate in the oxidative stress response and detoxification in *B. subtilis* (Fitzpatrick et al., 2003) what points it as an interesting target to control de pathogen survival. Moreover, seven of this *B. ovis* flavoproteins (Table 4.11) are underrepresented in alpha-proteobacteria, suggesting that they might be explored also as potential selective antimicrobial targets.

Among them are the pyridoxamine 5'-phosphate oxidase family protein, the NADPH dehydrogenase-Old yellow enzyme and the predicted nitroreductase family protein, all of them of still unclear function. This group is completed with the predicted salicylate hydroxylase, the FAD:protein FMN transferase, the blue-light-activated histidine kinase and the protein NrdI. Considering their above-mentioned envisaged roles for virulence upon infection in different bacteria (Table 4.10), these four proteins might be also of particular relevance as drug targets (Rhodes et al., 2014; Rinaldi et al., 2021).

Table 4.11. *Brucella ovis* ATCC 25840 flavoproteins lacking homologues in *O. aries* and Mammalia. Threshold set in at least 30 % sequence identity over 50 % of the query cover.

Flavoprotein	Protein Code	Flavoprotein	Protein Code
Potential L-gulonolactone oxidase FAD-binding oxygen oxidoreductase	ABQ62001.1	Peptide-methionine (S)-S-oxide reductase (quinone). MsrP catalytic subunit.	ABQ62365.1
UDP-N-acetylmuramate dehydrogenase	ABQ61769.1	Nitronate monooxygenase (formerly 2-nitropropane dioxygenase NPD)	ABQ62537.1
Predicted alkene reductase: N-ethylmaleimide reductase, glycerol trinitrate reductase or xenobiotic reductase B	ABQ62490.1	Predicted aerobic 5,6-dimethylbenzimidazole synthase (BluB)	ABQ62404.1
Predicted KsdD-like steroid dehydrogenase	ABQ62061.1	Predicted Salicylate hydroxylase	ABQ60137.1
Pyridoxamine 5'-phosphate oxidase family protein [a,b]	ABQ61684.1	Predicted Salicylate hydroxylase [a]	ABQ60978.1
Glycine oxidase ThiO	ABQ60316.1	4-hydroxybenzoate 3-monooxygenase	ABQ62030.1
Potential Aminoacetone oxidase family FAD-binding enzyme/ NAD(P)/FAD-dependent dehydrogenase	ABQ60616.1	Bacterial luciferase	ABQ60348.1
Potential Aminoacetone oxidase family FAD-binding enzyme/ NAD(P)/FAD-dependent dehydrogenase	ABQ60524.1	Cob(II)alamin reductase	ABQ60249.1
Predicted D-amino acid dehydrogenase small subunit	ABQ61937.1	Ferredoxin-$NADP^+$ reductase	ABQ61707.1
Predicted D-amino acid dehydrogenase	ABQ62519.1	Predicted nitroreductase family protein [a]	ABQ62091.1
Flavin reductase domain containing protein	ABQ60228.1	Methylenetetrahydrofolate-tRNA-(uracil54-C5-)-methyltransferase NAD(P)H oxidase	ABQ61275.1
Predicted monomeric Sarcosine oxidase	ABQ62932.1	Acetolactate synthase 3 catalytic subunit	ABQ60081.1
WrpA-type FMN-dependent NADH:quinone oxidoreductase	ABQ60884.1	Riboflavin synthase alpha subunit	ABQ60518.1
NADPH dehydrogenase (Old yellow enzyme) [a]	ABQ62422.1	Bifunctional riboflavin kinase/FAD synthase	ABQ62831.1
Predicted NAD(P)H nitroreductase [b]	ABQ60834.1	FAD:protein FMN transferase[a]	ABQ62066.1
Assimilatory sulphite reductase (NADPH) alpha component cluster [b]	WP_006015252.1	Blue-light-activated histidine kinase[a]	ABQ62113.1
	WP_006015255.1	Chorismate synthase	ABQ60200.1
	WP_006015257.1	Protein NrdI[a]	ABQ62891.1
Predicted thioredoxin-disulphide reductase	ABQ61134.1		

[a] Proteins underrepresented in alpha-proteobacteria.
[b] Proteins without homologues in any Eukarya.

In addition, Table 4.11 might also contain flavoenzymes with particular properties for their use in organic synthesis, biocatalysis, and/or bioremediation. Some of them might be predicted nitroreductase family protein or nitronate monooxygenase. If, as envisaged,

they contribute to the catabolism of nitroalkanes, widely used in chemical industry and as fuels, their low homology to other family members might provide them with particular stability or mechanistic features that would enlarge their applicative perspectives (Torres-Guzman et al., 2021). In any case, before used as either antimicrobial targets or biocatalyst, these flavoproteins should be exhaustively characterized at the structural and functional levels to confirm their relevance for bacteria survival, and investigated their species-specific features and/or the applicability of the chemical process they catalyze.

4.4 DISCUSSION

The predicted flavoproteins of *B. ovis* are envisaged to catalyze an important number of reactions in a large number of metabolic pathways, being particularly involved in the shuttle of electrons to the bacterial metabolism, the primary and energy metabolism, the metabolism of fats, carbohydrates, proteins and nucleotides, the oxidative stress response, or the tRNAs methylation (Figure 4.9B, Table 4.6), according with previous reports (Parsons & Dias, 1991; Myllykallio et al., 2002; Bornemann, 2002; Lipton & Bossy-Wetzel, 2002; Mansoorabadi et al., 2007; Nishimasu et al., 2009; Becker & Natarajan, 2012; Pinto & Cooper, 2014; Romero et al., 2018). Moreover, the *B. ovis* flavoproteome also contains enzymes that are candidates to favour the microbial metabolism in diverse environments, the xenobiotic metabolism for detoxification of aromatic compounds, the bacterial virulence or the activation of metabolites (pyruvate, folate, pyridoxal 5'-phosphate, vitamin B2, vitamin B12…). Therefore, flavoproteins and flavoenzymes are implicated in the transformation of a vast variety of metabolic bioactive compounds or are directly involved in suppressing the stress induced by the host cells upon infection, what can make some of these proteins, potential targets in the treatment of brucellosis. Noticeably, in *B. ovis*, 55% of 78 predicted flavoproteins belong to the core proteome of *Brucella*, whereas only 18% lack in 25% of the *Brucella* species here evaluated (Table 4.7). This indicates a heavy dependence of the *Brucella* metabolism on flavoproteins. Moreover, many of these core flavoproteins are particular of *Brucella*, since very few are found in all alpha-proteobacteria evaluated; namely Sdh, dihydrolipoyl dehydrogenases 2 and 3, thioredoxin-disulphide reductase and MurB. Nonetheless, the study of the *B. ovis* flavoproteome also shows some of its members are degraded, and probably unable to be functional, introducing variability in the capacities of this bacteria regarding to other members of the genus.

4.5 CONCLUSION

In the last decades many efforts have been done in sequencing different genomes. Many proteins with undetermined or putative functions have been identified, but so far little has been done yet to elucidate or corroborate their biological activity. In this context, it is of relevance to predict and evaluate the functionality of candidates to flavoproteins in particular organisms. Here we provide the list of proteins making the flavoproteome in *B. ovis*, as well as data of their potential activities and prevalence in different *Brucella* and alpha-proteobacteria species. Several predicted flavoproteins are highly divergent in this genus from revised proteins and for them is difficult to envisage a clear function. This will probably relate to modified activities or divergent processes and mechanisms still not identified. Based on the here compiled information we also identify some flavoproteins that might become potential antimicrobial and envisage that others might become new biocatalyst.

5.

The UDP-N-acetylglucosamine enolpyruvyl transferase from Brucella ovis: Insights into functional and structural features during the transformation of UDP-N-acetylglucosamine to enolpyruvyl-UDP-N-acetylglucosamine

5.1 SUMMARY

MurA (UDP-N-Acetylglucosamine enolpyruvyl transfer) is a pivotal enzyme that catalyzes the transfer of enolpyruvate from PEP to UNAG to synthesise UNAGEP, playing an indispensable role in the biosynthesis of the bacterial cell's PG layer. Therefore, it serves as an attractive template for the design of novel antibiotic drugs. Exploration of MurA sequences in several *Brucella* genera, as well as in other bacterial species, has revealed the presence of multiple copies within their genomes. While this phenomenon is typical among some Gram-positive bacteria, there is no bibliographic evidence addressing the study of multiple murA genes in Gram-negative bacteria. In our study, *B. ovis* was found to possess only one copy of murA, resulting in the production of the BoMurA protein. Comparative analysis revealed that BoMurA sequence shares a substantial degree of identity, exceeding 90% with other sequences in the *Brucella* genus and more than 40% with several bacterial genera. BomurA was cloned with a His-tagged and successfully overexpressed in *E. coli* as BoHTMurA. Subsequently, it was purified and characterized through SDS-PAGE, SEC, CN-PAGE, absorption, CD and fluorescence. These analyses confirmed that the purified protein is properly folded and exists in the monomeric form. On its side, thermal stability studies suggest that BoHTMurA unfolding does not occur cooperatively, and only envisage a slight protein stabilization in the presence of the UNAG substrate. Additionally, methodologies for measuring enzymatic activity to produce UNAGEP were standardized, being this product a critical component of the experimental development for the subsequent chapter (Chapter 6). Optimal conditions were identified wherein BoHTMurA produced the higher quantity of product within a 30 min reaction, comprising a mixture of 2 mM UNAG, 2 mM PEP, and 50 nM enzyme in 50 mM Bis-Tris Propane pH 7.0, at 37 ºC. Furthermore, the V_{max} under evaluated conditions was determined in the range of 1.6 µM min^{-1} with an apparent k_{cat} around 32 min^{-1}. These values are similar to those observed in other MurAs such as *S. aureus* and *S. pneumoniae*. The evaluation of the UNAGEP production by BoHTMurA was carried out using HPLC and NMR, confirming the formation of the product, but failing in the complete conversion and its purification. Lastly, despite multiple crystallization attempts, the structure of BoHTMurA could not be experimentally resolved. Nonetheless, theoretical models have been produced in its free form and in complex with its substrates. This combined approach, involving multiple sequence analyses and structural modeling, allowed us to identify the specific residues in BoMurA that are envisaged to interact with the UNAG substrate, as well as the regions and residues that play essential roles in the catalytic process. Notably, these regions exhibit a high degree of conservation among the MurA sequences examined in this study.

5.2 INTRODUCTION

UDP-N-acetylglucosamine enolpyruvyl transferase, also known as MurA (EC 2.5.1.7), catalyzes the first step in the cytoplasmic biosynthesis of the peptidoglycan (PG) precursor molecules by transferring the enolpyruvyl group of phosphenol pyruvate (PEP) to UDP-N-acetylglucosamine (UNAG) to produce enolpyruvyl-UDP-N-acetylglucosamine (UNAGEP) (Bensen et al., 2012). MurA is an extremely ubiquitous enzyme, highly conserved among bacteria, that is critical for survival and has no human homolog (Zoeiby et al., 2003). Sequence analysis has identified up to two genes encoding this enzyme in some Gram-positive bacteria: murA (murA1) and murZ (murA2), the second of which may have arisen from a gene duplication event, whereas most Gram negative bacteria have only one gene (Blake et al., 2009).

5.2.1 The MurA catalytic activity

MurA is therefore an enolpyruvyl transferase. The catalytic cycle model of enolpyruvyl transferases is based on the fact that the free enzyme (E) reversibly binds the first substrate (S1, UNAG in this case), forming a binary complex (E:S1), which undergoes a conformational change, resulting in the formation of the binding site for the second substrate (S2, PEP) (Figure 5.1). The second substrate can then bind, forming a ternary complex (E:S1:S2) that evolves into two reaction products (E:P1:P2). Lastly, the release of the products (E + P1 + P2) allows the enzyme to return to its original conformation. In particular, the reaction catalyzed by MurA enzymes is proposed to proceed via an addition-elimination mechanism (Marquardt et al. 1993).

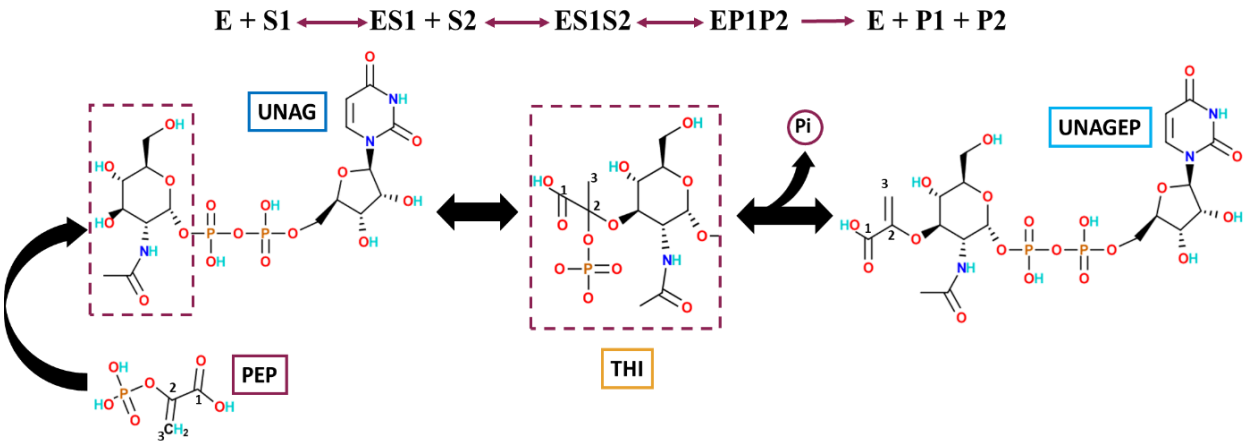

Figure 5.1. The MurA catalytic cycle. MurA catalyzes the transfer of the enolpyruvyl group of PEP to UNAG, while an inorganic phosphate is released from the THI to produce UNAGEP. The top panel shows the overall reaction scheme, while the bottom shows a scheme of the molecular chemical process. S1, S2, P1 and P2 account respectively for UNAG, PEP, Pi and UNAGEP.

Some studies suggest the existence of at least two intermediates in the MurA pathway, a phospholactoyl-enzyme tetrahedral intermediate (THI) and the subsequent phospholactoyl-UNAG intermediate (Brown et al., 1994). The reaction then proceeds through a THI, where the 3'-OH group of UNAG binds covalently to C2 of PEP, being its C3 then converted to a methyl group. During the breakdown of the THI, inorganic phosphate (Pi) is released and the C3 methyl group is deprotonated, resulting in the product UNAGEP (Eschenburg et al., 2003; Skarzynski et al., 1998) (Figure 5.1).

5.2.2 Structure of MurA enzymes

X-ray structures for several MurA proteins from different species, as well as in complexes with inhibitors or substrates, are available in the PDB (Tables 5.1 and 5.2). To describe the general structural features of MurA enzymes, the structures of *E. cloacae* MurA in the absence of ligands (PDB code 3SPB) (Skarzynski et al., 1998) and *E. coli* MurA (PDB code 1UAE) in complex with UNAG and [(1R)-1-hydroxypropyl]phosphonic acid (FFQ), a structural analog of PEP (Zhu et al., 2012), were here taken as models.

MurA proteins fold into two globular domains, each one consisting of six helices and three four-stranded β sheets (Figure 5.2). One striking feature of MurA structures is the six-fold repetition of one folding unit, or subdomain, consisting of β1, α1, β2, α2, β3 and β4 cores. Each domain has three folding units. The domains are connected by two strands, each of 3 and 4 amino acids in length, respectively. The active site is located in a deep cavity between the two domains, where the reaction occurs by an induced-fit mechanism involving conformational changes in the two domains (Yoon et al., 2008). The unbound "open" enzyme state first interacts with UNAG, forming a "closed" binary state where the second substrate, PEP, binds. In the course of the "open-closed" transition, a 10 residue loop located in Domain II and containing a Cys residue undergoes a drastic rotation. This rotation positions the side chain of the Cys residue towards the PEP binding site, and it could be inferred that such residue participates in the catalysis of the enzyme (Han et al., 2010).

Table 5.1 Summary of structural data for MurA enzymes available in the PDB.

Organism	% Identity to BoMurA	PDB Code	Ligand	Reference
Acinetobacter baumannii	50 %	5U4H	FMT, Na^{+}, 0V5	(Minasov et al. *To be published*)
Aliivibrio fischeri MJ11	49 %	3VCY	FFQ, GOL, $PO_4^{=}$, UD1	(Bensen et al., 2012)
Aquifex aeolicus VF5	46 %	2YVW	EPU, $PO_4^{=}$	(Kitamura, et al. *To be published*)
Bacillus anthracis	46 %	3SG1	PGE, PG4	(Minasov et al. *To be published*)
Campylobacter jejuni	45 %	5UJS	Cl^{-}	
Clostridioides difficile 630	48 %	6Q0A	EDO, EPZ	(Dopkins et al. *To be published*)
		6Q03		
		6Q0Y	EDO, UD1	
		6Q11	EDO, EPU, Na^{+}	
Enterobacter cloacae	49 %	1DLG	HAI, $PO_4^{=}$	(Schönbrunn et al., 2000)
		1EJC	GOL, $PO_4^{=}$	(Eschenburg & Schönbrunn, 2000)
		1EJD	HAI, $PO_4^{=}$	
		1EYN	2AN, GOL	(Schönbrunn et al., 2000)
		1Q3G	EDO, UDA	(Eschenburg et al., 2003)
		1Q36	FMT, SKP	
		1YBG	TAV	(Eschenburg et al., 2005)
		1RYW	EPU, GOL, $PO_4^{=}$	(Eschenburg et al., 2005)
		1NAW	HAI	(Schönbrunn et al., 1996)
		3KQA	Ca^{+2}, TR9	(Han et al., 2010)
		3KR6	FFQ, UD1	
		3LTH		
E. cloacae subsp. *cloacae* ATCC 13047		3SPB	Na^{+}	(Zhu et al., 2012)
		3SU9	ACT, EDO, EPZ	
		3SWA	EDO, UD1	
		3SWD	EPZ	
		3SWE	EPZ, GOL, $SO_4^{=}$	
		3SWG	EDO, EPZ, PEG, PG4, PGE	
		3SWI	Mg^{+2}, MOE, PG0, UD2, UPN	
		3SWQ	ACT, EDO, EPU, PEG, PGE	
		3UPK	EDO, PGE, UD1	
		3V5V	ACT, EDO, PEG, PGE	
		3V4T	ACT, EDO, UD1	
		4E7B	ACT, EDO, UPG	(Zhu et al. *To be published*)
		4E7C	ACT, EDO, UTP	
		4E7D		
		4E7E	ACT, EDO, UPG	
		4E7F	ACT, EDO, UDP	
		4E7G	ACT, EDO, PEG	
		4EII	EDO, GOL, PGE	
E. coli	49 %	1UAE	FFQ, UD1	(Skarzynski et al., 1996)
		1A2N	TET	(Skarzynski et al., 1998)
		2Z2C	UDC, UDP	(Steinbach et al. *To be published*)
E. coli K-12		3ISS	EPU, PO_3^{-}	(Jackson et al., 2009)
		3KQJ	GOL, UD1, $PO_4^{=}$	(Han et al. *To be published*)
E. coli O139:H28		5VM7		(Cui et al., 2017)
Haemophilus influenzae	50 %	2RL1	UD1, $SO_4^{=}$	(Yoon et al., 2008)
		2RL2	UD1, GG6, $SO_4^{=}$	
		3SWE	EPZ, $SO_4^{=}$, GOL	(Zhu et al., 2012)
L. monocytogenes	46 %	3R38	Cl^{-}, $SO_4^{=}$	(Halavaty et al. *To be published*)
Pseudomonas aeruginosa PAO1	52 %	5BQ2	EPU, Mg^{+2}	(Abendroth et al. *To be published*)
Pseudomonas putida	50 %	6CN1	EPU, Mg^{+2}, Cl^{-}, 0V5	(Minasov et al. *To be published*)
Stenotrophomonas maltophilia K279a	51 %	6WFM		(Abendroth et al. *To be published*)
Streptococcus pneumoniae TIGR4	47 %	5WI5	EPU, 0V5, Mg^{+2}	(Minasov et al. *To be published*)
Vibrio cholerae O1 biovar El Tor str. N16961	49 %	4R7U	UD1, PG4, FFQ, Na^{+}	(Nocek et al. *To be published*)

Table 5.2 Summary of ligands found in the MurA structures deposited in the PDB.

Code names for PDB ligands		
Code	Name	Formula
EPU	Uridine-Diphosphate-2(N-AcetylGlucosaminyl) Butiric Acid	$C_{20}H_{29}N_3O_{19}P_2$
EPZ	(2R)-2-{[(2R,3R,4R,5S,6R)-3-(acetylamino)-2-{[(S)-{[(R)-{[(2R,3S,4R,5R)-5-(2,4-dioxo-3,4-dihydropyrimidin-1(2H)-yl)-3,4-dihydroxytetrahydrofuran-2-yl]methoxy}(hydroxy)phosphoryl]oxy}(hydroxy)phosphoryl]oxy}-5-hydroxy-6-(hydroxymethyl)tetrahydro-2H-pyran-4-yl]oxy}propanoic acid	$C_{20}H_{31}N_3O_{19}P_2$
UDA	3'-1-Carboxy-1-phosphonooxy-ethoxy-uridine-diphosphate-N-acetylglucosamine	$C_{20}H_{32}N_3O_{23}P_3$
UDC	2-acetamido-3-O-[(2S,3S)-2-carboxy-3,4-dihydroxybutan-2-yl]-2-deoxy-alpha-D-glucopyranose	$C_{13}H_{23}NO_{10}$
UD1/UD2	Uridine-Diphosphate-N-Acetylglucosamine	$C_{17}H_{27}N_3O_{17}P_2$
UDP	Uridine-5'-Diphosphate	$C_9H_{14}N_2O_{12}P_2$
UPG	Uridine-5'-Diphosphate-Glucose	$C_{15}H_{24}N_2O_{17}P_2$
UPN	2-{[(2R,3R,4R,5R,6R)-3-(acetylamino)-2-{[(S)-{[(R)-{[(2R,3S,4R,5R)-5-(2,4-dioxo-3,4-dihydropyrimidin-1(2H)-yl)-3,4-dihydroxytetrahydrofuran-2-yl]methoxy}(hydroxy)phosphoryl]oxy}(hydroxy)phosphoryl]oxy}-5-hydroxy-6-(hydroxymethyl)tetrahydro-2H-pyran-4-yl]oxy}prop-2-enoic acid	$C_{20}H_{29}N_3O_{19}P_2$
UTP	Uridine 5'-Triphosphate	$C_9H_{15}N_2O_{15}P_3$
SKP	5-(1-Carboxy-1-phosphonooxy-ethoxyl)-4-hydroxy-3-phosphonooxy-cyclohex-1-enecarboxylic acid	$C_{10}H_{16}O_{14}P_2$
FMT	Formic Acid	CH_2O_2
FFQ	[(1R)-1-hydroxypropyl]phosphonic acid	$C_3H_9O_4P$
TAV	N-methyl-N-{2-[(2-naphthylsulfonyl)amino]-5-[(2-naphthylsulfonyl)oxy]benzoyl}-L-aspartic acid	$C_{32}H_{26}N_2O_{10}S_2$
TET	Uridine-diphosphate-2(N-acetylglucosaminyl-3-fluoro-2-phosphonooxy)propionic acid	$C_{20}H_{31}FN_3O_{23}P_3$
HAI	Cyclohexylammonium Ion	$C_6H_{14}N$
0V5	(2R)-2-(phosphonooxy)propanoic acid	$C_3H_7O_6P$
EDO	1,2-Ethanediol	C_2H_6O
MOE	Methoxy-Ethoxyl	$C_3H_7O_2$
GOL	Glycerol	$C_3H_8O_3$
$PO_4^{=}$	Phosphate Ion	O_4P^{-3}
PO_3^{-}	Phosphite Ion	O_3P^{-3}
PGE	Triethylene Glycol	$C_6H_{14}O_4$
PG4	Tetraethylene Glycol	$C_8H_{18}O_5$
PG0	2-(2-Methoxyethoxy)ethanol	$C_5H_{12}O_3$
2AN	8-Anilino-1-Naphthalene Sulfonate	$C_{16}H_{13}NO_3S$
TR9	(5S)-2,5-dihydroxy-3-methylcyclohex-2-ene-1,4-dione	$C_7H_8O_4$
ACT	Acetate Ion	$C_2H_3O_2$
$SO_4^{=}$	Sulfate Ion	O_4S^{-2}
PEG	Di(hidroxyenthyl) ether	$C_4H_{10}O_3$
GG6	[(1S,2S)-1,2-Dihydroxypropyl]phosphonic acid	$C_3H_9O_5P$

In most evaluated structures, the active Cys-loop consists of 10 amino acids (PGGCxIGxRP), anchored by Pro residues and containing three Gly residues, making it very flexible. The loop intermediate Cys is conserved in *E. coli* (Cys115), *E. cloacae* (Cys115), *S. pneumonia* (Cys116), *A. baumannii* (Cys116) and *H. influenzae* (Cys117) (Engel et al.,

2013; Skarzynski et al., 1998; Sonkar et al., 2017; Yoon et al., 2008; Zhu et al., 2012). This Cys residue has been proposed to play two distinct roles in catalysis. First, it participates as a general acid/base catalyst and enzyme nucleophile, although the latter role is not necessary for enzymatic activity. The thiol group of the Cys protonates the double bond of PEP at C3, and stabilizes the positive charge at C2 of the PEP cation electrostatically. The thiolate formed in this step acts as a general base during the elimination step by deprotonating the methyl group of the THI (Kim et al., 1996). The second role relates to product release: the conformation of the enzyme changes from the "closed" to the "open" state during the release of UNAGEP and Pi products. The enzyme exhibits a "staged conformation", when the Pi product binds to the polyanion binding site, which is located in a tunnel between the active site and the protein surface (Eschenburg et al., 2005; Jackson et al., 2009). Noticeably, in certain species, such as *M. tuberculosis*, *Borrelia burgdorferi* and *Chlamydia trachomatis*, the active site Cys residue is absent, being replaced by an aspartate residue (Asp117, Asp116 and Asp119 respectively). Despite the presence of this Asp, these MurA enzymes are also active (Jiang et al., 2011).

The Cys-loop in *E. coli* MurA contains three conserved glycine residues (Gly113, Gly114 and Gly118), which serve as hinge groups and allow the transition between loop states. The active site between the two domains stabilizes the binding of PEP by forming seven H-bonds with Lys22, Cys115, Arg120 and Arg397 (Sonkar et al., 2017). In addition, Arg120 may also contribute to stabilize the "closed" conformation through interactions with the phosphonate group of UNAG (Klein & Bachelier, 2006) (Figure 5.3).

The "open" conformation of the enzyme is believed to be stabilized by repulsive forces between the Arg397 and Lys48 residue pairs in the interdomain cleft. This repulsive force is neutralized when UNAG binds, enabling the two domains to approach each other. The N-acetylglucosamine moiety of the substrate interacts with several water molecules present in the active site pocket, forming three H-bonds that involve Asn23 and Asp305. UNAG also interacts with Arg91, Arg120, Ser162, Val163 and Gly164 upon binding (Schönbrunn et al., 1996; Skarzynski et al., 1996).

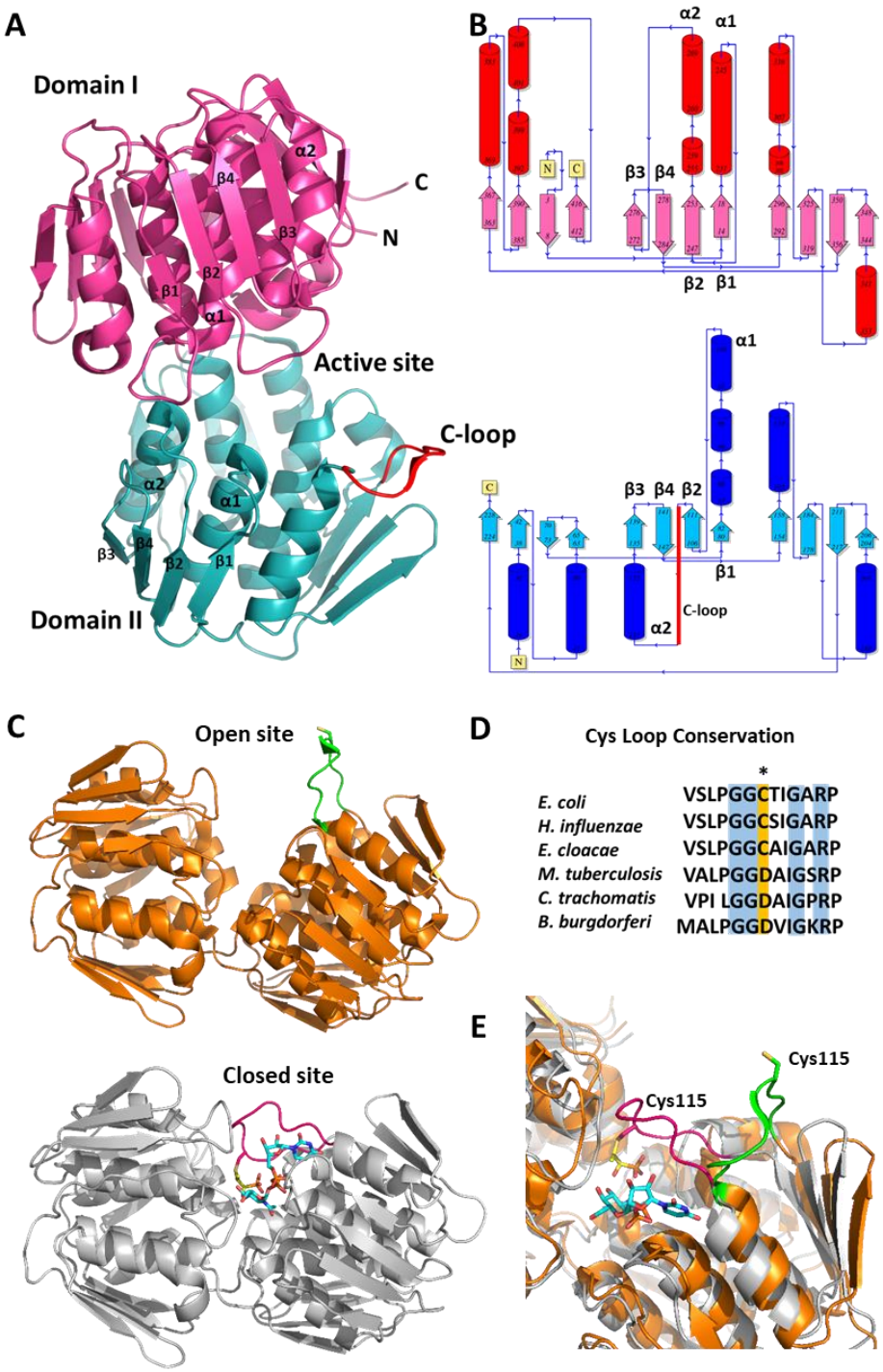

Figure 5.2. Structural organization of MurA enzymes. (A) Tertiary structure of the "open" conformation of *E. cloacae* MurA (3SPB), colored by domain as indicated in B. **(B)** Topology diagram of each domain as obtained by PDBsum software (Laskowski et al., 2018). Domains I and II are respectively colored with α-helixes/β-sheets in red/pink and dark/light blue, in both representations the conformational arrangement β1, α1, β2, α2, β3 and β4 is indicated and the Cys-loop is shown in red. **(C)** Cartoon representation of "open" conformation of *E. cloacae* MurA (3SPB) (orange) and "closed" conformation of *E. coli* MurA (1UAE) (grey). The Cys-loop is colored in green and pink, respectively and UNAG is depicted by carbon atoms in blue sticks. **(D)** Sequence alignment of the Cys-loop segment of 6 bacteria species containing either Cys or Asp as central residue. **(E)** Detail of an overlap of "open" and "closed" structures highlighting the two positions of the Cys-loop and Cys115 (sticks).

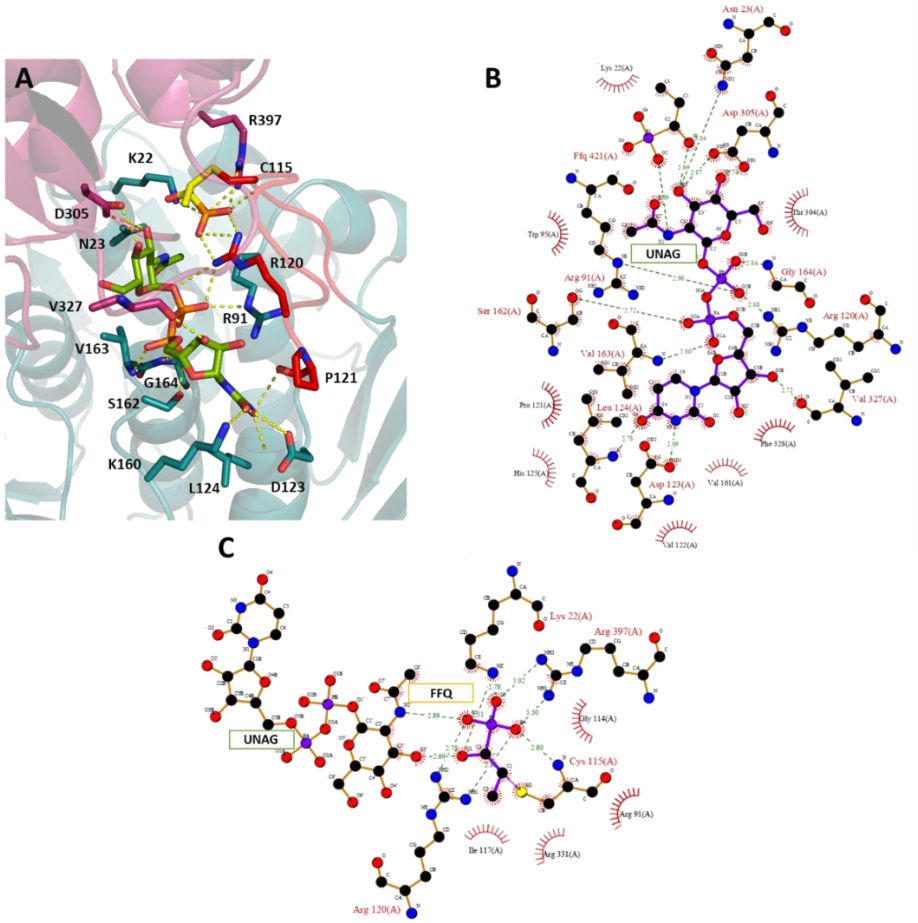

Figure 5.3. Site of interaction of *E. coli* MurA (1UAE) with bound UNAG and PEP structural analogue FFQ. (A) Detail of the H-bond network of domain I (pink) and domain II (blue) side-chains with UNAG (CPK colored green sticks) and FFQ (CPK colored yellow sticks). The Cys-loop residues are shown in CPK colored red sticks. **(B)** and **(C)** show the corresponding LIGPLOT diagrams of interactions.

5.2.3 Inhibition and resistance

Of all the enzymes involved in the PG synthesis pathway, only MurA is currently targeted by an antibiotic, fosfomycin, with a chemical structure unrelated to that of other known antibiotics. Fosfomycin is an old, low molecular weight (Mw) antibiotic agent that contains two critical groups, an epoxide and a phosphonic, which inhibit *E. coli* MurA by covalently binding to the thiol group of Cys115. It was discovered in 1969 as a phosphoenolpyruvate analog produced by *Streptomyces* spp. (de Oliveira et al., 2022; Falagas et al., 2016).

In vitro susceptibility data suggest that fosfomycin exhibits significant activity against Gram-positive pathogens, such as *Enterococcus* spp. (Allerberger & Klare, 1999), *S. aureus* (Alvarez et al., 1985) and *S. pneumoniae* as well as in Gram-negative pathogens including *E. coli*, *Proteus mirabilis*, *K. pneumoniae*, *Enterobacter* spp., *Citrobacter* spp., *Serratia marcescens*, *Neisseria meningitidis*, *Shigella* spp., and *Salmonella typhi*, which are

typically inhibited at fosfomycin concentrations ≤64 mg/ml (Michalopoulos et al., 2011). However, fosfomycin does not inhibit MurA enzymes whose catalytic residue is an Asp (Skarzynski et al., 1998).

The clinical efficacy of fosfomycin is compromised by both plasmid and genomic encoded resistance proteins that catalyze either the addition of thiols to the oxirane ring (Fillgrove et al., 2003), or the opening of the oxirane ring, thereby rendering it ineffective. This antibiotic modification can involve one of three different fosfomycin resistance proteins (FosA, FosB or FosX) (Castañeda-García et al., 2013). The genes that provide resistance to fosfomycin could be transferred together with other antibiotic-resistant genes, either in the same or in a conjugate plasmid (Falagas et al., 2019). FosX has been found in environmental microorganisms, such as *M. loti* and *Desulfitobacterium hafniense,* and in pathogens, such as *B. melitensis*, *Clostridium botulinum* and *L. monocytogenes* (Fillgrove et al., 2007; Zurfluh et al., 2020). As resistance to fosfomycin has been identified in many bacterial models that remain difficult to eliminate with conventional methods, it is necessary to develop new antibiotics. Therefore, in order to achieve this, it is of interest to better understand not only the mechanism of fosfomycin inhibition, but also its interplay with MurA in relation to its substrates.

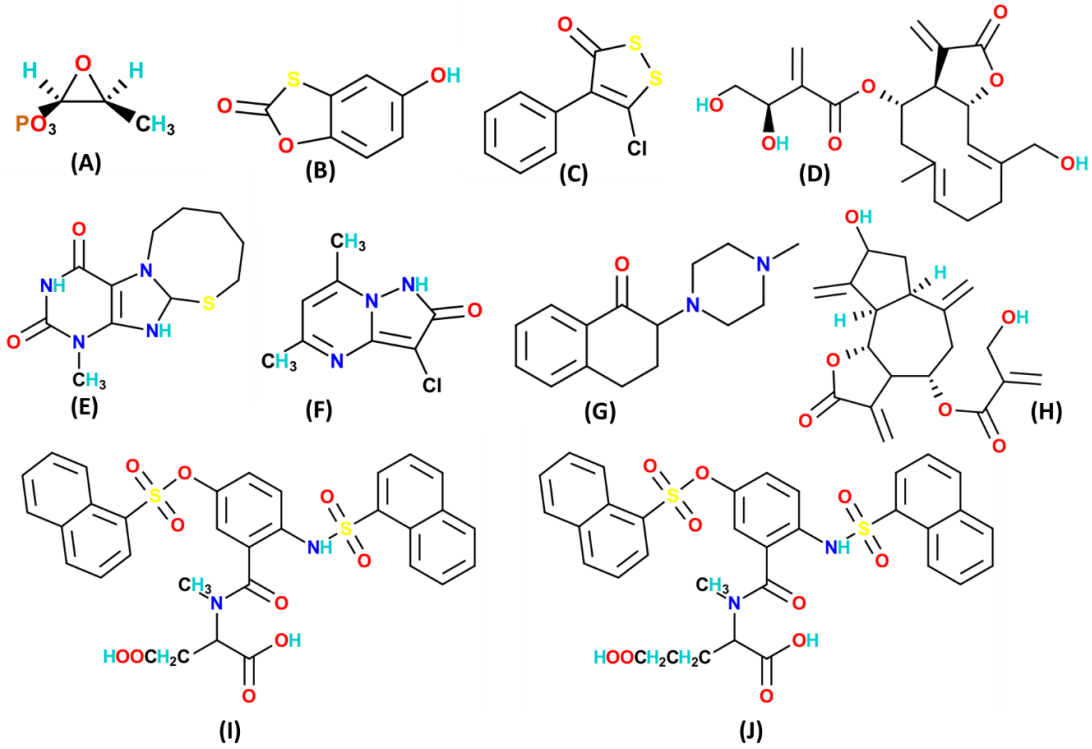

Figure 5.4. Inhibitors of MurA activities. (A) fosfomycin, **(B)** benzothioxalone, **(C)** RWJ-3981, **(D)** cnicin, **(E)** RWJ-140998, **(F)** RWJ-110192, **(G)** aminotetralones, **(H)** cynaropicrin, **(I)** sulfonyloxy anthranilic acid T6361 and **(J)** sulfonyloxy anthranilic acid T6362.

Considering this resistance to fosfomycin, other molecules capable of inhibiting MurA have been synthesized (Figure 5.4). Examples of these molecules are the cyclic disulfide RWJ-3981, the pyrazolopyrimidine RWJ-110192 and the purine analogues RWJ-140998, which have been tested on *E. coli* MurA and show higher inhibition compared to fosfomycin (Baum et al., 2001). Other successful compounds tested on *E. coli* MurA and *S. aureus* MurA and MurZ are derivatives of benzothioxalone and aminotetralone (Brown et al., 1995; Dunsmore et al., 2008). Sulfonyloxy anthranilic acid derivatives (compounds T6361 and T6362) also cause inhibition by affecting "open" to "closed" transitions (Eschenburg et al., 2005). Cnicin and cynaropicrin are also two potent natural inhibitors tested in *E. coli* and *P. aeruginosa* MurA that belong to the sesquiterpene lactone class (Eschenburg, et al., 2005).

Other miscellaneous compounds, such as heterocyclic systems, natural products, diketo acids and sulfones, have also been identified as MurA inhibitors (Figure 5.5). Some are now commercially available, such as the thimerosal (ethyl (2-mercaptobenzoato-S) mercury sodium salt), the thiram (1-(dimethylthiocarbamoyldisulfanyl)-N,N-dimethyl-methanethioamide) and the ebselen (consisting of a benzoisoselenazolone moiety) (Jin et al., 2009). In addition, there are some other natural compounds coming from plants, such as tulipalines and tuliposides derivatives (Mendgen et al., 2010). In this list, we can also find a fungal metabolite obtained from *Aspergillus terreus* and very similar to fosfomycin, the terreic acid (Han et al., 2010), and the feglymycin, a natural product isolated from *Streptomyces* spp. that comprises a 13-mer peptide whose structure consists of several non-proteinogenic amino acids and has been shown to inhibit both MurA and MurC of *E. coli* (Rausch et al., 2011).

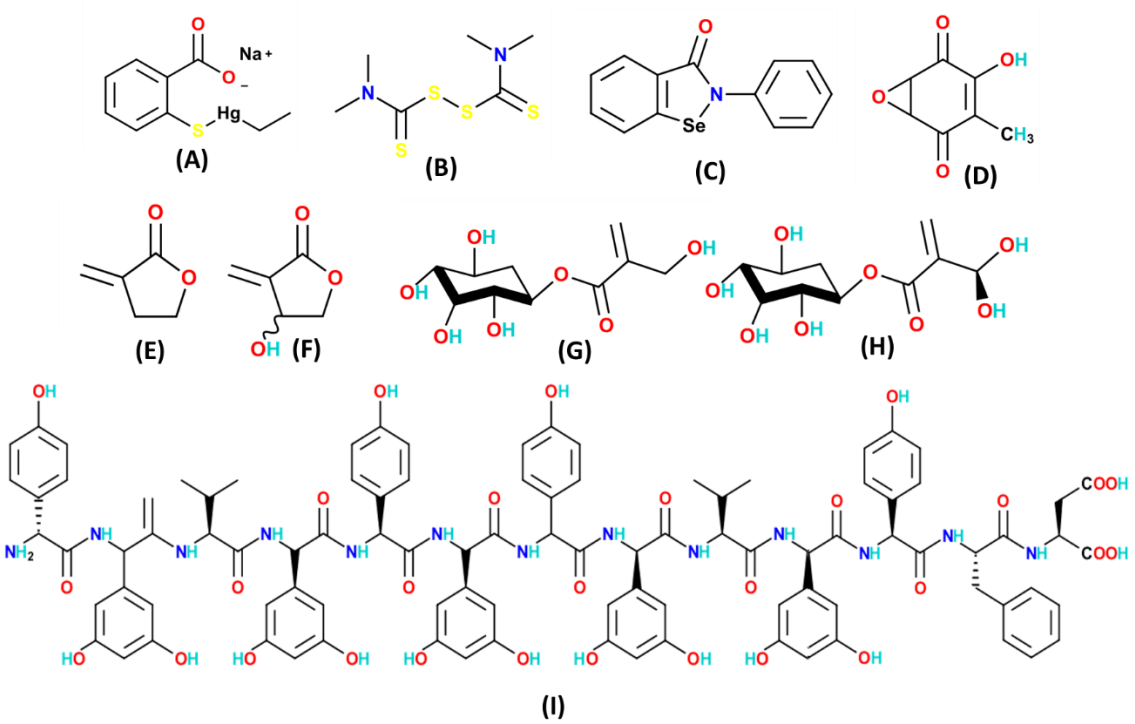

Figure 5.5. Miscellaneous inhibitors of MurA activity. (A) thimerosal, **(B)** thiram, **(C)** ebselen, **(D)** terreic acid, **(E)** tulipalines A, **(F)** tulipalines B, **(G)** 1-tuliposides A, **(H)** 1-tuliposides B and **(I)** feglymycin.

No studies have been reported so far regarding MurA of *B. ovis*, serving as motivation to functionally and structurally characterize it together with other Murs from the same organism (MurB and MurC) involved in the first stages of PG biosynthesis. In addition, UNAGEP is not commercially available and hast to be synthesized through MurA (Eniyan et al., 2016) for subsequent evaluations, as it serves as the substrate for the MurB activity, which will be discussed in the following chapter.

5.3 RESULTS

5.3.1 Overall characteristics of MurA from *B. ovis*

The *B. ovis* ATCC 25840 murA gene (BomurA), NCBI ID 45124764, is located on the chromosome I (NC_009505.1) with locus tag BOV_RS01375, in the specific region of 285774-284485. It is positioned between two coding sequences for proteins whose activity has not yet been described, and are therefore annotated as "hypothetical proteins" (Figure 5.6). The GC content of the murA gene was 60.93 %, and it is flanked by two small open reading frames (ORFs) that may form a single transcription unit. ProtParam analysis of the BoMurA sequence indicated that it was composed of 429 amino acids and 6,477 atoms, with a Mw of 45,719 Da and a theoretical pI of 6.57. The theoretical extinction coefficient for BoMurA at 280 nm computed in water was 15.9 $mM^{-1}cm^{-1}$. The instability index (II) was computed as 23.3, suggesting that BoMurA is a stable protein. The aliphatic index (100.8) and the GRAVY score (0.03) indicated that BoMurA is slightly hydrophobic. These data were useful for subsequent studies on enzyme production and biochemical and structural characterization. The BoMurA sequence envisages folding into an EPSP_synthase Pfam domain (PF00275), similar to other MurA proteins. The 3-phosphoshikimate 1-carboxyvinyltransferase (EPSP, AroA protein) is the representative member of this family, and is a key enzyme in the shikimate pathway for the biosynthesis of aromatic amino acids and other important metabolites in bacteria, plants, and fungi. The transfer of enolpyruvate from PEP to 3-phosphoshikimate is a key step that leads to the production of chorismate (a precursor for the synthesis of aromatic amino acids, folate, and other important metabolites) (Lee et al., 2017; Sonkar et al., 2017). MurA and EPSP synthase constitute then the enolpyruvyl transferases family of enzymes, which catalyze the chemically unusual reaction of enolpyruvyl transfer (Eschenburg et al., 2003).

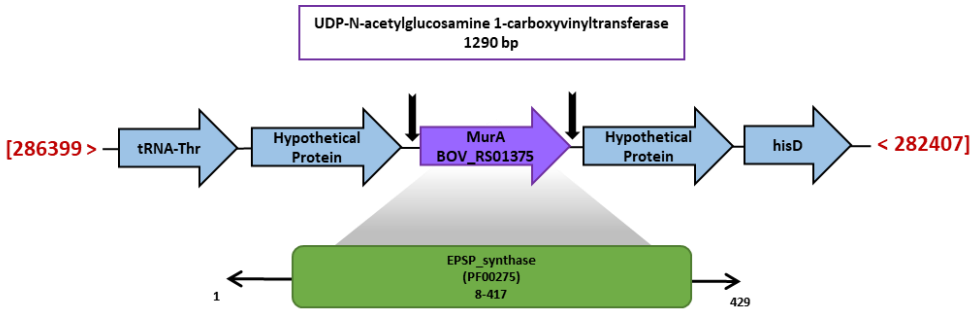

Figure 5.6. Genomic context of BoMurA and domain protein description. The genetic organization and transcriptional units of the conserved core of BoMurA are depicted by a purple arrow. Adjacent to this core, two genes are shown in blue upstream and downstream. Black arrows indicate the flanking ORFs. Furthermore, the red strip marks the specific location inside the genome (NC_009505.1: 286k-282k). The Pfam domain (PF00275) is represented in green.

5.3.2 Sequence and evolutionary analysis of MurA proteins in *Brucella* spp.

Currently, the NCBI database contains over 100 assembled genomes of different species and strains of *Brucella*. However, our sequence screening has focused on selecting evaluation models with almost complete sequencing and labeling information. As a result, we prioritized for our analysis genomes with RefSeq and GenBank annotations, and a verified taxonomic status. Using the BLASTp tool, 42 murA coding sequences from 38 species were retrieved (Table 5.3). *B. ovis*, like most *Brucella* species studied, and as expected for Gram-negative bacteria, has a single gene coding for MurA. However, our analysis indicated evidences for two murA copies in *B. anthropi*, *B. cytisi*, *B. pecoris* and *B. tritici*. This is not typical for Gram-negative bacteria and may be due to various evolutionary and adaptive factors (Brown et al., 1995; Du et al., 2000), suggesting unique characteristics for these *Brucella* species.

In multiple sequence alignment (MSA) (Figure 5.7), these sequences are herein called 1 and 2 (e. g. *B. anthropi*1 corresponds to ABS13059.1 and *B. anthropi*2 to ABS15831.1). BoMurA shares a significant degree of similarity with MurA homologues in other *Brucella*, with identities ranging from 87 to 100%. However, the identity goes down to ~53% when comparing with the four identified MurA2 sequences, tagged as *B. anthropi*2, *B. cytisi*2, *B. pecoris*2 and *B. tritici*2 (ABS15831.1, OIS93264.1, TNV13632.1 and KAB2666501.1, respectively). Nonetheless, as observed in the MSA WebLogo (Fig 5.9A), the residues mentioned in the introduction as involved in substrate binding remain 100% conserved in all *Brucella* sequences evaluated (Lys22, Asn23, Arg102, Cys126, Ile128, Arg131, Ser174, Thr316, Asp317, Asp381 and Leu382, considering BoMurA numbering). A second MSA was carried out only with MurA2 sequences from the *B. anthropi*, *B. cytisi*, *B. pecoris* and *B. tritici* strains (Figure 5.8), revealing a homogeneity of more than 95%.

Table 5.3. List of *Brucella* strains with complete assembled genome for which MurA sequences are evaluated in this study. *B. ovis* is highlighted in bold.

Strain	Protein Code	Strain	Protein Code
B. abortus	ACD71805.1	*B. pecoris*2	TNV13632.1
*B. anthropi*1	ABS13059.1	*B. tritici*1	KAB2667182.1
*B. anthropi*2	ABS15831.1	*B. tritici*2	KAB2666501.1
B. canis	ABX61351.1	*B. vulpis*	CUW49262.1
B. ceti	EEX86717.1	*B. pinnipedialis*	EEZ30437.1
B. cytisi1	OIS91003.1	*B. pituitosa*	KAB0572634.1
B. cytisi2	OIS93264.1	*B. pseudintermedia*	WP_121982858.1
B. daejeonensis	MBB5702445.1	*B. pseudogrignonensis*	OYR27879.1
B. endophytica	GGA87868.1	*B. rhizosphaerae*	OYR09882.1
B. gallinifaecis	TPF75555.1	*B. suis*	ABY37373.1
B. grignonensis	OYR10715.1	*B. thiophenivorans*	OYR20052.1
B. haematophila	TMV01134.1	*B.* sp. BO2	QPN26707.1
B. inopinata	SCD22730.1	*B.* sp. BO3	QMV25647.1
B. intermedia	KAB2732410.1	*B.* sp. BTU1	QWK77900.1
B. lupini	OYR29358.1	*B.* sp. F5/06	WP_006173703.1
B. melitensis	ACO00085.1	*B.* sp. NVSL 07-0026	EFG37237.2
B. microti	ACU47272.1	*B.* sp. 10RB9215	SBW15267.1
B. neotomae	EEY03874.1	*B.* sp. 2280	QGA57276.1
B. oryzae	PQA74623.1	*B.* sp. 458	QTN98180.1
B. ovis	**ABQ60706.1**	*B.* sp. 6810	QNQ61816.1
*B. pecoris*1	TNV09227.1	B. sp. 83/13	EEZ32282.1

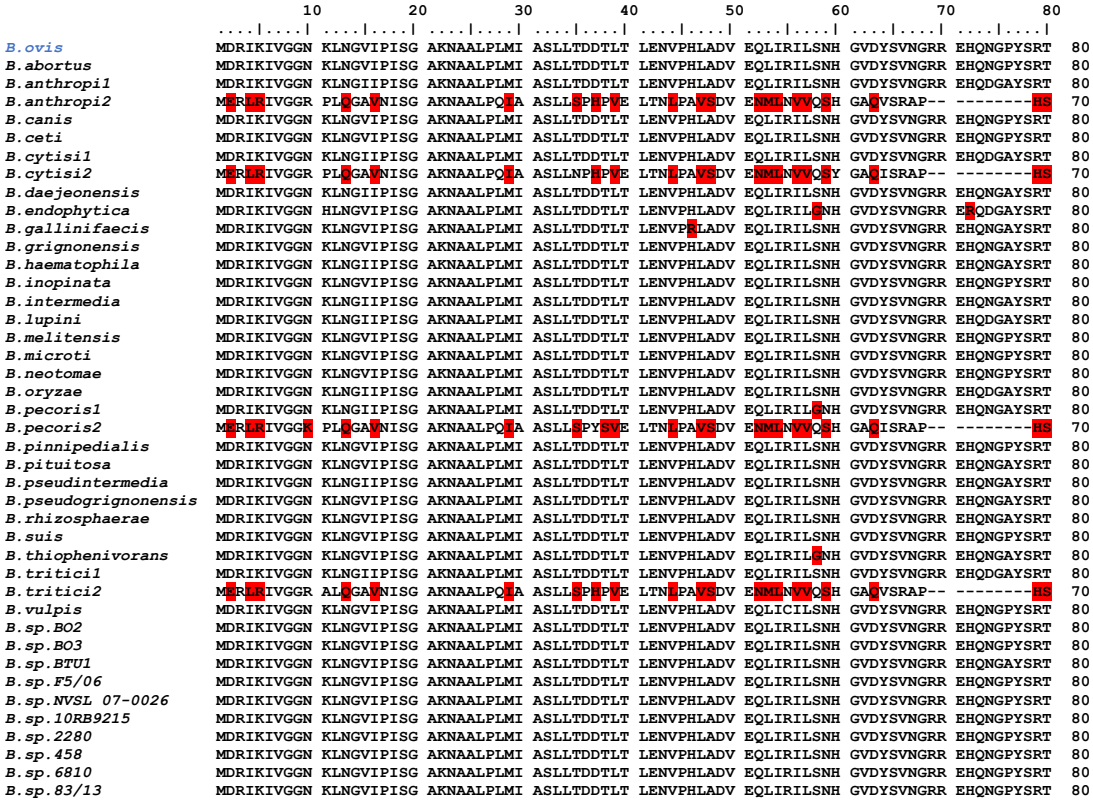

```
                                90        100       110       120       130       140       150       160
                     ....|....| ....|....| ....|....| ....|....| ....|....| ....|....| ....|....| ....|....|
B.ovis               IHFTARNIVD TTAPYELVSR MRASFWVIGP LLARMGEANV SLPGGCAIGT RPVDLLLDAL LALGAEIDIE NGYAKAKA-R 159
B.abortus            IHFTARNIVD TTAPYELVSR MRASFWVIGP LLARMGEANV SLPGGCAIGT RPVDLLLDAL LALGAEIDIE NGYAKAKA-R 159
B.anthropi1          IHFTARNIVT TTAPYELVSK MRASFWVIAP LLARMGEANV SLPGGCAIGT RPVDLLLEAL LALGADIEIE NGYAKAKA-R 159
B.anthropi2          TTVTATDVVG GETPYDTVRR MRAIVLVLAP LLARLGKVRV SLPGGCAIGA RPVDMHLKAL ATLGADVSID RGWIVASI-D 149
B.canis              IHFTARNIVD TTAPYELVSR MRASFWVIGP LLARMGEANV SLPGGCAIGT RPVDLLLDAL LALGAEIDIE NGYAKAKA-R 159
B.ceti               IHFTARNIVD TTAPYELVSR MRASFWVIGP LLARMGEANV SLPGGCAIGT RPVDLLLDAL LALGAEIDIE NGYAKAKA-R 159
B.cytisi1            IHFTARNIVT TTAPYELVSK MRASFWVIAP LLARMGEANV SLPGGCAIGT RPVDLLLEAF LALGADIEIE NGYAKAKA-K 159
B.cytisi2            TTITATDVVG GETPYDTVRR MRAIVLVLAP LLARLGKVRV SLPGGCAIGA RPVDMHLKAL ATLGADVSID RGWIVASI-D 149
B.daejeonensis       IHFTARNIVD TTAPYELVSK MRASFWVIGP LLARTGEATV SLPGGCAIGT RPVDLLLESL QALGAEIDIE NGYAKARAPK 160
B.endophytica        IHFTARNIVD TTAPYELVSK MRASFWVIGP LLARMGTANV SLPGGCAIGT RPVDLHLDSL AALGAEIDIE NGYVKATA-K 159
B.gallinifaecis      IHFTARNIVD TTAPYELVSK MRASFWVIGP LLARMGEANV SLPGGCAIGT RPVDLLLECL QALGAQIDIE NGYAKARAPK 160
B.grignonensis       IHFTARNIVD TVAPYELVSK MRASFWVIGP LLARMGEATV SLPGGCAIGT RPVDLLLECL QALGAQIDIE NGYAKARAPK 160
B.haematophila       IHFTARNIVD TTAPYELVSK MRASFWVIGP LLARMGEATV SLPGGCAIGT RPVDLLLDCL QALGAEIDIE NGYAKACAPK 160
B.inopinata          IHFTARNIVD TTAPYELVSK MRASFWVIGP LLARMGEANV SLPGGCAIGT RPVDLLLDAL LALGAEIDIE NGYAKAKA-R 159
B.intermedia         IHFTARNIVD TTAPYELVSK MRASFWVIGP LLARTGEATV SLPGGCAIGT RPVDLLLESL QALGAEIDIE NGYAKARAPK 160
B.lupini             IHFTARNIVT TTAPYELVSK MRASFWVIAP LLARMGEANV SLPGGCAIGT RPVDLLLEAL LALGADIEIE NGYAKAKA-R 159
B.melitensis         IHFTARNIVD TTAPYELVSR MRASFWVIGP LLARMGEANV SLPGGCAIGT RPVDLLLDAL LALGAEIDIE NGYAKAKA-R 159
B.microti            IHFTARNIVD TTAPYELVSR MRASFWVIGP LLARMGEANV SLPGGCAIGT RPVDLLLDAL LALGAEIDIE NGYAKAKA-R 159
B.neotomae           IHFTARNIVD TTAPYELVSR MRASFWVIGP LLARMGEANV SLPGGCAIGT RPVDLLLDAL LALGAEIDIE NGYAKAKA-R 159
B.oryzae             IHFTARNIVT TTAPYELVSK MRASFWVIAP LLARMGEANV SLPGGCAIGT RPVDLLLEAL LALGADIEIE NGYAKAKA-R 159
B.pecoris1           IHFTARNIVD TTAPYELVSK MRASFWVIGP LLARMGEATV SLPGGCAIGT RPVDLLLDCL QALGAEIDIE NGYAKARAPK 160
B.pecoris2           TTITATDLVV EETPYDTVRR MRAIVLVLAP LLARLGKVRV SLPGGCAIGA RPVDMHLKAL ATLGANVSID RGWIVASI-D 149
B.pinnipedialis      IHFTARNIVD TTAPYELVSR MRASFWVIGP LLARMGEANV SLPGGCAIGT RPVDLLLDAL LALGAEIDIE NGYAKAKA-R 159
B.pituitosa          IHFTARNIVD TVAPYELVSK MRASFWVIGP LLARMGEATV SLPGGCAIGT RPVDLLLECL QALGAQIDIE NGYAKARAPK 160
B.pseudintermedia    IHFTARNIVD TTAPYELVSK MRASFWVIGP LLARTGEATV SLPGGCAIGT RPVDLLLESL QALGAEIDIE NGYAKARAPK 160
B.pseudogrignonensis IHFTARNIVD TVAPYELVSK MRASFWVIGP LLARMGEATV SLPGGCAIGT RPVDLLLECL QALGAQIDIE NGYAKARAPQ 160
B.rhizosphaerae      IHFTARNIVD TTAPYELVSK MRASFWVIGP LLARMGEANV SLPGGCAIGT RPVDLLLECL QALGAQIDIE NGYAKARAPK 160
B.suis               IHFTARNIVD TTAPYELVSR MRASFWVIGP LLARMGEANV SLPGGCAIGT RPVDLLLDAL LALGAEIDIE NGYAKAKA-R 159
B.thiophenivorans    IHFTARTIVD TVAPYELVSK MRASFWVIGP LLARMGEATV SLPGGCAIGT RPVDLLLECL QALGAQIDIE NGYAKARAPK 160
B.tritici1           IHFTARNIVT TTAPYELVSK MRASFWVIAP LLARMGEANV SLPGGCAIGT RPVDLLLEAL LALGADIEIE NGYAKAKA-R 159
B.tritici2           TTIAATDLVG GETPYDTVRR MRAIVLVLAP LLARLGKVRV SLPGGCAIGA RPVDMHLKAL STLGADVSID RGWIVASI-D 149
B.vulpis             IHFTARNIVD TTAPYELVSK MRASFWVIGP LLARMGEANV SLPGGCAIGT RPVDLLLDAL LALGAEIDIE NGYAKAKA-R 159
B.sp.BO2             IHFTARNIVD TTAPYELVSR MRASFWVIGP LLARMGEANV SLPGGCAIGT RPVDLLLDAL LALGAEIDIE NGYAKAKA-R 159
B.sp.BO3             IHFTARNIVD TTAPYELVSR MRASFWVIGP LLARMGEANV SLPGGCAIGT RPVDLLLDAL LALGAEIDIE NGYAKAKA-R 159
B.sp.BTU1            IHFTARNIVD TVAPYELVSK MRASFWVIGP LLARMGEATV SLPGGCAIGT RPVDLLLECL QALGAQIDIE NGYAKARAPQ 160
B.sp.F5/06           IHFTARNIVD TTAPYEFVSR MRASFWVIGP LLARMGEANV SLPGGCAIGT RPVDLPLDAL LALGAEIDIE NGYAKAKA-R 159
B.sp.NVSL 07-0026    IHFTARNIVD TTAPYELVSR MRASFWVIGP LLARMGEANV SLPGGCAIGT RPVDLLLDAL LALGAEIDIE NGYAKAKA-R 159
B.sp.10RB9215        IHFTARNIVD TTAPYELVSR MRASFWVIGP LLARMGEANV SLPGGCAIGT RPVDLLLDAL LALGAEIDIE NGYAKAKA-R 159
B.sp.2280            IHFTARNIVD TTAPYELVSR MRASFWVIGP LLARMGEANV SLPGGCAIGT RPVDLLLDAL LALGAEIDIE NGYAKAKA-R 159
B.sp.458             IHFTARNIVD TTAPYELVSR MRASFWVIGP LLARMGEANV SLPGGCAIGT RPVDLLLDAL LALGAEIDIE NGYAKAKA-R 159
B.sp.6810            IHFTARNIVD TTAPYELVSR MRASFWVIGP LLARMGEANV SLPGGCAIGT RPVDLLLDAL LALGAEIDIE NGYAKAKA-R 159
B.sp.83/13           IHFTARNIVD TTAPYELVSR MRASFWVIGP LLARMGEANV SLPGGCAIGT RPVDLLLDAL LALGAEIDIE NGYAKAKA-R 159
                                                                          *

                               170       180       190       200       210       220       230       240
                     ....|....| ....|....| ....|....| ....|....| ....|....| ....|....| ....|....| ....|....|
B.ovis               NGLVGARYKF PKVSVGATHV MLMAATLAKG ETIIENAARE PEVANLADCL NAMGAKISGA GSSTIHVQGV TNLSGARVRI 239
B.abortus            NGLVGARYKF PKVSVGATHV MLMAATLAKG ETIIENAARE PEVANLADCL NAMGAKISGA GSSTIHVQGV TNLSGARVRI 239
B.anthropi1          NGLVGARYKF PKVSVGATHV MLMAAALAKG ETVIENAARE PEVVNLADCL NAMGAKITGA GTSTIHIDGV TNLSGARVRV 239
B.anthropi2          NGLIGRRIVL PAPSVGATAT AMMAATSARG ETEILNAARE PEIGDLAACL GAMGAQIEGA GTHRILIQGD TSWRTARHMG 229
B.canis              NGLVGARYKF PKVSVGATHV MLMAATLAKG ETIIENAARE PEVANLADCL NAMGAKISGA GSSTIHVQGV TNLSGARVRI 239
B.ceti               NGLVGARYKF PKVSVGATHV MLMAATLAKG ETIIENAARE PEVANLADCL NAMGAKISGA GSSTIHVQGV TNLSGARVRI 239
B.cytisi1            NGLVGARYKF PKVSVGATHV MLMAAALAKG ETVIENAARE PEVVNLADCL NAMGAKITGA GTSTIHIDGV TNLSGARVRV 239
B.cytisi2            NGLIGRRIVL PAPSVGATAT AMMAATSARG ETEILNAARE PEIGDLAACL GAMGAQIEGA GTHRILIQGD TSWQTARHMG 229
B.daejeonensis       GGLVGARYSF PKVSVGATHV MLMAAALARG ETTIENAARE PEVVNLADCL NAMGAKISGA GTGTIHVEGV TSLSGARVRV 240
B.endophytica        KGLIGTHYTF PKVSVGATHV LMMAATLAKG ETIISNAARE PEVVNLADCL NAMGANVTGA GTSTICIEGV ESLSGARVRV 239
B.gallinifaecis      GGLVGARYRF PKVSVGATHV MLMAAVLANG ETIIENPARE PEVVNLADCL NAMGAKITGA GTDTIHIQGV TNLSGARVRV 240
B.grignonensis       GGLVGARYRF PKVSVGATHV MLMAAVLAKG ETIIENPARE PEVVNLADCL NAMGAKITGA GTEAIHVQGV TSLSGARVRV 240
B.haematophila       GGLVGRRYRF PKVSVGATHV MLMAAVLAKG ETIIENPARE PEVVNLADCL NAMGAKITGA GTGTIHVQGV TSLSGARVRV 240
B.inopinata          SGLVGARYKF PKVSVGATHV MLMAATLAKG ETIIENAARE PEVANLADCL NAMGAKISGA GSSTIHVQGV TNLSGARVRI 239
B.intermedia         GGLVGARYSF PKVSVGATHV MLMAAALAKG ETIIENAARE PEVVNLADCL NAMGAKITGA GTSTIQVEGV TSLSGARVRV 240
B.lupini             NGLVGARYKF PKVSVGATHV MLMAAALAKG ETVIENAARE PEVVNLADCL NAMGAKITGA GTSTIHIDGV TNLSGARVRV 239
B.melitensis         NGLVGARYKF PKVSVGATHV MLMAATLAKG ETIIENAARE PEVANLADCL NAMGAKISGA GSSTIHVQGV TNLSGARVRI 239
B.microti            NGLVGARYKF PKVSVGATHV MLMAATLAKG ETIIENAARE PEVANLADCL NAMGAKISGA GSSTIHVQGV TNLSGARVRI 239
B.neotomae           NGLVGARYKF PKVSVGATQV MLMAATLAKG ETIIENAARE PEVANLADCL NAMGAKISGA GSSTIHVQGV TNLSGARVRI 239
B.oryzae             NGLVGARYKF PKVSVGATHV MLMAATLAKG ETIIENAARE PEVVNLADCL NAMGAKITGA GTGTIHVEGV TSLSGARVRV 239
B.pecoris1           GGLVGRRYRF PKVSVGATHV MLMAAALAKG ETVIENPARE PEVVNLADCL NAMGAKITGA GTDTIHIEGV TSLSGARVRV 240
B.pecoris2           NGLIGRRIVL PAPSVGATAT AMMAATSARG ETEILNAARE PEIADLAACL SAMGAQIEGA GTHRILVQGD TSWRPACHMG 229
B.pinnipedialis      NGLVGARYKF PKVSVGATHV MLMAATLAKG ETIIENAARE PEVANLADCL NAMGAKISGA GSSTIHVQGV TNLSGARVRI 239
B.pituitosa          GGLVGAHYRF PKVSVGATHV MLMAAVLANG ETIIENPARE PEVVNLADCL NAMGAKITGA GTETIHVQGV TSLSGARVRV 240
B.pseudintermedia    GGLVGARYRF PKVSVGATHV MLMAAALAKG ETIIENAARE PEVVNLADCL NAMGAKISGA GTSTIHVEGV TSLSGARVRV 240
B.pseudogrignonensis GGLIGARYRF PKVSVGATHV MLMAAVLAKG ETIIENPARE PEVVNLADCL NAMGAKITGA GTETIHVQGV TSLSGARVRV 240
B.rhizosphaerae      GGLIGRRYKF PKVSVGATHV MLMAAALARG ETVIENAARE PEVVNLADCL NAMGAKISGA GTGTIHVEGV TSLSGARVRV 240
B.suis               NGLVGARYKF PKVSVGATHV MLMAATLAKG ETIIENAARE PEVANLADCL NAMGAKISGA GSSTIHVQGV TNLSGARVRI 239
B.thiophenivorans    GGLVGTRYRF PKVSVGATHV MLMAAVLANG ETIIENPARE PEVVNLADCL NAMGAKITGA GTDTIHIQGV TSLSGARVRV 240
B.tritici1           NGLVGARYKF PKVSVGATHV MLMAAALAKG ETVIENAARE PEVVNLADCL NAMGAKITGA GTGTIHIDGV TNLSGARVRV 239
B.tritici2           SGLIGRRIVL PAPSVGATAT AMMAATSARG ETEILNAARE PETADLAACL GAMGAQTEGA GTHRILIQGD TSWRPARHMG 229
B.vulpis             NGLVGARYKF PKVSVGATHV MLMAATLAKG ETIIENAARE PEVANLADCL NAMGAKISGA GSSTIHVQGV TNLSGARVRI 239
B.sp.BO2             NGLVGARYKF PKVSVGATHV MLMAATLAKG ETIIENAARE PEVANLADCL NAMGAKISGA GSSTIHVQGV TNLSGARVRI 239
B.sp.BO3             NGLVGARYKF PKVSVGATHV MLMAATLAKG ETIIENAARE PEVANLADCL NAMGAKISGA GSSTIHVQGV TNLSGARVRI 239
B.sp.BTU1            GGLIGARYRF PKVSVGATHV MLMAAVLAKG ETIIENPARE PEVVNLADCL NAMGAKITGA GTETIHVQGV TSLSGARVRV 240
B.sp.F5/06           NGLVGARYKF PKVSVGATHV MLMAATLAKG ETIIENAARE PEVANLADCL NAMGAKISGA GSSTIHVQGV TNLSGARVRI 239
B.sp.NVSL 07-0026    NGLVGARYKF PKVSVGATHV MLMAATLAKG ETIIENAARE PEVANLADCL NAMGAKISGA GSSTIHVQGV TNLSGARVRI 239
B.sp.10RB9215        NGLVGARYKF PKVSVGATHV MLMAATLAKG ETIIENAARE PEVANLADCL NAMGAKISGA GSSTIHVQGV TNLSGARVRI 239
B.sp.2280            NGLVGARYKF PKVSVGATHV MLMAATLAKG ETIIENAARE PEVANLADCL NAMGAKISGA GSSTIHVQGV TNLSGARVRI 239
B.sp.458             NGLVGARYKF PKVSVGATHV MLMAATLAKG ETIIENAARE PEVANLADCL NAMGAKISGA GSSTIHVQGV TNLSGARVRI 239
B.sp.6810            NGLVGARYKF PKVSVGATHV MLMAATLAKG ETIIENAARE PEVANLADCL NAMGAKISGA GSSTIHVQGV TNLSGARVRI 239
B.sp.83/13           NGLVGARYKF PKVSVGATHV MLMAATLAKG ETIIENAARE PEVANLADCL NAMGAKISGA GSSTIHVQGV TNLSGARVRI 239
```

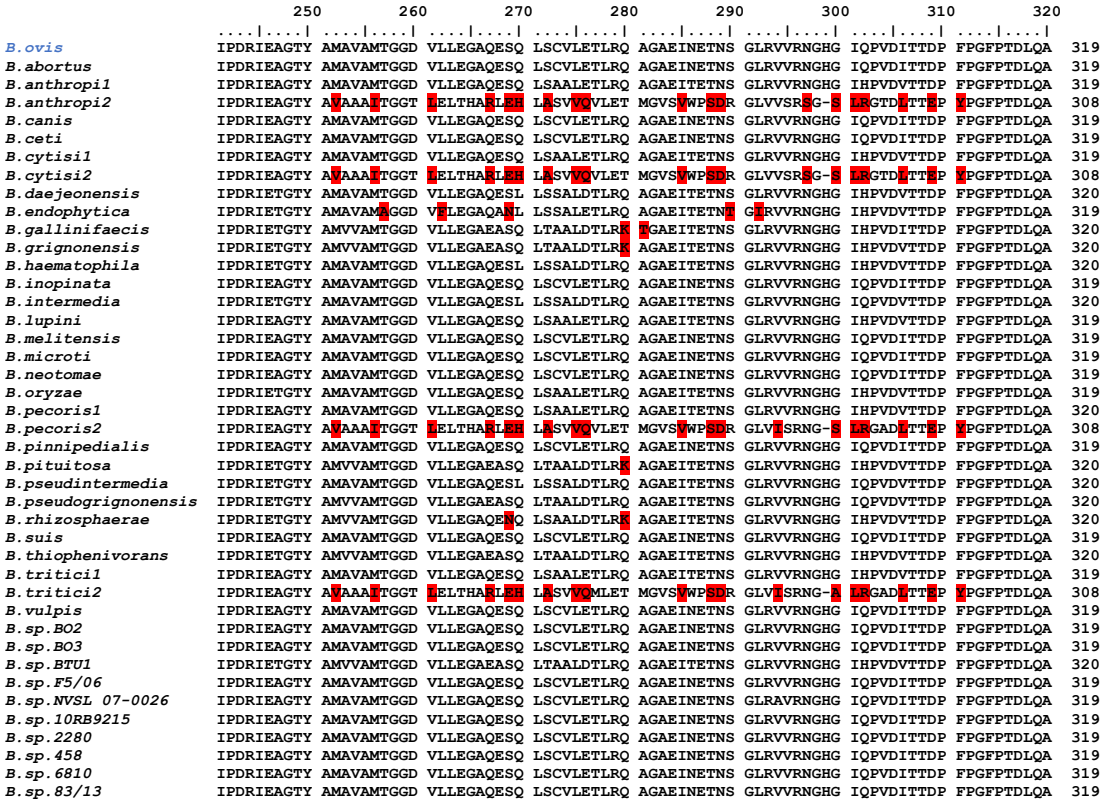
250 260 270 280 290 300 310 320
B.ovis IPDRIEAGTY AMAVAMTGGD VLLEGAQESQ LSCVLETLRQ AGAEINETNS GLRVVRNGHG IQPVDITTDP FPGFPTDLQA 319
B.abortus IPDRIEAGTY AMAVAMTGGD VLLEGAQESQ LSCVLETLRQ AGAEINETNS GLRVVRNGHG IQPVDITTDP FPGFPTDLQA 319
B.anthropi1 IPDRIEAGTY AMAVAMTGGD VLLEGAQESQ LSAALETLRQ AGAEITETNS GLRVVRNGHG IHPVDVTTDP FPGFPTDLQA 319
B.anthropi2 IPDRIEAGTY AVAAAITGGT LELTHARLEH LASVVQVLET MGVSVWPSDR GLVVSRSG-S LRGTDLTTEP YPGFPTDLQA 308
B.canis IPDRIEAGTY AMAVAMTGGD VLLEGAQESQ LSCVLETLRQ AGAEINETNS GLRVVRNGHG IQPVDITTDP FPGFPTDLQA 319
B.ceti IPDRIEAGTY AMAVAMTGGD VLLEGAQESQ LSCVLETLRQ AGAEINETNS GLRVVRNGHG IQPVDITTDP FPGFPTDLQA 319
B.cytisi1 IPDRIEAGTY AMAVAMTGGD VLLEGAQESQ LSAALETLRQ AGAEITETNS GLRVVRNGHG IHPVDVTTDP FPGFPTDLQA 319
B.cytisi2 IPDRIEAGTY AVAAAITGGT LELTHARLEH LASVVQVLET MGVSVWPSDR GLVVSRSG-S LRGTDLTTEP YPGFPTDLQA 308
B.daejeonensis IPDRIETGTY AMAVAMTGGD VLLEGAQESL LSSALDTLRQ AGAEITETNS GLRVVRNGHG IHPVDVTTDP FPGFPTDLQA 320
B.endophytica IPDRIETGTY AMAVAMAGGD VLLEGAQANL LSSALETLRQ AGAEITETNT GLRVVRNGHG IHPVDVTTDP FPGFPTDLQA 319
B.gallinifaecis IPDRIETGTY AMVVAMTGGD VLLEGAEASQ LTAALDTLRK TGAEITETNS GLRVVRNGHG IHPVDITTDP FPGFPTDLQA 320
B.grignonensis IPDRIETGTY AMVVAMTGGD VLLEGAEASQ LTAALDTLRK AGAEITETNS GLRVVRNGHG IHPVDVTTDP FPGFPTDLQA 320
B.haematophila IPDRIETGTY AMAVAMTGGD VLLEGAQESL LSSALDTLRQ AGAEITETNS GLRVVRNGHG IHPVDVTTDP FPGFPTDLQA 320
B.inopinata IPDRIEAGTY AMAVAMTGGD VLLEGAQESQ LSCVLETLRQ AGAEINETNS GLRVVRNGHG IQPVDITTDP FPGFPTDLQA 319
B.intermedia IPDRIETGTY AMAVAMTGGD VLLEGAQESL LSSALDTLRQ AGAEITETNS GLRVVRNGHG IQPVDVTTDP FPGFPTDLQA 320
B.lupini IPDRIEAGTY AMAVAMTGGD VLLEGAQESQ LSAALETLRQ AGAEITETNS GLRVVRNGHG IHPVDVTTDP FPGFPTDLQA 319
B.melitensis IPDRIEAGTY AMAVAMTGGD VLLEGAQESQ LSCVLETLRQ AGAEINETNS GLRVVRNGHG IQPVDITTDP FPGFPTDLQA 319
B.microti IPDRIEAGTY AMAVAMTGGD VLLEGAQESQ LSCVLETLRQ AGAEINETNS GLRVVRNGHG IQPVDITTDP FPGFPTDLQA 319
B.neotomae IPDRIEAGTY AMAVAMTGGD VLLEGAQESQ LSCVLETLRQ AGAEINETNS GLRVVRNGHG IQPVDITTDP FPGFPTDLQA 319
B.oryzae IPDRIETGTY AMAVAMTGGD VLLEGAQESQ LSAALETLRQ AGAEITETNS GLRVVRNGHG IHPVDVTTDP FPGFPTDLQA 319
B.pecoris1 IPDRIEAGTY AMAVAMTGGD VLLEGAQESQ LSAALETLRQ AGAEITETNS GLRVVRNGHG IHPVDVTTDP FPGFPTDLQA 320
B.pecoris2 IPDRIEAGTY AVAAAITGGT LELTHARLEH LASVVQVLET MGVSVWPSDR GLVISRNG-S LRGADLTTEP YPGFPTDLQA 308
B.pinnipedialis IPDRIEAGTY AMAVAMTGGD VLLEGAQESQ LSCVLETLRQ AGAEINETNS GLRVVRNGHG IQPVDITTDP FPGFPTDLQA 319
B.pituitosa IPDRIETGTY AMVVAMTGGD VLLEGAEASQ LTAALDTLRK AGAEITETNS GLRVVRNGHG IHPVDVTTDP FPGFPTDLQA 320
B.pseudintermedia IPDRIETGTY AMAVAMTGGD VLLEGAQESL LSSALDTLRQ AGAEITETNS GLRVVRNGHG IQPVDVTTDP FPGFPTDLQA 320
B.pseudogrignonensis IPDRIETGTY AMVVAMTGGD VLLEGAEASQ LTAALDTLRQ AGAEITETNS GLRVVRNGHG IQPVDVTTDP FPGFPTDLQA 320
B.rhizosphaerae IPDRIETGTY AMVVAMTGGD VLLEGAQENQ LSAALDTLRK AGAEITETNS GLRVVRNGHG IHPVDVTTDP FPGFPTDLQA 320
B.suis IPDRIEAGTY AMAVAMTGGD VLLEGAQESQ LSCVLETLRQ AGAEINETNS GLRVVRNGHG IQPVDITTDP FPGFPTDLQA 319
B.thiophenivorans IPDRIETGTY AMVVAMTGGD VLLEGAEASQ LTAALDTLRQ AGAEITETNS GLRVVRNGHG IHPVDVTTDP FPGFPTDLQA 320
B.tritici1 IPDRIEAGTY AMAVAMTGGD VLLEGAQESQ LSAALETLRQ AGAEITETNS GLRVVRNGHG IHPVDVTTDP FPGFPTDLQA 319
B.tritici2 IPDRIEAGTY AVAAAITGGT LELTHARLEH LASVVQMLET MGVSVWPSDR GLVISRNG-A LRGADLTTEP YPGFPTDLQA 308
B.vulpis IPDRIEAGTY AMAVAMTGGD VLLEGAQESQ LSCVLETLRQ AGAEINETNS GLRVVRNGHG IQPVDITTDP FPGFPTDLQA 319
B.sp.BO2 IPDRIEAGTY AMAVAMTGGD VLLEGAQESQ LSCVLETLRQ AGAEINETNS GLRVVRNGHG IQPVDITTDP FPGFPTDLQA 319
B.sp.BO3 IPDRIEAGTY AMAVAMTGGD VLLEGAQESQ LSCVLETLRQ AGAEINETNS GLRVVRNGHG IQPVDITTDP FPGFPTDLQA 319
B.sp.BTU1 IPDRIETGTY AMVVAMTGGD VLLEGAEASQ LTAALDTLRQ AGAEITETNS GLRVVRNGHG IHPVDVTTDP FPGFPTDLQA 320
B.sp.F5/06 IPDRIEAGTY AMAVAMTGGD VLLEGAQESQ LSCVLETLRQ AGAEINETNS GLRVVRNGHG IQPVDITTDP FPGFPTDLQA 319
B.sp.NVSL 07-0026 IPDRIEAGTY AMAVAMTGGD VLLEGAQESQ LSCVLETLRQ AGAEINETNS GLRAVRNGHG IQPVDITTDP FPGFPTDLQA 319
B.sp.10RB9215 IPDRIEAGTY AMAVAMTGGD VLLEGAQESQ LSCVLETLRQ AGAEINETNS GLRVVRNGHG IQPVDITTDP FPGFPTDLQA 319
B.sp.2280 IPDRIEAGTY AMAVAMTGGD VLLEGAQESQ LSCVLETLRQ AGAEINETNS GLRVVRNGHG IQPVDITTDP FPGFPTDLQA 319
B.sp.458 IPDRIEAGTY AMAVAMTGGD VLLEGAQESQ LSCVLETLRQ AGAEINETNS GLRVVRNGHG IQPVDITTDP FPGFPTDLQA 319
B.sp.6810 IPDRIEAGTY AMAVAMTGGD VLLEGAQESQ LSCVLETLRQ AGAEINETNS GLRVVRNGHG IQPVDITTDP FPGFPTDLQA 319
B.sp.83/13 IPDRIEAGTY AMAVAMTGGD VLLEGAQESQ LSCVLETLRQ AGAEINETNS GLRVVRNGHG IQPVDITTDP FPGFPTDLQA 319
330 340 350 360 370 380 390 400
B.ovis QFMGLMTRAK GTSHITETIF ENRFMHVQEL ARLGAKISLS GQTATVEGVE RLKGAQVMAT DLRASVSLVI AGLAAEGETI 399
B.abortus QFMGLMTRAK GTSHITETIF ENRFMHVQEL ARLGAKISLS GQTATVEGVE RLKGAQVMAT DLRASVSLVI AGLAAEGETI 399
B.anthropi1 QFMGLMTKAK GTSRITETIF ENRFMHVQEL ARLGAKISLS GQTATVEGVE RLKGAQVMAT DLRASVSLVI AGLAAEGETM 399
B.anthropi2 QFMALANCAE GASLIRETVF ESRFMHVPEL MRLGADIKLH GTTALVRGGR PLHGAQVMAT DLRASVSLVL AALVAEGETV 388
B.canis QFMGLMTRAK GTSHITETIF ENRFMHVQEL ARLGAKISLS GQTATVEGVE RLKGAQVMAT DLRASVSLVI AGLAAEGETI 399
B.ceti QFMGLMTRAK GTSHITETIF ENRFMHVQEL ARLGAKISLS GQTATVEGVE RLKGAQVMAT DLRASVSLVI AGLAAEGETI 399
B.cytisi1 QFMGLMTKAK GTSRITETIF ENRFMHVQEL ARLGAKISLS GQTATVEGVE RLKGAQVMAT DLRASVSLVI AGLAAEGETM 399
B.cytisi2 QFMALANCAE GASLIRETVF ESRFMHVPEL MRLGADIKLH GTTALVRGGR PLHGAQVMAT DLRASVSLVL AALVAEGETV 388
B.daejeonensis QFMGLMTKAK GTSRITETIF ENRFMHVQEL ARLGARISLS GQTATVEGVE RLKGAQVMAT DLRASVSLVI AGLAAEGETM 400
B.endophytica QFMGLMTKAK GTSRITETIF ENRFMHVQEL ARLGAKISLS GQVATVEGVE RLQGAQVMAT DLRASVSLVI AGLAAEGETY 399
B.gallinifaecis QFMGLMTMAK GTSHITETIF ENRFMHVQEL ARLGAKISLS GQTATVEGVE RLKGAQVMAT DLRASVSLVI AGLAAEGETT 400
B.grignonensis QFMGLMTMAK GTSRITETIF ENRFMHVQEL ARLGAKISLS GQTATVEGVE RLKGAQVMAT DLRASVSLVI AGLAAEGETI 400
B.haematophila QFMGLMTKAK GTSHITETIF ENRFMHVQEL ARLGAKISLS GQTATVEGVE RLKGAQVMAT DLRASVSLVI AGLAAEGETV 400
B.inopinata QFMGLMTRAK GTSHITETIF ENRFMHVQEL ARLGAKISLS GQTATVEGME RLKGAQVMAT DLRASVSLVI AGLAAEGETI 399
B.intermedia QFMGLMTKAK GTSRITETIF ENRFMHVQEL ARLGAKISLS GQTATVEGVE RLKGAQVMAT DLRASVSLVI AGLAAEGETM 400
B.lupini QFMGLMTKAK GTSRITETIF ENRFMHVQEL ARLGAKISLS GQTATVEGVE RLKGAQVMAT DLRASVSLVI AGLAAEGETM 399
B.melitensis QFMGLMTRAK GTSHITETIF ENRFMHVQEL ARLGAKISLS GQTATVEGVE RLKGAQVMAT DLRASVSLVI AGLAAEGETI 399
B.microti QFMGLMTRAK GTSHITETIF ENRFMHVQEL ARLGAKISLS GQTATVEGVE RLKGAQVMAT DLRASVSLVI AGLAAEGETI 399
B.neotomae QFMGLMTRAK GTSHITETIF ENRFMHVQEL ARLGAKISLS GQTATVEGVE RLKGAQVMAT DLRASVSLVI AGLAAEGETI 399
B.oryzae QFMGLMTKAK GTSRITETIF ENRFMHVQEL ARLGAKISLS GQTATVEGVE RLKGAQVMAT DLRASVSLVI AGLAAEGETL 399
B.pecoris1 QFMGLMTKAK GTSRITETIF ENRFMHVQEL ARLGAKISLS GQTATVEGVE RLKGAQVMAT DLRASVSLVI AGLAAEGETM 400
B.pecoris2 QFMALANCSE GASLIRETVF ESRFMHVPEL MRLGADIKLQ GTTALVRGGR PLHGAQVMAT DLRASVSLVL AALVAEGETV 388
B.pinnipedialis QFMGLMTRAK GTSHITETIF ENRFMHVQEL ARLGAKISLS GQTATVEGVE RLKGAQVMAT DLRASVSLVI AGLAAEGETI 399
B.pituitosa QFMGLMTMAK GTSRITETIF ENRFMHVQEL ARLGAKISLS GQTATVEGVE RLKGAQVMAT DLRASVSLVI AGLAAEGETI 400
B.pseudintermedia QFMGLMTKAK GTSRITETIF ENRFMHVQEL ARLGAKISLS GQTATVEGVE RLKGAQVMAT DLRASVSLVI AGLAAEGETM 400
B.pseudogrignonensis QFMGLMTKAK GTSRITETIF ENRFMHVQEL ARLGAKISLS GQTATVEGVE RLKGAQVMAT DLRASVSLVI AGLAAEGETI 400
B.rhizosphaerae QFMGLMTMAK GTSRITETIF ENRFMHVQEL ARLGAKISLS GQTATVEGVE RLKGAQVMAT DLRASVSLVI AGLAAEGETI 400
B.suis QFMGLMTRAK GTSHITETIF ENRFMHVQEL ARLGAKISLS GQTATVEGVE RLKGAQVMAT DLRASVSLVI AGLAAEGETI 399
B.thiophenivorans QFMGLMTMAK GTSHITETIF ENRFMHVQEL ARLGAKISLS GQTATVEGVE RLKGAQVMAT DLRASVSLVI AGLAAEGETI 400
B.tritici1 QFMGLMTKAK GTSRITETIF ENRFMHVQEL ARLGAKISLS GQTATVEGVE RLKGAQVMAT DLRASVSLVI AGLAAEGETL 399
B.tritici2 QFMALANCAE GASLIRETVF ESRFMHVPEL MRLGADIKLQ GTTALVRGGR PLHGAQVMAT DLRASVSLVL AALVAEGETV 388
B.vulpis QFMGLMTRAK GTSHITETIF ENRFMHVQEL ARLGAKISLS GQTATVEGVE RLKGAQVMAT DLRASVSLVI AGLAAEGETI 399
B.sp.BO2 QFMGLMTRAK GTSHITETIF ENRFMHVQEL ARLGAKISLS GQTATVEGVE RLKGAQVMAT DLRASVSLVI AGLAAEGETI 399
B.sp.BO3 QFMGLMTRAK GTSHITETIF ENRFMHVQEL ARLGAKISLS GQTATVEGVE RLKGAQVMAT DLRASVSLVI AGLAAEGETI 399
B.sp.BTU1 QFMGLMTKAK GTSRITETIF ENRFMHVQEL ARLGAKISLS GQTATVEGVE RLKGAQVMAT DLRASVSLVI AGLAAEGETI 400
B.sp.F5/06 QFMGLMTRAK GTSHITETIF ENRFMHVQEL ARLGAKISLS GQTATVEGVE RLKGAQVMAT DLRASVSLVI AGLAAEGETI 399
B.sp.NVSL 07-0026 QFMGLMTRAK GTSHITETIF ENRFMHVQEL ARLGAKISLS GQTATVEGVE RLKGAQVMAT DLRASVSLVI AGLAAEGETI 399
B.sp.10RB9215 QFMGLMTRAK GTSHITETIF ENRFMHVQEL ARLGAKISLS GQTATVEGVE RLKGAQVMAT DLRASVSLVI AGLAAEGETI 399
B.sp.2280 QFMGLMTRAK GTSHITETIF ENRFMHVQEL ARLGAKISLS GQTATVEGVE RLKGAQVMAT DLRASVSLVI AGLAAEGETI 399
B.sp.458 QFMGLMTRAK GTSHITETIF ENRFMHVQEL ARLGAKISLS GQTATVEGVE RLKGAQVMAT DLRASVSLVI AGLAAEGETI 399
B.sp.6810 QFMGLMTRAK GTSHITETIF ENRFMHVQEL ARLGAKISLS GQTATVEGVE RLKGAQVMAT DLRASVSLVI AGLAAEGETI 399
B.sp.83/13 QFMGLMTRAK GTSHITETIF ENRFMHVQEL ARLGAKISLS GQTATVEGVE RLKGAQVMAT DLRASVSLVI AGLAAEGETI 399

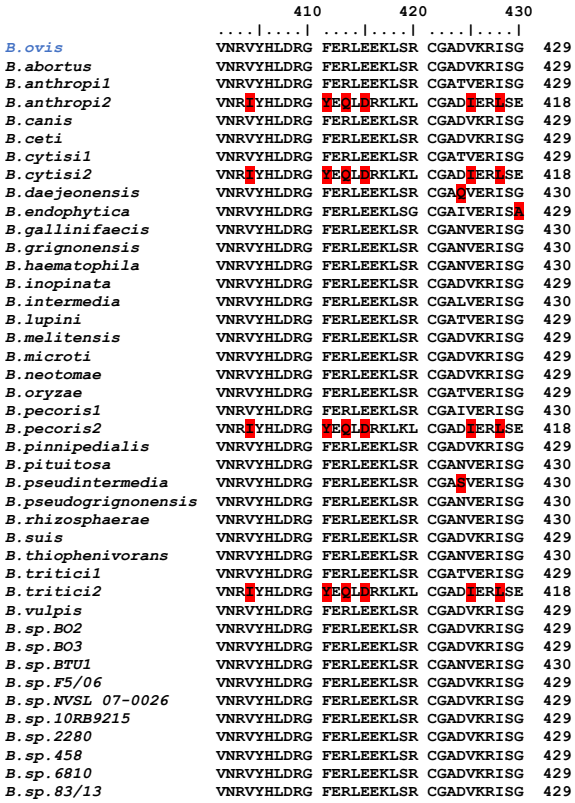

Figure 5.7. MurA sequence conservation within the *Brucella* genus. MSA (n=42) of MurAs from *Brucella* species in Table 5.3. The alignment was created with Clustal Omega. Residues that are not conserved in at least 90% of the sequences are highlighted in red. An asterisk marks the catalytic residue Cys.

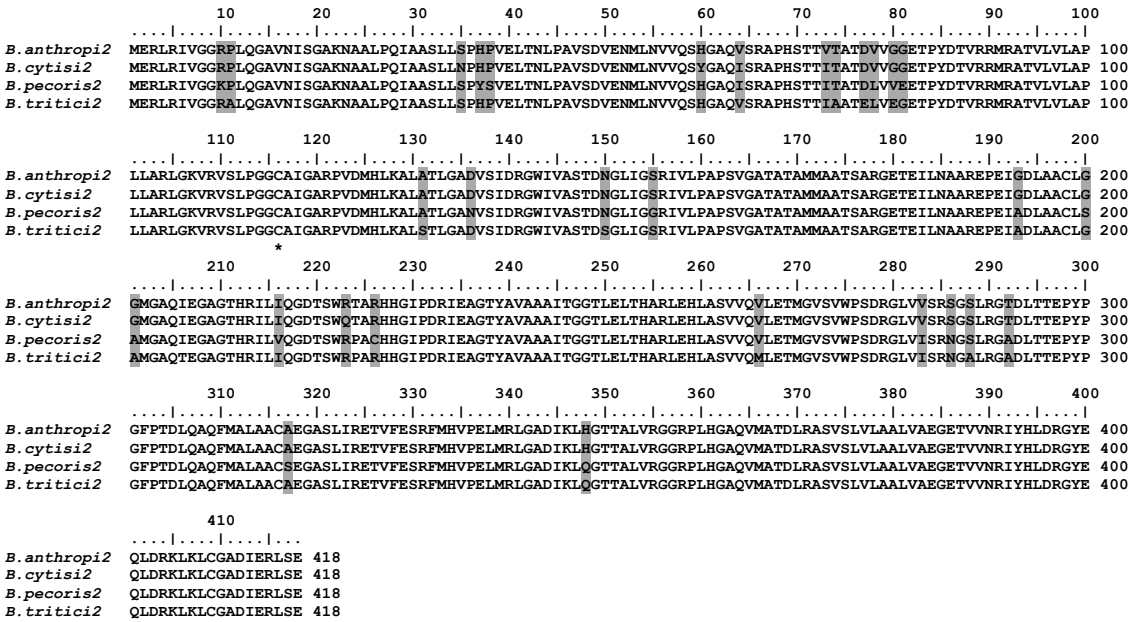

Figure 5.8. MurA2 sequence conservation within the *Brucella* genus. MSA (n=4) of MurA2s from *Brucella* species in Table 5.3. The alignment was created with Clustal Omega. Residues differing in some of the evaluated sequences are highlighted in grey. An asterisk marks the catalytic residue Cys

Phylogenetic analysis of MurA sequences from *Brucella* was performed using the MSA (Figure 5.7), bootstrap analysis of 500 replicates and rooting of the cladogram with *B.*

ovis SdhA as an outgroup sequence. The constructed tree exhibited three main clades (Figure 5.9B). Clade 1 (highlighted in red) represents the most divergent group and includes the MurA2s sequences of *B. precoris*, *B. tritici*, *B. cytisi* and *B. anthropi* sequence. Clade 2 (in blue) consists of 19 sequences, including MurA1 of *B. precoris*, *B. tritici*, *B. cytisi* and *B. anthropic, B. lupini, B. endophytica, B. oryzae, B. vulpis, B. daejeonensis, B. gallinifaecis, B. grignonensis, B. haematophila, B. intermedia, B. pituitosa, B. pseudintermedia, B. pseudogrignonensis, B. rhizosphaerae, B. thiophenivorans* and *B.* sp. BTU1 and is further divided into seven distinct clusters.

Clade 3 (green) encompasses the remaining MurA *Brucella* sequences. Within this clade, no further subclades are discernible beyond the grouping where BoMurA is found alongside *B. abortus*. Different branches are evident, but significant genetic or evolutionary differences are not pronounced enough to identify notable variations. Additionally, the bootstrap values decrease significantly throughout the tree after the initial sequence separation. As a result, it becomes challenging to determine the nearest evolutionary relatives in most cases. This pattern aligns with the high sequence similarity observed in the evaluated sequences in the MSA, leading to very few variable and informative sites for reconstructing the evolutionary history. Consequently, BoMurA clusters together with other significant pathogenic *Brucella* species that share highly similar sequences.

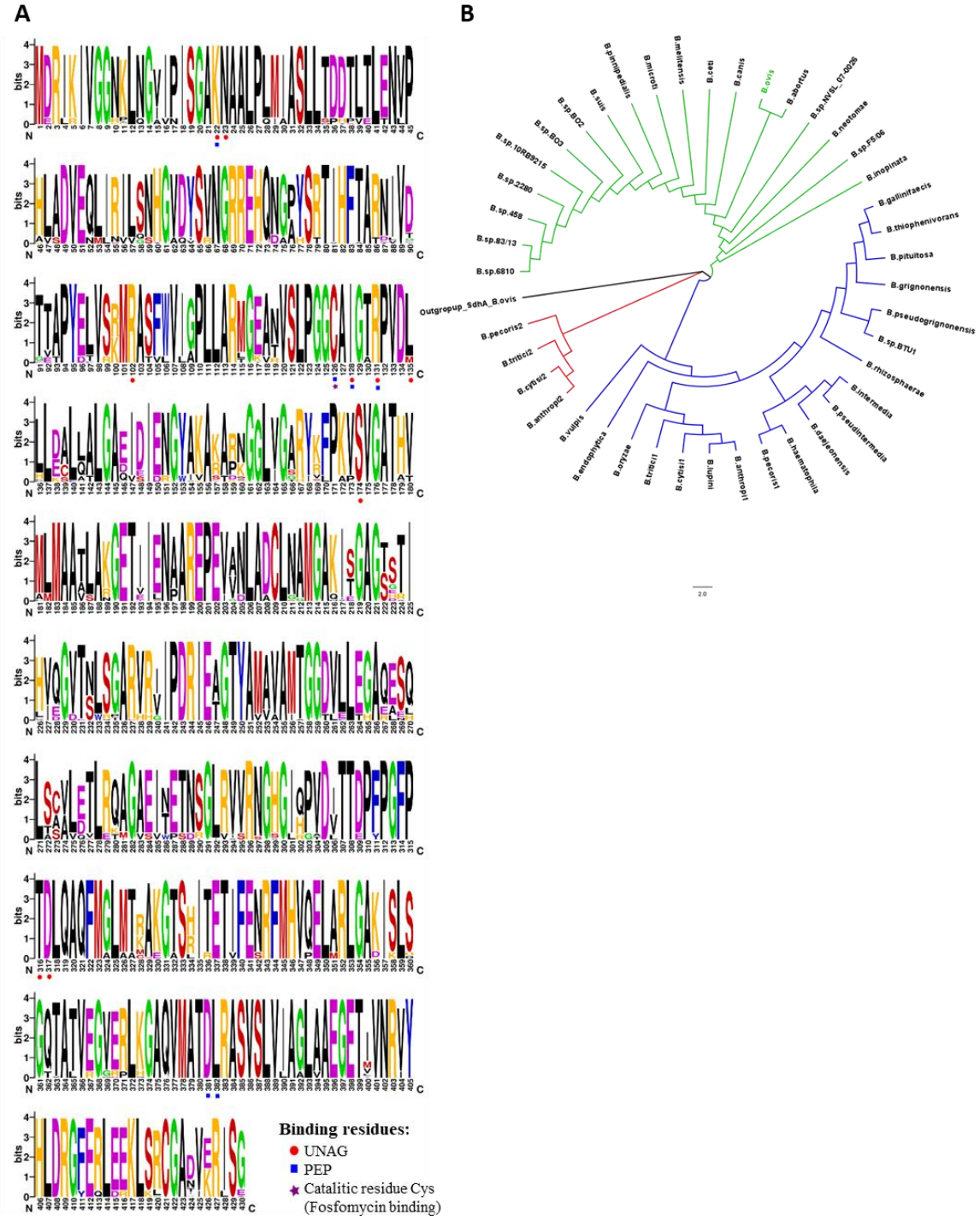

Figure 5.9. Residue conservation and evolution of MurA within *Brucella* spp. (A) Sequence Logo representing MSA of MurAs from *Brucella* (n=42). Logo generated with WebLogo. Residues presumably involved in substrate or inhibitor binding, by similarity with other MurA proteins, are indicated underneath the logo: Red circle, UNAG; blue square, PEP; purple stars, fosfomycin. **(B)** Phylogenetic relationship of MurAs from *Brucella*. Tree was built using the shown alignment, the Maximum Likelihood method and JTT matrix-based model with MEGA X. The tree with the highest log likelihood (-4850.34) is shown. This analysis involved the above aligned 42 MurA sequences from *Brucella* as well as the *B. ovis* SdhA sequence as outgroup. Branch lengths are proportional to the number of substitutions per site (scale beside). There was a total of 613 positions in the final dataset. The tree groups the sequences in three main clusters: Clade 1 (bootstrap = 100) in red color, Clade 2 (bootstrap > 77) in blue color, and Clade 3 (bootstrap > 66) in green color. This later cluster separates its branches in several subclades.

5.3.3 Sequence and evolutionary analysis of MurA proteins within bacterial species

Following the same approach, the next objective was to evaluate the sequence conservation in MurAs from different bacteria, for which an arbitrary number was chosen to compare with the BoMurA sequence. One set of chosen bacteria included the ESKAPE pathogens, an acronym that includes the scientific names of six highly virulent and antibiotic-resistant pathological bacteria according to the World Health Organization (WHO), and that includes: *Enterococcus faecium, S. aureus, K. pneumoniae, A. baumannii, P. aeruginosa* and *Enterobacter* spp. However, they are not the only bacteria of scientific interest, and we decided to expand the search to include pathogens for humans and animals as well as non-pathogenic bacteria. Altogether, a total of 74 MurA protein sequences from 62 bacterial species (Table 5.4) were collected to generate the MSA shown in Figure 5.10. The strains of *B. anthracis*, *B. licheniformis*, *B. subtilis*, *E. faecium, L. plantarum, L. monocytogenes*, *S. aureus*, *S. pneumoniae, S. paucimobilis* and *L. pneumophila* contain two isoforms of the murA gene, while *A. themocellus* possesses up to three, but the isoform 3 (WP_003512944.1) appears lacking the large portion of the N-terminal of the protein.

According to the literature, it is uncommon for bacteria to possess more than two copies of the MurA gene. However, it should be noted that there are variations among bacteria regarding the organization and complexity of their genomes. Certain bacteria may have larger and more intricate genomes, potentially leading to the presence of multiple copies of a particular gene, as is here the case of murA. Moreover, bacteria can occasionally acquire additional copies of genes through mechanisms such as gene duplication, recombination, or horizontal gene transfer (Griffiths & Gupta, 2006; Arber, 2014).

All sequences reveal >40% significant homology with BoMurA. Sequences with the highest percentage of similarity include *B. quintana* (WP_011179784.1, 76%), *B. schoenbuchensis* (WP_010704304.1, 76%), *G. oxydans* (WP_011252420.1, 66%), *N. gonorrhoeae* (WP_003688069.1, 66%), *P. zucieum* (ACG78612.1, 68%), *R. palustris* (WP_011160065.1, 78%), *R. pomeroyi* (WP_011241918.1, 66%), *S. meliloti* (WP_010968701.1, 84%) and *X. autotrophicus* (WP_012115108.1, 81%). In contrast, the sequences with the lowest similarity are *C. pecorum* (ETF39326.1, 46%), *C. trachomatis* (WP_009871813.1, 46%), *C. aggregans* (WP_015941285.1, 49%), *C. ammoniagenes* (WP_003847510.1, 55%), *F. tularensis* (CAG45938.1, 44%), *G. violaceus* (WP_011143118.1, 55%), *M. luteus* (WP_002856412.1, 47%), *P. gingivalis* (WP_005874334.1, 48%), *P. chlorophenolicus* (WP_015937434.1, 48%), *T. thermophilus*

(WP_011227732.1, 55%), *T. denticola* (WP_002669886.1, 48%); and the sequences classified as MurA2, such as *B. anthracis*2 (WP_000413260.1, 54%), *B. lincheniformis*2 (WP_003186058.1, 55%), *B. subtilis*2 (WP_003227628.1, 54%), *E. faecium*2 (SBA98256.1, 54%), *L. plantarum*2 (WP_003642050.1, 51%), *L. pneumophila*2 (WP_011214799.1, 41%), *L. monocytogenes*2 (WP_003734483.1, 54%), *S. paucimobilis*2 (EZP69702.1, 45%), *S. aureus*2 (WP_000046602.1, 54%) and *S. pneumoniae*2 (WP_001227083.1, 55%) (Figure 5.10).

Highly conserved residues and motifs are evident across the MSA (pink and gray residues in Figure 5.10), but particularly in the WebLogo shown in Figure 5.11A, which highlights them with green boxes. These highly conserved motifs are ^{44}GxKNxxL^{50}, ^{149}LPGG(C/D)xIG xxRPxDxLH^{164}, ^{353}TxPxPGFPTDxQ^{364} and ^{442}DLRAxxxLxxAGLxAxE^{458}, which are present in all the bacteria evaluated and contain the residues expected to be involved in enzyme catalysis (underlined) and, particularly the Cys/Asp catalytic residue shown in bold. In fact, the Cys-loop motif is prevalent in most bacteria, with the exception of *C. precorum*, *C. trachomatis*, *C. aggregans*, *C. ammoniagenes*, *L. plantarum*2, *M. marinum*, *M. tuberculosos*, *P. gingivalis*, and *T. denticola*, which show an "xGGDx" motif instead.

Phylogenetic analysis was performed using the MSA in Figure 5.9 with a bootstrap analysis of 500 replicates and rooting of the cladogram with the *B. ovis* SdhA as the outgroup sequence. The constructed tree exhibited six main clades (Figure 5.11B). Clade 1 (highlighted in cyan) stands as the most divergent, encompassing the single MurA sequence from *T. maritima*. Clade 2 (highlighted in red) comprises 11 MurA sequences spanning the Actinobacteria, Bacteroides, Chlamydiae, Chloroflex, Deinococcus-Thermus, and Spirochaetes phylum, along with 3 sequences from *F. tularensis*, *L. pneumophila*2, and *S. paucimobilis*2 of the Proteobacteria phylum. Clade 3 (in yellow) includes 6 sequences, encompassing representatives from the Cyanobacteria and Cercozoa phyla. Clade 4 (in purple) contains 19 sequences, all belonging to the Firmicutes phylum, subdivided into two subclades: one housing MurA1 sequences and the other MurA2 sequences. Clade 5 (in blue) comprises 15 Gram-negative bacteria sequences from the Proteobacteria phylum, including *L. pneumophila* MurA1. Finally, the Clade 6 (in green) encompasses the remaining sequences, all within the Proteobacteria phylum (excluding *A. aeolicus*). Notably, this clade features the MurA1 sequence of *S. paucimobilis* and as anticipated, it also contains BoMurA sequence.

Table 5.4. List of bacterial species for which MurA sequences are evaluated in this study. Column "Species Name" highligths in blue those species corresponding to virulent and antibiotic resistant bacterial pathogens known as ESKAPE, in light orange animal pathogens and in dark orange human pathogens. Column "Short Species Name" highlights in green those species for which MurA has been purified and structurally or functionally characterized. *B. ovis* is highlighted in bold.

Species Name	Short Species Name	Access Code	Gram	Phylum	Class
Acaryochloris marina	*A. marina*	ABW25985.1	negative	Cyanobacteria	Cyanophyceae
Acetivibrio thermocellus	*A. thermocellus*1	WP_003512944.1	positive	Firmicutes	Clostridia
	*A. thermocellus*2	WP_020457769.1			
	*A. thermocellus*3	ABN51679.1			
Acinetobacter baumannii	*A. baumannii*	WP_000357156.1	negative	Proteobacteria	Gammaproteobacteria
Aliivibrio fischeri	*A. fischeri*	WP_005417511.1	negative	Proteobacteria	Gammaproteobacteria
Anabaena PCC 7120 /*nostoc*	*Nostoc*	WP_010994351.1	negative	Cyanobacteria	--
Aquifex aeolicus	*A. aeolicus*	WP_010880817.1	negative	Aquificota	Aquificia
Azotobacter vinelandii	*A. vinelandii*	WP_012699937.1	negative	Proteobacteria	Alphaproteobacteria
Bacillus anthracis	*B. anthracis*1	WP_000411264.1	positive	Firmicutes	Bacilli
	*B. anthracis*2	WP_000413260.1			
Bacillus licheniformis	*B. licheniformis*1	WP_003185997.1	positive	Firmicutes	Bacilli
	*B. licheniformis*2	WP_003186058.1			
Bacillus subtilis	*B. subtilis*1	WP_003227695.1	positive	Firmicutes	Bacilli
	*B. subtilis*2	WP_003227628.1			
Bartonella quintana	*B. quintana*	WP_011179784.1	negative	Proteobacteria	Alphaproteobacteria
Bartonella schoenbuchensis	*B. schoenbuchensis*	WP_010704304.1	negative	Proteobacteria	Alphaproteobacteria
Brucella ovis (strain ATCC 25840)[a]	*B. ovis*	WP_002965536.1	negative	Proteobacteria	Alphaproteobacteria
Campylobacter sp	*Campylobacter*	WP_002857102.1	negative	Proteobacteria	Epsilonproteobacteria
Candidatus pelagibacter	*C. pelagibacter*	WP_008544542.1	negative	Proteobacteria	Alphaproteobacteria
Chlamydia pecorum[b]	*C. pecorum*	ETF39326.1	negative	Chlamydiae	Chlamydiia
Chlamydia trachomatis[b]	*C. trachomatis*	WP_009871813.1	negative	Chlamydiae	Chlamydiia
Chloroflexus aggregans	*C. aggregans*	WP_015941285.1	positive	Chloroflexi	Chloroflexi
Clostridioides difficile	*C. difficile*	CAJ66943.1	positive	Firmicutes	Clostridia
Corynebacterium ammoniagenes	*C. ammoniagenes*	WP_003847510.1	positive	Actinobacteria	Actinobacteria
Enterobacter cloacae	*E. cloacae*	WP_013098931.1	negative	Proteobacteria	Gammaproteobacteria
Enterococcus faecium	*E. faecium*1	SAM80470.1	positive	Firmicutes	Bacilli
	*E. faecium*2	SBA98256.1			
Escherichia coli	*E. coli*	WP_000357259.1	negative	Proteobacteria	Gammaproteobacteria
Francisella tularensis[a]	*F. tularensis*	CAG45938.1	negative	Proteobacteria	Gammaproteobacteria
Gloeobacter violaceus	*G. violaceus*	WP_011143118.1	negative	Cyanobacteria	Gloeobacteria
Gluconobacter oxydans	*G. oxydans*	WP_011252420.1	negative	Proteobacteria	Alphaproteobacteria
Haemophilus influenzae	*H. influenzae*	WP_005693405.1	negative	Proteobacteria	Gammaproteobacteria
Helicobacter pylori	*H. pylori*	WP_000346467.1	negative	Proteobacteria	Epsilonproteobacteria
Klebsiella pneumoniae	*K. pneumoniae*	WP_002918382.1	negative	Proteobacteria	Gammaproteobacteria
Lactiplantibacillus plantarum	*L. plantarum*1	WP_003644659.1	positive	Firmicutes	Bacilli
	*L. plantarum*2	WP_003642050.1			
Legionella pneumophila[a]	*L. pneumophila*1	WP_011215028.1	negative	Proteobacteria	Gammaproteobacteria
	*L. pneumophila*2	WP_011214799.1			
Listeria monocytogenes[b]	*L. monocytogenes*1	WP_003727894.1	positive	Firmicutes	Bacilli
	*L. monocytogenes*2	WP_003734483.1			
Micrococcus luteus	*M. luteus*	WP_002856412.1	positive	Actinobacteria	Actinomycetales
Mycobacterium marinum[a]	*M. marinum*	WP_012395668.1	positive	Actinobacteria	Actinobacteria
Mycobacterium tuberculosis[a]	*M. tuberculosis*	WP_003406845.1	positive	Actinobacteria	Actinobacteridae
Neisseria gonorrhoeae	*N. gonorrhoeae*	WP_003688069.1	negative	Proteobacteria	Betaproteobacteria
Paracoccus yeei	*P. yeei*	ATQ55765.1	negative	Proteobacteria	Alphaproteobacteria
Paulinella chromatophora	*P. chromatophora*	ACB42543.1	microalga	Cercozoa	Imbricatea
Phenylobacterium zucineum	*P. zucineum*	ACG78612.1	negative	Proteobacteria	Alphaproteobacteria
Porphyromonas gingivalis	*P. gingivalis*	WP_005874334.1	negative	Bacteroidetes	Bacteroidia
Pseudarthrobacter chlorophenolicus	*P. chlorophenolicus*	WP_015937434.1	positive	Actinobacteria	Actinomycetales
Pseudomonas aeruginosa	*P. aeruginosa*	WP_003094332.1	negative	Proteobacteria	Gammaproteobacteria
Pseudomonas putida	*P. putida*	WP_003255119.1	negative	Proteobacteria	Gammaproteobacteria
Rhodobacter capsulatus	*R. capsulatus*	WP_013068270.1	negative	Proteobacteria	Alphaproteobacteria
Rhodopseudomonas palustris	*R. palustris*	WP_011160065.1	negative	Proteobacteria	Alphaproteobacteria
Rickettsia rickettsii[b]	*R. rickettsii*	WP_012151046.1	negative	Proteobacteria	Alphaproteobacteria
Rickettsia typhi[b]	*R. typhi*	WP_011191016.1	negative	Proteobacteria	Alphaproteobacteria
Ruegeria pomeroyi	*R. pomeroyi*	WP_011241918.1	negative	Proteobacteria	Alphaproteobacteria
Salmonella enterica subsp. enterica serovar Typhimurium[a]	*S. enterica*	WP_000357288.1	negative	Proteobacteria	Gammaproteobacteria
Shigella dysenteriae serotype 1	*S. dysenteriae*	WP_000357268.1	negative	Proteobacteria	Gammaproteobacteria
Sinorhizobium meliloti	*S. meliloti*	WP_010968701.1	negative	Proteobacteria	Alphaproteobacteria
Sphingomonas paucimobilis	*S. paucimobilis*1	WP_037481860.1	negative	Proteobacteria	Alphaproteobacteria
	*S. paucimobilis*2	EZP69702.1			
Staphylococcus aureus	*S. aureus*1	WP_000358006.1	positive	Firmicutes	Bacilli
	*S. aureus*2	WP_000046602.1			
Stenotrophomonas maltophilia	*S. maltophilia*	WP_005408397.1	negative	Proteobacteria	Gammaproteobacteria
Streptococcus pneumoniae	*S. pneumoniae*1	WP_000358028.1	positive	Firmicutes	Bacilli
	*S. pneumoniae*2	WP_001227083.1			
Synechococcus sp.	*Synechococcus*	WP_011363859.1	negative	Cyanobacteria	--
Thermotoga marítima	*T. maritima*	WP_004082675.1	negative	Thermotogae	Thermotogae
Thermus thermophilus	*T. thermophilus*	WP_011227732.1	negative	Deinococcus-Thermus	Deinococci
Treponema denticola	*T. denticola*	WP_002669886.1	negative	Spirochaetes	Spirochaetia
Vibrio cholerae O1 biovar El Tor str. N16961	*V. cholerae*	WP_000410586.1	negative	Proteobacteria	Gammaproteobacteria
Wolbachia pipientis	*W. pipientis*	WP_010963092.1	negative	Proteobacteria	Alphaproteobacteria
Xanthobacter autotrophicus	*X. autotrophicus*	WP_012115108.1	negative	Proteobacteria	Alphaproteobacteria

[a]Facultative intracelular organism.
[b]Obligatory intracelular organism.

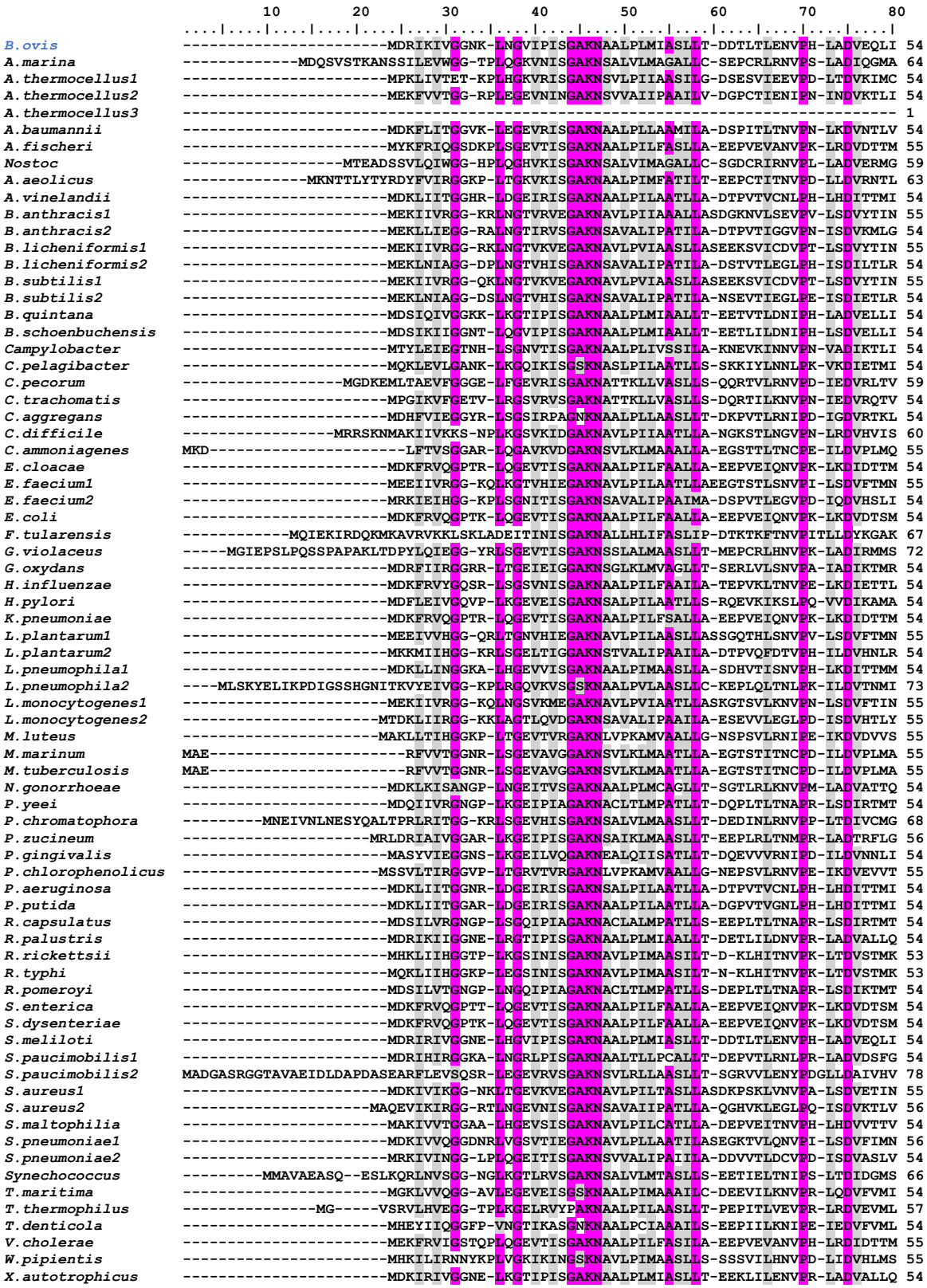
10 20 30 40 50 60 70 80
B.ovis
A.marina
A.thermocellus1
A.thermocellus2
A.thermocellus3
A.baumannii
A.fischeri
Nostoc
A.aeolicus
A.vinelandii
B.anthracis1
B.anthracis2
B.licheniformis1
B.licheniformis2
B.subtilis1
B.subtilis2
B.quintana
B.schoenbuchensis
Campylobacter
C.pelagibacter
C.pecorum
C.trachomatis
C.aggregans
C.difficile
C.ammoniagenes
E.cloacae
E.faecium1
E.faecium2
E.coli
F.tularensis
G.violaceus
G.oxydans
H.influenzae
H.pylori
K.pneumoniae
L.plantarum1
L.plantarum2
L.pneumophila1
L.pneumophila2
L.monocytogenes1
L.monocytogenes2
M.luteus
M.marinum
M.tuberculosis
N.gonorrhoeae
P.yeei
P.chromatophora
P.zucineum
P.gingivalis
P.chlorophenolicus
P.aeruginosa
P.putida
R.capsulatus
R.palustris
R.rickettsii
R.typhi
R.pomeroyi
S.enterica
S.dysenteriae
S.meliloti
S.paucimobilis1
S.paucimobilis2
S.aureus1
S.aureus2
S.maltophilia
S.pneumoniae1
S.pneumoniae2
Synechococcus
T.maritima
T.thermophilus
T.denticola
V.cholerae
W.pipientis
X.autotrophicus

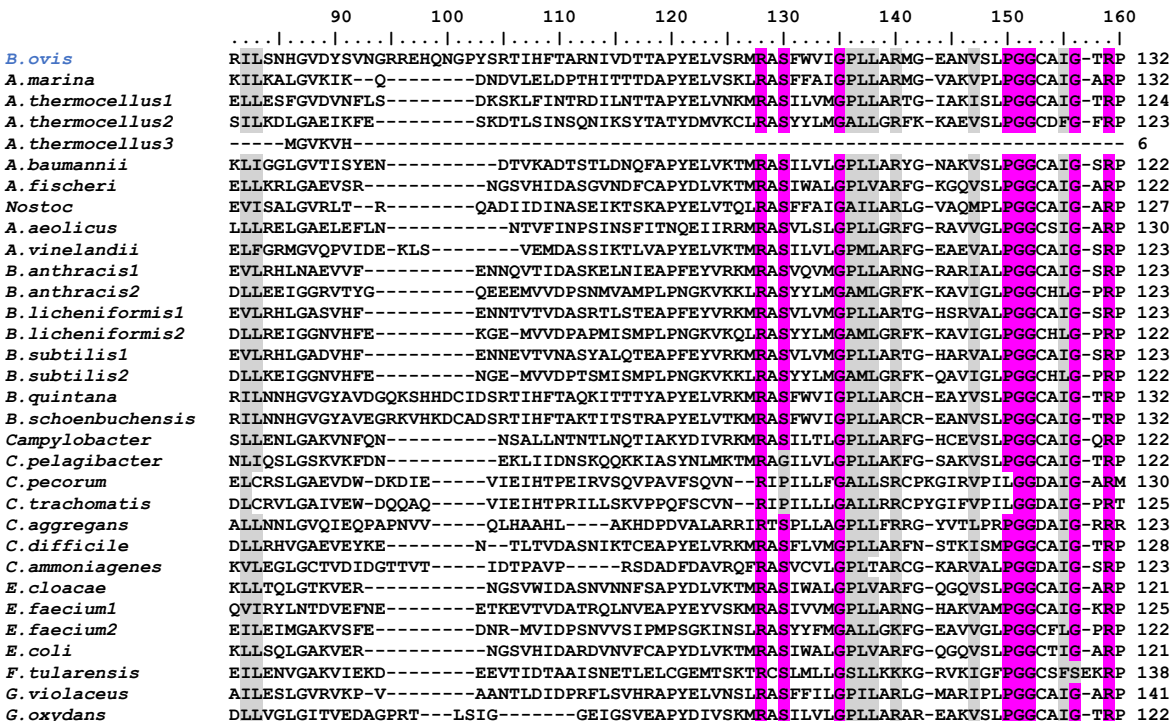
90 100 110 120 130 140 150 160
B.ovis RILSNHGVDYSVNGRREHQNGPYSRTIHFTARNIVDTTAPYELVSRMRASFWVIGPLLARMG-EANVSLPGGCAIG-TRP 132
A.marina KILKALGVKIK--Q--------DNDVLELDPTHITTTDAPYELVSKLRASFFAIGPLLARMG-VAKVPLPGGCAIG-ARP 132
A.thermocellus1 ELLESFGVDVNFLS--------DKSKLFINTRDILNTTAPYELVNKMRASILVMGPLLARTG-IAKISLPGGCAIG-TRP 124
A.thermocellus2 SILKDLGAEIKFE---------SKDTLSINSQNIKSYTATYDMVKCLRASYYLMGALLGRFK-KAEVSLPGGCDFG-FRP 123
A.thermocellus3 -----MGVKVH---------- 6
A.baumannii KLIGGLGVTISYEN----------DTVKADTSTLDNQFAPYELVKTMRASILVLGPLLARYG-NAKVSLPGGCAIG-SRP 122
A.fischeri ELLKRLGAEVSR----------NGSVHIDASGVNDFCAPYDLVKTMRASIWALGPLVARFG-KGQVSLPGGCAIG-ARP 122
Nostoc EVISALGVRLT--R--------QADIIDINASEIKTSKAPYELVTQLRASFFAIGAILARLG-VAQMPLPGGCAIG-ARP 127
A.aeolicus LLLRELGAELEFLN-----------NTVFINPSINSFITNQEIIRRMRASVLSLGPLLGRFG-RAVVGLPGGCSIG-ARP 130
A.vinelandii ELFGRMGVQPVIDE-KLS--------VEMDASSIKTLVAPYELVKTMRASILVLGPMLARFG-EAEVALPGGCAIG-SRP 123
B.anthracis1 EVLRHLNAEVVF----------ENNQVTIDASKELNIEAPFEYVRKMRASVQVMGPLLARNG-RARIALPGGCAIG-SRP 123
B.anthracis2 DLLEEIGGRVTYG---------QEEEMVVDPSNMVAMPLPNGKVKKLRASYYLMGAMLGRFK-KAVIGLPGGCHLG-PRP 123
B.licheniformis1 EVLRHLGASVHF----------ENNTVTVDASRTLSTEAPFEYVRKMRASVLVMGPLLARTG-HSRVALPGGCAIG-SRP 123
B.licheniformis2 DLLREIGGNVHFE---------KGE-MVVDPAPMISMPLPNGKVKQLRASYYLMGAMLGRFK-KAVIGLPGGCHLG-PRP 122
B.subtilis1 EVLRHLGADVHF----------ENNEVTVNASYALQTEAPFEYVRKMRASVLVMGPLLARTG-HARVALPGGCAIG-SRP 123
B.subtilis2 DLLKEIGGNVHFE---------NGE-MVVDPTSMISMPLPNGKVKKLRASYYLMGAMLGRFK-QAVIGLPGGCHLG-PRP 122
B.quintana RILNNHGVGYAVDGQKSHHDCIDSRTIHFTAQKITTTYAPYELVRKMRASFWVIGPLLARCH-EAYVSLPGGCAIG-TRP 132
B.schoenbuchensis RILNNHGVGYAVEGRKVHKDCADSRTIHFTAKTITSTRAPYELVTKMRASFWVIGPLLARCR-EANVSLPGGCAIG-TRP 132
Campylobacter SLLENLGAKVNFQN----------NSALLNTNTLNQTIAKYDIVRKMRASILTLGPLLARFG-HCEVSLPGGCAIG-QRP 122
C.pelagibacter NLIQSLGSKVKFDN----------EKLIIDNSKQQKKIASYNLMKTMRAGILVLGPLLAKFG-SAKVSLPGGCAIG-TRP 122
C.pecorum ELCRSLGAEVDW-DKDIE-----VIEIHTPEIRVSQVPAVFSQVN--RIPILLFGALLSRCPKGIRVPILGGDAIG-ARM 130
C.trachomatis DLCRVLGAIVEW-DQQAQ-----VIEIHTPRILLSKVPPQFSCVN--RIPILLLGALLRRCPYGIFVPILGGDAIG-PRT 125
C.aggregans ALLNNLGVQIEQPAPNVV-----QLHAAHL----AKHDPDVALARRIRTSPLLAGPLLFRRG-YVTLPRPGGDAIG-RRR 123
C.difficile DLLRHVGAEVEYKE--------N--TLTVDASNIKTCEAPYELVRKMRASFLVMGPLLARFN-STKISMPGGCAIG-TRP 128
C.ammoniagenes KVLEGLGCTVDIDGTTVT-----IDTPAVP-----RSDADFDAVRQFRASVCVLGPLTARCG-KARVALPGGDAIG-SRP 123
E.cloacae KLLTQLGTKVER-----------NGSVWIDASNVNNFSAPYDLVKTMRASIWALGPLVARFG-QGQVSLPGGCAIG-ARP 121
E.faecium1 QVIRYLNTDVEFNE--------ETKEVTVDATRQLNVEAPYEYVSKMRASIVVMGPLLARNG-HAKVAMPGGCAIG-KRP 125
E.faecium2 EILEIMGAKVSFE---------DNR-MVIDPSNVVSIPMPSGKINSLRASYYFMGALLGKFG-EAVVGLPGGCFLG-PRP 122
E.coli KLLSQLGAKVER-----------NGSVHIDARDVNVFCAPYDLVKTMRASIWALGPLVARFG-QGQVSLPGGCTIG-ARP 121
F.tularensis EILENVGAKVIEKD--------EEVTIDTAAISNETLELCGEMTSKTRCSLMLLGSLLKKKG-RVKIGFPGGCSFSEKRP 138
G.violaceus AILESLGVRVKP-V---------AANTLDIDPRFLSVHRAPYELVNSLRASFFILGPILARLG-MARIPLPGGCAIG-ARP 141
G.oxydans DLLVGLGITVEDAGPRT---LSIG-------GEIGSVEAPYDIVSKMRASILVLGPLLARAR-EAKVSLPGGCAIG-TRP 122
H.influenzae KILRQLGVVVDRDA---------TGAVLLDASNINHFTAPYELVKTMRASIWALAPLVARFH-QGQVSLPGGCSIG-ARP 123
H.pylori LLLQNLGASLEWLNP---------NTLQIGAKSLNHTEATYDLVRKMRASILVLGPLLARFK-ECLVSLPGGCAIG-ARP 123
K.pneumoniae KLLSQLGAKVER-----------NGSVWIDAGPVDVFCAPYDLVKTMRASIWALGPLVARFG-QGQVSLPGGCAIG-ARP 121
L.plantarum1 NVLKFLNTKIDFDE--------INKTIDIDASRQLSSEAPFQYVSKMRASIVVMGPLLARLG-HAKVAMPGGCAIG-SRP 125
L.plantarum2 LILESMNVHSTFE---------NDV-LTIDPTNIEESELPSHAIKSLRASYYFMGALLGRFN-RATVTFPGGDNIG-PRP 122
L.pneumophila1 ELLGQLGAHLIVDE-KMN--------VQVDSSQVNEFVAPYDLVKTMRASILVLGPMLARFG-KADVSLPGGCAIG-TRP 123
L.pneumophila2 QCMEALGKRFEF-I---------NTNTIKIGNREMDTLTIPKEAARQIRASIILLGPLVAQYP-KVILPLPGGCSIG-KRP 142
L.monocytogenes1 EVLKYLNADVSF----------VNDEVTVNATGEITSDAPFEYVRKMRASIVVMGPLLARTG-SARVALPGGCAIG-SRP 123
L.monocytogenes2 NILEELGGTVRYD---------NKT-AVIDPTDMISMPLPSGNVKKLRASYYLMGAMLGRFK-KAVIGLPGGCYLG-PRP 123
M.luteus SLLEIHGVSVEW-DKETG-----RITMDPAGVKSALTAEIDAHAGDSRIPILFCGPLMHAIG-EAFIPDLGGCKIG-DRP 127
M.marinum EVLRGLGATVELDGDVAR-----ITSPDEP-----KYDADFAAVRQFRASVCVLGPLVGRCK-RAKVALPGGDAIG-SRP 123
M.tuberculosis EVLRGLGATVELDGDVAR-----ITAPDEP-----KYDADFAAVRQFRASVCVLGPLVGRCK-RARVALPGGDAIG-SRP 123
N.gonorrhoeae KLLQGMGARVLTDN--IS-------EFEINGGTVNNTCAPYELVRTMRASILVLGPTLARFG-EAQVSLPGGCAIG-SRP 123
P.yeei ALLQSLGAEVASLQ--------DGQVLALSSHDLDNHTADYDIVRKMRASILVLGPMLARDG-HAVVSLPGGCAIG-ARP 124
P.chromatophora KILISLGVNLN--H--------GIESLRINSANLENIAPPYELVNCLRASFFCIGPLLARMG-ITQVPLPGGCRIG-TRP 136
P.zucineum KLLQRLGAEVVESDG------PEGSETLLTTREIVSGFAPYDLVRQMRASFNVLGPLLARSG-QAKVSLPGGCTIG-ARP 128
P.gingivalis DLLRNMGVKVKRPTRDTC-----VFQADNVNLDYIKSEQFLEKSRALRGSVLLVGPLISRFG-YAIFPKPGGDKIG-RRR 127
P.chlorophenolicus SLLQLHGVTVEK-DPVSG-----DLTLDPKAAKTASSTAIDAHAGDSRIPILLCGPLIHAIG-EAFIPDLGGCKIG-DRP 127
P.aeruginosa ELFGRMGVQPIIDE-KLN--------VEVDASSIKTLVAPYELVKTMRASILVLGPMLARFG-EAEVALPGGCAIG-SRP 123
P.putida ELFGRMGIEPVIDE-KLS---------VEIDPRTIKTLVAPYELVKTMRASILVLGPMVARFG-EAEVALPGGCAIG-SRP 123
R.capsulatus QLLASLGAEVTALQ--------DGKVLATSCHGAINPVADYDIVRKMRASNLVLGPLLARLG-HAVVSLPGGCAIG-ARP 124
R.palustris RILGNHGVDIMAAGKRPGDHEYQGQTLHISAKTIVDTTAPYDLVSKMRASFWVIAPLVARMH-EAKVSLPGGCAIG-TRP 132
R.rickettsii DLLRSHGADIEIIKH------QDEFELIIDTKNINNFTADYEIVRKMRASIWVLGPLLTKYG-KAKVSLPGGCAIG-ARQ 125
R.typhi DLLQNHGACIRIIEH------TDALEIIINTTNINKFTADYEIVRKMRASIWVLGPLLTKYG-KAKVSLPGGCAIG-ARQ 125
R.pomeroyi LLLQSLGAEVSSLQ--------DGKVLAMSSHDLTSHTADYDIVRKMRASNLVLGPMLARLG-QAVVSLPGGCAIG-ARP 124
S.enterica KLLSQLGAKVER-----------NGSVHIDASQVNVFCAPYDLVKTMRASIWALGPLVARFG-QGQVSLPGGCTIG-ARP 121
S.dysenteriae KLLSQLGAKVER-----------NGSVHIDARDVNVFCAPYDLVKTMRASIWALGPLVARFG-QGQVSLPGGCTIG-ARP 121
S.meliloti RILGNHGADISVNGRRERQGESYARTVHFTSRNIVSTTAPYELVSKMRASFWVIGPLLAREG-KARVSLPGGCAIG-TRP 132
S.paucimobilis1 HLLNQLGVSTMIEGARP---EDFGRVMTLRAGRVTSTEAPYDIVRKMRASILVLGPLLARAG-EARVSLPGGCAIG-NRP 129
S.paucimobilis2 GMLKTLGKTCRLEDSALV-----IEEATAP-----PSDLVWTG-RSIRNTLLILGALVARTG-AGSVPLPGGCDLG-DRK 145
S.aureus1 NVLTTLNADVTYKK--------DENAVVVDATKTLNEEAPYEYVSKMRASILVMGPLLARLG-HAIVALPGGCAIG-SRP 125
S.aureus2 SLLEDLNIKASLN---------GTE-LEVDTTEIQNAALPNNKVESLRASYYMMGAMLGRFK-KCVIGLPGGCPLG-PRP 124
S.maltophilia KLLGELGAKVTIDQGTLSR----GSAIVVDPRPVNQHVAPYELVKTMRASILVLGPLLARFG-AAEVSLPGGCAIG-SRP 128
S.pneumoniae1 QVVGGLNAKVDFDE--------EAHLVKVDATGDITEEAPYKYVSKMRASIVVLGPILARVG-HAKVSMPGGCTIG-SRP 126
S.pneumoniae2 EIMELMGATVKRY---------DDV-LEIDPRGVQNIPMPYGKINSLRASYYFYGSLLGRFG-EATVGLPGGCDLG-PRP 122
Synechococcus AILESLGVQVD--R--------QSDCIRLTAAELSGSAPPYELVNSLRASFFSIGPLLGRLG-HAQVPLPGGCRIG-ARP 134
T.maritima DILRSIGFRVEFE----------ENELKIKRENDISQEVPYELVRKMRASFNVLGPIAVRTG-RAKVALPGGCSIG-VRP 122
T.thermophilus ELLAHLGTQYAW-E--------GR-TLHLQTPEIKSTHAPYELVGQMRASFIVWGALLARAG-EGHVSMPGGCAFG-FRP 125
T.denticola QVFEALGGHYEKIEKNVF-----KLQIEKV----KTSKIPEDLATKIRASILFAGPLLARTG-KAVLPPPGGDVIG-RRR 123
V.cholerae ELLERLGAKVER-----------NGSVHVDAGPINQYCAPYDLVKTMRASIWALGPLVARFG-QGQVSLPGGCAIG-ARP 122
W.pipientis KLLESLGAEVNFMHNKN---YKANHTLKIDCSNINNHVMPYKTASKLRTSFLILGPMLSRFG-KARTAFPGGCNIG-KRP 130
X.autotrophicus RILGNHGVDITTNGKRNGDDPYAGQTLEIDARVIVDTTAPYDLVSRMRASFWVLGPLLARIG-VAKVSLPGGCAIG-TRP 132
*

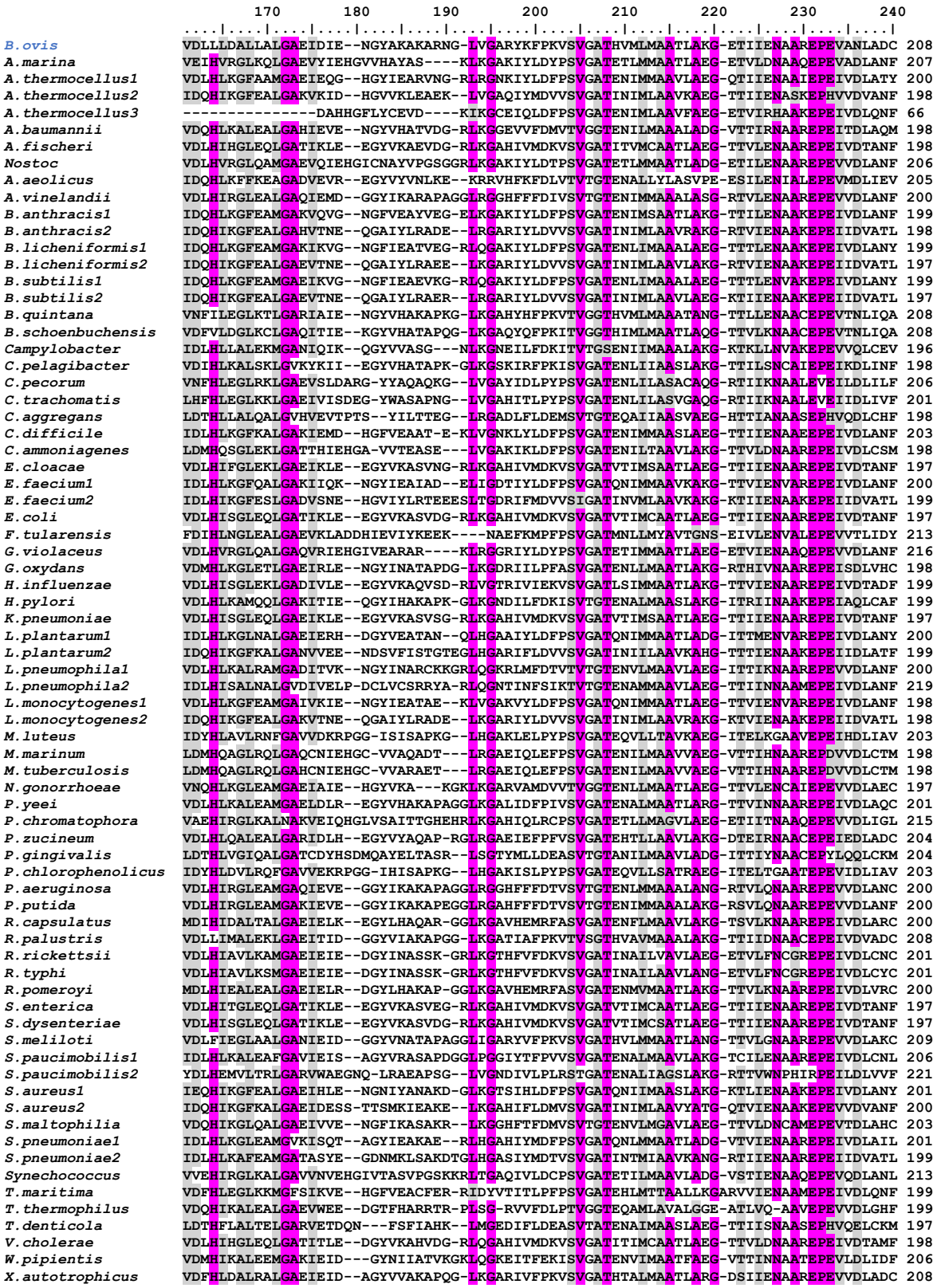
170 180 190 200 210 220 230 240
B.ovis VDLLLDALLALGAEIDIE--NGYAKAKARNG-LVGARYKFPKVSVGATHVMLMAATLAKG-ETIIENAAREPEVANLADC 208
A.marina VEIHVRGLKQLGAEVYIEHGVVHAYAS----KLKGAKIYLDYPSVGATETLMMAATLAEG-ETVLDNAAQEPEVADLANF 207
A.thermocellus1 VDLHLKGFAAMGAEIEQG--HGYIEARVNG-RLRGNKIYLDFPSVGATENIMMAAVLAEG-QTIIENAAIEPEIVDLATY 200
A.thermocellus2 IDQHIKGFEALGAKVKID--HGVVKLEAEK--LVGAQIYMDVVSVGATININMLAAVKAEG-TTIIENASKEPHVVDVANF 198
A.thermocellus3 ---------------DAHHGFLYCEVD----KIKGCEIQLDFPSVGATENIMLAAVFAEG-ETVIRHAAKEPEIVDLQNF 66
A.baumannii VDQHLKALEALGAHIEVE--NGYVHATVDG-RLKGGEVVFDMVTVGGTENILMAAALADG-VTTIRNAAREPEITDLAQM 198
A.fischeri VDLHIHGLEQLGATIKLE--EGYVKAEVDG-RLKGAHIVMDKVSVGATITVMCAATLAEG-TTVLENAAKEPEIVDTANF 198
Nostoc VDLHVRGLQAMGAEVQIEHGICNAYVPGSGGRLKGAKIYLDTPSVGATETLMMAATLADG-ETILENAAREPEVVDLANF 206
A.aeolicus IDQHLKFFKEAGADVEVR--EGYVYVNLKE--KRRVHFKFDLVTVTGTENALLYLASVPE-ESILENIALEPEVMDLIEV 205
A.vinelandii VDLHIRGLEALGAQIEMD--GGYIKARAPAGGLRGGHFFFDIVSVTGTENIMMAAALASG-RTVLENAAREPEVVDLANF 200
B.anthracis1 IDQHLKGFEAMGAKVQVG--NGFVEAYVEG-ELKGAKIYLDFPSVGATENIMSAATLAEG-TTILENAAKEPEIVDLANF 199
B.anthracis2 IDQHIKGFEALGAHVTNE--QGAIYLRADE--LRGARIYLDVVSVGATININMLAAVRAKG-RTVIENAAKEPEIIDVATL 198
B.licheniformis1 IDQHLKGFEAMGAKIKVG--NGFIEATVEG-RLQGAKIYLDFPSVGATENLIMAAALAEG-TTTLENAAKEPEIVDLANY 199
B.licheniformis2 IDQHIKGFEALGAEVTNE--QGAIYLRAEE--LKGARIYLDVVSVGATININMLAAVLAKG-RTVIENAAKEPEIIDVATL 197
B.subtilis1 IDQHLKGFEAMGAEIKVG--NGFIEAEVKG-RLQGAKIYLDFPSVGATENLIMAAALAEG-TTTLENVAKEPEIVDLANY 199
B.subtilis2 IDQHIKGFEALGAEVTNE--QGAIYLRAER--LRGARIYLDVVSVGATININMLAAVLAEG-KTIIENAAKEPEIIDVATL 197
B.quintana VNFILEGLKTLGARIAIE--NGYVHAKAPKG-LKGAHYHFPKVTVGGTHVMLMAAATANG-TTLLENAACEPEVTNLIQA 208
B.schoenbuchensis VDFVLDGLKCLGAQITIE--KGYVHATAPQG-LKGAQYQFPKITVGGTHIMLMAATLAQG-TTVLKNAACEPEVTNLIQA 208
Campylobacter IDLHLLALEKMGANIQIK--QGYVVASG---NLKGNEILFDKITVTGSENIIMAAALAKG-KTKLLNVAKEPEVVQLCEV 196
C.pelagibacter VDIHLKALSKLGVKYKII--EGYVHATAPK-GLKGSKIRFPKISVGATENLIIAASLAKG-TTILSNCAIEPEIKDLINF 198
C.pecorum VNFHLEGLRKLGAEVSLDARG-YYAQAQKG--LVGAYIDLPYPSVGATENLILASACAQG-RTIIKNAALEVEILDLILF 206
C.trachomatis LHFHLEGLKKLGAEIVISDEG-YWASAPNG--LVGAHITLPYPSVGATENLILASVGAQG-RTIIKNAALEVEIIDLIVF 201
C.aggregans LDTHLLALQALGVHVEVTPTS--YILTTEG--LRGADLFLDEMSVTGTEQAIIAASVAEG-HTTIANAASEPHVQDLCHF 198
C.difficile IDLHLKGFKALGAKIEMD--HGFVEAAT-E-KLVGNKLYLDFPSVGATENIMMAASLAEG-TTIIENAAEEPEIVDLANF 203
C.ammoniagenes LDMHQSGLEKLGATTHIEHGA-VVTEASE---LVGAKIKLDFPSVGATENILTAAVLAKG-TTVLDNAAREPEIVDLCSM 198
E.cloacae VDLHIFGLEKLGAEIKLE--EGYVKASVNG-RLKGAHIVMDKVSVGATVTIMSAATLAEG-TTIIENAAREPEIVDTANF 197
E.faecium1 IDLHLKGFQALGAKIIQK--NGYIEAIAD--ELIGDTIYLDFPSVGATQNIMMAAVKAKG-TTVIENVAREPEIVDLANF 200
E.faecium2 IDLHIKGFESLGADVSNE--HGVIYLRTEEESLTGDRIFMDVVSIGATINVMLAAVKAKG-KTIIENAAKEPEIIDVATL 199
E.coli VDLHISGLEQLGATIKLE--EGYVKASVDG-RLKGAHIVMDKVSVGATVTIMCAATLAEG-TTIIENAAREPEIVDTANF 197
F.tularensis FDIHLNGLEALGAEVKLADDHIEVIYKEEK----NAEFKMPFPSVGATMNLLMYAVTGNS-EIVLENVALEPEVVTLIDY 213
G.violaceus VDLHVRGLQALGAQVRIEHGIVEARAR----KLRGGRIYLDYPSVGATETIMMAATLAEG-ETVIENAAQEPEVVDLANF 216
G.oxydans VDMHLKGLETLGAEIRLE--NGYINATAPDG-LKGDRIILPFASVGATENLLMAATLAKG-RTHIVNAAREPEISDLVHC 198
H.influenzae VDLHISGLEKLGADIVLE--EGYVKAQVSD-RLVGTRIVIEKVSVGATLSIMMAATLAKG-TTVIENAAREPEIVDTADF 199
H.pylori VDLHLKAMQQLGAKITIE--QGYIHAKAPK-GLKGNDILFDKISVTGTENALMAASLAKG-ITRIINAAKEPEIAQLCAF 199
K.pneumoniae VDLHISGLEQLGAEIKLE--EGYVKASVSG-RLKGAHIVMDKVSVGATVTIMSAATLAEG-TTIIENAAREPEIVDTANF 197
L.plantarum1 IDLHLKGLNALGAEIERH--DGYVEATAN--QLHGAAIYLDFPSVGATQNIMMAATLADG-ITTMENVAREPEIVDLANY 200
L.plantarum2 IDQHIKGFKALGANVVEE--NDSVFISTGTEGLHGARIFLDVVSVGATININILAAVKAHG-TTTIENAAKEPEIIDLATF 199
L.pneumophila1 VDLHLKALRAMGADITVK--NGYINARCKKGRLQGKRLMFDTVTVTGTENVLMAAVLAEG-ITTIKNAAREPEVVDLANF 200
L.pneumophila2 IDLHISALNALGVDIVELP-DCLVCSRRYA-RLQGNTINFSIKTVTGTENAMMAAVLAEG-TTIINNAAMEPEIVDLANF 219
L.monocytogenes1 VDLHLKGFEAMGAIVKIE--NGYIEATAE--KLVGAKVYLDFPSVGATQNIMMAATLAEG-TTVIENVAREPEIVDLANF 198
L.monocytogenes2 IDQHIKGFEALGAKVTNE--QGAIYLRADE--LKGARIYLDVVSVGATININMLAAVRAKG-KTVIENAAKEPEIIDVATL 198
M.luteus IDYHLAVLRNFGAVVDKRPGG-ISISAPKG--LHGAKLELPYPSVGATEQVLLTAVKAEG-ITELKGAAVEPEIHDLIAV 203
M.marinum LDMHQAGLRQLGAQCNIEHGC-VVAQADT---LRGAEIQLEFPSVGATENILMAAVVAEG-VTTIHNAAREPDVVDLCTM 198
M.tuberculosis LDMHQAGLRQLGAHCNIEHGC-VVARAET---LRGAEIQLEFPSVGATENILMAAVVAEG-VTTIHNAAREPDVVDLCTM 198
N.gonorrhoeae VNQHLKGLEAMGAEIAIE--HGYVKA---KGKLKGARVAMDVVTVGGTENLLMAATLAEG-TTVLENCAIEPEVVDLAEC 197
P.yeei VDLHLKALEAMGAELDLR--EGYVHAKAPAGGLKGALIDFPIVSVGATENALMAATLARG-TTVINNAAREPEIVDLAQC 201
P.chromatophora VAEHIRGLKALNAKVEIQHGLVSAITTGHEHRLKGAHIQLRCPSVGATETLLMAGVLAEG-ETIITNAAQEPEVVDLIGL 215
P.zucineum VDLHLQALEALGARIDLH--EGYVYAQAP-RGLRGAEIEFPFVSVGATEHTLLAAVLAKG-DTEIRNAACEPEIEDLADC 204
P.gingivalis LDTHLVGIQALGATCDYHSDMQAYELTASR--LSGTYMLLDEASVTGTANILMAAVLADG-ITTIYNAACEPYLQQLCKM 204
P.chlorophenolicus IDYHLDVLRQFGAVVEKRPGG-IHISAPKG--LHGAKISLPYPSVGATEQVLLSATRAEG-ITELTGAATEPEVIDLIAV 203
P.aeruginosa VDLHIRGLEAMGAQIEVE--GGYIKAKAPAGGLRGGHFFFDTVSVTGTENLMMAAALANG-RTVLQNAAREPEVVDLANC 200
P.putida VDLHIRGLEAMGAKIEVE--GGYIKAKAPEGGLRGAHFFFDTVSVTGTENIMMAAALAKG-RSVLQNAAREPEVVDLANF 200
R.capsulatus MDIHIDALTALGAEIELK--EGYLHAQAR-GGLKGAVHEMRFASVGATENFLMAAVLAKG-TSVLKNAAREPEIVDLARC 200
R.palustris VDLLIMALEKLGAEITID--GGYVIAKAPGG-LKGATIAFPKVTVSGTHVAVMAAALAKG-TTIIDNAACEPEIVDVADC 208
R.rickettsii VDLHIAVLKAMGAEIEIE--DGYINASSK-GRLKGTHFVFDKVSVGATINAILVAVLAEG-ETVLFNCGREPEIVDLCNC 201
R.typhi VDLHIAVLKSMGAEIEIE--DGYINASSK-GRLKGTHFVFDKVSVGATINAILAAVLANG-ETVLFNCGREPEIVDLCYC 201
R.pomeroyi MDLHIEALEALGAEIELR--DGYLHAKAP-GGLKGAVHEMRFASVGATENMVMAATLAKG-TTVLKNAAREPEIVDLVRC 200
S.enterica VDLHITGLEQLGATIKLE--EGYVKASVEG-RLKGAHIVMDKVSVGATVTIMCAATLAEG-TTIIENAAREPEIVDTANF 197
S.dysenteriae VDLHISGLEQLGATIKLE--EGYVKASVDG-RLKGAHIVMDKVSVGATVTIMCSATLAEG-TTIIENAAREPEIVDTANF 197
S.meliloti VDLFIEGLAALGANIEID--GGYVNATAPAGGLIGARYVFPKVSVGATHVLMMAATLANG-TTVLGNAAREPEVVDLAKC 209
S.paucimobilis1 IDLHLKALEAFGAVIEIS--AGYVRASAPDGGLPGGIYTFPVVSVGATENALMAAVLAKG-TCILENAAREPEIVDLCNL 206
S.paucimobilis2 YDLHEMVLTRLGARVWAEGNQ-LRAEAPSG--LVGNDIVLPLRSTGATENALIAGSLAKG-RTTVWNPHIRPEILDLVVF 221
S.aureus1 IEQHIKGFEALGAEIHLE--NGNIYANAKD-GLKGTSIHLDFPSVGATQNIIMAASLAKG-KTLIENAAKEPEIVDLANY 201
S.aureus2 IDQHIKGFKALGAEIDESS-TTSMKIEAKE--LKGAHIFLDMVSVGATININMLAAVYATG-QTVIENAAKEPEVVDVANF 200
S.maltophilia VDQHIKGLQALGAEIVVE--NGFIKASAKR--LKGGHFTFDMVSVTGTENVLMGAVLAEG-TTVLDNCAMEPEVTDLAHC 203
S.pneumoniae1 IDLHLKGLEAMGVKISQT--AGYIEAKAE--RLHGAHIYMDFPSVGATQNLMMAATLADG-VTVIENAAREPEIVDLAIL 201
S.pneumoniae2 IDLHLKAFEAMGATASYE--GDNMKLSAKDTGLHGASIYMDTVSVGATINTMIAAVKANG-RTIIENAAREPEIIDVATL 199
Synechococcus VVEHIRGLKALGAVVNVEHGIVTASVPGSKKRLTGAQIVLDCPSVGATETILMAAVLADG-VSTIENAAQEPEVQDLANL 213
T.maritima VDFHLEGLKKMGFSIKVE--HGFVEACFER-RIDYVTITLPFPSVGATEHLMTTAALLKGARVVIENAAMEPEIVDLQNF 199
T.thermophilus VDQHIKALEALGAEVWEE--DGTFHARRTR-PLSG-RVVFDLPTVGGTEQAMLAVALGGE-ATLVQ-AAVEPEVVDLGHF 199
T.denticola LDTHFLALTELGARVETDQN---FSFIAHK--LMGEDIFLDEASVTATENAIMAASLAEG-TTIISNAASEPHVQELCKM 197
V.cholerae VDLHIHGLEQLGATITLE--DGYVKAHVDG-RLQGAHIVMDKVSVGATITIMCAATLAEG-TTVLDNAAREPEIVDTAMF 198
V.pipientis VDMHIKALEEMGAKIEID---GYNIIATVKGKLQGKEITFEKISVGATENVIMAATFAEG-VTTINNAATEPEVLDLIDF 206
X.autotrophicus VDFHLDALRALGAEIEID--AGYVVAKAPQG-LKGARIVFPKVSVGATHTALMAATLARG-DSIIENAAREPEVVDLADC 208

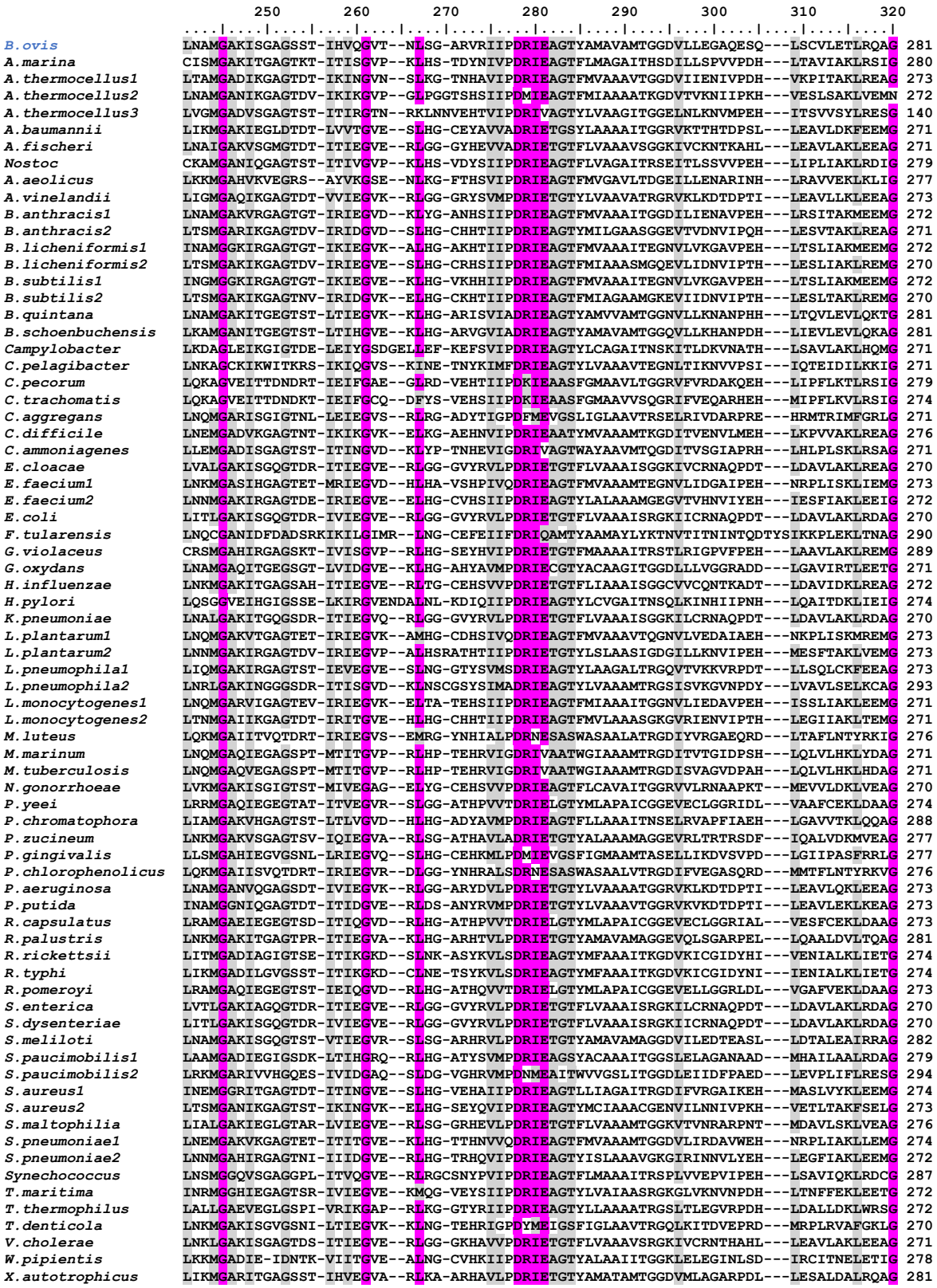
250 260 270 280 290 300 310 320
B.ovis LNAMGAKISGAGSST-IHVQGVT--NLSG-ARVRIIPDRIEAGTYAMAVAMTGGDVLLEGAQESQ---LSCVLETLRQAG 281
A.marina CISMGAKITGAGTKT-ITISGVP--KLHS-TDYNIVPDRIEAGTFLMAGAITHSDILLSPVVPDH---LTAVIAKLRSIG 280
A.thermocellus1 LTAMGADIKGAGTDT-IKINGVN--SLKG-TNHAVIPDRIEAGTFMVAAAVTGGDVIIENIVPDH---VKPITAKLREAG 273
A.thermocellus2 LNAMGANIKGAGTDV-IKIKGVP--GLPGGTSHSIIPDMIEAGTFMIAAAATKGDVTVKNIIPKH---VESLSAKLVEMN 272
A.thermocellus3 LVGMGADVSGAGTST-ITIRGTN--RKLNNVEHTVIPDRIVAGTYLVAAGITGGELNLKNVMPEH---ITSVVSYLRESG 140
A.baumannii LIKMGAKIEGLDTDT-LVVTGVE--SLHG-CEYAVVADRIETGSYLAAAAITGGRVKTTHTDPSL---LEAVLDKFEEMG 271
A.fischeri LNAIGAKVSGMGTDT-ITIEGVE--RLGG-GYHEVVADRIETGTYLCAAAVSGGKIVCKNTKAHL---LEAVLAKLEEAG 271
Nostoc CKAMGANIQGAGTST-ITIVGVP--KLHS-VDYSIIPDRIEAGTFLVAGAITRSEITLSSVVPEH---LIPLIAKLRDIG 279
A.aeolicus LKKMGAHVKVEGRS--AYVKGSE--NLKG-FTHSVIPDRIEAGTFMVGAVLTDGEILLENARINH---LRAVVEKLKLIG 277
A.vinelandii LIGMGAQIKGAGTDT-VVIEGVK--RLGG-GRYSVMPDRIETGTYLVAAVATRGRVKLKDTDPTI---LEAVLLKLEEAG 273
B.anthracis1 LNAMGAKVRGAGTGT-IRIEGVD--KLYG-ANHSIIPDRIEAGTFMVAAAVSGGNIVCKGAVPEH---LRSITAKMEEMG 272
B.anthracis2 LTSMGARIKGAGTDV-IRIDGVD--SLHG-CHHTIIPDRIEAGTYMILGAASGGEVTVDNVIPQH---LESVTAKLREAG 271
B.licheniformis1 INAMGGKIRGAGTGT-IKIEGVK--ALHG-AKHTIIPDRIEAGTFMVAAAITEGNVLVKGAVPEH---LTSLIAKMEEMG 272
B.licheniformis2 LTSMGAKIKGAGTDV-IRIEGVE--SLHG-CRHSIIPDRIEAGTFMIAAASMGQEVLIDNVIPTH---LESLIAKLREMG 270
B.subtilis1 INGMGGKIRGAGTGT-IKIEGVE--KLHG-VKHHIIPDRIEAGTFMVAAAITEGNVLVKGAVPEH---LTSLIAKMEEMG 272
B.subtilis2 LTSMGAKIKGAGTNV-IRIDGVK--ELHG-CKHTIIPDRIEAGTFMIAGAAMGKEVIIDNVIPTH---LESLTAKLREMG 270
B.quintana LNAMGAKITGEGTST-LTIEGVK--KLHG-ARISVIADRIEAGTYAMVVAMTGGNVLLKNANPHH---LTQVLEVLQKTG 281
B.schoenbuchensis LKAMGANITGEGTST-LTIHGVE--KLHG-ARVGVIADRIEAGTYAMAVAMTGGQVLLKHANPDH---LIEVLEVLQKAG 281
Campylobacter LKDAGLEIKGIGTDE-LEIYGSDGELLEF-KEFSVIPDRIEAGTYLCAGAITNSKITLDKVNATH---LSAVLAKLHQMG 271
C.pelagibacter LNKAGCKIKWITKRS-IKIQGVS--KINE-TNYKIMFDRIEAGTYLVAAAVTEGNLTIKNVVPSI---IQTEIDILKKIG 271
C.pecorum LQKAGVEITTDNDRT-IEIFGAE--GLRD-VEHTIIPDKIEAASFGMAAVLTGGRVFVRDAKQEH---LIPFLKTLRSIG 279
C.trachomatis LQKAGVEITTDNDKT-IEIFGCQ--DFYS-VEHSIIPDKIEAASFGMAAVVSQGRIFVEQARHEH---MIPFLKVLRSIG 274
C.aggregans LNQMGARISGIGTNL-LEIEGVS--RLRG-ADYTIGPDFMEVGSLIGLAAVTRSELRIVDARPRE---HRMTRIMFGRLG 271
C.difficile LNEMGADVKGAGTNT-IKIKGVK--ELKG-AEHNVIPDRIEAATYMVAAAMTKGDITVENVLMEH---LKPVVAKLREAG 276
C.ammoniagenes LLEMGADISGAGTST-ITINGVD--KLYP-TNHEVIGDRIVAGTWAYAAVMTQGDITVSGIAPRH---LHLPLSKLRSAG 271
E.cloacae LVALGAKISGQGTDR-ITIEGVE--RLGG-GVYRVLPDRIETGTFLVAAAISGGKIVCRNAQPDT---LDAVLAKLREAG 270
E.faecium1 LNKMGASIHGAGTET-MRIEGVD--HLHA-VSHPIVQDRIEAGTFMVAAAMTEGNVLIDGAIPEH---NRPLISKLIEMG 273
E.faecium2 LNNMGAKIRGAGTDE-IRIEGVE--ELHG-CVHSIIPDRIEAGTYLALAAAAMGEGVTVHNVIYEH---IESFIAKLEEIG 272
E.coli LITLGAKISGQGTDR-IVIEGVE--RLGG-GVYRVLPDRIETGTFLVAAAISRGKIICRNAQPDT---LDAVLAKLRDAG 270
F.tularensis LNQCGANIDFDADSRKIKILGIMR--LNG-CEFEIIFDRIQAMTYAAMAYLYKTNVTITNINTQDTYSIKKPLEKLTNAG 290
G.violaceus CRSMGAHIRGAGSKT-IVISGVP--RLHG-SEYHVIPDRIETGTFMAAAAITRSTLRIGPVFPEH---LAAVLAKLREMG 289
G.oxydans LNAMGAQITGEGSGT-LVIDGVE--KLHG-AHYAVMPDRIECGTYACAAGITGGDLLLVGGRADD---LGAVIRTLEETG 271
H.influenzae LNKMGAKITGAGSAH-ITIEGVE--RLTG-CEHSVVPDRIETGTFLIAAAISGGCVVCQNTKADT---LDAVIDKLREAG 272
H.pylori LQSGGVEIHGIGSSE-LKIRGVENDALNL-KDIQIIPDRIEAGTYLCVGAITNSQLKINHIIPNH---LQAITDKLIEIG 274
K.pneumoniae LNALGAKITGQGSDR-ITIEGVQ--RLGG-GVYRVLPDRIETGTFLVAAAISGGKILCRNAQPDT---LDAVLAKLRDAG 270
L.plantarum1 LNQMGAKVTGAGTET-IRIEGVK--AMHG-CDHSIVQDRIEAGTFMVAAAVTQGNVLVEDAIAEH---NKPLISKMREMG 273
L.plantarum2 LNNMGAKIRGAGTDV-IRIEGVP--ALHSRATHTIIPDRIETGTYLSLAASIGDGILLKNVIPEH---MESFTAKLVEMG 273
L.pneumophila1 LIQMGAKIRGAGTST-IEVEGVE--SLNG-GTYSVMSDRIEAGTYLAAGALTRGQVTVKKVRPDT---LLSQLCKFEEAG 273
L.pneumophila2 LNRLGAKINGGGSDR-ITISGVD--KLNSCGSYSIMADRIEAGTYLVAAAMTRGSISVKGVNPDY---LVAVLSELKCAG 293
L.monocytogenes1 LNQMGARVIGAGTEV-IRIEGVK--ELTA-TEHSIIPDRIEAGTFMIAAAITGGNVLIEDAVPEH---ISSLIAKLEEMG 271
L.monocytogenes2 LTNMGAIIKGAGTDT-IRITGVE--HLHG-CHHTIIPDRIEAGTFMVLAAASGKGVRIENVIPTH---LEGIIAKLTEMG 271
M.luteus LQKMGAIITVQTDRT-IRIEGVS--EMRG-YNHIALPDRNESASWASAALATRGDIYVRGAEQRD---LTAFLNTYRKIG 276
M.marinum LNQMGAQIEGAGSPT-MTITGVP--RLHP-TEHRVIGDRIVAATWGIAAAMTRGDITVTGIDPSH---LQLVLHKLYDAG 271
M.tuberculosis LNQMGAQVEGAGSPT-MTITGVP--RLHP-TEHRVIGDRIVAATWGIAAAMTRGDISVAGVDPAH---LQLVLHKLHDAG 271
N.gonorrhoeae LVKMGAKISGIGTST-MIVEGAG--ELYG-CEHSVVPDRIEAGTFLCAVAITGGRVVLRNAAPKT---MEVVLDKLVEAG 270
P.yeei LRRMGAQIEGEGTAT-ITVEGVR--SLGG-ATHPVVTDRIELGTYMLAPAICGGEVECLGGRIDL---VAAFCEKLDAAG 274
P.chromatophora LIAMGAKVHGAGTST-LTLVGVD--HLHG-ADYAVMPDRIEAGTFLLAAAITNSELRVAPFIAEH---LGAVVTKLQQAG 288
P.zucineum LNKMGAKVSGAGTSV-IQIEGVA--RLSG-ATHAVLADRIETGTYALAAAMAGGEVRLTRTRSDF---IQALVDKMVEAG 277
P.gingivalis LLSMGAHIEGVGSNL-LRIEGVQ--SLHG-CEHKMLPDMIEVGSFIGMAAMTASELLIKDVSVPD---LGIIPASFRRLG 277
P.chlorophenolicus LQKMGAIISVQTDRT-IRIEGVR--DLGG-YNHRALSDRNESASWASAALVTRGDIFVEGASQRD---MMTFLNTYRKVG 276
P.aeruginosa LNAMGANVQGAGSDT-IVIEGVK--RLGG-ARYDVLPDRIETGTYLVAAAATGGRVKLKDTDPTI---LEAVLQKLEEAG 273
P.putida INAMGGNIQGAGTDT-ITIDGVE--RLDS-ANYRVMPDRIETGTYLVAAAVTGGRVKVKDTDPTI---LEAVLEKLKEAG 273
R.capsulatus LRAMGAEIEGEGTSD-ITIQGVD--RLHG-ATHPVVTDRIELGTYMLAPAICGGEVECLGGRIAL---VESFCEKLDAAG 273
R.palustris LNKMGAKITGAGTPR-ITIEGVA--KLHG-ARHTVLPDRIETGTYAMAVAMAGGEVQLSGARPEL---LQAALDVLTQAG 281
R.rickettsii LITMGADIAGIGTSE-ITIKGKD--SLNK-ASYKVLSDRIEAGTYMFAAAITKGDVKICGIDYHI---VENIALKLIETG 274
R.typhi LIKMGADILGVGSST-ITIKGKD--CLNE-TSYKVLSDRIEAGTYMFAAAITKGDVKICGIDYNI---IENIALKLIETG 274
R.pomeroyi LRAMGAQIEGEGTST-IEIQGVD--RLHG-ATHQVVTDRIELGTYMLAPAICGGEVELLGGRLDL---VGAFVEKLDAAG 273
S.enterica LVTLGAKIAGQGTDR-ITIEGVE--RLGG-GVYRVLPDRIETGTFLVAAAISRGKILCRNAQPDT---LDAVLAKLRDAG 270
S.dysenteriae LITLGAKISGQGTDR-IVIEGVE--RLGG-GVYRVLPDRIETGTFLVAAAISRGKIICRNAQPDT---LDAVLAKLRDAG 270
S.meliloti LNAMGAKISGQGTST-VTIEGVR--SLSG-ARHRVLPDRIETGTYAMAVAMAGGDVILEDTEASL---LDTALEAIRRAG 282
S.paucimobilis1 LAAMGADIEGIGSDK-LTIHGRQ--RLHG-ATYSVMPDRIEAGSYACAAAITGGSLELAGANAAD---MHAILAALRDAG 279
S.paucimobilis2 LRKMGARIVVHGQES-IVIDGAQ--SLDG-VGHRVMPDNMEAITWVVGSLITGGDLEIIDFPAED---LEVPLIFLRESG 294
S.aureus1 INEMGGRITGAGTDT-ITINGVE--SLHG-VEHAIIPDRIEAGTLLIAGAITRGDIFVRGAIKEH---MASLVYKLEEMG 274
S.aureus2 LTSMGANIKGAGTST-IKINGVK--ELHG-SEYQVIPDRIEAGTYMCIAAACGENVILNNIVPKH---VETLTAKFSELG 273
S.maltophilia LIALGAKIEGLGTAR-LVIEGVE--RLSG-GRHEVLPDRIETGTFLVAAAMTGGKVTVNRARPNT---MDAVLSKLVEAG 276
S.pneumoniae1 LNEMGAKVKGAGTET-ITITGVE--KLHG-TTHNVVQDRIEAGTFMVAAAMTGGDVLIRDAVWEH---NRPLIAKLLEMG 274
S.pneumoniae2 LNNMGAHIRGAGTNI-IIIDGVE--RLHG-TRHQVIPDRIEAGTYISLAAAVGKGIRINNVLYEH---LEGFIAKLEEMG 272
Synechococcus LNSMGGQVSGAGGPL-ITVQGVE--RLRGCSNYPVIPDRIEAGTFLMAAAITRSPLVVEPVIPEH---LSAVIQKLRDCG 287
T.maritima INRMGGHIEGAGTSR-IVIEGVE--KMQG-VEYSIIPDRIEAGTYLVAIAASRGKGLVKNVNPDH---LTNFFEKLEETG 272
T.thermophilus LALLGAEVEGLGSPI-VRIKGAP--RLKG-GTYRIIPDRIEAGTYLLAAAATRGSLTLEGVRPDH---LDALLDKLWRSG 272
T.denticola LNKMGAKISGVGSNI-LTIEGVK--KLNG-TEHRIGPDYMEIGSFIGLAAVTRGQLKITDVEPRD---MRPLRVAFGKLG 270
V.cholerae LNKLGAKISGAGTDS-ITIEGVE--RLGG-GKHAVVPDRIETGTFLVAAAVSRGKIVCRNTHAHL---LEAVLAKLEEAG 271
W.pipientis LKKMGADIE-IDNTK-VIITGVE--ALNG-CVHKIIPDRIEAGTYALAAAIITGGKLELEGINLSD---IRCITNELETIG 278
X.autotrophicus LIKMGARITGAGSST-IHVEGVA--RLKA-ARHAVLPDRIETGTYAMATAMTGGDVMLAGARPDL---LESALDALRQAG 281

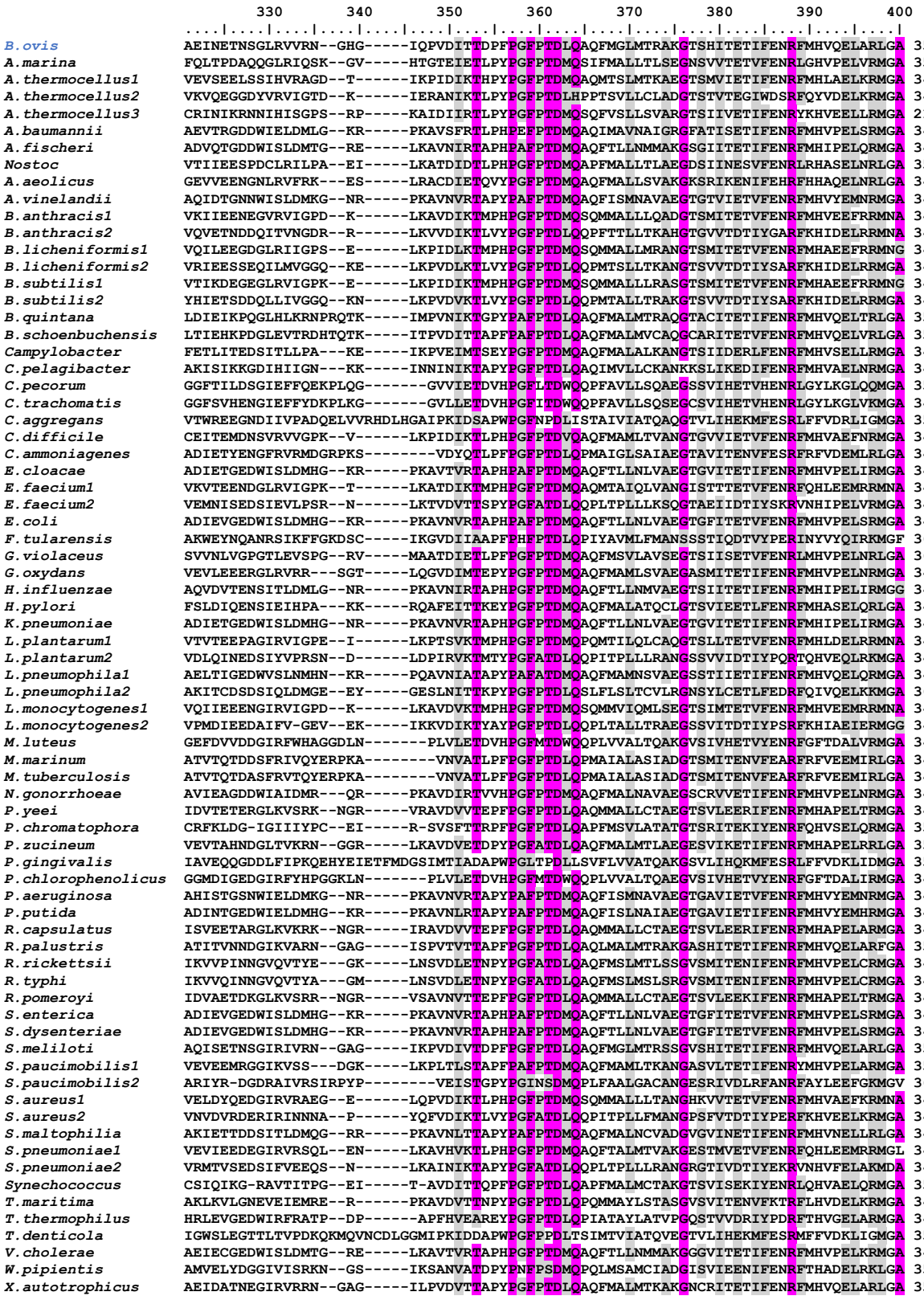
330 340 350 360 370 380 390 400
B.ovis AEINETNSGLRVVRN--GHG-----IQPVDITTDPFPGFPTDLQAQFMGLMTRAKGTSHITETIFENRFMHVQELARLGA 354
A.marina FQLTPDAQQGLRIQSK--GV-----HTGTEIETLPYPGFPTDMQSIFMALLTLSEGNSVVTETVFENRLGHVPELVRMGA 353
A.thermocellus1 VEVSEELSSIHVRAGD--T------IKPIDIKTHPYPGFPTDMQAQMTSLMTKAEGTSMVIETIFENRFMHLAELKRMGA 345
A.thermocellus2 VKVQEGGDYVRVIGTD--K------IERANIKTLPYPGFPTDLHPPTSVLLCLADGTSTVTEGIWDSRFQYVDELKRMGA 344
A.thermocellus3 CRINIKRNNIHISGPS--RP-----KAIDIIRTLPYPGFPTDMQSQFVSLLSVARGTSIIVETIFENRYKHVEELLRMGA 213
A.baumannii AEVTRGDDWIELDMLG--KR-----PKAVSFRTLPHPEFPTDMQAQIMAVNAIGRGFATISETIFENRFMHVPELSRMGA 344
A.fischeri ADVQTGDDWISLDMTG--RE-----LKAVNIRTAPHPAFPTDMQAQFTLLNMMAKGSGIITETIFENRFMHIPELQRMGA 344
Nostoc VTIIEESPDCLRILPA--EI-----LKATDIDTLPHPGFPTDMQAPFMALLTLAEGDSIINESVFENRLRHASELNRLGA 352
A.aeolicus GEVVEENGNLRVFRK---ES-----LRACDIETQVYPGFPTDMQAQFMALLSVAKGKSRIKENIFEHRFHHAQELNRLGA 349
A.vinelandii AQIDTGNNWISLDMKG--NR-----PKAVNVRTAPYPAFPTDMQAQFISMNAVAEGTGTVIETVFENRFMHVYEMNRMGA 346
B.anthracis1 VKIIEENEGVRVIGPD--K------LKAVDIKTMPHPGFPTDMQSQMMALLLQADGTSMITETVFENRFMHVEEFRRMNA 344
B.anthracis2 VQVETNDDQITVNGDR--R------LKVVDIKTLVYPGFPTDLQQPFTTLLTKAHGTGVVTDTIYGARFKHIDELRRMNA 343
B.licheniformis1 VQILEEGDGLRIIGPS--E------LKPIDLKTMPHPGFPTDMQSQMMALLMRANGTSMITETVFENRFMHAEEFRRMNG 344
B.licheniformis2 VRIEESSEQILMVGGQ--KE-----LKPVDLKTLVYPGFPTDLQQPMTSLLTKANGTSVVTDTIYSARFKHIDELRRMGA 343
B.subtilis1 VTIKDEGEGLRVIGPK--E------LKPIDIKTMPHPGFPTDMQSQMMALLLRASGTSMITETVFENRFMHAEEFRRMNG 344
B.subtilis2 YHIETSDDQLLIVGGQ--KN-----LKPVDVKTLVYPGFPTDLQQPMTALLTRAKGTSVVTDTIYSARFKHIDELRRMGA 343
B.quintana LDIEIKPQGLHLKRNPRQTK-----IMPVNIKTGPYPAFPTDLQAQFMALMTRAQGTACITETIFENRFMHVQELTRLGA 356
B.schoenbuchensis LTIEHKPDGLEVTRDHTQTK-----ITPVDITTAPFPAFPTDLQAQFMALMVCAQGCARITETVFENRFMHVQELVRLGA 356
Campylobacter FETLITEDSITLLPA---KE-----IKPVEIMTSEYPGFPTDMQAQFMALALKANGTSIIDERLFENRFMHVSELLRMGA 343
C.pelagibacter AKISIKKGDIHIIGN---KK-----INNINIKTAPYPGFPTDLQAQIMVLLCKANKKSLIKEDIFENRFMHVAELNRMGA 343
C.pecorum GGFTILDSGIEFFQEKPLQG-------GVVIETDVHPGFLTDWQQPFAVLLSQAEGSSVIHETVHENRLGYLKGLQQMGA 352
C.trachomatis GGFSVHENGIEFFYDKPLKG-------GVLLETDVHPGFITDWQQPFAVLLSQSEGCSVIHETVHENRLGYLKGLVKMGA 347
C.aggregans VTWREEGNDIIVPADQELVVRHDLHGAIPKIDSAPWPGFNPDLISTAIVIATQAQGTVLIHEKMFESRLFFVDRLIGMGA 351
C.difficile CEITEMDNSVRVVGPK--V------LKPIDIKTLPHPGFPTDVQAQFMAMLTVANGTGVVIETVFENRFMHVAEFNRMGA 348
C.ammoniagenes ADIETYENGFRVRMDGRPKS--------VDYQTLPFPGFPTDLQPMAIGLSAIAEGTAVITENVFESRFRFVDEMLRLGA 343
E.cloacae ADIETGEDWISLDMHG--KR-----PKAVTVRTAPHPAFPTDMQAQFTLLNLVAEGTGVITETIFENRFMHVPELIRMGA 343
E.faecium1 VKVTEENDGLRVIGPK--T------LKATDIKTMPHPGFPTDMQAQMTAIQLVANGISTTTETVFENRFQHLEEMRRMNA 345
E.faecium2 VEMNISEDSIEVLPSR--N------LKTVDVTTSPYPGFATDLQQPLTPLLLKSQGTAEIIDTIYSKRVNHIPELVRMGA 344
E.coli ADIEVGEDWISLDMHG--KR-----PKAVNVRTAPHPAFPTDMQAQFTLLNLVAEGTGFITETVFENRFMHVPELSRMGA 343
F.tularensis AKWEYNQANRSIKFFGKDSC-----IKGVDIIAAPFPHFPTDLQPIYAVMLFMANSSSTIQDTVYPERINYVYQIRKMGF 365
G.violaceus SVVNLVGPGTLEVSPG--RV-----MAATDIETLPFPGFPTDMQAQFMSVLAVSEGTSIISETVFENRLMHVPELNRLGA 362
G.oxydans VEVLEEERGLRVRR---SGT-----LQGVDIMTEPYPGFPTDMQAQFMAMLSVAEGASMITETIFENRFMHVPELNRMGA 343
H.influenzae AQVDVTENSITLDMLG--NR-----PKAVNIRTAPHPGFPTDMQAQFTLLNMVAEGTSIITETIFENRFMHIPELIRMGG 345
H.pylori FSLDIQENSIEIHPA---KK-----RQAFEITTKEYPGFPTDMQAQFMALATQCLGTSVIEETLFENRFMHASELQRLGA 346
K.pneumoniae ADIETGEDWISLDMHG--NR-----PKAVNVRTAPHPGFPTDMQAQFTLLNLVAEGTGVITETIFENRFMHIPELIRMGA 343
L.plantarum1 VTVTEEPAGIRVIGPE--I------LKPTSVKTMPHPGFPTDMQPQMTILQLCAQGTSLLTETVFENRFMHLDELRRMNA 345
L.plantarum2 VDLQINEDSIYVPRSN--D------LDPIRVKTMTYPGFATDLQQPITPLLLRANGSSVVIDTIYPQRTQHVEQLRKMGA 345
L.pneumophila1 AELTIGEDWVSLNMHN--KR-----PQAVNIATAPYPAFATDMQAQFMAMNSVAEGSSTIIETIFENRFMHVQELQRMGA 346
L.pneumophila2 AKITCDSDSIQLDMGE--EY-----GESLNITTKPYPGFPTDLQSLFLSLTCVLRGNSYLCETLFEDRFQIVQELKKMGA 366
L.monocytogenes1 VQIIEEENGIRVIGPD--K------LKAVDVKTMPHPGFPTDMQSQMMVIQMLSEGTSIMTETVFENRFMHVEEMRRMNA 343
L.monocytogenes2 VPMDIEEDAIFV-GEV--EK-----IKKVDIKTYAYPGFPTDLQQPLTALLTRAEGSSVITDTIYPSRFKHIAEIERMGG 343
M.luteus GEFDVVDDGIRFWHAGGDLN-------PLVLETDVHPGFMTDWQQPLVVALTQAKGVSIVHETVYENRFGFTDALVRMGA 349
M.marinum ATVTQTDDSFRIVQYERPKA--------VNVATLPFPGFPTDLQPMAIALASIADGTSMITENVFEARFRFVEEMIRLGA 343
M.tuberculosis ATVTQTDASFRVTQYERPKA--------VNVATLPFPGFPTDLQPMAIALASIADGTSMITENVFEARFRFVEEMIRLGA 343
N.gonorrhoeae AVIEAGDDWIAIDMR---QR-----PKAVDIRTVVHPGFPTDMQAQFMALNAVAEGSCRVVETIFENRFMHVPELNRMGA 342
P.yeei IDVTETERGLKVSRK--NGR-----VRAVDVVTEPFPGFPTDLQAQMMALLCTAEGTSVLEERIFENRFMHAPELTRMGA 347
P.chromatophora CRFKLDG-IGIIIYPC--EI-----R-SVSFTTRPFPGFPTDLQAPFMSVLATATGTSRITEKIYENRFQHVSELQRMGA 359
P.zucineum VEVTAHNDGLTVKRN--GGR-----LKAVDVETDPYPGFATDLQAQFMALMTLAEGESVIKETIFENRFMHAPELRRLGA 350
P.gingivalis IAVEQQGDDLFIPKQEHYEIETFMDGSIMTIADAPWPGLTPDLLSVFLVVATQAKGSVLIHQKMFESRLFFVDKLIDMGA 357
P.chlorophenolicus GGMDIGEDGIRFYHPGGKLN-------PLVLETDVHPGFMTDWQQPLVVALTQAEGVSIVHETVYENRFGFTDALIRMGA 349
P.aeruginosa AHISTGSNWIELDMKG--NR-----PKAVNVRTAPYPAFPTDMQAQFISMNAVAEGTGAVIETVFENRFMHVYEMNRMGA 346
P.putida ADINTGEDWIELDMHG--KR-----PKAVNLRTAPYPAFPTDMQAQFISLNAIAEGTGAVIETIFENRFMHVYEMHRMGA 346
R.capsulatus ISVEETARGLKVKRK--NGR-----IRAVDVVTEPFPGFPTDLQAQMMALLCTAEGTSVLEERIFENRFMHAPELARMGA 346
R.palustris ATITVNNDGIKVARN--GAG-----ISPVTVTTAPFPGFPTDLQAQLMALMTRAKGASHITETIFENRFMHVQELARFGA 354
R.rickettsii IKVVPINNGVQVTYE---GK-----LNSVDLETNPYPGFATDLQAQFMSLMTLSSGVSMITENIFENRFMHVPELCRMGA 346
R.typhi IKVVQINNGVQVTYA---GM-----LNSVDLETNPYPGFATDLQAQFMSLMSLSRGVSMITENIFENRFMHVPELCRMGA 346
R.pomeroyi IDVAETDKGLKVSRR--NGR-----VSAVNVTTEPFPGFPTDLQAQMMALLCTAEGTSVLEEKIFENRFMHAPELTRMGA 346
S.enterica ADIEVGEDWISLDMHG--KR-----PKAVNVRTAPHPAFPTDMQAQFTLLNLVAEGTGFITETVFENRFMHVPELSRMGA 343
S.dysenteriae ADIEVGEDWISLDMHG--KR-----PKAVNVRTAPHPAFPTDMQAQFTLLNLVAEGTGFITETVFENRFMHVPELSRMGA 343
S.meliloti AQISETNSGIRIVRN--GAG-----IKPVDIVTDPFPGFPTDLQAQFMGLMTRSSGVSHITETIFENRFMHVQELARLGA 355
S.paucimobilis1 VEVEEMRGGIKVSS---DGK-----LKPLTLSTAPFPAFPTDMQAQFMAMLTKANGASVLTETIFENRYMHVPELARMGA 351
S.paucimobilis2 ARIYR-DGDRAIVRSIRPYP--------VEISTGPYPGINSDMQPLFAALGACANGESRIVDLRFANRFAYLEEFGKMGV 365
S.aureus1 VELDYQEDGIRVRAEG--E------LQPVDIKTLPHPGFPTDMQSQMMALLLTANGHKVVTETVFENRFMHVAEFKRMNA 346
S.aureus2 VNVDVRDERIRINNNA--P------YQFVDIKTLVYPGFATDLQQPITPLLFMANGPSFVTDTIYPERFKHVEELKRMGA 345
S.maltophilia AKIETTDDSITLDMQG--RR-----PKAVNLTTAPYPAFPTDMQAQFMALNCVADGVGVINETIFENRFMHVNELLRLGA 349
S.pneumoniae1 VEVIEEDEGIRVRSQL--EN-----LKAVHVKTLPHPGFPTDMQAQFTALMTVAKGESTMVETVFENRFQHLEEMRRMGL 347
S.pneumoniae2 VRMTVSEDSIFVEEQS--N------LKAINIKTAPYPGFATDLQQPLTPLLLRANGRGTIVDTIYEKRVNHVFELAKMDA 344
Synechococcus CSIQIKG-RAVTITPG--EI-----T-AVDITTQPFPGFPTDLQAPFMALMCTAKGTSVISEKIYENRLQHVAELQRMGA 358
T.maritima AKLKVLGNEVEIEMRE--R------PKAVDVTTNPYPGFPTDLQPQMMAYLSTASGVSVITENVFKTRFLHVDELKRMGA 344
T.thermophilus HRLEVGEDWIRFRATP--DP------APFHVEAREYPGFPTDLQPIATAYLATVPGQSTVVDRIYPDRFTHVGELARMGA 344
T.denticola IGWSLEGTTLTVPDKQKMQVNCDLGGMIPKIDDAPWPGFPPDLTSIMTVIATQVEGTVLIHEKMFESRMFFVDKLIGMGA 350
V.cholerae AEIECGEDWISLDMTG--RE-----LKAVTVRTAPHPGFPTDMQAQFTLLNMMAKGGGVITETIFENRFMHVPELKRMGA 344
W.pipientis AMVELYDGGIVISRKN--GS-----IKSANVATDPYPNFPSDMQPQLMSAMCIADGISVIEENIFENRFTHADELRKLGA 351
X.autotrophicus AEIDATNEGIRVRRN--GAG-----ILPVDVTTAPYPGFPTDLQAQFMALMTKAKGNCRITETIFENRFMHVQELARLGA 354

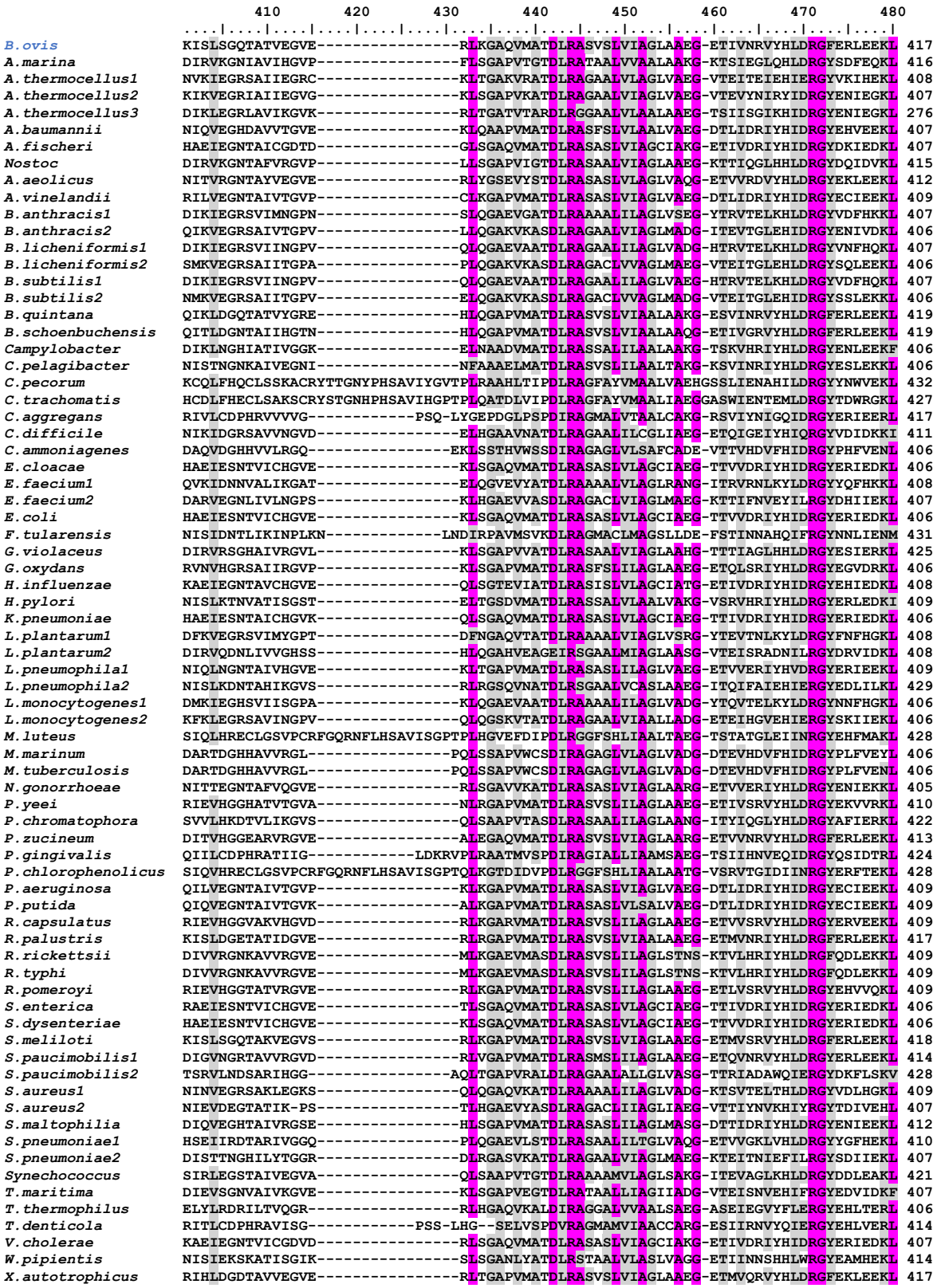
410 420 430 440 450 460 470 480
B.ovis KISLSGQTATVEGVE----------RLKGAQVMATDLRASVSLVIAGLAAEG-ETIVNRVYHLDRGFERLEEKL 417
A.marina DIRVKGNIAVIHGVP----------FLSGAPVTGTDLRATAALVVAALAAKG-KTSIEGLQHLDRGYSDFEQKL 416
A.thermocellus1 NVKIEGRSAIIEGRC----------KLTGAKVRATDLRAGAALVLAGLVAEG-VTEITEIEHIERGYVKIHEKL 408
A.thermocellus2 KIKVEGRIAIIEGVG----------KLSGAPVKATDLRAGAALVIAGLVAEG-VTEVYNIRYIDRGYENIEGKL 407
A.thermocellus3 DIKLEGRLAVIKGVK----------RLTGATVTARDLRGGAALVLAALAAEG-TSIISGIKHIDRGYENIEGKL 276
A.baumannii NIQVEGHDAVVTGVE----------KLQAAPVMATDLRASFSLVLAALVAEG-DTLIDRIYHIDRGYEHVEEKL 407
A.fischeri HAEIEGNTAICGDTD----------GLSGAQVMATDLRASASLVIAGCIAKG-ETIVDRIYHIDRGYDKIEDKL 407
Nostoc DIRVKGNTAFVRGVP----------LLSGAPVIGTDLRASAALVIAGLAAEG-KTTIQGLHHLDRGYDQIDVKL 415
A.aeolicus NITVRGNTAYVEGVE----------RLYGSEVYSTDLRASASLVLAGLVAQG-ETVVRDVYHLDRGYEKLEEKL 412
A.vinelandii RILVEGNTAIVTGVP----------CLKGAPVMATDLRASASLVIAGLVAEG-DTLIDRIYHIDRGYECIEEKL 409
B.anthracis1 DIKIEGRSVIMNGPN----------SLQGAEVGATDLRAGAALILAGLVSEG-YTRVTELKHLDRGYVDFHKKL 407
B.anthracis2 QIKVEGRSAIVTGPV----------LLQGAKVKASDLRAGAALVIAGLMADG-ITEVTGLEHIDRGYENIVDKL 406
B.licheniformis1 DIKIEGRSVIINGPV----------QLQGAEVAATDLRAGAALILAGLVADG-HTRVTELKHLDRGYVNFHQKL 407
B.licheniformis2 SMKVEGRSAIITGPA----------PLQGAKVKASDLRAGACLVVAGLMAEG-VTEITGLEHLDRGYSQLEEKL 406
B.subtilis1 DIKIEGRSVIINGPV----------QLQGAEVAATDLRAGAALILAGLVAEG-HTRVTELKHLDRGYVDFHQKL 407
B.subtilis2 NMKVEGRSAIITGPV----------ELQGAKVKASDLRAGACLVVAGLMADG-VTEITGLEHIDRGYSSLEKKL 406
B.quintana QIKLDGQTATVYGRE----------HLQGAPVMATDLRASVSLVIAALAAKG-ESVINRVYHLDRGFERLEEKL 419
B.schoenbuchensis QITLDGNTAIIHGTN----------HLQGAPVMATDLRASVSLVIAALAAQG-ETIVGRVYHLDRGFERLEEKL 419
Campylobacter DIKLNGHIATIVGGK----------ELNAADVMATDLRASSALILAALAAKG-TSKVHRIYHLDRGYENLEEKF 406
C.pelagibacter NISTNGNKAIVEGNI----------NFAAAELMATDLRASVSLILAALTAKG-KSVINRIYHLDRGYESLEKKL 406
C.pecorum KCQLFHQCLSSKACRYTTGNYPHSAVIYGVTPLRAAHLTIPDLRAGFAYVMAALVAEHGSSLIENAHILDRGYYNWVEKL 432
C.trachomatis HCDLFHECLSAKSCRYSTGNHPHSAVIHGPTPLQATDLVIPDLRAGFAYVMAALIAEGGASWIENTEMLDRGYTDWRGKL 427
C.aggregans RIVLCDPHRVVVVG----------PSQ-LYGEPDGLPSPDIRAGMALVTAALCAKG-RSVIYNIGQIDRGYERIEERL 417
C.difficile NIKIDGRSAVVNGVD----------ELHGAAVNATDLRAGAALILCGLIAEG-ETQIGEIYHIQRGYVDIDKKI 411
C.ammoniagenes DAQVDGHHVVLRGQ----------EKLSSTHVWSSDIRAGAGLVLSAFCADE-VTTVHDVFHIDRGYPHFVENL 406
E.cloacae HAEIESNTVICHGVE----------KLSGAQVMATDLRASASLVLAGCIAEG-TTVVDRIYHIDRGYERIEDKL 406
E.faecium1 QVKIDNNVALIKGAT----------ELQGVEVYATDLRAAAALVLAGLRANG-ITRVRNLKYLDRGYYQFHKKL 408
E.faecium2 DARVEGNLIVLNGPS----------KLHGAEVVASDLRAGACLVIAGLMAEG-KTTIFNVEYILRGYDHIIEKL 407
E.coli HAEIESNTVICHGVE----------KLSGAQVMATDLRASASLVLAGCIAEG-TTVVDRIYHIDRGYERIEDKL 406
F.tularensis NISIDNTLIKINPLKN----------LNDIRPAVMSVKDLRAGMACLMAGSLLDE-FSTINNAHQIFRGYNNLIENM 431
G.violaceus DIRVRSGHAIVRGVL----------KLSGAPVVATDLRASAALVIAGLAAHG-TTTIAGLHHLDRGYESIERKL 425
G.oxydans RVNVHGRSAIIRGVP----------KLSGAPVMATDLRASFSLILAGLAAEG-ETQLSRIYHLDRGYEGVDRKL 406
H.influenzae KAEIEGNTAVCHGVE----------QLSGTEVIATDLRASISLVLAGCIATG-ETIVDRIYHIDRGYEHIEDKL 408
H.pylori NISLKTNVATISGST----------ELTGSDVMATDLRASSALVLAALVAKG-VSRVHRIYHLDRGYERLEDKI 409
K.pneumoniae HAEIESNTAICHGVK----------QLSGAQVMATDLRASASLVLAGCIAEG-TTIVDRIYHIDRGYERIEDKL 406
L.plantarum1 DFKVEGRSVIMYGPT----------DFNGAQVTATDLRAAAALVIAGLVSRG-YTEVTNLKYLDRGYFNFHGKL 408
L.plantarum2 DIRVQDNLIVVGHSS----------HLQGAHVEAGEIRSGAALMIAGLAASG-VTEISRADNILRGYDRVIDKL 408
L.pneumophila1 NIQLNGNTAIVHGVE----------KLTGAPVMATDLRASASLILAGLVAEG-ETVVERIYHVDRGYERIEEKL 409
L.pneumophila2 NISLKDNTAHIKGVS----------RLRGSQVNATDLRSGAALVCASLAAEG-ITQIFAIEHIERGYEDLILKL 429
L.monocytogenes1 DMKIEGHSVIISGPA----------KLQGAEVAATDLRAAAALILAGLVADG-YTQVTELKYLDRGYNNFHGKL 406
L.monocytogenes2 KFKLEGRSAVINGPV----------QLQGSKVTATDLRAGAALVIAALLADG-ETEIHGVEHIERGYSKIIEKL 406
M.luteus SIQLHRECLGSVPCRFGQRNFLHSAVISGPTPLHGVEFDIPDLRGGFSHLIAALTAEG-TSTATGLEIINRGYEHFMAKL 428
M.marinum DARTDGHHAVVRGL----------PQLSSAPVWCSDIRAGAGLVLAGLVADG-DTEVHDVFHIDRGYPLFVEYL 406
M.tuberculosis DARTDGHHAVVRGL----------PQLSSAPVWCSDIRAGAGLVLAGLVADG-DTEVHDVFHIDRGYPLFVENL 406
N.gonorrhoeae NITTEGNTAFVQGVE----------RLSGAVVKATDLRASASLVIAGLAARG-ETVVERIYHLDRGYENIEKKL 405
P.yeei RIEVHGGHATVTGVA----------NLRGAPVMATDLRASVSLILAGLAAEG-ETIVSRVYHLDRGYEKVVRKL 410
P.chromatophora SVVLHKDTVLIKGVS----------QLSAAPVTASDLRASAALILAGLAANG-ITYIQGLYHLDRGYAFIERKL 422
P.zucineum DITVHGGEARVRGVE----------ALEGAQVMATDLRASVSLVIAGLAARG-ETVVNRVYHLDRGFERLEEKL 413
P.gingivalis QIILCDPHRATIIG----------LDKRVPLRAATMVSPDIRAGIALLIAAMSAEG-TSIIHNVEQIDRGYQSIDTRL 424
P.chlorophenolicus SIQVHRECLGSVPCRFGQRNFLHSAVISGPTQLKGTDIDVPDLRGGFSHLIAALAATG-VSRVTGIDIINRGYERFTEKL 428
P.aeruginosa QILVEGNTAIVTGVP----------KLKGAPVMATDLRASASLVIAGLVAEG-DTLIDRIYHIDRGYECIEEKL 409
P.putida QIQVEGNTAIVTGVK----------ALKGAPVMATDLRASASLVLSALVAEG-DTLIDRIYHIDRGYECIEEKL 409
R.capsulatus RIEVHGGVAKVHGVD----------RLKGARVMATDLRASVSLILAGLAAEG-ETVVSRVYHLDRGYERVEEKL 409
R.palustris KISLDGETATIDGVE----------RLRGAPVMATDLRASVSLVIAALAAEG-ETMVNRIYHLDRGFERLEEKL 417
R.rickettsii DIVVRGNKAVVRGVE----------MLKGAEVMASDLRASVSLILAGLSTNS-KTVLHRIYHLDRGFQDLEKKL 409
R.typhi DIVVRGNKAVVRGVE----------MLKGAEVMASDLRASVSLILAGLSTNS-KTVLHRIYHLDRGFQDLEKKL 409
R.pomeroyi RIEVHGGTATVRGVE----------RLKGAPVMATDLRASVSLILAGLAAEG-ETLVSRVYHLDRGYEHVVQKL 409
S.enterica RAEIESNTVICHGVE----------TLSGAQVMATDLRASASLVLAGCIAEG-TTIVDRIYHIDRGYERIEDKL 406
S.dysenteriae HAEIESNTVICHGVE----------KLSGAQVMATDLRASASLVLAGCIAEG-TTVVDRIYHIDRGYERIEDKL 406
S.meliloti KISLSGQTAKVEGVS----------RLKGAPVMATDLRASVSLVIAGLAAEG-ETMVSRVYHLDRGFERLEEKL 418
S.paucimobilis1 DIGVNGRTAVVRGVD----------RLVGAPVMATDLRASMSLILAGLAAEG-ETQVNRVYHLDRGYERLEEKL 414
S.paucimobilis2 TSRVLNDSARIHGG----------AQLTGAPVRALDLRAGAALALLGLVASG-TTRIADAWQIERGYDKFLSKV 428
S.aureus1 NINVEGRSAKLEGKS----------QLQGAQVKATDLRAAAALILAGLVADG-KTSVTELTHLDRGYVDLHGKL 409
S.aureus2 NIEVDEGTATIK-PS----------TLHGAEVYASDLRAGACLIIAGLIAEG-VTTIYNVKHIYRGYTDIVEHL 407
S.maltophilia DIQVEGHTAIVRGSE----------HLSGAPVMATDLRASASLILAGLMASG-DTTIDRIYHLDRGYENIEEKL 412
S.pneumoniae1 HSEIIRDTARIVGGQ----------PLQGAEVLSTDLRASAALILTGLVAQG-ETVVGKLVHLDRGYYGFHEKL 410
S.pneumoniae2 DISTTNGHILYTGGR----------DLRGASVKATDLRAGAALVIAGLMAEG-KTEITNIEFILRGYSDIIEKL 407
Synechococcus SIRLEGSTAIVEGVA----------QLSAAPVTGTDLRAAAAMVLAGLSAKG-ITEVAGLKHLDRGYDDLEAKL 421
T.maritima DIEVSGNVAIVKGVE----------KLSGAPVEGTDLRATAALLIAGIIADG-VTEISNVEHIFRGYEDVIDKF 407
T.thermophilus ELYLRDRILTVQGR----------RLHGAQVKALDIRAGGALVVAALSAEG-ASEIEGVYFLERGYEHLTERL 406
T.denticola RITLCDPHRAVISG----------PSS-LHG--SELVSPDVRAGMAMVIAACCARG-ESIIRNVYQIERGYEHLVERL 414
V.cholerae KAEIEGNTVICGDVD----------RLSGAQVMATDLRASASLVIAGCIAKG-ETIVDRIYHIDRGYERIEDKL 407
W.pipientis NISIEKSKATISGIK----------SLSGANLYATDLRSTAALVLASLVAGG-ETIINNSHHLWRGYEAMHEKL 414
X.autotrophicus RIHLDGDTAVVEGVE----------RLTGAPVMATDLRASVSLVIAGLAAEG-ETMVQRVYHLDRGFEKLEEKL 417

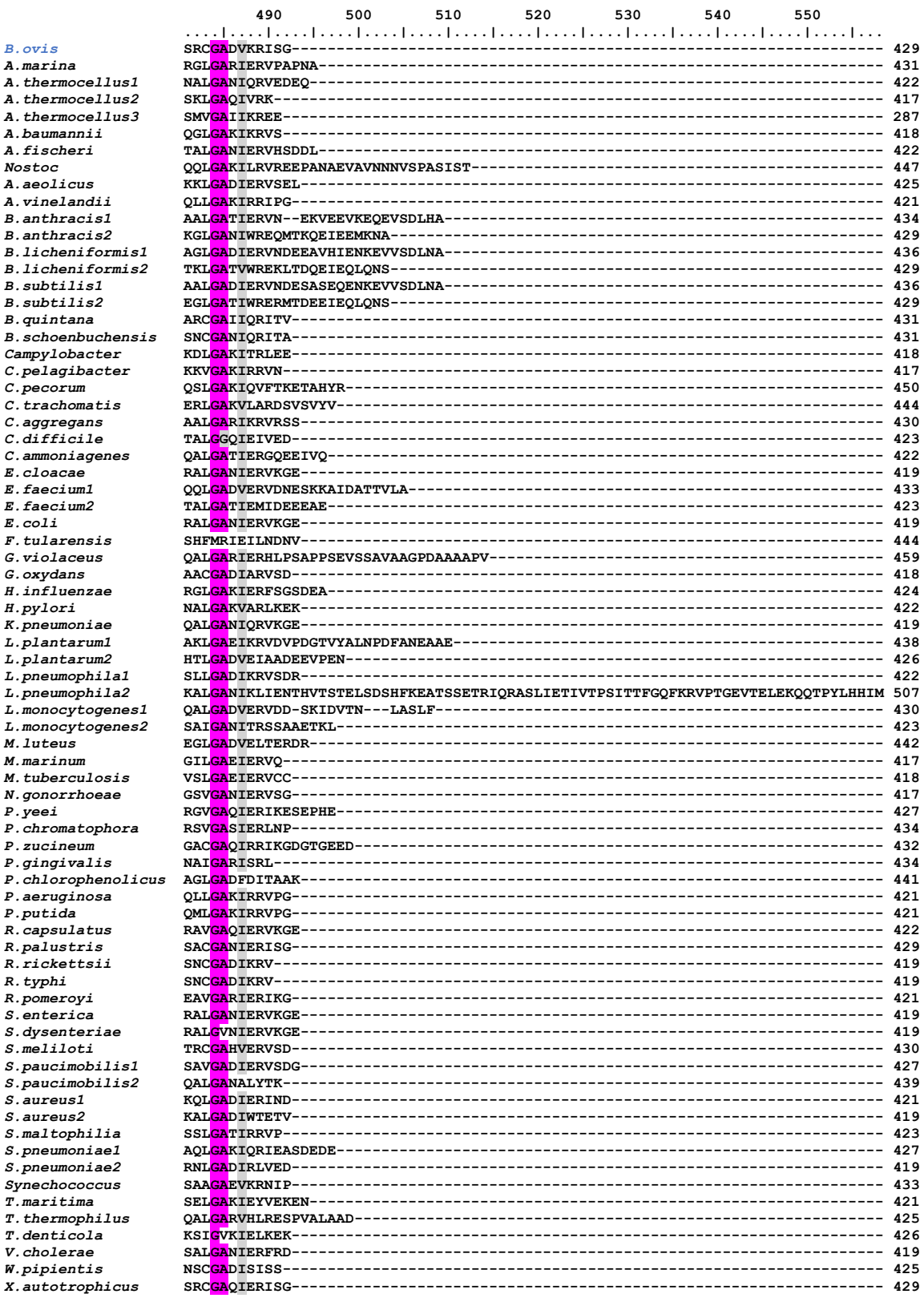

Figure 5.10. Conservation of MurA sequences within selected bacteria. MSA (n=74) of MurAs from species in Table 5.4. The alignment was constructed with Clustal Omega. Residues similar or identical in at least 90% of the sequences are highlighted in grey and purple, respectively. An asterisk marks the catalytic residue Cys/Asp.

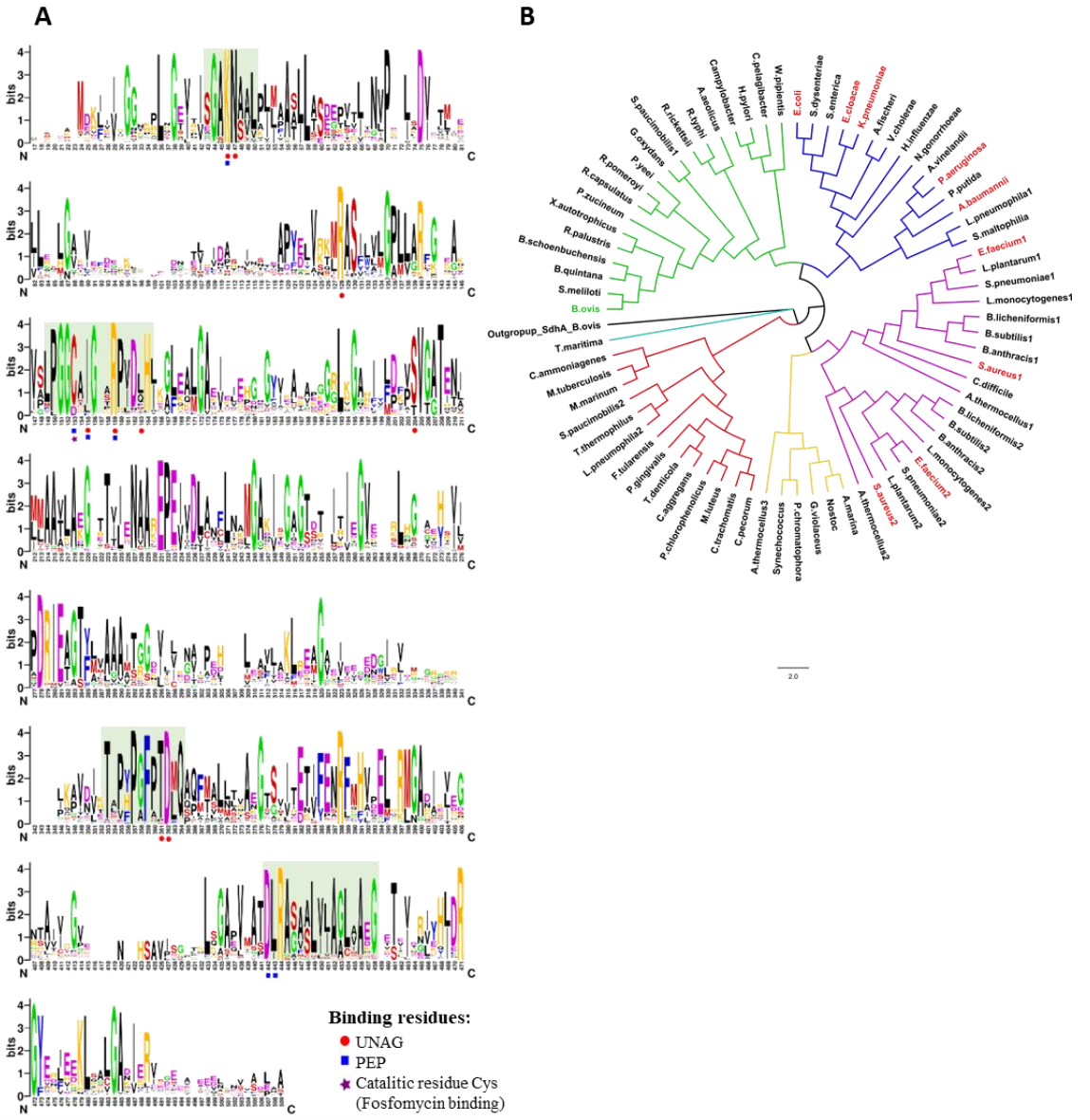

Figure 5.11. Residue conservation and phylogeny of MurA within the selected bacteria. (A) Sequence Logo representing MSA of MurA sequences from selected bacteria (n=74) from Figure 5.10. Green boxes highlight conserved motifs respectively involved in substrate binding. Other features and routine for logo generation as in Figure 5.7A. **(B)** Phylogeny of selected bacterial MurAs. The bootstrap consensus tree inferred from 500 replicates is taken to represent the evolutionary history of the taxa analyzed. The evolutionary history was inferred by using the Maximum Likelihood method and JTT matrix-based model with MEGA X. The tree with the highest log likelihood (-42195.71) is shown. The analysis involved 74 MurA sequences (Table 5.4), and the *B. ovis* SdhA was used as outgroup to highlight the evolutionary separation between clusters. ESKAPE pathogens are highlighted in bold red and *B. ovis* is highlighted in green. Branch lengths are proportional to the number of substitutions per site (scale beside). There were a total of 672 positions in the final dataset. The tree groups the sequences in seven main clusters: Clade 1 cyan, Clade 2 (bootstrap > 14) in red, Clade 3 (bootstrap > 67) in yellow, Clade 4 (bootstrap > 74) in purple, Clade 5 (bootstrap > 95) in blue and Clade 6 (bootstrap > 30) in green.

5.3.4 Heterologous production and hydrodynamic properties of BoHTMurA

To facilitate the purification of BoMurA, a 70 bp extension was added to the 5' end of the gene sequence, which included a 6-His tagged tail and a PreScission protease cleavage site with a NdeI restriction site (Figure 3.1A). The resulting BoHTMurA protein contains a 6-His tagged tail in the N-terminus, is composed of 455 amino acids and 6,837 atoms, and has a theoretical Mw and pI of 48,459.47 Da and 6.63, respectively. The theoretical extinction coefficient calculated at 280 nm is the same as that of the native form. In addition, the value was compared with that obtained through analysis of the ProtParam tool software, which calculated a value of 15.9 mM^{-1} cm^{-1}. The instability index (II) was computed as 23.42, indicating that the protein may be moderately unstable under certain conditions. The aliphatic index and GRAVY score were 97.36 and -0.012, respectively, suggesting that the protein may be slightly hydrophilic. Protein expression occurred within 16 h after induction with 1 mM IPTG at 20 ºC, resulting in approximately 4.5 g/L *E. coli* cells. A single-step purification of BoHTMurA was achieved by passing the crude extract through a Ni^{2+} affinity column (Figure 5.12A). The first peak of the chromatogram corresponded to contaminating proteins, while the protein eluted from the affinity column when the imidazole gradient was increased. No absorption peak was observed in fractions (22-32) where BoHTMurA was detected on 12% SDS-PAGE gels (Figure 5.12B) because it has only one tryptophan in its sequence and is not exposed to the solvent (Figure 5.12C). This observation agrees with the low molar extinction coefficient predicted for BoHTMurA at 280 nm. It was also observed that the protein yield was relatively low, 0.16 mg of BoHTMurA per liter of culture medium.

The purified BoHTMurA protein migrated with a Mw of 48.4 kDa on denaturing SDS-PAGE gel (Figure 5.13A, left inset). Upon size-exclusion chromatography (SEC), BoHTMurA eluted as a single broad peak at an elution volume corresponding to a calculated Mw of 46.6 kDa. Finally, BoHTMurA migrated as a single band in the CN-PAGE (Figure 5.13A, right inset). The predicted Mw by SDS-PAGE and SEC was consistent with the theoretical Mw of the protein monomer. In addition, the major SEC and CN-PAGE band indicated that purified BoHTMurA was a monomer.

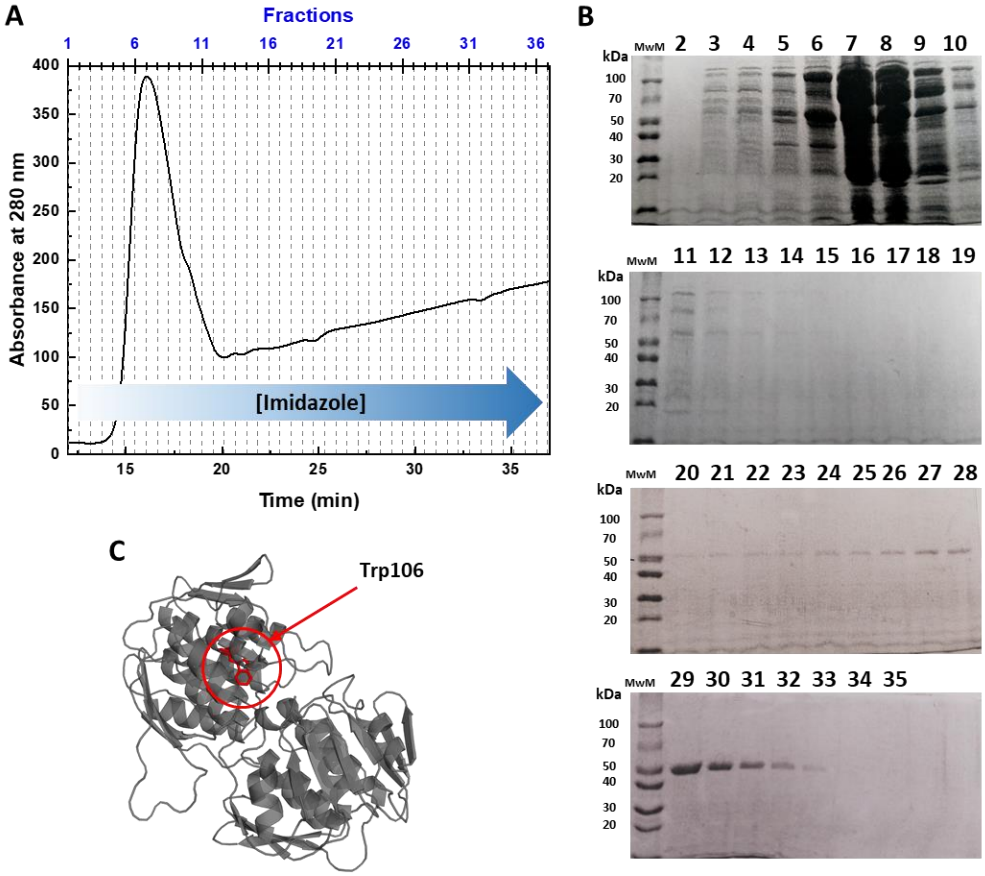

Figure 5.12. BoHTMurA purification using affinity chromatography. (A) Elution profile of the crude extract with the protein loaded onto a Ni affinity column and eluted with a gradient from 10 to 500 mM imidazole. **(B)** Analysis of fractions collected from the column using 12% SDS-PAGE gels. The molecular weight marker (MwM) is represented in lane 1. **(C)** Representation of the BoMurA structural model with the single tryptophan, Trp106, highlighted in red.

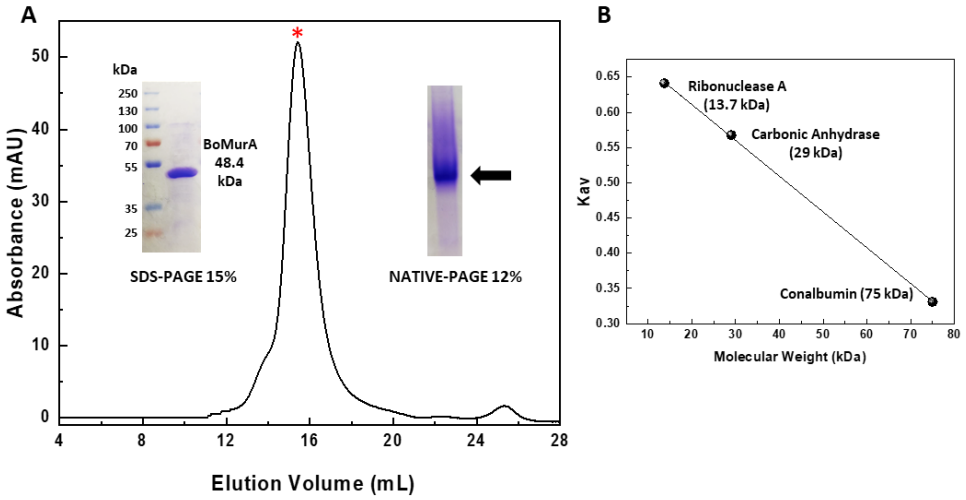

Figure 5.13. Hydrodynamic properties of BoHTMurA. (A) Elution profile of BoHTMurA on a 25 mL Superdex® 200 10/300 GL column at 4 °C. BoHTMurA (black line) eluted at 15.4 ml. The left inset shows a 15% SDS-PAGE of purified BoHTMurA: Left line, MwM PageRuler™ Plus; right line, purified BoHTMurA (48.4 kDa). The right inset shows a 12% CN-PAGE of purified BoHTMurA. **(B)** Calibration Plot of the Superdex® 200 10/300 GL column with Ribonuclease A (13.7 kDa), Carbonic Anhydrase (29 kDa) and Conalbumin (75 kDa).

5.3.5 Spectroscopic properties of BoHTMurA

The absorption spectrum of BoHTMurA purified to homogeneity was characterized by maximum at 278 nm (Figure 5.14A). Following the protocol 3.4.1.1.1, an experimental value of ε_{278}=16.9 ± 0.8 mM^{-1} cm^{-1} was determined in buffer 50 mM Bis-Tris Propane, 100 mM KCl, pH 8.0. As mentioned above, this is a relatively low value for a protein of 455 amino acids, but is consistent with BoHTMurA containing a single Trp residue. The BoHTMurA fluorescence emission spectrum exhibited an emission maximum at 330 nm upon excitation at 280 nm (Figure 5.14B), whereas the corresponding excitation spectrum showed two maxima at 230 and 278 nm. The far-UV CD spectrum of BoHTMurA showed two minima at 209.5 nm and 222 nm (Figure 5.14C), indicative of α-helix folding. The near-UV CD spectrum showed hardly any features, only a small broad band in the range of 285-310 nm (centered around at 292.5 nm). Again, this agrees with the low tryptophan content in the protein. Taken together, these data suggest that the purified BoHTMurA protein was in its folded state.

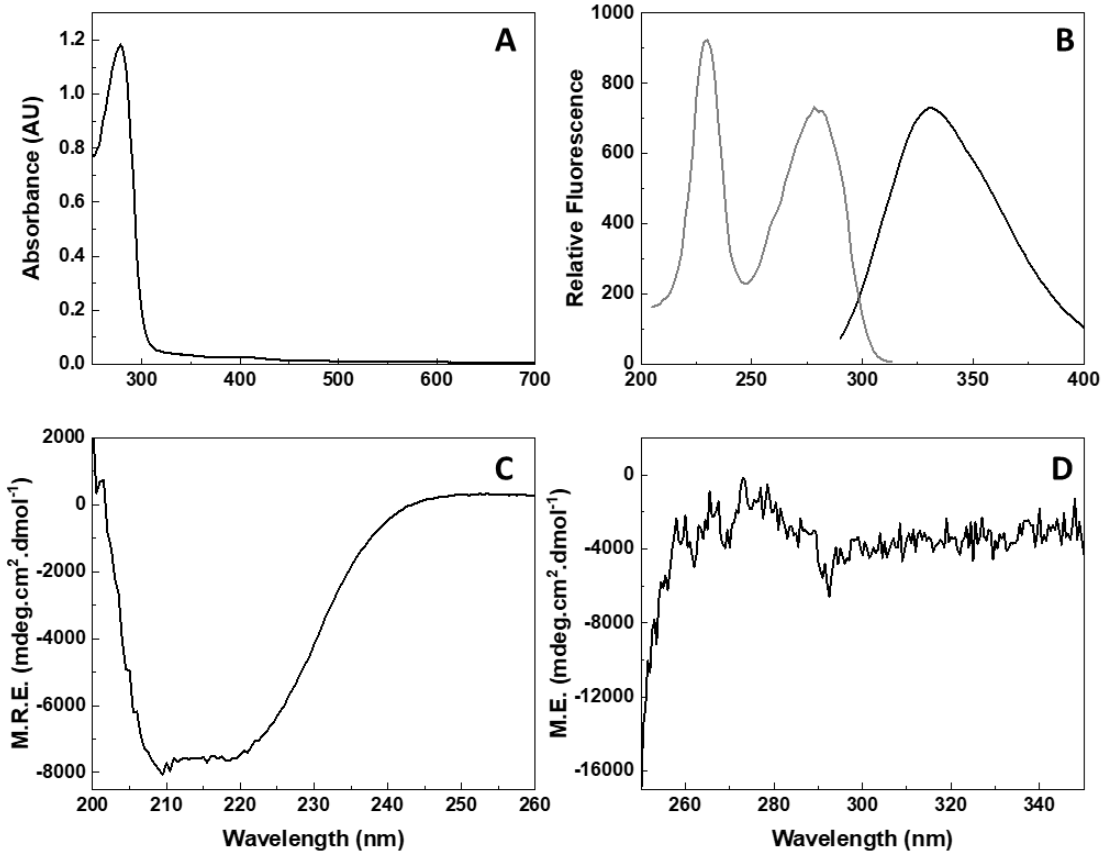

Figure 5.14. Spectroscopic properties of BoHTMurA. (A) UV-Visible absorption spectrum of BoHTMurA (70 µM). **(B)** Emission (black line) and excitation (grey line) fluorescence spectra of BoHTMurA (10 µM), λ_{ex}=280 nm, λ_{em}=330 nm. BoHTMurA CD spectra for the **(C)** far-UV (5 µM), and **(D)** near-UV/Vis (10 µM) regions, collected at 10 ºC. All measurements were performed in 50 mM Bis-Tris Propane, pH 8.0.

5.3.6 Thermal stability of BoHTMurA

The conformational stability of BoHTMurA in the absence and presence of UNAG was evaluated by following thermal protein unfolding. Denaturation curves were recorded through far-UV CD and fluorescence emission in 50 mM Bis-Tris Propane pH 8.0 (Figure 5.15). Throughout the process, BoHTMurA unfolded as the temperature increased. In far-UV CD denaturation curves at 208 nm suggested that BoHTMurA shifted from native to the unfolded state following a one-step transition process (N→U) with a T_m^{208nm} around 313 K, while curves at 222 nm best fit to a two-step model (N→I→U) with T_{m1}^{222nm} and T_{m2}^{222nm} being 316 K and 323 K, respectively. The presence of UNAG slightly increased T_m^{208nm} up to 315, as well as T_{m2}^{222nm} up to 328 K.

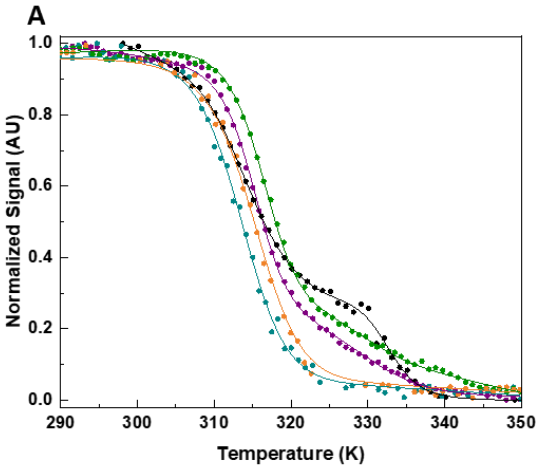

B

	BoHTMurA	BoHTMurA: UNAG		BoHTMurA	BoHTMurA: UNAG
T_{m1}^{208nm} (K)	313 ± 1	315 ± 1	ΔH_1^{208nm} (kcal/mol)	65 ± 1	63 ± 1
T_{m1}^{222nm} (K)	316 ± 1	316 ± 1	ΔH_1^{222nm} (kcal/mol)	93 ± 4	81 ± 8
T_{m2}^{222nm} (K)	323 ± 2	328 ± 1	$\Delta H2^{222nm}$ (kcal/mol)	21± 8	63 ± 1
T_{m1}FL (K)	317 ± 1	nd	ΔH_1 FL (kcal/mol)	44 ± 1	nd
T_{m2}FL (K)	331 ± 1	nd	ΔH_2 FL (kcal/mol)	118 ± 9	nd

Figure 5.15. Thermal stability of BoHTMurA. (A) Thermal denaturation profiles of BoHTMurA monitored using far-CD at 208 nm (cyan circles) and at 222 nm (purple circles), as well as fluorescence measurements (λ_{ex}=280 nm and λ_{em}=330 nm, black circles). Measurements, are also shown in the presence of UNAG (50 µM) for far-CD at 208 nm (orange circles) and 222 nm (green circles). Curves are shown roughly normalized from 0 to 1, and their individual fits are represented by the continuous lines. Curves recorded in 50 mM Bis-Tris Propane buffer, pH 8.0, from 283.15 to 363.15 K. Protein concentrations were 5 µM for far-CD assays, and 10 µM for fluorescence. UNAG concentrations were in 10-fold excess regarding BoHTMurA. **(B)** Resulting T_ms and ΔH values.

Although BoHTMurA has only a single Trp residue (Trp106) (Figure 5.12C), it is buried within the domain II of the protein and changes in its solvent accessibility are expected upon protein unfolding. Thus, the thermal denaturation curves were also followed by changes in its fluorescence. These curves best fit for a three-state unfolding process (N→I →U), represented by two different T_m values. T_{m1}^{FL} was set at 317 K, being this value relatively close to T_{m1}^{208nm} and T_{m1}^{222nm}. On the contrary, T_{m2}^{FL} at 331 K was considerably higher than those reported by CD denaturation curves. Altogether, these observations suggest that thermal unfolding does not occur cooperatively, with the protein going through at least three intermediate conformational states (N→I_1→I_2^{222nm}→I_3^{FL}→U) before reaching

complete unfolding. The potential stabilization of the protein upon UNAG binding was also evaluated by using the BoHTMurA:UNAG, showing that the presence of the substrate produced only a slight stabilization of the protein secondary structure (ΔT_{ms} in the range of +2 to +5).

5.3.7 Set up of a steady-state assay to measure BoHTMurA Activity

Steady-state kinetic parameters for BoHTMurA were determined by quantifying the Pi produced in the reaction using the malachite green assay. A calibration curve for Pi was constructed using a set of K_2HPO_4 solutions at different concentrations that were combined with the malachite green reagent, and by following the protocol described in section 3.7.1.2. The next equation was obtained for the calibration line (Figure 5.16A):

Eq. 3.22 $$[Pi] = ((Abs\lambda_{620nm}) + 0.2893)/0.0181$$

To identify the optimal conditions for BoHTMurA activity, its ability to produce Pi was evaluated using different buffers (Table 3.4), some of which have been used in the characterization of other MurA enzymes (see Table 5.5 below). In the assay, a mixture of 2.8 mM UNAG and 2.1 µM BoHTMurA was preincubated at 37 ºC for 10 min. The PEP substrate was then added to a final concentration of 2.8 mM in a total volume of 350 µL, and the reaction was allowed to proceed for 40 min. Finally, 700 µL of malachite green reagent were added to stop the reaction. Figure 5.16B summarizes the main results. The highest production of Pi was observed in 50 mM Bis-Tris Propane, pH 7.0, and 50 mM HEPES pH 6.8, both buffers having similar ionic strengths: 9 and 7 mM. A set of experiments was repeated using other buffers within this ionic strength range (Figure 5.16C). Again, 50 mM BIS-Tris Propane at pH 7.0 was the buffer in which BoHTMurA exhibited higher activity. The next step was to determine the potential influence of salts on the enzyme activity in this buffer. The assay was repeated in the presence of different KCl concentrations (Fig 5.16D), showing that KCl has a negative impact in ability of the enzyme to produce Pi. Therefore, 50 mM Bis-Tris Propane at pH 7.0 was selected as the optimal buffer for evaluating BoHTMurA activity.

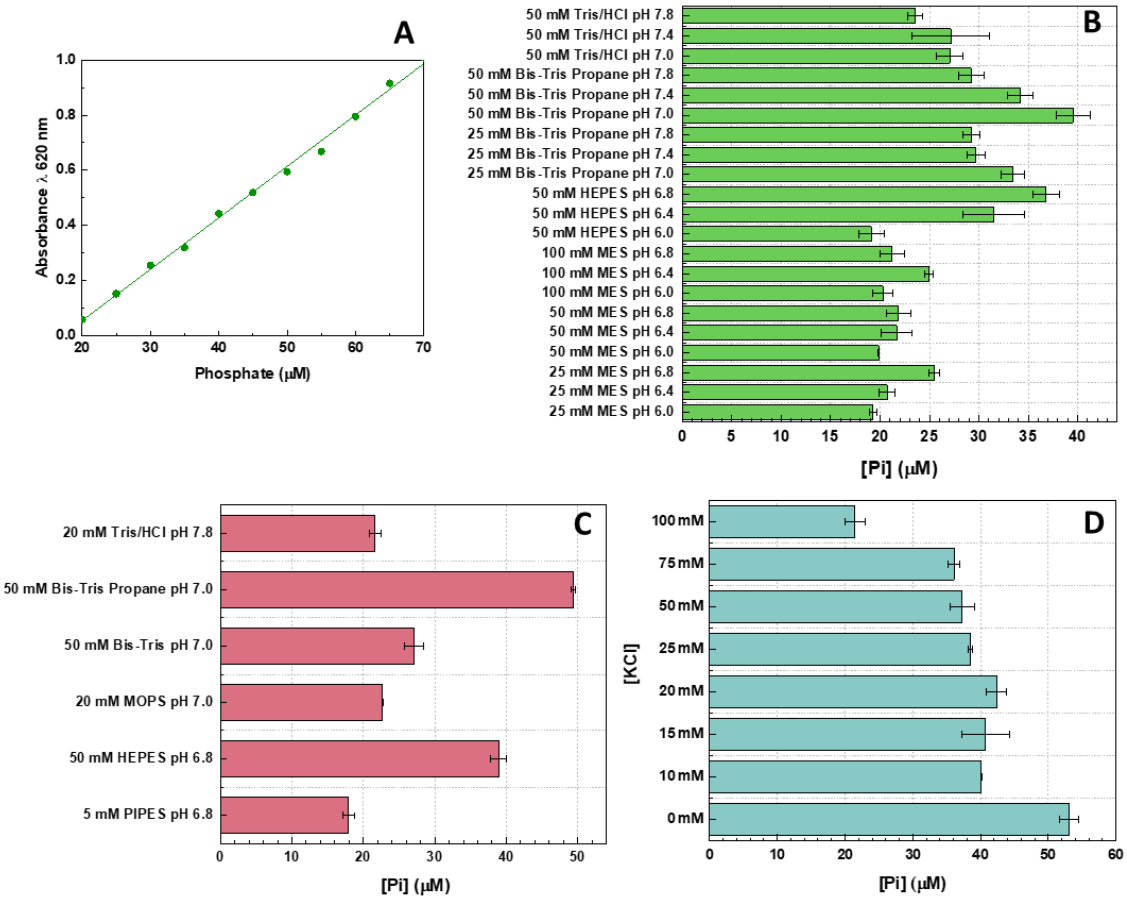

Figure 5.16. Quantification of Pi produced by BoHTMurA under various reaction conditions. (A) Calibration Plot using K_2HPO_4 and malachite green reagent. **(B)** Impact of buffer and pH on the production of Pi. **(C)** Impact of pH in the production of Pi in buffers with similar ionic strength. **(D)** Impact of KCl concentration on the production of Pi in 50 mM Bis-Tris Propane at pH 7.0.

Next, we optimized the amount of protein required to perform the activity assays. Since previous assays were conducted with 2.1 µM of BoHTMurA and the protein amounts used by other authors were generally lower (Table 5.5), varying amounts of enzyme were tested, ranging from 25 to 200 nM, in assay mixtures containing 2 mM of both UNAG and PEP substrates (Eniyan et al., 2016). The results of these assays are shown in Figure 5.17A, where it was found that the minimum quantity of BoHTMurA required for the efficient detection of the production of UNAGEP and Pi was 50 nM. Subsequently, the optimal incubation time for the reaction was determined to be 30 min (Figure 5.17B). Based on these results, we determined that the V_{max} of BoHTMurA is ~1.6 µM min^{-1} under the assayed conditions. Additionally, we calculated an apparent k_{cat} (catalytic constant) value of ~32 min^{-1}, which represents the turnover number of the enzyme. This kinetic characterization has laid the groundwork for ongoing kinetic studies, which are currently being conducted by other members of the team.

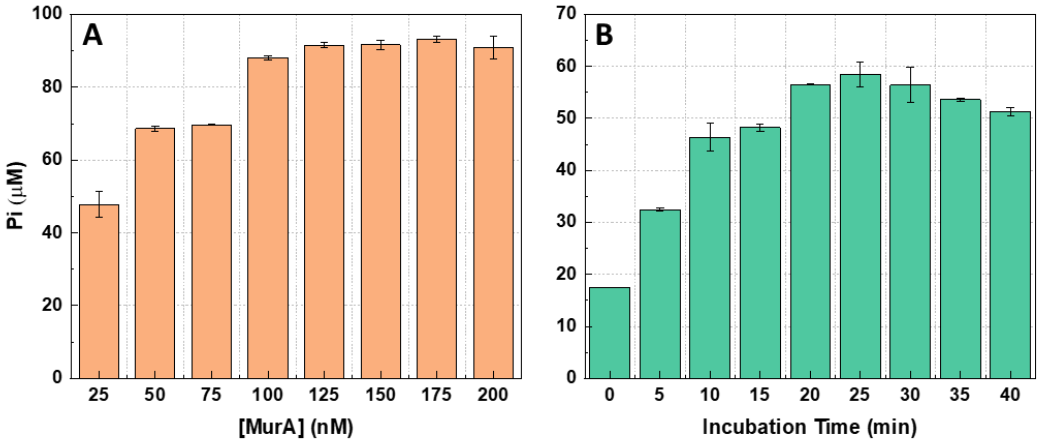

Figure 5.17. Quantification of Pi produced by BoHTMurA under various reaction conditions. Activity assays performed at different **(A)** enzyme concentrations and **(B)** incubation times. All measurements carried out using 2 mM UNAG and 2 mM PEP substrates in 50 mM Bis-Tris Propane at pH 7.0.

5.3.8 Synthesis and purification of UNAGEP

The UNAGEP product of MurA is the substrate of the following enzyme in the PG biosynthetic enzymatic chain, MurB. Since this is a non-commercial substrate we aimed to produce it to evaluate BoHTMurB and BoMurB activities. The protocol described in section 3.7.1.4 was followed to produce large UNAGEP amounts and the produced concentrated UNAGEP was quantified by measuring the absorbance at 262 nm. To confirm the presence and purity of the product in the reaction mixture, samples containing reaction mixtures as well as solutions of UNAG, PEP and the working buffer were subjected to several analyses.

Although different tests were carried out to visualize the formation of the UNAGEP product by HPLC, we did not reach adequate experimental conditions to observe uniform and separated peaks compared with the elution profiles of the PEP and UNAG substrates. In addition, the working buffer (50 mM Bis-Tris Propane pH 7.0) also absorbed at 260 nm, and all signals were obtained near this wavelength. Nonetheless, chromatograms confirmed the production of UNAGEP (Figure 5.18). Nonetheless, separating the UNAGEP product from the UNAG substrate by HPLC resulted quite challenging, requiring further optimizations of the experimental conditions to improve the separation and detection of the product peak.

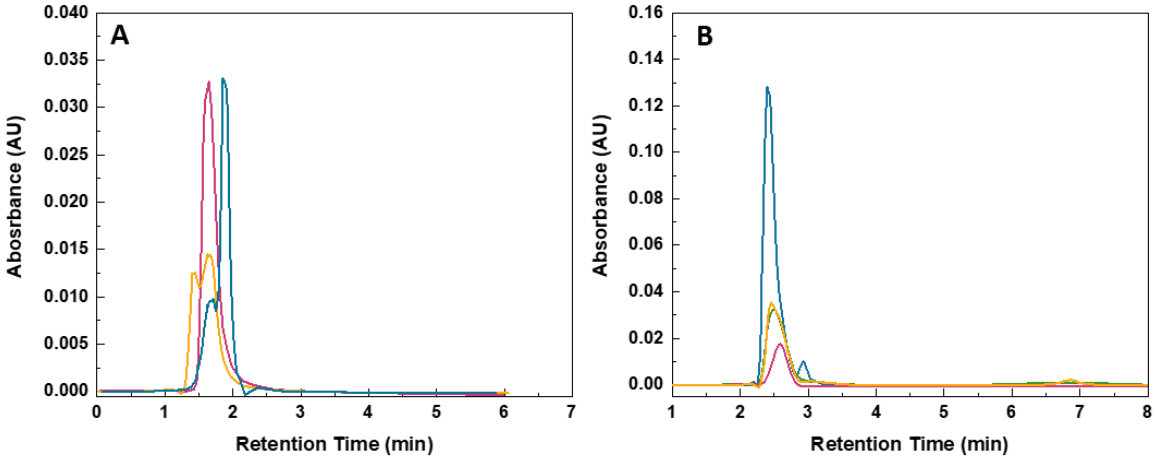

Figure 5.18. Reversed-phase HPLC analysis of various compounds using two different mobile phases: (A) 5 mM ammonium acetate (pH 6.0):methanol in ratio of 6:4, and **(B)** 100 mM ammonium acetate at pH 6.0:methanol in ratio of 3:7. Chromatograms corresponding to samples containing UNAG are in yellow, those for the product of the reaction are in blue (showing UNAGEP as well as UNAG) , Bis-Tris Propane is in pink and PEP is in green.

NMR was also used to identify the UNAGEP reaction product. Four samples were analyzed by ^{13}C-NMR: the UNAG and PEP substrates, the reaction buffer (BIS-Tris Propane) and the reaction mixture potentially containing UNAGEP. All of them were prepared at ~20 mg/mL in deuterated water. The obtained experimental spectra were compared to the simulated ^{13}C-NMR spectra obtained by using the ChemDraw Professional software (Cambridgesoft). UNAG and UNAGEP are registered at the PubChem database, taking from there their respective canonical SMILES to reconstruct the molecules on the ChemDraw software. The simulated spectrum of each molecule can be seen in Figure 5.19. UNAG is a large molecule with a Mw of 607.4 g/mol and 17 carbon atoms. With the addition of the enol-pyruvate group (3 carbons) from PEP to the molecule to form the UNAGEP, the Mw increased to 677.4 g/mol. The UNAG ^{13}C-NMR spectral profile shows 17 signals, one for each of the carbons (Figure 5.18A). The signals marked in green correspond to the uracil (δ = 102.4, 141.2, 150.8 and 163.5 ppm), being an aromatic ring, whose signals are expected to appear at a lower field when compared to the other C atoms. The acetyl group in orange is the most unshielded ^{13}C signal, having the highest chemical shift (δ = 174.6 ppm). Figure 5.19B shows a similar spectral profile, but with the addition of the signals that come from the enol-pyruvate moiety in purple, corresponding to δ = 103.4, 147.0 and 164.5 ppm. Upon addition of the enol-pyruvate group, the carbon atoms marked in pink within the glucosamine portion undergo changes in their signals. These changes are the result of modifications in the chemical environment surrounding the carbon nuclei. The introduction of three additional carbons to UNAG leads to alterations in the molecular structure. These

modifications can arise from variations in nearby functional groups, the presence of new chemical bonds, or adjustments in the hybridization of carbon atoms. Now, for the ribose group (unmarked colors), no relevant shifts were observed in its peaks.

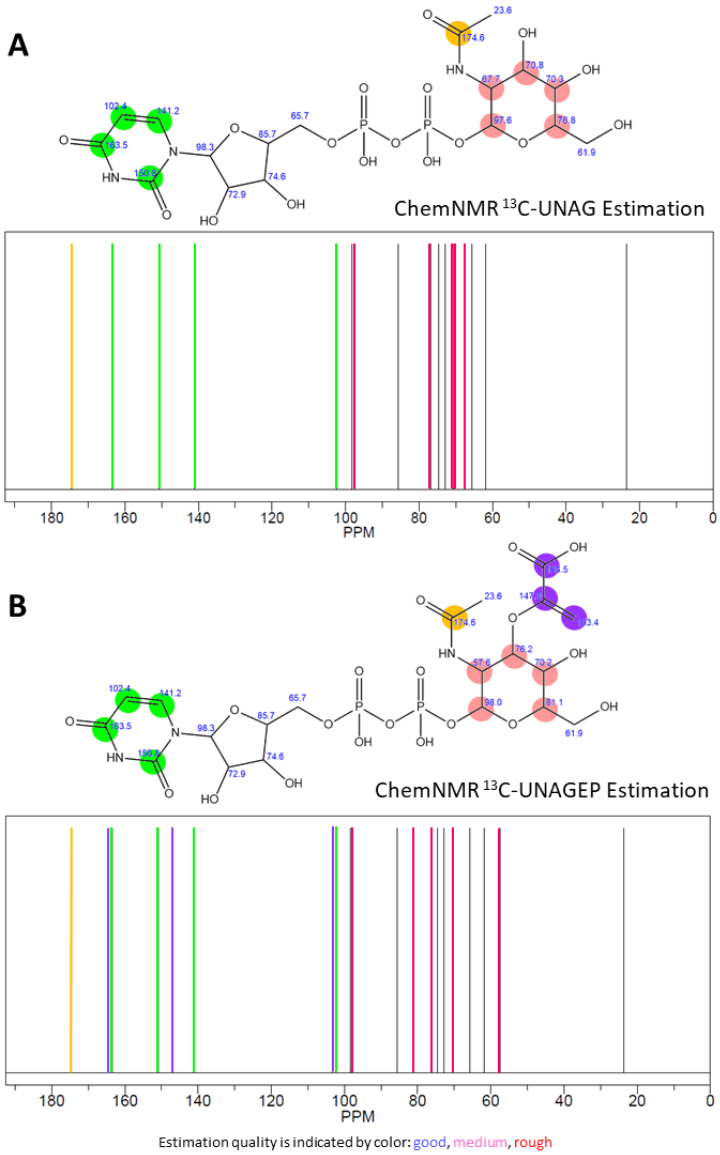

Figure 5.19. Simulated ^{13}C-NMR spectra. (A) UNAG and **(B)** UNAGEP. In upper panels are shown the molecules with predicted δ values (ppm) for each carbon (ChemDraw Professional, the good quality of the estimation is supported by the blue color of predicted δ values). In the molecular structure, the carbon atoms are highlighted in green spheres for the uracil group, in pink spheres for the glucosamine portion, in orange for the carbonyl group of the N-acetyl, and in purple for the enol-pyruvate group. The lower panels depict the simulation of the corresponding ^{13}C-NMR spectra, with each carbon signal indicated in the respective colors shown in the molecular structure.

The obtained experimental spectra are superimposed in Figure 5.20. The UNAG spectrum, represented in black, served as the control, while the spectrum of the reaction mixture is shown in red. In this mixture, UNAGEP, as well as potentially traces of substrates and Bis-Tris Propane buffer are expected to be present. The UNAG spectrum exhibits 17

peaks, corresponding to its 17 carbon atoms that form the molecule, whereas the spectrum of the mixture shows 21 peaks. Both spectra show 13 overlapping signals, while 7 signals are unique to each spectrum. The 3 carbons coming from the enol-pyruvate moiety correspond to the peaks marked with asterisks at δ = 171.6, 149.65, and 100.8 ppm. The black arrow signals represent the carbons from the glucosamine portion, which are located at δ = 69.64, 69.5, and 53.6 ppm in the UNAG control spectrum. However, in the UNAGEP spectrum, these signals shifted, being observed at δ = 62.6, 61.5, and 58.17 ppm, as indicated by the blue arrows. An additional peak at δ = 38.13 ppm, indicated by a green arrow, could potentially belong to traces of Bis-Tris Propane in the sample. Therefore, ^{13}C-NMR spectra confirm transformation of UNAG into UNAGEP, but also indicate that the product of the reaction is a mixture of both compounds.

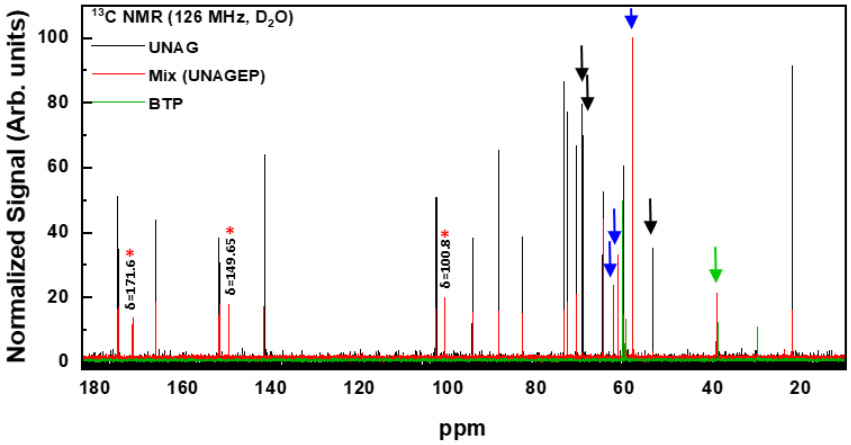

Figure 5.20. Superposition of ^{13}C-NMR spectra of substrates and reaction mixes. The figure shows the overlap of three spectra: UNAG (black), the reaction mixture (red), and BIS-Tris Propane (BTP) buffer (green). Overlapping signals correspond to the same carbons in the molecules, while non-overlapping signals indicate carbons from the PEP substrate (marked with a red asterisk) and displaced carbons. UNAG shows displaced signals marked with black arrows, UNAGEP with blue arrows, and a potential signal from BTP is indicated by a green arrow.

5.3.9 Crystallization of BoHTMurA

More than 700 crystallization conditions were explored to produce BoHTMurA crystals (3.9.2), but only a single one yielded crystals and diffraction patterns (Figure 5.21). These crystals appeared in a sitting drop with the condition H7 of the JBScreen Basic HTS, that contained a mixture of 0.5 µL of BoHTMurA and UNAG at final concentrations of 9.4 mg/ml and 1 mM, respectively, and 0.5 µl of 1 M sodium acetate, 50 mM cadmium sulfate and 100 mM HEPES (pH 7.5). The crystals were sent to the ALBA synchrotron for data collection on the BL13-Xaloc beamline. The best data were collected at 3 Å of resolution using a detector distance of 576.79 mm and 0.1° oscillation angle for a total of 900 images. The predicted space group was $P6_122$ and the data did not appear to be twinned. However,

despite the 49% sequence identity with the *E. coli* homologous enzyme, molecular replacement using this enzyme as a template (PDB 1UAE) yielded unsuccessful results.

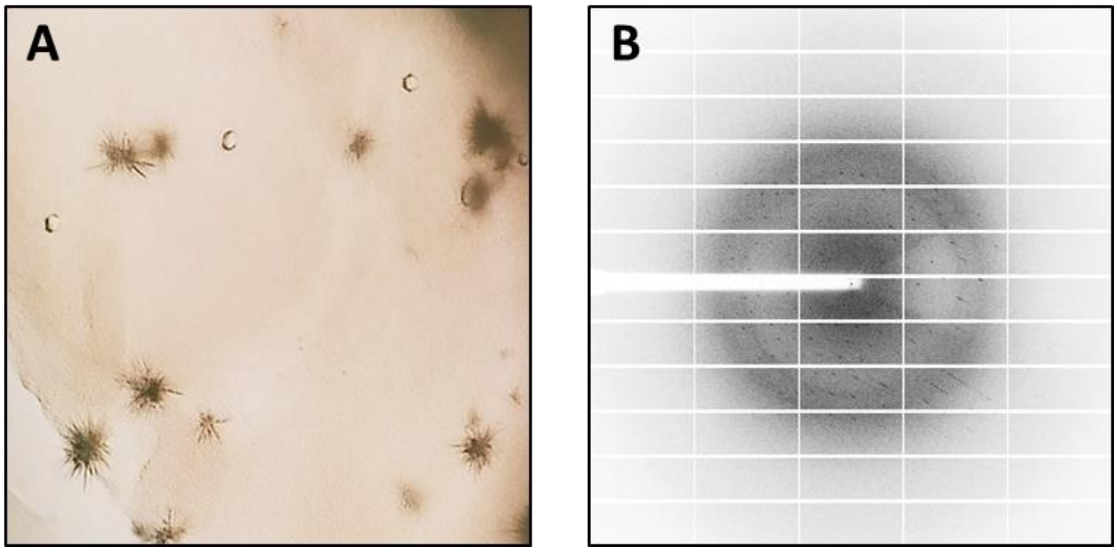

Figure 5.21. BoHTMurA crystals. (A) Small oval-shaped protein crystals were grown in the presence of UNAG in sitting drops in 96-well plates. Specifically, a solution of 60 µL of mother liquor, composed of 1 M sodium acetate, 50 mM cadmium sulphate and 100 mM HEPES (pH 7.5), was equilibrated against drops containing 0.5 µL of mother liquor and 0.5 µL of BoHTMurA (9.4 mg/ml) and UNAG (1 mM). **(B)** A diffraction pattern obtained from one of these crystals during the X-ray diffraction experiment.

Various efforts were made to optimize the crystallization conditions of BoHTMurA. The pH of the 100 mM HEPES buffer was adjusted in the range of 6.5-8.5. Additionally, the proportions of the two salts were changed from 0.7 to 1.3 M of sodium acetate and/or 30 to 70 mM of cadmium sulfate. These adjustments were made using 24-well hanging drop plates. Furthermore, an additive screen provided by Hampton Research was used to enhance the formation of BoHTMurA crystals. These additives were tested under the initial condition with and without UNAG. Unfortunately, successful replication of BoHTMurA crystal formation was not achieved.

5.3.10 Structural Models for BoMurA and Residue Conservation Analysis

Due to the unavailability of the crystal structure of BoHTMurA, a first homology modeling of BoMurA was performed using the free software I-TASSER. This resulted in two possible structures (Figure 5.22A and B) based on the previously described structures of *E. cloacae* (3SPB) and *E. coli* (1UAE) (Figure 5.2C). The first model generated represents the "closed" conformation of BoMurA, while the second model represents the "open" conformation. To assess and compare these models, a homology evaluation was conducted with the structure generated by the IA AlphaFold system, which was identified using the UniProt code A5VNK4 (MURA_BRUO2). The AlphaFold structure (Figure 5.22C)

corresponded to the "closed" conformation of MurA. Notably, the lower confidence scores were predominantly found in a loop situated at the back of domain II, opposite to the active site cavity. This loop comprises residues Arg70, Glu71, His72, Gln73, Asn74, Gly75, Pro76, and Tyr77, and its low confidence scores indicate that it is either not correctly predicted or that it is a flexible region of the protein. An analysis of the structural overlap between the "closed" model generated by I-TASSER and the model generated by AlphaFold (Figure 5.21D) using the TM-align algorithm launched with a score value of 0.97544. This means that the two models are very close, almost 95%.

Similar to other reported MurA structures, the BoMurA models consist of two globular domains (pink and yellow in Figure 5.22E) connected by a double-stranded linker. Each domain is comprised of three repeating subunits, resulting in a total of six subunits within the monomeric structure. The predicted catalytic site of the protein is located in a deep cavity at the interface between the two domains. It was also observed that the 122-132 Cys-loop retains 10 amino acids anchored by Pro residues (PGGCAIGTRP), being its intermediate cysteine at position 126.

For the analysis of residue conservation on the 3D structure, we used the ConSurf software, which plots the sequence conservation on the 3D structure, using as the 3D structure that of BoMurA in the AlphaFold database (A5VNK4) together with the MSAs above evaluated above for both *Brucella* (Figure 5.7) and the different bacteria (Figure 5.9). Figures 5.23 and 5.24 respectively plot the results of 3D residue conservation within *Brucella* and the bacterial species evaluated here, respectively. The results revealed a considerable degree of conservation in both cases, which is, as expected, higher when using *Brucella* species. In this latter case, 61.5% of the amino acids remained nearly unchanged, while the number decreases only to 48.3% (207 amino acids) when evaluating different bacteria. Moreover, the residues with an average conservation score are 34.1% (146 amino acids) and 51.3% (220 amino acids) for *Brucella* and bacteria analysis, respectively, while in both cases the number of highly variable residues is highly testimonial. Moreover, both analyses show that the most conserved residues accumulate mainly at the interface between the two domains, and particularly at the terminal ends of their α-helices that point towards the potential binding site for the substrates.

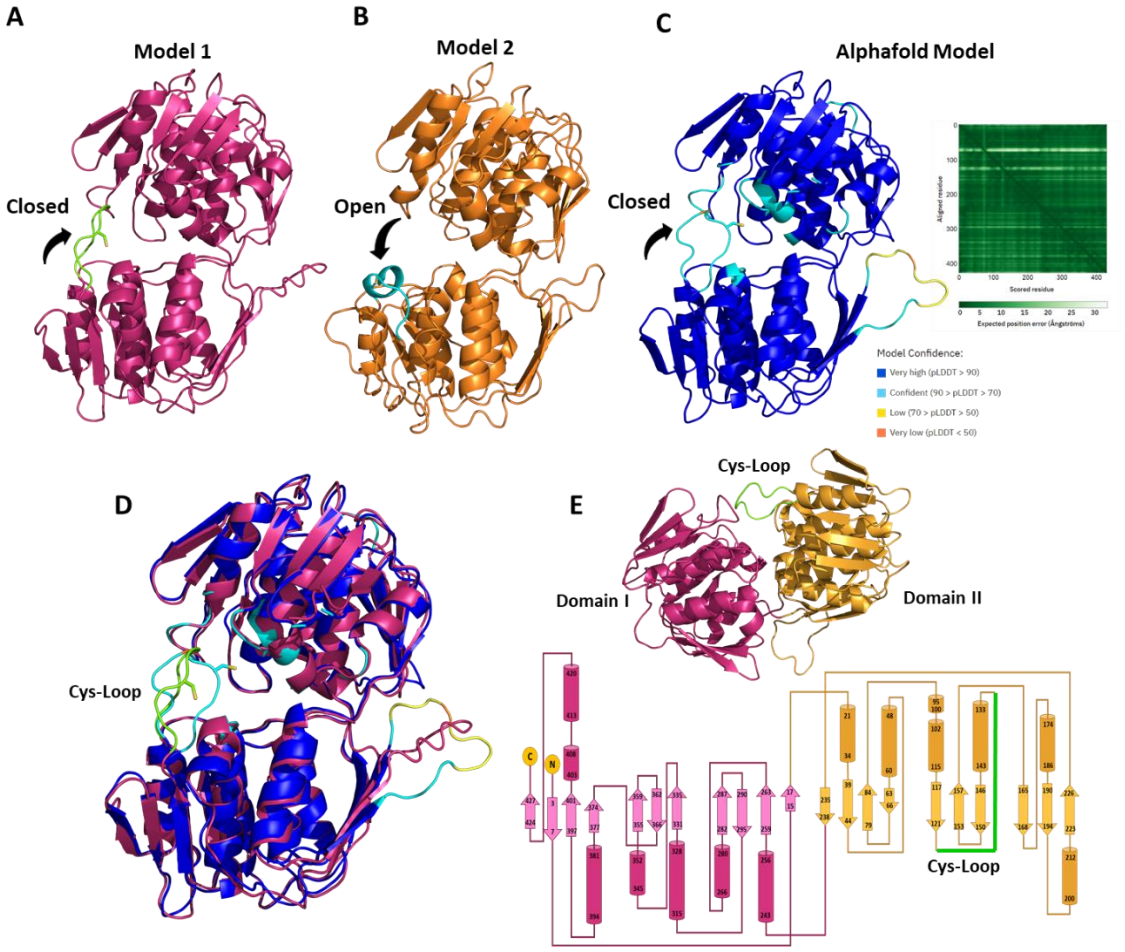

Figure 5.22. Features for the BoMurA structural model. (A) Model 1, representing the "closed" conformation (C-score of 1.59), and **(B)** Model 2, representing the "open" conformation (C-score of 0.24). Both models were generated using the I-TASSER software. In Model 1, the 122-132 Cys-loop is colored green, while in Model 2, it is colored cyan. **(C)** AlphaFold model (A5VNK4). The color of the structure is given in 4 colors that indicate the simulation confidence level: intense blue and light blue regions (pLDDT > 70) indicate high and reliable confidence levels. The yellow regions (70 > pLDDT > 50) indicate a lower confidence level, and the orange regions (pLDDT < 50) indicate structures that are not considered trustworthy. The green square represents the predicted aligned error. The color at position (x, y) indicates AlphaFold's expected position error at residue "x", when the predicted and true structures are aligned on residue "y". **(D)** Overlapping of "closed" models generated by I-TASSER and AlphaFold. The level of similarity evaluated with TM-align estimates a similarity of 97%. **(E)** Structural and topology diagram of domains I (residues 1 to 18, and 240 to 429) and domain II (residues 19 to 239) are respectively shown in pink and yellow. Cys-loop is represented in green.

To further explore the potential interaction of BoMurA with its substrate, a potential model of BoMurA in complex with UNAG and the Pi portion of PEP was produced upon overlapping with *A. fischeri* MurA (3VCY) (Figure 5.23C and 5.24C). The generated model revealed specific residues in close proximity to different regions of these ligands. In particular, Arg131, Pro132, Asp134, Leu135, Lys171, Ser173, Val174, and Gly175 are predicted to contribute to accommodate the UDP portion of UNAG, while Trp106, Thr315, Asp316, Ile338 and Arg341 should contribute to accommodate the N-acetylglucosamine portion of the substrate. Finally, Lys22, Asn23, Arg102, Cys126, and Ile128 surround the

cavity where PEP potentially binds. Noticeably, these residues are highly conserved among the different *Brucella* and bacteria evaluated, and are also consistent with those reported in analogous crystallographic structures (Figure 5.3A and B).

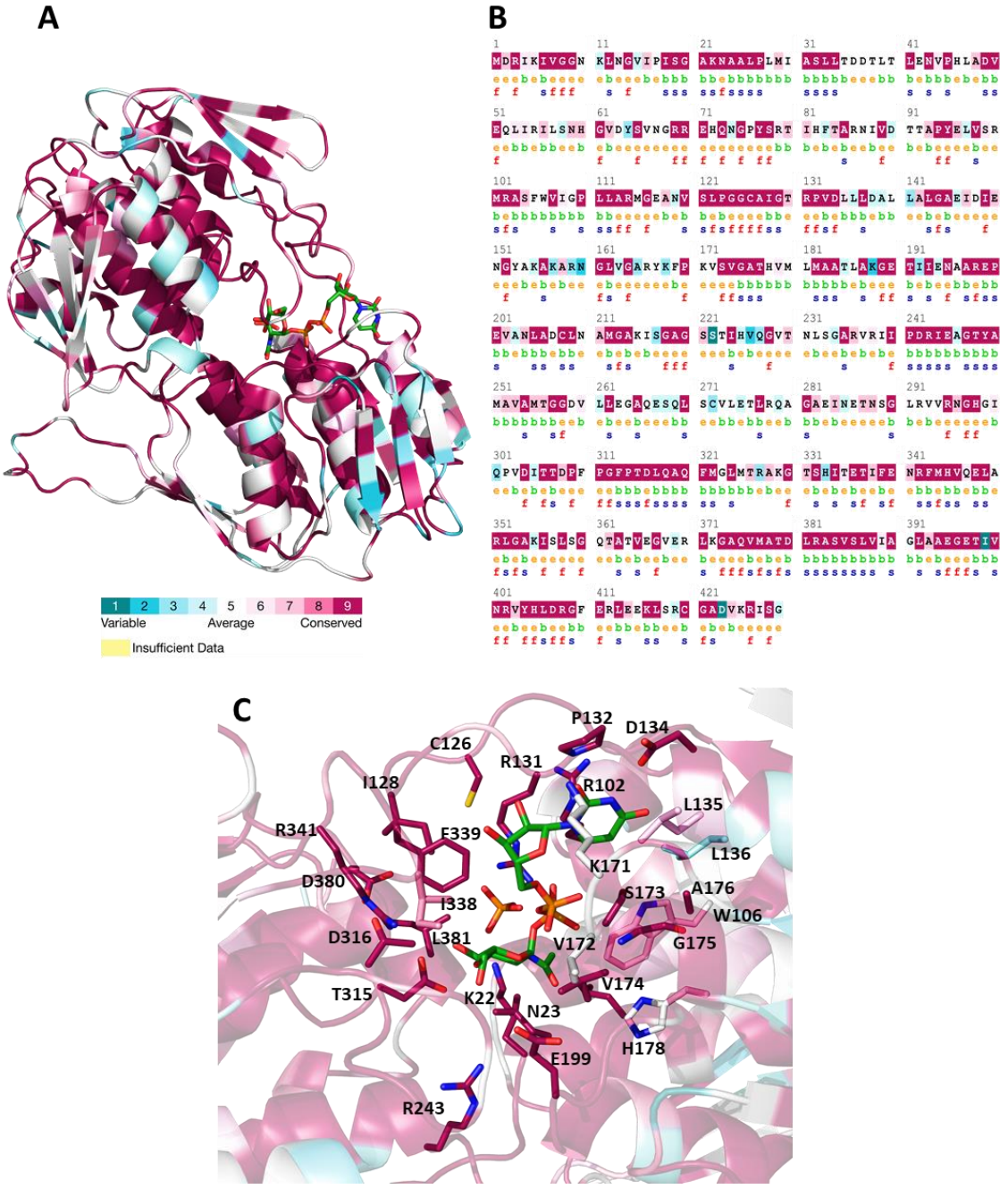

Figure 5.23. Evolutionary structural conservation analysis of BoMurA in the context of the *Brucella* genus. (A) Residue conservation score as calculated by the ConSurf server using the MurA sequences from *Brucella* in Table 5.3 and plotted on the AlphaFold structural model of BoMurA. Structure shown as cartoon colored according to conservation score (from deep teal as less conserved, to deep magenta as most conserved). **(B)** Plot of conservation scores on BoMurA sequence. Residues are also labelled regarding location ("b", buried; or "e", exposed) and predicted relevance as key structural (s) or functional (f) residues. **(C)** Detail of key residues implicated in the interaction with UNAG (CPK colored green sticks) and $PO_4^{=}$ (CPK colored orange sticks) at the enzyme active site. Positions of the substrates taken from an overlap with the 3D structure of *A. fischeri* (3VCY).

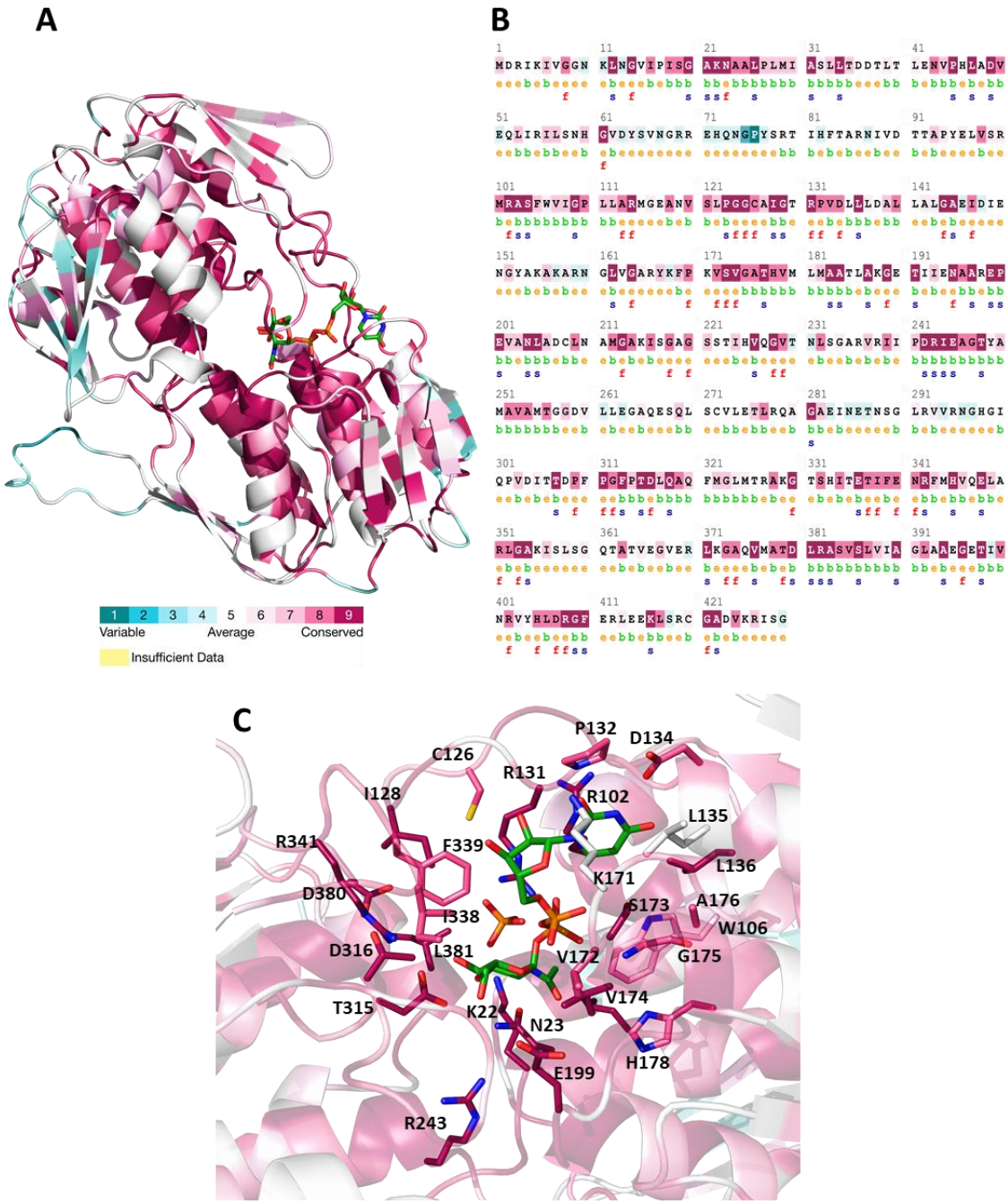

Figure 5.24. Evolutionary structural conservation analysis of BoMurA in the context of different bacteria sequences. (A) Residue conservation score as calculated by the ConSurf server using the MurA sequences from bacteria in Table 5.4, and plotted on the AlphaFold structural model of BoMurA. Structure shown as cartoon colored according to conservation score (from deep teal as less conserved, to deep magenta as most conserved). **(B)** Plot of conservation scores on BoMurA sequence. Residues are also labelled regarding location ("b", buried; or "e", exposed) and predicted relevance as key structural (s) or functional (f) residues. **(C)** Detail of key residues implicated in the interaction with UNAG (CPK colored green sticks) and $PO_4^{=}$ (CPK colored orange sticks) at the enzyme active site. The positions of the substrates are taken from an overlap with the structure of *A. fischeri* (3VCY).

5.4 DISCUSSION

Our analysis of MurA sequences from different *Brucella* species denoted a high degree of similarity among most of them (Figure 5.7), with phylogenetic bootstraps suggesting that these proteins are very close in evolution (Figure 5.8). Nonetheless, some singularities were clearly observed. Here, two copies or isoforms are detected in certain *Brucella* species, despite Gram-negative bacteria usually have a single gene encoding MurA. This raises questions about the evolutionary significance and functional implications of MurA in these species. Future investigations could explore whether these additional copies might confer any adaptive advantages, associated with unique characteristics or linked to different origins of these *Brucella* species, namely *B. antrophi*, *B. cytisi*, *B. pecoris*, and *B. tritic*i. In this context, it is worth noting that *B. anthropi* is typically found in soil and occasionally detected in healthcare environments (Aguilera-Arreola et al., 2018), and that *B. cytisi* and *B. tritici* are isolated from leguminous plants (Zurdo-Piñeiro et al., 2007). This could suggest that *Brucella* strains of rhizobial origin are more prone to harbor two types of MurA. Nonetheless, *B. pecoris*, found in ruminants (Kämpfer et al., 2011), also presents two MurA homologs, while *B. lupine* and *B. microti* are also isolated from soils (Trujillo et al., 2005; Scholz et al., 2008), and have only one copy of murA. Our sequence and phylogenetic analysis in the context of various bacteria reveals several species with more than one murA copy among Gram-positive bacteria. Gram-positive bacteria of the Firmicutes group, which have low percentages of G+C in their DNA, typically have two copies of this gene (Onyenwoke et al., 2004). *A. thermocellus*, *B. anthracis*, *B. licheniformis*, *B. subtilis*, *E. faecium*, *L. plantarum*, *L. monocytogenes*, *S. aureus*, and *S. pneumoniae* are all examples of this observation. Other bacterial species outside the Firmicutes group, such as *S. paucimobilis* and *L. pneumophila* of the Proteobacteria phylum, also contain two copies of the murA gene (Figure 5.10, Table 5.4). In general, both copies are expected to perform the same function, and can substitute for one another, being possible that such redundancy at the first committed step of PG biosynthesis might accommodate differential regulation (Du et al., 2000). In this context, the deletion of the murA gene in *E. coli* and of the two genes in *S. pneumoniae* has been shown to be lethal (Brown et al., 1995; Du et al., 2000). However, if the bacterium has two murA genes and only one of them is deleted, viability is not affected (McDevitt et al., 2002). When comparing to the pro-typical Gram-negative MurA, the MurA1 sequence typically exhibits higher sequence conservation than the similarly sized MurA2. Nonetheless, both MurA1/A2 enzymes share highly conserved structural features

and residues involved in ligand interactions, suggesting that it is unlikely that one of their encoding genes is a non-functional copy (Wanke et al., 1992).

Up to 3 different genes encoding murA have been identified in *A. thermocellus*: Cthe_2615 (WP_003512944.1), Cthe_2328 (WP_020457769.1) and Cthe_0441 (ABN51679.1). However, ABN51679.1 consists of only 287 aa and lacks the around first 150 residues (including the Cys loop), while the other 2 proteins are 422 and 417 aa long respectively. Since most MurA sequences exceed 400 aa, we suspect that Cthe_0441 is incomplete and may not be functional. However, these three genes sit in homogeneous operons, being AtMurA1 and AtMurA2 expressed together with proteins involved in PG metabolism and in sporulation, while AtMurA3 is expected to be expressed together with proteins involved in cell wall division such as FtsQ. Therefore, a function still not envisaged might be related to AtMurA3. Hence, the functional significance of multiple murA genes in *A. thermocellus* is still not entirely clear, and different gene copies may have distinct functions, such as playing different roles in cell wall synthesis or responding to different environmental conditions. Alternatively, the multiple full-length copies may serve as redundancy, ensuring that the bacterium can maintain cell wall integrity even if one copy becomes non-functional. The presence of more than one copy of the murA gene in a bacterial species may depend on factors such as the evolutionary history of the species, natural selection, and environmental stresses. Further work on the comparative characterization of these proteins within a single species needs to be done to determine whether they present kinetic parameters and/or substrate and product affinities that allow the bacteria to adapted to different ranges of substrate concentrations.

In the present study, BoHTMurA has been successfully purified to homogeneity, and although the obtained protein yield is not high, enough sample can be obtained to spectroscopically characterize the enzyme, evaluate its enzymatic activity and even to produce crystals. Spectroscopic characterization confirms the purification of folded protein and establishes its spectral properties (Figure 5.14), indicating that the protein has a high content of α-helix. We have also evaluated the thermal stability of BoHTMurA by different spectroscopic approaches, which come to show a multi-steps unfolding process. Such observations are in good agreement with folding of the protein into two almost independent domains, that apparently do not lose their secondary organizations, β-sheets and α-helices, simultaneously upon unfolding. Due to the key reaction catalyzed by BoHTMurA, it is an interesting target for antimicrobial drug discovery. In such searches, massive high-

throughput screening approaches have been efficiently used to identify compounds that bind to the protein by its thermal stabilization (Cremades et al., 2009). To evaluate whether this might be the case for BoHTMurA, we also evaluated the impact of its UNAG substrate binding on protein stabilization versus thermal denaturation. Noticeably, despite UNAG is a relatively large molecule, its presence produced in only a slight stabilization of the protein´s secondary structure. This suggests that in this particular case, efforts on searching for antimicrobials will rather require approaches by the massive search of compounds as direct inhibitors of its activity.

In this line, this study also aimed to standardize a protocol for measuring the BoHTMurA activity, that would in addition produce its UNAGEP product, that is not commercial but is the substrate of MurB. As activity measurement assay we chose the colorimetric Malachite green method to measure Pi released upon MurA activity. The best conditions here obtained for measuring BoHTMurA activity in this assay were obtained by pre-incubating the enzyme with 2 mM of UNAG at 37 °C for 10 min in 50 mM BIS-Tris Propane, pH 7.0, followed by the addition of 2 mM of PEP and allowing the reaction to continue for another 30 min. This approach enabled the roughly determination of a V_{max} value of 1.6 µM min^{-1} and an apparent k_{cat} of 32 min^{-1} for BoHTMurA. So far, kinetic parameters have been reported for a significant number of MurA enzymes from different species (Table 5.5). Noticeably, a great variability is observed in the k_{cat} values. MurA enzymes from Gram-negative bacteria such as *E. coli*, *E. cloacae* and *H. influenza*, which have a single copy of the protein, have the higher k_{cat} values, in the range of 180-534 min^{-1}. This suggests that these bacteria may have a high capacity to rapidly synthesize PG to build their cell wall. On the other hand, MurA from *M. tuberculosis* has a very low k_{cat} value, only 3 min^{-1}. It is important to keep in mind that *M. tuberculosis* is an intracellular organism that exhibits diverse physiological states and extremely slow growth. Its generation time is not less than 16 h. In contrast, bacteria like *E. coli* are fast growing and can have a generation time as short as 20 minutes (Zhu & Dai, 2018). In the Gram-positive bacteria, as *S. aureus* and *S. pneumoniae*, which harbor MurA1 and MurA2 isoforms, both exhibited comparable values for k_{cat} (25-68 min^{-1} range) and K_M. However, the MurA2 isoform of *S. pneumoniae* displays higher substrate specificity and almost twice the turnover rate compared to MurA1. On the other hand, MurAs from both organisms exhibit reduced catalytic activity and substrate specificity when compared to *E. coli* MurA. The presence of two MurA copies in *S. aureus* is functionally significant; a MurA1 knockout affects the growth rate and causes a

reduction in cellular PG content of up to 26%, whereas a MurA2 results in only a 3% reduction. Additionally, MurA1 was expressed at significantly higher levels than MurA2 (Kim et al., 1996; Du et al., 2000; Blake et al., 2009). As mentioned above, this also makes it plausible that the two MurA proteins in these bacteria play distinct roles in various stages of PG synthesis or other related metabolic processes. The k_{cat} values of both of these bacteria were similar to that here envisaged for BoHTMurA. In the case of K_M, the values so far reported are also highly varied, suggesting that the affinity of the different MurA enzymes for their substrates varies significantly among bacterial species. These different values may also be relevant for understanding the ability of bacteria to efficiently synthesize PG and build their cell wall, which may have implications for pathogenicity and antibiotic resistance. In addition, it is worth noting that the colorimetric assay using the Malachite green reagent to determine Pi standardized here has also been proved by other members of our group as an excellent method for the massive screening of large chemical libraries in solution (Moreno et al., 2023).

Table 5.5. List of bacterial species for which activities of MurA enzymes have been reported.

Organism	k_{cat}	K_M^{UNAG}	k_{cat}/K_M^{UNAG}	K_M^{PEP}	k_{cat}/K_M^{PEP}	K_d^{UNAG}	K_d^{PEP}	Experimental Conditions				Reference
	(min^{-1})	(μM)	($\mu M^{-1} \cdot min^{-1}$)	(μM)	($\mu M^{-1} \cdot min^{-1}$)	(μM)	(μM)	[Enzyme]	Final Vol.	Buffer	Incubation	
A. baumannii[b]	nd	1062±90	V_{max}= 0.236±0.005 nmolPi min^{-1}	1806±230	V_{max}= 0.052±0.002 nmolPi min^{-1}	nd	nd	3 μg/mL	50 μL	20 mM Tris-HCl pH 7.5,10 mM KCl, 1 mM DTT, 10% v/v glycerol	37 °C for 10 min	(Sonkar et al., 2017)
Borrelia burgdorferi	62.2±1.8	45±7	1.3	89±12	0.69	nd	nd	80 nM-1 μM	nd	50 mM Na·HEPES pH 7.0, 150 mM NaCl, 1 mM DTT	37 °C for 3 h	(Jiang et al., 2011)
E. coli	285	2500	0.11	1000	0.28	nd	nd	nd	100 μL	250 mM Tris pH 7.8	37 °C for 30 min	(Marquardt et al., 1992)
	228	15	15.2	0.4	570	nd	nd	0.01-0.05 U/mL	1 mL	100 mM Acetic acid, 50 mM Bis-Tris Propane, 50 mM Tris, pH 5.5-9.0, 20 mM KCl, 0.2 mM NADPH, 0.1 U/mL EcMurB	nd	(Kim et al., 1996; Marquardt et al., 1994)
	144	36±5	4	0.84±0.13	171	nd	nd	100 nM	100 μL	100 μM Tris-HCl pH 7.5	37 °C for 30 min	(Dube et al., 2010)
E. coli K12	534	5.7	93. 7	4.1	130	nd	nd	0.448 μM	70 μL	50 mM Tris-HCl pH 8.0, 2mM KCl, 2 mM DTT	37 °C for 30 min	(Dai et al., 2002)
E. cloacae	180±24	80±7	2.25	8.3±2.0	21.7	50	220	0.4 μM	nd	50 mM CABS pH 9.5-11/ 50 mM Tris pH 7.2-9.5/ 50 mM PIPES pH 5./-7.2 all containing 1 mM DTT and 2 mM EDTA	22 °C	(Krekel et al., 2000; Samland et al., 1999; Zhu et al., 2012)
Fusobacterium nucleatum[b]	nd	180	V_{max}= 0.077 mM $min^{-1}mg^{-1}$	77	V_{max}= 2.03 mM $min^{-1}mg^{-1}$	7±1	nd	2 μg/mL	100 μL	20 mM Tris-HCl pH 7.5, 1 mM DTT	37 °C for 30 min	(Kumar et al., 2017)
H. influenza	210	31	6.77	24	8.9	nd	nd	100 nM	100 μL	100 mM Tris-HCl pH 7.8	25 °C for 30 min	(Han et al., 2011)
M. tuberculosis	3.06	2048	1.4 x 10^{-3}	527.8	5.8 x 10^{-3}	nd	nd	125 nM	50 μL	50 mM Bis-Tris Propane pH 7.0	37 °C for 30 min	(Eniyan et al., 2016)
	nd	2743±231	7.2 x 10^{-4}	199±13	0.017	nd	nd	2 μg/mL	50 μL	50 mM Tris-HCl pH 7.5, 1 mM DTT	37 °C for 30 min	(Xu et al., 2014)
M. smegmatis	nd	2320±80	3.8 x 10^{-3}	121±14	0.058	nd	nd					
P. aeruginosa	108	17.8±2.5	6.06	0.45±0.07	240	nd	nd	100 nM	100 μL	100 μM Tris-HCl pH 7.5	37 °C for 30 min	(Dube et al., 2010)
S. aureus	67.8±1.2	123.8±8.2	0.5512	11.5±1.6	5.9	nd	nd	4 μg/mL	200 μL	50 mM HEPES pH 7.6, 250 mM methylthioguanosine, 0.1 U/mL purine-nucleoside phosphorylase, 100 uM DTT	nd	(Blake et al., 2009)
	45.6±1.2[a]	168.6±16.2[a]	0.271[a]	11.6±2.5[a]	3.94[a]	nd	nd					
Streptococcus mutans[b]	nd	120	V_{max}= 0.048±0.002 mM $min^{-1}mg^{-1}$	86	V_{max}= 0.098±0.001 mM $min^{-1}mg^{-1}$	nd	nd	1.84 μg/mL	100 μL	50 mM Tris-HCl pH 7.5,10 mM KCl, 1 mM DTT, 10% v/v glycerol	37 °C for 5 min	(Li et al., 2012)
S. pneumoniae	24.6±0.6	244±20	0.1	37±4	0.66	nd	nd	200 nM	200 μL	50 mM HEPES pH 7.5	room temperature	(Du et al., 2000)
	46.8±1.8[a]	119±16[a]	0.393[a]	11.1±2.3[a]	4.2[a]	nd	nd	50 nM				
Wolbachia[b]	nd	31.5	V_{max}= 1.4 mM $min^{-1}mg^{-1}$	9.19	V_{max}= 0.538 mM $min^{-1}mg^{-1}$	nd	nd	3 μg/mL	50 μL	50 mM Tris-HCl pH 7.5,10 mM KCl, 1 mM DTT, 10% v/v glycerol	37 °C for 10 min	(Shahab et al., 2014)

[a] Value corresponding to MurA2

[b] k_{cat}/K_M reported as V_{max} value with unusual units

One of our goals when producing BoHTMurA was also to produce UNAGEP, for its use as a BoMurB substrate. Nonetheless, up to the date, this has been proved a still challenging task. Reverse-phase HPLC showed that UNAG, UNAGEP, PEP, and BIS-Tris Propane eluted in a similar retention range, regardless of the mobile phase used. As a result, we concluded that, at this point, this technique requires further improvement to purify the UNAGEP produced for subsequent studies. In addition, we also used the NMR service at the University of Zaragoza to conduct a ^{13}C analysis for each of the components involved and to evaluate the level of UNAGEP production. The analysis yielded a positive result, since the signal corresponding to the three additional carbons expected in UNAGEP regarding UNAG was detected. Nonetheless, the obtained spectra for the reaction products showed a mixture of UNAG and UNAGEP, indicating that not all of the substrate was efficiently transformed in the UNAGEP product. Further work is needed to increase the amount of UNAGEP product and its separation from the UNAG substrate.

Moving to the structural properties of MurAs, more than 50 crystal structures for MurA enzymes are deposited on the PDB server (Table 5.1). Some of them have a percentage of identity with BoMurA close to 50%. The crystal structure of MurA from *P. aeruginosa* PAO1 (5BQ2) is the most similar to BoMurA, with 52% sequence identity. 32 crystal structures were obtained in the presence of some substrates or homologous molecules (Table 5.2). These structures provide information about the binding and catalytic mechanisms of MurA, and have been here used to infer potential residues that contribute to the interaction of BoMurA with its substrates. In the absence of a crystalline structure (since our attempts to obtain and experimental structure failed), BoMurA models obtained from I-TASSER and the AlphaFold database, were used here used. These models show that BoMurA folds into two globular domains linked by a connector, housing six subunits and a catalytic site nestled in a deep cavity. Structural conservation analysis using both different *Brucella* and bacterial species, highlighted particular residue conservation clustered around the substrates binding site, but also showed substantial conservation across the structure. Examination of predicted interactions with UNAG and the Pi portion of PEP revealed the proximity of specific residues to different substrate regions, pointing to molecular recognition of substrates being highly conserved among the evaluated MurA enzymes. Thus, key residues for BoMurA substrate binding and activity align in general with those documented for other MurA enzymes for which structures in the presence of ligands have been reported (Table 5.2).

5.5 CONCLUSION

The investigation into the diversity and functional significance of MurA enzymes across various *Brucella* and bacterial species has provided valuable insights into the complexity of the species specific potential regulation at the initial step of PG synthesis. The presence of multiple MurA copies or isoforms in certain bacteria, both Gram-positive and Gram-negative types, suggests the existence of intricate regulatory networks governing cell wall biosynthesis. The comparative analysis of MurA sequences, together with their kinetic parameters and structural information, underscores the importance of understanding these enzymes at both molecular and functional levels. The identification of conserved residues within critical regions of the protein structure emphasizes their pivotal roles in maintaining enzyme stability and substrate interaction. Additionally, the distinct kinetic properties observed among MurA enzymes from different bacterial species provide insight into their respective growth strategies and their efficiency in synthesizing PG. Furthermore, the successful purification and characterization of BoHTMurA, along with the elucidation of its response to thermal denaturation in the presence of substrate, will surely contribute to our understanding of the enzyme's functional behavior. These findings have enhanced our comprehension of BoMurA and PG biosynthesis, but most importantly, they have particularly provided to our research team with the tools to search for and to identify potential antimicrobial agents targeting BoMurA.

6.

The UDP-N-acetylglucosamine enolpyruvate reductase from Brucella ovis: Insights into functional and structural features during the transformation of enolpyruvyl-UDP-N-acetylglucosamine to UDP-N-acetylmuramic acid

6.1 SUMMARY

The biosynthesis of UNAM in bacteria represents a critical initial phase in the production of the PG. Within this process, the enzyme UDP-N-acetylglucosamine-enolpyruvate reductase (MurB) facilitates the reduction of UNAGEP to form UNAM, relying on NADPH and FAD as essential redox coenzyme and cofactor respectively. The exploration of MurB sequences across various *Brucella* genera and different bacterial species has unveiled a conserved operon, housing genes responsible for PG synthesis. Furthermore, MurBs can be categorized into type I and type II, with the latter further divided into subtypes IIa and IIb. *Brucella* MurBs fall under the category of type IIa, and comparative assessments show that their sequences exhibit a degree of identity exceeding 90%. Conversely, in other bacterial species, the identity percentage is notably high for both type IIa and IIb sequences. Two *B. ovis* MurB forms, denoted as BoHTMurB with a His-tagged and BoMurB without one, were here cloned and overexpressed in *E. coli*. They underwent purification and structural characterization, which included assessments by SDS-PAGE, SEC, CN-PAGE, absorption, CD, and fluorescence. These examinations unequivocally validated that both purified proteins are correctly folded and exist in monomeric state. On the other hand, thermal stability investigations indicate that the unfolding of BoHTMurB and BoMurB does not occur cooperatively, and they only hint at a marginal protein stabilization when UNAGEP and $NADP^+$ are present. The redox potential of the FAD cofactor in BoHTMurB was estimated in $E_{ox/hq}$ -256 ± 3 mV. Surprisingly, both BoHTMurB and BoMurB were capable of accepting electrons through photoirradiation as well as by sodium dithionite, indicating its ability to undergo reduction by non-physiological electron donors. Nonetheless, they did not oxidize their expected NAD(P)H coenzyme. Crystallizing the protein posed significant challenges, yet success was achieved in obtaining crystals of BoMurB by introducing UNAGEP into the crystallization conditions. The crystal structure unveiled a three-domain configuration and the binding of both FAD and UNAGEP. Multiple sequence analysis of both *Brucellas* and bacteria applied to the BoMurB crystal structure aided in identifying the extent of residue conservation within the active site cavities and its connection to the FAD cofactor.

6.2 INTRODUCTION

UDP-*N*-acetylglucosamine enolpyruvate reductase, also known as MurB (EC 1.3.1.98), is a highly conserved enzyme among bacterial species that is essential for maintaining bacterial cell integrity and for resistance to changes in osmotic pressure, whereas there are non-existing counterparts in eukaryotes. MurB is directly involved in the peptidoglycan (PG) biosynthetic pathway. It participates in the first stage, which occurs in the cytoplasm, where the monomeric building block N-acetylglucosamine–N-acetylmuramyl pentapeptide is formed. Due to its relevant role in bacterial viability, MurB enzymes are pointed as attractive targets for antimicrobial discovery (Ewing et al., 2017).

6.2.1 The MurB catalytic activity

MurB catalyzes the reduction of UDP-*N*-acetylglucosamine enolpyruvate (UNAGEP) to UDP-*N*-acetylmuramic acid (UNAM). The overall reaction involves a sequence of two half-reactions in a ping-pong bi-bi mechanism in which the enzyme-bound FAD serves as redox intermediate (Benson et al., 1993; Chen et al., 2013). In the first half-reaction, FAD is reduced to $FADH^-/H_2$ by the NADPH coenzyme. Specifically, a hydride, from the *4-pro-S* hydrogen of C4n of NADPH, is donated to the N5 atom of the isoalloxazine ring of FAD. In the second half-reaction, these two electrons are conveyed from the N5 of the reduced isoalloxazine to the C-3 of the enolpyruvyl moiety of UNAGEP producing UNAM while MurB returns to its oxidized state (Figure 6.1) (Moraes et al., 2015).

In addition, MurB enzymes have been reported to exhibit intrinsic NADPH oxidase activity (Zoeiby et al., 2003). When NADPH was added to purified MurB samples from different species, the yellow color was immediately bleached as consequence of the reduction of the FAD cofactor to $FADH^-$. This reduction can be followed by the quantitative decrease of oxidized FAD absorbance band I at ~460 nm. Under aerobic conditions, the yellow color was recovered, suggesting that reduction by NADPH was reversible. In addition, upon addition of the co-substrate UNAGEP, MurB-$FADH^-$ has been reported to become re-oxidized, establishing the FAD cofactor as a conduit of electrons from NADPH to the enolic site of UNAGEP during catalysis (Benson et al., 1993). On the other hand, MurB enzymes require monovalent cations, such as K^+, for activation, while divalent ions, such as Hg^{2+} and Pb^{2+}, either do not activate it or even produce its inhibition (Dhalla et al., 1995; Sylvester et al., 2001).

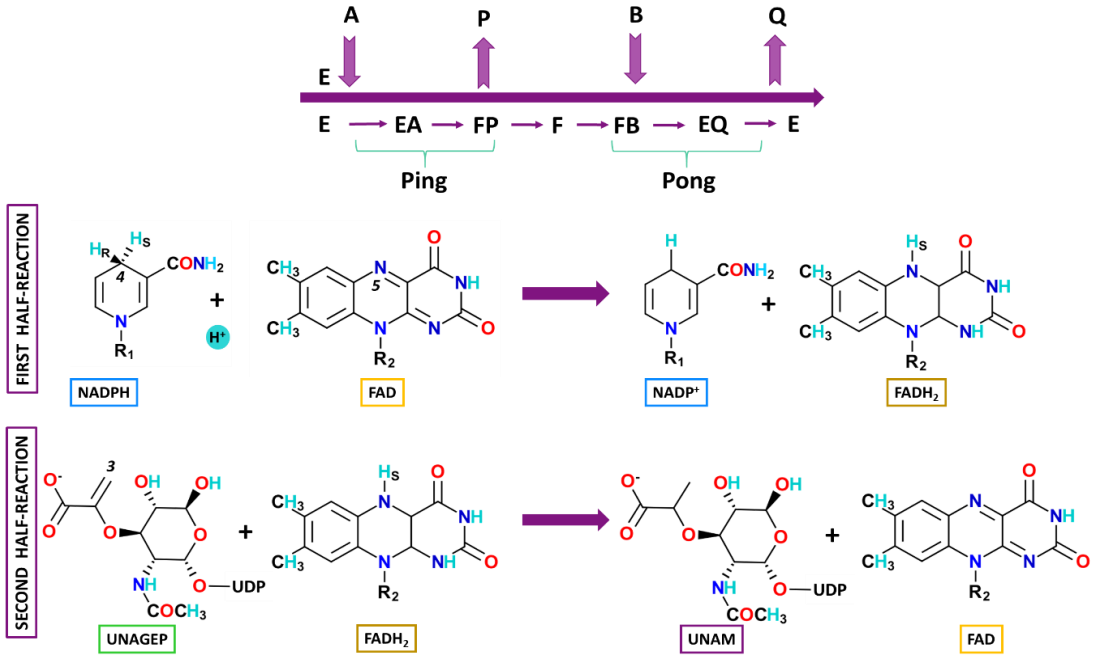

Figure 6.1. MurB enzymes catalyze the FAD and $NADP^+/H$ dependent reduction of UNAGEP to UNAM: The top panel shows a ping-pong Bi-Bi mechanism representation with Cleland's nomenclature with purple arrows. The underneath scheme shows the chemical structures for the first and second half reactions. In the flavin reductive process FAD is reduced to $FADH^-/H_2$ by NADPH, while in the re-oxidative process $FADH^-$ transfers two electrons to the UNAGEP enolpyruvyl group reducing it to a lactoyl group and thus converting UNAGEP to UNAM.

6.2.2 Structure and Classification

MurB is a mixed α+β protein composed of three domains. Domains I and II are involved in binding of the FAD cofactor, while domain III accommodates the coenzyme NADPH and the substrate UNAGEP. The cofactor FAD occupies the same binding site in the different structures reported for MurB (Benson et al., 1994, 1996, 2001). In addition, the conserved protein fold of the enzyme made it a member of a new superfamily of FAD binding proteins (Murzin, 1996). Sequence analysis allowed MurBs to be classified into two types. Type I is characterized by containing a tyrosine-rich loop (Tyr-loop), that is involved in opening the substrate-binding site, and a single split βαββ fold, found in the substrate-binding site, where the uridine moiety of UNAGEP is placed. These motifs are present in MurB from *E. coli*, *M. tuberculosis*, and *P. aeruginosa* (Constantine et al., 1997). In contrast, type II lacks the above mentioned traits and is found in *L. monocytogenes*, *S. aureus* and *Thermus caldophilus*. Both types of MurBs have similar overall folds, although they show differences at the substrate-binding regions, due mainly to the mentioned features in type II (Figure 6.2) (Benson et al., 1996, 2001; Eniyan et al., 2018; Nishida et al., 2006).

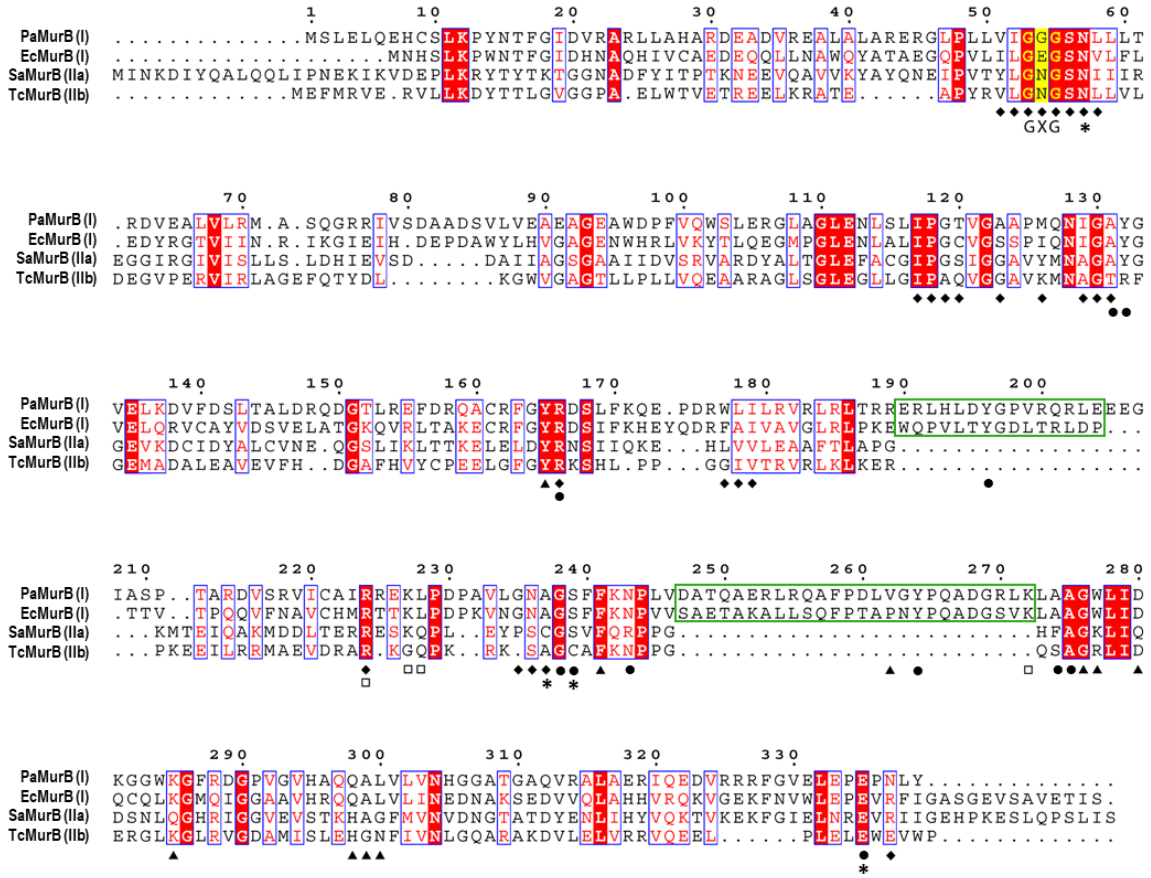

Figure 6.2. Sequence alignment of representative MurB enzymes with determined crystal structures. The sequences aligned are MurBs from *P. aeruginosa* (PaMurB, PDB code 4JAY), *E. coli* (EcMurB, PDB code 2MBR) as MurBs from type I; *S. aureus* (SaMurB, PDB code 1HSK) as MurB type IIa, and *Thermus caldophilus* (TcMurB, PDB code 2GQU) as MurB type IIb. Strictly conserved residues are shaded in red while conserved regions are boxed; the GXG motif involved in FAD-binding is annotated by letters underneath of the corresponding segment of alignment (PaMurB 53-55). Residues involved in cofactor and substrate binding are indicated with the following symbols: ♦, residues that interact with FAD in both PaMurB and EcMurB; ▲, residues that interact with UNAGEP in EcMurB; □, residues that interact with $NADP^+$; *, residues that interact with both UNAGEP and $NADP^+$ and ●, residues that coordinate the putative catalytic metal ion. Tyr-loop segments, only present in MurB type I, are boxed in green (figure adapted from Chen et al., 2013).

6.2.2.1 MurB Type I

This type of MurB presents a larger domain III than type II due to the presence of the aforementioned Tyr-loop. In these MurBs, the domain III is adjacent to the FAD pocket and can be visualized as two lobes. Figure 6.3 describes the general morphology of MurB type I from *P. aeruginosa* (PaMurB), whose structure was solved in complex with the coenzyme $NADP^+$ (PDB code 4JAY). Here, domain I is formed by residues 1-75 and 336-339, domain II comprises residues 76-191 and domain III, 192-335. In the domain III, lobe I consists of a linker (198-228) to domain II, that is structured in two helices, α5-α6, with Tyr196 sitting in α5. Lobe II, close to domain I, shows a β12-α7-β14-β13-α8 organization where Tyr264 sits in the β13 sheet. Substrate and coenzyme binding takes place between these two lobes.

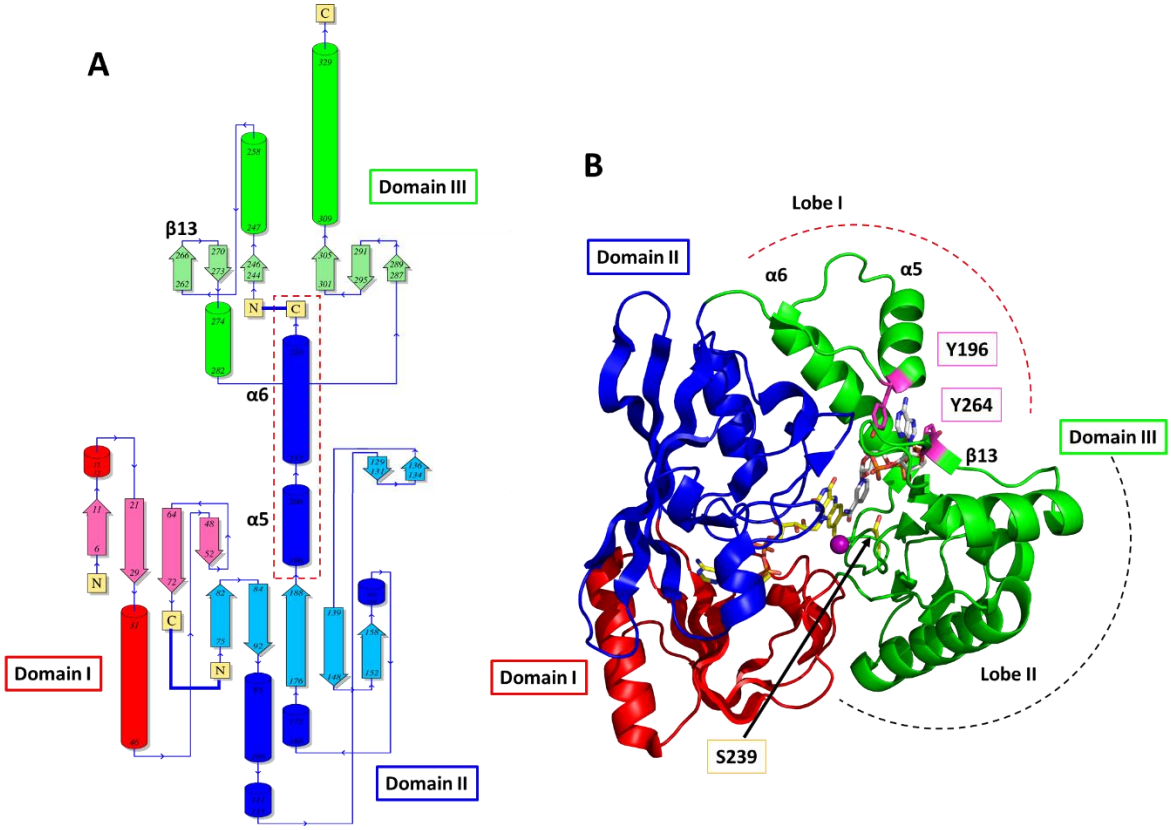

Figure 6.3 Crystal structure of PaMurB (4JAY), type I enzyme. (A) Topology diagram of each protein domain as obtained by PDBsum software (Laskowski et al., 2018). Domains I, II and III are respectively colored with α-helixes/β-sheets in red/pink, dark/light blue and dark/light green. The α-helices delimited in a red dashed rectangle, corresponding to residues 189-228, are identified by the PDBsum as part of domain II, while they are described in the literature as part of lobe I from domain III. **(B)** 3D structure of PaMurB colored by domain. FAD (CPK colored in yellow sticks), the $NADP^+$ (CPK colored in grey sticks) and K^+ ion (purple sphere) are also show. The residues Thr196 and Thr264 stacking the adenine of $NADP^+$ and Ser239 at the nicotinamide environment are shown in pink and yellow sticks, respectively.

The binding site and conformation for the FAD cofactor in PaMurB is similar to that found in other MurB structures (Benson et al., 1994, 1996, 2001). The FAD binding site is shown in figure 6.4, where N5 and O4 atoms of the isoalloxazine ring are stabilized by the guanidinium moiety of Arg224, and the polar backbone atoms of Gly130. The ribityl sugar moiety is stabilized through H-bonds to the carbonyl oxygen of Pro118 and the hydroxyl group of Ser56. The main chain atoms of residues 53-57 (GGGSN), which include the GxG motif, and found in the Rossmann fold, enclose the diphosphoadenine portion of the cofactor and are well conserved. In addition, Thr120 provides stabilizing interactions for the two phosphates, and the Ile179 backbone stabilizes the adenine conformation.

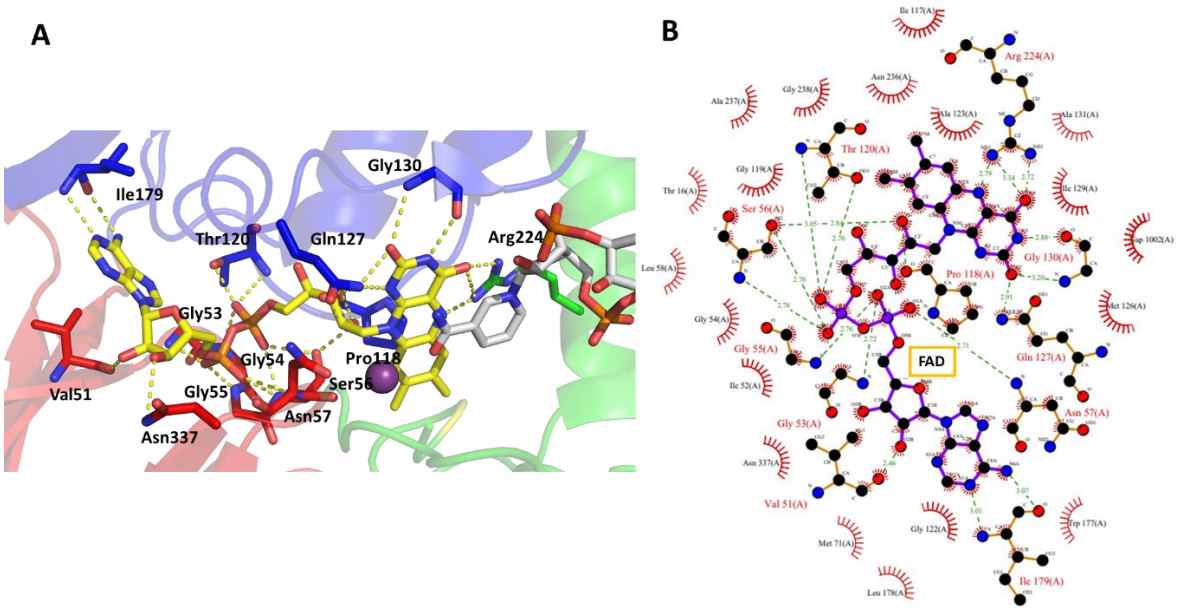

Figure 6.4. The FAD binding site in PaMurB (4JAY). (A) Detail of residues interacting with the FAD cofactor (CPK colored in yellow sticks). Domain I is show in red, domain II in blue, and domain III in green. $NADP^+$ is shown in CPK and colored in grey sticks. **(B)** LIGPLOT diagram of main interactions stablished by the FAD cofactor. FAD molecule is shown as purple ball-and-stick models. H-bonds and van der Waals interactions are indicated as green dashes and radiating red lines, respectively.

Regarding the $NADP^+$ binding site, residues Tyr132 and Arg166 interact with the ribose of the nicotinamide nucleotide moiety, while Lys227 stabilizes the pyrophosphate. The phosphoribose on the adenosine moiety hydrogen bonds with Tyr196, Asn243, and Lys272. The adenosine moiety, at the entrance of the substrate channel, adopts an anti-conformation with the adenine ring, by interacting with Tyr196 and Tyr264 of lobe 1 and the βαββ basset of lobe 2. Finally, a K^+ ion is located at the active site of PaMurB, in vicinity of the $NADP^+$ nicotinamide ring and the FAD isoalloxazine ring. This K^+ ion displays a pentagonal bipyramidal coordination with two main chain oxygen atoms (Ala237 and Ser239), the side chain carboxyl oxygen of Glu335, the side chain oxygen of Asn57 and the O7 of the nicotinamide ring (Figure 6.5) (Chen et al., 2013).

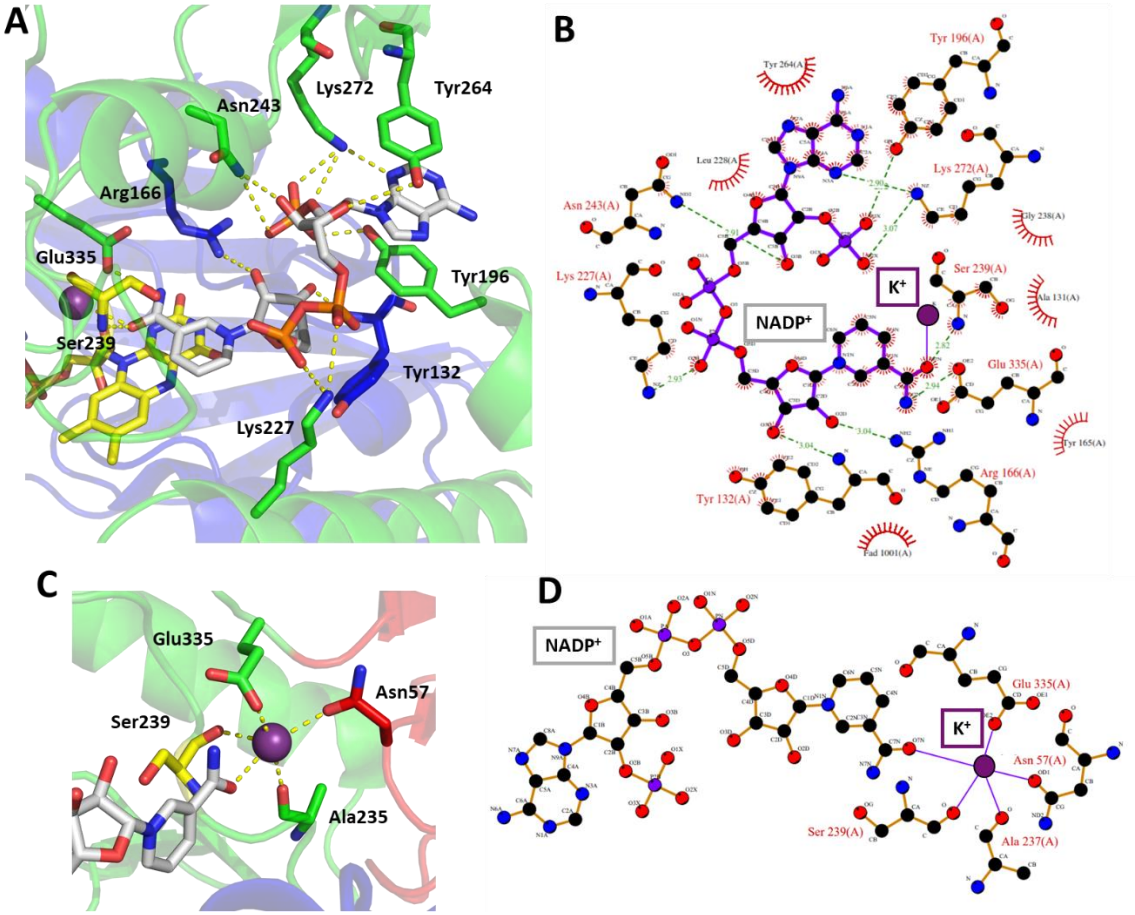

Figure 6.5. The $NADP^+$ and K^+ binding sites in PaMurB (4JAY). (A) Detail of residues interacting with the $NADP^+$ (CPK colored in grey sticks) and **(C)** the metal ion K^+ (purple sphere). Interactions are shown with yellow dashed lines, domain I is shown in red, domain II in blue, and domain III in green. The FAD and the catalytic residue Ser239 are shown in carbon atoms in yellow sticks. **(B)** and **(D)** LIGPLOT diagram of those interactions. $NADP^+$ molecule is shown as purple ball-and-stick models. H-bonds and van der Waals interactions are indicated as green dashes and radiating red lines, respectively.

6.2.2.2 MurB Type II

Type II MurBs are classified into groups IIa and IIb based on the nature of the catalytic residue at the active site that protonates the intermediate carbanion formed after hydride transfer to UNAGEP.

This residue is serine for MurB type IIa and cysteine for MurB type IIb (Benson et al., 1996). Both protein subtypes are structurally very similar, as shown in figure 6.6, where the crystal structure of MurB of *S. aureus* (SaMurB, PDB code 1HSK) (Benson et al., 2001), and that of *T. caldophilus* in complex with UNAGEP (TcMurB, PDB code 2GQU) (Kim et al., 2006) are shown as examples of types IIa and IIb, respectively. SaMurB type IIa is a 326 amino acid protein: domain I composed of residues 14-98 and 310-326, domain II made by residues 101-229, and domain III including residues 230-316. TcMurB is a protein of 265 amino acids: domain I composed of residues 3-65 and 263-267, domain II including residues

66-185 and domain III including residues 197-262. In both subtypes, domain III consist of a simple lobe, in contrast to type I MurBs.

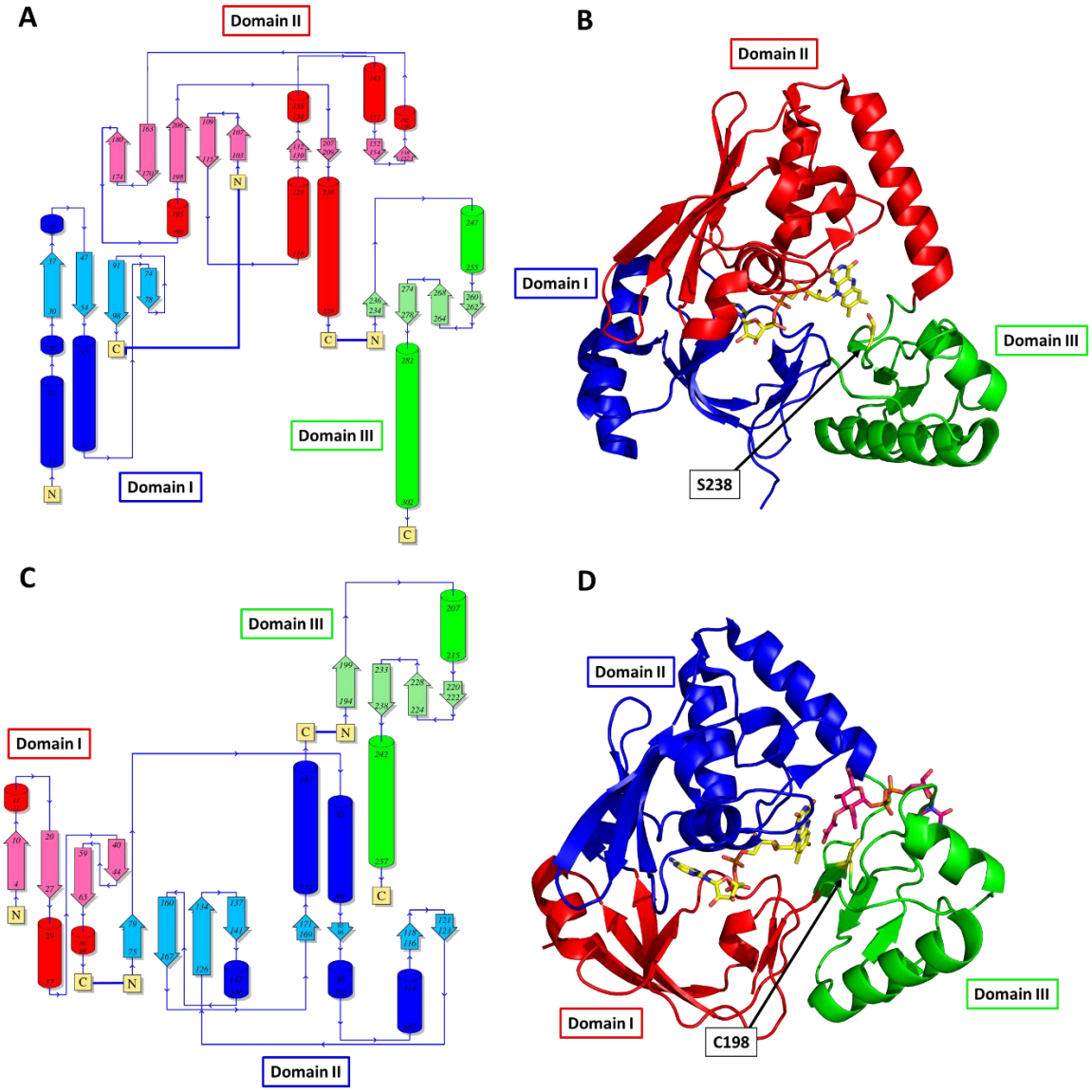

Figure 6.6. Crystal structure of SaMurB (1HSK) and TcMurB (2GQU) enzymes. (A) and **(C)** Topology diagrams and **(B)** and **(D)** cartoon representations of SaMurB and TcMurB, respectively. In (A) and (B) Domain I is colored in blue, II in red and III in green, while in (C) and (D) Domain I is colored in red, II in blue and III in green. FAD (CPK in yellow sticks) and UNAGEP (CPK in pink sticks, only in D) are also shown. The catalytic residues (Ser238 and Cys198 in yellow sticks) are indicated by black arrows. PDBsum software for topology diagram was used (Laskowski et al., 2018).

Conserved arginine residues also appear to contribute to the binding and stabilization of the reduced FAD cofactor during catalysis. Thus, the N5 and O4 atoms of the isoalloxazine ring sit at interacting distance with the guanidinium moiety of Arg225 in SaMurB and Arg187 in TcMurB. In addition, Gly153 of SaMurB and Gly117 of TcMurB interact with the N3 and O2 atoms. The hydroxyl groups of the ribityl moiety are stabilized

by Ser82 and Pro141 in SaMurB, and by Ser48 and Gly110 in TcMurB. The main chain atoms holding the conserved GxG motif (GNGSN), residues 79-83 in SaMurB and 45-49 in TcMurB, enclose the diphosphoadenine portion of FAD. In addition, Ser143 and Gln107 provide stabilizing interactions with the phosphates. Tyr77 of SaMurB, and Val43 and Gly264 of TcMurB, make contacts with the ribityl sugar, and Val199 and Val161 stabilize the adenine conformation (Figure 6.7).

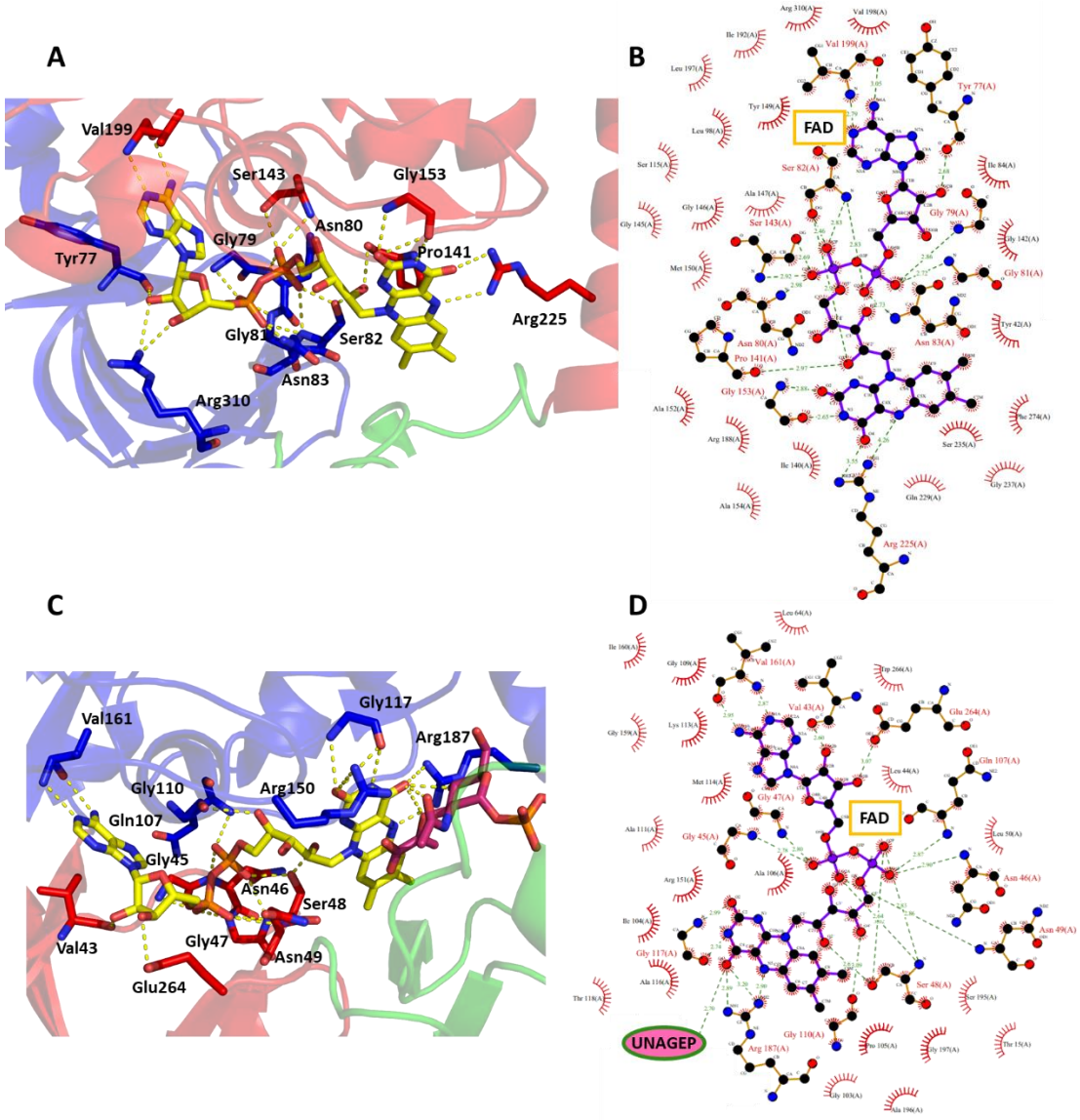

Figure 6.7. The FAD binding site in ScMurB (1HSK) and TcMurB (2GQU). (A) Detail of residues interacting with the FAD cofactor (CPK colored in yellow sticks) in type IIa ScMurB. Domain I is show in blue, domain II in red and domain III in green. **(C)** Detail of residues interacting with the FAD in type IIb TcMurB, UNAGEP (CPK colored in pink sticks). Domain I is shown in red, domain II in blue and domain III in green. LIGPLOT diagram of the interactions in **(B)** type IIa ScMurB and **(D)** type IIb TcMurB. FAD-binding sites show similar conformation, involving highly conserved H-bonds and van der Waals contacts in both MurBs. FAD is shown as purple ball-and-stick models. H-bonds and van der Waals interactions are indicated as green dashes and radiating red lines, respectively. In the crystal structure of TcMurB that contains UNAGEP, this substrate interacts also with O4 of the isoalloxazine ring of FAD.

Since TcMurB was solved in complex with its UNAGEP substrate, interactions between the protein-binding site and the substrate were identified (Figure 6.8). UNAGEP interacts with Arg119, Tyr150 and Arg151 residues of domain II and Cys198, Asn202, Asp213, His231, and Glu262 of domain III. During catalysis, Arg151 and Glu262 are proposed to stabilize the carbonic C2 of the enolpyruvyl portion of UNAGEP. The catalytic residue Cys198 participates as a promotor donor to quench the carbonic intermediate in the proton transfer to an enol that is formed during the second reduction step. In SaMurB, Ser238 occupies the position of Cys198 and therefore could play the same role in this organism (Benson et al., 2001; Kim et al., 2006). In this enzyme, Glu296 was also suggested to transfer a proton to the enolpyruvyl group of UNAGEP to stabilize the intermediate, while Try175 may bond with the N-acetyl moiety of UNAGEP. To probe the importance of both residues, E296A and Y175F mutants were generated and both showed loss of the ability to recognize the substrate (Nishida et al., 2006).

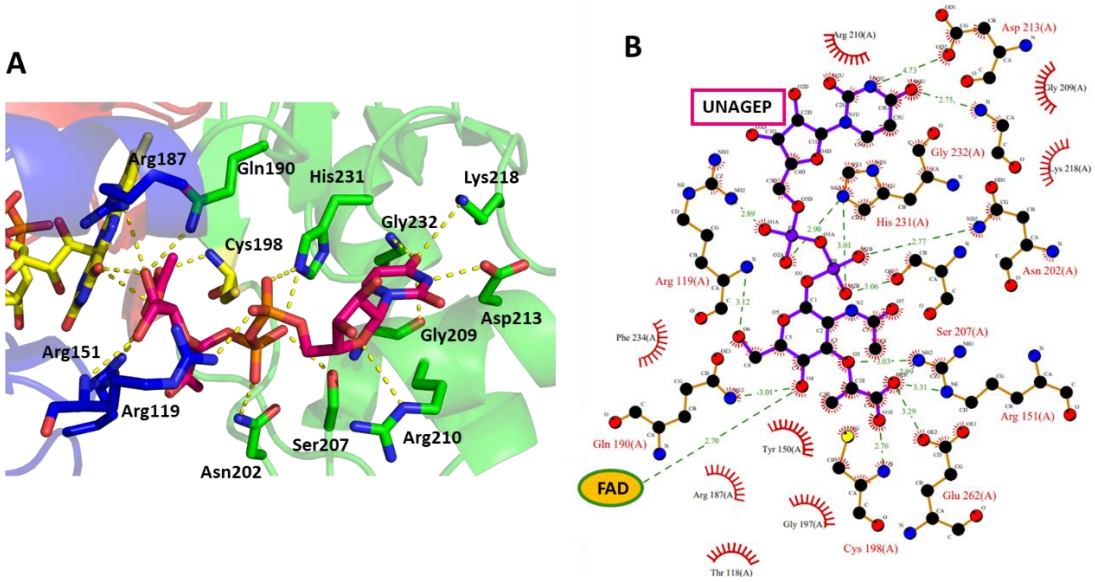

Figure 6.8. The interaction site of UNAGEP in TcMurB (4JAY). (A) Detail of residues interacting with UNAGEP (CPK colored in pink sticks). Domain I is shown in red, domain II in blue, and domain III in green. FAD and catalytic residue Cys198 are shown with carbon atoms in yellow sticks. **(B)** LIGPLOT diagram of the UNAGEP interaction. UNAGEP is shown as purple ball-and-stick model. H-bonds and van der Waals interactions are indicated as green dashes and radiating red lines, respectively.

Structural superposition of the reported complexes formed by MurB with $NADP^+$ (PaMurB, 4JAY) and with UNAGEP (TcMurB, 2GQU) showed that both substrates use the same binding pocket of the enzyme (Figure 6.9). The nicotinamide and enol pyruvyl moieties of the respective substrates being well aligned and positioned for hydride transfer to and from FAD. However, the flexibility of the substrate entrance channel allows the non-reactive parts of $NADP^+$ and UNAGEP to bind in different conformations. In addition, K^+ ion

observed in the TcMurB structure bound at the active site is thought to assist substrate orientation and binding (Constantine et al., 1997).

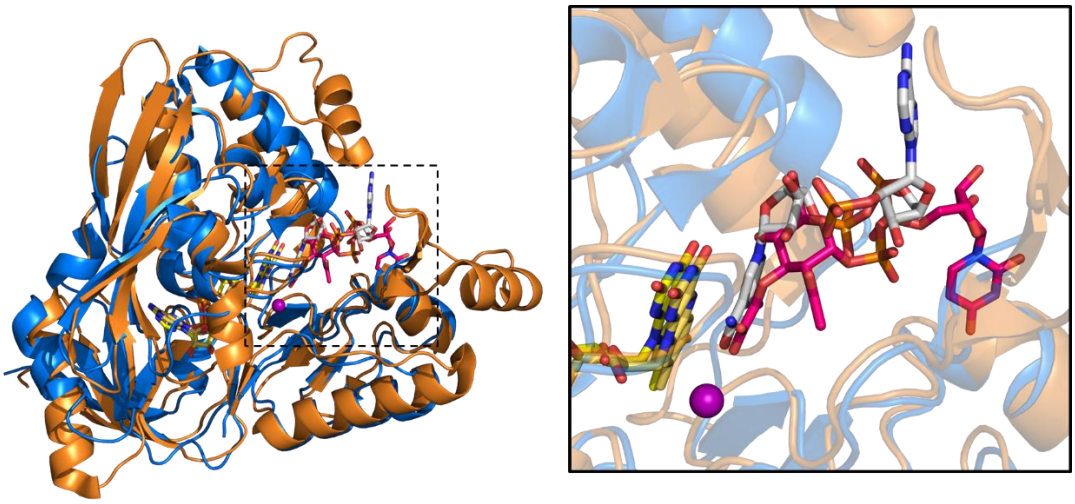

Figure 6.9. Structural superposition of PaMurB (4JAY) and TcMurB (2GQU). The two substrates use the same binding site but their conformation differ in the non-reactive parts. PaMurB structure is colored in orange, and TcMurB in blue. FAD (CPK in yellow sticks), UNAGEP (CPK in pink sticks), $NADP^+$ (CPK in grey sticks) and metal ion (purple sphere) are also shown.

Comparison of the structures of free and substrate-bound enzymes shows that in the presence of substrates, domain III undergoes rigid-body rotation towards domains I and II (Figure 6.6B). Thus, binding of the sugar substrate to MurB results in the closure of the substrate-binding channel over the substrate (Benson et al., 1996). In agreement, previous steady-state kinetic studies on EcMurB demonstrated weak and strong substrate inhibition by NADPH and UNAGEP, respectively, and the discovery of a ping-pong bi-bi double competitive substrate inhibition mechanism. Both molecules use the same binding pocket of the enzyme (Constantine et al., 1997) and therefore, cannot bind at once (Dhalla et al., 1995).

6.2.3 Inhibitors of MurB

Several compounds have been designed and synthesized as inhibitors of MurBs from different species (Figure 6.10). One of the most prominent is thiazolidinone, which is a biologically important heterocyclic ring with anti-inflammatory, antioxidant, antitumor, choleretic, and diuretic activities, among others. One of its derivatives, the 4-thiazolidinone has been considered a magic moiety because of its antimicrobial activities. The 4-thiazolidinone moiety has been proposed to mimic the diphosphate interactions of the UNAGEP substrate in the active site of MurB and can therefore be used in the design of inhibitors targeting MurB (Nirwan et al., 2019). In this category we can find also: i) the 2, 3, 5-Tri-substituted 4-thiazolidinones derivatives that inhibit the EcMurB enzyme at a low micromolar level when the R1 chain is substituted with n-butyl group, R2 is an aromatic

substituent and R3 is a methyl or hydrazide (Andres et al., 2000), ii) the 5-hydroxy-1H-pyrazol-3(2H)-one derivatives, with an inhibition score of IC_{50}^{S}=54 µM when R1 is a phenyl group and R2 (4-Cl) phenyl carboxamide (Gilbert et al., 2006), or iii) the 3, 5-dioxopyrazolidines derivatives, with R1 being 1,2-bis(4-chlorophenyl) inhibiting EcMurB and SaMurB with IC_{50}^{S} in the range of 4.1-6.8 µM and 4.3-10.3 µM, respectively. This last compound is a multi-target inhibitor, also proved in MurA and MurC (Yang et al., 2006).

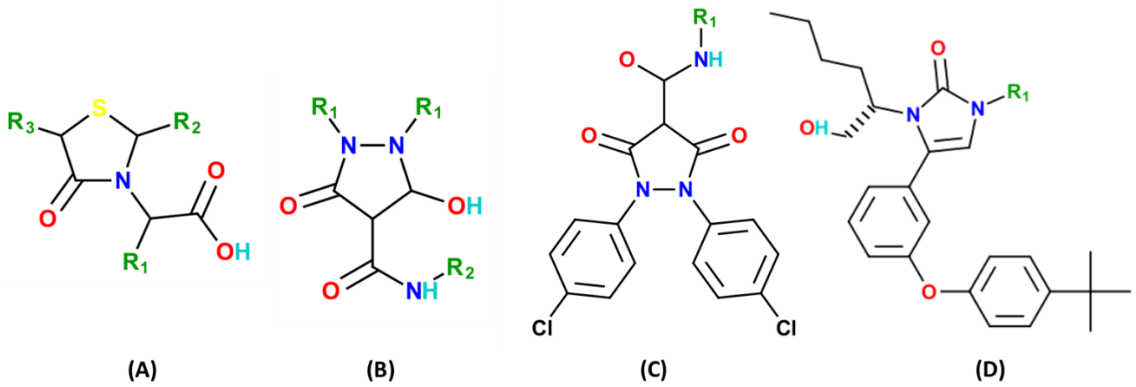

Figure 6.10. Inhibitors of MurB. Examples of derivatives of **(A)** 2, 3, 5-Tri-substituted 4-thiazolidinones, **(B)** 5-hydroxy-1H-pyrazol-3(2H)-one, **(C)** 3, 5-dioxopyrazolidines and **(D)** imidazolinones.

Other good MurB inhibitors are the imidazolinones derivatives. These compounds are heterocycles designed to mimic the diphosphate moiety of the UNAGEP substrate (Hrast et al., 2018). In this class of inhibitor, lipophilic compounds, where the substituent on R1 is allyl, benzyl, 3,4-dichlorobenzyl or 2-chlorophenethyl chains are essential for good MurB inhibition and to provide antibacterial activity of the whole cells (Bronson et al., 2003).

6.3 RESULTS

6.3.1 Overall characteristics of MurB from *B. ovis*

The *B. ovis* ATCC 25840 murB gene (BomurB), NCBI ID 45124764, localizes in chromosome I (NC_009505.1) with a locus tag BOV_RS06850, in the 1393194-1394162 specific region. A VIMSS analysis predicted that BomurB is located in an operon consisting of 15 genes organized in the following order: mraW, a hypothetical periplasmic protein, ftsI, murE, murF, mraY, murD, ftsW, murG, murC, murB, ddl, ftsQ, ftsA, and ftsZ (Figure 6.11). The ProtParam analysis of the BoMurB protein sequence indicated that it was composed of 322 amino acids and 4,889 atoms, with a Mw of 34,890 Da and a theoretical pI of 5.19. The theoretical extinction coefficient for apo-BoMurB at 280 nm, in water, was 21 mM^{-1} cm^{-1}. The instability index (II) was computed as 26.51, suggesting that BoMurB is a stable protein. The aliphatic index (83.29) and GRAVY score (-0.261) indicated that BoMurB is mainly hydrophilic. BoMurB sequence is organized in two Pfam domains. The first is a FAD_binding_4 Pfam domain (PF01565), commonly found in enzymes using FAD as a cofactor, many of them being oxygen-dependent oxidoreductases, while the second is a MurB_C domain (PF02873) unique to MurBs.

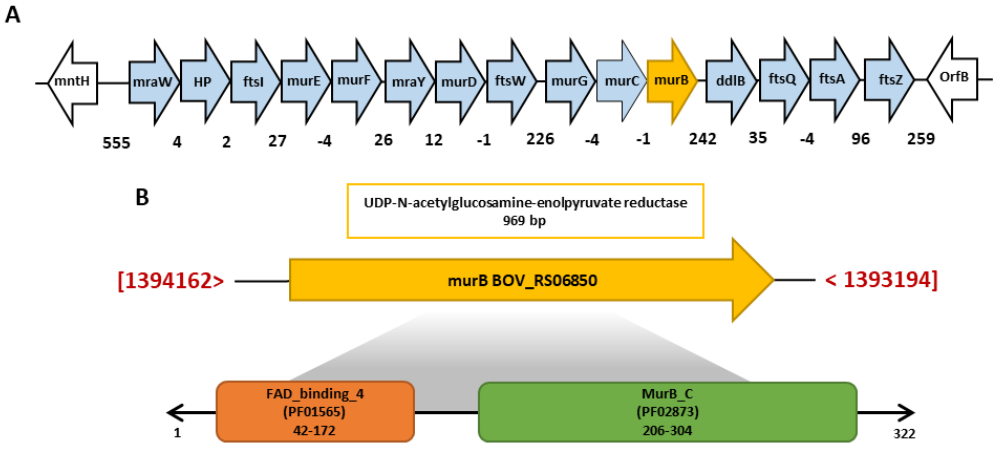

Figure 6.11. Genomic context of BoMurB and domain protein description. (A) Operon of genes involved in PG biosynthesis in *B. ovis*. The murB gene is shown in yellow. Nearby genes predicted to be in the same operon are colored in light blue. Genes upstream and downstream of the operon are shown in white. The arrowheads indicate the direction of transcription. The numbers below the genes indicate the intergenic distance between two adjacent genes. Negative numbers indicate overlapping genes. Each gene was labelled according to its name. **(B)** Genomic region that determines the precise location inside the genome (NC_009505.1: 1393M-13984M) flanked by a red strip of the 969 bp murB gene is shown by yellow arrow. Two boxes are displayed, indicating the Pfam domains associated with the 322 amino acids of the transcript: the FAD_binding_4 domain is shown in orange, and the MurB_C domain is highlighted in green.

6.3.2 Sequence and evolutionary analysis of MurB proteins in *Brucella* spp.

Following the methodology of section 5.3.2., 52 MurB protein sequences from 52 species of *Brucella* were retrieved (Table 6.1). *B. ovis*, as all studied brucellas, has a single gene coding for MurB. The BoMurB protein sequence exhibits significant resemblance to its counterparts in other *Brucella* species. *B. endophytica* displayed the lowest similarity to BoMurB (82% identity). On the other hand, *B. intermedia, B. haematophila, B. oryzae, B. gallinifaecis, B. tritici, B. rhizosphaerae, B. cytisi, B. pseudogringonensis, B. grignonensis, B. thiophenivorans, B. lupini, B. precoris, B. pituitosa, B. daejeonesis, B. anthropi* and *B. pseudointermedia* exhibited identity levels ranging from 90% to 95%, whereas the remaining species demonstrated identities exceeding 99%.

MSA and WebLogo analysis (Figure 6.12 and 6.13A) also revealed that the residues predicted to form the protein active site remain conserved across all examined *Brucella* sequences. Specifically, the amino acids expecting to contribute to the interaction with UNAGEP (including Tyr185, Phe237, Asn246, Asp250, Arg255, His268, and Cys269), $NADP^+$ (Arg222, Val225, and Gln226) as well as those interacting with both substrates (Arg186, Gly234, Ser235, Asn239, Ser244, Ala245, and Glu305) demonstrate complete conservation (100%). However, it's noteworthy that in the FAD binding site, the conservation pattern is not maintained for Asn209 and Asn210. From this analysis, it is apparent that the sequences of MurB in *Brucella* genus will produce proteins exhibiting high structural similarity. In addition, this sequence analysis classifies BoMurBs within type II, as they lack the Tyr-loop in their sequences. Moreover, they are categorized as type IIa due to the complete preservation of their catalytic residue as a serine, Ser235.

The MSA from Figure 6.12 was used for the phylogenetic analysis of MurB sequences from *Brucella*. The resulting tree revealed the presence of seven main clades (Figure 6.13B). Clade 1 (highlighted in red) comprises the only sequence of *B. endophytica* while, in agreement with the lower sequence identity with the rest of evaluated sequences it was the one more divergent in the tree (bootstrap > 98). For the rest of clades bootstrap values are below 70, also in agreement with the evaluated sequences having high identity among them. Nonetheless, the presented tree shows a single sequence in Clade 2 (highlighted in blue), that from *B. haematophila*. Clade 3 (highlighted in green) is composed of sequences from *B. thiophenivorans, B. gallinifaecis, B. pseudogrignonensis, B. grignonensis, B. pituitosa* and *B. rhizosphaerae.* Clade 4 (highlighted in yellow) includes *B. daejeonensis, B. oryzae, B. tritici, B. precoris, B. pseudintermedia, B. intermedia, B. lupine, B. anthropi* and

B. cytisi. Clade 5 (highlighted in pink) is relatively small, containing four sequences from *B.* sp. F96/2, *B.* sp. F23/97 and *B.* sp. UK1/97. Clade 6 (in cyan) contains the sequences *B. suis*, *B.* sp. 04-5288, *B. canis*, *B.* sp. 83/13, *B.* sp. BO2, *B.* sp. 458, *B. inopinata*, *B.* sp. 191011898, *B.* sp. 09RB8910, *B.* sp. 2280, *B.* sp. 6810 and *B.* sp. 10RB9215. And finally, the Clade 7 (in purple) contains the rest of the sequences, including *B. neotomae*, *B. ovis*, *B. melitensis*, *B. pinnipedialis* and *B. ceti*.

Table 6.1. List of *Brucella* strains with complete assembled genome for which MurB protein sequences are evaluated in this study. *B. ovis* is highlighted in bold.

Strain	Protein Code	Strain	Protein Code
B.abortus	CAJ11404.1	*B.tritici*	KAB2686354.1
B.anthropi	ABS14462.1	*B.vulpis*	CUW48863.1
B.canis	ABX62493.1	*B.*sp.BO2	QPN28988.1
B.ceti	EEH14089.1	*B.*sp.BO3	QMV26646.1
B.cytisi	OIS95238.1	*B.*sp.BTU1	QWK81521.1
B.daejeonensis	MBB5702670.1	*B.*sp.B13-0095	OEI83815.1
B.endophytica	GGA97327.1	*B.*sp.F5/06	ENT09866.1
B.gallinifaecis	TPF76630.1	*B.*sp.F5/99	EEY26588.1
B.grignonensis	OYR13668.1	*B.*sp.F8/99	ENT15393.1
B.haematophila	RIA06604.1	*B.*sp.F23/97	ENT08624.1
B.inopinata	SCD23702.1	*B.*sp.F96/2	ENT16331.1
B.intermedia	NVM40739.1	*B.*sp.NVSL 07-0026	EFG38343.2
B.lupini	OYR31771.1	*B.*sp.UK1/97	ENT22012.1
B.melitensis	AAL51762.1	*B.*sp.UK40/99	ENT22623.1
B.microti	ACU48407.1	*B.sp.04-5288*	ERU00206.1
B.neotomae	EEY04970.1	*B.*sp.09RB8471	APX70440.1
B.oryzae	PQA73407.1	*B.*sp.09RB8910	APY14490.1
B. ovis	**ABQ61769.1**	*B.*sp.10RB9215	SBW14254.1
B.pecoris	TNV09893.1	*B.*sp.191011898	CAB4326117.1
B.pinnipedialis	EEZ31531.1	*B.*sp.2002734562	AOG44048.1
B.pituitosa	KAB0571875.1	*B.*sp.2280	QGA56279.1
B.pseudintermedia	WP_176023020.1	*B.*sp.458	QTN99157.1
B.pseudogrignonensis	NNV22441.1	*B.*sp.56/94	ENT00829.1
B.rhizosphaerae	OYR12758.1	*B.*sp.63/311	ENT05230.1
B.suis	ABY38519.1	*B.*sp.6810	QNQ62927.1
B.thiophenivorans	OYR22275.1	*B.*sp.83/13	EEZ33319.1

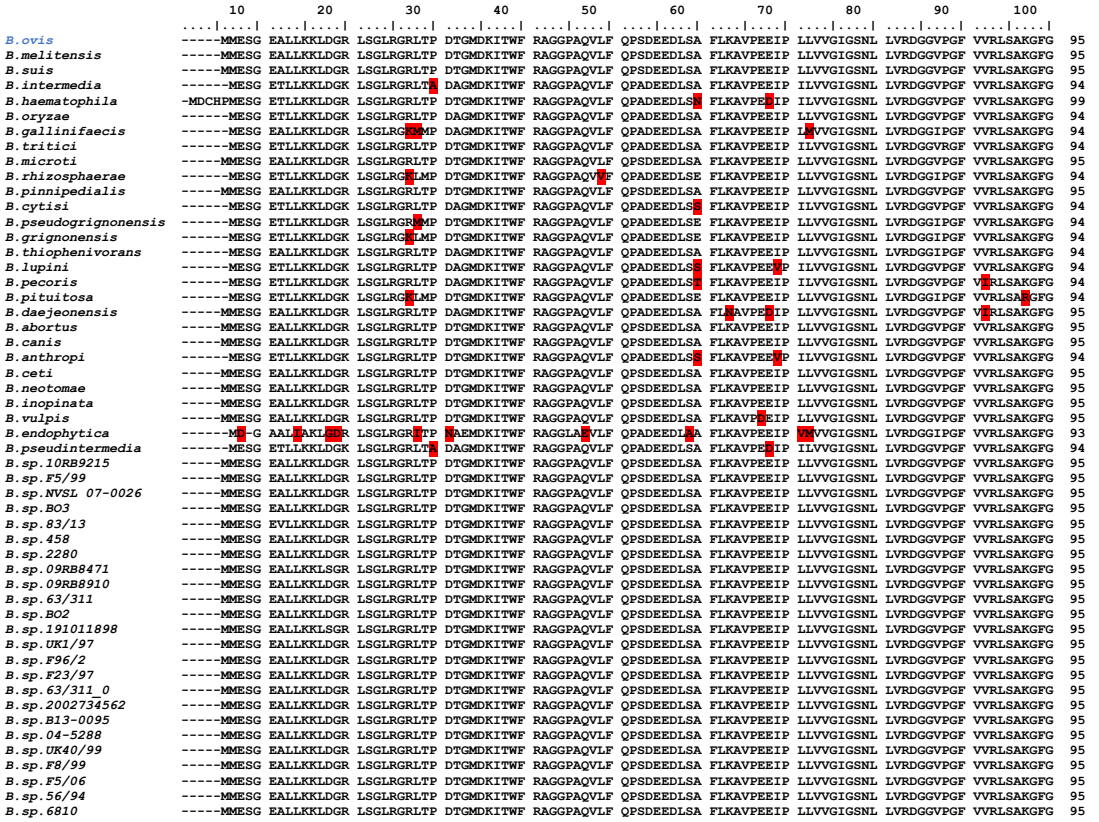

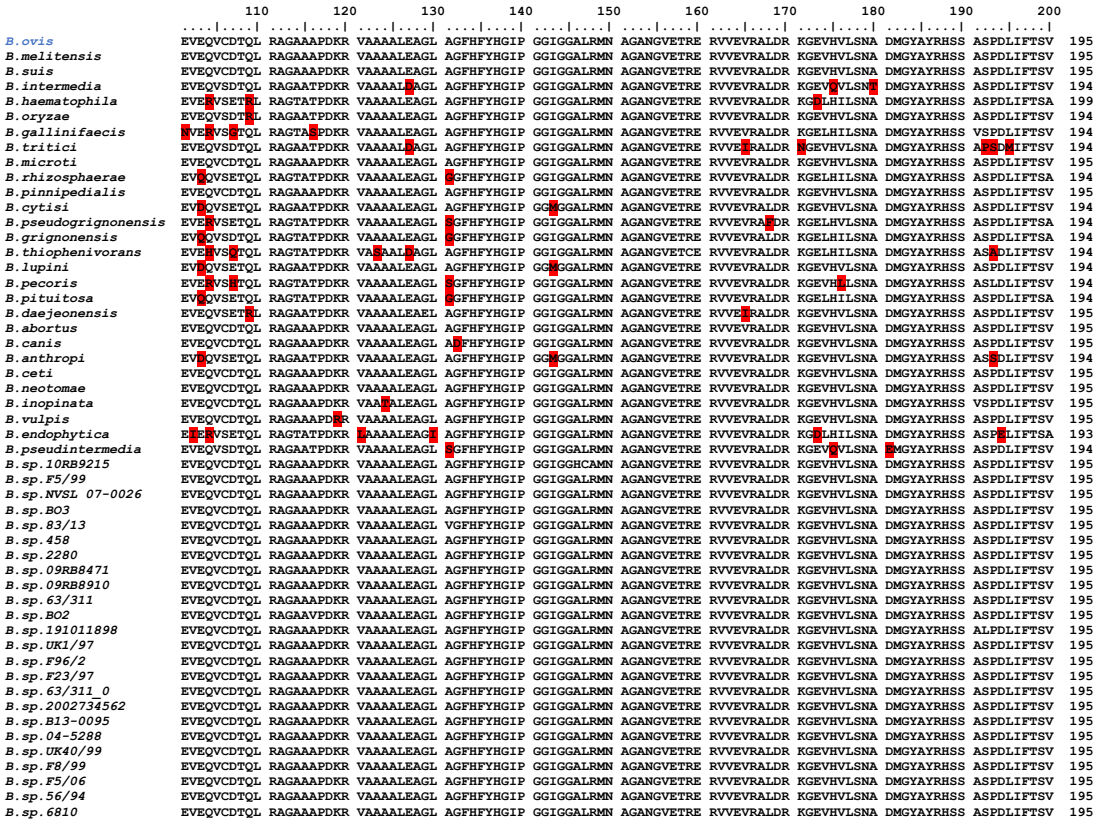

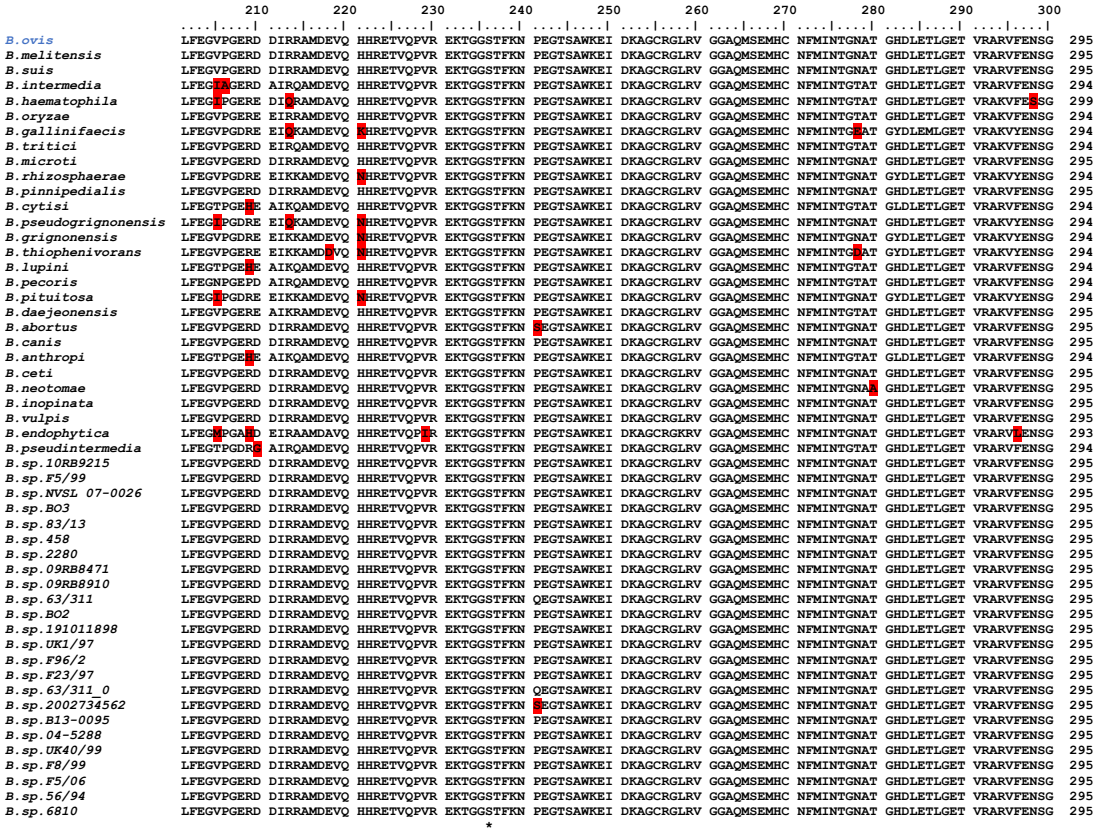

Figure 6.12. MurB sequence conservation within the *Brucella* genus. MSA (n=52) of MurBs from *Brucella* species in Table 6.1. The alignment was constructed with Clustal Omega. Residues not conserved in at least 90% of the sequences are highlighted in red. The Ser catalytic residue is marked with an asterisk.

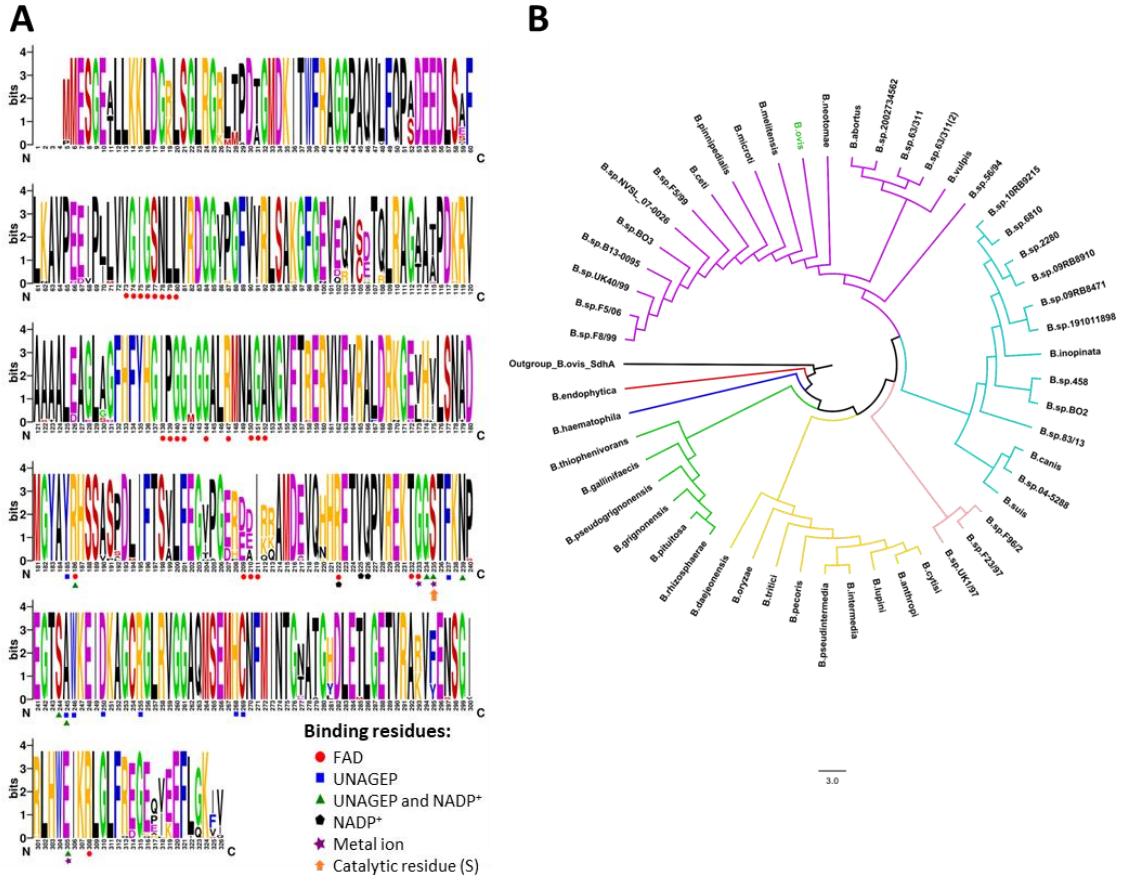

Figure 6.13. Residue conservation and evolution of MurB within *Brucella* spp. (A) Sequence Logo representing the MSA of MurBs from *Brucella* (n=52). Logo generated with WebLogo. Residues presumably involved in cofactor and substrate binding, by similarity with other MurB proteins, are indicated underneath the logo: Red circle, FAD; blue square, UNAGEP; green triangles, UNAGEP and $NADP^+$; black pentagon, $NADP^+$; purple stars, catalytic metal ion; catalytic residue (Ser), orange arrow. **(B)** Phylogenetic relationship of MurBs from *Brucella*. Tree was built using the above shown MSA, the Maximum Likelihood method and JTT matrix-based model with MEGA X. The tree with the highest log likelihood (-4086.20.78) is shown. Bootstrap analysis of 500 replicates. This analysis involved the above aligned 52 MurA sequences from *Brucella* as well as the *B. ovis* SdhA sequence as outgroup. Branch lengths are proportional to the number of substitutions per site (scale beside). There was a total of 613 positions in the final dataset. The tree groups the sequences in seven main clusters: Clade 1 (bootstrap > 98) in red color, Clade 2 (bootstrap > 34) in blue, Clade 3 (bootstrap > 69) in green, Clade 4 (bootstrap > 38) in yellow, Clade 5 (bootstrap > 64) in pink, Clade 6 in cyan and Clade 7 in purple, these last two clades diverged in some subclades.

6.3.3 Sequence and evolutionary analysis of MurB proteins within bacterial species

Conservation of residues in MurB sequences from various bacteria was also examined. The analysed sequences included representatives from the ESKAPE group, as well as other pathogens and non-pathogens found in humans and animals. A total of 57 MurB protein sequences were collected and categorized into two types, type I and type II, based on the presence of the Tyr-loop. According to the detailed information provided in Table 6.2, 17 sequences were classified as type I, while 42 sequences were classified as type II. Furthermore, within the type II ones, 36 sequences belong to group IIa, including BoMurB,

and 4 sequences to group IIb. Notably, the sequence of *A. phagocytophilum* showed a tyrosine residue at the position expected for either the catalytic serine or cysteine (Figure 6.14). Type IIa and IIb MurB homologues from *B. quintana* (WP_038525224.1), *B. schoenbuchensis* (WP_010703986.1) and *S. meliloti* (WP_010969746.1) show the highest sequence identity (76%) to BoMurB, while the remaining MurB type II sequences show identities ranging from 71 to 48%. Sequences with lower identity percentages (≤ 40%) regarding BoMurB correspond to the MurB type I sequences. Despite variations in identity among the evaluated sequences, a significant number of highly conserved residues and motifs are preserved (pink and grey residues in Figure 6.14). The WebLogos obtained from the MSA for sequences of type I (Figure 6.15A) and type II (Figure 6.15B) show some of these conserved residues and motifs corresponding to the FAD binding site: namely ^{69}GxGSNxLxxxxxG^{82}, ^{133}GLExLxLIPGxxG(A/S)xPxQNxGAYGxE^{158} and ^{188}YRxS^{191} for type I and ^{107}GxGSNx(L/I)xxDxG^{118}, ^{164}GLEFxxGIPGxxGGAxxMNAGxxG^{187} and ^{220}YRxS^{223} for type II. Additionally, the motifs ^{268}xxxGSFF(K/T)NPxV^{279}, ^{304}(P/V)x(Y/F)P(Q/A)xxG^{311}, ^{315}KLAA(G/A)WLI(D/E)xxxxKG^{329}, ^{349}(Q/H)(A/T)L^{351} and ^{383}LxPE^{386} in type I MurBs and ^{277}xxGSxF(K/R)(N/R)P^{285}, ^{310}GL(K/R)G^{313}, ^{322}SxxHx(N/G)F^{328} and ^{360}LxxE^{363} in type II sequences, which are envisaged to be involved in substrate and metal ion binding. These motifs contain an important number of residues (underlined) that will surely play relevant roles in the structural organization of MurB in different species as well as in the reaction MurB catalyzes. It is worth to note that the WebLogo analysis was conducted without the MurB sequence from *M. lutaus* (WP_010080355.1). This particular sequence was excluded because of its lengthy nature, caused by the insertion of two loops not found in any other sequence, that resulted in two long gaps in the Logo.

Table 6.2. List of bacteria species for which MurB sequences are evaluated in this study. Column "Species Name" highlights in blue those species corresponding to virulent and antibiotic resistant bacterial pathogens known as ESKAPE; in light orange animal pathogens and in dark orange human pathogens. Column "Short Species Name" highlights in green those species for which MurB has been purified and structurally or functionally characterized. *B. ovis* is highlighted in bold.

Type	Species Name	Short Species Name	Access Code	Gram	Phylum	Class
I	*Acinetobacter baumannii*	*A.baumannii*	WP_001166922.1	negative	Proteobacteria	Gammaproteobacteria
	Azotobacter vinelandii	*A.vinelandii*	WP_012700115.1	negative	Proteobacteria	Alphaproteobacteria
	Corynebacterium ammoniagenes	*C.ammoniagenes*	WP_168939647.1	positive	Actinobacteria	Actinobacteria
	Enterobacter sp. *Bisph*1	*Enterobacter*	WP_039054657.1	negative	Proteobacteria	Gammaproteobacteria
	Escherichia coli	*E.coli*	WP_001016699.1	negative	Proteobacteria	Gammaproteobacteria
	Haemophilus influenzae	*H.influenzae*	WP_005694036.1	negative	Proteobacteria	Gammaproteobacteria
	Klebsiella pneumoniae	*K.pneumoniae*	WP_002883510.1	negative	Proteobacteria	Gammaproteobacteria
	Mycobacterium marinum[a]	*M.marinum*	WP_012392749.1	positive	Actinobacteria	Actinobacteria
	Mycobacterium tuberculosis[a]	*M.tuberculosis*	WP_003402354.1	positive	Actinobacteria	Actinobacteridae
	Micrococcus luteus	*M.luteus*	WP_010080355.1	positive	Actinobacteria	Actinomycetales
	Neisseria gonorrhoeae	*N.gonorrhoeae*	WP_003692788.1	negative	Proteobacteria	Betaproteobacteria
	Porphyromonas gingivalis	*P.gingivalis*	WP_004585516.1	negative	Bacteroidetes	Bacteroidia
	Pseudarthrobacter chlorophenolicus	*P.chlorophenolicus*	ACL40701.1	positive	Actinobacteria	Actinomycetales
	Pseudomonas aeruginosa	*P.aeruginosa*	WP_003106928.1	negative	Proteobacteria	Gammaproteobacteria
	Salmonella enterica subsp. enterica serovar Typhimurium[a]	*S.enterica*	WP_000149795.1	negative	Proteobacteria	Gammaproteobacteria
	Shigella dysenteriae serotype 1	*S.dysenteriae*	WP_001016672.1	negative	Proteobacteria	Gammaproteobacteria
	Vibrio cholerae O1 biovar El Tor str. N16961	*V.cholerae*	NP_229972.1	negative	Proteobacteria	Gammaproteobacteria
IIa	*Acaryochloris marina*	*A.marina*	WP_012162328.1	negative	Cyanobacteria	Cyanophyceae
	Acetivibrio thermocellus	*A.thermocellus*	ABN51353.1	positive	Firmicutes	Clostridia
	Anabaena PCC 7120 */nostoc*	*Nostoc*	WP_010999192.1	negative	Cyanobacteria	--
	Anaplasma phagocytophilum[b]	*A.phagocytophilum*	WP_011450845.1	negative	Proteobacteria	Alphaproteobacteria
	Bacillus licheniformis	*B.licheniformis*	WP_003181550.1	positive	Firmicutes	Bacilli
	Bacillus subtilis	*B.subtilis*	WP_003232182.1	positive	Firmicutes	Bacilli
	Bartonella quintana	*B.quintana*	WP_038525224.1	negative	Proteobacteria	Alphaproteobacteria
	Bartonella schoenbuchensis	*B.schoenbuchensis*	WP_010703986.1	negative	Proteobacteria	Alphaproteobacteria
	***Brucella ovis* (strain ATCC 25840)**[a]	***B.ovis***	**ABQ61769.1**	**negative**	**Proteobacteria**	**Alphaproteobacteria**
	Campylobacter sp.	*Campylobacter*	WP_002858257.1	negative	Proteobacteria	Epsilonproteobacteria
	Candidatus pelagibacter	*C.pelagibacter*	MAJ22417.1	negative	Proteobacteria	Alphaproteobacteria
	Chloroflexus aggregans	*C.aggregans*	WP_015941573.1	positive	Chloroflexi	Chloroflexi
	Enterococcus faecium	*E.faecium*	WP_070703712.1	positive	Firmicutes	Bacilli
	Francisella tularensis[a]	*F.tularensis*	WP_003022017.1	negative	Proteobacteria	Gammaproteobacteria
	Gloeobacter violaceus	*G.violaceus*	WP_011142314.1	negative	Cyanobacteria	Gloeobacteria
	Gluconobacter oxydans	*G.oxydans*	WP_011251756.1	negative	Proteobacteria	Alphaproteobacteria
	Helicobacter pylori	*H. pylori*	WP_000894903.1	negative	Proteobacteria	Epsilonproteobacteria
	Lactiplantibacillus plantarum	*L.plantarum*	WP_003641067.1	positive	Firmicutes	Bacilli
	Legionella pneumophila[a]	*L.pneumophila*	WP_016357031.1	negative	Proteobacteria	Gammaproteobacteria
	Listeria monocytogenes[c]	*L.monocytogenes*	WP_010990117.1	positive	Firmicutes	Bacilli
	Paracoccus yeei	*P.yeei*	WP_099649959.1	negative	Proteobacteria	Alphaproteobacteria
	Paulinella chromatophora	*P.chromatophora*	YP_002049066.1	microalga	Cercozoa	Imbricatea
	Phenylobacterium zucineum	*P.zucineum*	WP_012522872.1	negative	Proteobacteria	Alphaproteobacteria
	Rhodobacter capsulatus	*R.capsulatus*	WP_013066566.1	negative	Proteobacteria	Alphaproteobacteria
	Rhodopseudomonas palustris	*R.palustris*	WP_042441207.1	negative	Proteobacteria	Alphaproteobacteria
	Rickettsia rickettsii[c]	*R.rickettsii*	WP_012150547.1	negative	Proteobacteria	Alphaproteobacteria
	Rickettsia typhi[c]	*R.typhi*	WP_011190706.1	negative	Proteobacteria	Alphaproteobacteria
	Ruegeria pomeroyi	*R.pomeroyi*	WP_011046943.1	negative	Proteobacteria	Alphaproteobacteria
	Sinorhizobium meliloti	*S.meliloti*	WP_010969746.1	negative	Proteobacteria	Alphaproteobacteria
	Sphingomonas paucimobilis	*S.paucimobilis*	WP_007405407.1	negative	Proteobacteria	Alphaproteobacteria
	Staphylococcus aureus	*S.aureus*	WP_000608440.1	positive	Firmicutes	Bacilli
	Streptococcus pneumoniae	*S.pneumoniae*	WP_000116181.1	positive	Firmicutes	Bacilli
	Synechococcus sp.	*Synechococcus*	WP_011126906.1	negative	Cyanobacteria	--
	Thermotoga maritima	*T.maritima*	AAD36780.1	negative	Thermotogae	Thermotogae
	Treponema denticola	*T.denticola*	WP_002680945.1	negative	Spirochaetes	Spirochaetia
	Xanthobacter autotrophicus	*X.autotrophicus*	ABS65582.1	negative	Proteobacteria	Alphaproteobacteria
IIb	*Chlamydia pecorum*[c]	*C. pecorum*	WP_024010151.1	negative	Chlamydiae	Chlamydiia
	Chlamydia trachomatis[c]	*C. trachomatis*	WP_009873442.1	negative	Chlamydiae	Chlamydiia
	Thermus thermophiles	*T.thermophilus*	WP_011228429.1	negative	Deinococcus-Thermus	Deinococci
	Wolbachia pipientis	*W.pipientis*	WP_010082163.1	negative	Proteobacteria	Alphaproteobacteria

[a] Facultative intracellular organism.
[b] Tyr as proton donor, neither Ser (type IIa) nor Cys (type IIb).
[c] Obligatory intracellular organism.

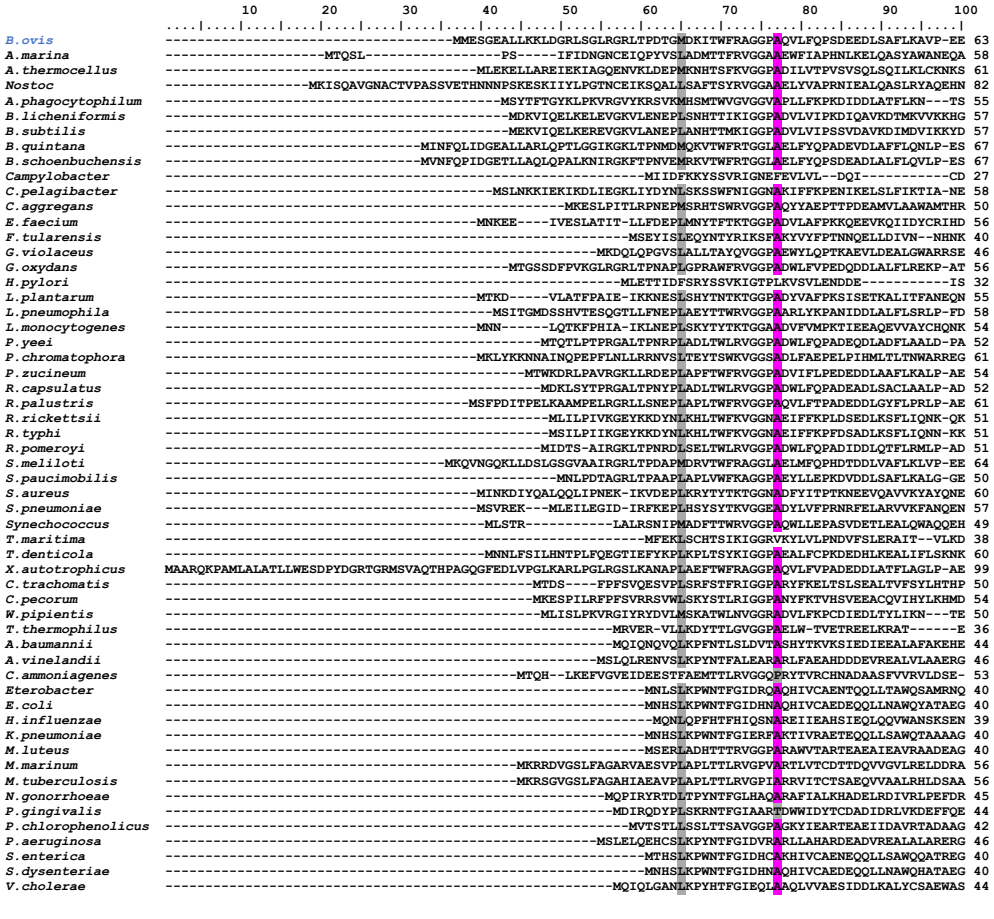
B.ovis
A.marina
A.thermocellus
Nostoc
A.phagocytophilum
B.licheniformis
B.subtilis
B.quintana
B.schoenbuchensis
Campylobacter
C.pelagibacter
C.aggregans
E.faecium
F.tularensis
G.violaceus
G.oxydans
H.pylori
L.plantarum
L.pneumophila
L.monocytogenes
P.yeei
P.chromatophora
P.zucineum
R.capsulatus
R.palustris
R.rickettsii
R.typhi
R.pomeroyi
S.meliloti
S.paucimobilis
S.aureus
S.pneumoniae
Synechococcus
T.maritima
T.denticola
X.autotrophicus
C.trachomatis
C.pecorum
W.pipientis
T.thermophilus
A.baumannii
A.vinelandii
C.ammoniagenes
Eterobacter
E.coli
H.influenzae
K.pneumoniae
M.luteus
M.marinum
M.tuberculosis
N.gonorrhoeae
P.gingivalis
P.chlorophenolicus
P.aeruginosa
S.enterica
S.dysenteriae
V.cholerae

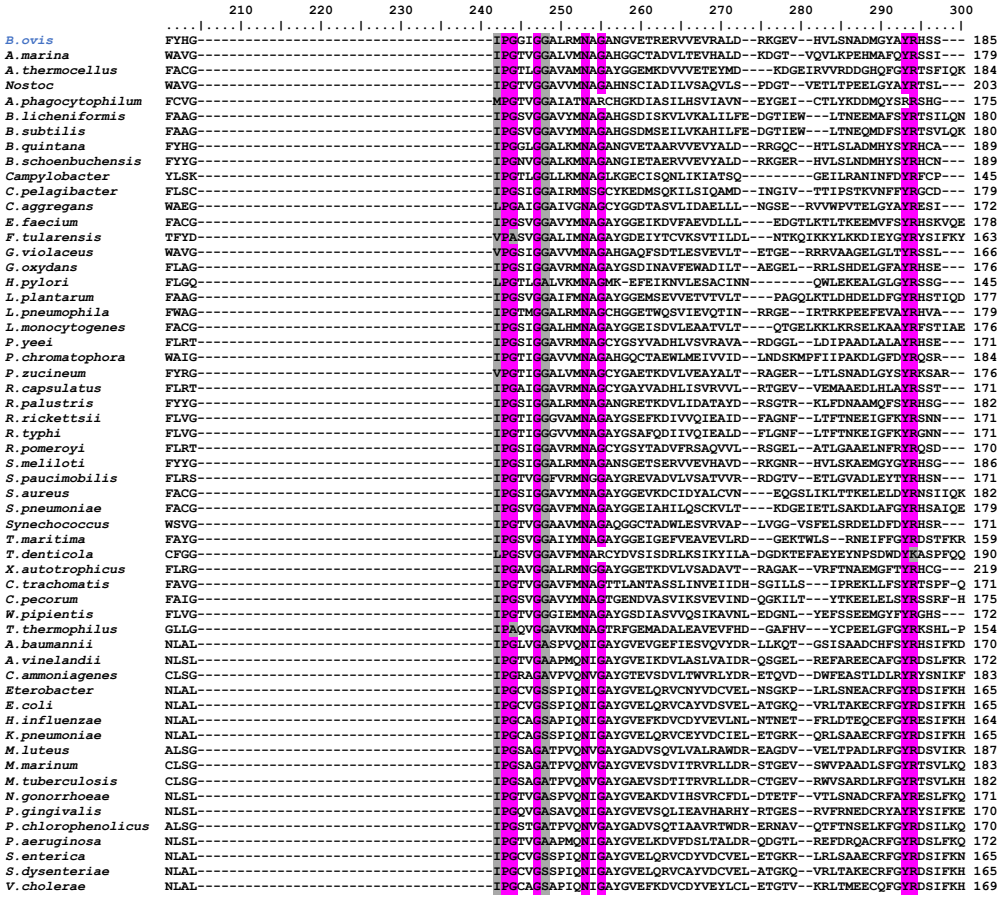
210 220 230 240 250 260 270 280 290 300
B.ovis FYHG---------- IPGGIGGALRMNAGANGVETRERVVEVRALD--RKGEV--HVLSNADMGYAYRHSS--- 185
A.marina WAVG---------- IPGTVGGALVMNAGAHGGCTADVLTEVHALD--KDGT--VQVLKPEHMAFQYRSSI--- 179
A.thermocellus FACG---------- IPGTLGGAVAMNAGAYGGEMKDVVVETEYMD----KDGEIRVVRDDGHQFGYRTSFIQK 184
Nostoc WAVG---------- IPGTVGGAVVMNAGAHNSCIADILVSAQVLS--PDGT--VETLTPEELGYAYRTSL--- 203
A.phagocytophilum FCVG---------- MPGTVGGAIATNARCHGKDIASILHSVIAVN--EYGEI--CTLYKDDMQYSRRSHG--- 175
B.licheniformis FAAG---------- IPGSVGGAVYMNAGAHGSDISKVLVKALILFE-DGTIEW---LTNEEMAFSYRTSILQN 180
B.subtilis FAAG---------- IPGSVGGAVYMNAGAHGSDMSEILVKAHILFE-DGTIEW---LTNEQMDFSYRTSVLQK 180
B.quintana FYHG---------- IPGGLGGALKMNAGANGVETAARVVEVYALD--RRGQC--HTLSLADMHYSYRHCA--- 189
B.schoenbuchensis FYYG---------- IPGNVGGALKMNAGANGIETAERVVEVYALD--RKGER--HVLSLNDMHYSYRHCN--- 189
Campylobacter YLSK---------- IPGTLGGLLKMNAGLKGECISQNLIKIATSQ---------GEILRANINFDYRFCP--- 145
C.pelagibacter FLSC---------- IPGSIGGAIRMNSGCYKEDMSQKILSIQAMD--INGIV--TTIPSTKVNFFYRGCD--- 179
C.aggregans WAEG---------- LPGAIGGAIVGNAGCYGGDTASVLIDAELLL--NGSE--RVVWPVTELGYAYRESI--- 172
E.faecium FACG---------- IPGSVGGAVYMNAGAYGGEIKDVFAEVDLLL----EDGTLKTLTKEEMVFSYRHSKVQE 178
F.tularensis TFYD---------- VPASVGGALIMNAGAYGDEIYTCVKSVTILDL---NTKQIKKYLKKDIEYGYRYSIFKY 163
G.violaceus WAVG---------- VPGSIGGAVVMNAGAHGAQFSDTLESVEVLT--ETGE--RRRVAAGELGLTYRSSL--- 166
G.oxydans FLAG---------- IPGSIGGAVRMNAGAYGSDINAVFEWADILT--AEGEL--RRLSHDELGFAYRHSE--- 176
H.pylori FLGQ---------- LPGTLGALVKMNAGMK-EFEIKNVLESACINN--------QWLEKEALGLGYRSSG--- 145
L.plantarum FAAG---------- IPGSVGGAIFMNAGAYGGEMSEVVETVTVLT----PAGQLKTLDHDELDFGYRHSTIQD 177
L.pneumophila FWAG---------- IPGTMGGALRMNAGCHGGETWQSVIEVQTIN--RRGE--IRTRKPEEFEVAYRHVA--- 179
L.monocytogenes FACG---------- IPGSIGGALHMNAGAYGGEISDVLEAATVLT----QTGELKKLKRSELKAAYRFSTIAE 176
P.yeei FLRT---------- IPGSIGGAVRMNAGCYGSYVADHLVSVRAVA--RDGGL--LDIPAADLALAYRHSE--- 171
P.chromatophora WAIG---------- IPGTIGGAVVMNAGAHGQCTAEWLMEIVVID--LNDSKMPFIIPAKDLGFDYRQSR--- 184
P.zucineum FYRG---------- VPGTIGGALVMNAGCYGAETKDVLVEAYALT--RAGER--LTLSNADLGYSYRKSAR--- 176
R.capsulatus FLRT---------- IPGAIGGAVRMNAGCYGAYVADHLISVRVVL--RTGEV--VEMAAEDLHLAYRSST--- 171
R.palustris FYYG---------- IPGSIGGALRMNAGANGRETKDVLIDATAYD--RSGTR--KLFDNAAMQFSYRHSG--- 182
R.rickettsii FLVG---------- IPGTIGGGVAMNAGAYGSEFKDIVVQIEAID--FAGNF--LTFTNEEIGFKYRSNN--- 171
R.typhi FLVG---------- IPGTIGGGVVMNAGAYGSAFQDIIVQIEALD--FLGNF--LTFTNKEIGFKYRCNN--- 171
R.pomeroyi FLRT---------- IPGSIGGAVRMNAGCYGSYTADVFRSAQVVL--RSGEL--ATLGAAELNFRYRQSD--- 170
S.meliloti FYYG---------- IPGSIGGALRMNAGANSGETSERVVEVHAVD--RKGNR--HVLSKAEMGYGYRHSG--- 186
S.paucimobilis FLRS---------- IPGAVGGALRMNGGAYGGETKDVLVSADAVT--RAGAK--VRFTNAEMGFTYRHCG--- 219
S.aureus FACG---------- IPGSIGGAVYMNAGAYGGEVKDCIDYALCVN----EQGSLIKLTTKELELDYRNSIIQK 182
S.pneumoniae FACG---------- IPGSVGGAVFMNAGAYGGEIAHILQSCKVLT----KDGEIETLSAKDLAFGYRHSAIQE 179
Synechococcus WSVG---------- IPGTVGGAAVMNAGAQGGCTADWLESVRVAP--LVGG-VSFELSRDELDFDYRHSR--- 171
T.maritima FAYG---------- IPGSVGGAIYMNAGAYGGEIGEFVEAVEVLRD---GEKTWLS--RNEIFFGYRDSTFKR 159
T.denticola CFGG---------- LPGSVGGAVFMNARCYDVSISDRLKSIKYILA-DGDKTEFAEYEYNPSDWDYKASPFQQ 190
X.autotrophicus FLRG---------- IPGAVGGALRMNGGAYGGETKDVLVSADAVT--RAGAK--VRFTNAEMGFTYRHCG--- 219
C.trachomatis FAVG---------- IPGTVGGAVFMNAGTTLANTASSLINVEIIDH-SGILLS---IPREKLLFSYRTSPF-Q 171
C.pecorum FAIG---------- IPGSVGGAVYMNAGTGENDVASVIKSVEVIND-QGKILT---YTKEELELSYRSSRF-H 175
W.pipientis FLVG---------- IPGTVGGGIEMNAGAYGSDIASVVQSIKAVNL-EDGNL--YEFSSEEMGYFYRGHS--- 172
T.thermophilus GLLG---------- IPAQVGGAVKMNAGTRFGEMADALEAVEVFHD--GAFHV---YCPEELGFGYRKSHL-P 154
A.baumannii NLAL---------- IPGLVGASPVQNIGAYGVEVGEFIESVQVYDR-LLKQT--GSISAADCHFSYRHSIFKD 170
A.vinelandii NLSL---------- IPGTVGAAPMQNIGAYGVEIKDVLASLVAIDR-QSGEL--REFAREECAFGYRDSLFKR 172
C.ammoniagenes CLSG---------- IPGRAGAVPVQNVGAYGTEVSDVLTWVRLYDR-ETQVD--DWFEASTLDLRYRYSNIKF 183
Eterobacter NLAL---------- IPGCVGSSPIQNIGAYGVELQRVCNYVDCVEL-NSGKP--LRLSNEACRFGYRDSIFKH 165
E.coli NLAL---------- IPGCVGSSPIQNIGAYGVELQRVCAYVDSVEL-ATGKQ--VRLTAKECRFGYRDSIFKH 165
H.influenzae NLAL---------- IPGCAGSAPIQNIGAYGVEFKDVCDYVEVLNL-NTNET--FRLDTEQCEFGYRESIFKH 164
K.pneumoniae NLAL---------- IPGCAGSSPIQNIGAYGVELQRVCEYVDCIEL-ETGRK--QRLSAAECRFGYRDSIFKH 165
M.luteus ALSG---------- IPGSAGATPVQNVGAYGADVSQVLVALRAWDR-EAGDV--VELTPADLRFGYRDSVIKR 187
M.marinum CLSG---------- IPGSAGATPVQNVGAYGVEVSDVITRVRLLDR-STGEV--SWVPAADLSFGYRTSVLKQ 183
M.tuberculosis CLSG---------- IPGSAGATPVQNVGAYGAEVSDTITRVRLLDR-CTGEV--RWVSARDLRFGYRTSVLKH 182
N.gonorrhoeae NLSL---------- IPGTVGASPVQNIGAYGVEAKDVIHSVRCFDL-DTETF--VTLSNADCRFAYRESLFKQ 171
P.gingivalis NLSL---------- IPGQVGASAVQNIGAYGVEVSQLIEAVHARHY-RTGES--RVFRNEDCRYAYRYSIFKE 170
P.chlorophenolicus ALSG---------- IPGSTGATPVQNVGAYGADVSQTIAAVRTWDR-ERNAV--QTFTNSELKFGYRDSILKQ 170
P.aeruginosa NLSL---------- IPGTVGAAPMQNIGAYGVELKDVFDSLTALDR-QDGTL--REFDRQACRFGYRDSLFKQ 172
S.enterica NLAL---------- IPGCVGSSPIQNIGAYGVELQRVCDYVDCVEL-ETGKR--LRLSAAECRFGYRDSIFKN 165
S.dysenteriae NLAL---------- IPGCVGSSPIQNIGAYGVELQRVCAYVDCVEL-ATGKQ--VRLTAKECRFGYRDSIFKH 165
V.cholerae NLAL---------- IPGCAGSAPIQNIGAYGVEFKDVCDYVEYLCL-ETGTV--KRLTMEECQFGYRDSIFKH 169
310 320 330 340 350 360 370 380 390 400
B.ovis -----ASPDL------IFTSVLFEGVPG---------- ERDDIRRAMDEVQHHRETV------QPVR-EKTGGSTFKN 235
A.marina -----LQQS-----PKPVLLGVEQLHAN---------- QSAEQVKATTQSHLDHRLS-------TQPYDWPSCGSVFRN 231
A.thermocellus NS----------GIVIKTSMKLKKG---------- NKEEIKALMDDLTQRRQEK------QPLE-MPSAGSIFRN 232
Nostoc -----LQGS-----NRVVTQATEQLQPG---------- FDPAYVTATTKQHKQMRLT-------TQPYNFPSCGSVFRN 255
A.phagocytophilum -----LEGRW------VFVEARFVGNPA---------- ELNTIRNTMSELLIKRNAT------QPIYYGKSIGYIFQD 226
B.licheniformis KRP----------GICLEAVLQLEQK---------- ERDQIVAQMQKNKDYRKET------QPVS-NPCAGSIFRN 229
B.subtilis KRP----------GVCLEAVLQLEQK---------- DKESIVQQMQSNKDYRKNT------QPYS-SPCAGSIFRN 229
B.quintana -----VPEDF------IFTAALLEGKPG---------- NKGDIRAAMDEVALHRESV------QPVR-EKTGGSTFRN 239
B.schoenbuchensis -----VSEEL-----IFTAAVLEGKPG---------- DKDNIHAAMNEVVLHREKV------QPVR-EKTGGSTFRN 239
Campylobacter ----------LNTHFFWAEFK---------- LNFGFDTLKDEALKNARSN-------QPSG--ASFGSIFKN 188
C.pelagibacter -----LSEDL-----IFLSVTLKGNIK---------- QKKEINEKMKKFINDKEKS------QPNK-IKTCGSTFKN 229
C.aggregans -----LKRPGADGVPPLVLAGRFRLHR---------- ADPKVLMARIGAIAAERKR-------KTPAG-SSCGSVFKN 227
E.faecium LR----------AIVLEARFSLQTG---------- DYEAIKARMDELTELRQSK------QPLE-YPSCGSVFKR 226
F.tularensis MKD----------ICILSAEFEFEYK---------- SKQEIKAKLDDIYSRRLSN------LPQ--KPTAGSVFKR 211
G.violaceus -----LQQR-----DWVVLSARLRLAPG---------- HQPARLIEHIDEFNTFRHR------TQPSGFPNCGSVFRN 218
G.oxydans -----LPEGS------VVIRASLRGTPD---------- NADAIRSRIADIRASREAS------QPVR-ARTGGSTFRN 226
H.pylori ----------FSGVVLRARFK---------- KTHGFREGVLKACQSMRKS-------HPKL--PNFGSCFKN 188
L.plantarum YD----------DIVVSVTFGLKPG---------- NQTKIQARMDELNTLRAAK------QPLE-WPSCGSVFKR 225
L.pneumophila ----GLGD------EWFISAKLQLSPG---------- NKET-SLQLIKDLLAHRAK-------TQPTNEYNCGSVFRN 229
L.monocytogenes KN----------YIVLDATFSLALE---------- EKNLIQAKMDELTAAREAK------QPLE-YPSCGSVFKR 224
P.yeei -----LPPGC------VLTRATFRANRG---------- EPADLAAKMQDQLARRDAS------QPTR-DRSAGSTFRN 221
P.chromatophora -----LQEE-----NLVVISARFRLKPG---------- FLPVKLLNKTKTNLSNRIN-------SQPYKNPSCGSVFRN 236
P.zucineum ----AAAEPL------IFLGALFEGRPD---------- DPAAIEARMAEITERREKT------QPIR-EKTGGSTFKN 227
R.capsulatus -----LPDQA-----VIVSATFRAAAG---------- DPAALAARMEEQIAKRDAS------QPTK-ARSAGSTFRN 221
R.palustris -----ADPAL------IFTSARLRGTPA---------- TPDHIRAKMNEVQAHRELA------QPIR-EKTGGSTFKN 232
R.rickettsii -----LPKNL------IILKVIFKINKG---------- DSENILLRMNEINNARSST------QPIK-ERTGGSTFAN 221
R.typhi -----LPKDL------ILLKAIFKANKG---------- DSQNILLKMNKINTTRSST------QPIK-ERTGGSTFKN 221
R.pomeroyi -----LPEGA-----VLVSASLQGVPG---------- DPEALHARMQAQLDKRDQT------QPTK-ERSAGSTFRN 220
S.meliloti -----AAKEL------IFTHAIFEGYAE---------- DKTKIRTDMDAVRQHRETV------QPIR-EKTGGSTFKN 236
S.paucimobilis -----LTDGT-----VVVEATFQGQAA---------- EPEIIQAEMDRIAAAREAS------QPLR-SKTGGSTFRN 221
S.aureus EH----------LVVLEAAFTLAPG---------- KMTEIQAKMDDLTERRESK------QPLE-YPSCGSVFQR 230
S.pneumoniae SG----------AVVLSVKFALAPG---------- THQVIKQEMDRLTHLRELK------QPLE-YPSCGSVFKN 227
Synechococcus -----LQDE-----ELVVLSARFRLEPG---------- HDPEEITRITSGNLSHRTS-------TQPYTQPSCGSVFRN 223
T.maritima EK----------LIITRVMMSFKKE---------- KKETIKAKMDDYMRRRLEK------QPLD-LPSAGSVFKR 207
T.denticola NPVSTEITKN----RKIVLSAVFTLTHG---------- IKEEIAVKTEEKVQDRISK------GHFK-EPSAGSTFKN 247
X.autotrophicus -----VPADV------VFTRAVFEGRPG---------- DPAVIAAEMAKITESREAT------QPIK-SRTGGSTFKN 269
C.trachomatis KKP----------AFIASATFQLTKD---------- PQAAKRAKALIEE--RILK------QPYE-YPSAGCIFRN 218
C.pecorum HRP----------EFILSATFQLTKN---------- PLAPHKVKTALQH--RIAT------QPCS-LPSAGCVFRN 222
W.pipientis -----LKGNW------IFVEAEFKGVNS---------- EYELILQRLKEVIERKNKS------QPIR-GKTAGCIFRN 222
T.thermophilus PG----------GIVTRVRLKLKER---------- PKEEILRRMAEVD--RARK-----GQPK--RKSAGCAFRN 200
A.baumannii D----------PARYIITHVTFKLLKQ-----ANLKLNYGDLKQAVG---------- DNLTAENLQNQVIHIRQSK-----LPDPKEYPNVGSFFKN 237
A.vinelandii Q----------AGRWLILRVRFALQRT-----PRLHLDYGPVRQWLAERGV-------ESPTPRDVSRAICAIRQEK-----LPDPAVLGNAGSFFKN 243
C.ammoniagenes TQ----------RAVVLAIEMQLTTD---GLSAPLNFRQLTE-----NPG------ERRAVEEVREMVLQLRRGKGMVL-NATDKDTWSAGSFFKN 254
Eterobacter EY----------QNRYAITAVGLRLAKA-----WQP-LDYGDLTRLDP---------- ASVTPQQVFDTVCKMRTSK-----LPDPKVNGNAGSFFKN 232
E.coli EY----------QDRFAIVAVGLRLPKE-----WQPVLTYGDLTRLDP---------- TTVTPQQVFNAVCHMRTTK-----LPDPKVNGNAGSFFKN 233
H.influenzae RY----------QQGYVITAVGLKLKKD-----WQPILKYGSLVEFDP---------- KTVTAKQIFDEVCHIRQSK-----LPDPNEVGNAGSFFKN 232
K.pneumoniae EY----------QDRYAIVAIGLSLAKT-----WQPVLSYGDLTRLDP---------- QTVTPQQVFDAVCHMRMTK-----LPDPKINGNAGSFFKN 233
M.luteus SML----ETDAPSPRWIVLSIDLRLRRASSDAEPTAPVRYGQLAAALD-VEEG-------AHAPLAVVRREVLALRAAKGMVS-DLADPDTWSTGSYFTN 274
M.marinum ADG----L----ALPAVVLEVEFALDAS----GRSAPLRYGELTAALG-MNSG-------ERGEPRAVRDAVLALRARKGMVL-DAADHDTWSVGSFFTN 262
M.tuberculosis ADG----L----AVPTVVLEVEFALDPS----GRSAPLRYGELIAALN-ATSG-------ERADPQAVREAVLALRARKGMVL-DPTDHDTWSVGSFFTN 261
N.gonorrhoeae EG----------KGRYVIVSVVFALKTH-----FVPNLGYGDLAAKVAELSAG-------REATAKDVSDAVSAIRNSK-----LPDPKVLGNVGSFFKN 244
P.gingivalis PD----------YAEWAIMYVDYRLRLR-----PSFSLEYKALAKVLEEERI---------TPTLQSIRDTVIRIRNSK-----LPDPATIGNAGSFFVN 241
P.chlorophenolicus TTV----N---GSPRYVVLTVEFQLPLG----RMSAPIRYAELARSLG-VEAG-------KRAYSNDVRREVLRLRASKGMVL-DAADRDTYSTGSFFTN 250
P.aeruginosa E----------PDRWLILRVRLRLTRR-----ERLHLDYGPVRQRLEEEGI---------ASPTARDVSRVICAIRREK-----LPDPAVLGNAGSFFKN 243
S.enterica EY----------QDRVAIVAVGLRLSKQ-----WQPVLTYGDLTCLDP---------- KTVTAQQVFDAVCHMRTTK-----LPDPKVNGNAGSFFKN 233
S.dysenteriae EY----------QDRFAIVAVGLRLPKE-----WQPVLTYGDLTRLEP---------- TTVTPQQVFNAVCHMRTTK-----LPDPKVNGNAGSFFKN 233
V.cholerae QL----------YQKAVVTAVGLKFAKA-----WQPIIQYGPLKDLS---------- SDCAIHDVYQRVCATRMEK-----LPDPAVMGNAGSFFKN 236
*

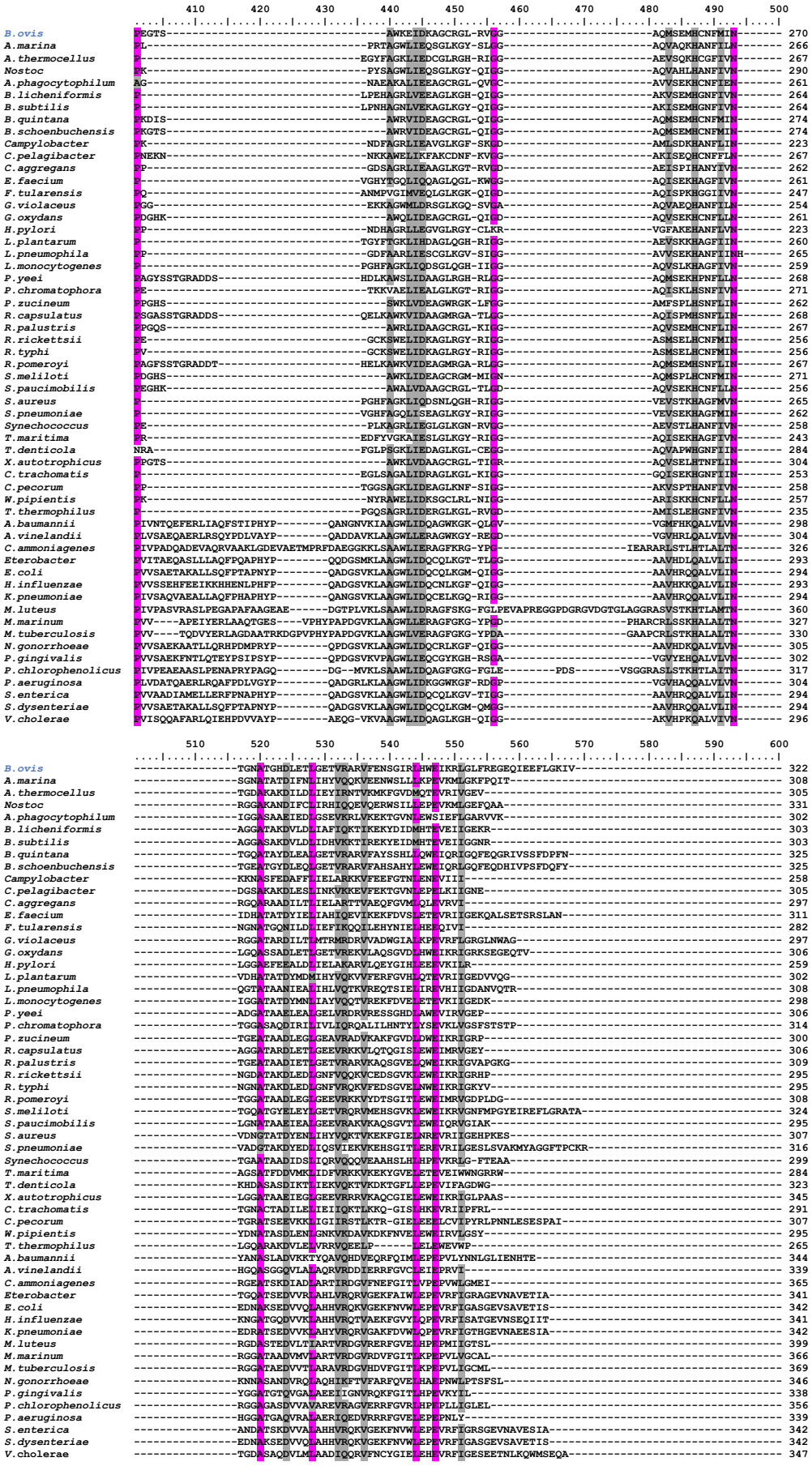

Figure 6.14. Conservation of MurB sequence within selected bacteria. MSA (n=57) of MurBs from species in Table 6.2. The alignment was constructed with Clustal Omega. Residues similar or identical in at least 90% of the sequences are highlighted in grey and purple, respectively. The Ser/Cys catalytic residue is marked with an asterisk.

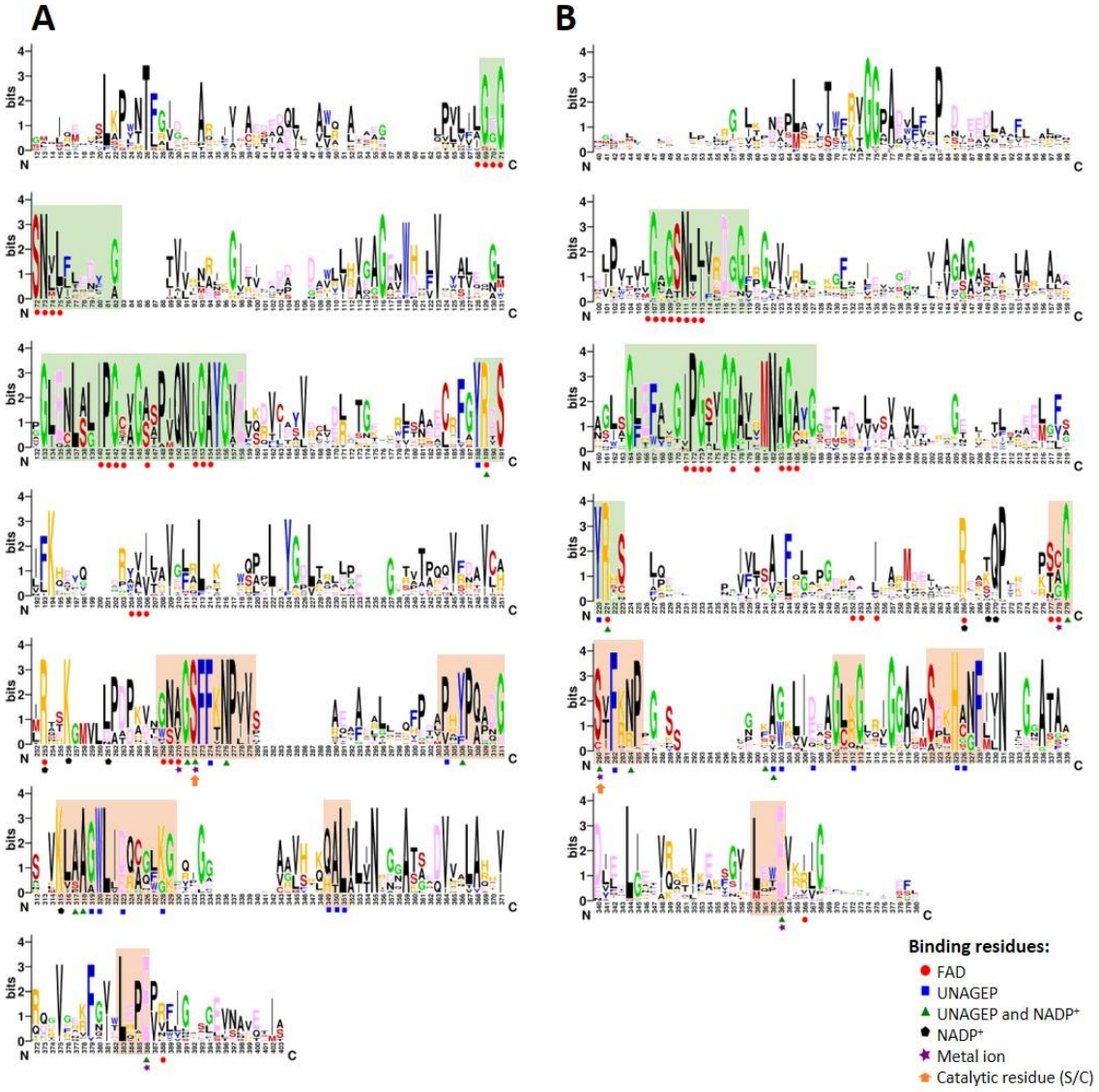

Figure 6.15. Residue conservation of MurB sequences within selected bacteria. Logos for MurB of **(A)** type I (n=16) and **(B)** type II (n=40) constructed from Figure 6.12 MSA, excluding the *M. luteus* sequence. Green and orange boxes highlight conserved motifs respectively involved in FAD or substrate binding. Other features and routine for logo generation as in Figure 6.13A.

The MSA of Figure 6.14 was used to phylogenetically evaluate these sequences. The resulting tree grouped the sequences in seven primary clades (Figure 6.16). The most divergent clade (Clade 1) contains only one taxa, MurB type IIa from *T. maritima*, the only sequence evaluated from the thermotogae phylum. Clade 2 is also quite divergent regarding the remaining sequences and only contains the sequence of MurB type IIa from the proteobacteria *F. tularensis*, respectively. Clade 3 is formed by 8 sequences, all of them being MurB type IIa of the Firmicute phylum. Clade 4 has the single sequence of MurB type IIa from *T. denticola*, the only spirochaete here included. Clade 5 groups the MurB type II sequences from the proteobacteria *Campylobacter* and *H. pylori*. The remaining sequences

group in the two most populated clades. Clade 6 (cyan) groups all MurB type I evaluated sequences, including five from the Actinobacteria phylum, one from the Bacteroidetes phylum and eleven from the Proteobacteria phylum. Finally, Clade 7 contains the remaining sequences, grouping both type IIa and IIb sequences that belong to the Cercozoa, Chlamydiae, Chloroflex, Cyanobacteria, Deinococcus-Thermus and, particularly, Proteobacteria (that group all together) phylum. As expected, the BoMurB sequence is positioned in this later clade.

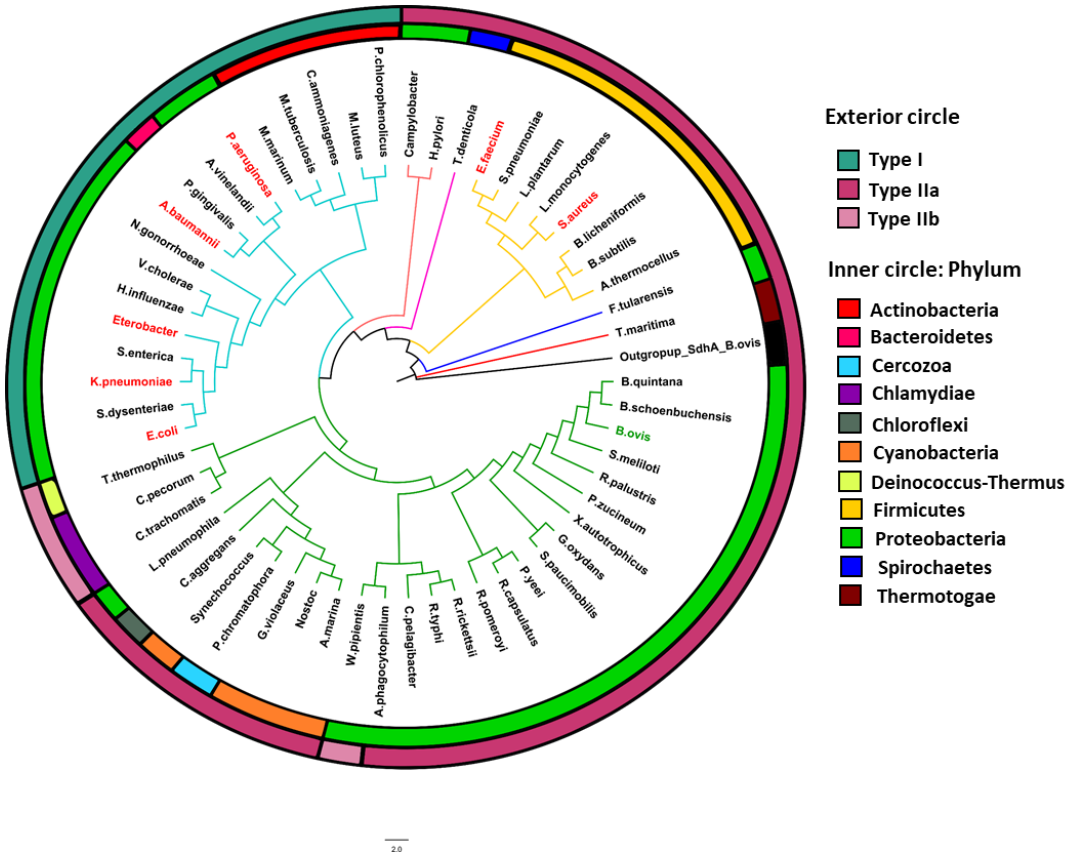

Figure 6.16. Phylogeny of MurB sequences within the selected bacterial. The evolutionary history was inferred by using the Maximum Likelihood method and JTT matrix-based model. The tree with the highest log likelihood (-32082.59) is shown. A bootstrap analysis of 500 replicates was conducted. The analysis involved 57 MurB sequences (Table 6.2), and *B. ovis* SdhA was used as outgroup to highlight the evolutionary separation between clusters. ESKAPE pathogens are highlighted in red and *B. ovis* is highlighted in green. Branch lengths are proportional to the number of substitutions per site (scale beside). There was a total of 623 positions in the final dataset. The type and phylum of the bacteria are denoted by colors on the outer and inner ring, respectively, of the external circle. The tree groups the sequences in seven main clusters: Clade 1in red color, Clade 2 in blue, Clade 3 in yellow, Clade 4 in pink, Clade 5 in coral, Clade 6 in cyan and Clade 7 in green. These last two clades have other subclades.

6.3.4 Heterologous production and hydrodynamic properties of BoHTMurB and BoMurB

In the initial approach, and in order to facilitate the purification of BoMurB, a 70 bp extension was added to the 5' end of the BomurB gene sequence, which included a 6-His

tagged tail and a PreScission protease cleavage site followed by a NdeI restriction site (Figure 3.1B). The resulting protein, BoHTMurB, contained a 6-His tagged tail at the N-terminus, was expected to be composed of 348 amino acids and 5,249 atoms, and for its theoretical Mw and pI values of 37,630.6 Da and 6.15, were respectively estimated. The calculated theoretical extinction coefficient at 280 nm not differed regarding the native form without the His-tag extension. Its instability index (II) was computed as 26.15, pointing to the protein potentially being moderately unstable under certain conditions. The aliphatic index and GRAVY score were 80.14 and -0.294, respectively, suggesting that the protein might be slightly hydrophilic.

BoHTMurB expression occurred within 5 h of induction with 1 mM IPTG at 30 ºC, resulting in approximately 4.5 g/L *E. coli* cells. Initially, the crude extract was loaded onto a Ni^{2+} affinity column, and upon elution with an imidazole gradient. The chromatogram showed a main peak followed by some shoulders (Figure 6.17A) with positive fractions showing an intense yellow color that was related to fractions containing FAD bound to BoHTMurB. The collected fractions were subjected to analysis by 12% SDS-PAGE gel (Figure 6.17B), where those showing bands compatible with BoHTMurB also showed contaminations of different Mw. These fractions were pooled, concentrated while removing imidazole, and subsequently loaded onto an SEC column (Figure 6.18).

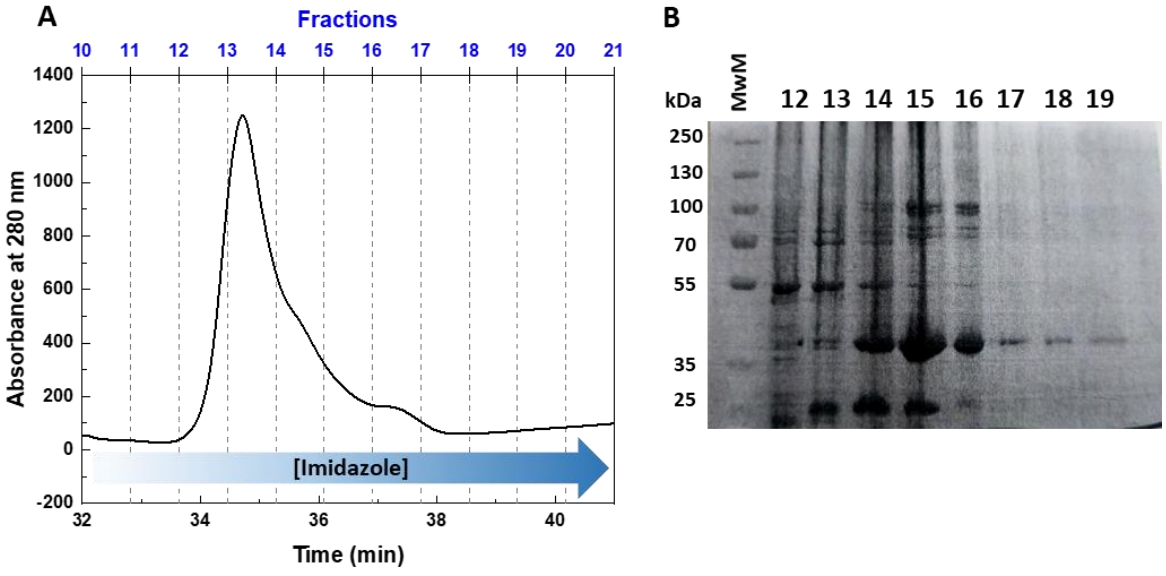

Figure 6.17. BoHTMurB purification using affinity chromatography and evaluation by SDS-PAGE. (A) Elution profile of the crude extract with the protein loaded onto a Ni^{2+} affinity column and eluted with a gradient from 10 to 500 mM imidazole. **(B)** Analysis of several fractions collected from the column using 12% SDS-PAGE gels. The MwM is represented in lane 1.

SEC purification of pooled BoHTMurB fractions separated a main yellow peak that eluted at a volume consistent with a molecule of Mw of ~39 kDa, in agreement with the predicted theoretical Mw of the BoHTMurB peptidic chain plus the Mw of its FAD cofactor. Moreover, when evaluating this peak by SDS-PAGE it also migrated with a Mw of 37.6 kDa (Figure 6.18A, left inset). The SDS-PAGE of this central peak additionally showed two small bands at ~25 and ~10 kDa. The nature of these extra bands in the pure protein sample were analyzed using MALDI-TOF. The outcomes unveiled a set of peptides that correspond to various segments of BoHTMurB (Table 6.3). The peptides detected within "Band No. 2" span regions from the N-terminal to the middle section of the protein (domains I and II), whereas those present in "Band No. 3" are indicative of a segment within domain II. This observation hints at potential proteolytic cleavage of the protein, a phenomenon previously reported in MurBs from other species (Anwar & Vlaovic, 1979; Benson et al., 1993). During CN-PAGE (Figure 6.18A, right inset), two bands were observed, again the weaker bands might be due to shorter versions of MurB as consequence of proteolysis.

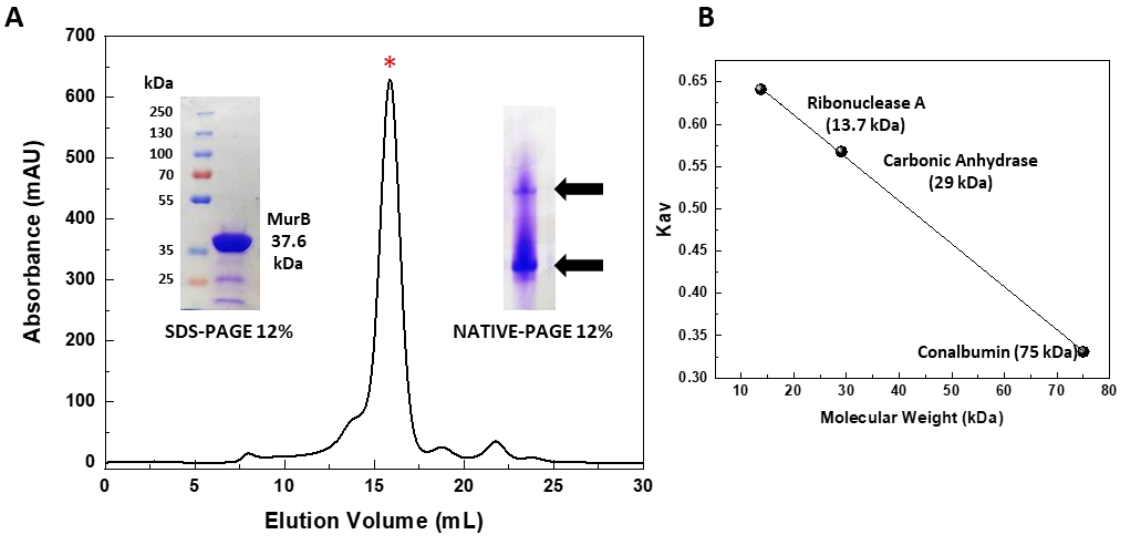

Figure 6.18. Hydrodynamic properties of BoHTMurB. (A) Elution profile of BoHTMurB on a 25 mL Superdex® 200 10/300 GL column at 4 °C. BoHTMurB (black line) elutes at 15.9 ml. The left inset shows a 12% SDS-PAGE of purified BoHTMurB: Left line, Mw marker PageRuler^{TM} Plus; right line, purified BoHTMurB (37.6 kDa). The right inset shows a 12% CN-PAGE of purified BoHTMurB. **(B)** Calibration Plot of the Superdex® 200 10/300 GL column with Ribonuclease A (13.7 kDa), Carbonic Anhydrase (29 kDa) and Conalbumin (75 kDa).

The same growth conditions as BoHTMurB were used for BoMurB biomass production. Due to the absence of the His-tag, protein purification required multiple steps. Ammonium sulfate to 80% was used to initially remove impurities, resulting in a yellow precipitate and clear supernatant. The obtained precipitate was resuspended in the working buffer, and the sample was loaded onto a DEAE-Sepharose column and eluted using a

reverse ammonium sulfate gradient. The collected yellow fractions were transferred to a second DEAE-Sepharose column, but this time they were eluted with a linear KCl gradient. The collected BoMurB fractions were concentrated. This sample was loaded onto a Hi-Trap QFF column, using another linear KCl gradient. The final SEC column showed improved purification, yielding a distinct ~35 kDa BoMurB band with reduced contaminating proteins (Figure 6.19).

Table 6.3. Results of MALDI-TOF mass spectrometry for three separate bands of BoMurB.

MASCOT SEARCH RESULTS			
SAMPLE	**PEPTIDE**	**SCORE**	**PROTEIN HITS Bacteria (*Brucella*)**
Band No. 1 (~37.6 kDa)	**K.ITWFR.A**	**31**	MURB_BRUMB: UDP-N-acetylenolpyruvoylglucosamine reductase OS=Brucella melitensis biotype 2 (strain ATCC 23457) OX=546272 GN=murB PE=3 SV=1 MURB_BRUME: UDP-N-acetylenolpyruvoylglucosamine reductase OS=Brucella melitensis biotype 1 (strain 16M / ATCC 23456 / NCTC 10094) OX=224914 G MURB_BRUSU: UDP-N-acetylenolpyruvoylglucosamine reductase OS=Brucella suis biovar 1 (strain 1330) OX=204722 GN=murB PE=3 SV=1 MURB_BRUC2: UDP-N-acetylenolpyruvoylglucosamine reductase OS=Brucella canis (strain ATCC 23365 / NCTC 10854) OX=483179 GN=murB PE=3 SV=1 MURB_BRUO2: UDP-N-acetylenolpyruvoylglucosamine reductase OS=Brucella ovis (strain ATCC 25840 / 63/290 / NCTC 10512) OX=444178 GN=murB PE=3 S MURB_BRUSI: UDP-N-acetylenolpyruvoylglucosamine reductase OS=Brucella suis (strain ATCC 23445 / NCTC 10510) OX=470137 GN=murB PE=3 SV=1
	R.LHWEIK.R	**36**	
	R.ETVQPVR.E	**36**	
	R.VFENSGIR.L	**33**	
	K.NPEGTSAWK.E	**48**	
	R.LTPDTGMDK.I + Oxidation (M)	**34**	
	R.DGGVPGFVVR.L	**57**	
	R.MNAGANGVETR.E	**79**	
	R.EGEQIEEFLGK.I	**72**	
	K.GFGEVEQVCDTQLR.A	**76**	
	K.AVPEEIPLLVVGIGSNLLVR.D	**51**	
	R.AGGPAQVLFQPSDEEDLSAFLK.A	**69**	
Band No. 2 (~25 kDa)	**K.ITWFR.A**	**31**	MURB_BRUAB: UDP-N-acetylenolpyruvoylglucosamine reductase OS=Brucella abortus biovar 1 (strain 9-941) OX=262698 GN=murB PE=3 SV=1 MURB_BRUMB: UDP-N-acetylenolpyruvoylglucosamine reductase OS=Brucella melitensis biotype 2 (strain ATCC 23457) OX=546272 GN=murB PE=3 SV=1 MURB_BRUME: UDP-N-acetylenolpyruvoylglucosamine reductase OS=Brucella melitensis biotype 1 (strain 16M / ATCC 23456 / NCTC 10094) OX=224914 G MURB_BRUSI: UDP-N-acetylenolpyruvoylglucosamine reductase OS=Brucella suis (strain ATCC 23445 / NCTC 10510) OX=470137 GN=murB PE=3 SV=1 MURB_BRUSU: UDP-N-acetylenolpyruvoylglucosamine reductase OS=Brucella suis biovar 1 (strain 1330) OX=204722 GN=murB PE=3 SV=1 MURB_BRUA1: UDP-N-acetylenolpyruvoylglucosamine reductase OS=Brucella abortus (strain S19) OX=430066 GN=murB PE=3 SV=1 MURB_BRUA2: UDP-N-acetylenolpyruvoylglucosamine reductase OS=Brucella abortus (strain 2308) OX=359391 GN=murB PE=3 SV=1 MURB_BRUC2: UDP-N-acetylenolpyruvoylglucosamine reductase OS=Brucella canis (strain ATCC 23365 / NCTC 10854) OX=483179 GN=murB PE=3 SV=1 MURB_BRUO2: UDP-N-acetylenolpyruvoylglucosamine reductase OS=Brucella ovis (strain ATCC 25840 / 63/290 / NCTC 10512) OX=444178 GN=murB PE=3 S
	R.ETVQPVR.E	**32**	
	R.DGGVPGFVVR.L	**41**	
	R.MNAGANGVETR.E	**57**	
	K.GFGEVEQVCDTQLR.A	**79**	
	K.AVPEEIPLLVVGIGSNLLVR.D	**32**	
	R.AGGPAQVLFQPSDEEDLSAFLK.A	**74**	
	R.HSSASPDLIFTSVLFEGVPGER.D	**49**	
Band No. 3 (~10 kDa)	**K.GFGEVEQVCDTQLR.A**	**79**	MURB_BRUAB: UDP-N-acetylenolpyruvoylglucosamine reductase OS=Brucella abortus biovar 1 (strain 9-941) OX=262698 GN=murB PE=3 SV=1 MURB_BRUMB: UDP-N-acetylenolpyruvoylglucosamine reductase OS=Brucella melitensis biotype 2 (strain ATCC 23457) OX=546272 GN=murB PE=3 SV=1 MURB_BRUME: UDP-N-acetylenolpyruvoylglucosamine reductase OS=Brucella melitensis biotype 1 (strain 16M / ATCC 23456 / NCTC 10094) OX=224914 G MURB_BRUSI: UDP-N-acetylenolpyruvoylglucosamine reductase OS=Brucella suis (strain ATCC 23445 / NCTC 10510) OX=470137 GN=murB PE=3 SV=1 MURB_BRUA1: UDP-N-acetylenolpyruvoylglucosamine reductase OS=Brucella abortus (strain S19) OX=430066 GN=murB PE=3 SV=1 MURB_BRUA2: UDP-N-acetylenolpyruvoylglucosamine reductase OS=Brucella abortus (strain 2308) OX=359391 GN=murB PE=3 SV=1 MURB_BRUO2: UDP-N-acetylenolpyruvoylglucosamine reductase OS=Brucella ovis (strain ATCC 25840 / 63/290 / NCTC 10512) OX=444178 GN=murB PE=3 S
	R.HSSASPDLIFTSVLFEGVPGER.D	**54**	
	R.VAAAALEAGLAGFHFYHGIPGGIGGALR.M	**42**	

Individual ions scores > 39 indicate identity or extensive homology ($p<0.05$).

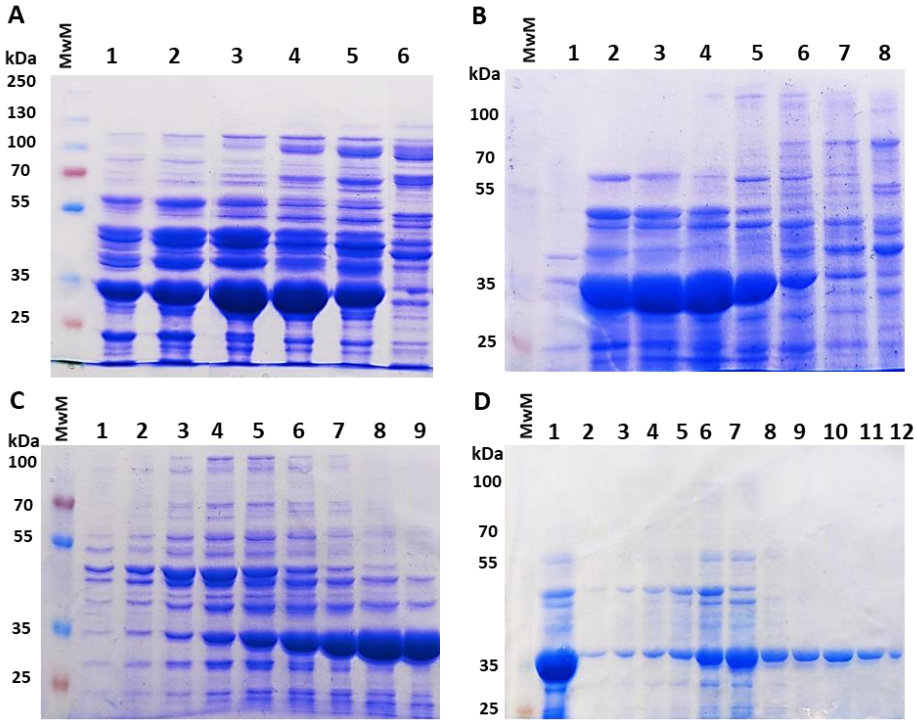

Figure 6.19. SDS-PAGE analysis of the obtained fractions after each BoMurB purification step. Fraction analysis for the elution profile of BoMurB from the **(A)** DEAE-Sepharose1 column (lane 2-6: different fractions**), (B)** DEAE-Sepharose2 column (lane 1: flow-through sample; lane 2-8: yellow fractions), **(C)** Hi-Trap QFF column (lane 1-9: yellow fractions) and **(D)** Superdex® 200 10/300 GL column (lane 1: concentrated sample before loading; lane 2-12: yellow fractions). All gels shown MwM PageRuler^{TM} Plus in the first line.

6.3.5 Spectroscopic properties of BoHTMurB and BoMurB

The absorption spectrum of BoHTMurB purified to homogeneity was characterized by maxima at 270, 380 and 463 nm, a shoulder at 490 nm, and an Abs_{270}/Abs_{463} ratio of 5.1 (Figure 6.20A), while that of BoMurB showed maxima at 270, 385 and 462 nm, a shoulder at 489 nm, and an Abs_{270}/Abs_{462} ratio of 5.5 (Figure 6.21A). Following the protocol reported in section 3.4.1.1.2, the flavin cofactor became released, obtaining for it a spectrum with maxima at 374 nm and 450 nm, thus confirming BoHTMurB has FAD as cofactor. This allowed for the determination of the experimental ε_{462nm} = 12.2 ± 0.3 $mM^{-1}cm^{-1}$ for BoHTMurB and ε_{463nm} = 11.2 ± 0.4 $mM^{-1}cm^{-1}$ for BoMurB, in 50 mM Bis-Tris propane, 100 mM KCl and 1 mM DTT, pH 8.0.

Photoreduction of BoHTMurB and BoMurB showed the proteins' capacity to undergo reduction by accepting electrons through photoirradiation (Figure 6.20B and 6.21B). Likewise, both photoreduced proteins reverted to their original spectra when exposed to molecular oxygen. Additionally, throughout the photoreduction and reoxidation, the proteins did not exhibit any evidence of stabilization of anionic or neutral FAD semiquinone states.

The BoHTMurB fluorescence emission spectrum exhibited a maximum at 331 nm upon excitation in the aromatic region consistent with at least one tryptophan residue in a folded environment (Figure 6.20C), as well as a maximum at 528 nm when exciting in the flavin band I region (Figure 6.20D). BoMurB fluorescence emission spectrum exhibits maxima at 330 and 527 nm upon respective excitation at 280 nm (Figure 6.21C) and 460 nm (Fig 6.21D). Some differences were observed in the fluorescence quantum yield of both proteins. However, during fluorescence measurements using the Cary Eclipse fluorimeter, a voltage of 600 V (the default setting for the PMT detector) was selected for the 10 µM BoHTMurB sample. Nonetheless, when measuring the BoMurB sample at the same concentration, the signal was excessively high, which required a reduction in the PMT detector voltage to 400 V. This suggests that the presence of the His-tail in BoHTMurB shields exposure of FAD to the solvent, resulting in quenched fluorescence, and therefore BoMurB shows more fluorescence versus BoHTMurB.

The far-UV CD spectrum of BoHTMurB showed two minima at 208 and 221.5 nm (Figure 6.20E), indicative of α-helixes contributing to the conformation of the folded protein. The near-UV/Vis CD spectra displayed two maxima peaks at 299 and 407 nm and three minima at 271.5, 368 and 466.5 nm (Figure 6.20F). In BoMurB, far-UV CD spectrum showed minima at 207 and 221 nm (Figure 6.21 E), and near-UV/Vis CD spectrum displayed two maxima peaking at 299.5 and 414 nm and three minima at 268.5, 360 and 460.5 nm (Figure 6.21F).

Altogether this spectroscopic characterization indicates that purified samples of BoHTMurB and BoMurB are properly folded and incorporate one FAD molecule per protein molecule, being this FAD cofactor able to exchange two-electrons at a time upon photoirradiation and reoxidation by molecular oxygen.

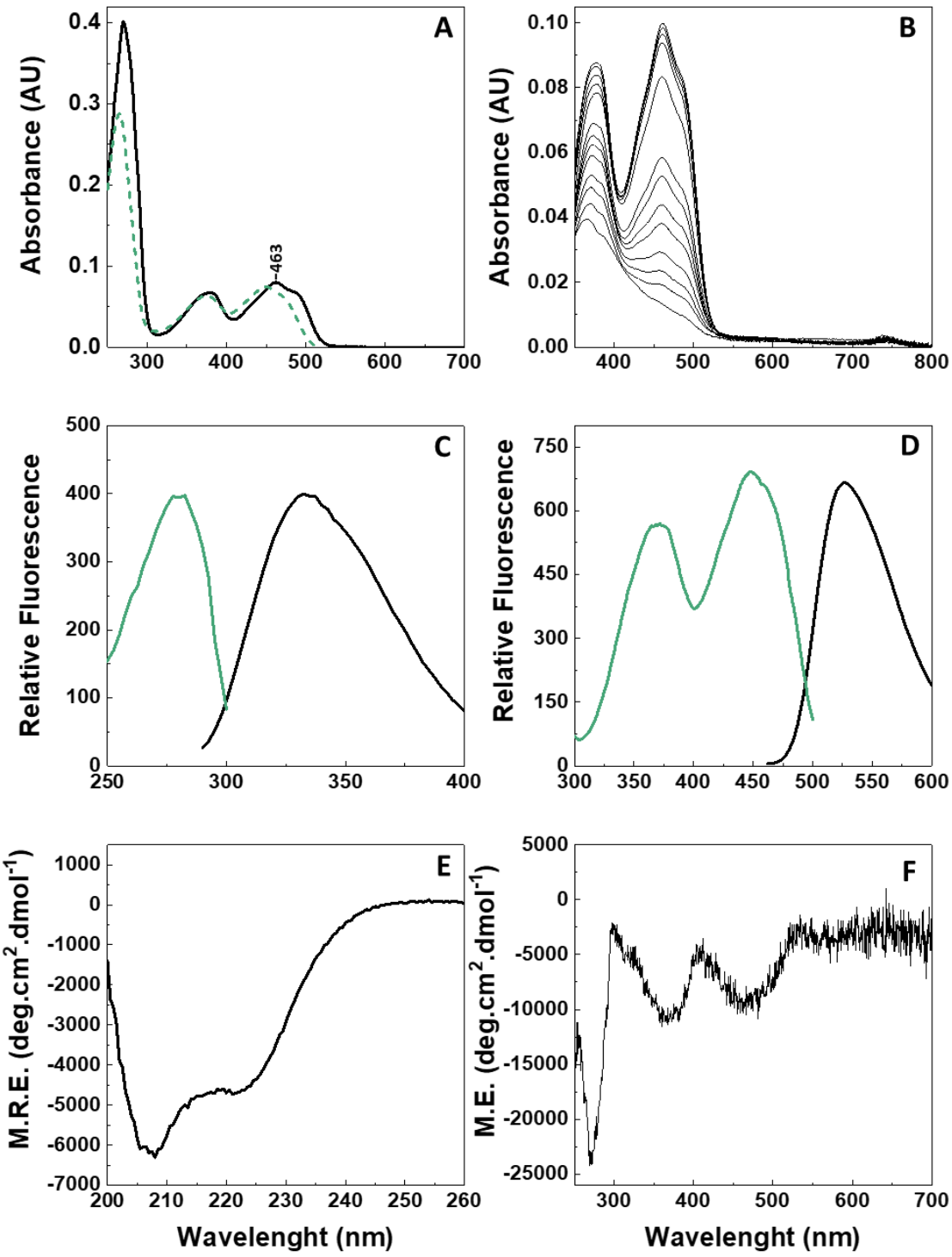

Figure 6.20. Spectral properties of BoHTMurB. (A) UV-Visible absorption spectra of BoHTMurB (6.5 µM) (black line) in 50 mM Bis-Tris Propane, 100 mM KCl, 1 mM DTT, pH 8.0, at 25 °C for a folded sample, and of its released FAD (green dotted line) after incubation for 5 min at 90 °C. **(B)** Spectral evolution for the photoreduction of BoHTMurB (7.8 µM) in the visible region. Spectra recorded in 50 mM Bis-Tris Propane, 100 mM KCl, 1 mM DTT pH 8.0, 20% glycerol, and 50 mM EDTA. Emission fluorescence spectra when exciting in the **(C)** aromatic region, λ_{ex} = 280 nm (10 µM) and in the **(D)** flavin region, λ_{ex} = 460 nm (10 µM). The corresponding excitation spectra (green lines) are shown when collecting emission at 330 and 528 nm respectively. Spectra were collected at 600 V. CD spectra for the **(E)** far-UV (5 µM), and **(F)** near-UV/Vis (10 µM) regions. Emission and CD spectra were recorded in 10 mM potassium phosphate, pH 8.0, at 10 °C.

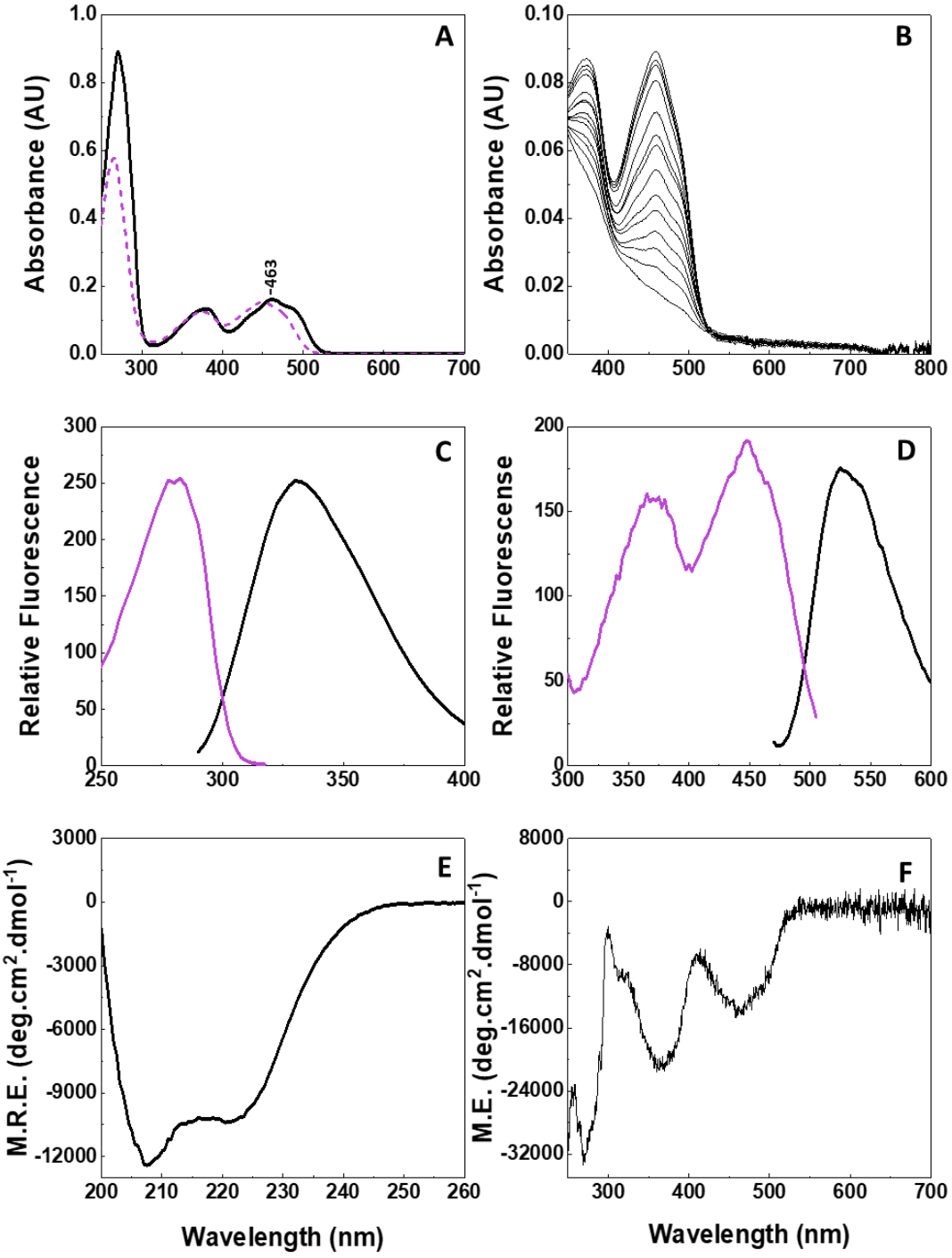

Figure 6.21. Spectral properties of BoMurB. (A) UV-Visible absorption spectra of BoMurB (14.3 µM) (black line) in 50 mM Bis-Tris Propane, 100 mM KCl, 1 mM DTT, pH 8.0, at 25 °C for a folded sample, and of its released FAD (purple dotted line) after incubation for 5 min at 90 °C. **(B)** Spectral evolution for the photoreduction of BoMurB (8 µM) in the visible region. Spectra recorded in 50 mM Bis-Tris Propane, 100 mM KCl, 1 mM DTT pH 8.0, 20% glycerol, 50 mM EDTA. Emission fluorescence spectra of BoMurB when exciting in the **(C)** aromatic region, λ_{ex} = 280 nm (10 µM) and in the **(D)** flavin region, λ_{ex} = 460 nm (10 µM). The corresponding excitation spectra (purple lines) are shown when collecting emission at 330 and 528 nm respectively. Results were collected at 400 V. CD spectra for the **(E)** far-UV (5 µM), and (**F)** near-UV/Vis (20 µM) regions. Emission and CD spectra were recorded in 10 mM potassium phosphate, pH 8.0, at 10 °C.

6.3.6 Mid-point reduction potential of BoHTMurB

The redox potential of the FAD cofactor within BoHTMurB was determined with the xanthine/xanthine oxidase system (Figure 6.22A) using as dye the obligatory two-electron exchanger phenosafranin ($E_{ox/rd}$=-252 mV). Along reduction of the system spectral changes for BoHTMurB indicate that its FAD cofactor is accepting two electrons simultaneously, without stabilization of any semiquinone intermediate. The plot of 12.5In($PheS_{ox}/PheS_{rd}$) *versus* 12.5In(FAD_{ox}/FAD_{rd}) showed a line whose slope close to unity further supports both the dye and the flavin exchanging two electrons at a time. Derived data from this plot allowed to estimate a mid-point potential for the two electrons exchange of the BoHTMurB FAD cofactor, $E_{ox/hq}$, in -256 ± 3 mV. This value in slightly more negative than that of the free FAD cofactor (E_m=-219 mV, (Maklashina & Cecchini, 2020)) and close to the value reported for MurB from *E. coli* ($E_{ox/hq}$=-234 mV) (Benson et al., 1997). In addition, the cyclic voltammogram of BoHTMurB demonstrates the presence of a redox couple with well-defined oxidation and reduction peaks (Figure 6.22B), and allow to estimate its mid-point around -200 mV under the evaluated conditions.

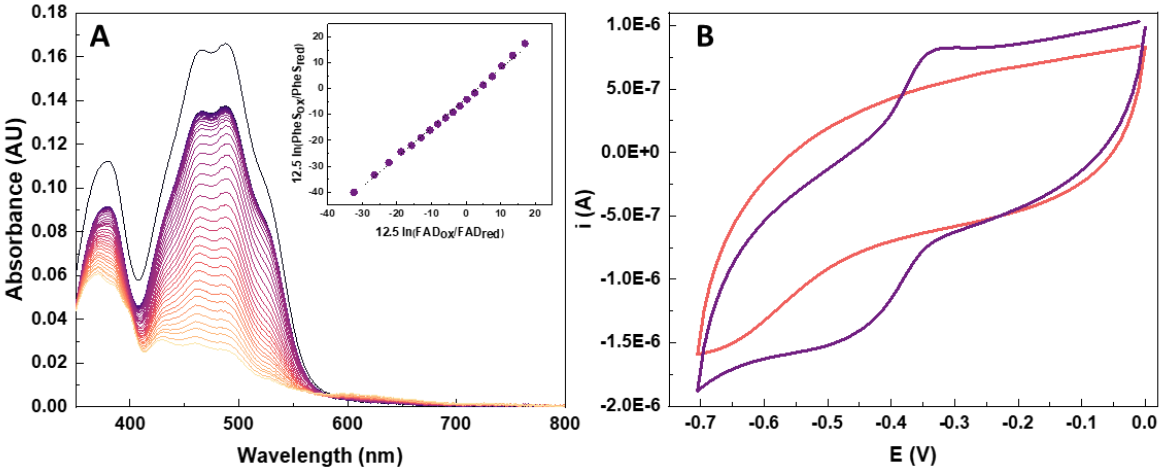

Figure 6.22. BoHTMurB redox potential. (A) Spectral evolution upon mid-point reduction potential assessment using phenosafranin as a dye. The black spectrum represents BoHTMurB before mixing with xanthine oxidase, while colored visible absorption spectra in purple degradation correspond to different time points along protein reduction. Samples were premixed with benzyl viologen, xanthine and phenosafranin, made anaerobic by several cycles of vacuum application and bubbled with O_2–free argon, and subsequently mixed with xanthine oxidase. Spectra were recorded every 5 min for up to 2 h in 50 mM Bis-Tris Propane, 100 mM KCl, 1mM DTT, pH 8.0 at 25 °C. The inset shows the logarithm of the ratios of oxidized/reduced dye and oxidized/reduced BoHTMurB at different time points. **(B)** Cyclic voltammogram of BoHTMurB as recorded at 25 °C under anaerobic conditions by applying a potential between 0 and -700 mV with a scan rate of 120 mV/sec (purple). A control experiment in the absence of the protein is shown in pink. The supporting electrolyte was 50 mM phosphate buffer pH 7.4 with 100 mM KCl, and the reference electrode was Ag/AgCl.

6.3.7 Thermal stability of BoHTMurB and BoMurB

BoHTMurB and BoMurB conformational stability in the absence and presence of UNAG, UNAGEP and $NADP^+$ was evaluated by following thermal protein unfolding. Denaturation curves were recorded through far-UV CD and fluorescence emission in 10 mM potassium phosphate, pH 8.0. The thermal denaturation curves allowed them to follow changes in secondary structure by CD, as well as in fluorescence of tryptophan's and FAD upon release from the protein environment (Table 6.3 and Figure 6.23).

BoHTMurB when it is free of substrate shows a three-state unfolding process (N→I→U), represented by two different T_m values. While T_{m1}^{222nm} was a set at 314 K, T_{m2}^{FLTrp} and T_{m2}^{FLFAD} were set at 318 K. In the case of BoMurB, the curves obtained from multiple experiments in far-CD did not exhibit values that aligned with the fluorescence data, and, in numerous instances, the signal obtained was insufficient. When following fluorescence of Trp two T_{ms} were detected, T_{m1}^{FLTrp} at 309 K and T_{m2}^{FLTrp} at 318 K. This last temperature was also consistent with T_{m2}^{FLFAD}. Therefore, a three steps unfolding process also applied for BoMurB. When assessing the complex with UNAG, there were no noticeable difference in the T_m values for BoHTMurB. This suggests that UNAG likely does not bind the enzyme, or if it does, the interaction is weak. Nonetheless, when evaluating BoMurB:UNAG the fluorescence analysis revealed two T_m values in each assay: T_{m2}^{FLTrp} at 317 K and T_{m2}^{FLTrp} at 321 K, corresponding to the T_{m2}^{FLFAD} and T_{m3}^{FLFAD} at 327 K. Since both set of T_m values differed among them and increased regarding the free enzyme, UNAG has a stabilizing impact on BoMurB and includes one additional step in the denaturation process. This suggests that UNAG binds BoMurB but not BoHTMurB.

BoHTMurB exhibits three T_m values in presence of UNAGEP: T_{m1}^{FLTrp} at 313 K and T_{m2}^{FLTrp} at 318 K, which align with T_{m2}^{222nm} and T_{m2}^{FLFAD}, to finally also show a T_{m3}^{FLFAD} at 330 K. For BoMurB, the T_ms were closer to those for the complex with UNAG, obtaining the T_{m1}^{FLTrp} at 316 K and T_{m2}^{FLTrp} at 322 K. This temperature is close to T_{m2}^{FLFAD} at 321 K, but finally, T_{m3}^{FLFAD} at 329 K was observed. Indeed, this observation suggests that UNAGEP has a stabilizing effect on a portion of the propeller structure, allowing some tryptophan as well as FAD two retain some "protein environment" at higher temperatures, thus producing the observed denaturation in three steps ($N \rightarrow I_1^{FLTrp} \rightarrow I_2^{FLFAD} \rightarrow U$).

The presence of $NADP^+$ also slightly stabilizes some elements of the helical secondary structure for BoHTMurB, as shown by the increased T_m values, all of which are close to 318 K, suggesting a two species mechanism (N→U). For BoMurB, T_{m1}^{FLTrp}

corresponds to this same value of 319 K; however, T_{m2}^{FLTrp} and T_{m}^{FLFAD} are close to 324 K, proposing an overall N→I→U mechanism.

In the last evaluations, mixtures of both substrates/analogues with the protein were used. BoHTMurB:UNAG:$NADP^+$ exhibits an identical mechanism to that obtained in the presence of $NADP^+$, corresponding to a N→U process. Once again, it is confirmed that the presence of UNAG in the reaction does not promote the stabilization of the His-tag protein. In contrast, when BoHTMurB is mixed with UNAGEP and $NADP^+$, it unfolds with two additional intermediates, just like in its complex with only UNAGEP. Therefore, the additional presence of $NADP^+$ does not provide extra stability to the BoHTMurB:UNAGEP mixture, as envisaged since both substrates should bind at the same binding site.

For the BoMurB:UNAG:$NADP^+$ complex, an optimal signal was not obtained in any of denaturation curves in multiple trails. In contrast, for the complex with UNAGEP and $NADP^+$, multiple T_m values were obtained for different transition states. T_{m1}^{FLTrp} and T_{m2}^{FLTrp} had values of 321 and 324 K, respectively, close to those detected in the BoMurB:$NADP^+$ mixture. However, the fluorescence assay curve for FAD also displayed two T_m values: T_{m2}^{FLFAD}, with a value close to T_{m2}^{FLTrp}, and T_{m3}^{FLTrp} at 331 K. This indicates a three-step mechanism with more than one intermediate (N→I_1^{FLTrp}→I_2^{FLFAD}→U), as observed in the complexes with UNAG and UNAGEP. The stabilization of proteins in the presence of UNAGEP and UNAGEP:$NADP^+$ is evident in the fluorescence evaluation at 280 nm. As depicted in Figure 6.23B, two of the three tryptophan residues are situated in the binding sites. Trp34 is positioned very close to the isoalloxazine ring of FAD, while Trp242 may be involved in interactions with UNAGEP or $NADP^+$ molecules. Therefore, when the enzyme is free of substrate, this specific Trp242 will become exposed to the substrate more rapidly than when the enzyme interacts with its substrate.

Table 6.3. Effect of substrates in BoHTMurB and BoMurB thermal stability parameters. Values were obtained by independently fitting of far-CD (222 nm) as well as tryptophan and FAD fluorescence thermal denaturation curves. Data obtained in 10 mM potassium phosphate buffer, pH 8.0, from 283.15 to 363.15 K. Error in T_m determination is within ±1.

	CD ^{222nm}			FL^{Trp}			FL^{FAD}			Global Mechanism
	T_{m1}	T_{m2}	T_{m3}	T_{m1}	T_{m2}	T_{m3}	T_{m1}	T_{m2}	T_{m3}	
BoHTMurB	314				318			318		N→I→D
BoHTMurB:UNAG	315				318			319		N→I→D
BoHTMurB:UNAGEP		318		313	318			319	330	N→I_1→I_2→D
BoHTMurB:UNAG:NADP$^+$		318			318			318		N→D
BoHTMurB:UNAGEP:NADP$^+$		318		316	320			321	330	N→I_1→I_2→D
BoHTMurB:NADP$^+$		317			318			318		N→D
BoMurB	nd	nd	nd	309	318			318		N→I→D
BoMurB:UNAG	nd	nd	nd	317	321			320	327	N→I_1→I_2→D
BoMurB:UNAGEP	nd	nd	nd	316	322			321	329	N→I_1→I_2→D
BoMurB:UNAG:NADP$^+$	nd	nd	nd	nd	nd	nd	nd	nd	nd	nd
BoMurB:UNAGEP:NADP$^+$	nd	nd	nd	321	324			322	331	N→I_1→I_2→D
BoMurB:NADP$^+$	nd	nd	nd	319	323			324		N→I→D

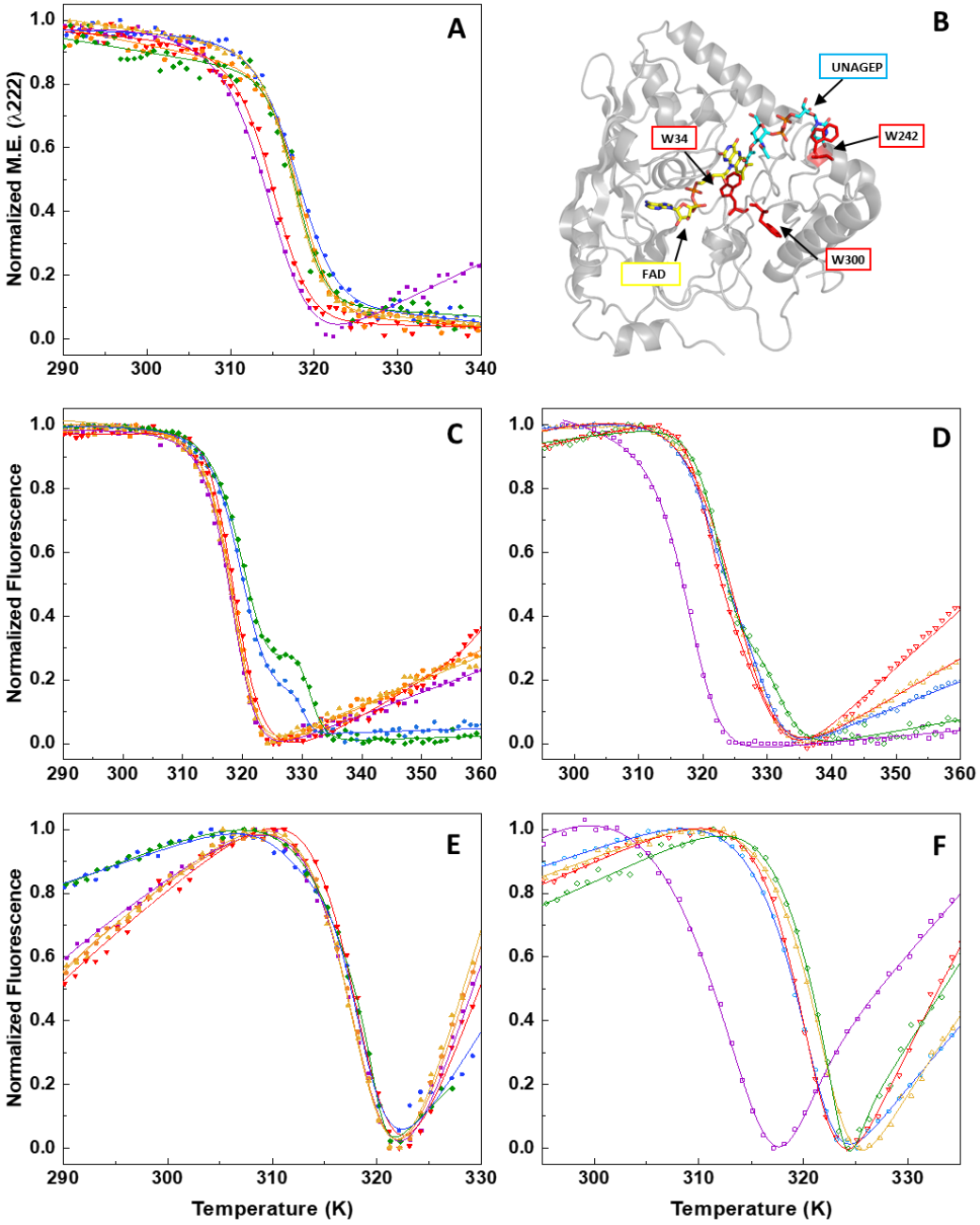

Figure 6.23. Impact of ligands on the thermal stability of BoHTMurB and BoMurB. Thermal unfolding curves for (**A) (C) (E)** BoHTMurB and **(D) (F)** BoMurB. Curves were monitored using (A) far-CD at 222 nm, (C) and (D) Trp fluorescence (λ_{ex}=280 nm and λ_{em}=330 nm) and (E) and (F) FAD fluorescence (λ_{ex}=460 nm and λ_{em}=527 nm). **(B)** Crystal structure of BoMurB showing the position of tryptophans, (Trp34, Trp242 and Trp300) highlighted in red. FAD is shown in yellow CPK and UNAGEP in cyan CPK. The denaturation curves of BoHTMurB and BoMurB without substrate are represented by purple full and empty squares; in the presence of UNAG are represented by red full and empty inverted triangles; in the presence of UNAGEP are represented by blue full and empty circles; in the presence of UNAG and $NADP^+$ are represented by orange full and empty pentagons; in the presence of UNAGEP and $NADP^+$ are represented by green full and empty rhombus; in the presence of $NADP^+$ are represented by yellow full and empty triangles. Curves are shown roughly normalized from 0 to 1, and their individual fits are represented by the continuous lines. Curves recorded in 10 mM potassium phosphate buffer, pH 8.0, from 283.15 to 363.15 K. Protein concentrations were 5 µM for far-CD assays, and 10 µM for fluorescence. UNAG and UNAGEP concentrations were in 10-fold excess regarding enzyme concentration and $NADP^+$ in 20-fold excess.

6.3.8 Reduction of BoMurB proteins by physiological and non-physiological hydride/electron donors.

MurB enzymes are reported to use the NADPH coenzyme as a source of electrons for the reduction of their FAD cofactor to subsequently catalyze the reduction of UNAGEP to UNAM (Figure 6.1). Therefore, we moved to evaluate the efficiency of purified BoHTMurB and BoMurB samples in transforming NADPH into $NADP^+$, by following the absorption decrease at 340 nm of the NADPH substrate upon its oxidation. Assays were carried out under both aerobic and anaerobic conditions, as well as in the presence of the UNAGEP oxidizing substrate, the BoMurA/UNAG/PEP system producing UNAGEP, and even in the presence of the BoMurC enzyme expected to use the UNAM product of BoMurB. Under any of the evaluated conditions oxidation of NADPH was detected (Figure 6.24). This was an unexpected result. In the same way, we conducted experiments with NADH instead of NADPH, but no oxidation of the reagent was again observed.

Trying to find an explanation to the lack of observed activity, we further evaluated the kinetics of the reduction of BoHTMurB samples by non-physiological electron donors by following spectral evolution along time for the FAD cofactor upon photoreduction and reduction by the sodium dithionite ($Na_2S_2O_4$, a commonly used and versatile reducing agent for flavoproteins) (Figure 6.25). Photoreduction of BoHTMurB samples to the hydroquinone state was achieved within the observation chamber of the stopped-flow equipment upon 8 h of continuous photoirradiation by the system source lamp (Figure 6.25A). Spectral evolution at the flavin band I was consistent with at least two distinct major phases (Figure 6.25B). The first phase, covering the 0-2300 s range, courses with a slight decrease in the FAD band absorption, hardly consistent with FAD reduction, and fits to a one-step process with an apparent observed rate constant ($^{app}k_{obs1}$) around 4.4 x 10^{-2} min^{-1} (Figure 6.25C). After this, a lag phase of around 700 s is observed before the start of the second phase (Figure 6.25B). In this later phase reduction of FAD to the hydroquinone state is nearly achieved in the evaluated time (3000-8000 s) with at least two processes with $^{app}k_{obs2}$ and $^{app}k_{obs3}$ values of around 7.7x10^{-2} min^{-1} and 1.3x10^{-4} min^{-1} (Figure 6.25C). It is worth to note that traces of semiquinone stabilization were not detected at any point of the overall photoreductive process.

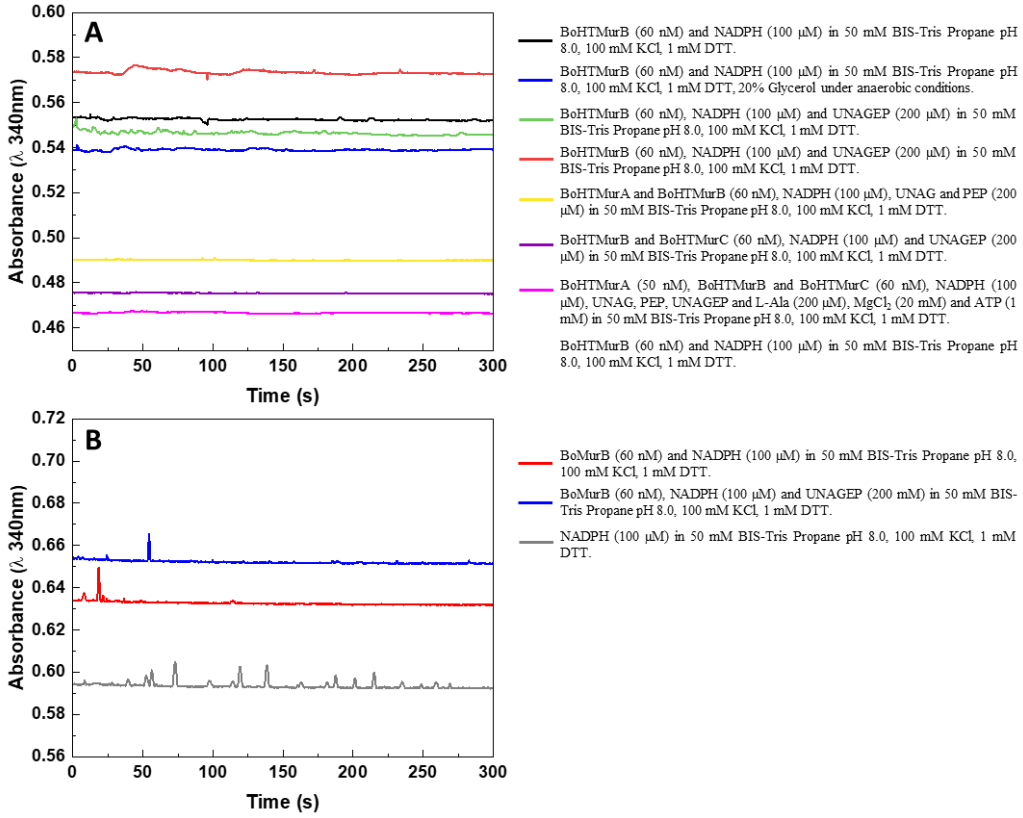

Figure 6.24. Steady-state evaluation of BoHTMurB and BoMurB ability to oxidize NADPH. (A) Evolution of the absorption of BoHTMurB at 340 nm under different mixtures conditions. **(B)** Evolution of the absorption of BoMurB at 340 nm under different aerobic conditions.

We also investigated the fast spectral evolution for the BoHTMurB reduction by sodium dithionite ($Na_2S_2O_4$) (Figure 6.25E). The obtained spectra displayed a lag period before the bleaching of the FAD band was observed. Nonetheless, on starting the reductive process reaction proceeded up to achieving full reduction of the protein to the semiquinone state, following a single kinetic process with an $^{app}k_{obs1}$ of 594 min^{-1}.

Altogether, photoirradiation as well as reduction assays using sodium dithionite or the xanthine/xanthine oxidase system indicate that the produced BoHTMurB samples are able to achieve flavin reduction. Nonetheless, the lack of capacity of the enzyme to oxidize NADPH under the assayed conditions suggests that we might be missing some key component of the physiological system.

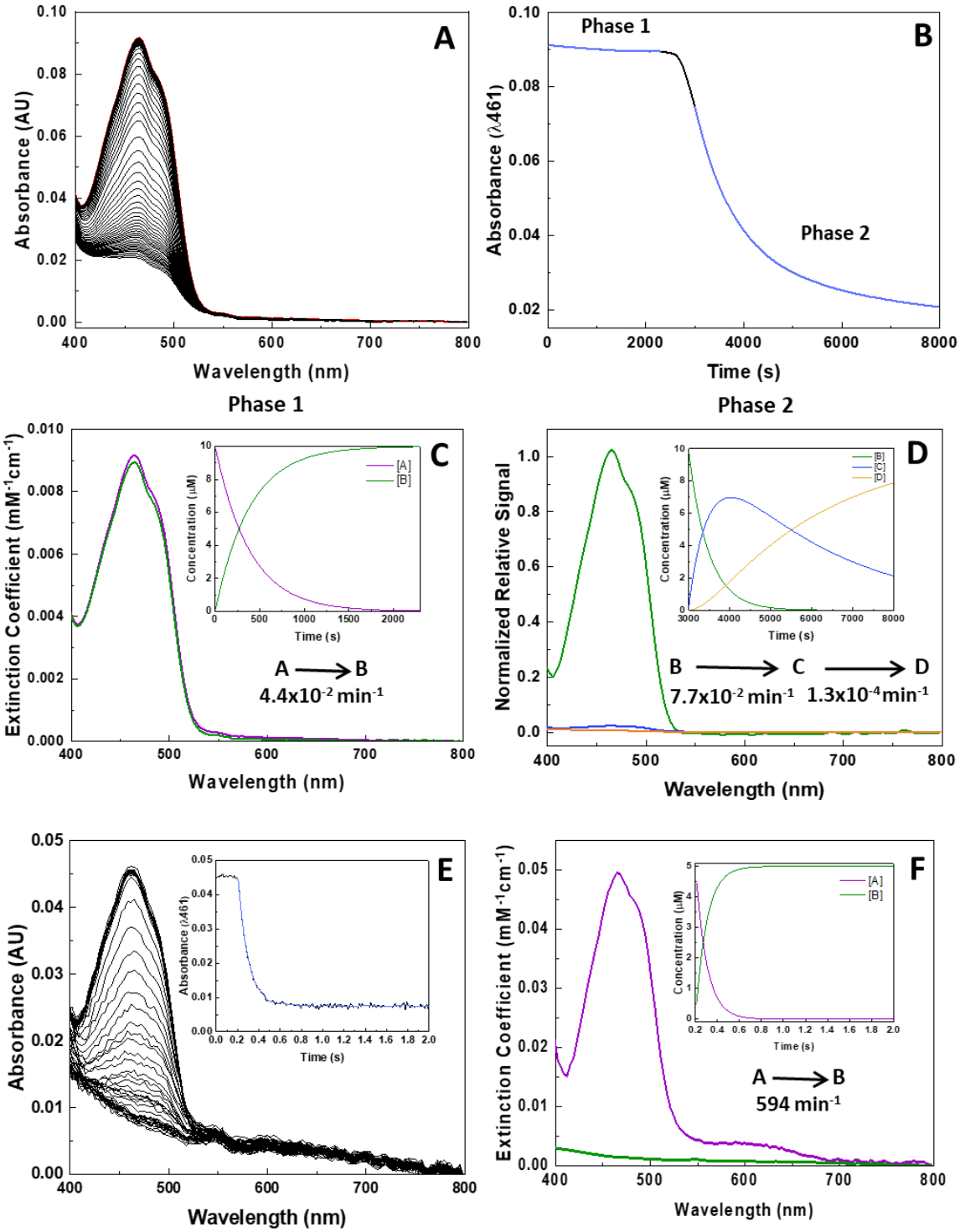

Figure 6.25. Kinetics for the reduction of BoHTMurB by non-physiological electron donors. (A) Spectral evolution upon photoreduction of BoHTMurB (~10 µM) by the stopped-flow equipment light source in the 400-800 nm region, in 50 mM Bis-Tris Propane, 100 mM KCl, 1 mM DTT pH 8.0, 20% glycerol, 50 mM EDTA at 25 °C. Spectra are shown at different times in the 0-8000 s range after samples entering the mixing chamber. **(B)** The right panel shows the absorbance time evolution at 461 nm corresponding to panel (A), schematizing the main phases of the process. **(C)** Spectroscopic species identified along spectral evolution when fitting the decay observed in the phase 1 corresponding to the 0-2300 s range to a one step reaction model (A→B). (D) Spectroscopic species identified along spectral evolution when fitting the decay observed in the phase 2, 3000-8000 s range, to a two-step reaction model (A→B→C). **(E)** Spectral evolution of BoHTMurB (5 µM) upon mixing with dithionite (150 µM) in 50 mM Bis-Tris Propane, 100 mM KCl, 1 mM DTT, pH 8.0

at 25 °C. Spectra are shown at different times in the 0-2 s range after mixing. The inset shows the time dependent absorbance evolution at 461 nm. **(F)** Features of spectroscopic species identified when fitting the decay observed in the 0.2-2 s range to a one step reduction model (A→B). Insets in (C), (D) and (F) show the evolution of the detected species along the reaction course.

6.3.9 Crystallization of BoHTMurB and BoMurB and crystal structure of the BoMurB:UNAGEP complex

More than 700 different crystallization conditions were tested using commercial kits in an attempt to produce suitable BoHTMurB crystals (3.9.2). Initially, the concentration of protein in each drop was varied, starting with 10 mg/ml, followed by 14, 18, 20, and 24 mg/ml. However, after several months of incubation, none of the conditions exhibited positive signs of crystal formation. Subsequently, the experiment was repeated with 0.5 - 1 mM of UNAGEP added to the selected crystallization conditions. The UNAGEP was previously obtained through the enzymatic reaction of BoHTMurA with its substrates UNAG and PEP, as described in section 3.7.1.1, and as shown in the previous chapter will contain a UNAGEP/UNAG mixture.

This modification resulted in the formation of small crystals resembling fine needles, which appeared in the JBScreen PEG Salt B7 (20% PEG 3350 and 200 mM lithium sulfate) and F7 (20% PEG 5000 and 200 mM lithium sulfate), as well as in the JBScreen Classic HTS1 B7 (30% PEG 3000, 100 mM Tris pH 8.5, and 200 mM lithium sulfate), C1 (16% PEG 4000, 100 mM Tris pH 8.5, and 200 mM lithium sulfate) (Figure 6.26A and B), C4 (20% PEG 4000, 100 mM Tris pH 8.5, and 200 mM lithium sulfate), E10 (25% PEG MME 5000, 100 mM Tris pH 8.5, and 200 mM lithium sulfate), and G12 (18% PEG 8000, 100 mM Tris pH 8.5, and 200 mM lithium sulfate) conditions. Although the crystals exhibited irregular growth patterns, some of them were frozen with 20% of glycerol and sent to the Alba Synchrotron for data collection in the Xaloc-MX13 beamline. The diffraction patterns showed spots not resolved, with streaks and very poor spot shapes (Figure 6.26). This issue can be attributed to the occurrence of twinning crystals, a phenomenon characterized by symmetrical intergrowth between two or more adjacent crystals.

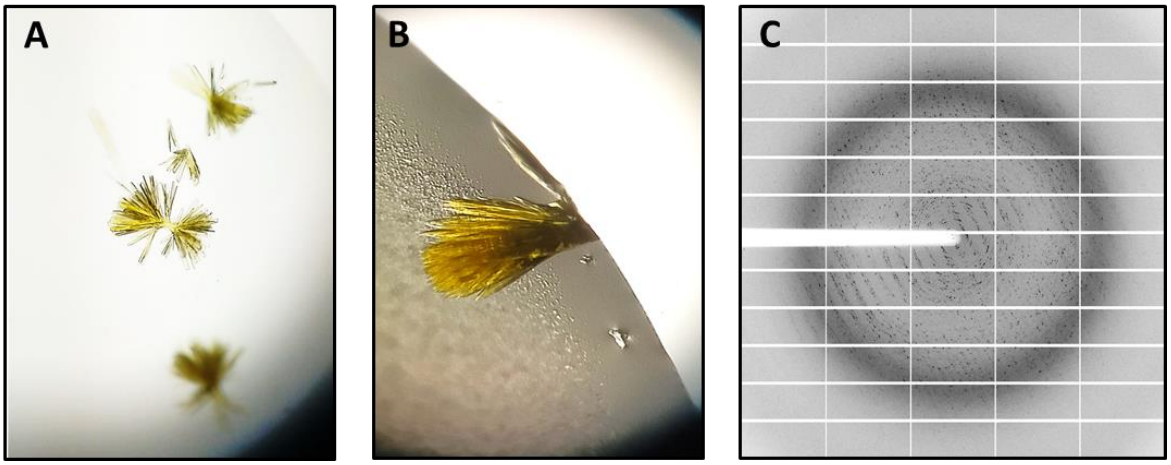

Figure 6.26. BoHTMurB crystals and diffraction pattern. Fibrous needles of BoHTMurB crystals obtained in the presence of UNAGEP by vapor diffusion method in **(A)** sitting drops in 96 wells plates and **(B)** hanging drops in 24 wells plates. 60 or 500 µL of mother liquor (20 % PEG 4000, 200 mM lithium sulfate, 100 mM Tris pH 8.5) were placed in equilibrium against drops containing 1 µL of BoHTMurB (14 mg/ml) and 1 µL of UNAGEP/UNAG (1 mM). **(C)** Pattern obtained from a crystal upon X-ray diffraction.

The conditions described above (including UNAGEP/UNAG) were used to produce BoMurB crystals. Surprisingly, some remarkable crystals were obtained within 4 days (Figure 6.27A). These crystals were cryoprotected with 20% ethylene glycol and sent to the ALBA Synchrotron for data collection in the Xaloc-MX13 beamline. The best data collection reached a resolution of 1.9 Å form 1500 diffraction patterns. The phase problem was solved using the molecular replacement technique, taking as a model the AlphaFold structure for BoMurB (code A5VRH5). The data collection and refinement statistics are presented in Table 6.4.

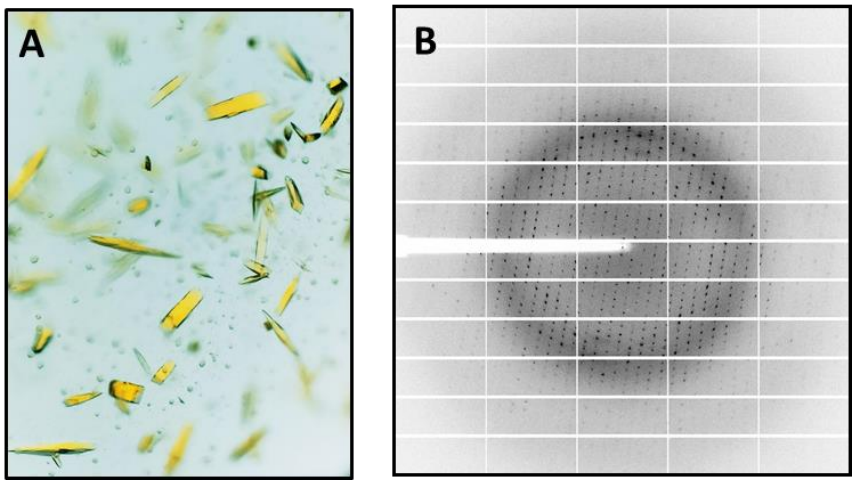

Figure 6.27. BoMurB Crystals and a diffraction pattern. (A) Crystals of BoMurB obtained in the presence of UNAGEP by the vapor diffusion method with sitting drops in 96 wells plates. 60 µl of mother liquor of JBScreen Classic HTS 1, C1 (16 % PEG 4000, 200 mM lithium sulfate, 100 mM Tris pH 8.5) were placed in equilibrium against drops containing 1 µl of BoMurB (25 mg/ml) and 1 µl of UNAGEP/UNAG (1 mM). **(B)** Diffraction pattern obtained from a crystal upon X-ray diffraction.

Table 6.4. Data collection and refinement statistics for BoMurB:UNAGEP complex

Data collection statistics	
Space group	C121
Unit cell parameters	
a, Å	120.03
b, Å	37.53
c, Å	77.9
Wavelength, Å	0.979185
Resolution, Å	77.89-2.10
	(2.21-2.10)
No. of unique reflections	18694
Redundancy	2.7 (2.5)
Completeness, %	90.7 (97.7)
Mn(I)/sd	7.2 (2.1)
R_{merge} [a]	0.080 (0.416)
Refinement Statistics	
Resolution range, Å	60.01-2.10
Protein non-hydrogen atoms	2452
Ligand non-hydrogen atoms	154
Solvent non-hydrogen atoms	103
R_{work} (%)	23.6
R_{free} [b] (%)	27.4
RMSD bond lenght, Å	0.006
RMSD bond angels, °	0.678
Average B-factor, Å^2	38.23

Values in parentheses correspond to the highest resolution shell.
[a] Rsym = Σ| I - Iav |/ Σ I, where the summation is over symmetry equivalent reflections.
[b] R calculated for 5% of data excluded from the refinement

The crystallographic BoMurB model is composed of 322 amino acids, adopts a three-domain structure and shows one molecule of FAD and one molecule of UNAGEP. Its domain I (residues 1-88 at the N-terminus and residues 303-310) consists of three α-helices and six β-strands, which form a four-stranded mixed β-sheet and a two-stranded parallel β-sheet. Domain II (residues 89-221) is comprised of a five-stranded antiparallel β-sheet and seven α-helices. Domain III (residues 222-302 and 311-322 at the C-terminus) includes a three-stranded antiparallel β-sheet and two α-helices (Figure 6.28A and B). The binding pocket for the FAD cofactor is formed mainly by domains I and II, with additional contributions from domain III and the loop connecting domains II and III. Domains II and III together create the substrate binding pocket.

The FAD cofactor is bound by the protein in a folded conformation, which is held in place by a network of H-bond interactions (Figure 6.28C). Specific interactions occur: Gly147 and Arg218 engage with the isoalloxazine ring, Asn74 and Ser73 interact with the ribityl chain, Gly72, Ile71, Gly70, and Gly137 interact with the pyrophosphate moiety,

Val68 binds to the adenine nucleotide, and Phe192 stacks with the adenosine ring of FAD. In addition, four water molecules are H-bonded to some O and N atoms of the isoalloxazine ring. The UNAGEP substrate, interacts with residues Asn149, Tyr181, Arg182, His217, Arg218, and Gln222 from domain II, and residues Ser231, Asn235, Arg251, Met263, His264, and Cys265 from domain III. Additionally, nine water molecules establish interactions with atoms within the UNAGEP substrate (Figure 6.28D).

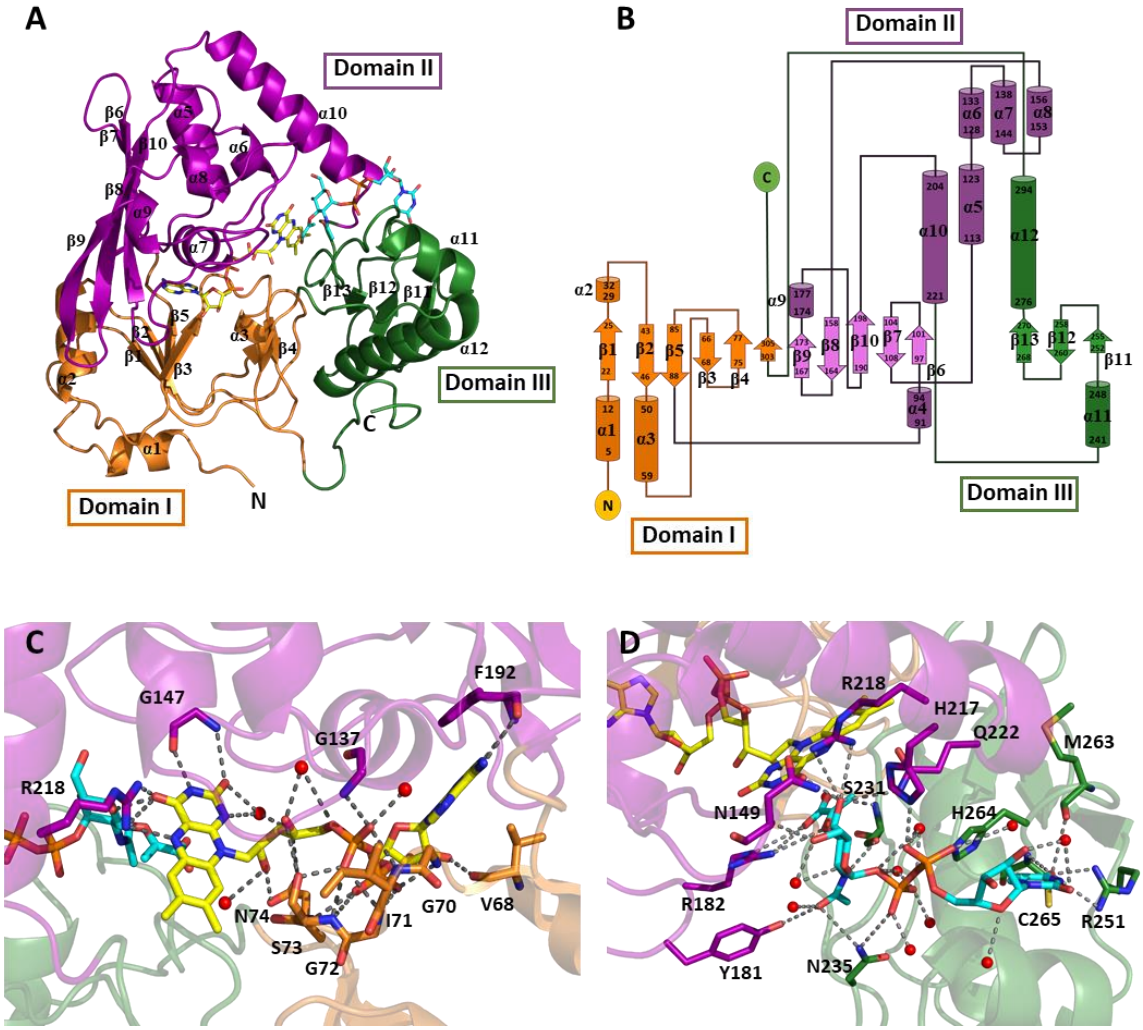

Figure 6.28. BoMurB:UNAGEP complex structural features. (A) Crystal structure of BoMurB with bound FAD cofactor (CPK in yellow sticks) and its substrate UNAGEP (CPK in cyan sticks) and **(B)** topology diagram. Domain I, II and II are colored in orange, purple and green, respectively. Detail of **(C)** the FAD-binding site and **(D)** the UNAGEP-binding site. Residues involved in H-bonds (dotted grey lines) are shown in sticks. Water molecules are represented as red spheres.

The superposition of several MurB type IIa structures (Figure 6.29A) without UNAGEP, on that of BoMurB, shows low RMSD values. For *B. lincheniformis* (BlMurB, 4PYT), a value of 0.9 Å was observed with 239 aligned Cα-atoms; for *S. aureus* (SaMurB, 1HSK), a value of 1.06 Å was obtained with 243 aligned Cα-atoms, both sequences show a

33% of sequence identity with BoMurB. In the case of *L. monocytogenes* (LmMurB, 3TX1), a value of 0.95 Å was obtained with 246 aligned Cα-atoms and 35% sequence identity. These results indicate that the structures are remarkably similar to each other and that the presence of the UNAGEP substrate has little effect on the free structure. Finally, it is worth to note that the sequence of *T. caldophilus* (TcMurB, 2GQU) (Figure 6.29B), classified as MurB type IIb, shares the highest identity percentage with BoMurB (37%) and exhibits an RMSD value of 0.95 Å, with 182 Cα-atoms aligned. This structure has also been solved with its substrate and among other significant differences, the TcMurB structure exhibits a smaller size compared to BoMurB, leading to a lack of structural overlap in regions near the N- and C-termini. Notably, differences are also evident in amino acid regions 89-106 and 54-66 (based on BoMurB numbering), where the loops are significantly shorter in TcMurB.

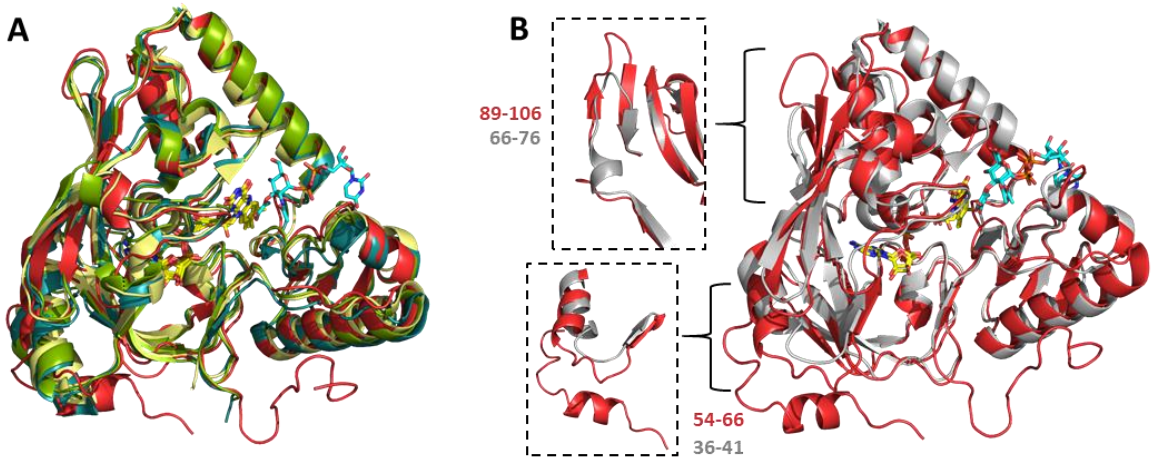

Figure 6.29. Structural comparison of MurBs type II with BoMurB:UNAGEP. (A) Ribbon representation of the superposition of BoMurB (in red color) with the MurBs type IIa: BlMurB (4PYT, in pale yellow color), LmMurB (3TX1, in green color), SaMurB (1HSK, in blue color) and **(B)** with the MurB type IIb, TcMurB (2GQU in grey color). FAD and UNAGEP are represented in yellow and cyan sticks, respectively.

6.3.10 Structural Residue Conservation Analysis

The evolutionary conservation of residues was also plotted on the structure of BoMurB to better evaluate conservation at the binding sites cofactor and substrates. When using the MSA including only *Brucella* species, the highest conservation scores were observed in approximately 68.6% of the amino acids. They were mainly located within the active site cavity, the binding sites of cofactor and substrates, and particularly pointing towards the protein inside. In contrast, residues with the most variable scores make up only 5% of the entire protein structure and sit in general towards its surface. Residues with an average conservation score constitute 26.4% of the structure, totaling 85 amino acids that are in general in the more external structural parts of the protein (Figure 6.30A and B).

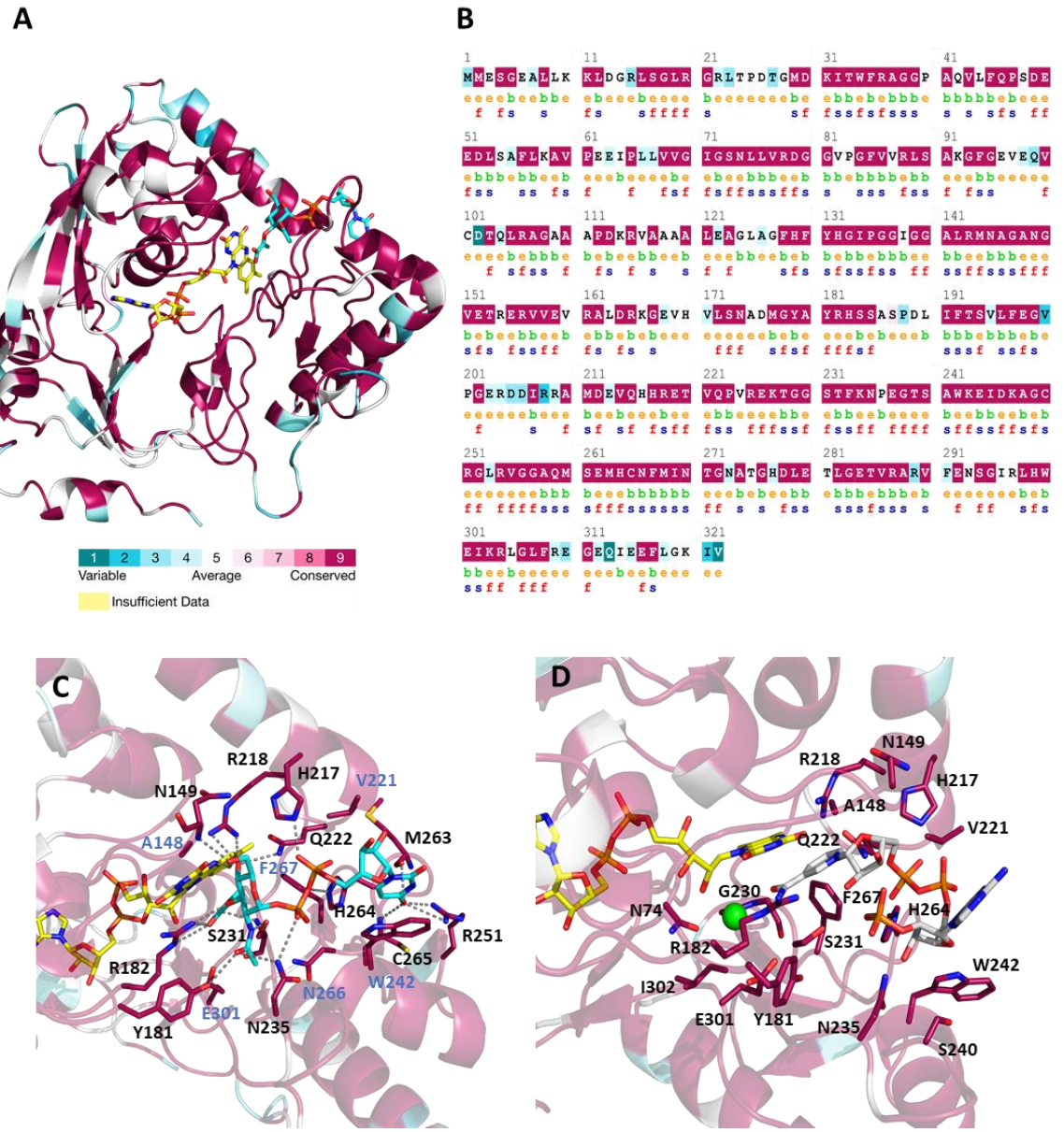

Figure 6.30. Evolutionary structural conservation analysis of BoMurB and *Brucella* sequences. (A) Residue conservation score as calculated by the ConSurf server and plotted on the structural model of BoMurB. Structure shown as cartoon colored according to conservation score (from deep teal as less conserved, to deep magenta as most conserved). **(B)** Plot of conservation scores on BoMurB sequence. Residues are also labelled regarding location ("b", buried; or "e", exposed) and predicted relevance as key structural (s) or functional (f) residues. **(C)** Detail of key residues implicated in the interaction with UNAGEP (CPK colored in cyan sticks). Residues involved in H-bonds (dotted grey lines) are labelled in black, residues close to the UNAGEP but without H-bond are labelled in blue. **(D)** Detail of key residues potentially contributing to $NADP^+$ (CPK colored in grey sticks) interaction. The position of $NADP^+$ is taken from an overlap with the structure of PaMurB (4JAY). FAD is shown in CPK colored yellow sticks.

A similar analysis of bacterial species also revealed a considerable degree of conservation in the structure. Specifically, 44.4% (143 amino acids) of the residues display the highest level of conservation, 54% (174 amino acids) exhibit an average conservation score, and only 1.3% (4 amino acids) are characterized by the most variable conservation

scores (Figure 6.31A and B). The protein residues identified in BoMurB and other species as essential for both structure and function remain conserved across the evaluated bacterial species.

The 12 residues H-bonding the UNAGEP substrate exhibit significant high conservation scores. This observation holds not only within the sequences of *Brucella* species but also for bacteria as a whole (Figure 6.30C and 6.31C). Interestingly, only one pair of residues (His217 and Met263) achieve average scores in the broader bacterial context (Figure 6.31C). Out of these 12 residues, four, namely Arg151, Arg187, Gln190, and Asn202, align consistently with those previously reported in TcMurB:UNAGEP structure (Figure 6.8). It is important to note that this structure is classified as type IIb, which could lead to some variability in the binding site sequences. When comparing these residues to the structure of a type IIa enzyme, like LmMurB, we observe complete conservation of seven residues, Asn133, Tyr169, Arg170, Arg207, Gln211, Ser220, and His253, mirroring their presence in BoMurB.

Furthermore, we examined possible interactions with $NADP^+$ and K^+, by overlapping the BoMurB structure with that of PaMurB (4JAY). It is important to note that PaMurB belongs to type I, and therefore, the presence of loops (α5 from lobe I and β13 from lobe II) in the vicinity of the UNAGEP-NADPH binding sites does not align with the BoMurB structure. This comparative analysis unveiled residues situated in different regions of the substrate, many of which participate in the interaction with UNAGEP. Specifically, residues Ala148, Asn149, Arg218, Glu222, and Phe267 have been identified in the vicinity of the ribose portion. His217, Val221, Asn235, and His264 are found in the area expected for the pyrophosphate moiety, while Ser240 and Trp242 locate close to the phosphoribose moiety of the coenzyme. Notably, none of these residues shows homology with the ones described in the PaMurB structure. Finally, with regards to the K^+ binding site, three out of five residues, Asn74, Glu231, and Ser231 have the potential bind the ion in BoMurB (Figure 6.30 and 6.31D).

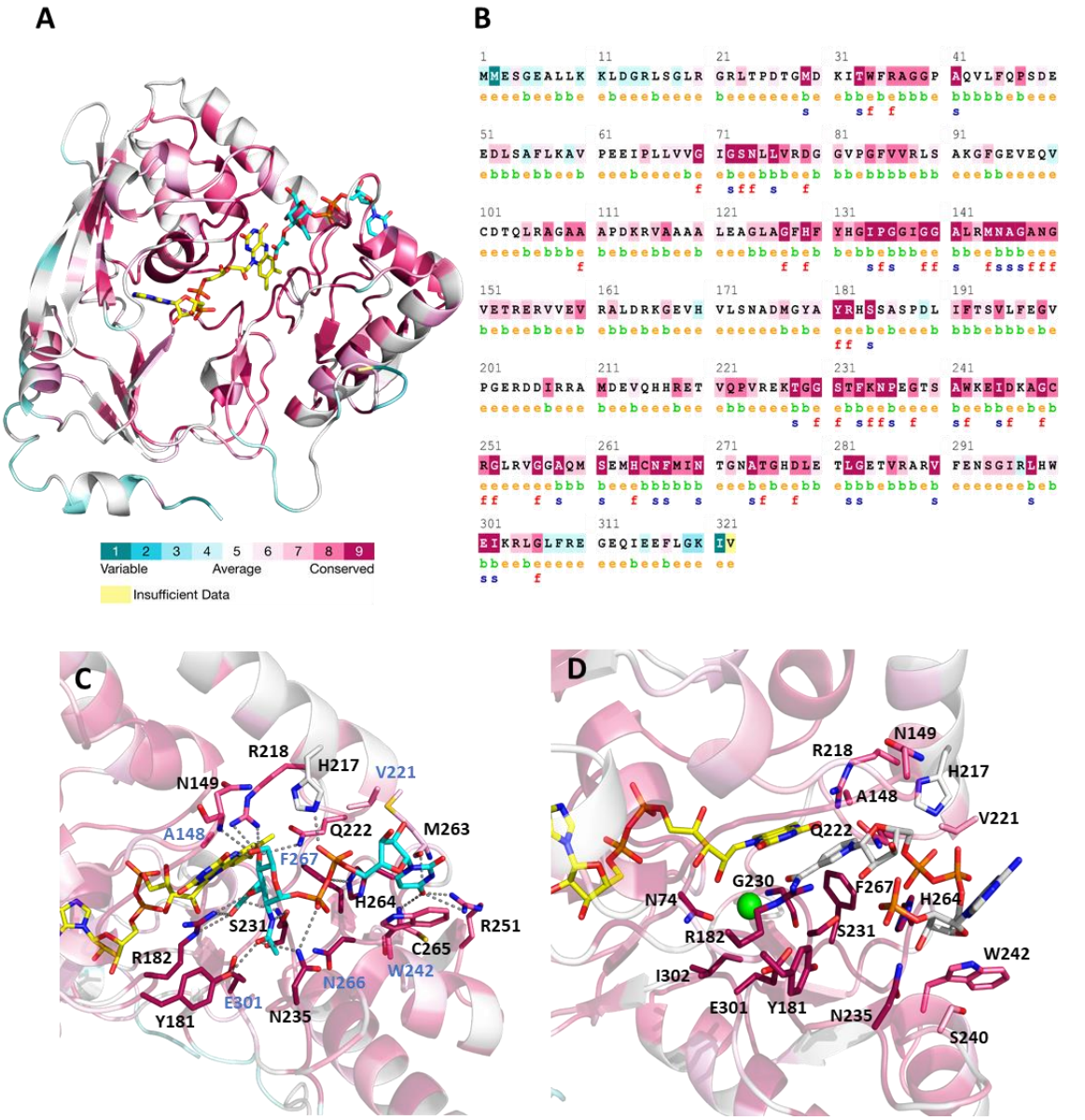

Figure 6.31. Evolutionary Structural conservation analysis of BoMurB and different bacteria sequences. **(A)** Residue conservation score as calculated by the ConSurf server and plotted on the structural model of BoMurB. Structure shown as cartoon colored according to conservation score (from deep teal as less conserved, to deep magenta as most conserved). **(B)** Plot of conservation scores on BoMurB sequence. Residues are also labelled regarding location ("b", buried; or "e", exposed) and predicted relevance as key structural (s) or functional (f) residues. **(C)** Detail of key residues implicated in the interaction with UNAGEP (CPK colored in cyan sticks). Residues involved in H-bonds (dotted grey lines) are labelled in black, residues close to the UNAGEP but without H-bond are labelled in blue. **(D)** Detail of key residues potentially contributing to $NADP^+$ (CPK colored in grey sticks) interaction. The position of $NADP^+$ is taken from an overlap with the structure of PaMurB (4JAY). FAD is shown in CPK colored yellow sticks.

6.4 DISCUSSION

The analysis of MurB sequences among various *Brucella* and bacterial species indicates significant similarity among most of them (Figure 6.12 and 6.14). Additionally, phylogenetic bootstraps demonstrate evolutionary proximity among these proteins (Figure 6.13B and 6.16). However, certain strains of *Bacillus*, including *B. cereus*, *B. thuringiensis subp. konkukian*, *B. anthracis*, and *B. thiaminlyticus*, are expected to have two MurB isoforms. Moreover, a gene with an unique fusion ORF that encodes a fused MurB/C protein was identified in some Verrucomicrobia and Methylacidiphilales (Naqvi et al., 2016). Regarding genome organization, the murB gene is present in most *Brucella* strains in an operon closely resembling that of *B. ovis* (Figure 6.11). A similar operon organization is also observed in *B. licheniformis*, *B. quintana*, *C. aggregans*, *C. pelagibacter*, *G. oxydans*, *L. pneumophila*, *P. zucineum*, and *R. capsulatus*. All of these bacteria have type IIa MurB, despite they do not share any other relevant characteristics. On the contrary, the arrangement of the murB gene differs in other bacteria. In some bacteria, like *C. ammoniagenes*, *M. marinum*, *R. palustris*, *S. pneumoniae*, and *C. trachomatis*, murB is not in any operon. In the case of *S. enterica*, *S. dysenteriae*, *V. cholerae*, *K. pneumoniae*, *E. coli*, and *Enterobacter*, the murB gene co-transcribes along with birA. BirA is a bifunctional protein that displays biotinidase activity and functions as a DNA-binding transcriptional repressor within the biotin operon. As a result, this arrangement is considered as a regulon (Eisenberg et al., 1982). Consequently, additional variability to that provided by the different proteins' types (I, IIa and IIb) might be also envisaged to *in vivo* regulate MurB functionality within different species when considering potential regulation of MurB expression.

BoHTMurB and BoMurB were here successfully purified to homogeneity by the first time. Moreover, spectroscopic and structural conformation assessments indicated that the purified proteins were optimally folded with minimal differences between the two forms of the enzyme (Figures 6.20 and 6.21). The thermal stability of both proteins was assessed through thermal unfolding, where denaturation curves were recorded using far-UV CD and fluorescence emission. When evaluating complexes with mixtures of substrates and proteins, specific unfolding mechanisms and T_m values were observed for each case. The data suggests that $NADP^+$ and particularly UNAGEP have a stabilizing effect on the secondary structure and tertiary conformation of these proteins, influencing the exposure of tryptophan residues (Trp34, Trp242 and Trp300) to the solvent and affecting the release of FAD. These results also indicate that BoMurB is able to bind both substrates (Figure 6.23 and Table 6.3).

Unexpectedly, when subjected to reduction/oxidation tests with the substrates of the reaction it catalyzes, NADPH and UNAGEP, the purified enzyme did not display the expected activity under any of the evaluated conditions (Figure 6.24). Thus, all our attempts to detect the BoHTMurB and BoMurB physiological FAD dependent redox activity failed, apparently by NAD(P)H being unable to reduce it within BoMurB. Thus, despite binding was envisaged by thermal denaturation, the conformation achieved does not appear to get close to that competent for hydride transfer. However, we found several non-physiological electron donors that were able to achieve full flavin reduction (Figure 6.25) and were able to determine its midpoint reduction potential, indicating that the BoMurB FAD cofactor is active from the redox point of view. Noticeably, in most of these situations, reduction occurs after an activation lag phase, without stabilization of any semiquinone intermediate and involving electron donors that do not involve hydride transfer processes as the one expected from the NADPH coenzyme. At this stage, the lag phases detected during reduction by non-physiological electron donors remain unclear, as well the reason why the purified BoMurB does not undergo NADPH oxidation, both in the absence and presence of UNAGEP under any of the evaluated conditions. In this context, it must be notice that kinetic parameters for MurB enzymes have only been reported in three bacterial species (Table 6.5). This includes MurB type I from *E. coli*, the most extensively studied, and MurBs type IIa from *S. pneumoniae* and *S. aureus*, both gram-positive. Considering the potential of MurB as an antimicrobial drug target and the fact that the PDB contains up to 17 MurB structures from 8 distinct species (Table 6.6 and 6.7), this is an astonishing observation. In addition, it is also worth to mention that the reported kinetic parameters for these MurB enzymes show a large dispersion in both k_{cat} and K_m values, differing not only among bacterial species but also within a single species. Variations reported within a single species appear in some cases due to varying experimental conditions, but notable differences are also found among measures carried out by different research groups using similar experimental conditions.

Table 6.5. Kinetic parameters reported for MurB enzymes in different bacterial species.

Organism	Type	k_{cat} (min^{-1})	K_m^{NADPH} (μM)	k_{cat}/K_m^{NADPH} ($\mu M^{-1}.min^{-1}$)	K_m^{UNAGEP} (μM)	k_{cat}/K_m^{UNAGEP} ($\mu M^{-1}.min^{-1}$)	K_d^{NADP+} (μM)	K_d^{UNAGEP} (μM)	Ki^{NADPH} (μM)	Ki^{UNAGEP} (μM)	Salt in media	Experimental Conditions	pH	Reference
E.coli	I	1300	20	65	12	104	2.4	4.1	nd	nd	20 mM KCl	50 mM Tris-HCl, 0.5 mM DTT, 100 μM UNAGEP, 150 μM NADPH. Total volume 500 μl, room T.	8.0	(Benson et al., 1993; 1997)
		840	17	49	2.2	382	0.7	2.7	nd	880 ± 160	50 mM KCl	50 mM Bis-Tris Propane, 125 μM UNAGEP, 150 μM NADPH, 1 μg MurB. Total volume 1 mL, pre 37° 10 min	8.0	(Axley et al., 1997)
		2160	22	98			nd	nd	nd		50 mM KCl	50 mM Bis-Tris Propane, 125 μM UNAGEP, 150 μM NADPH, 1 μg MurB. Total volume of 1 mL, pre 37° 10 min	8.0	(Dhalla et al., 1995)
		3420			20	171	nd	nd		330 ± 40				
		3720	17	219	24	155	nd	nd	910 ± 670	73 ± 19				
		840	43	20			nd	nd	580 ± 180		2 mM KCl			
		960			46	21	nd	nd		300 ± 80				
		2460	20	123	42	59	nd	nd	490 ± 120	430 ± 140			9.0	
		2100	17	124			nd	nd	1600 ± 580		50 mM KCl		7.0	
		2880			18	1160	nd	nd		81 ± 11				
		3060	17	180	19	161	nd	nd	250 ± 60	8 ± 2				
		1920	100	19			nd	nd	nd				6.0	
		2400			25	96	nd	nd		10 ± 3				
		900	11	82			nd	nd	nd	nd	10 mM KCl	50 mM Tris-HCl, 50 μM NADPH, 50 μM UNAGEP. Total volume 200 μl, room T.	8.0	(Yang et al., 2006)
		1080			15	72								
S. aureus	IIa		4.1		0.53	nd	16	41	nd	nd	20 mM KCl	50 mM Tris-HCl, 0.5 mM DTT, 100 μM UNAGEP, 150 μM NADPH, 3-30 pmol MurB. Total volume 100 μl. Monitoring 30-60s for 5 min, room T.	8.0	(Nishida et al., 2006)
		40 [a]	38 [a]	1 [a]		nd	nd	nd	nd	nd				
		270	3.7	73			nd	nd	nd	nd	10 mM KCl	50 mM Tris-HCl,50 μM NADPH, 50 μM UNAGEP. Total volume 200 μl, room T.	8.0	(Yang et al., 2006)
		474			41	11								
			40		15									Benson 2001 Pers comm
S. pneumoniae		798	53	15	nd	nd	nd	nd	nd	nd	no KCl	50 mM Bis-Tris propane, 200 μM UNAGEP, 200 μM NADPH, 0.2 μg/ml enzyme. 37 °C for 20–60 s.	8.0	(Sylvester et al., 2001)
		1080	79	14	89	12	nd	nd	nd	nd	100 mM KCl			

[a] Value corresponding to the enzyme NADPH oxidase activity in the absence of UNAGEP under aerobic conditions.

Sequence and structural analysis within evaluated MurBs also reveals significant conservation in specific segments. For instance, Gly-rich regions play crucial rol in the FAD binding and stabilization of Gly70 and Gly74 (BoMurB numbering) are strictly conserved according to the MSA and WebLogo results, enabling them to contact the pyrophosphate and the ribose 2'-hydroxyl of the adenosine moiety of FAD. Similarly, Gly136, Gly137, and Gly140 promote the tight packing of the propeller against the β-sheet, with Gly147 forming H-bonds with the isoalloxazine ring. Additionally, Arg182 is another highly conserved residue, H-bonding with both the O2 atom of the isoalloxazine and the O3' of ribityl, contributing to charge compensation, much like Arg218 (Figures 6.12 and 6.13A) (Dym & Eisenberg, 2001). However, there is some variability in the substrate binding residues, which are more divergent in the bacterial MSA and WebLogo results (Figures 6.14 and 6.15). In this context, among the amino acids, Phe and Leu stand out as the most conserved, known for their hydrophobic characteristics that generally enhance complex stability. Additionally, Glu residues play a crucial role in stabilizing substrate charge due to their negative charge. Similarly, the catalytic residue distinctive to MurBs, in the case of BoMurB, is Ser231, which forms H-bonds with the N-Acetyl portion and the enol-pyruvyl of the glucosamine of UNAGEP (Figure 6.32A). This is in contrast to the structure of PaMurB (4JAY), where the Ser239 residue H-bonds with the amide of the nicotinamide group of $NADP^+$ and with the K^+ ion (Figure 6.32B).

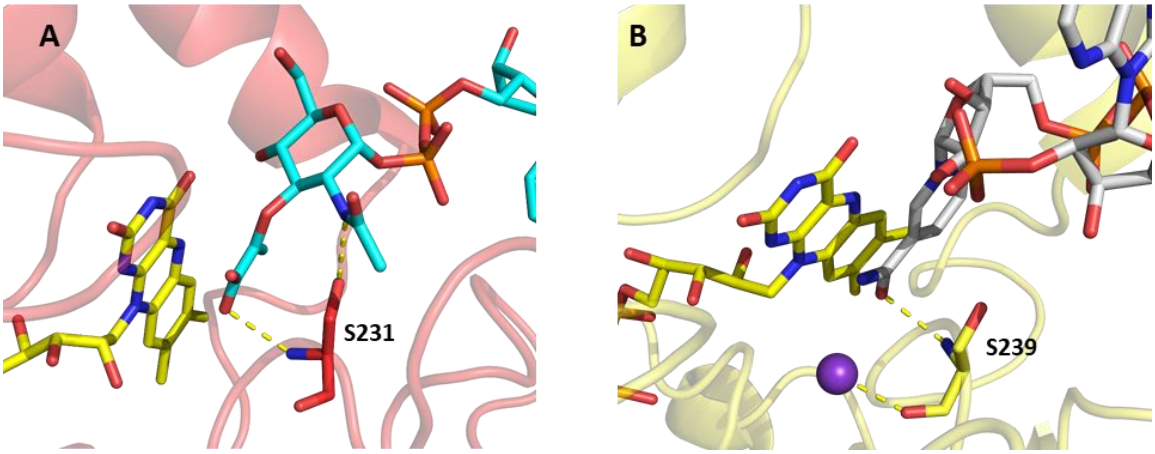

Figure 6.32. Interactions between the catalytic residue and substrates in BoMurB and PaMurB (4JAY). **(A)** Ser231 of BoMurB structure (in red), is shown interacting with N-Acetyl and enol-pyruvyl portion of UNAGEP (CPK in cyan sticks). **(B)** Ser239 of PaMurB structure (in yellow), is shown interacting with amide portion of $NADP^+$ (CPK in grey sticks) and the K^+ ion (purple sphere). FAD (CPK in yellow sticks).

Noticeably, the absence of the 6-His tagged tail and the presence of UNAGEP facilitated the generation of suitable crystals that allowed to solve the structure of the BoMurB:UNAGEP complex. The structural model revealed the three-domain structure typical for type IIa MurB enzymes, including the FAD cofactor and one bound molecule of UNAGEP substrate. The comparative analysis revealed significant structural similarities and a high degree of conservation in specific residues, especially when compared to other MurB proteins, particularly those of the type IIa enzymes. Consequently, the residues that make up the active site and establish H-bonds with FAD in BoMurB are strongly conserved when compared to other MurB proteins. As a result, the residues that make up the active site are mostly highly conserved, both in *Brucella* alignments and in bacteria (Figure 6.30C and 6.31C), and it is determined which residues establish H-bonds with UNAGEP. However, there are some amino acids that do not show a high degree of conservation, such as His217 and Met263. An overlay with the structure of SaMurB, of type IIa as BoMurB (Table 6.6), reveals that in these positions, are residues Arg224 and Lys270, respectively (Figure 6.33A). His and Arg residues share the ability to form H-bonds with substrates due to the functional groups in their side chains, as well as their capacity to donate or accept protons. As there are non reported crystallographic structures of type II MurBs in complex with $NADP^+$ and K^+(Tables 6.6 and 6.7), we used the type I PaMurB structure in complex with $NADP^+$ to speculate on their potential binding mode. Overlapping these structures envisages differences in substrate binding due to the presence of two loops in PaMurB, which are in close proximity to the UNAGEP/NADPH binding site (Figure 6.33B). While BoMurB residues interacting with UNAGEP differed from PaMurB, some showed potential ability for K^+ binding and the reported binding site in PaMurB. The absence of $NADP^+$-bound type II MurB crystallographic structures limits in-depth analysis, particularly for amino acids potentially interacting with the adenosine moiety, which appears solvent-accessible (Figure 6.30D and 6.31D). This exposure may result from variations in loop orientations near α11-α12 and β12-β13 chains in domains II and III.

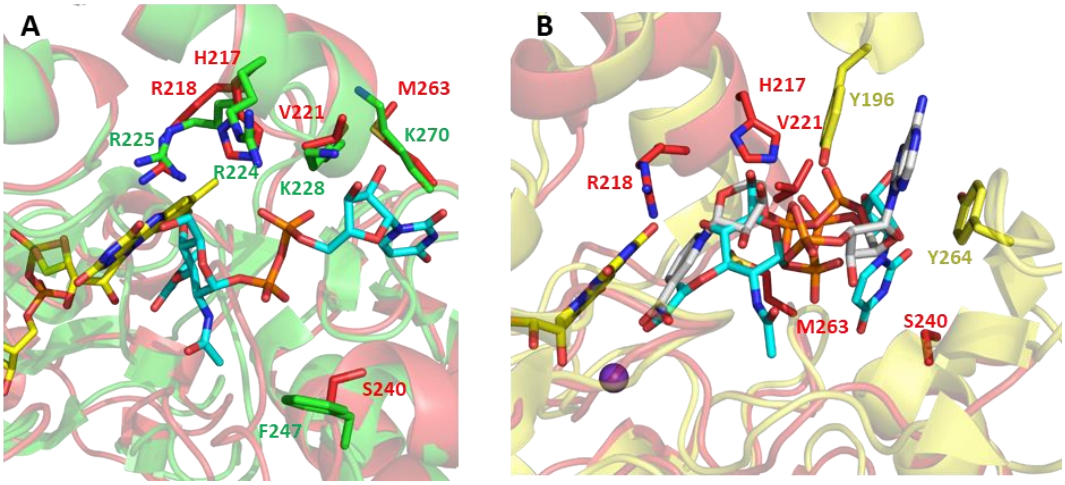

Figure 6.33. Structural superposition of BoMurB with SaMurB (1HSK) and PaMurB (4JAY). (A) BoMurB structure is colored in red, and SaMurB in green. Special residues with divergent score in ConSurf analysis are shown in sticks. **(B)** PaMurB structure is colored in yellow. The two substrates use the same binding site but their conformation differ in the non-reactive parts. FAD (CPK in yellow sticks), UNAGEP (CPK in pink sticks), the $NADP^+$ (CPK in grey sticks) and metal ion (purple sphere) are also shown.

Table 6.6. Summary of structural data for MurB proteins available in the PDB.

Type	Organism	% Identity to BoMurB	PDB	Ligand	Reference
I	*Escherichia coli*	24%	1MBB	EEB, FAD	(Lees et al., 1996)
	Escherichia coli		1MBT	FAD, $SO_4^=$	(Benson et al., 1996)
	Escherichia coli S229A mutant		1UXY	EPU, FAD	(Benson et al., 1997)
	Escherichia coli		2MBR		
	Escherichia coli		2Q85	973, FAD	(Mansour et al. *To be published*)
	Mycobacterium tuberculosis H37Rv	26%	5JZX	FAD, K^+	(Eniyan et al., 2018)
	Pseudomonas aeruginosa PAO1	28%	4JAY	B3P, FAD, K^+, NAP	(Chen et al., 2013)
			4JB1	FAD, GOL, NAP	
			7OSQ	0JI, FAD	(Acebrón-García-de-Eulate et al., 2022)
			7OR2	9FH, FAD	
			7ORZ	0IM, FAD, GOL	
	Vibrio cholerae O1 biovar El Tor str. N16961	24%	3I99	FAD, $PO_4^=$	(Zhang et al. *To be published*)
IIa	*Bacillus licheniformis*	33%	4PYT	Cl^-, FAD, Mg^{+2}	(Auldridge et al., 2015)
	Listeria monocytogenes	35%	3TX1	FAD, GOL, $PO_4^=$	(Filippova et al. *To be published*)
	Staphylococcus aureus	33%	1HSK	FAD	(Benson et al., 2001)
IIb	*Thermus caldophilus*	37%	2GQU	EPU, FAD	(Kim et al., 2006)
			2GQT	Ca^{+2}, FAD	

Table 6.7. Summary of ligands found in the MurB structures deposited in the PDB.

Code names for PDB ligands		
Code	**Name**	**Formula**
973	(5Z)-3-(4-Chlorophenyl)-4-Hydroxy-5-(1-NaphthylMethylene)Furan-2(5H)-One	$C_{21}\,H_{13}\,Cl\,O_3$
0IM	1-phenyl-5-(trifluoromethyl)pyrazole-4-carboxylic acid	$C_{11}\,H_7\,F_3\,N_2\,O_2$
0JI	5-methyl-1-phenyl-1,2,3-triazole-4-carboxylic acid	$C_{11}\,H_{10}\,N_2\,O_2$
9FH	5-methyl-1-phenyl-pyrazole-4-carboxylic acid	$C_{10}\,H_9\,N_3\,O_3$
B3P	2-[3-(2-Hydroxy-1,1-DihydroxyMethyl-Ethylamino)-Propylamino]-2-HydroxyMethyl-Propane-1,3-Diol	$C_{11}\,H_{26}\,N_2\,O_6$
EEB	Uridine-Diphosphate-3(N-AcetylGlucosaminyl) Butiric Acid	$C_{21}\,H_{33}\,N_3\,O_{19}\,P_2$
EPU	Uridine-Diphosphate-2(N-AcetylGlucosaminyl) Butiric Acid	$C_{20}\,H_{29}\,N_3\,O_{19}\,P_2$
FAD	Flavin-Adenine Dinucleotide	$C_{27}\,H_{33}\,N_9\,O_{15}\,P_2$
GOL	Glycerol	$C_3\,H_8\,O_3$
NAP	Nicotinamide-Adenine-Dinucleotide Phosphate	$C_{21}\,H_{28}\,N_7\,O_{17}\,P_3$
$PO_4^{=}$	Phosphate Ion	$O_4\,P^{-3}$
$SO_4^{=}$	Sulfate Ion	$O_4\,S^{-2}$

6.5 CONCLUSIONS

The analysis of MurB sequences in various *Brucella* and bacterial species revealed significant similarity and evolutionary proximity among these proteins, particularly within types. Nonetheless, they might be differently regulated at the expression level, since the genomic context of murB varies across bacteria. Highly conserved glycine-rich regions play a crucial role in binding and stabilizing FAD within MurB proteins. Amino acids involved in substrate binding exhibit some variability, with Phe, Leu, and Glu being among the most conserved and Cys or Ser acting as catalytic residue. The BoMurB samples produced in this study have been shown to be adequately folded, being even able to produce crystals that allowed to solve its 3D structure in complex with the UNAGEP substrate. However, efforts to measure its physiological NADPH-dependent redox enzymatic activity have been unfruitful. Nonetheless, the oxido-reduction ability of its flavin cofactor has been proved by the use of several non-physiological electron donors. Inability of BoMurB to become reduced by NADPH was an unexpected result, but the bibliographic search of kinetic parameters for MurB enzymes came out with data only limited to three species, despite much more 3D structures are found in the PDB. Here, we have also solved the crystal structure BoMurB in complex with UNAGEP. It shows overall folding and features similar to other type IIa MurBs, and places the substrate in a competent position for catalysis. Comparison of this structure with others for type I enzymes in complex with $NADP^+$, clearly envisages a different binding mode at the adenosine moiety of the coenzyme among type I and type II enzymes, and as consequence potential differences in the access of the coenzyme nicotinamide redox active moiety to the active site.

7.

The UDP-N-acetylmuramoyl:L-alanine ligase from Brucella ovis: Insights into functional and structural features in the transformation of UDP-N-acetylmuramic acid to UDP-N-acetylmuramyl-L-alanine

7.1 SUMMARY

UDP-N-acetylmuramoyl:l-alanine ligase (MurC), plays a crucial role in the biosynthesis pathway that starts from UNAG and leads to the formation of the UNAM:pentapeptide unit. This unit serves as the fundamental building block for the PG layer present in the cell walls of all bacteria. The investigation into MurC sequences from diverse bacterial species, including *Brucella*, highlights significant similarity, indicating evolutionary closeness. Phylogenetic analysis supports this relationship. Genomic organization reveals the presence of the MurC gene in *Brucella* strains, often arranged in operons resembling those of other bacteria involved in PG biosynthesis. The protein was cloned with a 6-His tagged (BoHTMurC) and successfully overexpressed in *E. coli*. Subsequently, it was purified and structurally characterized through SDS-PAGE, SEC, CN-PAGE, absorption, CD and fluorescence evaluations. These analyses confirmed that the purified protein exhibits correct folding, and allowed to evaluate its thermal stability. The kinetic characterization of BoHTMurC could not be carried out due to the unavailability of the UNAM substrate. However, a bibliographic analysis was conducted on the kinetic constants discovered for MurCs from species such as *E. coli*, *S. aureus*, *V. spinosum*, *M. tuberculosis*, and *C. trichomantis*. A wide variability in the obtained values was observed, despite similarities in the applied methodologies. The k_{cat} of *E. coli* was calculated, with its highest value reaching 980 min^{-1}, surpassing the others. Crystallographic studies allowed the successful crystallization of BoMurC; however, the achieved resolution of its structure was 3.2 Å. The squences of BoMurC and BoMurB, underwent modeling to assess a potential complex formation between the two proteins, as suggested in various bacterial models. Additionally, a docking analysis between the monomers was conducted, uncovering strong interactions within the formed complexes.

7.2 INTRODUCTION

Mur ligases play an essential role in PG biosynthesis by catalyzing the stepwise formation of the peptide moiety of the PG disaccharide peptide monomer unit (see Chapter 1, Section 1.4). Once UDP-N-acetylmuramic acid (UNAM) has been formed by the sequential action of MurA and MurB, four Mur specific peptide ligases, designated as MurC, MurD, MurE and MurF, catalyze the assembly of the peptide moiety of the monomeric unit by the successive addition of L-alanine, D-glutamic acid, meso-diaminopimelic acid or L-lysine, and D-alanyl-D-alanine to UNAM (Fiuza et al., 2008). All of these Mur-ligases contribute to the formation of non-ribosomal peptide bonds with the concomitant hydrolysis of ATP, and their reaction mechanisms involve the activation of the carboxyl group of the UDP-precursor by ATP, generating an acyl phosphate intermediate and ADP. The acyl phosphate then undergoes nucleophilic attack on the amino group of the condensing amino acid, leading to the formation of a tetrahedral intermediate, which eventually breaks down into an amide, or peptide, and Pi.

7.2.1 The MurC catalytic activity

The UDP-N-acetylmuramoyl:L-alanine ligase (MurC, EC 6.3.2.8) catalyzes the ATP-dependent ligation of L-alanine and UNAM to form UDP-N-acetylmuramyl-L-alanine (UNAM-Ala), creating an amide bond between L-alanine and UNAM. Mechanistic studies on *E. coli* MurC demonstrated an ordered Ter-Ter mechanism, where ATP is the first substrate to bind, followed by UNAM and then L-Ala. These studies support an enzyme-catalyzed reaction comprised by at least two distinct chemical steps: activation of the free UNAM carboxylate by phosphoryl transfer from ATP (forming an acyl phosphate UNAM intermediate), followed by nucleophilic attack on the acyl phosphate group by L-Ala to form a new amide bond with the incoming L-alanine amino acid (Figure 7.1). MurC activities have been shown to require divalent cations and are highly dependent on Mg^{2+} concentrations. MurC enzymes have been reported to exhibit maximum activity in the presence of $MgCl_2$, although they can also use $MnCl_2$. Moreover, monovalent ions, such as K^+ and NH_4^+, appear to be slightly better than some divalent ions when replacing Mg^{2+} (Emanuele et al., 1996; Deva et al., 2003).

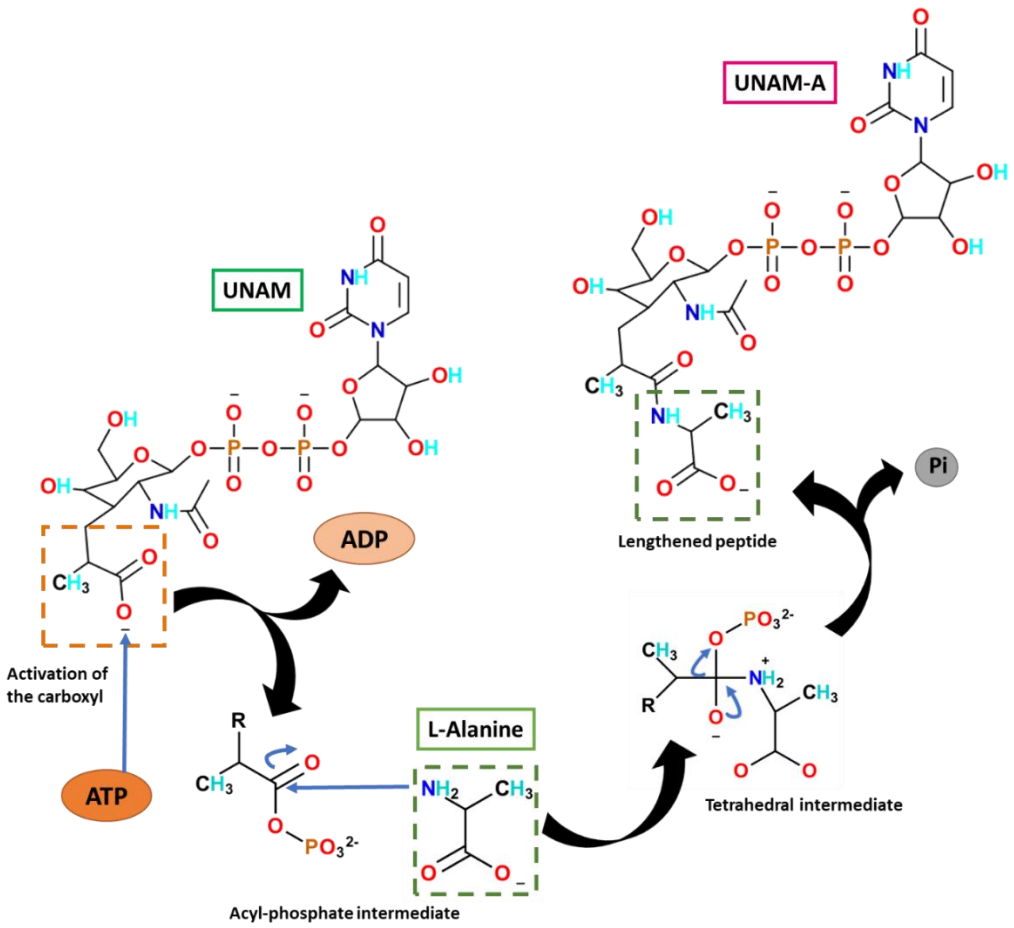

Figure 7.1. MurC catalytic cycle. Scheme of the reaction catalyzed by MurC, including activation of the carboxyl group of UNAM by transfer of the γ-phosphate of ATP, formation of the acyl-phosphate intermediate, nucleophilic attack by the amino group of the condensing amino acid, formation of the THI with the new peptide bond, and production of lengthened peptide and Pi.

Although, L-alanine is the most common amino acid encountered at position 1 of the tetrapeptide, glycine and L-serine can also be alternatives in some species. This could result from variations in the substrate specificity of MurC enzymes, unusual high concentrations of the alternative amino acids in the intracellular pool, or a combination of both factors (Hesse et al., 2003).

7.2.2 Structure of MurC enzymes

All four Mur ligases (EC numbers 6.3.2.*), MurC, MurD, MurE, and MurF, are topologically similar to one another, even though they display low sequence identity (Fiuza et al., 2008). Each ligase is composed of three domains: a N-terminal Rossmann-fold domain responsible for binding the UNAM substrate, a central domain (similar to ATP-binding domains of several ATPases and GTPases), and a C-terminal domain (similar to dihydrofolate reductase fold) that binds the incoming amino acid (Figure 7.2A).

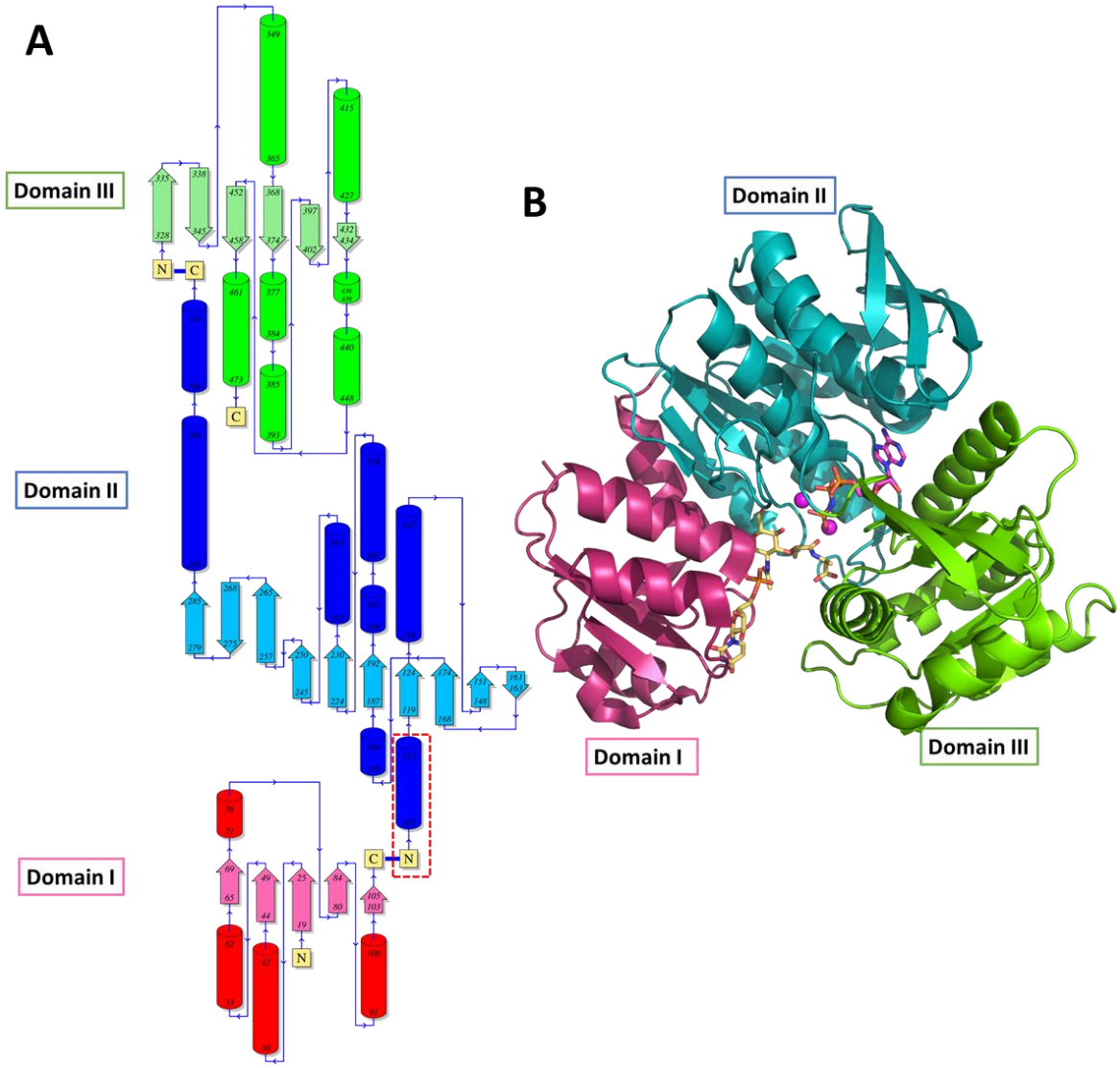

Figure 7.2. Structure of HiMurC (1P3D). (A) Topologic diagram of each domain obtained using PDBsum software (Laskowski et al., 2018). Domains I, II and III are colored red/pink, dark/light blue and dark/light green, respectively for α-helixes (dark colors) and β-sheets (light colors). The alpha-helix delimited in the red dashed rectangle, corresponding to residues 107-117, is identified by PDBsum as part of domain II, whereas in the literature, it is described as part of domain I. **(B)** Tertiary structure colored by domain. UNAM (CPK in yellow sticks), the ATP analog AMP-PNP (CPK in pink sticks) and metal ions (Mn^{+2}, pink spheres) are also shown.

The three domains of MurC enzymes are illustrated by the structure of MurC from *Haemophilus influenzae* (HiMurC with PDB code 1P3D) (Figure 7.2) in complex with UNAM, Mn^{+2} and ANP-PNP (phosphoaminophosphonic acid-adenylate ester) (Mol et al., 2003). Domain I folds into five central β-sheets and four surrounding α-helices with a Rossmann fold architecture typical of dinucleotide-binding proteins. It binds the phosphate groups of the nucleotide moiety of UNAM through a glycine-rich loop, between β1 and α1, which is the GxGxxG fingerprint motif typical of dinucleotide-binding domains. Domain II is the largest, being the ATP-binding domain, and folds in a seven stranded parallel β-sheet (β6-β12) surrounded by five α-helices and is flanked by an antiparallel 3 stranded β-sheet

(β13-β15). The C-terminal domain of MurC (domain III) consists of a central 6 β-sheet, flanked by 5 α-helices. Residues from domain III provide key interactions that orient and position the incoming amino acid ligand with the growing PG chain, in addition to providing contacts with the ribose sugar and the phosphate group of AMP-PNP. Domain III also contains a classic Rossmann dinucleotide-binding fold, but it lacks the GxGxxG fingerprint motif.

Figure 7.3 shows how HiMurC binds the UDP half of the UNAM substrate. The uracil ring sits in a site formed by the β2-α2 and β4-α4 loops, between the side-chains of Ile50 on one side and Ala86 and Ile87 on the other side, and with its N1 atom H-bonding the side-chain of His70. On its side, the sugar hydroxyl groups are positioned towards the carboxylate oxygens of Asp49. The alpha-phosphate of the UDP portion interacts with the main chain atoms of Ala29, whereas the beta-phosphate is located between Gly30 and Ser84. The N-acetylmuramic acid portion of UNAM extends towards the cleft formed among the three MurC domains, becoming stabilized by two Arg and one His residues from domain III.

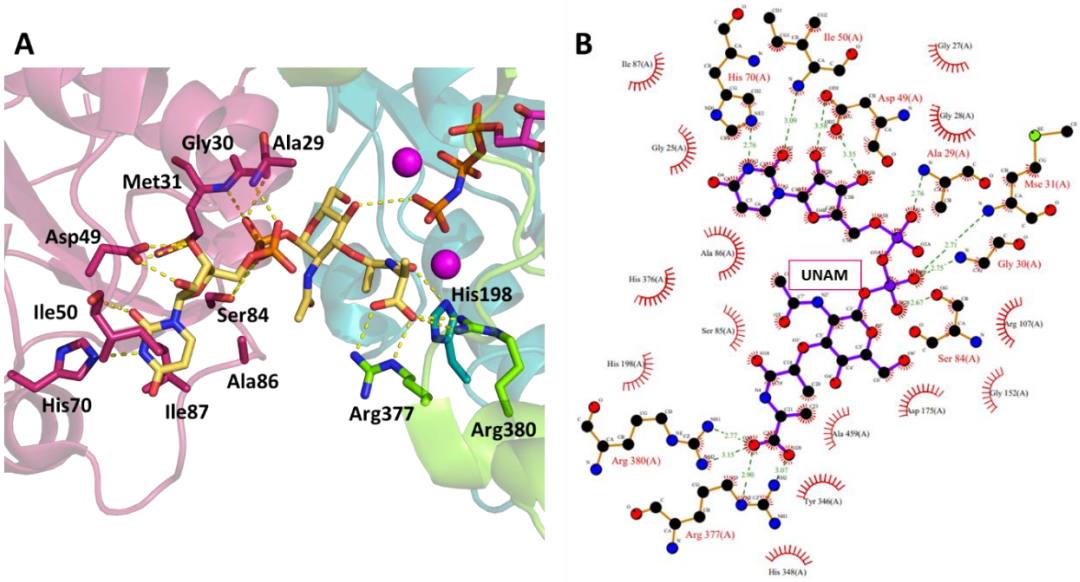

Figure 7.3. The site of interaction of HiMurC (1P3D) with UNAM. (A) Detail of residues interacting with the UNAM substrate (CPK in yellow sticks). **(B)** LIGPLOT diagram of interaction. The UNAM molecule is represented as a purple ball-and-stick model. H-bonds and van der Waals interactions are indicated by green dashes and radiating red lines, respectively.

The HiMurC structure in complex with the ANP-PNP (ATP non-hydrolysable analog) places the ATP-binding site at the interface between domains I and II (Figure 7.4). Nonetheless, the substrate adenine ring and α- and β-phosphates bind particularly to the ATP-binding domain (domain II). A glycine-rich loop linking strand β6 and helix α6 results a key binding determinant to α- and β-phosphates. This motif is equivalent in location and

sequence to the classical mononucleotide-binding P-loop (AGTHGKTTTT) observed in many kinases and ATPases, and is present as a consensus sequence of the other Mur ligases (Bertrand et al., 1999; Gordon et al., 2001). In particular, Thr131 H-bonds to an α-phosphate oxygen, and Thr130 and Lys129 to two oxygen atoms of the β-phosphate group. In addition, two metal atoms (Mn^{2+}) contribute to linking the β- and γ-phosphates to different residues of domain II, while water-mediated interactions of the metals with the side chains of Glu176, Asp197, and His348 are also detected. The adenine ring of AMP-PNP is inserted into a pocket of domain II, between the peptide backbone of Gly128 and the side chain of His291, and its N7 and exocyclic N6 atoms H-bond N2 and O1 atoms, respectively, of the strictly conserved Asn295. Finally, the ribose is H-bonded to Thr356 and Asp345 in domain III, while the side-chain of Arg326, also in domain III, balances the negative charge of the α-phosphate.

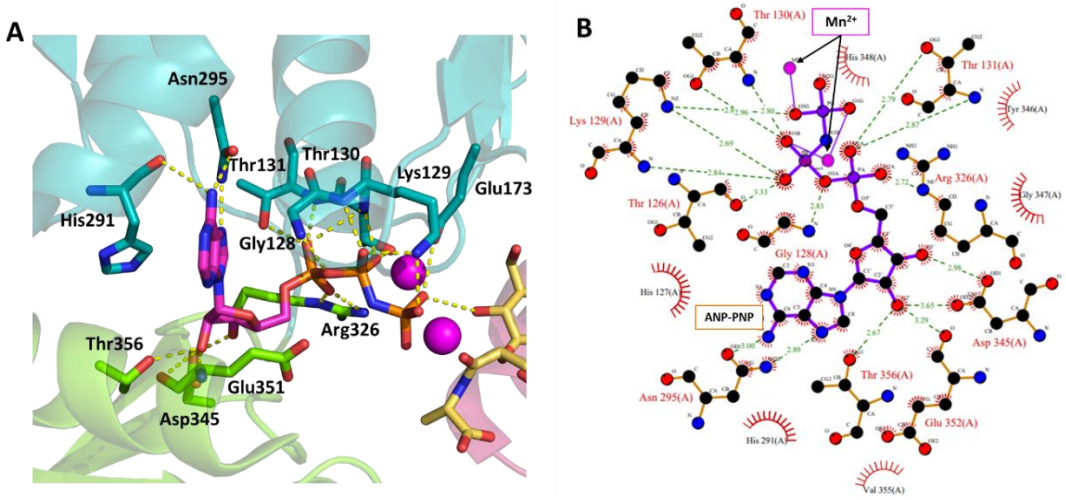

Figure 7.4. The site of interaction of ANP-PNP in HiMurC (1P3D). (A) Detail of residues interacting with ANP-PNP (CPK in pink sticks), the P-loop in domain II is shown in blue, domain III in green and Mn^{2+} in pink spheres. **(B)** LIGPLOT diagram of the interaction. The ANP-PNP molecule is represented as a purple ball-and-stick model. H-bonds and van der Waals interactions are indicated as green dashes and radiating red lines, respectively.

The binding site for the amino acid substrate has not yet been determined experimentally. A structural comparison with other Mur ligases has helped to identify the potential L-Ala binding site as formed by two loops on the upper surface of domain III that sit adjacent to the active site (Bertrand et al., 1999; Gordon et al., 2001). Thus, His376, Arg377 and Arg380 residues in the β18-α12 loop are proposed to interact with the L-Ala carboxylate, along with Tyr346 and His348 in the adjacent β17-α11 loop.

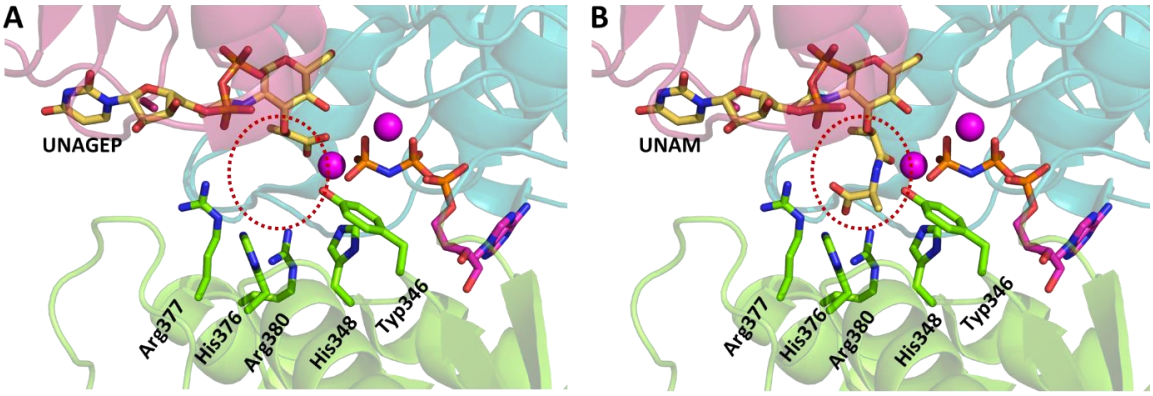

Figure 7.5. The potential site of interaction of L-alanine in domain III. HiMurC binding sites for **(A)** UNAGEP (1P31) and **(B)** UNAM (1P3D). Both ligands are shown in yellow sticks (carbon atoms), ANP-PNP is in pink sticks (carbon atoms) and Mn^{2+} is in pink spheres. The dashed red line represents the L-Ala carboxylate binding site.

4.2.3 Inhibitors of MurC

A series of compounds have been designed and synthesized as MurC inhibitors from different species. Many examples of these drugs (Figure 7.6) are pyrazolopyrimidines derivatives, known to possess antimicrobial and antifungal activities (Khobragade et al., 2010). These molecules have been reported to inhibit the PG biosynthesis *in vivo* by targeting *E. coli* and *P. aerugiunosa* MurCs (Hameed et al., 2014). Some others such as benzylidine rhodamine and its analogues also show optimal inhibition against Gram-positive methicillin resistant *S. aureus* (MRSA) and MurC enzymes (Bryskier, 2005; Maddila et al., 2020), but unfortunately, they show toxicity in hamster cells (Sim et al., 2002). Since several acyl phosphate intermediates are formed in the metabolic pathway of Mur ligases, phosphinate inhibitors have been developed that mimic the tetrahedral reaction center of the transition state (Marmor et al., 2001; Štrancar et al., 2006, 2007), and so far these are the most efficient compounds and are not toxic for the host. In addition, novel series of benzene-1,3 dicarboxylic acid 2,5-dimethylpyrrole have been designed as transition-state analogs against multiple bacterial Mur ligases (Humljan et al., 2008; Perdih et al., 2014).

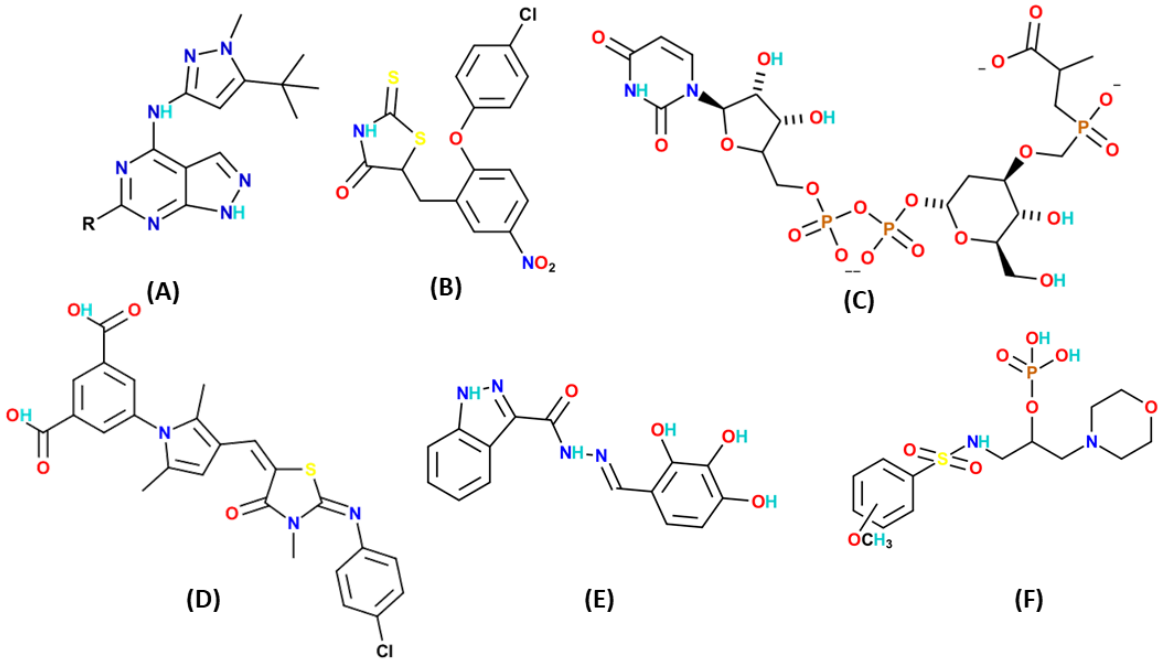

Figure 7.6. Inhibitors of MurC activity. Examples of derivatives of **(A)** pyrazolopyrimidines, **(B)** benzylidene rhodamine, **(C)** phosphinate, **(D)** benzene-1,3 dicarboxylic acid 2,5-dimethylpyrrole, **(E)** N-acylhydrazones and **(F)** phosphorylated hydroxyethylamines.

Since Mur ligases share a similar structure and activity, most inhibitors developed recently aim to inhibit all ligases equally. Some examples of these multi targets drugs are: the N-acylhydrazone scaffold compounds, which bind to ATP sites and were shown to be successful inhibitors of MurC and MurD (Šink et al., 2008), phosphorylated hydroxyethylamines derivatives that inhibit MurC to MurF (Sadeghian et al., 2010), feglymycin (see Chapter 5, section 5.2.3), which inhibit MurA and MurC in *E. coli* (Rausch et al., 2011) and 3, 5-dioxopyrazolidines derivatives (see Chapter 6, section 6.2.3) tested to inhibit MurB and MurC enzymes (Yang et al., 2006).

7.3 RESULTS

7.3.1 Overall characteristics of MurC from *B. ovis*

The *B. ovis* ATCC 25840 murC gene (BomurC), NCBI ID 45124764, is localized in the chromosome I (NC_009505.1) with a locus tag named BOV_RS06855, in the specific region from 1394162 to1395577. BomurC is part of the same operon mentioned in Section 6.3.1, positioned upstream of BomurB. ProtParam analysis of the BoMurC sequence indicated that it consists of 471 amino acids and 7,145 atoms, with a Mw of 50,794 Da and a theoretical pI of 5.86. The theoretical extinction coefficient for BoMurC at 280 nm computed in water is 31.5 $mM^{-1}cm^{-1}$. The instability index (II) was computed as 38.48, suggesting that BoMurC is a stable protein. It is also mainly hydrophobic, as evidenced by its aliphatic index of 93.82 and GRAVY score of -0.054. These findings provide useful information for studying enzyme production as well as biochemical and structural characterization. The BoMurC sequence envisages folding in three domains: the first, a Rossmann-fold Mur_ligase Pfam domain (PF01225), that binds the UNAM substrate; the second, referred to as Mur_ligase_M (PF08245), is responsible for ATP binding; and the third, the Mur_ligase_C (PF02875), binds the incoming amino acid.

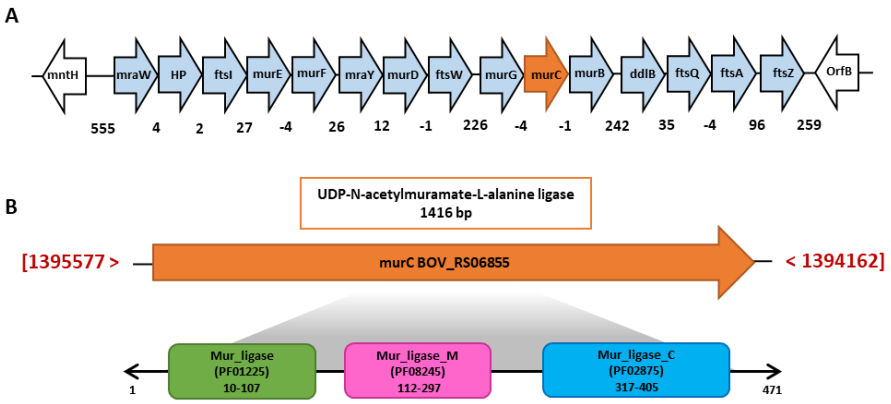

Figure 7.7. Genomic context of BoMurC and domain protein description. (A) Operon that contains several of the genes involved in PG biosynthesis in *B. ovis*. The murC gene is shown in orange. Nearby genes predicted to be in the same operon are colored in light blue. Genes upstream and downstream of the operon are shown in white. The arrowhead indicates the direction of transcription. The numbers below the genes indicate the intergenic distance between two adjacent genes. Negative numbers indicate overlapping genes. Each gene was labelled according to its name. **(B)** Genomic region that determines the precise location inside the genome (NC_009505.1: 1392M-1398M) flanked by a red strip of the 1416 bp murC gene is shown by orange arrow. Three boxes are displayed, indicating the Pfam domains associated with the 471 amino acids of the transcript: the three different Mur_ligase domains are shown in green, pink and blue boxes.

7.3.2 Sequence and evolutionary analysis of MurC proteins in *Brucella* spp.

Following the approach outlined in chapter 5, section 5.3.2., the murC coding sequences from 52 *Brucella* species were retrieved (Table 7.1). *B. ovis*, like most Brucellae studied, has a single gene coding for MurC. Figure 7.8 shows that BoMurC exhibits

significant resemblance to MurC counterparts found in other *Brucella* species. Among these species, *B. endophytica* displayed the lowest similarity (85% identity). On the other hand, *B. anthropi*, *B. daejeonesis*, *B. gallinifaecis*, *B. grignonensis*, *B. thiophenivorans*, *B. lupini*, *B. oryzae*, *B. precoris*, *B. pituitosa*, *B. pseudogringonensis*, *B. rhizosphaerae*, *B. tritici* and *B.* sp. BTU1 exhibited identity levels to BoMurC ranging from 92 to 94%, whereas the remaining species demonstrated identities exceeding 95%. Furthermore, the WebLogo analysis (Figure 7.9A) revealed that particularly the active site residues remain conserved across all examined *Brucella* sequences. Specifically, several amino acids implicated in substrate/product binding exhibit 100% conservation. These residues included Ile18, Gly19, Met20, Asp38, Gln39, His59, Ser73, Ala75, Ile76, and His187 (BoMurC numbering) for the UNAM substrate; Tyr337, His339, His369, Arg370, and Arg373 for the added L-Ala; Gly117, Lys118, Thr119, Thr120, His286, Asn290, Asp336, Arg321, and Val347 for the ATP substrate; and Glu165, Glu186, and His339 for the metal ion binding.

Table 7.1. List of *Brucella* strains with complete assembled genome for which MurC sequences are evaluated in this study. *B. ovis* is highlighted in bold.

Strain	Protein Code	Strain	Protein Code
B.abortus	ACD72850.1	*B.tritici*	KAB2686355.1
B.anthropi	WP_061346008.1	*B.vulpis*	CUW48864.1
B.canis	ABX62494.1	*B.*sp.BO2	EFM58165.1
B.ceti	EEH14090.1	*B.*sp.BO3	QMV26647.1
B.cytisi	OIS95237.1	*B.*sp.BTU1	QWK76880.1
B.daejeonensis	MBB5702669.1	*B.*sp.B13-0095	OEI83816.1
B.endophytica	GGA97321.1	*B.*sp.F5/06	ENT09867.1
B.gallinifaecis	TPF76629.1	*B.*sp.F5/99	EEY26589.1
B.grignonensis	OYR13669.1	*B.*sp.F8/99	ENT15394.1
B.haematophila	RIA06605.1	*B.*sp.F23/97	ENT08625.1
B.inopinata	WP_008506257.1	*B.*sp.F96/2	ENT16332.1
B.intermedia	QNQ39870.1	*B.*sp.NVSL 07-0026	EFG38344.1
B.lupini	OYR31772.1	*B.*sp.UK1/97	ENT22013.1
B.melitensis	AAL51761.1	*B.*sp.UK40/99	ENT22624.1
B.microti	ACU48408.1	*B.*sp.04-5288	ERU00207.1
B.neotomae	EEY04971.1	*B.*sp.09RB8471	APX70439.1
B.oryzae	PQA73408.1	*B.*sp.09RB8910	APY14489.1
B. ovis	**ABQ61623.1**	*B.*sp.10RB9215	SBW14256.1
B.pecoris	TNV09892.1	*B.*sp.191011898	CAB4326116.1
B.pinnipedialis	EEY00763.1	*B.*sp.2002734562	AOG44049.1
B.pituitosa	KAB0571874.1	*B.*sp.2280	QGA56280.1
B.pseudintermedia	KAB2685281.1	*B.*sp.458	QTN99158.1
B.pseudogrignonensis	OYR29943.1	*B.*sp.56/94	ENT00830.1
B.rhizosphaerae	OYR12759.1	*B.*sp.63/311	ENT05231.1
B.suis	ABY38520.1	*B.*sp.6810	QNQ62928.1
B.thiophenivorans	OYR22276.1	*B.*sp.83/13	EEZ33320.1

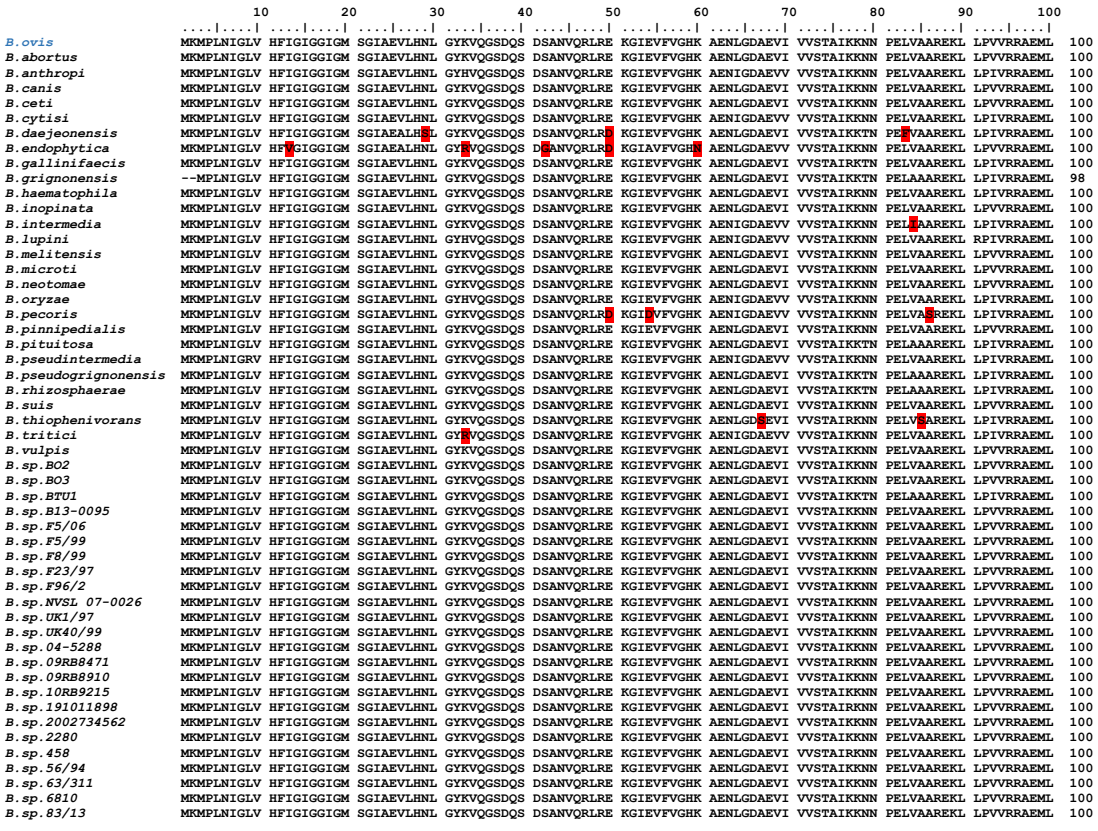
10 20 30 40 50 60 70 80 90 100
B.ovis MKMPLNIGLV HFIGIGGIGM SGIAEVLHNL GYKVQGSDQS DSANVQRLRE KGIEVFVGHK AENLGDAEVI VVSTAIKKNN PELVAAREKL LPVVRRAEML 100
B.abortus MKMPLNIGLV HFIGIGGIGM SGIAEVLHNL GYKVQGSDQS DSANVQRLRE KGIEVFVGHK AENLGDAEVI VVSTAIKKNN PELVAAREKL LPVVRRAEML 100
B.anthropi MKMPLNIGLV HFIGIGGIGM SGIAEVLHNL GYHVQGSDQS DSANVQRLRE KGIEVFVGHK AENIGDAEVV VVSTAIKKNN PELVAAREKL LPIVRRAEML 100
B.canis MKMPLNIGLV HFIGIGGIGM SGIAEVLHNL GYKVQGSDQS DSANVQRLRE KGIEVFVGHK AENLGDAEVI VVSTAIKKNN PELVAAREKL LPVVRRAEML 100
B.ceti MKMPLNIGLV HFIGIGGIGM SGIAEVLHNL GYKVQGSDQS DSANVQRLRE KGIEVFVGHK AENLGDAEVI VVSTAIKKNN PELVAAREKL LPVVRRAEML 100
B.cytisi MKMPLNIGLV HFIGIGGIGM SGIAEVLHNL GYKVQGSDQS DSANVQRLRE KGIEVFVGHK AENIGDAEVV VVSTAIKKNN PELVAAREKL LPIVRRAEML 100
B.daejeonensis MKMPLNIGLV HFIGIGGIGM SGIAEALHSL GYKVQGSDQS DSANVQRLRD KGIEVFVGHK AENLGDAEVI VVSTAIKKTN PEIVAAREKL LPIVRRAEML 100
B.endophytica MKMPLNIGLV HFVGIGGIGM SGIAEALHNL GYEVQGSDQS DSANVQRLRD KGIAVFVGHN AENLGDAEVV VVSTAIKKNN PELVAAREKL LPVVRRAEML 100
B.gallinifaecis MKMPLNIGLV HFIGIGGIGM SGIAEVLHNL GYKVQGSDQS DSANVQRLRE KGIEVFVGHK AENLGDAEVI VVSTAIRKTN PELVAAREKL LPIVRRAEML 100
B.grignonensis --MPLNIGLV HFIGIGGIGM SGIAEVLHNL GYKVQGSDQS DSANVQRLRE KGIEVFVGHK AENLGDAEVI VVSTAIKKTN PELAAAREKL LPIVRRAEML 98
B.haematophila MKMPLNIGLV HFIGIGGIGM SGIAEVLHNL GYKVQGSDQS DSANVQRLRE KGIEVFVGHK AENLGDAEVI VVSTAIRKNN PELVAAREKL LPIVRRAEML 100
B.inopinata MKMPLNIGLV HFIGIGGIGM SGIAEVLHNL GYKVQGSDQS DSANVQRLRE KGIEVFVGHK AENLGDAEVI VVSTAIKKNN PELVAAREKL LPVVRRAEML 100
B.intermedia MKMPLNIGLV HFIGIGGIGM SGIAEVLHNL GYKVQGSDQS DSANVQRLRE KGIEVFVGHK AENIGDAEVV VVSTAIKKNN PELIAAREKL LPIVRRAEML 100
B.lupini MKMPLNIGLV HFIGIGGIGM SGIAEVLHNL GYHVQGSDQS DSANVQRLRE KGIEVFVGHK AENIGDAEVV VVSTAIKKNN PELVAAREKL RPIVRRAEML 100
B.melitensis MKMPLNIGLV HFIGIGGIGM SGIAEVLHNL GYKVQGSDQS DSANVQRLRE KGIEVFVGHK AENLGDAEVI VVSTAIKKNN PELVAAREKL LPVVRRAEML 100
B.microti MKMPLNIGLV HFIGIGGIGM SGIAEVLHNL GYKVQGSDQS DSANVQRLRE KGIEVFVGHK AENLGDAEVI VVSTAIKKNN PELVAAREKL LPVVRRAEML 100
B.neotomae MKMPLNIGLV HFIGIGGIGM SGIAEVLHNL GYKVQGSDQS DSANVQRLRE KGIEVFVGHK AENLGDAEVI VVSTAIKKNN PELVAAREKL LPVVRRAEML 100
B.oryzae MKMPLNIGLV HFIGIGGIGM SGIAEVLHNL GYHVQGSDQS DSANVQRLRE KGIEVFVGHK AENIGDAEVV VVSTAIKKNN PELVAAREKL LPIVRRAEML 100
B.pecoris MKMPLNIGLV HFIGIGGIGM SGIAEVLHNL GYKVQGSDQS DSANVQRLRD KGIDVFVGHK AENIGDAEVV VVSTAIKKNN PELVASREKL LPIVRRAEML 100
B.pinnipedialis MKMPLNIGLV HFIGIGGIGM SGIAEVLHNL GYKVQGSDQS DSANVQRLRE KGIEVFVGHK AENLGDAEVI VVSTAIKKNN PELVAAREKL LPVVRRAEML 100
B.pituitosa MKMPLNIGLV HFIGIGGIGM SGIAEVLHNL GYKVQGSDQS DSANVQRLRE KGIEVFVGHK AENLGDAEVI VVSTAIKKTN PELAAAREKL LPIVRRAEML 100
B.pseudintermedia MKMPLNIGRV HFIGIGGIGM SGIAEVLHNL GYKVQGSDQS DSANVQRLRE KGIEVFVGHK AENIGDAEVV VVSTAIKKNN PELVAAREKL LPIVRRAEML 100
B.pseudogrignonensis MKMPLNIGLV HFIGIGGIGM SGIAEVLHNL GYKVQGSDQS DSANVQRLRE KGIEVFVGHK AENLGDAEVI VVSTAIKKTN PELAAAREKL LPIVRRAEML 100
B.rhizosphaerae MKMPLNIGLV HFIGIGGIGM SGIAEVLHNL GYKVQGSDQS DSANVQRLRE KGIEVFVGHK AENLGDAEVI VVSTAIKKTN PELAAAREKL LPIVRRAEML 100
B.suis MKMPLNIGLV HFIGIGGIGM SGIAEVLHNL GYKVQGSDQS DSANVQRLRE KGIEVFVGHK AENLGDAEVI VVSTAIKKNN PELVAAREKL LPVVRRAEML 100
B.thiophenivorans MKMPLNIGLV HFIGIGGIGM SGIAEVLHNL GYKVQGSDQS DSANVQRLRE KGIEVFVGHK AENLGDSEVI VVSTAIRKNN PELVSAREKL LPIVRRAEML 100
B.tritici MKMPLNIGLV HFIGIGGIGM SGIAEVLHNL GYEVQGSDQS DSANVQRLRE KGIEVFVGHK AENIGDAEVV VVSTAIKKNN PELVAAREKL LPIVRRAEML 100
B.vulpis MKMPLNIGLV HFIGIGGIGM SGIAEVLHNL GYKVQGSDQS DSANVQRLRE KGIEVFVGHK AENLGDAEVI VVSTAIKKNN PELVAAREKL LPVVRRAEML 100
B.sp.BO2 MKMPLNIGLV HFIGIGGIGM SGIAEVLHNL GYKVQGSDQS DSANVQRLRE KGIEVFVGHK AENLGDAEVI VVSTAIKKNN PELVAAREKL LPVVRRAEML 100
B.sp.BO3 MKMPLNIGLV HFIGIGGIGM SGIAEVLHNL GYKVQGSDQS DSANVQRLRE KGIEVFVGHK AENLGDAEVI VVSTAIKKNN PELVAAREKL LPVVRRAEML 100
B.sp.BTU1 MKMPLNIGLV HFIGIGGIGM SGIAEVLHNL GYKVQGSDQS DSANVQRLRE KGIEVFVGHK AENLGDAEVI VVSTAIKKTN PELAAAREKL LPIVRRAEML 100
B.sp.B13-0095 MKMPLNIGLV HFIGIGGIGM SGIAEVLHNL GYKVQGSDQS DSANVQRLRE KGIEVFVGHK AENLGDAEVI VVSTAIKKNN PELVAAREKL LPVVRRAEML 100
B.sp.F5/06 MKMPLNIGLV HFIGIGGIGM SGIAEVLHNL GYKVQGSDQS DSANVQRLRE KGIEVFVGHK AENLGDAEVI VVSTAIKKNN PELVAAREKL LPVVRRAEML 100
B.sp.F5/99 MKMPLNIGLV HFIGIGGIGM SGIAEVLHNL GYKVQGSDQS DSANVQRLRE KGIEVFVGHK AENLGDAEVI VVSTAIKKNN PELVAAREKL LPVVRRAEML 100
B.sp.F8/99 MKMPLNIGLV HFIGIGGIGM SGIAEVLHNL GYKVQGSDQS DSANVQRLRE KGIEVFVGHK AENLGDAEVI VVSTAIKKNN PELVAAREKL LPVVRRAEML 100
B.sp.F23/97 MKMPLNIGLV HFIGIGGIGM SGIAEVLHNL GYKVQGSDQS DSANVQRLRE KGIEVFVGHK AENLGDAEVI VVSTAIKKNN PELVAAREKL LPVVRRAEML 100
B.sp.F96/2 MKMPLNIGLV HFIGIGGIGM SGIAEVLHNL GYKVQGSDQS DSANVQRLRE KGIEVFVGHK AENLGDAEVI VVSTAIKKNN PELVAAREKL LPVVRRAEML 100
B.sp.NVSL 07-0026 MKMPLNIGLV HFIGIGGIGM SGIAEVLHNL GYKVQGSDQS DSANVQRLRE KGIEVFVGHK AENLGDAEVI VVSTAIKKNN PELVAAREKL LPVVRRAEML 100
B.sp.UK1/97 MKMPLNIGLV HFIGIGGIGM SGIAEVLHNL GYKVQGSDQS DSANVQRLRE KGIEVFVGHK AENLGDAEVI VVSTAIKKNN PELVAAREKL LPVVRRAEML 100
B.sp.UK40/99 MKMPLNIGLV HFIGIGGIGM SGIAEVLHNL GYKVQGSDQS DSANVQRLRE KGIEVFVGHK AENLGDAEVI VVSTAIKKNN PELVAAREKL LPVVRRAEML 100
B.sp.04-5288 MKMPLNIGLV HFIGIGGIGM SGIAEVLHNL GYKVQGSDQS DSANVQRLRE KGIEVFVGHK AENLGDAEVI VVSTAIKKNN PELVAAREKL LPVVRRAEML 100
B.sp.09RB8471 MKMPLNIGLV HFIGIGGIGM SGIAEVLHNL GYKVQGSDQS DSANVQRLRE KGIEVFVGHK AENLGDAEVI VVSTAIRKNN PELVAAREKL LPVVRRAEML 100
B.sp.09RB8910 MKMPLNIGLV HFIGIGGIGM SGIAEVLHNL GYKVQGSDQS DSANVQRLRE KGIEVFVGHK AENLGDAEVI VVSTAIKKNN PELVAAREKL LPVVRRAEML 100
B.sp.10RB9215 MKMPLNIGLV HFIGIGGIGM SGIAEVLHNL GYKVQGSDQS DSANVQRLRE KGIEVFVGHK AENLGDAEVI VVSTAIKKNN PELVAAREKL LPVVRRAEML 100
B.sp.191011898 MKMPLNIGLV HFIGIGGIGM SGIAEVLHNL GYKVQGSDQS DSANVQRLRE KGIEVFVGHK AENLGDAEVI VVSTAIRKNN PELVAAREKL LPVVRRAEML 100
B.sp.2002734562 MKMPLNIGLV HFIGIGGIGM SGIAEVLHNL GYKVQGSDQS DSANVQRLRE KGIEVFVGHK AENLGDAEVI VVSTAIKKNN PELVAAREKL LPVVRRAEML 100
B.sp.2280 MKMPLNIGLV HFIGIGGIGM SGIAEVLHNL GYKVQGSDQS DSANVQRLRE KGIEVFVGHK AENLGDAEVI VVSTAIKKNN PELVAAREKL LPVVRRAEML 100
B.sp.458 MKMPLNIGLV HFIGIGGIGM SGIAEVLHNL GYKVQGSDQS DSANVQRLRE KGIEVFVGHK AENLGDAEVI VVSTAIRKNN PELVAAREKL LPVVRRAEML 100
B.sp.56/94 MKMPLNIGLV HFIGIGGIGM SGIAEVLHNL GYKVQGSDQS DSANVQRLRE KGIEVFVGHK AENLGDAEVI VVSTAIKKNN PELVAAREKL LPVVRRAEML 100
B.sp.63/311 MKMPLNIGLV HFIGIGGIGM SGIAEVLHNL GYKVQGSDQS DSANVQRLRE KGIEVFVGHK AENLGDAEVI VVSTAIKKNN PELVAAREKL LPVVRRAEML 100
B.sp.6810 MKMPLNIGLV HFIGIGGIGM SGIAEVLHNL GYKVQGSDQS DSANVQRLRE KGIEVFVGHK AENLGDAEVI VVSTAIKKNN PELVAAREKL LPVVRRAEML 100
B.sp.83/13 MKMPLNIGLV HFIGIGGIGM SGIAEVLHNL GYKVQGSDQS DSANVQRLRE KGIEVFVGHK AENLGDAEVI VVSTAIKKNN PELVAAREKL LPVVRRAEML 100

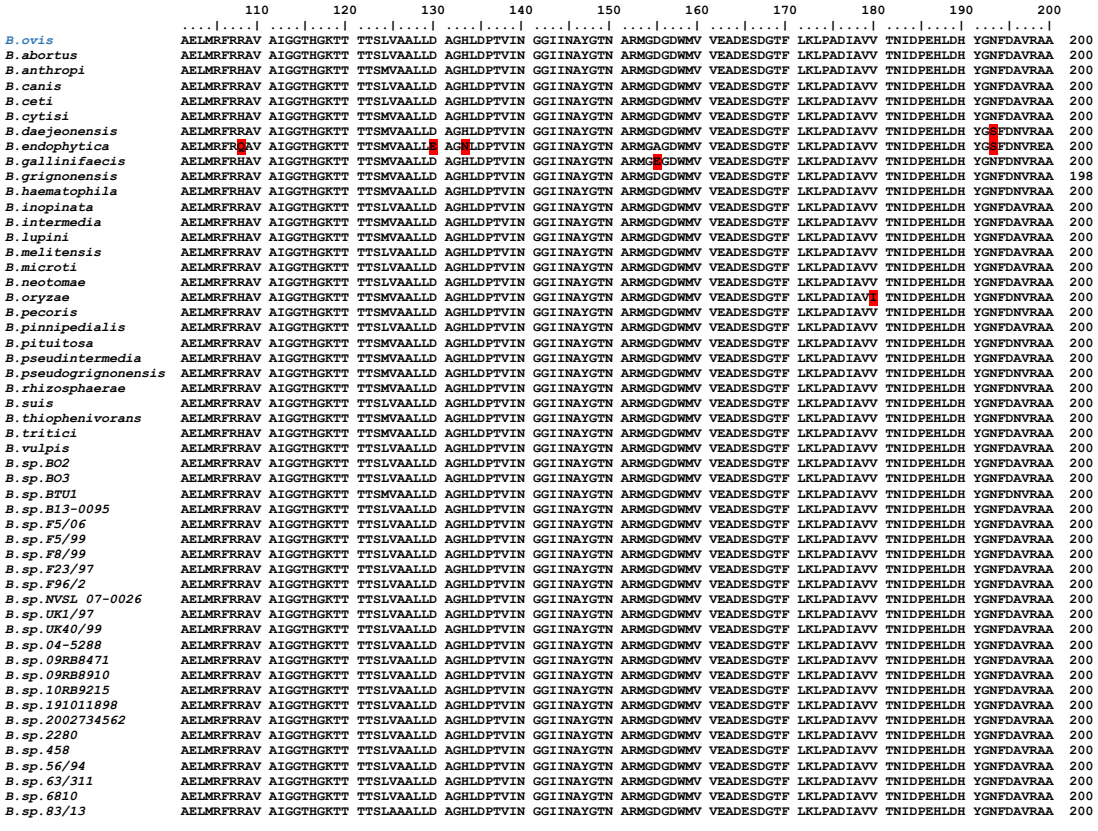
110 120 130 140 150 160 170 180 190 200
B.ovis AELMRFRRAV AIGGTHGKTT TTSLVAALLD AGHLDPTVIN GGIINAYGTN ARMGDGDWMV VEADESDGTF LKLPADIAVV TNIDPEHLDH YGNFDAVRAA 200
B.abortus AELMRFRRAV AIGGTHGKTT TTSLVAALLD AGHLDPTVIN GGIINAYGTN ARMGDGDWMV VEADESDGTF LKLPADIAVV TNIDPEHLDH YGNFDAVRAA 200
B.anthropi AELMRFRHAV AIGGTHGKTT TTSMVAALLD AGHLDPTVIN GGIINAYGTN ARMGDGDWMV VEADESDGTF LKLPADIAVV TNIDPEHLDH YGNFDAVRAA 200
B.canis AELMRFRRAV AIGGTHGKTT TTSLVAALLD AGHLDPTVIN GGIINAYGTN ARMGDGDWMV VEADESDGTF LKLPADIAVV TNIDPEHLDH YGNFDAVRAA 200
B.ceti AELMRFRRAV AIGGTHGKTT TTSLVAALLD AGHLDPTVIN GGIINAYGTN ARMGDGDWMV VEADESDGTF LKLPADIAVV TNIDPEHLDH YGNFDAVRAA 200
B.cytisi AELMRFRHAV AIGGTHGKTT TTSMVAALLD AGHLDPTVIN GGIINAYGTN ARMGDGDWMV VEADESDGTF LKLPADIAVV TNIDPEHLDH YGNFDAVRAA 200
B.daejeonensis AELMRFRRAV AIGGTHGKTT TTSMVAALLD AGHLDPTVIN GGIINAYGTN ARMGDGDWMV VEADESDGTF LKLPADIAVV TNIDPEHLDH YGSFDNVRAA 200
B.endophytica AELMRFRAAV AIGGTHGKTT TTSMVAALLS AGNLDPTVIN GGIINAYGTN ARMGAGDWMV VEADESDGTF LKLPADIAVV TNIDPEHLDH YGSFDNVREA 200
B.gallinifaecis AELMRFRHAV AIGGTHGKTT TTSMVAALLD AGHLDPTVIN GGIINAYGTN ARMGEGDWMV VEADESDGTF LKLPADIAVV TNIDPEHLDH YGNFDNVRAA 200
B.grignonensis AELMRFRRAV AIGGTHGKTT TTSMVAALLD AGHLDPTVIN GGIINAYGTN ARMGDGDWMV VEADESDGTF LKLPADIAVV TNIDPEHLDH YGNFDNVRAA 198
B.haematophila AELMRFRHAV AIGGTHGKTT TTSMVAALLD AGHLDPTVIN GGIINAYGTN ARMGDGDWMV VEADESDGTF LKLPADIAVV TNIDPEHLDH YGNFDNVRAA 200
B.inopinata AELMRFRRAV AIGGTHGKTT TTSLVAALLD AGHLDPTVIN GGIINAYGTN ARMGDGDWMV VEADESDGTF LKLPADIAVV TNIDPEHLDH YGNFDAVRAA 200
B.intermedia AELMRFRHAV AIGGTHGKTT TTSMVAALLD AGHLDPTVIN GGIINAYGTN ARMGDGDWMV VEADESDGTF LKLPADIAVV TNIDPEHLDH YGNFDAVRAA 200
B.lupini AELMRFRHAV AIGGTHGKTT TTSMVAALLD AGHLDPTVIN GGIINAYGTN ARMGDGDWMV VEADESDGTF LKLPADIAVV TNIDPEHLDH YGNFDAVRAA 200
B.melitensis AELMRFRRAV AIGGTHGKTT TTSLVAALLD AGHLDPTVIN GGIINAYGTN ARMGDGDWMV VEADESDGTF LKLPADIAVV TNIDPEHLDH YGNFDAVRAA 200
B.microti AELMRFRRAV AIGGTHGKTT TTSLVAALLD AGHLDPTVIN GGIINAYGTN ARMGDGDWMV VEADESDGTF LKLPADIAVV TNIDPEHLDH YGNFDAVRAA 200
B.neotomae AELMRFRRAV AIGGTHGKTT TTSLVAALLD AGHLDPTVIN GGIINAYGTN ARMGDGDWMV VEADESDGTF LKLPADIAVV TNIDPEHLDH YGNFDAVRAA 200
B.oryzae AELMRFRHAV AIGGTHGKTT TTSMVAALLD AGHLDPTVIN GGIINAYGTN ARMGDGDWMV VEADESDGTF LKLPADIAVI TNIDPEHLDH YGNFDNVRAA 200
B.pecoris AELMRFRRAV AIGGTHGKTT TTSMVAALLD AGHLDPTVIN GGIINAYGTN ARMGDGDWMV VEADESDGTF LKLPADIAVV TNIDPEHLDH YGNFDNVRAA 200
B.pinnipedialis AELMRFRRAV AIGGTHGKTT TTSLVAALLD AGHLDPTVIN GGIINAYGTN ARMGDGDWMV VEADESDGTF LKLPADIAVV TNIDPEHLDH YGNFDAVRAA 200
B.pituitosa AELMRFRRAV AIGGTHGKTT TTSMVAALLD AGHLDPTVIN GGIINAYGTN ARMGDGDWMV VEADESDGTF LKLPADIAVV TNIDPEHLDH YGNFDNVRAA 200
B.pseudintermedia AELMRFRHAV AIGGTHGKTT TTSMVAALLD AGHLDPTVIN GGIINAYGTN ARMGDGDWMV VEADESDGTF LKLPADIAVV TNIDPEHLDH YGNFDAVRAA 200
B.pseudogrignonensis AELMRFRRAV AIGGTHGKTT TTSMVAALLD AGHLDPTVIN GGIINAYGTN ARMGDGDWMV VEADESDGTF LKLPADIAVV TNIDPEHLDH YGNFDNVRAA 200
B.rhizosphaerae AELMRFRRAV AIGGTHGKTT TTSMVAALLD AGHLDPTVIN GGIINAYGTN ARMGDGDWMV VEADESDGTF LKLPADIAVV TNIDPEHLDH YGNFDNVRAA 200
B.suis AELMRFRRAV AIGGTHGKTT TTSLVAALLD AGHLDPTVIN GGIINAYGTN ARMGDGDWMV VEADESDGTF LKLPADIAVV TNIDPEHLDH YGNFDAVRAA 200
B.thiophenivorans AELMRFRRAV AIGGTHGKTT TTSMVAALLD AGHLDPTVIN GGIINAYGTN ARMGDGDWMV VEADESDGTF LKLPADIAVV TNIDPEHLDH YGNFDNVRAA 200
B.tritici AELMRFRHAV AIGGTHGKTT TTSMVAALLD AGHLDPTVIN GGIINAYGTN ARMGDGDWMV VEADESDGTF LKLPADIAVV TNIDPEHLDH YGNFDAVRAA 200
B.vulpis AELMRFRRAV AIGGTHGKTT TTSLVAALLD AGHLDPTVIN GGIINAYGTN ARMGDGDWMV VEADESDGTF LKLPADIAVV TNIDPEHLDH YGNFDAVRAA 200
B.sp.BO2 AELMRFRRAV AIGGTHGKTT TTSLVAALLD AGHLDPTVIN GGIINAYGTN ARMGDGDWMV VEADESDGTF LKLPADIAVV TNIDPEHLDH YGNFDAVRAA 200
B.sp.BO3 AELMRFRRAV AIGGTHGKTT TTSLVAALLD AGHLDPTVIN GGIINAYGTN ARMGDGDWMV VEADESDGTF LKLPADIAVV TNIDPEHLDH YGNFDAVRAA 200
B.sp.BTU1 AELMRFRRAV AIGGTHGKTT TTSMVAALLD AGHLDPTVIN GGIINAYGTN ARMGDGDWMV VEADESDGTF LKLPADIAVV TNIDPEHLDH YGNFDNVRAA 200
B.sp.B13-0095 AELMRFRRAV AIGGTHGKTT TTSLVAALLD AGHLDPTVIN GGIINAYGTN ARMGDGDWMV VEADESDGTF LKLPADIAVV TNIDPEHLDH YGNFDAVRAA 200
B.sp.F5/06 AELMRFRRAV AIGGTHGKTT TTSLVAALLD AGHLDPTVIN GGIINAYGTN ARMGDGDWMV VEADESDGTF LKLPADIAVV TNIDPEHLDH YGNFDAVRAA 200
B.sp.F5/99 AELMRFRRAV AIGGTHGKTT TTSLVAALLD AGHLDPTVIN GGIINAYGTN ARMGDGDWMV VEADESDGTF LKLPADIAVV TNIDPEHLDH YGNFDAVRAA 200
B.sp.F8/99 AELMRFRRAV AIGGTHGKTT TTSLVAALLD AGHLDPTVIN GGIINAYGTN ARMGDGDWMV VEADESDGTF LKLPADIAVV TNIDPEHLDH YGNFDAVRAA 200
B.sp.F23/97 AELMRFRRAV AIGGTHGKTT TTSLVAALLD AGHLDPTVIN GGIINAYGTN ARMGDGDWMV VEADESDGTF LKLPADIAVV TNIDPEHLDH YGNFDAVRAA 200
B.sp.F96/2 AELMRFRRAV AIGGTHGKTT TTSLVAALLD AGHLDPTVIN GGIINAYGTN ARMGDGDWMV VEADESDGTF LKLPADIAVV TNIDPEHLDH YGNFDAVRAA 200
B.sp.NVSL 07-0026 AELMRFRRAV AIGGTHGKTT TTSLVAALLD AGHLDPTVIN GGIINAYGTN ARMGDGDWMV VEADESDGTF LKLPADIAVV TNIDPEHLDH YGNFDAVRAA 200
B.sp.UK1/97 AELMRFRRAV AIGGTHGKTT TTSLVAALLD AGHLDPTVIN GGIINAYGTN ARMGDGDWMV VEADESDGTF LKLPADIAVV TNIDPEHLDH YGNFDAVRAA 200
B.sp.UK40/99 AELMRFRRAV AIGGTHGKTT TTSLVAALLD AGHLDPTVIN GGIINAYGTN ARMGDGDWMV VEADESDGTF LKLPADIAVV TNIDPEHLDH YGNFDAVRAA 200
B.sp.04-5288 AELMRFRRAV AIGGTHGKTT TTSLVAALLD AGHLDPTVIN GGIINAYGTN ARMGDGDWMV VEADESDGTF LKLPADIAVV TNIDPEHLDH YGNFDAVRAA 200
B.sp.09RB8471 AELMRFRRAV AIGGTHGKTT TTSLVAALLD AGHLDPTVIN GGIINAYGTN ARMGDGDWMV VEADESDGTF LKLPADIAVV TNIDPEHLDH YGNFDAVRAA 200
B.sp.09RB8910 AELMRFRRAV AIGGTHGKTT TTSLVAALLD AGHLDPTVIN GGIINAYGTN ARMGDGDWMV VEADESDGTF LKLPADIAVV TNIDPEHLDH YGNFDAVRAA 200
B.sp.10RB9215 AELMRFRRAV AIGGTHGKTT TTSLVAALLD AGHLDPTVIN GGIINAYGTN ARMGDGDWMV VEADESDGTF LKLPADIAVV TNIDPEHLDH YGNFDAVRAA 200
B.sp.191011898 AELMRFRRAV AIGGTHGKTT TTSLVAALLD AGHLDPTVIN GGIINAYGTN ARMGDGDWMV VEADESDGTF LKLPADIAVV TNIDPEHLDH YGNFDAVRAA 200
B.sp.2002734562 AELMRFRRAV AIGGTHGKTT TTSLVAALLD AGHLDPTVIN GGIINAYGTN ARMGDGDWMV VEADESDGTF LKLPADIAVV TNIDPEHLDH YGNFDAVRAA 200
B.sp.2280 AELMRFRRAV AIGGTHGKTT TTSLVAALLD AGHLDPTVIN GGIINAYGTN ARMGDGDWMV VEADESDGTF LKLPADIAVV TNIDPEHLDH YGNFDAVRAA 200
B.sp.458 AELMRFRRAV AIGGTHGKTT TTSLVAALLD AGHLDPTVIN GGIINAYGTN ARMGDGDWMV VEADESDGTF LKLPADIAVV TNIDPEHLDH YGNFDAVRAA 200
B.sp.56/94 AELMRFRRAV AIGGTHGKTT TTSLVAALLD AGHLDPTVIN GGIINAYGTN ARMGDGDWMV VEADESDGTF LKLPADIAVV TNIDPEHLDH YGNFDAVRAA 200
B.sp.63/311 AELMRFRRAV AIGGTHGKTT TTSLVAALLD AGHLDPTVIN GGIINAYGTN ARMGDGDWMV VEADESDGTF LKLPADIAVV TNIDPEHLDH YGNFDAVRAA 200
B.sp.6810 AELMRFRRAV AIGGTHGKTT TTSLVAALLD AGHLDPTVIN GGIINAYGTN ARMGDGDWMV VEADESDGTF LKLPADIAVV TNIDPEHLDH YGNFDAVRAA 200
B.sp.83/13 AELMRFRRAV AIGGTHGKTT TTSLAAALLD AGHLDPTVIN GGIINAYGTN ARMGDGDWMV VEADESDGTF LKLPADIAVV TNIDPEHLDH YGNFDAVRAA 200

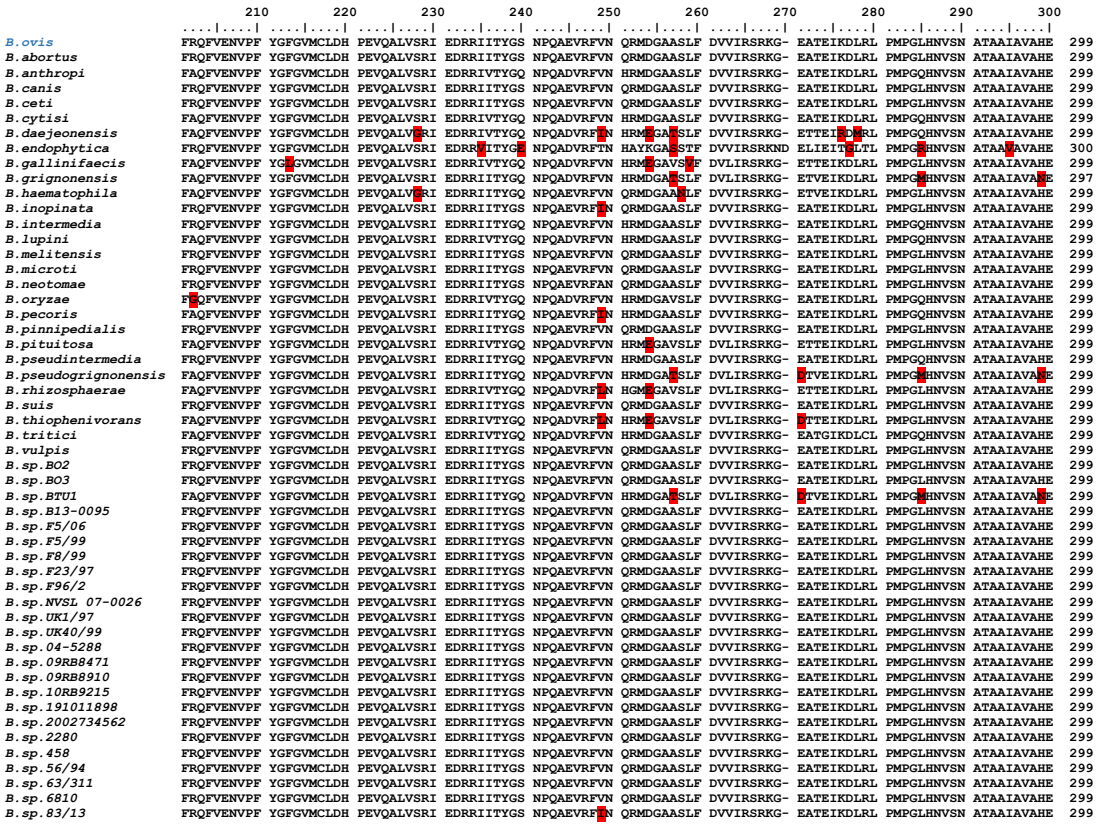

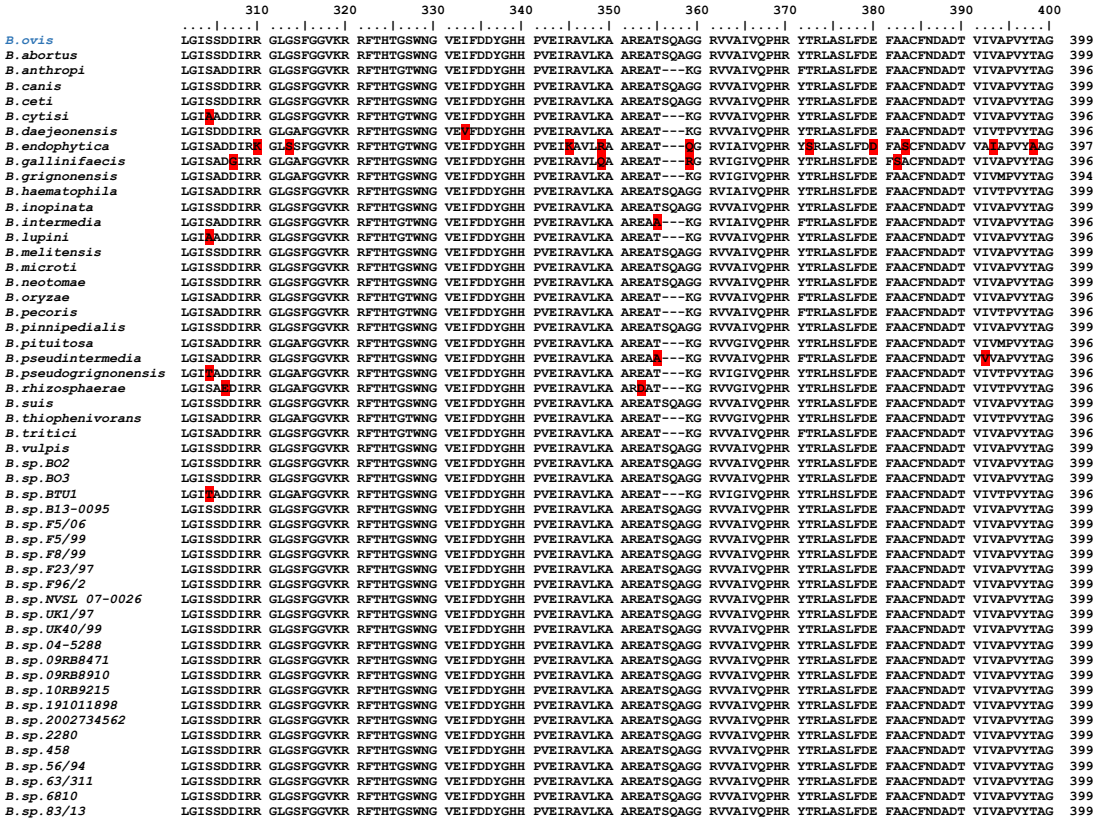

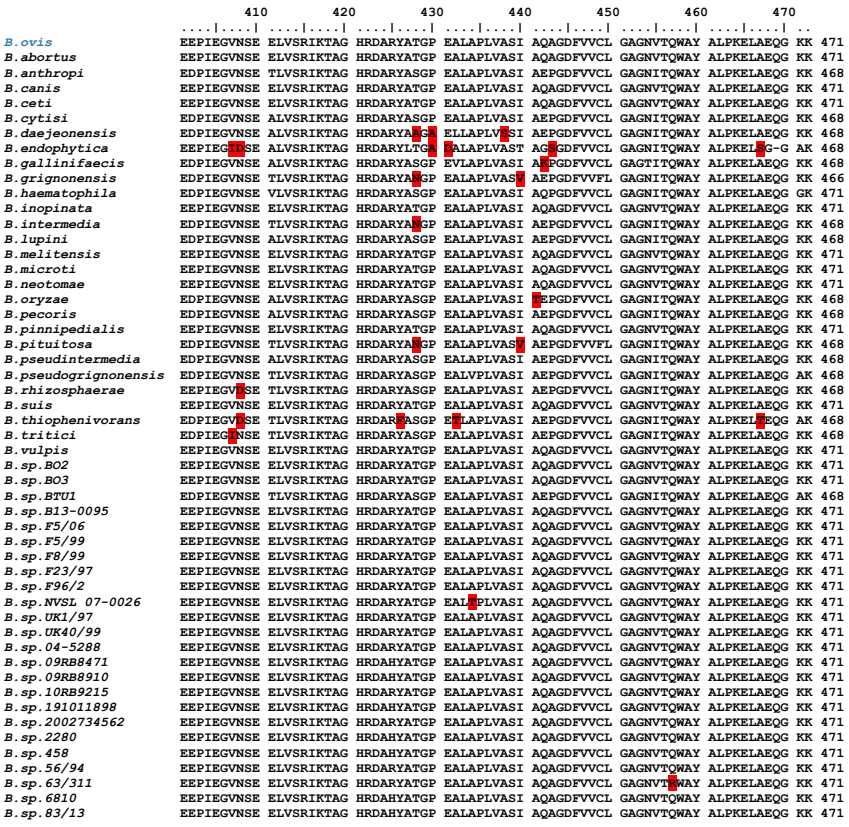

Figure 7.8. MurC sequence conservation within the *Brucella* genus. MSA (n=52) of MurCs from *Brucella* species in Table 7.1. The alignment was constructed with Clustal Omega. Residues that are not conserved in at least 90% of the sequences are highlighted in red.

The phylogenetic analysis of MurC sequences from *Brucella*, as shown in Figure 7.9, involved several steps, including bootstrap analysis of 500 replicates and rooting the cladogram using *B. ovis* SdhA as an outgroup sequence. The resulting tree displayed only two primary clades (Figure 7.9 B). Clade 1 is highlighted in red and comprises 17 sequences, while clade 2 is shown in purple and encompasses the remaining sequences. The notably low bootstrap values in this case may be attributed to the high degree of sequence conservation observed among protein sequences across different Brucellae. This high conservation implies that these sequences have changed little over evolutionary time, making it challenging to establish distinct and robust phylogenetic relationships. Consequently, the low bootstrap values suggest that the branching patterns in the tree may not be well-supported by sequence data alone.

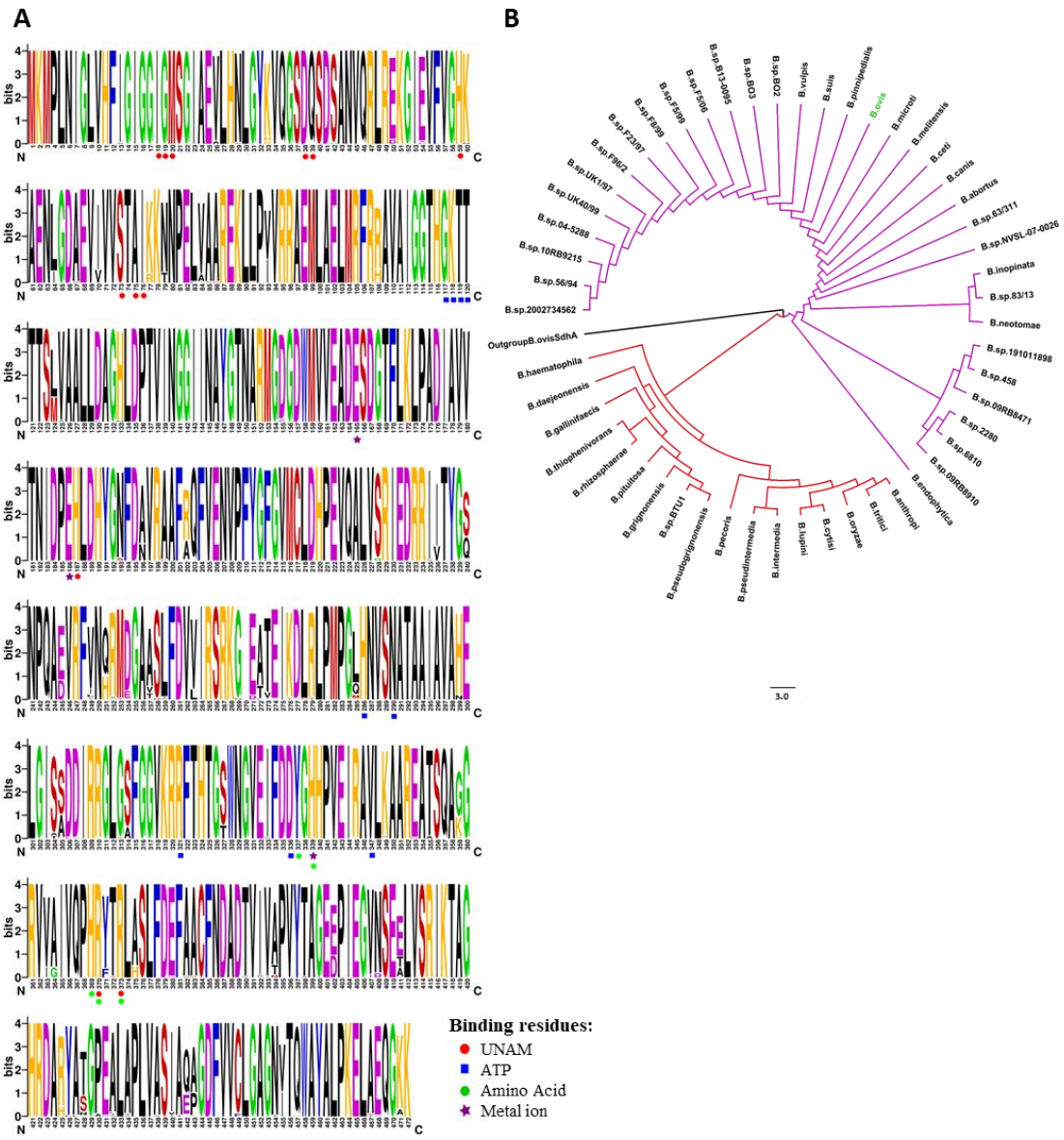

Figure 7.9. Residue conservation and evolution of MurC within *Brucella* spp. (A) Sequence Logo representing MSA of MurCs from *Brucella* (n=52). Logo generated with WebLogo. Residues presumably involved in substrates binding, by similarity with other MurC proteins, are indicated underneath the logo: Red circle, UNAM; blue square, ATP; green circle, amino acid; purple stars, metal ion. **(B)** Phylogenetic relationship of MurCs from *Brucella*. Tree was built using the shown alignment, the Maximum Likelihood method and JTT matrix-based model with MEGA X. The tree with the highest log likelihood (-4455.72) is shown. This analysis involved the above aligned 52 MurA sequences from *Brucella* as well as the *B. ovis* SdhA sequence as an outgroup. Branch lengths are proportional to the number of substitutions per site (scale beside). There was a total of 613 positions in the final dataset. The tree groups the sequences in two main clusters: Clade 1 (bootstrap > 24) in red color, Clade 2 (bootstrap > 12) in purple.

7.3.3 Sequence and evolutionary analysis of MurC proteins within bacterial species

The conservation of residues in MurC sequences from various bacteria was also studied. The sequences included representatives from the ESKAPE group, as well as other pathogens and non-pathogens found in humans and animals. A total of 64 MurC protein sequences were collected and analysed by MSA. BoMurC shares the highest similarity with the MurC homologues of *S. meliloti* (WP_003529126.1, 84%), *B. schoenbuchensis*

(WP_010703987.1, 80%), *B. quintana* (WP_011179602.1, 79%), *R. palustris* (WP_011159069.1, 77%), *X. autotrophicus* (WP_012113212.1, 76%) and *G. oxydans* (WP_011251755.1, 76%), *P. zucineum* (WP_012522873.1, 71%), *S. paucimobilis* (WP_030539649.1, 71%). MurC sequences with the lowest similarity relative to BoMurC were those of *S. aureus* (WP_000150168.1, 45%), *C. aggregans* (WP_015941572.1, 45%) and *T. denticola* (WP_010956876.1, 41%). Indeed, the percentage of identity among most sequences is approximately 50%, indicating that a significant number of residues are highly conserved across the evaluated sequences (pink and grey residues in Figure 7.10).

The WebLogo obtained from the MSA highlights in green boxes the conserved motifs ^{33}GxGGxGMxxxAxxL^{46}, ^{50}GxxVxVGSD^{57}, ^{158}(V/I)xGTHGKTTTTx(M/L)^{170}, ^{209}(V/I)xEADESD^{216}, ^{230}TNI(D/E)x(D/E)HxDxY^{240}, ^{393}FxGxxRRF^{400}, ^{422}DDY(A/G)HHPxE^{430} and ^{460}FQPHR(Y/F)(S/T)RT^{448}, which are present in MurC of all evaluated bacteria and contain the residues expected to be involved in enzyme catalysis (underlined). It is important to note that the MSA and WebLogo analysis were specifically conducted using only the segments corresponding to MurC of *C. pecorum* (WP_024010182.1) and *C. trachomatis* (WP_010725335.1). The reason for this choice is that these particular sequences belong to fused multi-domain proteins with a Ddl (D-Ala:D-Ala ligase) domain, resulting in proteins with an extension of more than 800 amino acids.

Table 7.2. List of bacteria species for which MurC sequences are evaluated in this study. The "Species Name" column highlights in blue those species corresponding to virulent and antibiotic resistant bacterial pathogens known as ESKAPE; in light orange animal pathogens and in dark orange human pathogens. The "Short Species Name"columnhighlights in green those species for which MurC has been purified and structurally or functionally characterized. *B. ovis* is highlighted in bold.

Species Name	Short Species Name	Access Code	Gram	Phylum	Class
Acaryochloris marina	*A.marina*	WP_012162329.1	negative	Cyanobacteria	Cyanophyceae
Acetivibrio thermocellus	*A.thermocellus*	WP_003512921.1	positive	Firmicutes	Clostridia
Acinetobacter baumannii	*A.baumannii*	WP_000075476.1	negative	Proteobacteria	Gammaproteobacteria
Acinetobacter baylyi	*A.baylyi*	WP_004923336.1	negative	Proteobacteria	Gammaproteobacteria
Anabaena PCC 7120 /*nostoc*	*Nostoc*	WP_010999191.1	negative	Cyanobacteria	--
Azotobacter vinelandii	*A.vinelandii*	WP_012699972.1	negative	Proteobacteria	Alphaproteobacteria
Bacillus licheniformis	*B.licheniformis*	AOP16355.1	positive	Firmicutes	Bacilli
Bacillus subtilis	*B.subtilis*	WP_003229274.1	positive	Firmicutes	Bacilli
Bartonella quintana	*B.quintana*	WP_011179602.1	negative	Proteobacteria	Alphaproteobacteria
Bartonella schoenbuchensis	*B.schoenbuchensis*	WP_010703987.1	negative	Proteobacteria	Alphaproteobacteria
***Brucella ovis* (strain ATCC 25840)[a]**	***B.ovis***	**ABQ61623.1**	**negative**	**Proteobacteria**	**Alphaproteobacteria**
Campylobacter sp.	*Campylobacter*	WP_010891904.1	negative	Proteobacteria	Epsilonproteobacteria
Candidatus pelagibacter	*C.pelagibacter*	MAK19408.1	negative	Proteobacteria	Alphaproteobacteria
Chlamydia pecorum[bc]	*C. pecorum*	WP_024010182.1	negative	Chlamydiae	Chlamydiia
Chlamydia trachomatis[bc]	*C. trachomatis*	WP_010725335.1	negative	Chlamydiae	Chlamydiia
Chloroflexus aggregans	*C.aggregans*	WP_015941572.1	positive	Chloroflexi	Chloroflexi
Corynebacterium ammoniagenes	*C.ammoniagenes*	WP_003845226.1	positive	Actinobacteria	Actinobacteria
Corynebacterium glutamicum	*C.glutamicum*	NP_601359.1	positive	Actinobacteria	Actinobacteria
Enterobacter sp. Bisph1	*Enterobacter*	WP_039057447.1	negative	Proteobacteria	Gammaproteobacteria
Enterococcus faecium	*E.faecium*1	SAM75441.1	positive	Firmicutes	Bacilli
	*E.faecium*2	WP_002296400.1			
Escherichia coli	*E.coli*	WP_001096049.1	negative	Proteobacteria	Gammaproteobacteria
Francisella tularensis[a]	*F.tularensis*	WP_003021772.1	negative	Proteobacteria	Gammaproteobacteria
Gloeobacter violaceus	*G.violaceus*	WP_011142313.1	negative	Cyanobacteria	Gloeobacteria
Gluconobacter oxydans	*G.oxydans*	WP_011251755.1	negative	Proteobacteria	Alphaproteobacteria
Haemophilus influenzae	*H.influenzae*	WP_005693453.1	negative	Proteobacteria	Gammaproteobacteria
Helicobacter pylori	*H. pylori*	WP_000894779.1	negative	Proteobacteria	Epsilonproteobacteria
Klebsiella pneumoniae	*K.pneumoniae*	WP_004219314.1	negative	Proteobacteria	Gammaproteobacteria
Lactiplantibacillus plantarum	*L.plantarum*	WP_011101415.1	positive	Firmicutes	Bacilli
Legionella pneumophila[a]	*L.pneumophila*	WP_010948314.1	negative	Proteobacteria	Gammaproteobacteria
Listeria monocytogenes[b]	*L.monocytogenes*	WP_003727366.1	positive	Firmicutes	Bacilli
Micrococcus luteus	*M.luteus*	WP_012750916.1	positive	Actinobacteria	Actinomycetales
Mycobacterium leprae[a]	*M.leprae*	WP_010908022.1	positive	Actinobacteria	Actinobacteria
Mycobacterium bovis[a]	*M.bovis*	WP_003411159.1	positive	Actinobacteria	Actinobacteria
Mycobacterium marinum[a]	*M.marinum*	WP_012394858.1	positive	Actinobacteria	Actinobacteria
Mycobacterium tuberculosis[a]	*M.tuberculosis*	WP_003411159.1	positive	Actinobacteria	Actinobacteridae
Neisseria gonorrhoeae	*N.gonorrhoeae*	YP_208580.3	negative	Proteobacteria	Betaproteobacteria
Paracoccus yeei	*P.yeei*	AYF01650.1	negative	Proteobacteria	Alphaproteobacteria
Paulinella chromatophora	*P.chromatophora*	YP_002049067.1	microalga	Cercozoa	Imbricatea
Phenylobacterium zucineum	*P.zucineum*	WP_012522873.1	negative	Proteobacteria	Alphaproteobacteria
Porphyromonas gingivalis	*P.gingivalis*	WP_012457660.1	negative	Bacteroidetes	Bacteroidia
Proteus mirabilis[a]	*P.mirabilis*	WP_004244115.1	negative	Proteobacteria	Gammaproteobacteria
Pseudarthrobacter chlorophenolicus	*P.chlorophenolicus*	WP_015936780.1	positive	Actinobacteria	Actinomycetales
Pseudomonas aeruginosa	*P.aeruginosa*	WP_003094121.1	negative	Proteobacteria	Gammaproteobacteria
Psychrobacter arcticus	*P.arcticus*	WP_011281010.1	negative	Proteobacteria	Gammaproteobacteria
Rhodobacter capsulatus	*R.capsulatus*	WP_013066564.1	negative	Proteobacteria	Alphaproteobacteria
Rhodopseudomonas palustris	*R.palustris*	WP_011159069.1	negative	Proteobacteria	Alphaproteobacteria
Rickettsia rickettsii[b]	*R.rickettsii*	WP_012150546.1	negative	Proteobacteria	Alphaproteobacteria
Rickettsia typhi[b]	*R.typhi*	WP_011190705.1	negative	Proteobacteria	Alphaproteobacteria
Ruegeria pomeroyi	*R.pomeroyi*	WP_011190705.1	negative	Proteobacteria	Alphaproteobacteria
Salmonella enterica subsp. enterica serovar Typhimurium[a]	*S.enterica*	WP_001096070.1	negative	Proteobacteria	Gammaproteobacteria
Shigella dysenteriae serotype 1	*S.dysenteriae*	WP_001096057.1	negative	Proteobacteria	Gammaproteobacteria
Sinorhizobium meliloti	*S.meliloti*	WP_003529126.1	negative	Proteobacteria	Alphaproteobacteria
Sphingomonas paucimobilis	*S.paucimobilis*	WP_030539649.1	negative	Proteobacteria	Alphaproteobacteria
Staphylococcus aureus	*S.aureus*	WP_000150168.1	positive	Firmicutes	Bacilli
Streptococcus pneumoniae	*S.pneumoniae*	WP_000048090.1	positive	Firmicutes	Bacilli
Synechococcus sp.	*Synechococcus*	WP_011126907.1	negative	Cyanobacteria	--
Thermotoga maritima	*T.maritima*	WP_004082924.1	negative	Thermotogae	Thermotogae
Thermus thermophilus	*T.thermophilus*	WP_011228428.1	negative	Deinococcus-Thermus	Deinococci
Treponema denticola	*T.denticola*	WP_010956876.1	negative	Spirochaetes	Spirochaetia
Vibrio cholerae O1 biovar El Tor str. N16961	*V.cholerae*	WP_000152804.1	negative	Proteobacteria	Gammaproteobacteria
Wolbachia pipientis	*W.pipientis*	WP_010962635.1	negative	Proteobacteria	Alphaproteobacteria
Xanthobacter autotrophicus	*X.autotrophicus*	WP_012113212.1	negative	Proteobacteria	Alphaproteobacteria
Yersinia pestis[a]	*Y.pestis*	WP_002216457.1	negative	Proteobacteria	Gammaproteobacteria

[a]Facultative intracelular organism.
[b]Obligatory intracelular organism.
[c]Bifunctional enzyme MurC/Ddl

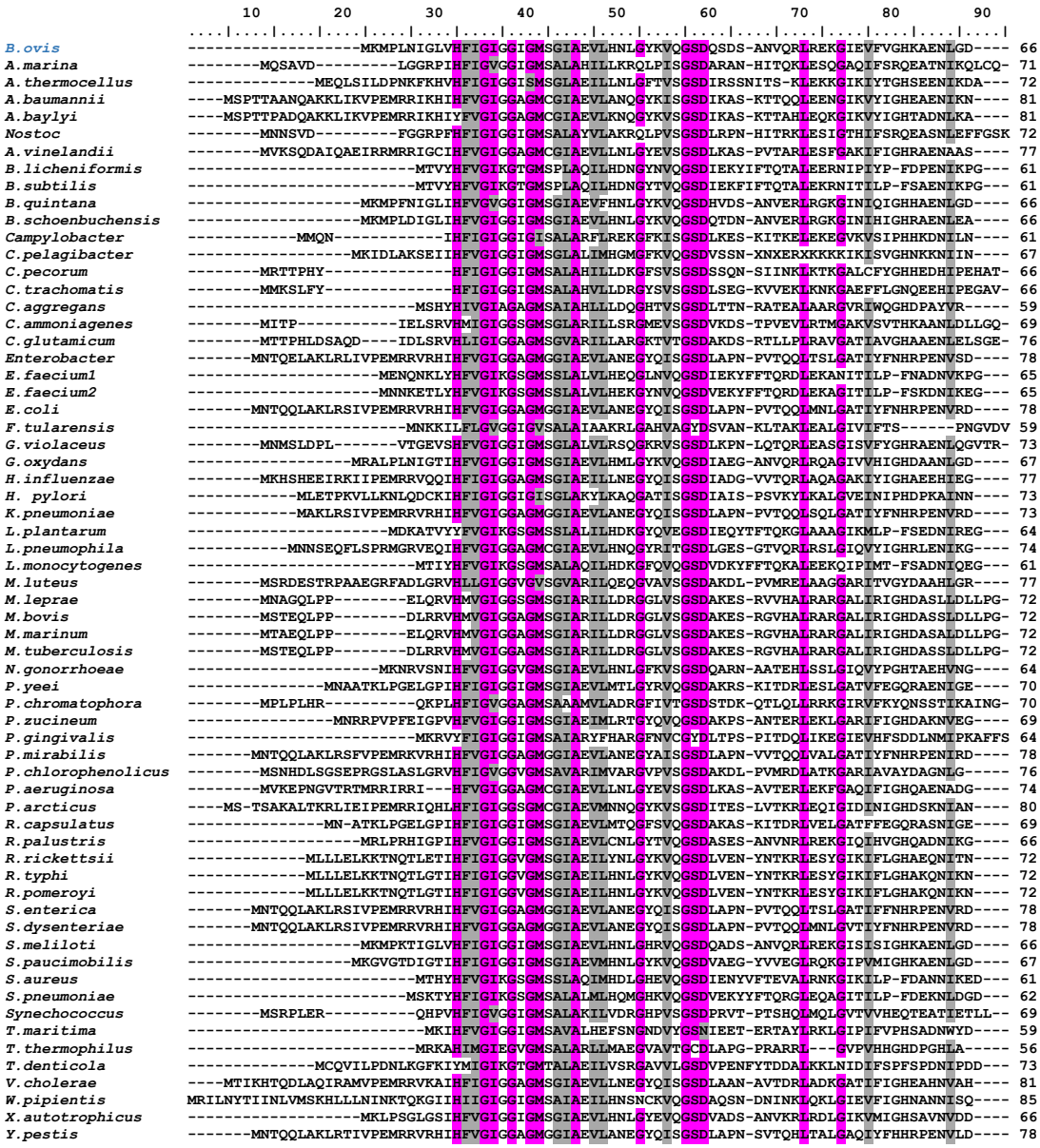
10 20 30 40 50 60 70 80 90
B.ovis
A.marina
A.thermocellus
A.baumannii
A.baylyi
Nostoc
A.vinelandii
B.licheniformis
B.subtilis
B.quintana
B.schoenbuchensis
Campylobacter
C.pelagibacter
C.pecorum
C.trachomatis
C.aggregans
C.ammoniagenes
C.glutamicum
Enterobacter
E.faecium1
E.faecium2
E.coli
F.tularensis
G.violaceus
G.oxydans
H.influenzae
H. pylori
K.pneumoniae
L.plantarum
L.pneumophila
L.monocytogenes
M.luteus
M.leprae
M.bovis
M.marinum
M.tuberculosis
N.gonorrhoeae
P.yeei
P.chromatophora
P.zucineum
P.gingivalis
P.mirabilis
P.chlorophenolicus
P.aeruginosa
P.arcticus
R.capsulatus
R.palustris
R.rickettsii
R.typhi
R.pomeroyi
S.enterica
S.dysenteriae
S.meliloti
S.paucimobilis
S.aureus
S.pneumoniae
Synechococcus
T.maritima
T.thermophilus
T.denticola
V.cholerae
W.pipientis
X.autotrophicus
Y.pestis

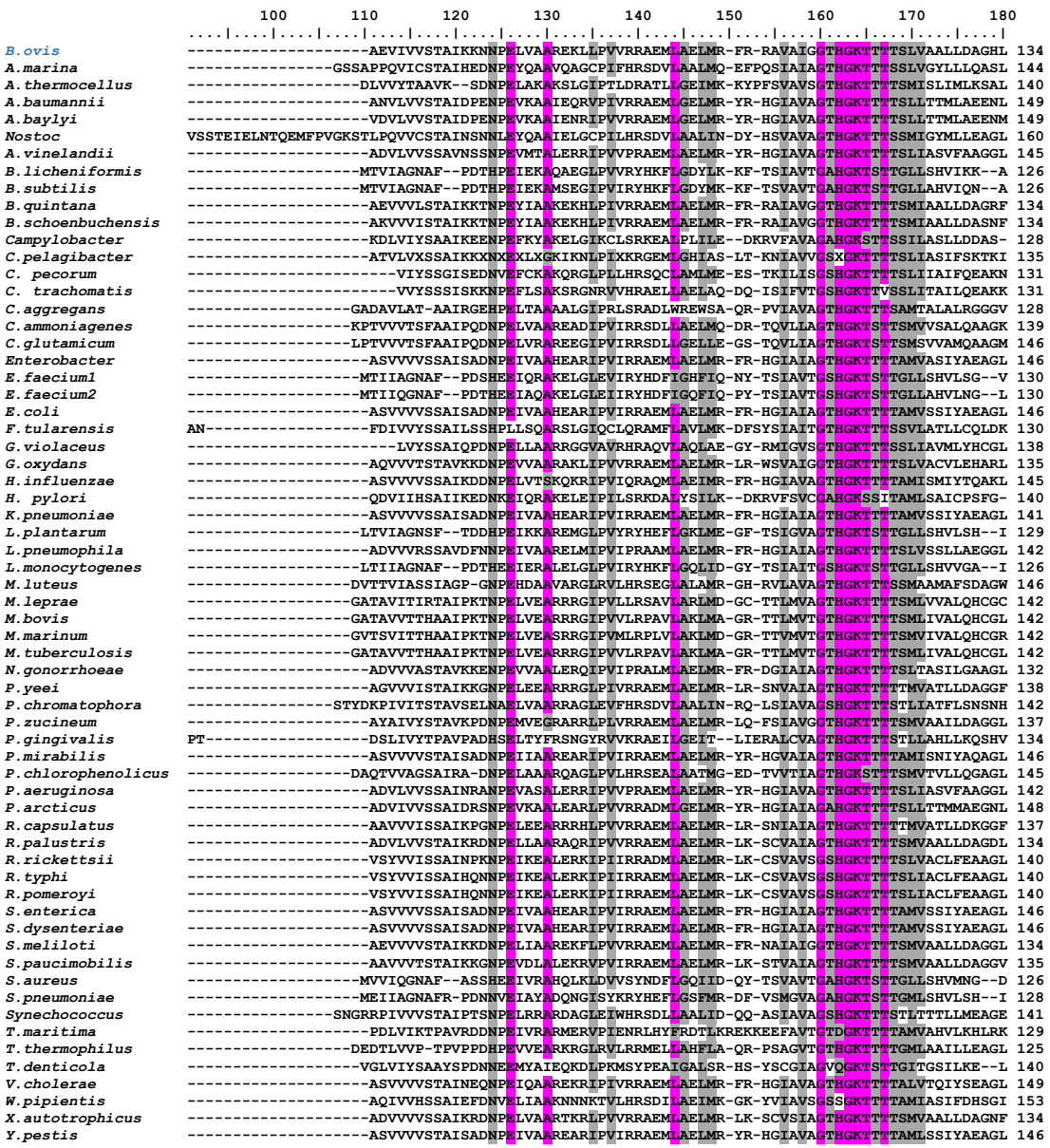
100 110 120 130 140 150 160 170 180
B.ovis
A.marina
A.thermocellus
A.baumannii
A.baylyi
Nostoc
A.vinelandii
B.licheniformis
B.subtilis
B.quintana
B.schoenbuchensis
Campylobacter
C.pelagibacter
C. pecorum
C. trachomatis
C.aggregans
C.ammoniagenes
C.glutamicum
Enterobacter
E.faecium1
E.faecium2
E.coli
F.tularensis
G.violaceus
G.oxydans
H.influenzae
H. pylori
K.pneumoniae
L.plantarum
L.pneumophila
L.monocytogenes
M.luteus
M.leprae
M.bovis
M.marinum
M.tuberculosis
N.gonorrhoeae
P.yeei
P.chromatophora
P.zucineum
P.gingivalis
P.mirabilis
P.chlorophenolicus
P.aeruginosa
P.arcticus
R.capsulatus
R.palustris
R.rickettsii
R.typhi
R.pomeroyi
S.enterica
S.dysenteriae
S.meliloti
S.paucimobilis
S.aureus
S.pneumoniae
Synechococcus
T.maritima
T.thermophilus
T.denticola
V.cholerae
W.pipientis
X.autotrophicus
Y.pestis

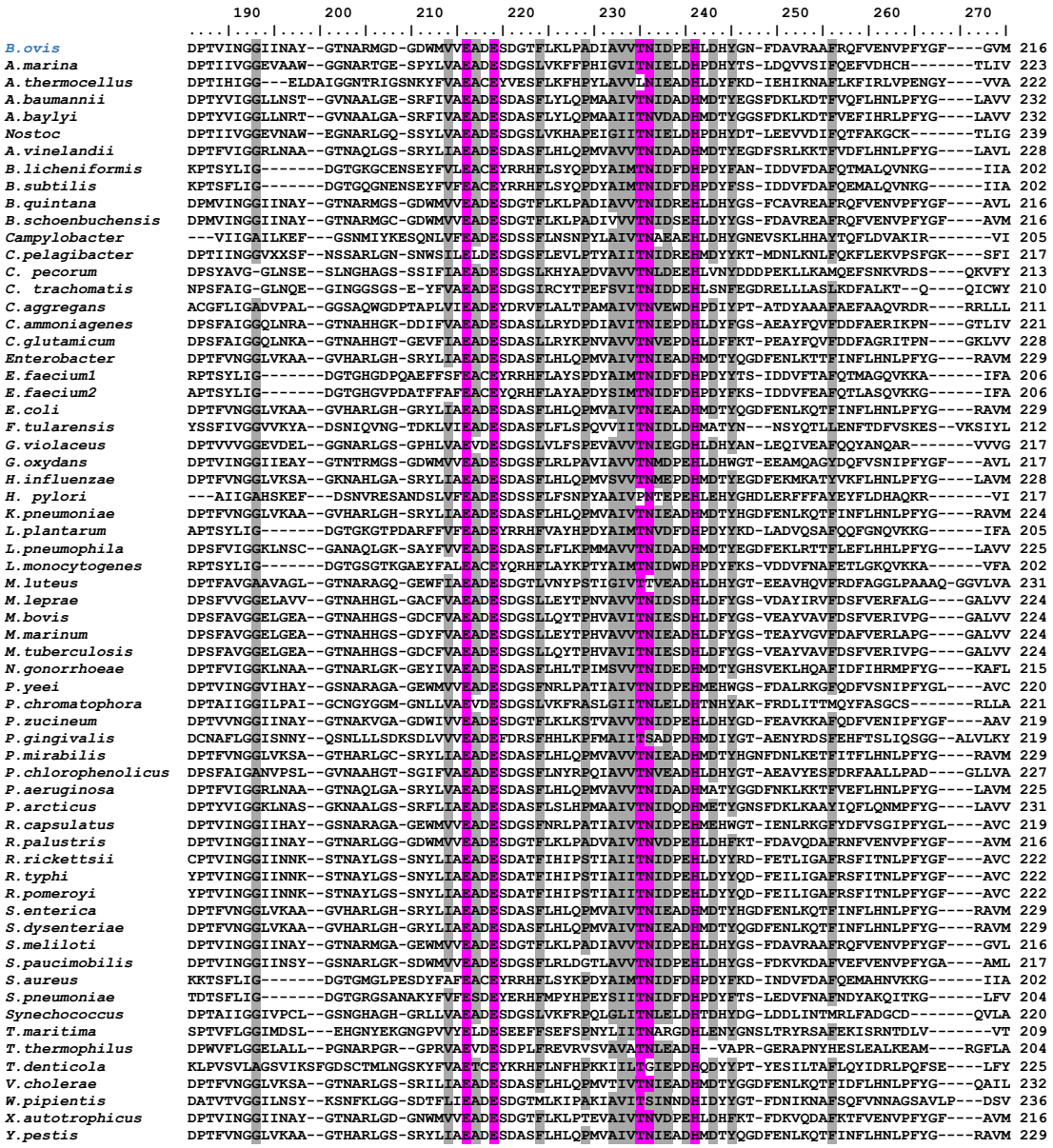
190 200 210 220 230 240 250 260 270
B.ovis DPTVINGGIINAY--GTNARMGD-GDWMVVEADESDGTFLKLPADIAVVTNIDPEHLDHYGN-FDAVRAAFRQFVENVPFYGF----GVM 216
A.marina DPTIIVGGEVAAW--GGNARTGE-SPYLVAEADESDGSLVKFFPHIGVITNIELDHPDHYTS-LDQVVSIFQEFVDHCH-------TLIV 223
A.thermocellus DPTIHIGG---ELDAIGGNTRIGSNKYFVAEACEYVESFLKFHPYLAVVLNIEADHLDYFKD-IEHIKNAFLKFIRLVPENGY----VVA 222
A.baumannii DPTYVIGGLLNST--GVNAALGE-SRFIVAEADESDASFLYLQPMAAIVTNIDADHMDTYEGSFDKLKDTFVQFLHNLPFYG----LAVV 232
A.baylyi DPTYVIGGLLNRT--GVNAALGA-SRFIVAEADESDASFLYLQPMAAIITNVDADHMDTYGGSFDKLKDTFVEFIHRLPFYG----LAVV 232
Nostoc DPTIIVGGEVNAW--EGNARLGQ-SSYLVAEADESDGSLVKHAPEIGIITNIELDHPDHYDT-LEEVVDIFQTFAKGCK-------TLIG 239
A.vinelandii DPTFVIGGRLNAA--GTNAQLGS-SRYLIAEADESDASFLHLQPMVAVVTNIDADHMDTYEGDFSRLKKTFVDFLHNLPFYG----LAVL 228
B.licheniformis KPTSYLIG-------DGTGKGCENSEYFVLEACEYRRHFLSYQPDYAIMTNIDFDHPDYFAN-IDDVFDAFQTMALQVNKG------IIA 202
B.subtilis KPTSFLIG-------DGTGQGNENSEYFVFEACEYRRHFLSYQPDYAIMTNIDFDHPDYFSS-IDDVFDAFQEMALQVNKG------IIA 202
B.quintana DPMVINGGIINAY--GTNARMGS-GDWMVVEADESDGTFLKLPADIAVVTNIDREHLDHYGS-FCAVREAFRQFVENVPFYGF----AVL 216
B.schoenbuchensis DPMVINGGIINAY--GTNARMGC-GDWMVVEADESDGTFLKLPADIVVVTNIDSEHLDYYGS-FDAVREAFRQFVENVPFYGF----AVM 216
Campylobacter ---VIIGAILKEF---GSNMIYKESQNLVFEADESDSSFLNSNPYLAIVTNAEAEHLDHYGNEVSKLHHAYTQFLDVAKIR-------VI 205
C.pelagibacter DPTIINGGVXXSF--NSSARLGN-SNWSILELDESDGSFLEVLPTYAIITNIDREHMDYYKT-MDNLKNLFQKFLEKVPSFGK----SFI 217
C. pecorum DPSYAVG-GLNSE--SLNGHAGS-SSIFIAEADESDGSLKHYAPDVAVVTNLDEEHLVNYDDDPEKLLKAMQEFSNKVRDS----QKVFY 213
C. trachomatis NPSFAIG-GLNQE--GINGGSGS-E-YFVAEADESDGSIRCYTPEFSVITNIDDEHLSNFEGDRELLLASLKDFALKT--Q----QICWY 210
C.aggregans ACGFLIGADVPAL--GGSAQWGDPTAPLVIEADEYDRVFLALTPAMAIVTNVEWDHPDIYPT-ATDYAAAFAEFAAQVRDR----RRLLL 211
C.ammoniagenes DPSFAIGGQLNRA--GTNAHHGK-DDIFVAEADESDASLLRYDPDIAVITNIEPDHLDYFGS-AEAYFQVFDDFAERIKPN----GTLIV 221
C.glutamicum DPSFAIGGQLNKA--GTNAHHGT-GEVFIAEADESDASLLRYKPNVAVVTNVEPDHLDFFKT-PEAYFQVFDDFAGRITPN----GKLVV 228
Enterobacter DPTFVNGGLVKAA--GVHARLGH-SRYLIAEADESDASFLHLQPMVAIVTNIEADHMDTYQGDFENLKTTFINFLHNLPFYG----RAVM 229
E.faecium1 RPTSYLIG-------DGTGHGDPQAEFFSFEACEYRRHFLAYSPDYAIMTNIDFDHPDYYTS-IDDVFTAFQTMAGQVKKA------IFA 206
E.faecium2 APTSYLIG-------DGTGHGVPDATFFAFEACEYQRHFLAYAPDYSIMTNIDFDHPDYFKS-IDDVFEAFQTLASQVKKG------IFA 206
E.coli DPTFVNGGLVKAA--GVHARLGH-GRYLIAEADESDASFLHLQPMVAIVTNIEADHMDTYQGDFENLKQTFINFLHNLPFYG----RAVM 229
F.tularensis YSSFIVGGVVKYA--DSNIQVNG-TDKLVIEADESDASFLFLSPQVVIITNIDLDHMATYN---NSYQTLLENFTDFVSKES--VKSIYL 212
G.violaceus DPTVVVGGEVDEL--GGNARLGS-GPHLVAEVDESDGSLVLFSPEVAVVTNIEGDHLDHYAN-LEQIVEAFQQYANQAR-------VVVG 217
G.oxydans DPTVINGGIIEAY--GTNTRMGS-GDWMVVEADESDGSFLRLPAVIAVVTNMDPEHLDHWGT-EEAMQAGYDQFVSNIPFYGF----AVL 217
H.influenzae DPTFVNGGLVKSA--GKNAHLGA-SRYLIAEADESDASFLHLQPMVSVVTNMEPDHMDTYEGDFEKMKATYVKFLHNLPFYG----LAVM 228
H. pylori ---AIIGAHSKEF---DSNVRESANDSLVFEADESDSSFLFSNPYAAIVPNTEPEHLEHYGHDLERFFFAYEYFLDHAQKR-------VI 217
K.pneumoniae DPTFVNGGLVKAA--GVHARLGH-SRYLIAEADESDASFLHLQPMVAIVTNIEADHMDTYHGDFENLKQTFINFLHNLPFYG----RAVM 224
L.plantarum APTSYLIG-------DGTGKGTPDARFFVFEADEYRRHFVAYHPDYAIMTNVDFDHPDYYKD-LADVQSAFQQFGNQVKKG------IFA 205
L.pneumophila DPSFVIGGKLNSC--GANAQLGK-SAYFVVEADESDASFLFLKPMMAVVTNIDADHMDTYEGDFEKLRTTFLEFLHHLPFYG----LAVV 225
L.monocytogenes RPTSYLIG-------DGTGSGTKGAEYFALEACEYQRHFLAYKPTYAIMTNIDWDHPDYFKS-VDDVFNAFETLGKQVKKA------VFA 202
M.luteus DPTFAVGAAVAGL--GTNARAGQ-GEWFIAEADESDGTLVNYPSTIGIVTTVEADHLDHYGT-EEAVHQVFRDFAGGLPAAAQ-GGVLVA 231
M.leprae DPSFVVGGELAVV--GTNAHHGL-GACFVAEADESDGSLLEYTPNVAVVTNIDSDHLDFYGS-VDAYIRVFDSFVERFALG----GALVV 224
M.bovis DPSFAVGGELGEA--GTNAHHGS-GDCFVAEADESDGSLLQYTPHVAVITNIESDHLDFYGS-VEAYVAVFDSFVERIVPG----GALVV 224
M.marinum DPSFAVGGELGEA--GTNAHHGS-GDYFVAEADESDGSLLEYTPHVAVVTNIEADHLDFYGS-TEAYVGVFDAFVERLAPG----GALVV 224
M.tuberculosis DPSFAVGGELGEA--GTNAHHGS-GDCFVAEADESDGSLLQYTPHVAVITNIESDHLDFYGS-VEAYVAVFDSFVERIVPG----GALVV 224
N.gonorrhoeae DPTFVIGGKLNAA--GTNARLGK-GEYIVAEADESDASFLHLTPIMSVVTNIDEDHMDTYGHSVEKLHQAFIDFIHRMPFYG----KAFL 215
P.yeei DPTVINGGVIHAY--GSNARAGA-GEWMVVEADESDGSFNRLPATIAIVTNIDPEHMEHWGS-FDALRKGFQDFVSNIPFYGL----AVC 220
P.chromatophora DPTAIIGGILPAI--GCNGYGGM-GNLLVAEVDESDGSLVKFRASLGIITNLELDHTNHYAK-FRDLITTMQYFASGCS-------RLLA 221
P.zucineum DPTVVNGGIINAY--GTNAKVGA-GDWIVVEADESDGTFLKLKSTVAVVTNIDPEHLDHYGD-FEAVKKAFQDFVENIPFYGF----AAV 219
P.gingivalis DCNAFLGGISNNY--QSNLLLSDKSDLVVVEADEFDRSFHHLKPFMAIITSADPDHMDIYGT-AENYRDSFEHFTSLIQSGG--ALVLKY 219
P.mirabilis DPTFVNGGLVKSA--GTHARLGC-SRYLIAEADESDASFLHLQPMVAVVTNIEADHMDTYHGNFDNLKETFITFLHNLPFYG----RAVM 229
P.chlorophenolicus DPSFAIGANVPSL--GVNAAHGT-SGIFVAEADESDGSFLNYRPQIAVVTNVEADHLDHYGT-AEAVYESFDRFAALLPAD----GLLVA 227
P.aeruginosa DPTFVIGGRLNAA--GTNAQLGA-SRYLVAEADESDASFLHLQPMVAVVTNIDADHMATYGGDFNKLKKTFVEFLHNLPFYG----LAVM 225
P.arcticus DPTYVIGGKLNAS--GKNAALGS-SRFLIAEADESDASFLSLHPMAAIVTNIDQDHMETYGNSFDKLKAAYIQFLQNMPFYG----LAVV 231
R.capsulatus DPTVINGGIIHAY--GSNARAGA-GEWMVVEADESDGSFNRLPATIAIVTNIDPEHMEHWGT-IENLRKGFYDFVSGIPFYGL----AVC 219
R.palustris DPTVINGGIINAY--GTNARLGG-GDWMVVEADESDGTFLKLPADVAIVTNVDPEHLDHFKT-FDAVQDAFRNFVENVPFYGF----AVM 216
R.rickettsii CPTVINGGIINNK--STNAYLGS-SNYLIAEADESDATFIHIPSTIAIITNIDPEHLDYYRD-FETLIGAFRSFITNLPFYGF----AVC 222
R.typhi YPTVINGGIINNK--STNAYLGS-SNYLIAEADESDATFIHIPSTIAIITNIDPEHLDYYQD-FEILIGAFRSFITNLPFYGF----AVC 222
R.pomeroyi YPTVINGGIINNK--STNAYLGS-SNYLIAEADESDATFIHIPSTIAIITNIDPEHLDYYQD-FEILIGAFRSFITNLPFYGF----AVC 222
S.enterica DPTFVNGGLVKAA--GVHARLGH-SRYLIAEADESDASFLHLQPMVAIVTNIEADHMDTYHGDFENLKQTFINFLHNLPFYG----RAVM 229
S.dysenteriae DPTFVNGGLVKAA--GVHARLGH-GRYLIAEADESDASFLHLQPMVAIVTNIEADHMDTYQGDFENLKQTFINFLHNLPFYG----RAVM 229
S.meliloti DPTVINGGIINAY--GTNARMGA-GEWMVVEADESDGTFLKLPADIAVVTNIDPEHLDHYGS-FDAVRAAFRQFVENVPFYGF----GVL 216
S.paucimobilis DPTVINGGIINSY--GSNARLGK-SDWMVVEADESDGSFLRLDGTLAVVTNIDPEHLDHYGS-FDKVKDAFVEFVENVPFYGA----AML 217
S.aureus KKTSFLIG-------DGTGMGLPESDYFAFEACEYRRHFLSYKPDYAIMTNIDFDHPDYFKD-INDVFDAFQEMAHNVKKG------IIA 202
S.pneumoniae TDTSFLIG-------DGTGRGSANAKYFVFESDEYERHFMPYHPEYSIITNIDFDHPDYFTS-LEDVFNAFNDYAKQITKG------LFV 204
Synechococcus DPTAIIGGIVPCL--GSNGHAGH-GRLLVAEADESDGSLVKFRPQLGLITNLELDHTDHYDG-LDDLINTMRLFADGCD-------QVLA 220
T.maritima SPTVFLGGIMDSL---EHGNYEKGNGPVVYELDESEEFFSEFSPNYLIITNARGDHLENYGNSLTRYRSAFEKISRNTDLV-------VT 209
T.thermophilus DPWVFLGGELALL--PGNARPGR--GPRVAEVDESDPLFREVRVSVAVATNLEADH--VAPR-GERAPNYHESLEALKEAM----RGFLA 204
T.denticola KLPVSVLAGSVIKSFGDSCTMLNGSKYFVAETCEYKRHFLNFHPKKIILTGIEPDHQDYYPT-YESILTAFLQYIDRLPQFSE----LFY 225
V.cholerae DPTFVNGGLVKSA--GTNARLGS-SRILIAEADESDASFLHLQPMVTIVTNIEADHMDTYGGDFENLKQTFIDFLHNLPFYG----QAIL 232
W.pipientis DATVTVGGILNSY--KSNFKLGG-SDTFLIEADESDGTMLKIPAKIAVITSINNDHIDYYGT-FDNIKNAFSQFVNNAGSAVLP---DSV 236
X.autotrophicus DPTVINGGIINAY--GTNARLGD-GNWMVVEADESDGTFLKLPTEVAIVTNVDPEHLDHFKT-FDKVQDAFKTFVENVPFYGF----AVM 216
Y.pestis DPTFVNGGLVKAA--GTHARLGS-SRYLIAEADESDASFLHLQPMVAIVTNIEADHMDTYQGDFENLKQTFINFLHNLPFYG----RAVM 229

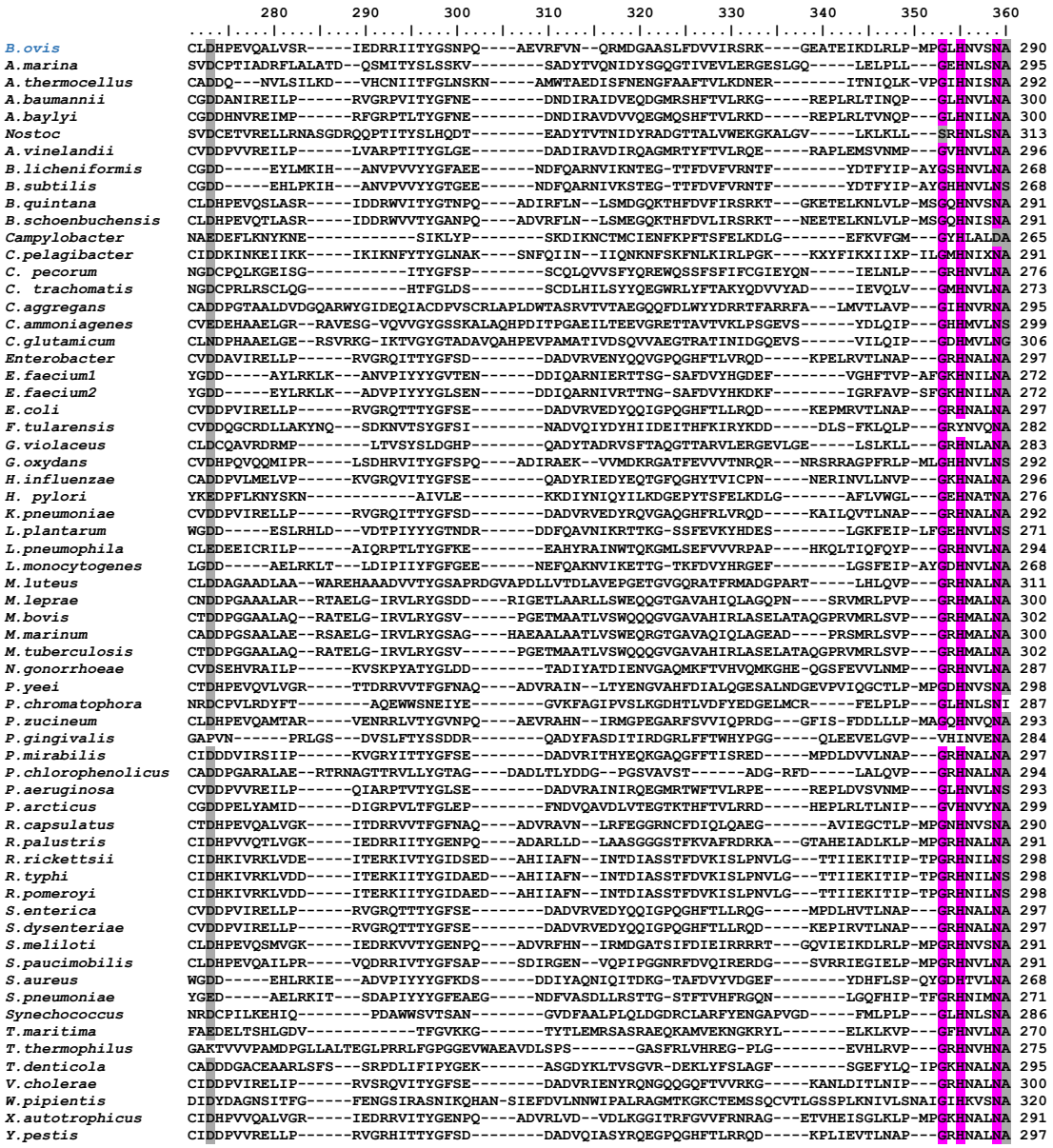
280 290 300 310 320 330 340 350 360
B.ovis CLDHPEVQALVSR-----IEDRRIITYGSNPQ----AEVRFVN--QRMDGAASLFDVVIRSRK----GEATEIKDLRLP-MPGLHNVSNA 290
A.marina SVDCPTIADRFLALATD--QSMITYSLSSKV--------SADYTVQNIDYSGQGTIVEVLERGESLGQ-----LELPLL---GEHNLSNA 295
A.thermocellus CADDQ---NVLSILKD---VHCNIITFGLNSKN-----AMWTAEDISFNENGFAAFTVLKDNER--------ITNIQLK-VPGIHNISNA 292
A.baumannii CGDDANIREILP------RVGRPVITYGFNE--------DNDIRAIDVEQDGMRSHFTVLRKG-----REPLRLTINQP---GLHNVLNA 300
A.baylyi CGDDHNVREIMP------RFGRPTLTYGFNE--------DNDIRAVDVVQEGMQSHFTVLRKD-----REPLRLTVNQP---GLHNILNA 300
Nostoc SVDCETVRELLRNASGDRQQPTITYSLHQDT--------EADYTVTNIDYRADGTTALVWEKGKALGV-----LKLKLL---SRHNLSNA 313
A.vinelandii CVDDPVVREILP------LVARPTITYGLGE--------DADIRAVDIRQAGMRTYFTVLRQE-----RAPLEMSVNMP---GVHNVLNA 296
B.licheniformis CGDD-----EYLMKIH---ANVPVVYYGFAEE------NDFQARNVIKNTEG-TTFDVFVRNTF--------YDTFYIP-AYGSHNVLNA 268
B.subtilis CGDD-----EHLPKIH---ANVPVVYYGTGEE------NDFQARNIVKSTEG-TTFDVFVRNTF--------YDTFYIP-AYGHHNVLNS 268
B.quintana CLDHPEVQSLASR-----IDDRWVITYGTNPQ----ADIRFLN--LSMDGQKTHFDVFIRSRKT---GKETELKNLVLP-MSGQHNVSNA 291
B.schoenbuchensis CLDHPEVQTLASR-----IDDRWVVTYGANPQ----ADVRFLN--LSMEGQKTHFDVLIRSRKT---NEETELKNLVLP-MSGQHNISNA 291
Campylobacter NAEDEFLKNYKNE----------SIKLYP--------SKDIKNCTMCIENFKPFTSFELKDLG-------EFKVFGM---GYHLALDA 265
C.pelagibacter CIDDKINKEIIKK-----IKIKNFYTYGLNAK----SNFQIIN--IIQNKNFSKFNLKIRLPGK----KXYFIKXIIXP-ILGMHNIXNA 291
C. pecorum NGDCPQLKGEISG----------ITYGFSP--------SCQLQVVSFYQREWQSSFSFIFCGIEYQN-----IELNLP---GRHNVLNA 276
C. trachomatis NGDCPRLRSCLQG----------HTFGLDS--------SCDLHILSYYQEGWRLYFTAKYQDVVYAD-----IEVQLV---GMHNVLNA 273
C.aggregans CADDPGTAALDVDGQARWYGIDEQIACDPVSCRLAPLDWTASRVTVTAEGQQFDLWYYDRRTFARRFA---LMVTLAVP---GIHNVRNA 295
C.ammoniagenes CVEDEHAAELGR--RAVESG-VQVVGYGSSKALAQHPDITPGAEILTEEVGRETTAVTVKLPSGEVS------YDLQIP---GHHMVLNS 299
C.glutamicum CLNDPHAAELGE--RSVRKG-IKTVGYGTADAVQAHPEVPAMATIVDSQVVAEGTRATINIDGQEVS------VILQIP---GDHMVLNG 306
Enterobacter CVDDAVIRELLP------RVGRQITTYGFSD--------DADVRVENYQQVGPQGHFTLVRQD-----KPELRVTLNAP---GRHNALNA 297
E.faecium1 YGDD-----AYLRKLK---ANVPIYYYGVTEN------DDIQARNIERTTSG-SAFDVYHGDEF--------VGHFTVP-AFGKHNILNA 272
E.faecium2 YGDD-----EYLRKLK---ADVPIYYYGLSEN------DDIQARNIVRTTNG-SAFDVYHKDKF--------IGRFAVP-SFGKHNILNA 272
E.coli CVDDPVIRELLP------RVGRQTTTYGFSE--------DADVREVDYQQIGPQGHFTLLRQD-----KEPMRVTLNAP---GRHNALNA 297
F.tularensis CVDDQGCRDLLAKYNQ---SDKNVTSYGFSI--------NADVQIYDYHIIDEITHFKIRYKDD-----DLS-FKLQLP---GRYNVQNA 282
G.violaceus CLDCQAVRDRMP--------LTVSYSLDGHP--------QADYTADRVSFTAQGTTARVLERGEVLGE-----LSLKLL---GRHNLANA 283
G.oxydans CVDHPQVQQMIPR-----LSDHRVITYGFSPQ----ADIRAEK--VVMDKRGATFEVVVTNRQR---NRSRRAGPFRLP-MLGHHNVLNS 292
H.influenzae CADDPVLMELVP------KVGRQVITYGFSE--------QADYRIEDYEQTGFQGHYTVICPN-----NERINVLLNVP---GKHNALNA 296
H. pylori YKEDPFLKNYSKN----------AIVLE---------KKDIYNIQYILKDGEPYTSFELKDLG-------AFLVWGL---GEHNATNA 276
K.pneumoniae CVDDPVIRELLP------RVGRQITTYGFSD--------DADVRVEDYRQVGAQGHFRLVRQD-----KAILQVTLNAP---GRHNALNA 292
L.plantarum WGDD-----ESLRHLD---VDTPIYYYGTNDR------DDFQAVNIKRTTKG-SSFEVKYHDES--------LGKFEIP-LFGEHNVLNS 271
L.pneumophila CLEDEEICRILP------AIQRPTLTYGFKE--------EAHYRAINWTQKGMLSEFVVVRPAP----HKQLTIQFQYP---GRHNVLNA 294
L.monocytogenes LGDD-----AELRKLT---LDIPIIYFGFGEE------NEFQAKNVIKETTG-TKFDVYHRGEF--------LGSFEIP-AYGDHNVLNA 268
M.luteus CLDDAGAADLAA--WAREHAAADVVTYGSAPRDGVAPDLLVTDLAVEPGETGVGQRATFRMADGPART-----LHLQVP---GRHNALNA 311
M.leprae CNDDPGAAALAR--RTAELG-IRVLRYGSDD----RIGETLAARLLSWEQQGTGAVAHIQLAGQPN----SRVMRLPVP---GRHMALNA 300
M.bovis CTDDPGGAALAQ--RATELG-IRVLRYGSV------PGETMAATLVSWQQQGVGAVAHIRLASELATAQGPRVMRLSVP---GRHMALNA 302
M.marinum CADDPGSAALAE--RSAELG-IRVLRYGSAG----HAEAALAATLVSWEQRGTGAVAQIQLAGEAD----PRSMRLSVP---GRHMALNA 300
M.tuberculosis CTDDPGGAALAQ--RATELG-IRVLRYGSV------PGETMAATLVSWQQQGVGAVAHIRLASELATAQGPRVMRLSVP---GRHMALNA 302
N.gonorrhoeae CVDSEHVRAILP------KVSKPYATYGLDD--------TADIYATDIENVGAQMKFTVHVQMKGHE-QGSFEVVLNMP---GRHNVLNA 287
P.yeei CTDHPEVQVLVGR-----TTDRRVVTFGFNAQ----ADVRAIN--LTYENGVAHFDIALQGESALNDGEVPVIQGCTLP-MPGDHNVSNA 298
P.chromatophora NRDCPVLRDYFT--------AQEWWSNEIYE--------GVKFAGIPVSLKGDHTLVDFYEDGELMCR-----FELPLP---GLHNLSNI 287
P.zucineum CLDHPEVQAMTAR-----VENRRLVTYGVNPQ----AEVRAHN--IRMGPEGARFSVVIQPRDG---GFIS-FDDLLLP-MAGQHNVQNA 293
P.gingivalis GAPVN------PRLGS---DVSLFTYSSDDR--------QADYFASDITIRDGRLFFTWHYPGG-----QLEEVELGVP---VHINVENA 284
P.mirabilis CIDDDVIRSIIP------KVGRYITTYGFSE--------DADVRITHYEQKGAQGFFTISRED-----MPDLDVVLNAP---GRHNALNA 297
P.chlorophenolicus CADDPGARALAE--RTRNAGTTRVLLYGTAG----DADLTLYDDG--PGSVAVST------ADG-RFD-----LALQVP---GRHNALNA 294
P.aeruginosa CVDDPVVREILP------QIARPTVTYGLSE--------DADVRAINIRQEGMRTWFTVLRPE-----REPLDVSVNMP---GLHNVLNS 293
P.arcticus CGDDPELYAMID------DIGRPVLTFGLEP--------FNDVQAVDLVTEGTKTHFTVLRRD-----HEPLRLTLNIP---GVHNVYNA 299
R.capsulatus CTDHPEVQALVGK-----ITDRRVVTFGFNAQ----ADVRAVN--LRFEGGRNCFDIQLQAEG-------AVIEGCTLP-MPGNHNVSNA 290
R.palustris CIDHPVVQTLVGK-----IEDRRIITYGENPQ----ADARLLD--LAASGGGSTFKVAFRDRKA---GTAHEIADLKLP-MPGRHNALNA 291
R.rickettsii CIDHKIVRKLVDE-----ITERKIVTYGIDSED---AHIIAFN--INTDIASSTFDVKISLPNVLG---TTIIEKITIP-TPGRHNILNS 298
R.typhi CIDHKIVRKLVDD-----ITERKIITYGIDAED---AHIIAFN--INTDIASSTFDVKISLPNVLG---TTIIEKITIP-TPGRHNILNS 298
R.pomeroyi CIDHKIVRKLVDD-----ITERKIITYGIDAED---AHIIAFN--INTDIASSTFDVKISLPNVLG---TTIIEKITIP-TPGRHNILNS 298
S.enterica CVDDPVIRELLP------RVGRQTTTYGFSE--------DADVREVDYQQIGPQGHFTLLRQG-----MPDLHVTLNAP---GRHNALNA 297
S.dysenteriae CVDDPVIRELLP------RVGRQTTTYGFSE--------DADVREVDYQQIGPQGHFTLLRQD-----KEPIRVTLNAP---GRHNALNA 297
S.meliloti CLDHPEVQSMVGK-----IEDRKVVTYGENPQ----ADVRFHN--IRMDGATSIFDIEIRRRRT---GQVIEIKDLRLP-MPGRHNVSNA 291
S.paucimobilis CLDHPEVQAILPR-----VQDRRIVTYGFSAP----SDIRGEN--VQPIPGGNRFDVQIRERDG----SVRRIEGIELP-MPGRHNVLNA 291
S.aureus WGDD-----EHLRKIE---ADVPIYYYGFKDS------DDIYAQNIQITDKG-TAFDVYVDGEF--------YDHFLSP-QYGDHTVLNA 268
S.pneumoniae YGED-----AELRKIT---SDAPIYYYGFEAEG-----NDFVASDLLRSTTG-STFTVHFRGQN--------LGQFHIP-TFGRHNIMNA 271
Synechococcus NRDCPILKEHIQ--------PDAWWSVTSAN--------GVDFAALPLQLDGDRCLARFYENGAPVGD-----FMLPLP---GLHNLSNA 286
T.maritima FAEDELTSHLGDV----------TFGVKKG-------TYTLEMRSASRAEQKAMVEKNGKRYL-------ELKLKVP---GFHNVLNA 270
T.thermophilus GAKTVVVPAMDPGLLALTEGLPRRLFGPGGEVWAEAVDLSPS-------GASFRLVHREG-PLG--------EVHLRVP---GRHNVHNA 275
T.denticola CADDDGACEAARLSFS---SRPDLIFIPYGEK-------ASGDYKLTVSGVR-DEKLYFSLAGF--------SGEFYLQ-IPGKHNALNA 295
V.cholerae CIDDPVIRELIP------RVSRQVITYGFSE--------DADVRIENYRQNGQQGQFTVVRKG-----KANLDITLNIP---GRHNALNA 300
W.pipientis DIDYDAGNSITFG-----FENGSIRASNIKQHAN-SIEFDVLNNWIPALRAGMTKGKCTEMSSQCVTLGSSPLKNIVLSNAIGIHKVSNA 320
X.autotrophicus CIDHPVVQALVGR-----IEDRRVITYGENPQ----ADVRLVD--VDLKGGITRFGVVFRNRAG---ETVHEISGLKLP-MPGKHNALNA 291
Y.pestis CIDDPVVRELLP------RVGRHITTYGFSD--------DADVQIASYRQEGPQGHFTLRRQD-----KPLIEVTLNAP---GRHNALNA 297

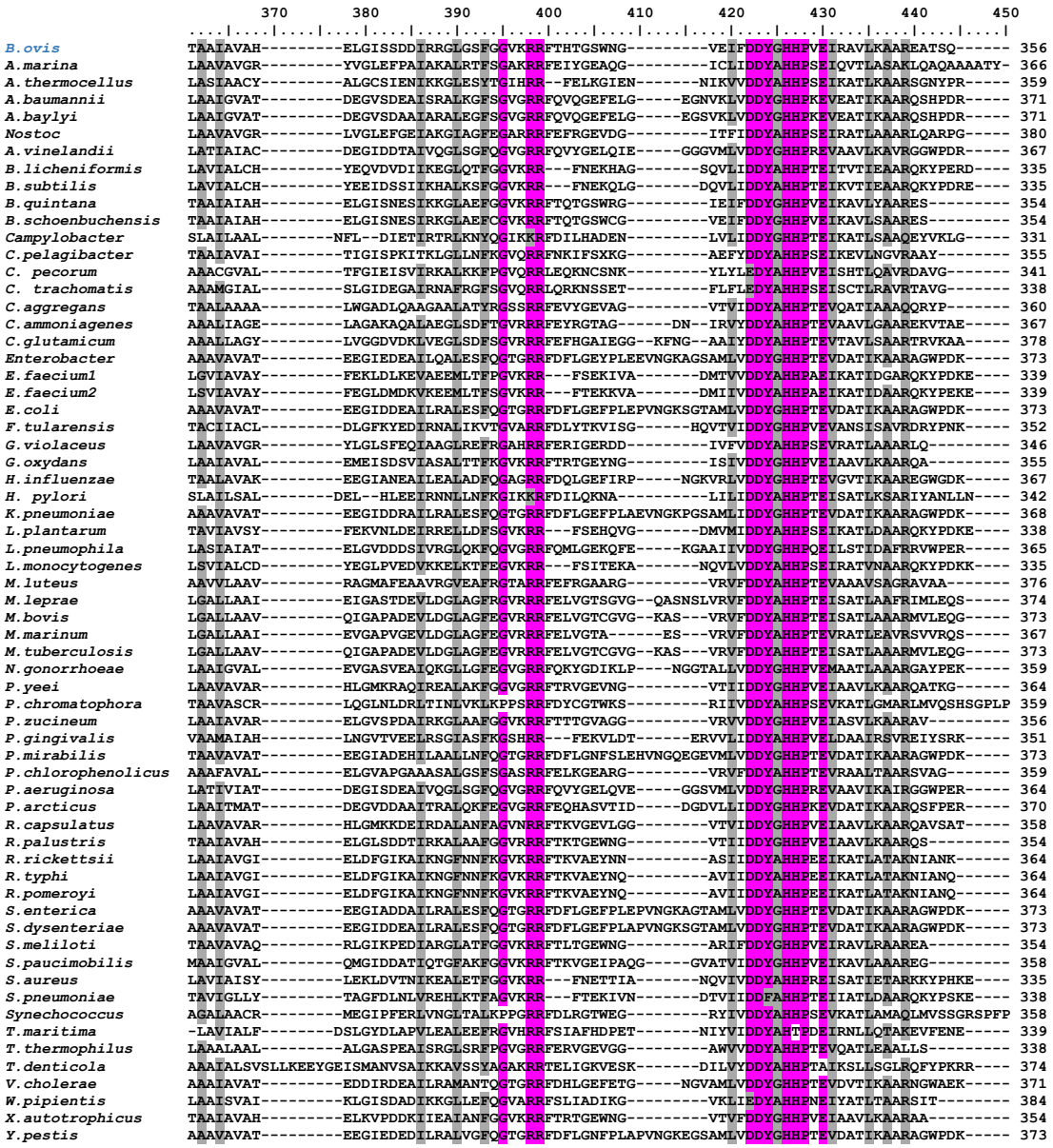
370 380 390 400 410 420 430 440 450
B.ovis TAAIAVAH--------ELGISSDDIRRGLGSFGGVKRRFTHTGSWNG---------VEIFDDYGHHPVEIRAVLKAAREATSQ------ 356
A.marina LAAVAVGR---------YVGLEFPAIAKALRTFSGAKRRFEIYGEAQG---------ICLIDDYAHHPSEIQVTLASAKLQAQAAAATY- 366
A.thermocellus LASIAACY---------ALGCSIENIKKGLESYTGIHRR--FELKGIEN-------NIKVVDDYAHHPSEIKATLKAARSGNYPR----- 359
A.baumannii LAAIGVAT---------DEGVSDEAISRALKGFSGVGRRFQVQGEFELG-----EGNVKLVDDYGHHPKEVEATIKAARQSHPDR----- 371
A.baylyi LAAIGVAT---------DEGVSDAAIARALEGFSGVGRRFQVQGEFELG-----EGSVKLVDDYGHHPKEVEATIKAARQSHPDR----- 371
Nostoc LAAVAVGR---------LVGLEFGEIAKGIAGFEGARRRFEFRGEVDG---------ITFIDDYAHHPSEIRATLAAARLQARPG----- 380
A.vinelandii LATIAIAC---------DEGIDDTAIVQGLSGFQGVGRRFQVYGELQIE-----GGGVMLVDDYGHHPREVAAVLKAVRGGWPDR----- 367
B.licheniformis LAVIALCH---------YEQVDVDIIKEGLQTFGGVKRR---FNEKHAG-------SQVLIDDYAHHPTEITVTIEAARQKYPERD---- 335
B.subtilis LAVIALCH---------YEEIDSSIIKHALKSFGGVKRR---FNEKQLG-------DQVLIDDYAHHPTEIKVTIEAARQKYPDRE---- 335
B.quintana TAAIAIAH---------ELGISNESIKKGLAEFGGVKRRFTQTGSWRG---------IEIFDDYGHHPVEIKAVLYAARES--------- 354
B.schoenbuchensis TAAIAIAH---------ELGISNESIRKGLAEFCGVKRRFTQTGSWCG---------VEIFDDYGHHPVEIKAVLSAARES--------- 354
Campylobacter SLAILAAL--------NFL--DIETIRTRLKNYQGIKKRFDILHADEN---------LVLIDDYGHHPTEIKATLSAAQEYVKLG----- 331
C.pelagibacter TAAIAVAI---------TIGISPKITKLGLLNFKGVQRRFNKIFSXKG---------AEFYDDYAHHPSEIKEVLNGVRAAY--------- 355
C. pecorum AAACGVAL---------TFGIEISVIRKALKKFPGVQRRLEQKNCSNK---------YLYLEDYAHHPVEISHTLQAVRDAVG------- 341
C. trachomatis AAAMGIAL---------SLGIDEGAIRNAFRGFSGVQRRLQRKNSSET---------FLFLEDYAHHPSEISCTLRAVRTAVG------- 338
C.aggregans TAALAAAA---------LWGADLQAAGAALATYRGSSRRFEVYGEVAG---------VTVIDDYAHHPTEVQATIAAAQQRYP------- 360
C.ammoniagenes AAALIAGE---------LAGAKAQALAEGLSDFTGVRRRFEYRGTAG------DN--IRVYDDYAHHPTEVAAVLGAARERKVTAE----- 367
C.glutamicum AAALLAGY---------LVGGDVDKLVEGLSDFSGVRRRFEFHGAIEGG--KFNG--AAIYDDYAHHPTEVTAVLSAARTRVKAA----- 378
Enterobacter AAAVAVAT---------EEGIEDEAILQALESFQGTGRRFDFLGEYPLEEVNGKAGSAMLVDDYGHHPTEVDATIKAARAGWPDK----- 373
E.faecium1 LGVIAVAY---------FEKLDLKEVAEEMLTFPGVKRR---FSEKIVA-------DMTVVDDYAHHPAEIKATIDGARQKYPDKE---- 339
E.faecium2 LSVIAVAY---------FEGLDMDKVKEEMLTFSGVKRR---FTEKKVA-------DMIIVDDYAHHPAEIKATIDAARQKYPEKE---- 339
E.coli AAAVAVAT---------EEGIDDEAILRALESFQGTGRRFDFLGEFPLEPVNGKSGTAMLVDDYGHHPTEVDATIKAARAGWPDK----- 373
F.tularensis TACIIACL---------DLGFKYEDIRNALIKVTGVARRFDLYTKVISG------HQVTVIDDYGHHPVEVANSISAVRDRYPNK----- 352
G.violaceus LAAVAVGR---------YLGLSFEQIAAGLREFRGAHRRFERIGERDD---------IVFVDDYAHHPSEVRATLAAARLQ--------- 346
G.oxydans LAAIAVAL---------EMEISDSVIASALTTFKGVKRRFTRTGEYNG---------ISIVDDYGHHPVEIAAVLKAARQA--------- 355
H.influenzae TAALAVAK---------EEGIANEAILEALADFQGAGRRFDQLGEFIRP-----NGKVRLVDDYGHHPTEVGVTIKAAREGWGDK----- 367
H. pylori SLAILSAL--------DEL--HLEEIRNNLLNFKGIKKRFDILQKNA---------LILIDDYAHHPTEISATLKSARIYANLLN---- 342
K.pneumoniae AAAVAVAT---------EEGIDDRAILRALESFQGTGRRFDFLGEFPLAEVNGKPGSAMLIDDYGHHPTEVDATIKAARAGWPDK----- 368
L.plantarum TAVIAVSY---------FEKVNLDEIRRELLDFSGVKRR---FSEHQVG-------DMVMIDDYAHHPSEIKATLDAARQKYPDKE---- 338
L.pneumophila LASIAIAT---------ELGVDDDSIVRGLQKFQGVGRRFQMLGEKQFE-----KGAAIIVDDYGHHPQEILSTIDAFRRVWPER----- 365
L.monocytogenes LSVIALCD---------YEGLPVEDVKKELKTFEGVKRR---FSITEKA-------NQVLVDDYAHHPSEIRATVNAARQKYPDKK---- 335
M.luteus AAVVLAAV---------RAGMAFEAAVRGVEAFRGTARRFEFRGAARG---------VRVFDDYAHHPTEVAAAVSAGRAVAA-------- 376
M.leprae LGALLAAI---------EIGASTDEVLDGLAGFRGVRRRFELVGTSGVG--QASNSLVRVFDDYAHHPTEISATLAAFRIMLEQS----- 374
M.bovis LGALLAAV---------QIGAPADEVLDGLAGFEGVRRRFELVGTCGVG--KAS---VRVFDDYAHHPTEISATLAAARMVLEQG----- 373
M.marinum LGALLAAI---------EVGAPVGEVLDGLAGFEGVRRRFELVGTA------ES---VRVFDDYAHHPTEVRATLEAVRSVVRQS----- 367
M.tuberculosis LGALLAAV---------QIGAPADEVLDGLAGFEGVRRRFELVGTCGVG--KAS---VRVFDDYAHHPTEISATLAAARMVLEQG----- 373
N.gonorrhoeae LAAIGVAL---------EVGASVEAIQKGLLGFEGVGRRFQKYGDIKLP----NGGTALLVDDYGHHPVEMAATLAAARGAYPEK----- 359
P.yeei LAAVAVAR---------HLGMKRAQIREALAKFGGVGRRFTRVGEVNG---------VTIIDDYGHHPVEIAAVLKAARQATKG------ 364
P.chromatophora TAAVASCR---------LQGLNLDRLTINLVKLKPPSRRFDYCGTWKS---------RIIVDDYAHHPSEVKATLGMARLMVQSHSGPLP 359
P.zucineum LAAIAVAR---------ELGVSPDAIRKGLAAFGGVKRRFTTTGVAGG---------VRVVDDYGHHPVEIASVLKAARAV--------- 356
P.gingivalis VAAMAIAH---------LNGVTVEELRSGIASFKGSHRR---FEKVLDT------ERVVLIDDYAHHPVELDAAIRSVREIYSRK----- 351
P.mirabilis TAAVAVAT---------EEGIADEHILAALLNFQGTGRRFDFLGNFSLEHVNGQEGEVMLVDDYGHHPTEVDATIKAARAGWPDK----- 373
P.chlorophenolicus AAAFAVAL---------ELGVAPGAAASALGSFSGASRRFELKGEARG---------VRVFDDYAHHPTEVRAALTAARSVAG------- 359
P.aeruginosa LATIVIAT---------DEGISDEAIVQGLSGFQGVGRRFQVYGELQVE-----GGSVMLVDDYGHHPREVAAVIKAIRGGWPER----- 364
P.arcticus LAAITMAT---------DEGVDDAAITRALQKFEGVGRRFEQHASVTID-----DGDVLLIDDYGHHPKEVDATIKAARQSFPER----- 370
R.capsulatus LAAVAVAR---------HLGMKKDEIRDALANFAGVNRRFTKVGEVLGG--------VTVIDDYGHHPVEIAAVLKAARQAVSAT----- 358
R.palustris TAAIAVAH---------ELGLSDDTIRKALAAFGGVRRRFTKTGEWNG---------VTIIDDYGHHPVEIAAVLKAARQS--------- 354
R.rickettsii LAAIAVGI---------ELDFGIKAIKNGFNNFKGVKRRFTKVAEYNN---------ASIIDDYAHHPEEIKATLATAKNIANK------ 364
R.typhi LAAIAVGI---------ELDFGIKAIKNGFNNFKGVKRRFTKVAEYNQ---------AVIIDDYAHHPEEIKATLATAKNIANQ------ 364
R.pomeroyi LAAIAVGI---------ELDFGIKAIKNGFNNFKGVKRRFTKVAEYNQ---------AVIIDDYAHHPEEIKATLATAKNIANQ------ 364
S.enterica AAAVAVAT---------EEGIADDAILRALESFQGTGRRFDFLGEFPLEPVNGKAGTAMLVDDYGHHPTEVDATIKAARAGWPDK----- 373
S.dysenteriae AAAVAVAT---------EEGIDDEAILRALESFQGTGRRFDFLGEFPLAPVNGKSGTAMLVDDYGHHPTEVDATIKAARAGWPDK----- 373
S.meliloti TAAVAVAQ---------RLGIKPEDIARGLATFGGVKRRFTLTGEWNG---------ARIFDDYGHHPVEIRAVLRAAREA--------- 354
S.paucimobilis MAAIGVAL---------QMGIDDATIQTGFAKFGGVKRRFTKVGEIPAQG-----GVATVIDDYGHHPVEIKAVLAAAREG--------- 358
S.aureus LAVIAISY---------LEKLDVTNIKEALETFGGVKRR---FNETTIA-------NQVIVDDYAHHPREISATIETARKKYPHKE---- 335
S.pneumoniae TAVIGLLY---------TAGFDLNLVREHLKTFAGVKRR---FTEKIVN-------DTVIIDDFAHHPTEIIATLDAARQKYPSKE---- 338
Synechococcus AGALAACR---------MEGIPFERLVNGLTALKPPGRRFDLRGTWEG---------RYIVDDYAHHPSEVKATLAMAQLMVSSGRSPFP 358
T.maritima -LAVIALF--------DSLGYDLAPVLEALEEFRGVHRRFSIAFHDPET-------NIYVIDDYAHTPDEIRNLLQTAKEVFENE----- 339
T.thermophilus LAAALAAL---------ALGASPEAISRGLSRFPGVGRRFERVGEVGG---------AWVVDDYAHHPTEVQATLEAALLS--------- 338
T.denticola AAAIALSVSLLKEEYGEISMANVSAIKKAVSSYAGAKRRTELIGKVESK-------DILVYDDYAHHPTAIKSLLSGLRQFYPKRR---- 374
V.cholerae AAAIAVAT---------EDDIRDEAILRAMANTQGTGRRFDHLGEFETG-----NGVAMLVDDYGHHPTEVDVTIKAARNGWAEK----- 371
W.pipientis LAAISVAI---------KLGISDADIKKGLLEFQGVARRFSLIADIKG---------VKLIEDYAHHPNEIYATLTAARSIT-------- 384
X.autotrophicus TAAIAVAH---------ELKVPDDKIIEAIANFGGVKRRFTRTGEWNG---------VTVFDDYGHHPVEIAAVLKAARAA--------- 354
Y.pestis AAAVAVAT---------EEGIEDEDILRALVGFQGTGRRFDFLGNFPLAPVNGKEGSAMLVDDYGHHPTEVDATIKAARAGWPDK----- 373

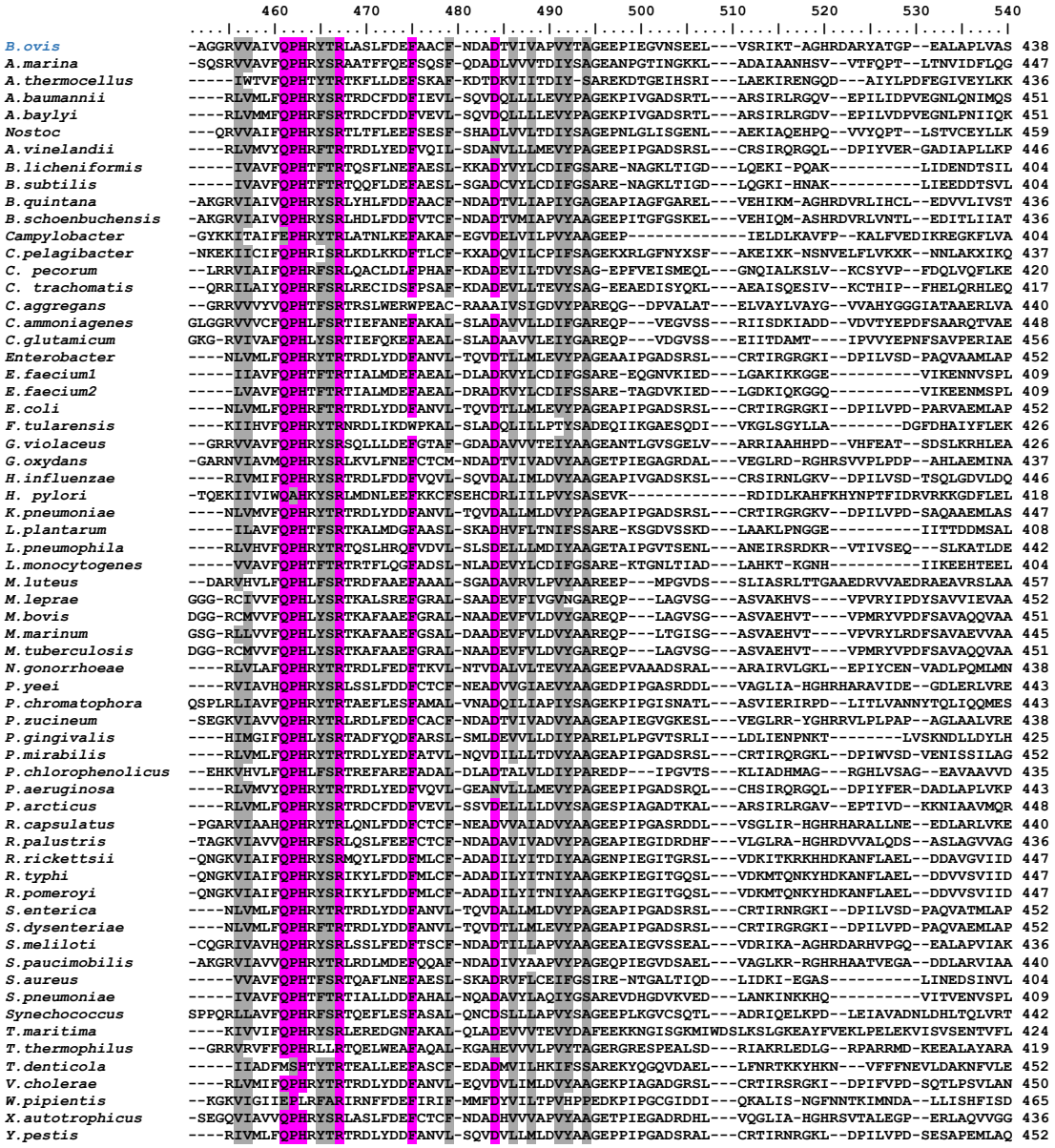
460 470 480 490 500 510 520 530 540
B.ovis -AGGRVVAIVQPHRYTRLASLFDEFAACF-NDADTVIVAPVYTAGEEPIEGVNSEEL---VSRIKT-AGHRDARYATGP--EALAPLVAS 438
A.marina -SQSRVVAVFQPHRYSRAATFFQEFSQSF-QDADLVVVTDIYSAGEANPGTINGKKL---ADAIAANHSV--VTFQPT--LTNVIDFLQG 447
A.thermocellus -----IWTVFQPHTYTRTKFLLDEFSKAF-KDTDKVIITDIY-SAREKDTGEIHSRI---LAEKIRENGQD---AIYLPDFEGIVEYLKK 436
A.baumannii ----RLVMLFQPHRYSRTRDCFDDFIEVL-SQVDQLLLLEVYPAGEKPIVGADSRTL---ARSIRLRGQV--EPILIDPVEGNLQNIMQS 451
A.baylyi ----RLVMMFQPHRFSRTRDCFDDFVEVL-SQVDQLLLLEVYPAGEKPIVGADSRTL---ARSIRLRGDV--EPILVDPVEGNLPNIIQK 451
Nostoc ---QRVVAIFQPHRYSRTLTFLEEFSESF-SHADLVVLTDIYSAGEPNLGLISGENL---AEKIAQEHPQ--VVYQPT--LSTVCEYLLK 459
A.vinelandii ----RLVMVYQPHRFTRTRDLYEDFVQIL-SDANVLLLMEVYPAGEEPIPGADSRSL---CRSIRQRGQL--DPIYVER-GADIAPLLKP 446
B.licheniformis -----IVAVFQPHTFTRTQSFLNEFAESL-KKADYVYLCDIFGSARE-NAGKLTIGD---LQEKI-PQAK----------LIDENDTSIL 404
B.subtilis -----IVAVFQPHTFTRTQQFLDEFAESL-SGADCVYLCDIFGSARE-NAGKLTIGD---LQGKI-HNAK----------LIEEDDTSVL 404
B.quintana -AKGRVIAIVQPHRYSRLYHLFDDFAACF-NDADTVLIAPIYGAGEAPIAGFGAREL---VEHIKM-AGHRDVRLIHCL--EDVVLIVST 436
B.schoenbuchensis -AKGRVIAIVQPHRYSRLHDLFDDFVTCF-NDADTVMIAPVYAAGEEPITGFGSKEL---VEHIQM-ASHRDVRLVNTL--EDITLIIAT 436
Campylobacter -GYKKITAIFEPHRYTRLATNLKEFAKAF-EGVDELVILPVYAAGEEP------------IELDLKAVFP--KALFVEDIKREGKFLVA 404
C.pelagibacter -NKEKIICIFQPHRISRLKDLKKDFTLCF-KKADQVILCPIFSAGEKXRLGFNYXSF---AKEIXK-NSNVELFLVKXK--NNLAKXIKQ 437
C. pecorum --LRRVIAIFQPHRFSRLQACLDLFPHAF-KDADEVILTDVYSAG-EPFVEISMEQL---GNQIALKSLV--KCSYVP--FDQLVQFLKE 420
C. trachomatis --QRRILAIYQPHRFSRLRECIDSFPSAF-KDADEVLLTEVYSAG-EEAEDISYQKL---AEAISQESIV--KCTHIP--FHELQRHLEQ 417
C.aggregans --GRRVVVYVQPHTFSRTRSLWERWPEAC-RAAAIVSIGDVYPAREQG--DPVALAT---ELVAYLVAYG--VVAHYGGGIATAAERLVA 440
C.ammoniagenes GLGGRVVVCFQPHLFSRTIEFANEFAKAL-SLADAVVLLDIFGAREQP---VEGVSS---RIISDKIADD--VDVTYEPDFSAARQTVAE 448
C.glutamicum GKG-RVIVAFQPHLYSRTIEFQKEFAEAL-SLADAAVVLEIYGAREQP---VDGVSS---EIITDAMT----IPVVYEPNFSAVPERIAE 456
Enterobacter ----NLVMLFQPHRYTRTRDLYDDFANVL-TQVDTLLMLEVYPAGEAAIPGADSRSL---CRTIRGRGKI--DPILVSD-PAQVAAMLAP 452
E.faecium1 -----IIAVFQPHTFTRTIALMDEFAEAL-DLADKVYLCDIFGSARE-EQGNVKIED---LGAKIKKGGE----------VIKENNVSPL 409
E.faecium2 -----LVAVFQPHTFTRTIALMDEFAEAL-DRADKVYLCDIFSSARE-TAGDVKIED---LGDKIQKGGQ----------VIKEENMSPL 409
E.coli ----NLVMLFQPHRFTRTRDLYDDFANVL-TQVDTLLMLEVYPAGEAPIPGADSRSL---CRTIRGRGKI--DPILVPD-PARVAEMLAP 452
F.tularensis ----KIIHVFQPHRYTRNRDLIKDWPKAL-SLADQLILLPTYSADEQIIKGAESQDI---VKGLSGYLLA--------DGFDHAIYFLEK 426
G.violaceus --GRRVVAVFQPHRYSRSQLLLDEFGTAF-GDADAVVVTEIYAAGEANTLGVSGELV---ARRIAAHHPD--VHFEAT--SDSLKRHLEA 426
G.oxydans -GARNVIAVMQPHRYSRLKVLFNEFCTCM-NDADTVIVADVYAAGETPIEGAGRDAL---VEGLRD-RGHRSVVPLPDP--AHLAEMINA 437
H.influenzae ----RIVMIFQPHRYSRTRDLFDDFVQVL-SQVDALIMLDVYAAGEAPIVGADSKSL---CRSIRNLGKV--DPILVSD-TSQLGDVLDQ 446
H. pylori -TQEKIIVIWQAHKYSRLMDNLEEFKKCFSEHCDRLIILPVYSASEVK------------RDIDLKAHFKHYNPTFIDRVRKKGDFLEL 418
K.pneumoniae ----NLVMVFQPHRYTRTRDLYDDFANVL-TQVDALLMLDVYPAGEAPIPGADSRSL---CRTIRGRGKV--DPILVPD-SAQAAEMLAS 447
L.plantarum -----ILAVFQPHTFSRTKALMDGFAASL-SKADHVFLTNIFSSARE-KSGDVSSKD---LAAKLPNGGE----------IITTDDMSAL 408
L.pneumophila ----RLVHVFQPHRYTRTQSLHRQFVDVL-SLSDELLLMDIYAAGETAIPGVTSENL---ANEIRSRDKR--VTIVSEQ---SLKATLDE 442
L.monocytogenes -----VVAVFQPHTFTRTRTFLQGFADSL-NLADEVYLCDIFGSARE-KTGNLTIAD---LAHKT-KGNH----------IIKEEHTEEL 404
M.luteus --DARVHVLFQPHLFSRTRDFAAEFAAAL-SGADAVRVLPVYAAREEP---MPGVDS---SLIASRLTTGAAEDRVVAEDRAEAVRSLAA 457
M.leprae GGG-RCIVVFQPHLYSRTKALSREFGRAL-SAADEVFIVGVNGAREQP---LAGVSG---ASVAKHVS----VPVRYIPDYSAVVIEVAA 452
M.bovis DGG-RCMVVFQPHLYSRTKAFAAEFGRAL-NAADEVFVLDVYGAREQP---LAGVSG---ASVAEHVT----VPMRYVPDFSAVAQQVAA 451
M.marinum GSG-RLLVVFQPHLYSRTKAFAAEFGSAL-DAADEVFVLDVYAAREQP---LTGISG---ASVAEHVT----VPVRYLRDFSAVAEVVAA 445
M.tuberculosis DGG-RCMVVFQPHLYSRTKAFAAEFGRAL-NAADEVFVLDVYGAREQP---LAGVSG---ASVAEHVT----VPMRYVPDFSAVAQQVAA 451
N.gonorrhoeae ----RLVLAFQPHRYTRTRDLFEDFTKVL-NTVDALVLTEVYAAGEEPVAAADSRAL---ARAIRVLGKL--EPIYCEN-VADLPQMLMN 438
P.yeei ----RVIAVHQPHRYSRLSSLFDDFCTCF-NEADVVGIAEVYAAGEDPIPGASRDDL---VAGLIA-HGHRHARAVIDE--GDLERLVRE 443
P.chromatophora QSPLRLIAVFQPHRYTRTAEFLESFAMAL-VNADQILIAPIYSAGEKPIPGISNATL---ASVIERIRPD--LITLVANNYTQLIQQMES 443
P.zucineum -SEGKVIAVVQPHRYTRLRDLFEDFCACF-NDADTVIVADVYAAGEAPIEGVGKESL---VEGLRR-YGHRRVLPLPAP--AGLAALVRE 438
P.gingivalis ----HIMGIFQPHLYSRTADFYQDFARSL-SMLDEVVLLDIYPARELPLPGVTSRLI---LDLIENPNKT--------LVSKNDLLDYLH 425
P.mirabilis ----RLVMLFQPHRYTRTRDLYEDFATVL-NQVDILLLTDVYAAGEAPIPGADSRSL---CRTIRQRGKL--DPIWVSD-VENISSILAG 452
P.chlorophenolicus --EHKVHVLFQPHLFSRTREFAREFADAL-DLADTALVLDIYPAREDP---IPGVTS---KLIADHMAG---RGHLVSAG--EAVAAVVD 435
P.aeruginosa ----RLVMVYQPHRYTRTRDLYEDFVQVL-GEANVLLLMEVYPAGEEPIPGADSRQL---CHSIRQRGQL--DPIYFER-DADLAPLVKP 443
P.arcticus ----RLVMLFQPHRYSRTRDCFDDFVEVL-SSVDELLLLDVYSAGESPIAGADTKAL---ARSIRLRGAV--EPTIVD--KKNIAAVMQR 448
R.capsulatus -PGARVIAAHQPHRYTRLQNLFDDFCTCF-NEADVVAIADVYAAGEEPIPGASRDDL---VSGLIR-HGHRHARALLNE--EDLARLVKE 440
R.palustris -TAGKVIAVVQPHRFSRLQSLFEEFCTCF-NDADAVIVADVYPAGEAPIEGIDRDHF---VLGLRA-HGHRDVVALQDS--ASLAGVVAG 436
R.rickettsii -QNGKVIAIFQPHRYSRMQYLFDDFMLCF-ADADILYITDIYAAGENPIEGITGRSL---VDKITKRKHHDKANFLAEL--DDAVGVIID 447
R.typhi -QNGKVIAIFQPHRYSRIKYLFDDFMLCF-ADADILYITNIYAAGEKPIEGITGQSL---VDKMTQNKYHDKANFLAEL--DDVVSVIID 447
R.pomeroyi -QNGKVIAIFQPHRYSRIKYLFDDFMLCF-ADADILYITNIYAAGEKPIEGITGQSL---VDKMTQNKYHDKANFLAEL--DDVVSVIID 447
S.enterica ----NLVMLFQPHRYTRTRDLYDDFANVL-TQVDALLMLDVYPAGEAPIPGADSRSL---CRTIRNRGKI--DPILVSD-PAQVATMLAP 452
S.dysenteriae ----NLVMLFQPHRFTRTRDLYDDFANVL-TQVDTLLMLEVYPAGEAPIPGADSRSL---CRTIRGRGKI--DPILVPD-PAQVAEMLAP 452
S.meliloti -CQGRIVAVHQPHRYSRLSSLFEDFTSCF-NDADTILLAPVYAAGEEAIEGVSSEAL---VDRIKA-AGHRDARHVPGQ--EALAPVIAK 436
S.paucimobilis -AKGRVIAVVQPHRYTRLRDLMDEFQQAF-NDADIVYAAPVYPAGEQPIEGVDSAEL---VAGLKR-RGHRHAATVEGA--DDLARVIAA 440
S.aureus -----VVAVFQPHTFSRTQAFLNEFAESL-SKADRVFLCEIFGSIRE-NTGALTIQD---LIDKI-EGAS----------LINEDSINVL 404
S.pneumoniae -----IVAVFQPHTFTRTIALLDDFAHAL-NQADAVYLAQIYGSAREVDHGDVKVED---LANKINKKHQ----------VITVENVSPL 409
Synechococcus SPPQRLLAVFQPHRFSRTQEFLESFASAL-QNCDSLLLAPVYSAGEEPLKGVCSQTL---ADRIQELKPD--LEIAVADNLDHLTQLVRT 442
T.maritima ----KIVVIFQPHRYSRLEREDGNFAKAL-QLADEVVVTEVYDAFEEKKNGISGKMIWDSLKSLGKEAYFVEKLPELEKVISVSENTVFL 424
T.thermophilus --GRRVRVFFQPHRLLRTQELWEAFAQAL-KGAHEVVVLPVYTAGERGRESPEALSD---RIAKRLEDLG--RPARRMD-KEEALAYARA 419
T.denticola -----IIADFMSHTYTRTEALLEEFASCF-EDADMVILHKIFSSAREKYQGQVDAEL---LFNRTKKYHKN---VFFFNEVLDAKNFVLE 452
V.cholerae ----RLVMIFQPHRYTRTRDLYDDFANVL-EQVDVLIMLDVYAAGEKPIAGADGRSL---CRTIRSRGKI--DPIFVPD-SQTLPSVLAN 450
W.pipientis --KGKVIGIIEPLRFARIRNFFDEFIRIF-MMFDYVILTPVHPPEDKPIPGCGIDDI---QKALIS-NGFNNTKIMNDA--LLISHFISD 465
X.autotrophicus -SEGQVIAVVQPHRYSRLASLFDEFCTCF-NDADHVVVAPVYAAGETPIEGADRDHL---VQGLIA-HGHRSVTALEGP--ERLAQVVGG 436
Y.pestis ----RIVMLFQPHRYTRTRDLYDDFANVL-SQVDVLLMLDVYAAGEPPIPGADSRAL---CRTIRNRGKL--DPILVPD-SESAPEMLAQ 452

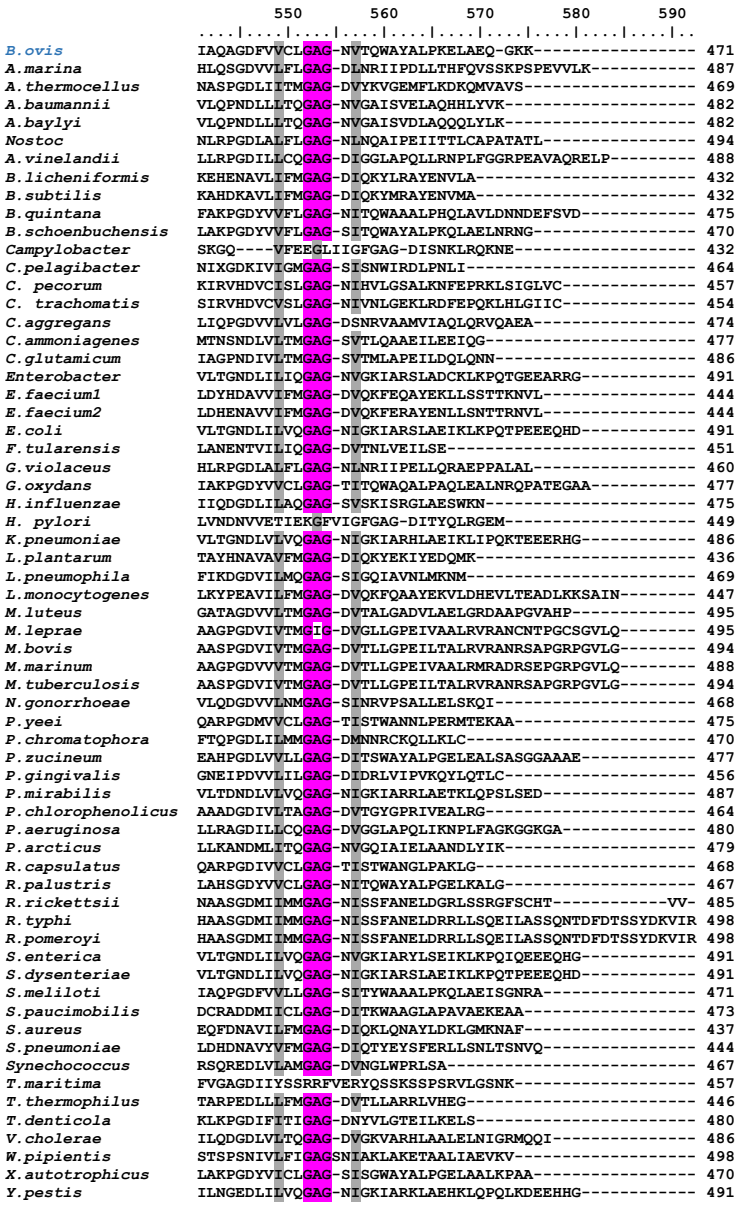

Figure 7.10. Conservation of MurC sequences within selected bacteria. MSA (n=64) of MurCs from species in Table 7.2. The alignment was constructed with Clustal Omega. Residues similar or identical in at least 90% of the sequences are highlighted in grey and purple, respectively.

The phylogenetic analysis was performed using the MSA in Figure 7.10 with a bootstrap analysis of 500 replicates and rooting of the cladogram with *B. ovis* ihfB protein as an outgroup sequence (Figure 7.11). The constructed tree reveals six distinct clades (Figure 7.11B). Clade 1 (highlighted in red) is the most divergent, contains the sequences from phylum spirochaetes and firmicutes, as well as the specific species: *T. denticola*, *L. plantarum*, *S. pneumoniae*, *E. faecium* 1 and 2, *L. monocytogenes*, *S. aureus*, *B. subtilis* and *B. licheniformis*. Clade 2 (in blue) comprises only the sequence of *A. thermocellus*, forming a separate branch from the other groups. Clade 3 (in yellow) consists of 17 sequences from various phyla, including actinobacteria, cercozoa, chlamydiae, chloroflexi, cyanobacteria

and deinococcus-thermus. Clade 4 (in green) with the sequences of *F. tularensis*, *P. gingivalis*, *T. maitima*, *H. pylory* and *Campylobacter*. Clade 5 (in cyan) is composed of 16 sequences of gammaproteobacteria and Clade 6 (in purple) contains 16 sequences of alphaproteobacteria. In this last clade, MurC of *B. ovis* was localized. Low bootstrap values among clades again agree with sequence conservation being in general at least around 50%.

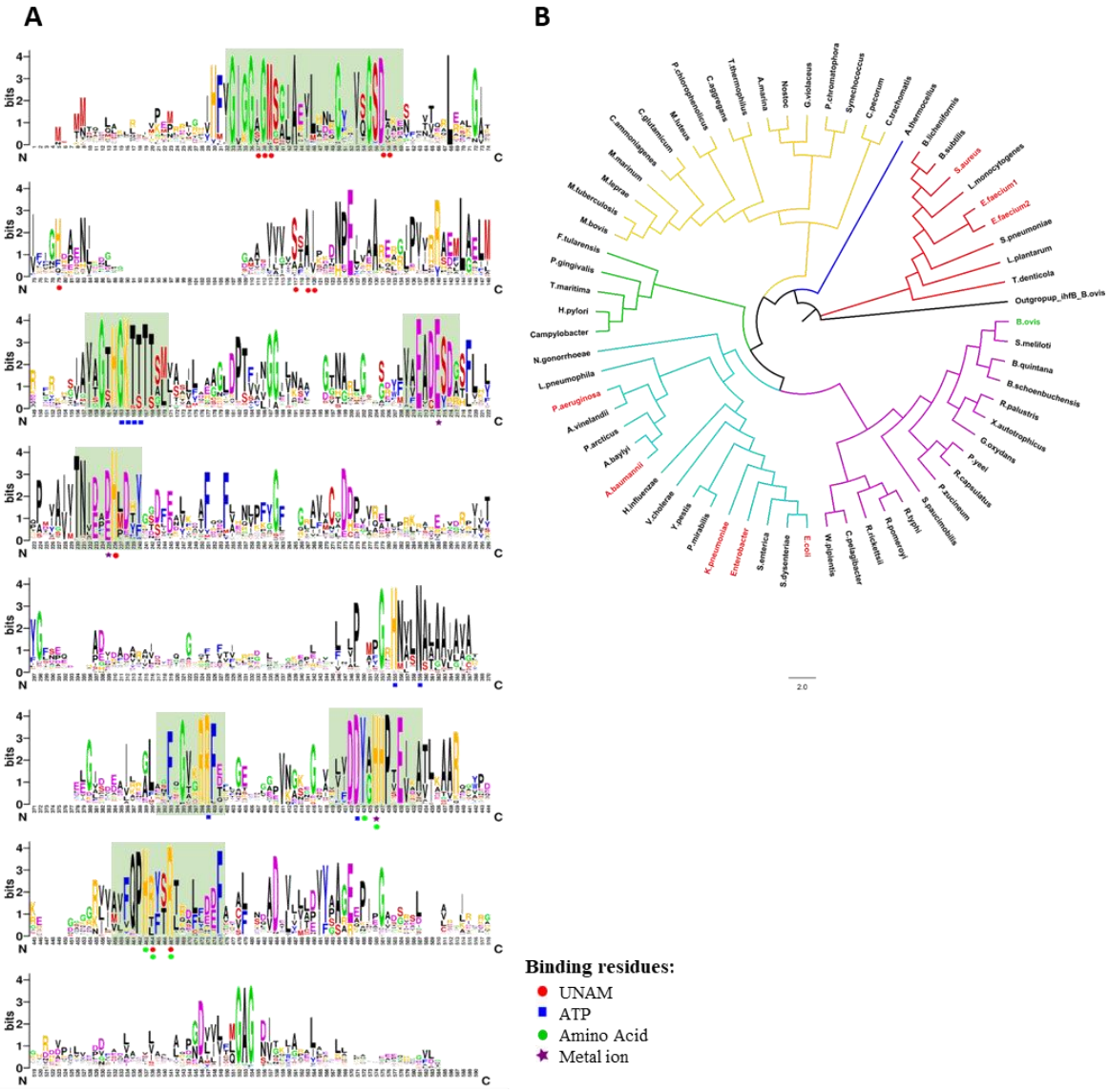

Figure 7.11. Residue conservation and phylogeny of MurC within the selected bacteria. (A) Sequence Logo representing MSA of MurC sequences from selected bacteria (n=64) from Figure 7.10. Green boxes highlight conserved motifs respectively involved in substrate binding. Other features and routine for logo generation as in Figure 7.9A. **(B)** Phylogeny of selected bacterial MurCs. The bootstrap consensus tree inferred from 500 replicates is taken to represent the evolutionary history of the taxa analyzed. The evolutionary history was inferred by using the Maximum Likelihood method and JTT matrix-based model with MEGA X. The analysis involved 64 MurC sequences (Table 7.2), and the *B. ovis* ihfB was used as outgroup to highlight the evolutionary separation between clusters. ESKAPE pathogens are highlighted in red and *B. ovis* is highlighted in green. Branch lengths are proportional to the number of substitutions per site (scale beside). There were a total of 939 positions in the final dataset. The tree groups the sequences in six main clusters: Clade 1 (bootstrap > 65) in red color, Clade 2 (bootstrap > 44) in blue, Clade 3 (bootstrap > 23) in yellow, Clade 4 (bootstrap > 9) in green, Clade 5 (bootstrap > 98) in cyan and Clade 6 (bootstrap > 58) in purple.

7.3.4 Heterologous production and hydrodynamic properties of BoHTMurC

To facilitate the purification of the BomurC, a 70 bp extension was added to the 5' end of the gene sequence, which included a 6-His tagged tail and a PreScission protease cleavage site with an NdeI restriction site (Figure 3.1C). The resulting BoHTMurC protein contains a 6-His tagged tail at the N-terminus, is composed of 497 amino acids and 7,505 atoms, and has theoretical Mw and pI of 53,533.7 Da and 6.05, respectively. The theoretical extinction coefficient at 280 nm is the same as that of the native form. In addition, the value was compared with that obtained through analysis of the ProtParam tool software, which calculated a value of 31.5 $mM^{-1}cm^{-1}$. The instability index (II) was computed as 37.61, indicating that the protein may be moderately unstable under certain conditions. The aliphatic index and GRAVY score were respectively 91.07 and -0.088, suggesting that the protein might be slightly hydrophilic. Protein expression occurred within 12 h of induction with 1 mM IPTG at 18 ºC, resulting in approximately 6 g/L *E. coli* cells. Initially, the crude extract was loaded onto an Ni affinity column. Upon elution with an imidazole gradient, the chromatogram showed a main peak followed by a broad band (Figure 7.12A). The collected fractions were subjected to analysis by 12% SDS-PAGE (Figure 7.12B), revealing a substantial amount of protein present in each well. The band spanning from the well of fraction 7 to 15 is compatible with the BoHTMurC Mw, and also showed contaminations mainly with proteins of lower Mw. These fractions were pooled, concentrated while removing imidazole, and subsequently loaded onto an SEC column (Figure 7.12).

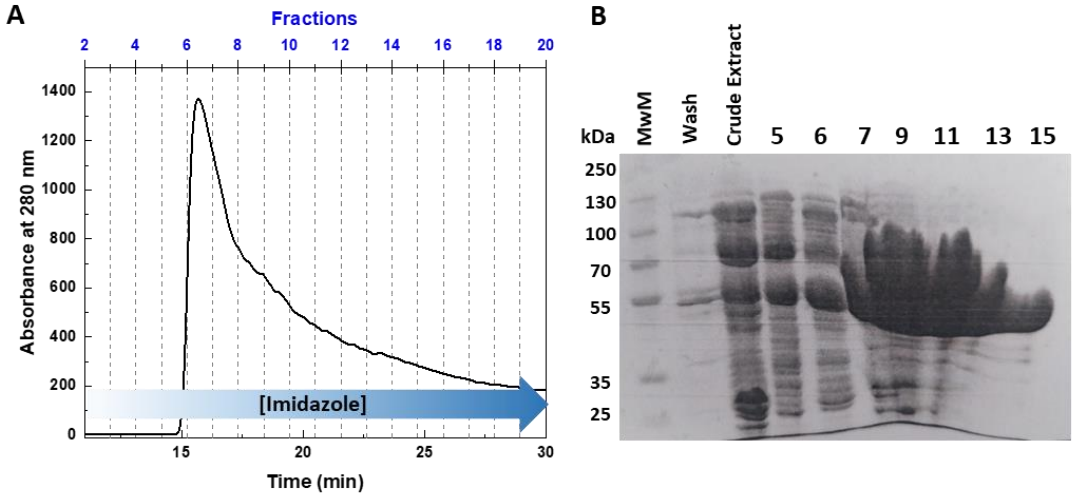

Figure 7.12. BoHTMurC purification using affinity chromatography and evaluation by SDS-PAGE. (A) Elution profile of the crude extract with the protein loaded onto a Ni affinity column and eluted with a gradient from 10 to 500 mM imidazole. **(B)** Analysis of fractions collected from the column using 12% SDS-PAGE gels. The MwM is represented in lane 1.

Purified BoHTMurC migrated with an apparent Mw of 53.5 kDa on denaturing SDS-PAGE (Figure 7.13A, left inset). Upon SEC, the protein was eluted as a single peakwith at an elution volume corresponding to a calculated Mw of 46.6 kDa (Figure 7.13). Noticeably, the peak was preceded by a broad tail. During CN-PAGE analysis, BoHTMurC exhibits migration as multiple bands (Figure 7.13A, right inset). This, together with the front tail in the SEC, suggested that the purified protein might exist as an oligomer in solution. The protein yield was high, reaching 24.25 mg per L of culture (~36 g of biomass).

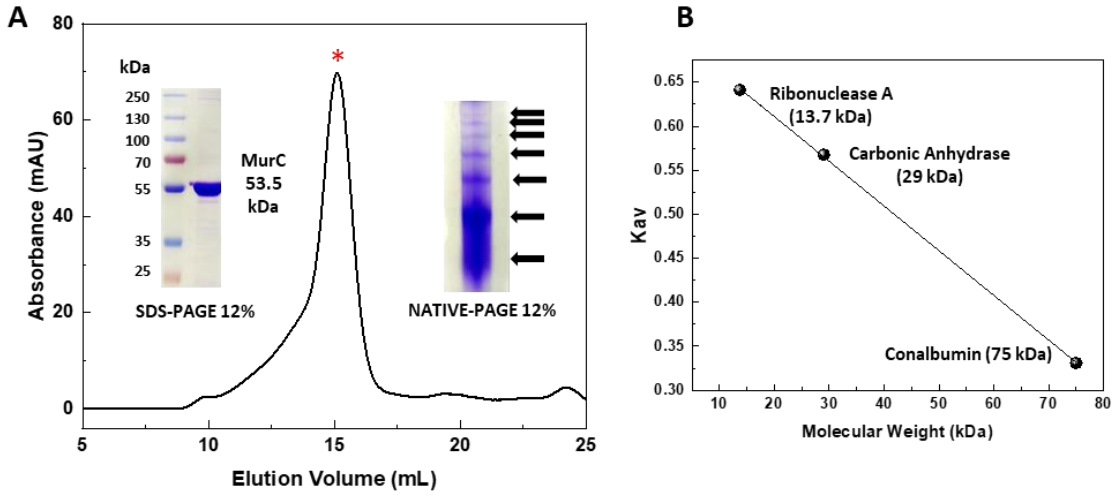

Figure 7.13. Hydrodynamic properties of BoHTMurC. (A) Elution profile of BoHTMurC on a 25 mL Superdex® 200 10/300 GL column at 4 °C. BoHTMurC (black line) elutes at 14.9 ml. The left inset shows a 15% SDS-PAGE of purified BoHTMurC: Left line, MwM PageRuler^{TM} Plus; right line, purified BoHTMurC (48.4 kDa). The right inset shows a 12% CN-PAGE of purified BoHTMurC. **(B)** Calibration Plot of the Superdex® 200 10/300 GL column with Ribonuclease A (13.7 kDa), Carbonic Anhydrase (29 kDa) and Conalbumin (75 kDa).

7.3.5 Spectroscopic properties of BoHTMurC

The absorption spectrum of BoHTMurC purified to homogeneity was characterized by a maximum at 280 nm (Figure 7.14A). Following the 3.4.1.1.1, protocol an experimental value of ε_{280}=31.8±0.6 mM^{-1} cm^{-1} was determined in 50 mM Tris-HCl, 100 mM KCl, pH 8.0. The BoHTMurC fluorescence spectrum exhibited an emission maximum at 329 nm upon excitation at 280 nm (Figure 7.14B), whereas the corresponding excitation spectrum showed two maxima at 229 and 280 nm. The far-UV CD spectrum of BoHTMurC showed two minima at 209 nm and 222 nm (Figure 7.14C), indicative of α-helix folding. The near-UV CD spectrum hardly showed features, only a small broad band in the 280-305 nm range (centered around at 293 nm). Altogether these data indicate that the purified BoHTMurC protein is in its folded state.

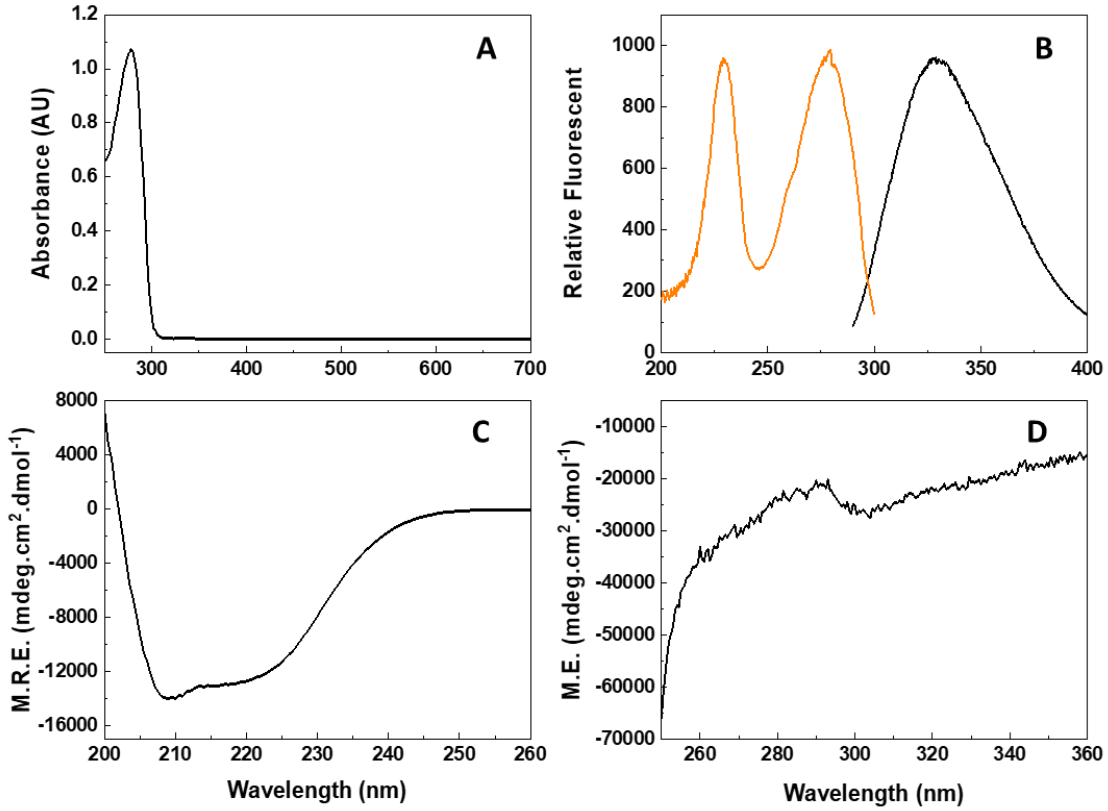

Figure 7.14. Spectroscopic properties of BoHTMurC. (A) UV-Visible absorption spectrum of BoHTMurC (33.7 µM) in 50 mM Tris-HCl, 100 mM KCl, 1 mM DTT, pH 8.0, at 25 °C for a folded sample. **(B)** Emission (black line) and excitation (orange line) fluorescence spectra of BoHTMurC for aromatic region, λ_{ex} = 280 nm, λ_{em} = 330 nm (10 µM) in 10 mM potassium phosphate, pH 8.0. BoHTMurC CD spectra for the **(C)** far-UV (5 µM), and **(D)** near-UV/Vis (10 µM) regions in 10 mM potassium phosphate, pH 8.0.

7.3.6 Thermal stability of BoHTMurC

To assess the stability of BoHTMurC, thermal denaturation was followed by using two techniques: far-UV CD and DSC. The CD denaturation curves at 208 nm indicated the presence of three unfolding states (N→I→U). The first transition, T_{m1} was measured at 312 K, while the second transition, T_{m2} occurred at 324 K. This suggest a multi-step process during thermal denaturation. This distinct T_m values reflect different energy requirements for the unfolding of various structural elements within the protein. This may indicate the presence of intermediate states or specific structural domains with varying stability. In contrast, the 222 nm denaturation curve showed a direct shift from the native state to the unfolded state (N→U) with a T_m of 321 K. This suggests that certain secondary structure elements within BoHTMurC might unravel cooperatively during this thermal denaturation process.

The DSC analysis yielded a single T_m value of 327 K, slightly higher than the T_{m2} observed in the CD analysis. DSC measures the heat capacity change associated with thermal unfolding, and the higher T_m might be indicative of a major cooperative unfolding event in

BoHTMurC. Nevertheless, it is essential to consider that the discrepancies in T_m values between CD and DSC analyses could arise from variances in the methodologies and the particular structural components examined by each method.

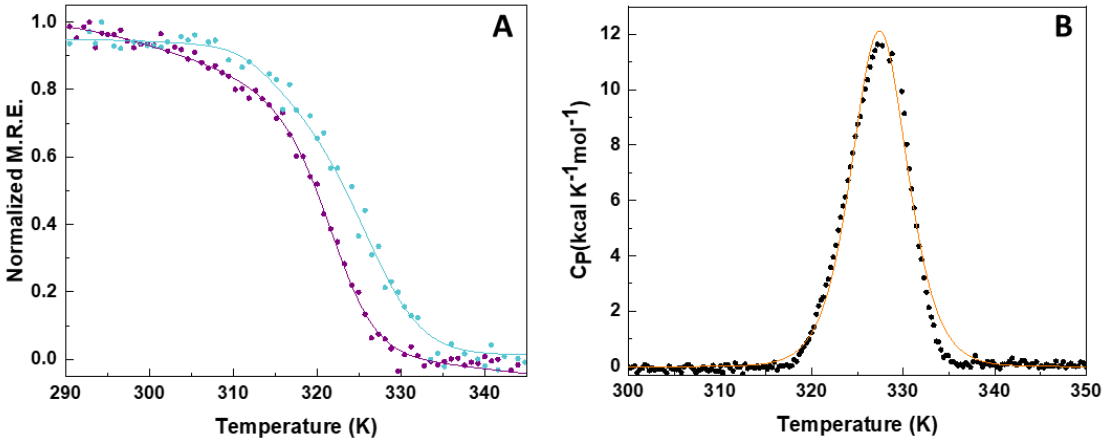

CD			DSC
T_{m1}^{208nm} (K)	T_{m2}^{208nm} (K)	T_m^{222nm} (K)	T_m (K)
312 ± 1	324 ± 1	321 ± 1	327 ± 1
$\Delta H1^{208nm}$ (kcal/mol)	$\Delta H2^{208nm}$ (kcal/mol)	ΔH^{222nm} (kcal/mol)	ΔH (kcal/mol)
87 ± 4	46 ± 2	68 ± 1	95 ± 1

Figure 7.15. Thermal stability of BoHTMurC. (A) Thermal denaturation profiles of BoHTMurC monitored using far-CD (5 µM) at 208 nm (cyan circles) and at 222 nm (purple circles). **(B)** DSC denaturation profile of BoHTMurC (20 µM). The table presents the resulting T_{ms} and ΔH values for each experiment. Curves are shown roughly normalized from 0 to 1, and their individual fits are represented by the continuous lines. CD curves recorded in 10 mM potassium phosphate, pH 8.0 and DSC in 50 mM BIS-Tris Propane buffer, pH 8.0, from 283.15 to 350.15 K.

7.3.7 Crystallization of BoMurC

More than 700 different crystallization conditions were tested using commercial kits in an attempt to solve the BoMurC structure by X ray diffraction (section 3.9.2). An initial protein concentration of 10 mg/ml was employed for the crystallization trials. Crystals were successfully obtained in the Proplex G7 condition (3M sodium formate, 100 mM Tris pH 7.5). Subsequently, these crystals, after freezing in cryo solutions containing 20% glycerol, were sent to the ALBA synchrotron for data collection in the XALOC-MX13 beamline. Unfortunately, the resulting x ray diffraction patterns were of poor quality, showing weak signals with resolutions between 6-8 Å.

Based on these results, the following strategies were applied to optimize the quality of the crystals:

1. The 6-His tail of BoHTMurC was removed using the protocol described in section 3.9.1, and the resulting protein was used to generate new crystals.

2. Different additives from a commercial kit by Hampton Research were added to the Proplex G7 condition.
3. Alternatively, crystals were subjected to dehydration using glycerol, ethanol, methanol, and propanol (the range starts at 5% and increases in increments of 5, up to 30%).
4. ATP, $MgCl_2$ or L-Alanine were added to the condition at the final concentration of 1 mM.

Despite implementing all these strategies, both individually and in combination, BoHTMurC and BoMurC crystals displayed low resolution diffraction signals. The best data were collected at a resolution of 3.2 Å for a total of 1000 images. The phase problem was solved by the molecular replacement approach, taking as a model the predicted structure for BoMurC in the Alphafold Protein Structure Database (code A5VRH6). The data collection and refinement statistics are summarized in Table 7.3.

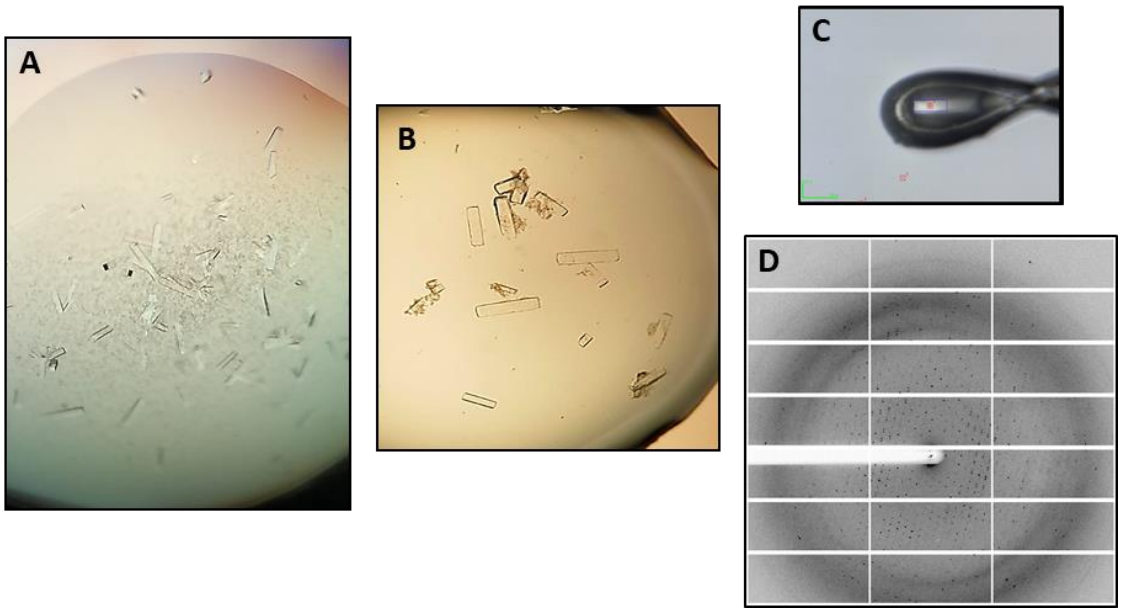

Figure 7.16. BoMurC crystals and diffraction pattern. (A) Crystals of protein formed by the vapor diffusion method in hanging drops set in 24 well plates. 500 µL of mother liquor (3M sodium formate, 100 mM Tris/HCl pH 7.5) were placed in equilibrium against drops containing 2 µL of BoMurC (15 mg/mL) and 2 µL of mother liquor. **(B)** Crystals during dehydration with 20% glycerol. **(C)** Loop containing one protein crystal and **(D)** diffraction pattern obtained from a crystal during the X-ray experiment.

Table 7.3. Data collection and refinement statistics for BoMurC.

Data collection statistics	
Space group	P 43 21 2
Unit cell parameters	
a, Å	192.51
b, Å	192.51
c, Å	76.36
Wavelength, Å	0.979261
Resolution, Å	192051-3.3
	(3.48-3.3)
No. of unique reflections	22228
Redundancy	11 (11.4)
Completeness, %	100 (100)
Mn(l)/sd	11 (1)
R_{merge} [a]	0.123 (2.345)
Refinement Statistics	
Resolution range, Å	136.12-3.3
Protein non-hydrogen atoms	7155
Ligand non-hydrogen atoms	-
Solvent non-hydrogen atoms	-
R_{work} (%)	20.5
R_{free} [b] (%)	30.0
rmsd bond lenght, Å	0.006
rmsd bond angels, °	1.34
Average B-factor, Å^2	153.9

Values in parentheses correspond to the highest resolution shell.
[a] Rsym = Σ| I - Iav |/ Σ I, where the summation is over symmetry equivalent reflections.
[b] R calculated for 5% of data excluded from the refinement

Similar to other resolved MurC structures, and despite the low resolution achieved, it can be concluded that the BoMurC crystallographic model is composed of 471 amino acids that fold in the expected three contiguous domains (Figure 7.17A). The first domain (residues 1-106 at the N-terminus), exhibits a Rossmann-type structure, characterized by five-stranded parallel β-sheet flanked by five α-helices and serves as the UNAGEP-binding region. The second domain (residues 107-318) is comprised by six-stranded parallel β-sheet plus a separate three-stranded antiparallel β-sheet, surrounded by seven α-helices. The core of the domain is typical of the mononucleotide-binding domains in a number of ATP- and GTP-dependent enzymes, so acts as the ATP-binding region. The third domain (residues 319-471 at the C-terminus), also has a Rossmann-type fold, includes a six-stranded β-sheet flanked by six α-helices and serves as the L-Alanine binding domain (Figure 7.17B).

The crystalline asymmetric unit (a.u.) of BoMurC shows two molecules (Figure 7.17C) and the crystal packing analysis using PISA (Krissinel & Henrick, 2005) did not identify any potential higher order oligomers in the crystal lattice. However, the protein appears to form higher organizations than the monomer in solution as observed by CN-PAGE and SEC (Figure 7.13A, right inset). The interface between the two molecules of a.u.

in BoMurC crystals is formed by interleaving of loops from outer region of domain II of one molecule with loops from domain III of the second molecule. The most relevant interactions involve Asn241, Gln243, Ala244 and Arg265 from the loop between strand β11, β12 and β13 from domain II, that interacts with Asn385', Ala387', His420' and Arg421' from the loops between α15-β18 and α16-β19 from domain III in the second BoMurC molecule.

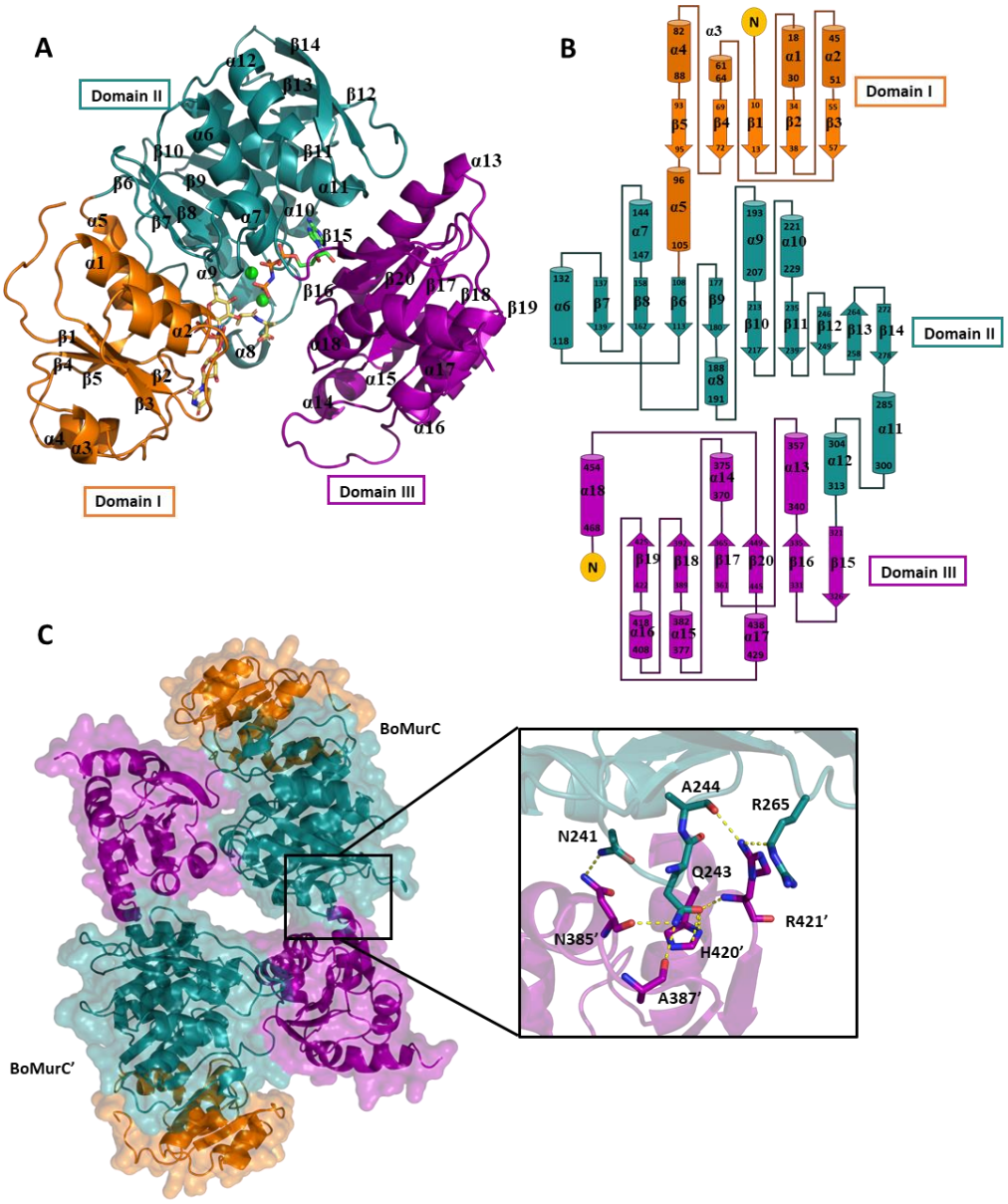

Figure 7.17. BoMurC structural features. (A) Crystal structure and **(B)** topology diagram of each BoMurC domain. Domains I, II and III are colored in orange, blue and purple, respectively. **(C)** Surface representation of the crystallographic BoMurC dimeric organization, showing the two molecules as BoMurC and BoMurC'. The part of the dimer interface, where loops from domain II (blue) of BoMurC interlock with loops from domain III (purple) of BoMurC' is highlighted. The positions of the substrates are taken from an overlap with the HiMurC (1P3D). UNAM (CPK in yellow sticks), ANP-PNP (CPK in green sticks) and Mn^{2+} in green spheres.

Multiple structures of various organisms have been resolved (Table 7.3), with many of them involving some ligands (Table 7.4). When comparing a BoMurC monomer with these structures, we observe a wide range of RMSD values, but it is essential to consider that the BoMurC structure was not resolved at high resolution. Additionally, it is worth noting that the structures obtained for *P. aeruginosa* (PaMurC: 5VVW, 6X9N, and 6X9F) and *A. baumannii* (AbMurC: 6CAU), despite having high sequence identity, only domains I and II were crystallized and solved.

The structural comparison with the structure of *Y. pestis* (YpMurC, 4HV4), yielded a RMSD value of 1.12 Å for 366 aligned Cα-atoms and 44% sequence identity, with *E. coli* (EcMurC, 2F00), a value of 1.16 Å for 369 aligned Cα-atoms and 43% sequence identity, and finally, with *M. tuberculosis* (MtMurC, 7BVA), a value of 1.92 Å for 406 Cα-atoms and 40% sequence identity (Figure 7.18A). The alignment with the structures of PaMurC (5VVW), with identity of 50% and AbMurC with 46%, reveal RMSD values of 2.51 Å for 264 aligned Cα-atoms and 1.02 Å for 269 aligned Cα-atoms, respectively, since only domains I and II of these proteins are solved (Figure 7.18B).

For the sequences of *H. influenzae* there are two types of crystal forms. The apo-HiMurC structure (1GQQ), which has an "open" conformation where the AA-binding domain does not interact with either the UDP-binding or the ATP-binding domain, resulting in a large empty cavity in the inter-domain space. The other form is the ligand-bound HiMurC (1GQY), where HiMurC is in complex with phosphomethylphosphonic acid adenylate ester. The UNAM and AA-binding domains have rearranged to interact tightly with the ATP-binding domain. This decreases the enclosed inner space by the three domains substantially, showing a "closed" conformation (Seo et al., 2021a). The RMSD values were 6.42 Å for 414 aligned Cα-atoms for the open conformation (1GQQ) and 1.24 Å for 390 aligned Cα-atoms for the closed conformation (1GQY), both with 43% sequence identity (Figure 7.18C).

Finally, structures with the lowest identity percentage are *T. maritima* (TcMurC, 1J6U) and *P. arcticus* (ParMurC, 3HN7) with values of 32 and 28%, respectively. The RMSD values were remarkably high, 2.06 Å for 333 aligned Cα-atoms and 3.66 Å for 289 aligned Cα-atoms, respectively (Figure 7.18D).

Table 7.3. Summary of structural data for MurC proteins from different species in the PDB.

Organism	% Identity to BoMurC	PDB Code	Ligand	Sequence Length	Reference
Haemophilus influenzae	43%	1GQY	ACP, Mg^{+2}	475	(Skarzynski et al. *To be published*)
		1GQQ			
Haemophilus influenzae	42%	1P31	EPU, Mg^{+2}		(Mol et al., 2003)
		1P3D	ANP, MN, UMA		
Thermotoga maritima	32%	1J6U	MSE	469	(Spraggon et al., 2004)
Escherichia coli	43%	2F00	Mg^{+2}	491	(Deva et al., 2006)
Yersinia pestis CO92	44%	4HV4	AMP, BME	494	(Halavaty et al. *To be published*)
Pseudomonas aeruginosa PAO1	50%	5VVW	EDO	315	(Horanyi et al. *To be published*)
	47%	6X9N	Cl^-, DMS, EDO, UYD, VAL	318	
		6X9F	Cl^-, DMS, EDO, UXP	311	
		8DOF	T4L, EDO, SO_4	318	
	51%	8EGM	WIU, $SO_4^=$	316	(Abendroth et al. *To be published*)
		8EGN	WIR, $SO_4^=$		
		8EWA	WIY, $SO_4^=$, Cl^-		
Acinetobacter baumannii	46%	6CAU	ANP, Mg^{+2}	328	(Horanyi et al. *To be published*)
Mycobacterium tuberculosis variant bovis AF2122/97	40%	7BVA	Zn^{+2}	519	(Seo et al., 2021)
		7BVB	UD1, Zn^{+2}		
Psychrobacter arcticus 273-4	28%	3HN7	MSE	524	(Das et al., 2011)

Table 7.4 Summary of ligands found in the MurC structures in the PDB.

Code names for PDB ligands		
Code	**Name**	**Formula**
ACP	Phospho Methil Phosphonic Acid Adenylate Ester	$C_{11}\ H_{18}\ N_5\ O_{12}\ P_3$
ANP	Phospho Minol Phosphonic Acid Adenylate Ester	$C_{10}\ H_{17}\ N_6\ O_{12}\ P_3$
UMA	Uridine-5'-Diphosphate-N-Acetylmuramoyl-L-Alanine	$C_{23}\ H_{36}\ N_4\ O_{20}\ P_2$
AMP	Adenosine Mono Phosphate	$C_{10}\ H_{14}\ N_5\ O_7\ P$
BME	Beta-Mercaptoethanol	$C_2\ H_6\ O\ S$
EDO	1,2-Ethanediol	$C_2\ H_6\ O$
EPU	Uridine-Diphosphate-2(N-AcetylGlucosaminyl) Butiric Acid	$C_{20}\ H_{29}\ N_3\ O_{19}\ P_2$
UYD	(2R)-2-({4-[(5-tert-butyl-1-methyl-1H-pyrazol-3-yl)amino]-1H-pyrazolo[3,4-d]pyrimidin-6-yl}amino)-2-phenylethan-1-ol	$C_{21}\ H_{26}\ N_8\ O$
UXP	[(2R)-1-{4-[(5-cyclopropyl-1H-pyrazol-3-yl)amino]-2H-pyrazolo[3,4-d]pyrimidin-6-yl}piperidin-2-yl]methanol	$C_{17}\ H_{22}\ N_{38}\ O$
MSE	L-Peptide Linking	$C_5\ H_{11}\ N\ O_2\ Se$
DMS	Dimethyl Sulfoxide	$C_2\ H_6\ O\ S$
UD1	Uridine-Diphosphate-N-Acetylglucosamine	$C_{17}\ H_{27}\ N_3\ O_{17}\ P_2$
VAL	Valine	$C_5\ H_{11}\ N\ O_2$
T4L	(2R)-2-cyclohexyl-2-[(4-{[5-(propan-2-yl)-1H-pyrazol-3-yl]amino}-1H-pyrazolo[3,4-d]pyrimidin-6-yl)amino]ethan-1-ol	$C_{19}\ H_{28}\ N_8\ O$
WIU	(2R)-2-({4-[(5-tert-butyl-1-methyl-1H-pyrazol-3-yl)amino]-1H-pyrazolo[3,4-d]pyrimidin-6-yl}amino)-2-phenylethyl (2-aminoethyl)carbamate	$C_{24}\ H_{32}\ N_{10}\ O_2$
WIR	(1R,2S)-1-({4-[(5-tert-butyl-1-methyl-1H-pyrazol-3-yl)amino]-1H-pyrazolo[3,4-d]pyrimidin-6-yl}amino)-2,3-dihydro-1H-inden-2-ol	$C_{22}\ H_{26}\ N_8\ O$
WYI	(2R)-2-({4-[(5-tert-butyl-1-methyl-1H-pyrazol-3-yl)amino]-1H-pyrazolo[3,4-d]pyrimidin-6-yl}amino)-2-phenylethyl (2R)-2-(aminomethyl)morpholine-4-carboxylate	$C_{27}\ H_{36}\ N_{10}\ O_3$
$SO_4^=$	Sulphate Ion	$O_4\ S^{-2}$

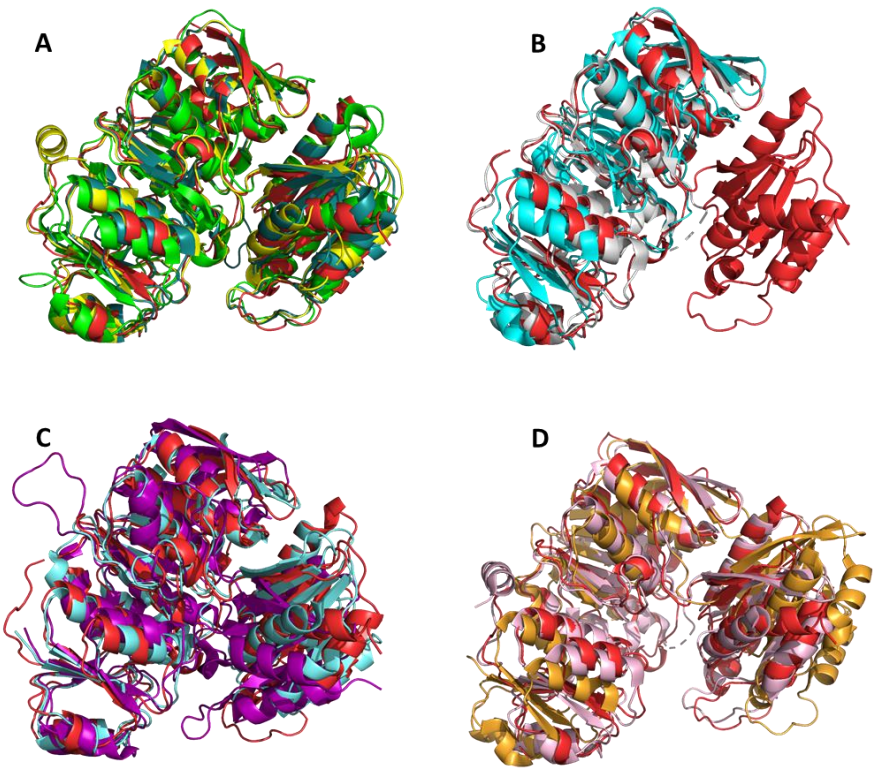

Figure 7.18. Structural comparison of several MurCs with BoMurC. (A) Ribbon representation of the superposition of BoMurC (in red color) with YpMurC (4HV4, in deep teal blue color), EcMurC (2F00, in yellow color) and MtMurB (7BVA, in green color); **(B)** PaMurC (5VVW, in cyan color), AbMurC (6CAU, in grey color); **(C)** TcMurC (1J6U, in light blue color) and ParMurC (3HN7, in purple color); **(D)** HiMurC in "closed" conformation (1GQY, in pink color) and "open" conformation (1GQQ, in yellow color).

7.3.8 BoMurB:MurC complex and molecular docking

Using the Google DeepMind software AlphaFold2.ipynb (Jumper et al., 2021), which incorporates AlphaFold-Multimer (Evans et al., 2021), we conducted the modeling of a complex between BoMurB and BoMurC. The program generated a total of 5 potential structures, with the highest-ranking model shown in the Figure 7.19A. In this model, the active site of BoMurC opens to accommodate a BoMurB monomer. Specifically, BoMurB's Domain III is located within the cavity between the BoMurC domains. However, for a UNAM transfer competent interaction to occur, BoMurB would be expected to rotate and adjust in such a way that BoMurB's Domain II migrates towards BoMurC's Domain I (Figure 7.19B), positioning their product and substrate binding sites in a conformation competent for their transfer. Additionally, regions in both proteins have been identified that exhibit lower confidence in predictions. This decrease in confidence suggests that these segments might be more flexible or possibly interacting with other molecules.

To grasp an idea of the conformational changes in the "hypothetical complex," the model was compared with some MurB-MurC fused protein structures from other bacterial models found in the AlphaFold database. Most of these hybrid proteins exhibit an "open"

conformation, as depicted in Figure 7.19C, such as the protein OLB01401.1, from *V. bacterium* (A0A1Q6VKM2), where the positions of the two monomers are contiguous. It is suggested that during the UNAM transfer reaction the MurB monomer may need to rotate 90º around the vertical axis, as indicated by an arrow.

A more thorough search of these hybrid proteins in the AlphaFold database was conducted, identifying a few models whose conformational arrangement is akin to the one we propose BoMurB:BoMurC should adopt. The model of the fused protein OYW27287.1 from *Caulobacter sp.* (A0A257X1B9) was found to adopt a conformation in line with our objectives, in which the protein segment corresponding to MurB is oriented toward the catalytic center of MurC (Figure 7.19D). However, in this model, it is observed that the active site of MurB is exposed to the solvent, so we assume that the MurB monomer would have to undergo a 180º rotation to facilitate substrate conversion and allow UNAM to be transferred to MurC's Domain I.

The study of the potential interaction between BoMurB and BoMurC, was also carried out based on docking approach using PyDockWeb software (Jiménez-García et al., 2013). Initially, we performed the analysis based on potential interacting residues between the two monomers in the model generated by AlphaFold. The results revealed very high interaction energies, as shown in Figure 7.20A and Table 7.5. Consequently, we implemented multiple amino acid restraints to guide the rigid-body docking process. These restraints focused on surface residues from domains II and III of BoMurB, aligning them with domain I of BoMurC, to facilitate product-substrate transfer.

As a result of these adjustments, the obtained values reflected more negative binding energies, indicating a favorable interaction between the molecules. This suggests that the molecules may have a tendency to come together and form a stable complex. The more negative the binding energy, the stronger the interaction, with highly negative values indicating an exceptionally strong binding. Furthermore, we assessed various positional arrangements for the complex, ensuring the selection of configurations consistent with biologically plausible scenarios (Figure 7.20B-F). With the exception of the first conformation (Fig.7.20A), the active sites of BoMurB and BoMurC were found to be within a distance of less than 15 Å apart.

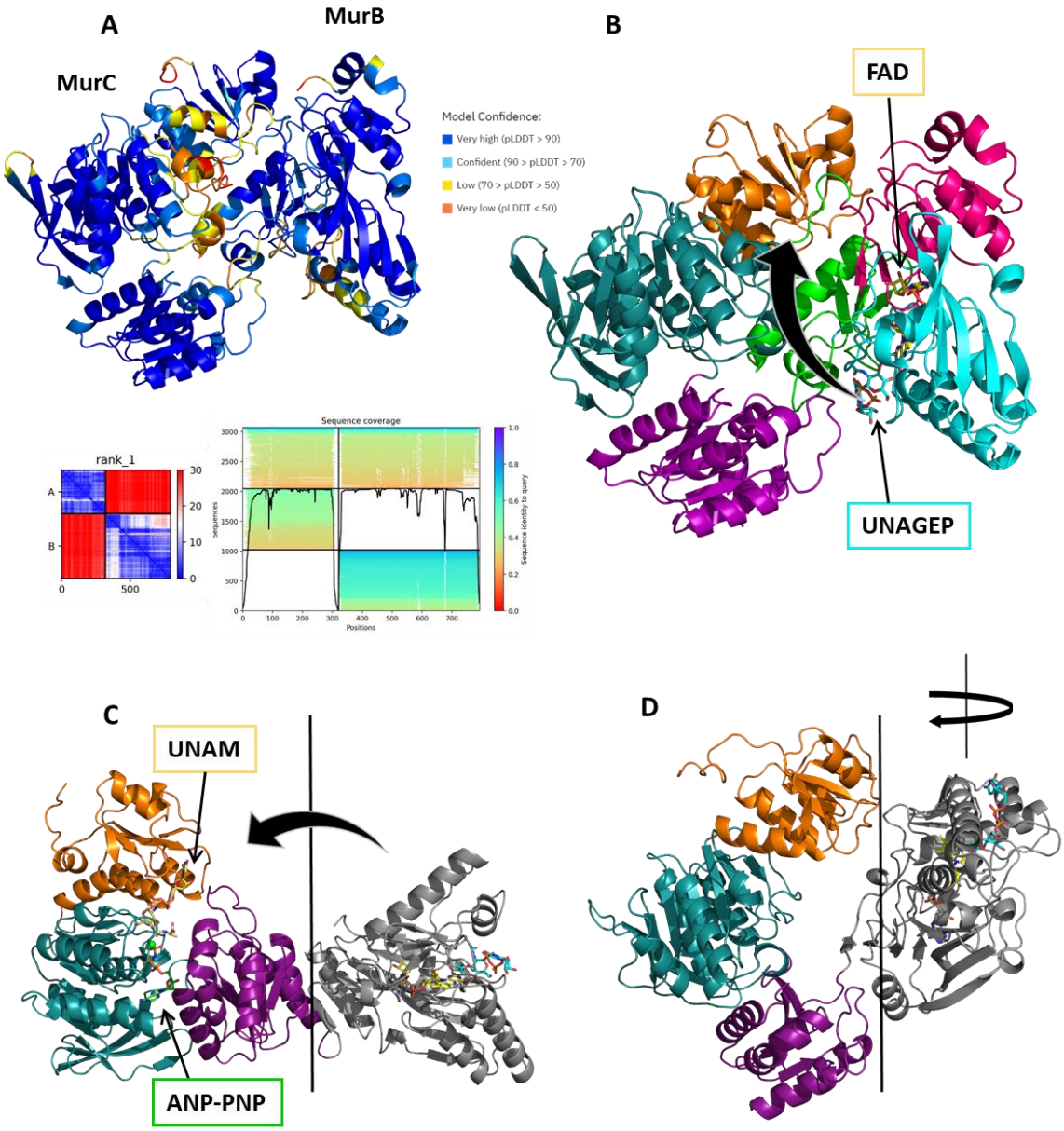

Figure 7.19. Exploring structural features of the potential MurB:MurCinteraction. (A) AlphaFold model of BoMurB:BoMurC complex. The color of the structure is given in 4 colors that indicate the simulation confidence level: intense blue and light blue regions (pLDDT > 70) indicate high and reliable confidence levels. The yellow regions (70 > pLDDT > 50) indicate a lower confidence level, and the orange regions (pLDDT < 50) indicate structures that are not considered trustworthy. The blue/red square represents the prediction aligned error (PAE) score for the model. This score displays the calculated error of the predicted distance for each pair of residues. Both axes indicate the position of the individual amino acids. The uncertainty in the predicted distance of two amino acids is color coded from blue (0 Å) to red (30 Å), as shown in the right bar. The color of the intersection of a horizontal line drawn from the position of an amino acid on the y-axis and a vertical line from the position of another amino acid on the x-axis indicates the error in the predicted distance between these two residues. The panel of sequence coverage used a MSA as input for the network and shows adequate coverage of both sequences. **(B)** Model colored by domains. Domains I, II and III of BoMurC are colored in orange, blue and purple, respectively. BoMurB domains I, II and III are colored in pink, cyan and green. **(C)** AlphaFold model of *V. bacterium* fussed MurBC (A0A1Q6VKM2), and **(D)** AlphaFold model of *Caulobacter* sp. fussed MurBC (A0A257X1B9). The positions of the MurC substrates are taken from an overlap with the structure of HiMurC (1P3D). UNAM (CPK colored yellow sticks), ANP-PNP (CPK colored green sticks) and Mn^{2+} in green spheres. The monomer corresponding to MurB is shown in grey. UNAGEP (CPK in cyan sticks) and FAD (CPK in yellow sticks) were taken from BoMurB crystal structure.

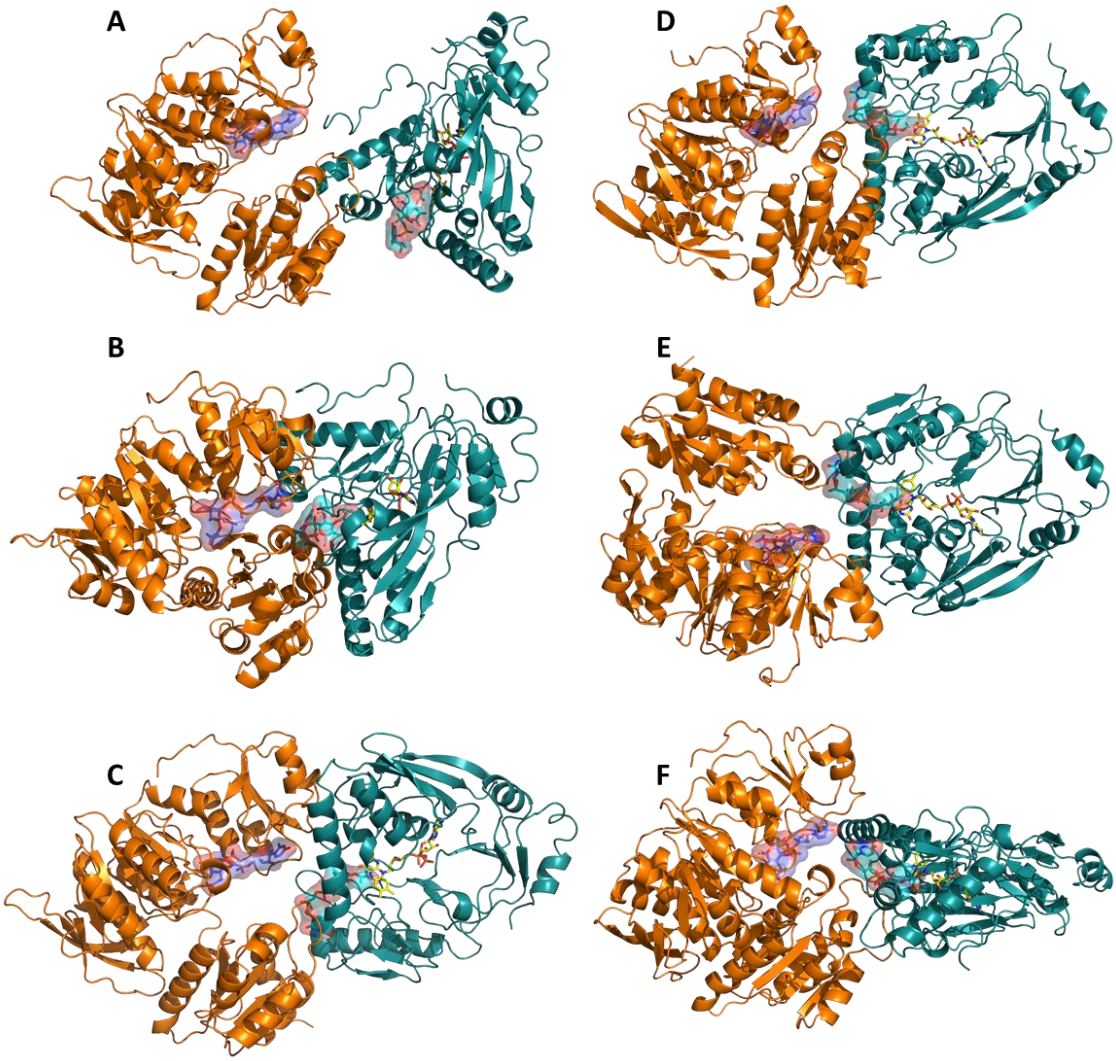

Figure 7.20. Models of BoMurB:BoMurC docking complex obtained using PyDock. BoMurB in orange and BoMurC in deepteal. UNAGEP molecules on both enzymes are depicted inside surfaces. UNAGEP (CPK in cyan sticks) and FAD (CPK in yellow sticks) in BoMurB were taken from its crystal structure and, UNAGEP (CPK in blue sticks) in BoMurC from HiMurC (1P31).

Table 7.5 Energy values of selected poses obtained in the BoMurB:BoMurC molecular docking.

Conformation	Electrostatic energy	Desolvation energy	Van der Waals energy	relRST	Total	Residue Restraints	
						Receptor BoMurC	Ligand BoMurB
A	-17.869	13.501	6.21	33.333	-37.08	Q39, S40, A398, G399,E400, E401, P402, E409, G428,N453, Q456	E237, G238, T239, N293, S294, G295,I295, R297, K320, I321, V322
B	-29.068	17.604	47.517	73.684	-80.396	S40, A43, Q46, E50, G58, H59, K60, A61, K318, R319, P429, E430	N149, G150, V151, E152, A180,H216, H217, R218, E219, T220, E237, I296, L298, H299
C	-13.309	15.743	9.095	52.632	-49.288		
D	-32.039	16.02	-16.743	75	-92.693	P394, P402, E404, G405, E409, T427, A431, L461, E464, E467, Q468	L125, A126,G127, N149,V151, E155, R156, P201, E203, I207, A210, E213
E	-10.67	7.622	16.792	75	-76.369		
F	-20.91	17.379	52.488	68.571	-66.853	D38, Q39, S40, D41, V57, G58, H59, K60, I76, K77, K78, N79, N80, P81	D205, D206, R209, D212, E213, H216, E219, T220

7.3.9 Structural Residue Conservation Analysis

The ConSurf server was used as a tool to plot the evolutionary conservation of every amino acid residue in the structure of BoMurC. Using the MSA including only *Brucella* species, the highest conservation scores were observed in approximately 76.8% of the amino acids. They were mainly located within the active site cavity or facing the interior of the protein. In contrast, residues with the most variable scores make up only 5.3% of the entire protein structure and are generally located towards the surface of the protein. On the other hand, residues with an average conservation score constitute 16.8% of the structure, totaling 85 amino acids, and are generally found in the more external structural parts of the protein (Figure 7.21A and B). The analysis of the bacterial sequences also reveals a considerable degree of conservation. Specifically, 42.5% (200 amino acids) of the residues display the highest level of conservation, 56.7% (267 amino acids) exhibit an average conservation score, and only 0.8% (4 amino acids) are characterized by the most variable conservation scores (Figure 7.22A and B). The protein residues previously identified in other species as essential for both structure and function remain conserved across the evaluated bacterial species.

To investigate the potential interactions of UNAM and ATP substrates with BoMurC, the crystallographic BoMurC structure was overlapped with that of HiMurC (1P3D) to position these substrates in the active site. Significantly, in the vicinity of the UDP portion, the amino acid residues Asp38, Gln39, His59, Arg96, and the Gly-rich loop ^{14}GIGGIG^{19} (situated between β1 and α1) were identified as crucial for binding. On the other hand, Glu162, Asp164, Tyr336, Arg372, and His338 were found to be in close proximity to the N-acetylmuramic acid portion. These observations suggest that these amino acid residues will play a vital role in substrate binding and, consequently, in the function of BoMurC. For a more detailed visualization of these interactions, see Figure 7.21 and 7.22, which represent the key residues predicted at the UNAM and ATP substrates binding sites in panels C and D. As can be observed in both the analyses conducted on *Brucellas* and bacteria, the active site of BoMurC is remarkably conserved, and the residues potentially involved in substrate binding and catalysis exhibit a high degree of convergence in their score values.

Additionally, considering the models generated by PyDock for potential interactions between BoMurB and BoMurC, we highlight the conservation of surface residues of bacterial sequences, in domains I and III of BoMurC, that are putatively involved in complex formation. These residues are indicated in the structure with arrows and outlined in the alignment, colored orange and purple, respectively (Figure 7.22A and B).

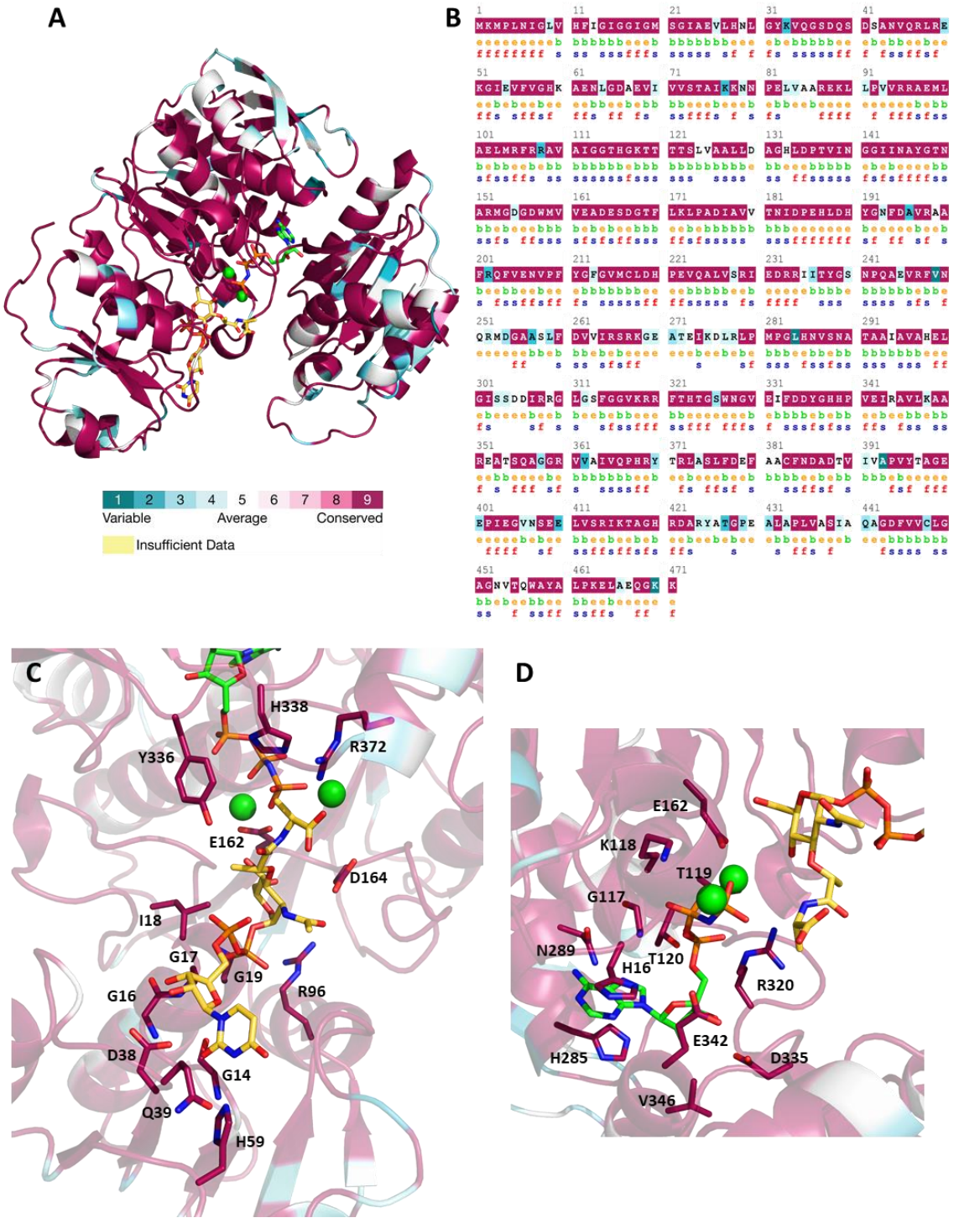

Figure 7.21. Evolutionary structural conservation analysis of BoMurC and *Brucella* sequences. (A) Residue conservation score as calculated by the ConSurf server and plotted on the structural model of BoMurC. Structure shown as cartoon colored according to conservation score (from deep teal as less conserved, to deep magenta as most conserved). **(B)** Plot of conservation scores on BoMurC sequence. Residues are also labelled regarding location ("b", buried; or "e", exposed) and predicted relevance as key structural (s) or functional (f) residues. **(C)** Detail of key residues implicated in the interaction with UNAM (CPK colored yellow sticks) and **(D)** ANP-PNP (CPK colored green sticks) and Mn^{2+} in green spheres. The positions of the substrates are taken from an overlap with the structure of HiMurC (1P3D).

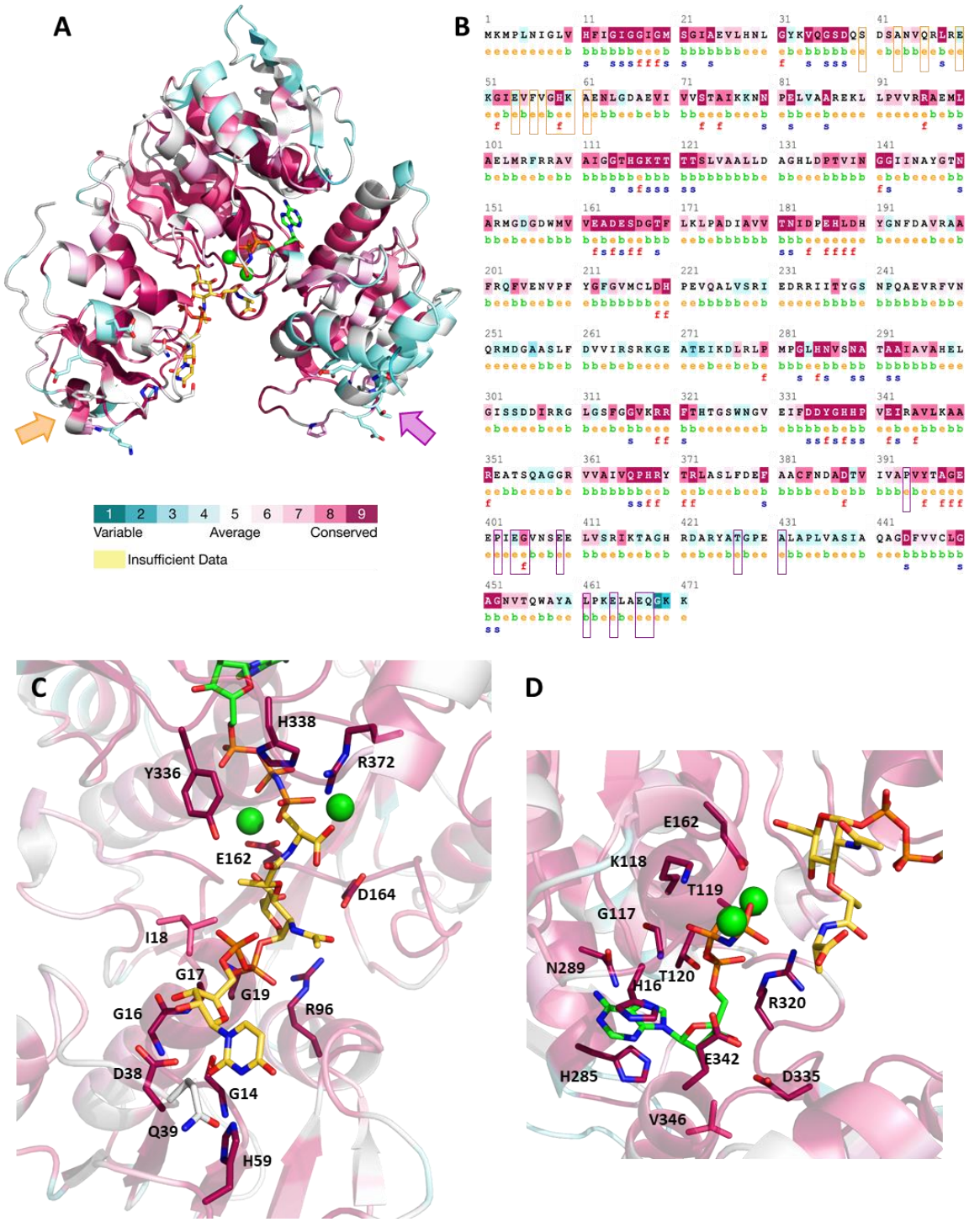

Figure 7.22. Evolutionary Structural conservation analysis of BoMurC and different bacterial sequences. (A) Residue conservation score as calculated by the ConSurf server and plotted on the structural model of BoMurC. Structure shown as cartoon colored according to conservation score (from deep teal as less conserved, to deep magenta as most conserved). **(B)** Plot of conservation scores on BoMurC sequence. Residues are also labelled regarding location ("b", buried; or "e", exposed) and predicted relevance as key structural (s) or functional (f) residues. The residues presumed to be involved in the formation of the BoMurB:BoMurC complex are detailed in sticks in (A), with those belonging to domain I indicated by an orange arrow and those of domain III in purple. In (B), the residues are highlighted within the blocks. **(C)** Detail of key residues implicated in the interaction with UNAM (CPK colored yellow sticks) and **(D)** ANP-PNP (CPK colored green sticks) and Mn^{2+} in green spheres. The positions of the substrates are taken from an overlap with the structure of HiMurC (1P3D).

7.4 DISCUSSION

Examination of MurC sequences in diverse *Brucella* and bacterial species unveiled noteworthy similarity across the majority of the sequences (Figure 7.8 and 7.10). Furthermore, phylogenetic bootstraps underscore a considerable degree of evolutionary closeness among these proteins (Figure 7.9B and 7.11B). In our study, we found no evidence for the presence of multiple MurC isoforms in the strains we examined. In terms of genome organization, the murC gene is found in the majority of *Brucella* strains, typically arranged in an operon closely resembling that of *B. ovis* (Figure 7.7). As discussed in Chapter 5, a similar operon organization is also observed in *B. licheniformis*, *B. quintana*, *C. aggregans*, *C. pelagibacter*, *G. oxydans*, *L. pneumophila*, *P. zucineum*, and *R. capsulatus* accompanied with the murB gene. On the other hand, in the remaining bacteria, murC is located in conjunction with the ligases murD, murE, murF, and murG. Numerous studies support the hypothesis that Mur enzymes interact with one another, forming complexes that enhance the cytoplasmic PG biosynthesis process through sequential reactions. This concept is supported by the observation that in many eubacteria, mur genes are located within a single operon as part of the well conserved division cell wall (dcw) cluster (Mingorance et al., 2004). The formation of heteromeric protein complexes is frequently enhanced by the arrangement of subunit-encoding genes, either within operons or clusters that predominantly preserve the necessary gene expression sequence. This organization facilitates the ordered translation and efficient assembly of complexes, which holds substantial significance in various biological processes. In the context of PG biosynthesis, the rapid turnover rates may benefit from the establishment of multiprotein complexes that can channel pathway intermediates from one protein to the next (Natan et al., 2017).

In the current investigation, BoHTMurC has been effectively purified to a state of homogeneity with outstanding performance. Subsequently, an evaluation of its structure was conducted using spectroscopic techniques, and thermal denaturation experiments. These analyses confirmed that the protein had undergone correct folding (Figure 7.14), and contained a high content of α-helix. The thermal stability of BoHTMurC was assessed using CD and DSC. Monitoring protein unfolding at 208 nm exhibited two distinct transitions: at 312 K, and at324 K. This second T_m closely matched the transition observed at 222 nm in the CD analysis which was 327 K. These different techniques reveal a potential complex multi-step unfolding process that should be studied in further detail.

In this study, the kinetic characterization of BoMurC was not feasible because all experiments required the UNAM substrate, which is not commercially available. The catalytic constants reported to date for MurC span only five different species and display highly variable values (Table 7.6). Although the calculated k_{cat} in some *E. coli* assays was significantly higher than that for *S. aureus* or *M. tuberculosis*, the calculated K_ms for *E. coli* were lower than those obtained for *S. aureus* or *V. spinosorum*. Most assays follow a similar experimental dynamic pattern. Although the commonly used protocol to determine MurC catalytic constants involves mixing substrates with radioactively labeled amino acids, the products have been detected by HPLC or TLC.

On the other hand, another way to measure MurC activity is by quantifying Pi derived from ATP, using the same protocol described in Chapter 5 with malachite green. This method was employed to determine the catalytic constants for *E. coli*, complemented with HPLC (Deng et al., 2004), and *M. tuberculosis* (Munshi et al., 2013). Another possibility is the method described by Rausch et al., 2011, where the production of NAD^+ is monitored at 340 nm by UV-visible spectroscopy in a cascade reaction involving MurC substrates, pyruvate kinase (PK), and lactate dehydrogenase (LDH). A noteworthy point in the table is the calculation of K_m for certain amino acids such as L-serine and glycine. Although it is reported that MurC prefers to use L-Ala (Hesse et al., 2003), it is not ruled out that it may use these amino acids to initiate the UNAM-pentapeptide.

Table 7.6. List of bacterial species for which activities of MurC enzymes have been reported.

Organism	k_{cat}	K_m^{ATP}	k_{cat}/K_m^{ATP}	K_m^{UNAM}	k_{cat}/K_m^{UNAM}	$K_m^{L\text{-}Ala}$	$k_{cat}/K_m^{L\text{-}Ala}$	$K_m^{L\text{-}Ser}$	$k_{cat}/K_m^{L\text{-}Ser}$	K_m^{Gly}	k_{cat}/K_m^{Gly}	Experimental Conditions				Reference
	(min^{-1})	(μM)	($\mu M^{-1}.min^{-1}$)	(μM)	($\mu M^{-1}.min^{-1}$)	(μM)	($\mu M^{-1}.min^{-1}$)	(μM)	($\mu M^{-1}.min^{-1}$)	(μM)	($\mu M^{-1}.min^{-1}$)	[MurC]	Final Vol.	Buffer	Incubation	
E.coli[b]	nd	100	V_{max}= 32640 nmol min^{-1} mM^{-1} mg of $protein^{-1}$	90	V_{max}= 36267 nmol min^{-1} mM^{-1} mg of $protein^{-1}$	110	V_{max}= 29673 nmol min^{-1} mM^{-1} mg of $protein^{-1}$	nd	nd	nd	nd	nd	50 μL	100 mM Tris/HCl pH 7.8, 5 mM ATP, 20 mM $MgCl_2$, 20 mM $(NH_4)_2SO_4$, 1 mM L-l-aminoethylphosphpnic acid, 0.5 mM UNAM, 0,5 mM L-(^{14}C)Ala	37 °C for 30 min	(Bouhss et al., 1997)
	20.41	63.8	0.32	34.3	0.6	22.9	0.9	nd	nd	nd	nd	24 nM	nd	50 mM Tris/HCl pH 8.0, 2.5 mM DTT, 740 μM ATP, 10 mM $MgCl_2$, 20 mM $(NH_4)_2HCO_2$, 228 μM UNAM, 660 μM L-Ala	nd	(Deng et al., 2004)
	980 ± 40	130 ± 10	7.53	44 ± 3	22.27	48 ± 6	20.41	1200	0.81	10000	0.098	1000 U	80 mL	100 mM Tris/HCl pH 8.0, 20 mM $MgCl_2$, 40 mM$(NH_4)_2SO_4$, 1 mM DTT, 2.5 mM β-mercaptoethanol, 20 mM ATP, 15.3 mM UNAM, 20 mM L-Ala	25 °C for 24 h	(Emanuele et al., 1996)
	411	92	4.46	58	7.08	87	4.72	1990	0.2	7890	0.052	1.36 μg	20 μL	50 mM Tris/HCl pH 8.5, 20 mM $MgCl_2$, 25 mM $(NH_4)_2SO_4$, 1 mM DTT, 5 mM ATP, 1 mM UNAM, 1 mM L-(^{14}C)Ala (9.26 mCi/mmol)	5 min	(Gubler et al., 1996)
	928	450	2.06	100	9.28	20	46.4	nd	nd	nd	nd	nd	50 μL	100 mM Tris/HCl buffer, 5 mM ATP, 20 mM $MgCl_2$, 0.5 $mg.mL^{-1}$ BSA, 0.5 mM UNAM, 1 mM L-(^{14}C)Ala (2 kBq)	37 °C for 30 min	(Liger et al., 1995)
	930[a]	132.3[a]	7.02[a]	170[a]	5.47[a]	78.1[a]	11.9[a]	nd	nd	nd	nd	20 nM	50 μL	50 mM Tris/HCl pH 8.0, 10 mM $MgCl_2$,10 mM $(NH_4)_2SO_4$, 400 μM L-Ala or/and 400 μM ATP 400 μM UNAM, 2.5 mM DTT, 1 mM PEP, 1 mM NADH, 10 U/mL lactic dehydrogenase, 10 U/mL pyruvate kinase	37 °C for 20 min	(Rausch et al., 2011)
S. aureus[b]	84[a]	280.2[a]	0.3[a]	263.1[a]	0.32[a]	221.6[a]	0.38[a]	nd	nd	nd	nd					
	nd	67	nd	51	nd	150	nd	29000	nd	nd	nd	368 μg	500 μL	40 mM Tris/HCl pH 8.5, μmoles ATP, 1 μmoles $MgCl_2$, 10 μmoles $(NH_4)_2SO_4$, 100 μmoles UNAM, 180 μmoles DL-(^{14}C)Ala (500,000 cpm), 2 μmoles cycloserine	37 °C for 2 h	(Mizuno et al., 1973)
	nd	2000 ± 300	V_{max}= 1.4 ± 0.24 μmol min^{-1} mM^{-1} mg of $protein^{-1}$	280 ± 20	V_{max}= 10 ± 1.0 μmol min^{-1} mM^{-1} mg of $protein^{-1}$	440 ± 130	V_{max}= 6.4 ± 1.9 μmol min^{-1} mM^{-1} mg of $protein^{-1}$	nd	nd	nd	nd	nd	50 μL	100 mM Tris/HCl pH 8.6, 4 mM ATP, 5 mM $MgCl_2$, 20 mM $(NH_4)_2SO_4$, 2.5 mM DTT, 2 mM UNAM, 2 mM L-Ala	37 °C for 30 min	(Patin et al., 2010)
V. spinosum.	480	470 ± 160	1.02	90 ± 25	5.3	25 ± 10	19.2	nd	nd	nd	nd	nd	40 μL	100 mM Tris/HCl pH 9.0, 3 mM ATP, 10 mM $MgCl_2$, 10 mM $(NH_4)_2SO_4$, 0.5 $mg.mL^{-1}$ BSA, 0.9 mM UNAM, 0.3 mM L-(^{14}C)Ala (400 Bq)	37 °C for 30 min	(Naqvi et al., 2016)
M. tuberculosis	1	67.7	0.906	23.5	0.0448	43	0.024	99.7	0.0125	146.5	0.0104	100-200 ng	50 μL	50 mM Bis/Tris 8.5, 1 mM ATP, 5 mM $MgCl_2$, 0.1 mM UNAM, 1 mM amino acids	37 °C for 30 min	(Munshi et al., 2013)
C. trichomantis[b]	nd	162 ± 40	V_{max}= 456 nmol min^{-1} mM^{-1} mg of $protein^{-1}$	196 ± 65	V_{max}= 376 nmol min^{-1} mM^{-1} mg of $protein^{-1}$	124 ± 37	V_{max}= 595 nmol min^{-1} mM^{-1} mg of $protein^{-1}$	242 ± 67	V_{max}= 316 nmol min^{-1} mM^{-1} mg of $protein^{-1}$	1170 ± 190	V_{max}= 176 nmol min^{-1} mM^{-1} mg of $protein^{-1}$	nd	50 μL	200 mM Tris/HCl pH 8.6, 2.5 mM ATP, 20 mM $MgCl_2$, 40 mM $(NH_4)_2SO_4$, 2 mM UNAM, 10 mM L-(^{14}C)Ala (3.4 kBq; 5.5 GBq $mmol^{-1}$)	37 °C for 30 min	(Hesse et al., 2003)

[a] Value was determinated by monitoring the NAD^+ production of couplig assay with PK and LDH

[b] k_{cat}/K_M reported as v_{max} valu

The crystallization of BoMurC (with and without a 6-His tag) was partially successful. The X-ray diffraction of the first crystals obtained was of insufficient resolution. Several optimizations of the crystallization trials were attempted and by dehydration using alcohols and ethylene glycol as a cryoprotectant, the diffraction resolution of the crystals improved from 8 Å to 3.5 Å. The crystallographic structure at 3.3 Å suggested a potential dimeric arrangement, but an analysis conducted by PISA software indicated that this potential arrangement was unstable in solution (Figure 7.17). However, a CN-PAGE (Figure 7.13A, right inset) assay suggested that BoMurC could form dimers or tetramers. In this sense, EcMurC (PDB 2F00) presents two molecules in the a.u. of its crystals as BoMurC, and in solution, it demonstrates a dynamic equilibrium between monomeric and dimeric forms. Biochemical studies have revealed a binding affinity (K_d) of approximately 1 mM, and it appears to retain activity in both monomeric and dimeric states (Emanuele et al., 1996). The dimer interface of EcMurC is formed by the interlocking of loops from domain II of one molecule with loops from domain I of the second molecule. Specifically, residues Met16, Val19, Val81, Met111, and Ile106 from one protomer interact with the Phe223-Tyr224 pair. Notably, these residues are part of a conserved PFYG motif found in nearly 50% of known MurC sequences. Furthermore, Arg17 and Arg18 extend toward the second molecule, establishing salt bridges with adjacent Glu306 and Glu307 residues (Deva et al., 2006). This dimer interface is also observed in the HiMurC 1GQY structure (residues 209-212) but is conspicuously absent in other crystal structures like TcMurC (Mol et al., 2003; Spraggon et al., 2004). For instance, in the crystal structure of MtMurC, two monomers are present in the a.u., but there are no notable interactions between these monomers, indicating a lack of dimer formation (Seo et al., 2021).

In some cases, pairs of mur genes are fused to encode a single chimeric polypeptide. Chimeric Mur enzymes are notably concentrated within specific phyla: MurE-MurF combinations are prevalent in Proteobacteria; MurG-MurC combinations are abundant in Actinobacteria; MurD-FtsW combinations are observed in Proteobacteria and Actinobacteria; MurC-MurB combinations are prominent in Verrucomicrobia, like the VspiD_010100018130 gene of *V. spinosum* that expresses a bifunctional protein (WP_009962545.1) (Naqvi et al., 2016); and MurC-Ddl combinations are found in Chlamydiae and Firmicutes, since the case of KW36_rs04145 in *C. trachomatis* which encodes a fusion protein (WP_010725335.1) (Hesse et al., 2003). In bacteria that produce PG, Ddl is an indispensable enzyme, and the ligation of two D-Ala residues by Ddl proteins

is exceptionally specific. The addition of D-Ala-D-Ala to PG monomers holds immense importance for the survival of bacteria, as it plays a critical role in linking the pentapeptide chains of PG monomers in the periplasm. Specifically, it facilitates the cross-linking of the penultimate D-Ala of one peptide chain to diaminopimelic acid in another chain (McCoy & Maurelli, 2005). Further examination of protein sequences in the Uniprot database has revealed the relative distribution of these chimeric Mur types. Among these, MurE-MurF chimeras are the most abundant, accounting for 64% of all chimeras. They are followed by MurC-Ddl chimeras at 11%, MurC-MurB chimeras at 11%, MurG-MurC chimeras at 9%, and MurD-FtsW chimeras at 3% (Shirakawa et al., 2023). In addition, in *S. pneumoniae*, it has been demonstrated that MurC, MurD, MurE, MurF, and MurG exhibit robust interactions when paired as binary complexes, and these interactions are primarily localized to loop regions. What is intriguing is that MurC, MurD, and MurE display a 10-fold higher affinity for each other when compared to their affinity for MurF and MurG. This observation implies that the Mur ligases, which are responsible for catalyzing the initial steps in the PG biosynthesis pathway, might potentially form a subcomplex. Such a subcomplex could play a crucial role in facilitating the biosynthesis of Lipid II (Miyachiro et al., 2019). An analysis of the crystal structure of a MurE-MurF complex from *B. pertussis* revealed that it adopts an elongated conformation where the domains open up and extend. It has been demonstrated that Mur ligases often alter their conformation depending on ligand binding, with apo forms being more "open," and ligand-bound forms exhibiting domain closure. Overlaying it with ligand-bound structures of MurE from different bacteria such as *A. baumannii*, *T. maritima*, and *S. aureus* allowed the identification of a potential rotation of the N-terminal domain that facilitates interaction with the monomer of MurF. The interface between MurE and MurF comprises a predominantly helical region covering a hydrophobic patch, forming a tight nonpolar pocket. The two binding sites are approximately 50 Å apart from each other (measured from the central region of each cleft) (Figure 7.23A, B and C). This arrangement establishes an organization where the orientation between the two proteins could potentially be stabilized, favoring the transfer of ligands (Shirakawa et al., 2023). In addition, the crystal structure of the association of two proteins forming a binary complex has been identified within the group of enzymes contributing to the peptidoglycan machinery in bacteria. These enzymes are GatD (Glutamine amidotransferase) and MurT (lipid II isoglutaminyl synthase or glutamine-hydrolysing) from *S. aureus*. Together, these two proteins catalyze the amination of α-D-isoglutamic acid in precursor peptides of the cell wall in an ATP-

dependent reaction. The structure of the GatD:MurT complex (6GS2) assembles into a curved boomerang-like configuration, with GatD coupled to the C-terminal domain of MurT. Small-angle X-ray scattering (SAXS) data confirm that the complex adopts an open conformation, suggesting flexibility between the monomers. However, the observed change in protein solubility clearly indicates a significant conformational rearrangement in the protein upon binding ATP and Lipid II. This change leads to a "closed" state in the presence of ligands, as simulated in Figure 7.23E (Nöldeke et al., 2018).

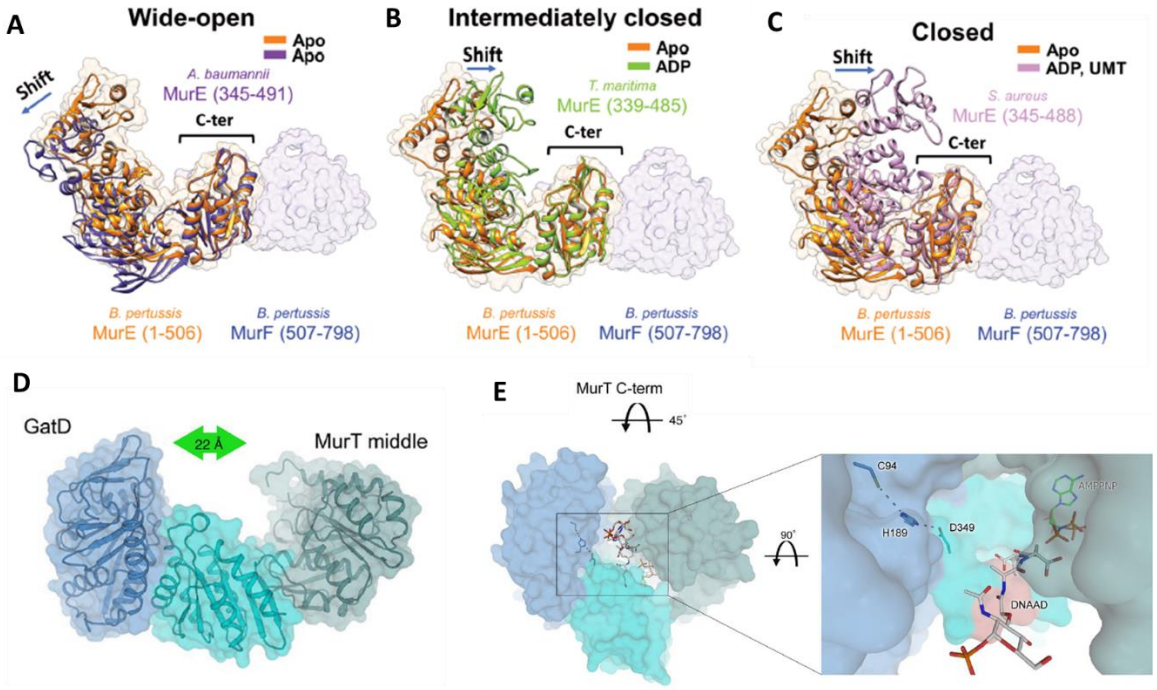

Figure 7.23. Superposition of the MurE:MurFΔ6 structure with that of MurE from different species and conformation of the GatD:MurT complex in solution and putative conformational changes upon ligand engagement. The structural alignment between the C-terminal region of MurE from MurE:MurFΔ6 (residues 360 to 506, orange) and MurE from **(A)** *A. baumannii* (PDB ID: 7D27, residues 345 to 491 - RMSD: 0.837 Å), in purple, and in the apo form **(B)** *T. maritima* (PDB ID: 4BUB, residues 340 to 485 - RMSD: 1.041 Å) in green with ADP bound and **(C)** *S. aureus* (PDB ID: 4C12, residues 345 to 488 - RMSD: 0.967 Å) in violet with ADP and UMT, reveals the variety of N-terminal and central domain conformations in MurE that depend on the presence of substrate and/or nucleotides. This ranges from a widely open conformation in apo-form (A) to intermediately closed (B) with ADP and to closed (C) conformation in the presence of ADP and UMT. The MurE:MurFΔ6 structure, crystallized in the apo form, is in an open conformation (Shirakawa et al., 2023). **(D)** GatD:MurT crystal structure after refinement against SAXS data. While the overall organization and shape of the complex remain similar, the increased diameter of the GatD and MurT middle domain envelopes as well as the smaller gap of 22 Å between them suggest that some flexibility between domains exists in solution. **(E)** Putative model of an active conformation of GatD:MurT with the domain movement modeled after the *S. aureus* MurE structure. The GatD catalytic triad and the bound AMPPNP molecule are shown as colored sticks, the relevant muramyltripeptide portion of the superimposed substrate of MurE (MurNAc-L-Ala-γ-D-Glu-L-Lys, but lacking UDP) is shown in grey stick representation for reference. The DNAAD motif, suggested to be involved in substrate binding is highlighted in salmon (right) (Nöldeke et al., 2018).

In the case of the BoMurB:BoMurC complex modeled by AlphaFold in the absence of ligands, it is observed that the BoMurC monomer is in an "open" position toward

BoMurB. However, it is unlikely that BoMurB is situated "nested" within the active site of BoMurC. Therefore, this modeling does not align with the examples mentioned earlier for similar protein complexes. Possibly, the BoMurB monomer should position itself to the side of BoMurC, where it interacts with the C-terminal domain, maintaining an "open" conformation. Later, when ligands bind, BoMurB will transition to a "closed" conformation. BoMurB might rotate to meet BoMurC in the "open" state, and the UNAM produced by BoMurB will migrate towards BoMurC, as we proposed that in can occur with the OLB01401.1 protein of *V. bacterium* in Figure 7.19C. In this example, in the case of a hybrid protein, the MurB portion, when passing the product, must transit to another conformation to allow MurC to close. In the case of non-hybrid proteins, such as BoMurB and BoMurC, the formation of the complex may occur in several steps. It is not ruled out that BoMurC undergoes different conformations, such as "open→intermediate→closed," similar to MurE from *B. pertussis* (Figure 7.23A, B, and C). Meanwhile, BoMurB may dissociate and separate or remain interacting with some domain of BoMurC. The latter scenario is also a plausible hypothesis.

The results of the docking between these proteins show highly negative interaction energies (Table 7.5), suggesting that the generated complexes are stable, thermodynamically favorable, and likely spontaneous, indicating a strong affinity between them. In Figure 7.20, a series of conformations is proposed where the active sites of both proteins are within at least 15 Å of each other. Although ligand transfer can occur over a wide range of distances, its specificity will depend on multiple factors, including the structural and chemical characteristics of the active sites, as well as the three-dimensional orientation of the proteins at the time of interaction and ligand transfer. In some cases, transfers can occur at short distances, with binding sites in direct or very close contact. In other cases, transfers may occur at greater distances, and the formation of protein-protein complexes may involve conformational changes or structural adjustments to facilitate the process.

Despite all these data compilation, we cannot definitively assert if there is an interaction between BoMurB and BoMurC, as we suspect there might be. Further experiments, both *in situ* and *in silico,* are needed.

7.5 CONCLUSION

The examination of MurC sequences across *Brucella* and bacterial species reveals significant similarity, indicating evolutionary closeness. In terms of genomic organization, the MurC gene is commonly found in *Brucella* strains, typically arranged in an operon resembling that of *B. ovis*. Similar operon structures are observed in various bacteria participating in PG biosynthesis. This suggests a potential interaction and complex formation among Mur enzymes, BoHTMurC, successfully purified, exhibits correct folding. Although, given the absence of UNAM in our hands, we were not able to measure the BoMurC kinetic parameters, a thorough bibliographic analysis was undertaken to examine the kinetic constants associated with different species. Despite similarities in the methodologies employed, a substantial variability in the values obtained was observed. The crystallization of both variants of BoMurC yielded single crystals. However, the diffraction of these crystals initially did not give a meaningful signal at first. Various optimizations, including dehydration with alcohols and ethylene glycol, improved the diffraction resolution. The resulting crystals suggested a potential dimeric arrangement with two apo BoMurC molecules in the a.u. Chimeric Mur enzymes, formed by fusion of mur gene pairs, show diverse distributions among bacterial phyla. Robust interactions among Mur enzymes in other bacterial models and the identification of a binary complex underscore the complexity of their conformations and catalytic way functions. AlphaFold modeling of the BoMurB:BoMurC complex suggests an "open" conformation, and protein docking analysis indicates stable complexes with highly negative interaction energies. Docking results indicated highly negative interaction energies, implying stable and thermodynamically favorable complexes with a strong affinity between BoMurB and BoMurC. However, the existence of this interaction requires further validation through experimental approaches.

8.

Decoding the redox conformational mechanism in Ferredoxin flavin-thioredoxin reductase from Gloeobacter violaceus

8.1 SUMMARY

In this study, we performed in-depth analysis of several variants of the cyanobacterial ferredoxin-dependent flavoenzyme thioredoxin reductase (FFTR) from *Gloeobacter violaceus*. We analyzed two mutant versions of the protein C-terminal tail with a focus on understanding the role of Trp315 and the C-terminal tail in protein conformation and function. We also evaluated a third mutant, in which the redox-active CxxC motif within the redox-active disulfide domain of the protein was replaced by a SXXC motif (Cys135Ser replacement). The effects of these modifications on the electronic environment of FAD isoalloxazine and on the stability of its semiquinone state during the GvFFTR redox cycle were analyzed, as well as their impact on the flavin reductive-half reaction. Although mutations at the C-terminal tail exhibit changes in the bound FAD spectroscopic properties, the absence of Trp315 and the C-terminal tail did not lead to significant changes in overall protein folding. Nonetheless, removal of Trp315 has a relevant impact on the midpoint reduction potential of the FAD cofactor of GvFFTR, and removal of the C-terminal tail abolishes FAD semiquinone stabilization. Noticeably, both features considerably enhance the ability of flavin to accept electrons. In contrast, the mutation at the CxxC motif hardly affected the FAD midpoint reduction potential and the spectroscopic properties of the oxidized protein. However, the C135S replacement makes the FAD of GvFFTR less prone to reduction, and its semiquinone/hydroquinone transition exhibits, in addition to the neutral semiquinone band, a new peak at 506 nm that might be related to the SxxC motif stacking against the FAD isoalloxazine. These findings provide valuable insights into the role of specific residues in modulating spectroscopic, functional, and structural characteristics of cyanobacterial-type FFTR enzymes.

8.2 INTRODUCTION

8.2.1 FFTR structure-function relationship in the Trxs/TrxR system in *Gloeobacter violaceus*

Some cyanobacterial genomes such as those of *Gloeobacter* and *Prochlorococcus* were reported to lack NADPH-thioredoxin reductases (NTR) and ferredoxin-thioredoxin reductases (FTR) enzymes, but contained instead a flavoenzyme thioredoxin reductase (originally labelled as deeplyrooted thioredoxin reductase or DTR) with non-identified electron donor but showing features like those of FFTR in *Clostridium pasteurianum* (Hammel et al., 1983). More recent studies suggested this enzyme being a Fdx flavin-thioredoxin reductase (FFTR) and, consequently, the enzyme initially called *Gloeobacter violaceus* DTR (GvDTR) was renamed as FFTR (GvFFTR) (Buey et al., 2021). The GvFFTR crystalline structure (PDB code 5J60) is a homodimer, with each protomer comprising two main domains connected by two antiparallel β strands and each containing one redox-active centre (Buey et al., 2017, 2021). The FAD-binding domain contains FAD as redox cofactor, while the redox-active disulfide domain has a CxxC motif where the two cysteine residues are forming a reversible disulfide bond. All reported structures of FFTR homodimers show a central core region where the FAD-binding domains of each protomer attach to each other, while their redox-active disulfide domains display an overall "open conformation" that positions their CxxC motifs of the redox-active disulfide domain more than 30 Å away from their corresponding FAD expected electron donors (Figure 8.1) (Buey et al., 2017, 2018, 2021). In addition, the C-terminal tail (P313-H317) of each GvFFTR protomer has a highly conserved tryptophan, Trp315, that π-stacks to the isoalloxazine ring of the FAD of the neighbour protomer (Figure 8.1), suggesting for both, the C-tail and W315, potential physiological roles during electron transfer (ET) events.

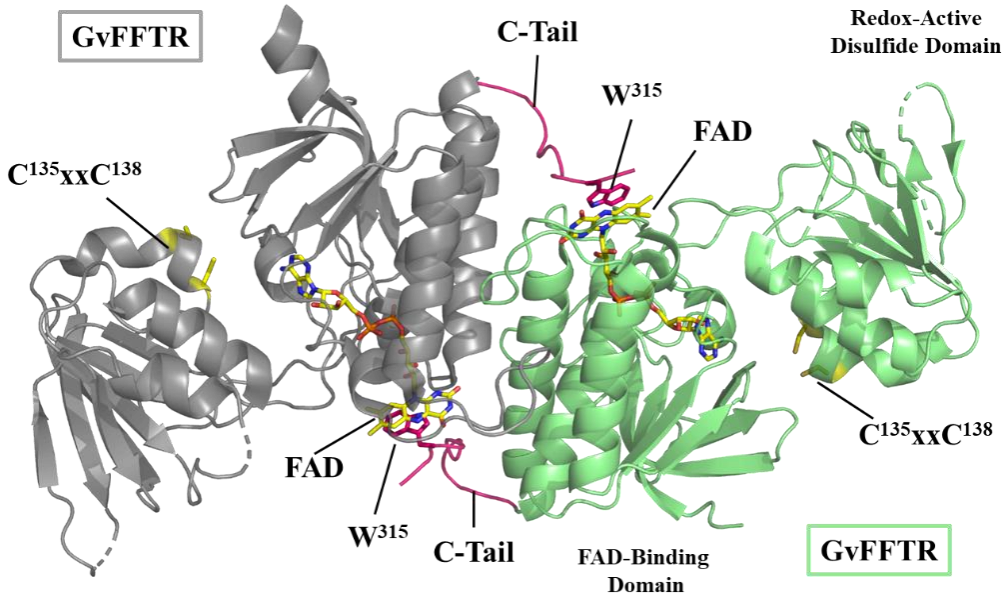

Figure 8.1. Crystal structure of the GvFFTR homodimer (PDB code 5J60). The two protomers within the dimer are respectively displayed in grey and green cartoon. Missing loops are represented as dashed lines. The C-tails (P313-H317) and the Trp315 aromatic residues (in sticks) are CPK colored with carbons in pink. Cys residues of CxxC motif and FAD are CPK colored with carbons in yellow.

Two Fdxs from *G. violaceus* (GvFdx1 and GxFdx2) were explored as potential partners of GvFFTR. Isothermal titration calorimetric assays revealed a broad affinity of GvFdx1 (having a plant-type Fdx fold and containing [2Fe-2S]) for GvFFTR (K_d 3.9 µM), whereas interaction with GvFdx2 was negligible. Crystallographic assays led to the resolution of the structure for a GvFFTR-GvFdx1 complex (PDB code 6XTF) where each GvFFTR protomer adopted an open conformation with the two redox centers (the isoalloxazine ring of FAD and cysteines of the CxxC motif) again far away. GvFdx1 binding to GvFFTR was primarily electrostatic and occurred at the grove of the two domains of each GvFFTR protomer (Figure 8.2). Noticeably, while the FAD isoalloxazine is involved in the interaction with GvFdx1, it preserves its stacking to Trp315 of the opposite monomer. The electron density was clear enough in this structure to show the C-7 and C-8 methyl groups of the isoalloxazine ring of GvFFTR oriented towards the [2Fe-2S] of GvFdx1, envisaging a potential adequate orientation for ET from reduced GvFdx1 to the FAD of GvFFTR (Buey et al., 2021).

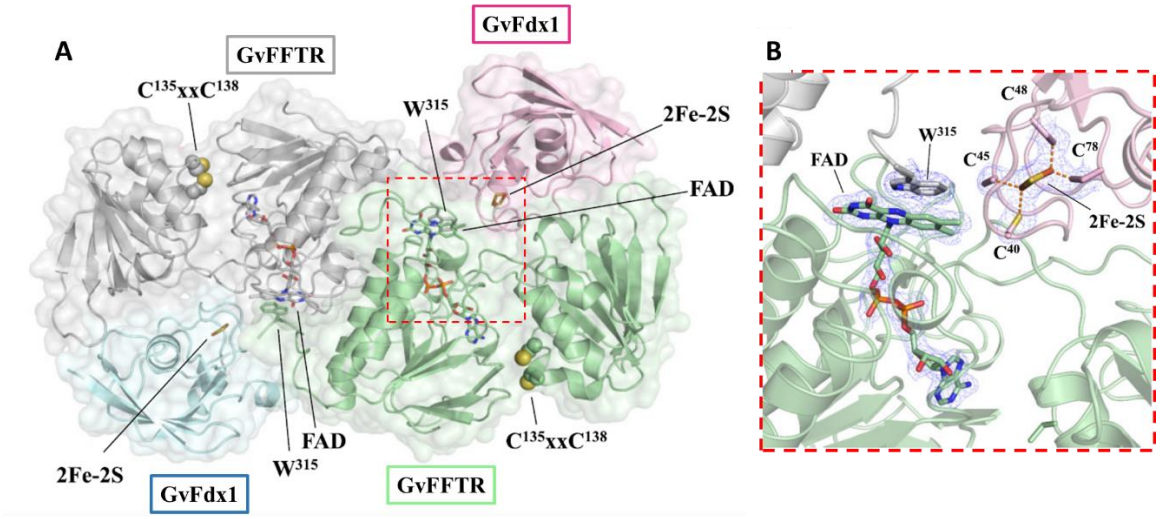

Figure 8.2. Crystal structure of the GvFFTR-GvFdx1 complex (PDB code 6XTF). (A) Cartoon diagram of the GvFFTR homodimer with protomers respectively colored in green and grey, each bound to a GvFdx1 molecule colored in magenta and blue, respectively. **(B)** Detail of the GvFFTR-GvFdx1 interaction regions showing the FAD and [2Fe-2S] electron density maps. The [2Fe-2S] cluster, coordinated by four Cys residues, sits at the surface of the protein and close to the GvFFTR-GvFdx1interface. The FAD cofactor, the [2Fe-2S] cluster and the Cys residues binding it, as well as the Trp315 side chain are shown in CPK sticks, while Cys residues of the CxxC motif are shown as spheres (Figure taken from Buey et al., 2021).

8.2.2 The catalytic activity of GvFFTR

GvFFTR lacks the NTR activity, when using *E. coli* NTR (EcNTR) as a positive control in a reduction-coupled NAD(P)H oxidation experiment with 5,5'-dithiobis (2-nitrobenzoic acid) (DTNB) (Holmgren & Bjornstedt, 1995). In addition, a mutant lacking the C-tail (313-317 residues), GvFFTR_Δtail, was produced to assess functional characteristics of the protein (Figure 8.3). Since NADPH was incapable of reducing GvFFTR_WT and GvFFTR_Δtail, assays with sodium dithionite (DTH) were performed, observing an increase in the rate of flavin reduction of the mutant up to 10 times regarding that of the wild type. These results suggested that the exclusive C-tail in GvFFTR has a direct connection with enzymatic activity and could constitute a regulatory mechanism. Furthermore, visible absorption spectra showed two peaks in the UV-visible region at 391 and 458 nm for the WT that were displaced to 380 and 450 nm for the GvFFTR_Δtail mutant, probably due to a larger exposition of the FAD to the solvent in the mutant (Buey et al., 2017).

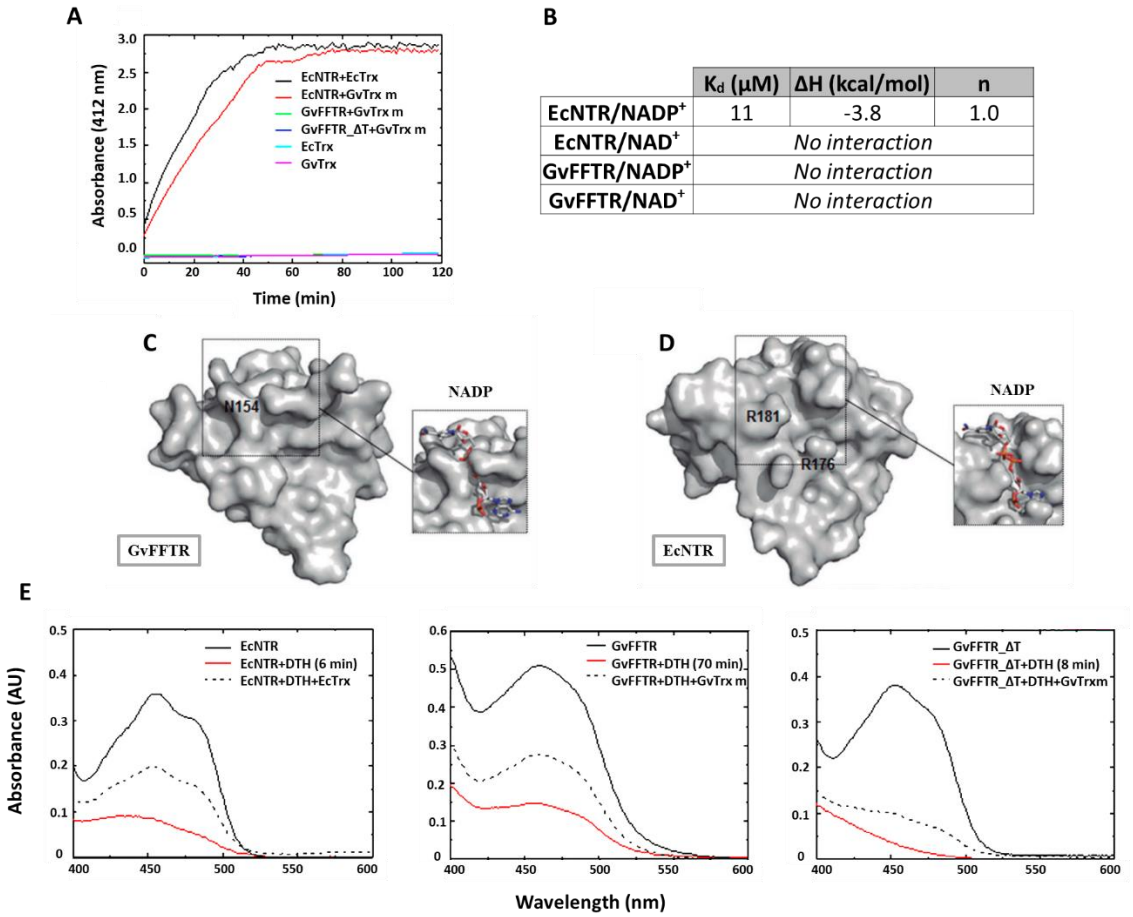

	K_d (μM)	ΔH (kcal/mol)	n
EcNTR/NADP$^+$	11	-3.8	1.0
EcNTR/NAD$^+$	*No interaction*		
GvFFTR/NADP$^+$	*No interaction*		
GvFFTR/NAD$^+$	*No interaction*		

Figure 8.3. (A) Absorbance changes at 412 nm as a consequence of DTNB reduction by using NADPH as source of reducing equivalents for GvFFTR and EcNTR in the presence of EcTrx or GvTrxm. **(B)** Summary of dissociation constants (K_d), binding enthalpy (ΔH), and stoichiometry (n) of the binding to GvFFTR and EcNTR of NAD(P)$^+$. Relative error in K_d is 15%; absolute errors in ΔH and n are 0.3 kcal/mol and 0.1, respectively. **(C)** Surface representation of the potential NADP$^+$ binding domain in GvFFTR. Position of Asn154, which substitutes for the second conserved Gly in the GxGxxG/A motif of pyridine nucleotide binding proteins is labeled. **(D)** Surface representation of the NADP$^+$ binding domain in EcNTR. Positions of Arg176 and Arg181 involved in electrostatic interactions with the coenzyme are labeled. The binding pocket for NAD(P)H is particularly altered in GvFFTR, lacking the residues involved in electrostatic interaction with the pyrophosphate bridge of NADP$^+$/H. (NADP$^+$ is shown in CPK sticks) **(E)** Visible absorption spectra of EcNTR, GvFFTR, and GvFFTR_Δtail at the flavin band I. Oxidized flavoenzymes are represented by a black line. Red lines show the corresponding absorption spectra after incubation with DTH under anaerobic conditions for the following times: 6 min for EcNTR, 70 min for GvFFTR, and 8 min for GvFFTR_Δtail. The spectra obtained after addition of homologous Trxm to the reduced system (less than 3 min) are displayed as dashed black lines (Figure adapted from Buey et al., 2016).

Moreover, while photoreduction of GvFFTR WT stabilized a large amount of neutral semiquinone, this state was hardly populated upon photoreduction of GvFFTR_Δtail (Figure 8.4). Therefore, a role for the C-tail in the stabilization of the neutral semiquinone, and therefore in the flavin chemistry is envisaged.

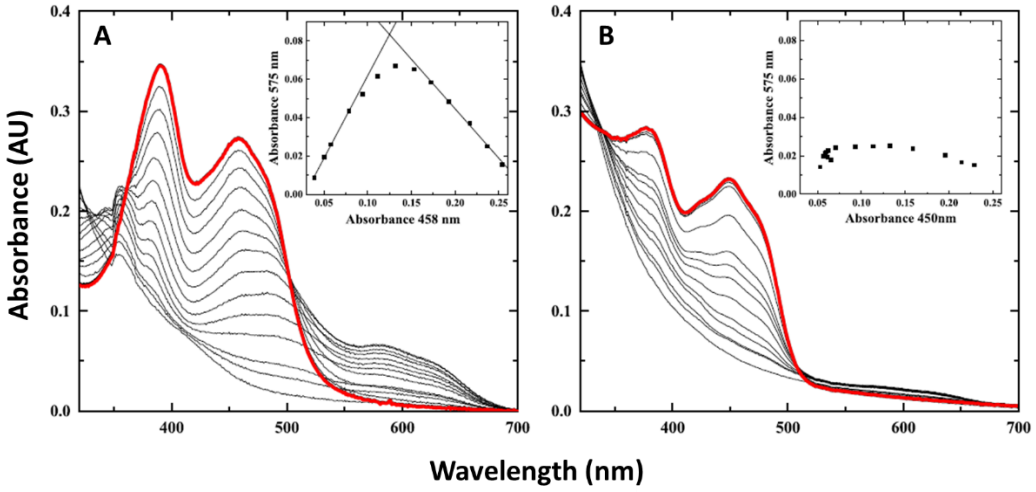

Figure 8.4. Flavin spectral evolution for the photoreduction of GvFFTR and GvFFTR_Δtail. (A) Absorption spectrum of oxidized flavin in GvFFTR WT sample shows maxima of bands II and I at 391 and 458 nm, respectively. Flavin reduction occurs with stabilization of neutral semiquinone as shown by appearance of isosbestic points at 361 and 502 nm (for oxidized/semiquinone transition) and 324 nm (for semiquinone/hydroquinone transition). **(B)** The flavin reduction in GvFFTR_Δtail (with maxima at 380 and 450 nm) occurs without semiquinone stabilization, as shown by the isosbestic points at 340 and 509 nm for the oxidized/hydroquinone transition. The bold red lines show the spectra after one cycle of whole protein photoreduction followed by molecular oxygen reoxidation, which are identical to the initial spectra. The insets show the absorption at the neutral semiquinone band maxima (575 nm) relative to absorption at the flavin I band maxima (450 nm) together with photoreduction. Experiments were performed under anaerobic conditions in the presence of 5-deazariboflavin and EDTA. (Figure taken from Buey et al., 2021).

Altogether, these observations allowed to propose an action mechanism for GvFFTR that is summarized in Figure 8.5 (Buey et al., 2021). This model agrees with two GvFdx1 molecules sequentially binding GvFFTR in its open conformation and delivering each one electron to the FAD cofactor through the transient stabilization of its semiquinone state, probably by the action of the C-tail. Then, once the FAD is in its hydroquinone state, a conformational change that would bring the CxxC motif at redox-active disulfide domain into close contact of the flavin isoalloxazine is expected, namely closed conformation, in order to allow reduction of the CxxC motif. Finally, upon reduction of the CxxC motif to a dithiol, recovering of the open conformation must be achieved redox-active disulfide domain to pass the electros to Trx. Thus, GvFFTR should adopt open and closed conformations during the catalytic cycle, but so far structural data are reduced to the open oxidized conformation, and it is not clear whether removal of the C-tail from the stacking position onto the isoalloxazine occurs at any point (Buey et al., 2017, 2018, 2021). Nonetheless, a recent study using atomic force microscopy has reported different relative dispositions in solution for the redox-active disulfide and FAD-binding domains for flavin-reduced homodimers, indicating a dynamic disposition of disulfide domains regarding the central

protein core (Marcuello et al., 2021). Furthermore, this study also detected morphological changes upon the interaction of FFTRs with their protein partners.

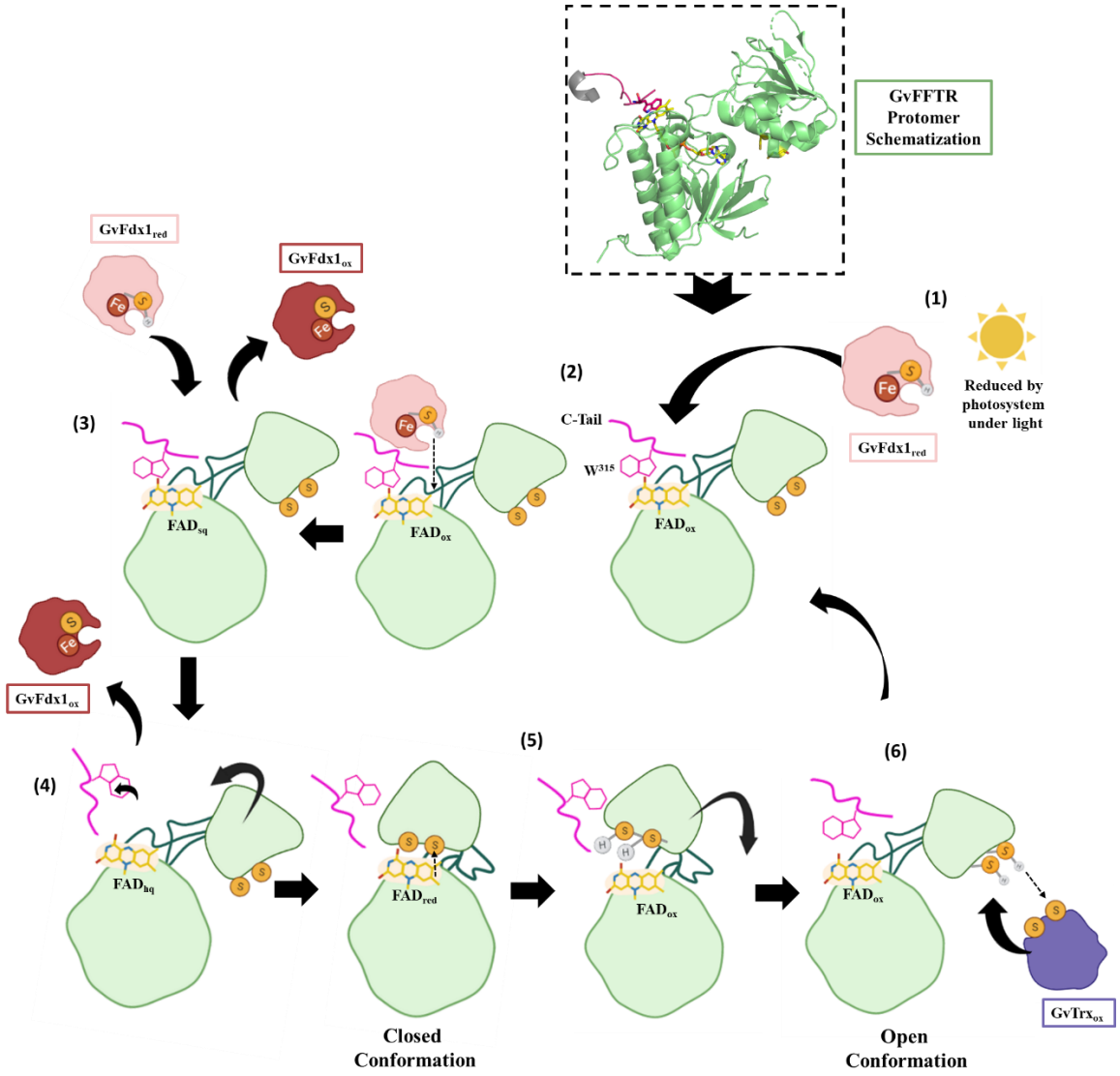

Figure 8.5. Potential model for the catalytic cycle of GvFFTR (exemplified by a single protomer from PDB code 6XTF). (1) GvFdx1 becomes reduced by photosystem I; **(2)** Reduced GvFdx1 binds to GvFFTR in its open-conformation, transfers one electron to its FAD cofactor, generates the FAD semiquinone state and leaves the complex as $GvFdx1_{ox}$; **(3)** A second $GvFdx1_{red}$ protein binds to GvFFTR with its FAD in semiquinone state that is reduced to the hydroquinone state and $GvFdx1_{ox}$ leaves the complex; **(4)** A conformational rearrangement from an open to a closed conformation is envisaged to allow the coupling of the redox-active disulfide domain to the reduced isoalloxazine of FAD; **(5)** electrons are transferred from reduced FAD to the CxxC motif of the redox-active disulfide domain, thus becoming a dithiol; **(6)** Conformational rearrangement takes place to the open conformation to allow dithiol–disulfide exchange between GvFFTR and oxidized GvTrx, recovering GvFFTR its oxidized state **(2)**. The scheme only shows the cycle of a functional unit, while for the neighboring protomer only the C-tail is displayed in pink with Trp315 highlighted as lines.

In the present study we aimed to enhance our understanding of the role played by the C-terminal tail and Trp315 in setting the chemical properties of FAD within GvFFTR, as well as in the redox chemistry of the protein when reduced by GvFdx1. To achieve these

objectives, a comparative analysis of several features of wild-type, GvFFTR_WT, two of its variants at the FAD isolloxazine region, namely GvFFTR_Δtail, GvFFTR_W315A and a variant at the disulfide domain, namely GvFFTR_C135S (where Cys135 is replaced by Ser, making the 135-CxxC-138 motif a SxxC motif) is herein presented. Such structural insights shed light on the intriguing variations in their mechanisms and functions.

8.3 RESULTS

8.3.1 Spectroscopic properties of GvFdx1 and GvFFTR variants

Absorption spectra of both GvFFTR_WT and GvFFTR_Δtail in solution were reported in a previous study (Buey et al., 2021). Here, we expanded this analysis to GvFFTR_W315A and GvFFTR_C135S mutated versions of the enzyme. The primary objective of the GvFFTR_W315A modification was analyze the specific impact of the Trp315 side chain within the C-terminal tail of the protein. Since stacking of this Trp against the isoalloxazine of the neighbor protomer seems to be critical to set the redox cofactor properties, we might anticipate relevant changes as a result of this single alteration. The GvFFTR_W315A$_{ox}$ homodimer showed two peaks in the visible absorption spectrum with their maxima occurring at 380 and 450 nm, corresponding respectively to bands II and I of its FAD cofactor (Figure 8.6A, orange line). Previous work reported these bands at exactly the same wavelengths for GvFFTR_Δtail$_{ox}$, while they appeared at 391 and 458 nm for GvFFTR_WT$_{ox}$ (Figure 8.6A, blue and green and lines, respectively). Moreover, the blue-shifted change in the bands II and I for both mutants resembles the spectrum of free FAD. This indicates that in these mutants the isoalloxazine is solvent accessible and confirms that the Trp315 side chain modulates the isoalloxazine electronic environment within GvFFTR_WT. On the contrary, the absorption spectrum of the GvFFTR_C135S mutant highly resembles that of GvFFTR_WT (Figure 8.6A, pink).

To further evaluate the relevance of the Trp315, the C-terminal tail and the disulfide motif on the FAD cofactor chemistry, we performed photoreduction experiments on the new produced variants. Stepwise photoreduction of GvFFTR_W315A shows the transient appearance of a 550–700 nm long-wavelength absorbance band, with a maximum at 577 nm and a shoulder at 620 nm, with concurrent decrease of the absorption intensity at bands II and I (Figure 8.6B). These observations indicate that photoreduction of FAD within GvFFTR_W315A occurs through a mechanism involving the one-electron-reduced neutral semiquinone (FAD$_{sq}$) state. GvFFTR_WT has been reported to effectively stabilize such neutral FAD$_{sq}$ state up to 80% (Buey et al., 2021), while indicate that replacement of Trp315

by Ala leads to decrease in the maximal FAD_{sq} stabilized to around 60 %. Noticeably, the GvFFTR_Δtail mutant showed only marginal stabilization of this state (Buey et al., 2021). Despite the still high proportion of FAD_{sq} stabilized in GvFFTR_W315A, its spectral shape diverges when compared to that of GvFFTR_WT (compare Figure 8.6B with Figure 8.4A). Thus, GvFFTR_W315A photoreduction exhibits isosbestic points at 342 and 502 nm for the oxidized/semiquinone (ox/sq) transition and 342 nm for the semiquinone/hydroquinone (sq/hq) transition, values that slightly differ from those reported for GvFFTR_WT (361 and 502 nm for ox/sq and 324 nm for sq/hq) and GvFFTR_Δtail (340 and 509 nm for the ox/hq). Collectively, these observations suggest some contribution of Trp315 in the neutral FAD_{sq} stabilization, but particularly indicate that the C-terminal tail is a key element in stabilizing it within FFTR. This emphasizes the significant contribution of these two features to the FAD chemistry within the protein. Regarding the GvFFTR_C135S mutant, its photoreduction resembles that of GvFFTR_WT, exhibiting isosbestic points at 351 and 506 nm for ox/sq and stabilizing nearly 70% of the neutral FAD_{sq} (Figure 8.6C). Nonetheless, a peak at 506 nm, not detected upon GvFFTR_WT photoreduction, is observed for its sq/hq transition (compare Figure 8.6C with Figure 8.4A). This later observation envisages that the replacement in the CxxC motif at the disulfide domain somehow impacts the environment of the $FAD_{sq/hq}$ states in GvFFTR. Photoreduction was also conducted on oxidized GvFdx1 ($GvFdx1_{ox}$), which exhibits absorption maxima at 330 nm and 422 in the visible region, along with a shoulder around 462 nm (Figure 8.6D) (Buey et al., 2021). Upon photoreduction these distinctive spectral features experience bleaching, indicating that the reduction of the iron-sulfur center [2Fe-2S] in $GvFdx1_{ox}$ can be achieved by light irradiation. In all proteins here photoreduced, re-oxidation was induced by admission of air in the dark (not shown).

To complete the spectroscopic characterization of these GvFFTR forms, fluorescence experiments were conducted. When excited in the near-UV at 280 nm, GvFFTR_WT exhibited fluorescence emission centered at 333 nm with a shoulder at 352 nm. The corresponding excitation spectrum at the maximum excitation wavelength exhibits a peak at approximately 290 nm (Figure 8.6E). These emission and excitation spectral features suggest a prominent role of Trp residues in shaping the fluorescence spectrum of GvFFTR_WT. The peak at 333 nm and the shoulder around 352 nm are consistent with the characteristic fluorescence of buried and solvent-exposed Trp side chains, respectively. Consistent with this observation, each GvFFTR protomer contains five Trp residues, two of which are buried, two are solvent exposed, and one (Trp315) directly stacks against the FAD isoalloxazine.

On its side, within the flavin fluorescence range, the intensity of both visible emission and excitation spectra for GvFFTR_WT remains significantly low, indicating that the isoalloxazine's fluorescence is strongly quenched by the protein environment (Figure 8.6F, green color). Distinct alterations were evident in fluorescence spectra of GvFFTR_Δtail and GvFFTR_W315A compared to GvFFTR_WT. In both mutants, the overall emission intensity in the aromatic region significantly decreased relative to GvFFTR_WT (Figure 8.6E), although the peak/shoulder ratios remained largely unchanged (1.2, 1.1 and 1.1 for GvFFTR_WT, GvFFTR_Δtail and GvFFTR_W315A). These findings suggest that the side chain of Trp315, absent in the mutants, highly contributes to the overall Trp fluorescence in GvFFTR_WT. Interestingly, both mutants displayed a considerable increase in the flavin fluorescence quantum yield, with the effect being more pronounced in GvFFTR_Δtail (Figure 8.6F). The observed alteration in FAD fluorescence properties is likely a result of the loss of the Trp315-isoalloxazine interaction and of an increased exposure to solvent. This implies that both the C-terminal tail and the Trp315 side chain contribute to quench the isoalloxazine fluorescence in FFTR_WT by shielding it from the surrounding solvent. It is also noticeable the higher quantum yield exhibited by both mutants in comparison to free FAD. This observation aligns well with the concept of its adenine nucleotide portion folding over the isoalloxazine in the free cofactor, thus resulting in the fluorescence quenching of the latter but not in the mutated proteins. These findings confirm that FAD remains firmly bound in both GvFFTR mutants, where it retains an extended conformation while its isoalloxazine is solvent accessible. On its side, fluorescent properties of GvFFTR_C135S also resemble very much those of GvFFTR_WT, with the flavin fluorescence remaining highly quenched (Figure 8.6F).

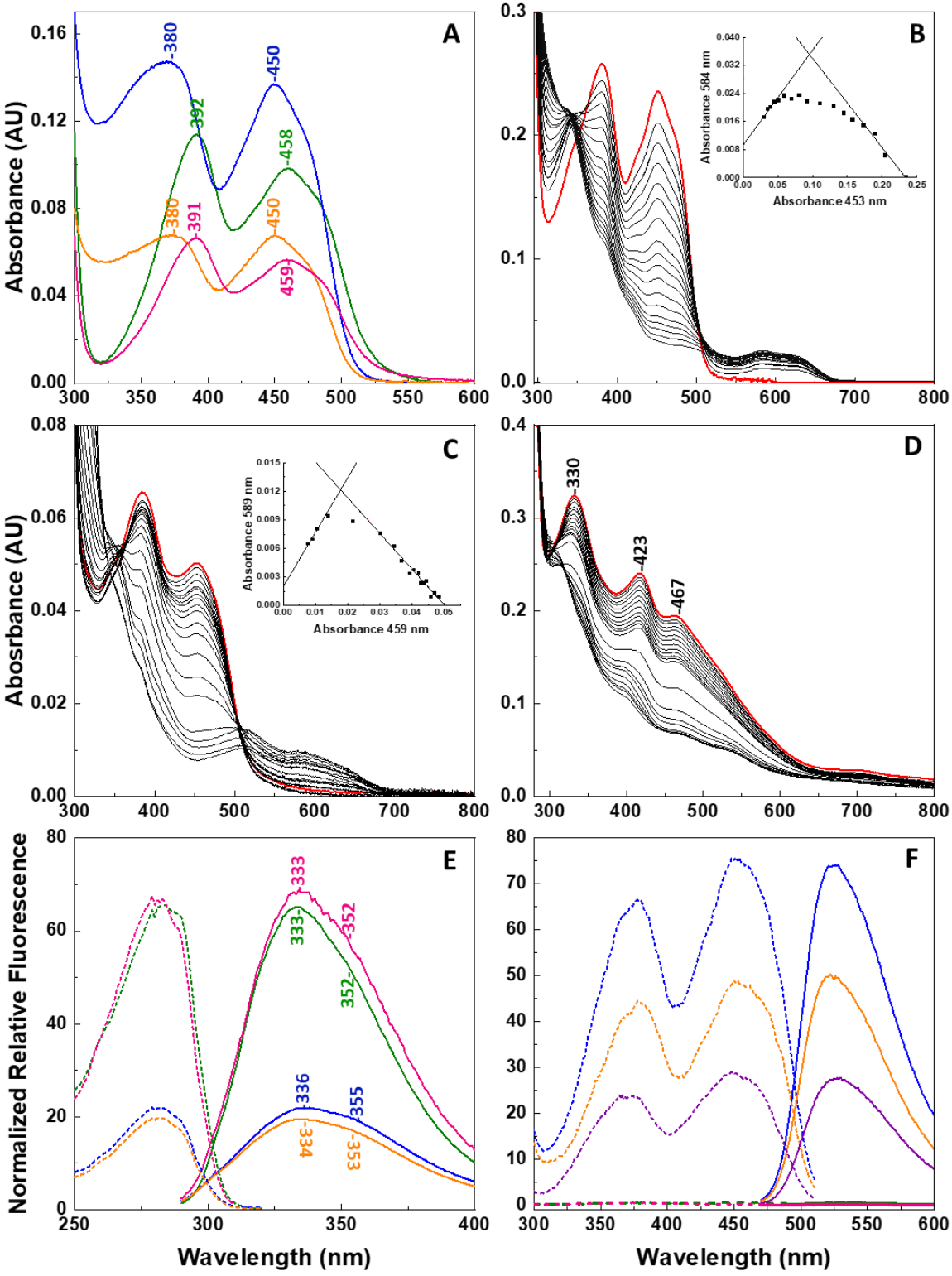

Figure 8.6. Spectroscopic properties of GvFFTR C-tail variants and GvFdx1. (A) Visible absorption spectra of oxidized GvFFTR_WT (green line, ~4.9 µM homodimer, herein all GvFFTR concentrations correspond to the homodimer ones), GvFFTR_Δtail (blue line, ~5 µM), GvFFTR_W315A (orange line, ~2.6 µM) and GvFFTR_C135S (magenta line, ~2.6 µM). Spectral evolution along photoreduction of **(B)** GvFFTR_W315A (~9 µM) and **(C)** GvFFTR_C135S (~2.4 µM). The inset shows the absorption at the neutral semiquinone band maximum (584 nm and 589 nm respectively) relative to absorption at the flavin band I maximum (453 nm and 459 nm respectively). **(D)** Spectral evolution along photoreduction of GvFdx1 (~25 µM). Photoreductions were performed under anaerobic conditions in the presence of 5-dRf (4 µM) and EDTA

(3 mM). Red spectra correspond to initial oxidized ones before addition of additives for photoreduction. Absorption and photoreduction spectra were recorded in 20 mM Tris/HCl, 150 mM NaCl, pH 8.0. **(E)** Far UV and **(F)** visible fluorescence spectra of GvFFTR_WT (green), GvFFTR_Δtail (blue), GvFFTR_W315A (orange) and GvFFTR_C135S (magenta line). Solid lines show the fluorescence emission spectra when exciting at 280 nm and 600 V in (E) and 460 nm and 700 V in (F), whereas dashed lines correspond to excitation spectra when collecting fluorescence at 333 (E) and 527 (F) nm. Panel (F) also shows the corresponding spectra for a free FAD solution (violet). Fluorescence spectra were recorded in 10 mM potassium phosphate, pH 8.0, at 25 °C and relative fluorescence is shown as normalized by protein concentration. In (A) and (E) relevant peaks in spectra are highlighted.

The collective evidences from these spectroscopic studies strongly suggest that while the absence of the Trp315 and of the C-terminal tail influences the electronic environment of the isoalloxazine in GvFFTR, it does not induce substantial conformational changes in the overall protein folding. Thus, it can be inferred that, as in GvFFTR_WT, the redox-active disulfide domains within the homodimer would maintain in GvFFTR_Δtail and GvFFTR_W315A the open conformation that positions the CxxC motifs distantly from their corresponding flavin partners in the resting state. This is consistent with previous findings from small-angle X-ray scattering (SAXS) studies, which demonstrated that deletion of the C-terminal tail has minimal impact on the overall structure of GvFFTR_Δtail. Additionally, the results indicate that the behavior of GvFFTR is similar to its *Clostridium acetobutylicum* homologue, despite the absence of the C-terminal tail extension in the latter (Buey et al., 2018, 2021). Both enzymes retain the open conformation, characterized by the positioning of their CxxC motifs away from the corresponding flavin redox partners, suggesting that this open conformation might be a conserved feature among related FFTR enzymes. On the contrary, the appearance of a band at 506 nm upon formation of the neutral FAD_{sq}/FAD_{hq} states in the GvFFTR_C135S mutant envisages alteration in its isoalloxazine environment upon reduction when compared to the WT protein. This is an interesting observation due to the long distance between the isoalloxazine and the introduced Ser135 in the open GvFFTR conformation. Therefore, this observation might be suggestive of a potential conformational change that migth allow formation of some type of charge transfer complex between the reduced isoalloxazine and either the Ser introduced at position 135 or the Thiol group of Cys138.

8.3.2 Insights into the reductive half-reaction mechanism: GvFFTR ability to become reduced by unspecific reductants

To test the impact of GvFFTR mutations on its FAD cofactor ability to accept electrons, spectral evolution of the reduction of the flavin of GvFFTR by DTH was first evaluated. DTH is a potent reductant (E^o=*-660 mV*) that rapidly reduces enzyme-bound flavins (particularly if their *midpoint reduction potential* values are in the -200 to +100 mV

range) (Moran, 2019). Noticeably, a large excess of DTH (50 mM) over GvFFTR_WT is required to initiate flavin reduction, and even with this excess, the process is extremely slow (Figure 8.7A). The neutral FAD_{sq} state is stabilized during the reduction, but it hardly evolves to achieve full reduction. Different behaviours are detected for the other evaluated mutants. GvFFTR_Δtail and GvFFTR_W315A become faster and fully reduced without apparent FAD_{sq} stabilization by using much lower concentrations of the reductant (5 mM) (Figure 8.7B and C). This is consistent with an earlier report of faster chemical reduction (using sodium dithionite) of GvFFTR_Δtail compared to GvFFTR_WT (Buey et al., 2021). Nonetheless, these two mutants differ in the overall spectral time evolution for FAD reduction. While the GvFFTR_Δtail process shows two phases of very different rates, separated by a lag period and accounting each for nearly half of the FAD band I reduction (insets Figure 8.7B), FAD reduction in GvFFTR_W315A appears to occur in a continuous phase (inset Figure 8.7C). GvFFTR_C135S was also able to nearly achieve the FAD_{hq} state without FAD_{sq} stabilization, and, as for GvFFTR_Δtail, two phases separated by a lag phase described the process (Figure 8.7D). Noticeably, for this mutant the first FAD reductive phase was much faster than the second, which was nearly as slow as the GvFFTR_WT reduction and also considerably slower than in the other two mutants (inset Figure 8.7D). Considering that $GvFFTR_{ox}$ is a dimer, the two phase reduction processes observed for GvFFTR_Δtail and GvFFTR_C135S, together with the absence of FAD_{sq} stabilization at any of the phases, suggest that, particularly in these two mutants, reduction by DTH of each FAD protomer within the GvFFTR dimer might occur at very different rates. Finally, reduction by DTH of GvFFTR_C135S presented another interesting feature, being the only variant that upon mixing with the reductant displayed an initial lag period, followed by an increase in the absorption at the ixoalloxazine band before it starts to apparently become slightly reduced (see below Figure 8.8). Collectively, these observations envisage that the C-terminal tail, the Trp315 residue, and the CxxC motif play relevant roles in modulating redox properties of the FAD cofactor within GvFFTR. This envisages that they might contribute to set its midpoint reduction potential, the access of reductants to the isoalloxazine and/or the cooperativity in the redox process occurring at both protomers.

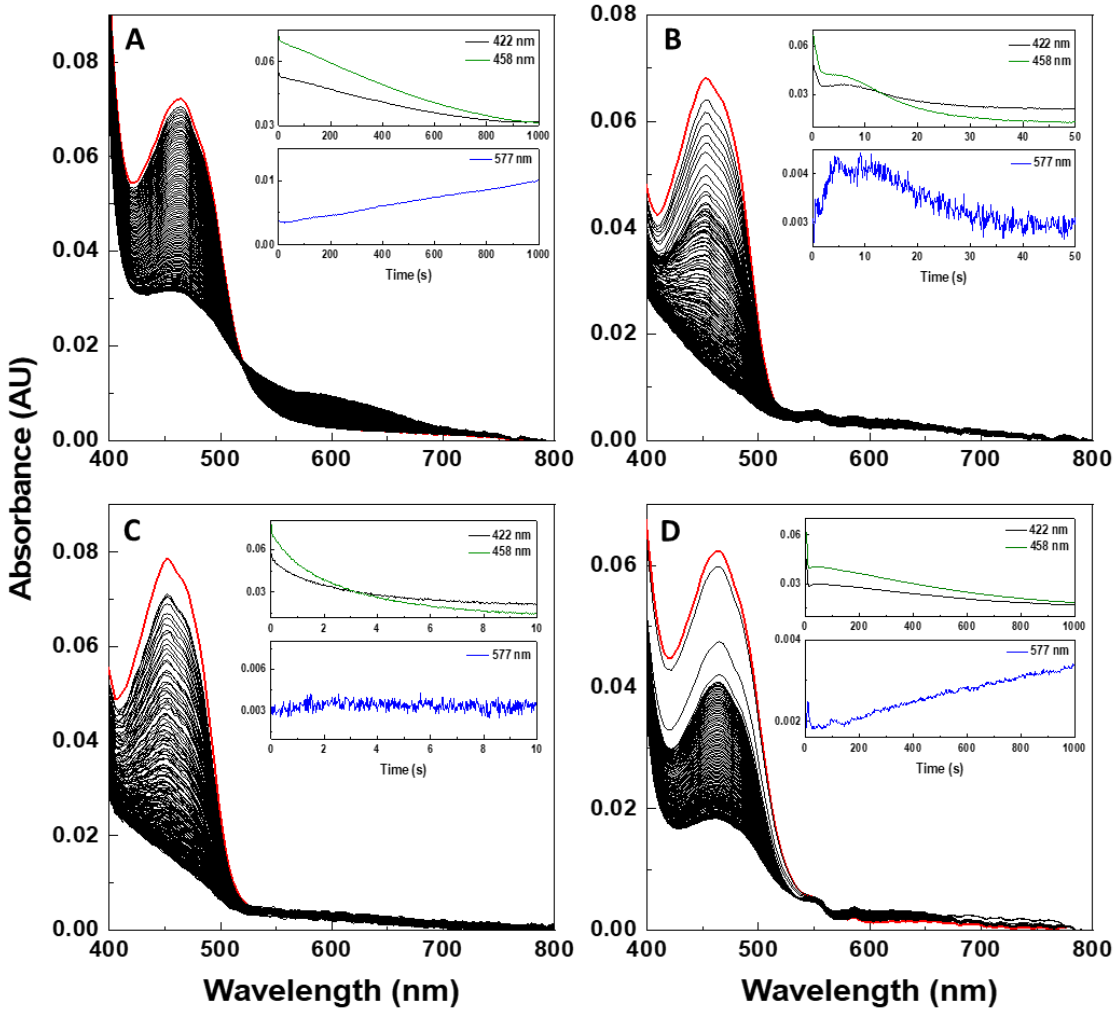

Figure 8.7. Spectral evolution upon GvFFTR reduction by sodium dithionite. Spectral evolution observed when mixing **(A)** GvFFTR_WT (~3.7 µM) with 50 mM sodium dithionite, **(B)** GvFFTR_Δtail (~3.4 µM) with 5 mM sodium dithionite, **(C)** GvFFTR_W315A (~3.1 µM) with 5 mM DTH and **(D)** GvFFTR_C135S (~3.1 µM) with 25 mM DTH in the stopped-flow equipment (final concentrations after mixing are indicated). DTH solutions were prepared in 20 mM Tris/HCl, 150 mM KCl, pH 8.0 under anaerobic conditions at 25 °C. Insets in panels portray kinetic traces at 422 nm (black), 458 nm (green) and 577 nm (blue). In all panels the first spectrum after mixing is shown in red line.

8.3.3 Insights into the reductive half-reaction mechanism: Light irradiation favors electron transfer from GvFdx1$_{rd}$ to GvFFTR

Previous studies have shown that GvFdx1$_{rd}$ serves as a functional electron-delivering partner to GvFFTR (Buey et al., 2021). To gain further insights into the ET from [2Fe-2S] GvFdx1$_{rd}$ to the FAD in GvFFTR, we investigate here such process by anaerobic mixing of GvFdx1$_{rd}$ (generated by photoreduction) and each of the GvFFTR$_{ox}$ mutants (WT, Δtail, W325A and C135S) (Figure 8.9). Spectral evolution upon mixing of the proteins at equimolecular amounts of their redox centers ([2Fe-2S] and FAD) is consistent with complete reduction up to the FAD$_{hq}$ state being achieved for GvFFTR_WT, GvFFTR_Δtail and GvFFTR_W315A variants (Figure 8.9A-C). This was an unexpected finding because,

under such conditions, the amount of $GvFdx1_{rd}$ in the mixture would provide only one of the two electrons required for the full reduction of the FAD within each GvFFTR_WT protomer. Furthermore, it was unforeseen that $GvFdx1_{rd}$ could effectively reduce the GvFFTR_Δtail and GvFFTR_W315A mutants, since isothermal calorimetry studies suggest that, differently to GvFFTR_WT, they exhibit either a lack of specific interaction with $GvFdx1_{ox}$ and, if there is any interaction, it occurs with a negligible change in enthalpy under the tested conditions (personal communication). Furthermore, activity assays using $GvFdx1_{rd}$ to provide reducing equivalents to GvFFTR demonstrate that these mutants were unable to effectively reduce Trx (Buey et al., 2021) (personal communication). Noticeably, when similarly mixing $GvFdx_{rd}$ with GvFFTR_C135S several differences in spectral evolution are observed (Figure 8.8 and 8.9D); i) the initial spectra after mixing showed absorbance increase at the flavin band I, a feature not observed for any of the other GvFFTR variants; ii) reduction was only achieved by a few isoalloxazine molecules; and iii) absorption changes were hardly observed in the 580-600 nm region where FAD_{sq} stabilization might be occurring along the process.

To better interpret the observed behaviors, several controls in the absence of $GvFdx1_{rd}$ were performed. Interestingly, despite de absence of the protein electron donor, these controls reveal that GvFFTR_WT reduction occurring through the neutral FAD_{sq} state. This reduction process is more pronounced in the 5-dRF/EDTA presence, but it is also observed to a lesser extent in their absence, particularly in the case of GvFFTR_Δtail and GvFFTR_W315A mutants (Figure 8.9E-H, 8.11 and 8.12). Since all GvFFTR variants are capable of undergoing photoreduction (Figure 8.6B-C, and 8.4), it is interpreted that prolonged exposure to the detection light source (150 W Xenon Lamp) within the observation chamber during the mixing and recording time promoted FAD photoreduction. This phenomenon is not uncommon among flavoproteins and has been reported for NTRs in the absence of their NADPH electron donor (Zanetti et al., 1968). Nonetheless, the kinetics of light-induced reduction differs among the evaluated GvFFTR variants. Derived absorption spectra for the kinetically distinguishable spectroscopic species and their interconversion k_{obs} values indicate that reduction is faster and achieves a greater degree of isoalloxazine reduction in GvFFTR_Δtail and GvFFTR_W315A compared to GvFFTR_WT and, particularly, GvFFTR_C135S (Figure 8.9E-H, 8.11 and 8.12). This agrees with above observations when using DTH as reductant (Figure 8.7).

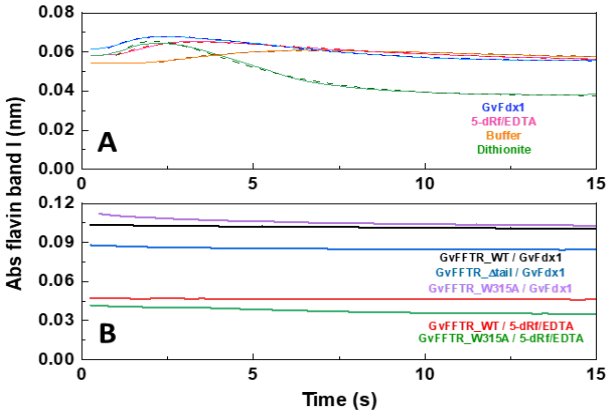

C

GvFFTR_C135S mixed with	$k_{obsA\rightarrow B}$ (s^{-1})	$k_{obsB\rightarrow C}$ (s^{-1})
GvFdx1	0.50	0.35
5-dRf/EDTA	0.58	0.18
Buffer	0.35	0.12
Sodium dithionite	0.58	0.54

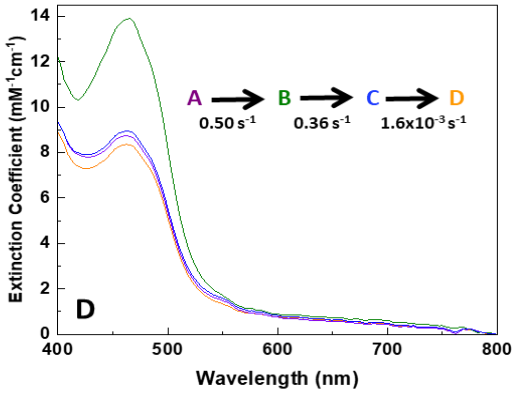

Figure 8.8. Analysis of the absorption evolution in mixes of GvFFTR_C135S. Traces showing absorption changes observed in the initial times upon mixing **(A)** GvFFTR_C135S (~3 µM) with GvFdx1 (1:1), 5-dRf/EDTA, buffer and DTH and **(B)** GvFFTR_WT, GvFFTR_Δtail and/or GvFFTR_W315A with either GvFdx1 (1:1) and with 5-dRf/EDTA. **(C)** Derived observed rate constants for initial absorption increase ($k_{obsA\rightarrow B,1}$) and subsequent absorption decrease ($k_{obsB\rightarrow C,1}$) in the different mixings of GvFFTR_C135S as evaluated in the first 40 s after mixing. **(D)** Absorption spectra for the kinetically distinguishable spectroscopic species obtained by the global-fitting analysis of processes observed upon mixing GvFFTR_C135S with GvFdx1 Errors in given k_{obs} values are within 10% of the value.

Furthermore, in the GvFFTR_WT controls, the photoreduction process best fit a single-step process, with the derived spectroscopic species compatible with the establishment of a $FAD_{ox/sq}$ equilibrium that is apparently displaced towards FAD_{ox}, while a subsequent very slow and slight increase in the FAD_{sq} band is detected over time (inset Figure 8.11A). On the contrary, reduction of GvFFTR_Δtail and GvFFTR_W315A by photoirradiation is best described by a three-step model (insets Figure 8.9F-, Figure 8.13B-C). The derived spectroscopic species for the mutants suggest that the reduction process extends beyond the FAD_{sq}, reaching even FAD_{hq} in GvFFTR_W315A (Figure 7.11B-C and 7.13B-C). Therefore, in the C-terminal tail GvFFTR mutants, the initial step involves formation of FAD_{sq}, the intermediate step results in minor spectroscopic changes which may reflect reorganization of the flavin electrostatics and/or of its environment, and the final step, which is much slower, involves the incorporation of a second electron to the FAD_{sq} to yield FAD_{hq}.

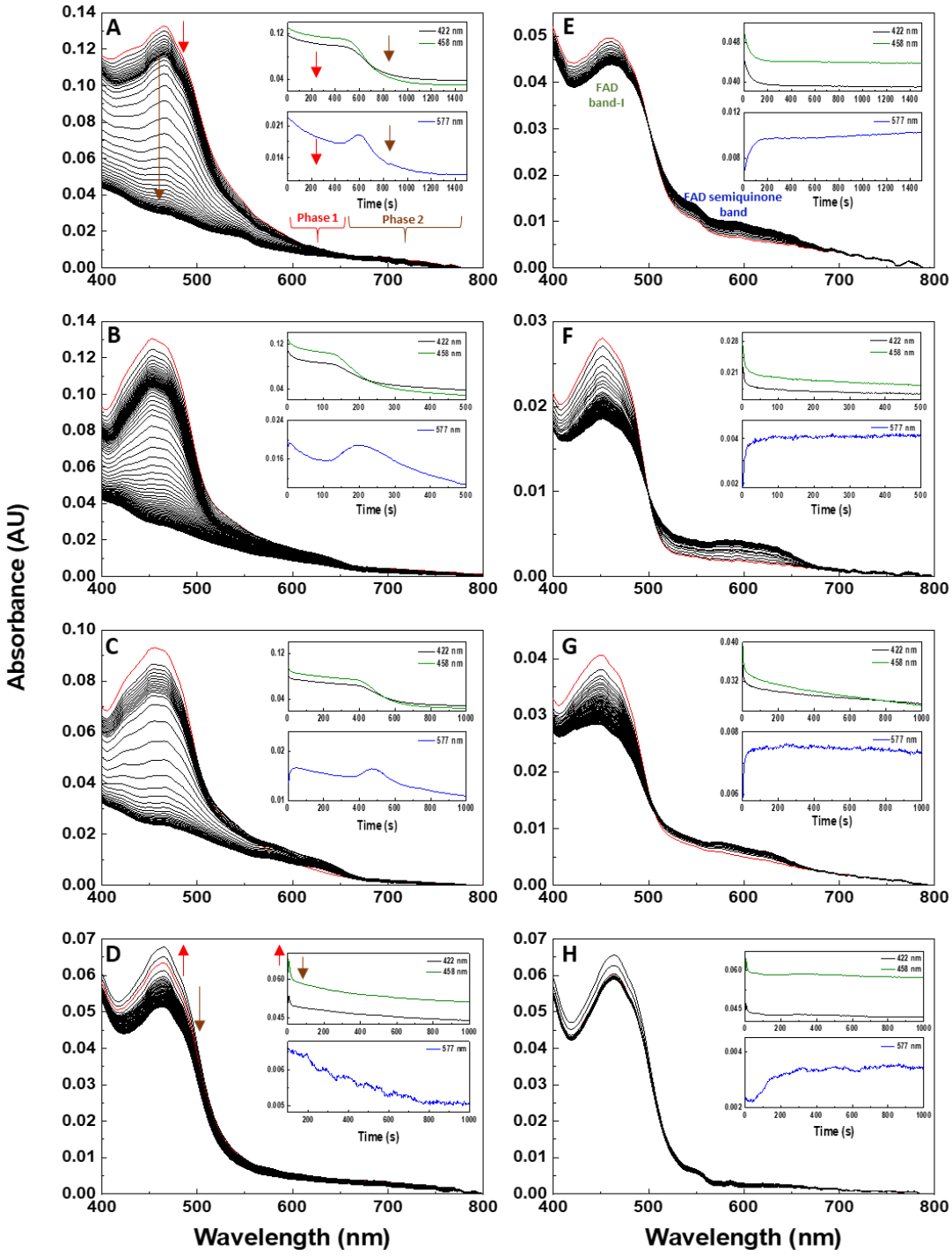

Figure 8.9. Reduction of GvFFTR homodimers by GvFdx1$_{rd}$ upon mixing on a stopped-flow equipment. Spectral evolution observed upon mixing GvFdx1$_{rd}$ with oxidized **(A)** GvFFTR_WT, **(B)** GvFFTR_Δtail, **(C)** GvFFTR_W315A and **(D)** GvFFTR_C135S (equimolar concentration of both proteins, ~5-10 μM GvFdx1$_{rd}$ and ~2.5-5 μM FFTR consider as final concentration of homdimer after mixing) in the stopped-flow equipment under anaerobic conditions. For (A), (B), (C) and (D) at least two major main stages or phases are envisaged, being the first and second indicated by arrows and brackets in panels (A) and (D) and respectively colored in red and brown. Controls showing spectral evolution elicited by the equipment light source in the absence of the electron donor protein in **(E)** GvFFTR_WT (~2.5 μM), **(F)** GvFFTR_Δtail (~1.1 μM), **(G)** GvFFTR_W315A (~1.3 μM) and **(H)** GvFFTR_C135S (~3 μM) upon mixing flavoprotein solutions with buffer solution in the absence of Fdx1$_{rd}$. All measurements were carried out in 20 mM Tris/HCl, 150 mM KCl, pH 8.0 under anaerobic conditions at 25 °C, and contained 1.5 mM EDTA and 2 μM 5-dRf. The corresponding

insets portray kinetic traces at 422 nm (black), 458 nm (green) and 577 nm (blue) nm, following respectively maximal absorption wavelengths for oxidized GvFdx1, band-I of oxidized flavin and band of neutral semiquinone flavin. In all panels the first spectrum after mixing is shown in red line.

Overall, the easier reduction observed in these mutants compared to WT suggests for them less negative midpoint reduction potentials, particularly for the $E_{sq/hq}$ pair. This also agrees with their considerably lower ability to stabilize FAD_{sq} as compared to GvFFTR_WT. Finally, GvFFTR_C135S is the variant less prone to isoalloxazine reduction upon photoirradiation and, again, the only one were initial spectra upon mixing produced an increase in the flavin band I absorption (Figure 8.8, 8.9H, 8.11D and 8.12D). This might envisage a potential change in the isoalloxazine environment upon light photoirradiation, producing a conformation apparently less prone for FAD reduction than GvFFTR_WT. Regarding light-induced reduction in the mixing chamber, it is worth noting that photoreduction of $GvFdx1_{ox}$ was also detected in the stopped-flow chamber (Figure 8.10E). Therefore, when going back to the reactions of $GvFFTR_{ox}$ variants with $GvFdx1_{rd}$, the results indicate that, under our experimental conditions, not only $GvFdx1_{rd}$ but also photoirradiation contribute to generate the FAD_{hq} state in GvFFTR_WT, GvFFTR_Δtail and GvFFTR_W315A (Figure 8.9A-C, 8.10). Furthermore, it is observed that in any of these cases FAD_{sq} accumulates in the presence of GvFdx1, suggesting that photoirradiation of reoxidized $GvFdx1_{rd}$ within the stopped-flow chamber contributes to achieve a second flavin reduction cycle, potentially by the same GvFdx1 molecule that has been re-reduced. Here, we also must consider that absorption changes in the flavin band I region (exemplified in Figure 8.9 insets at 422 and particularly the flavin band I), either upon ET from $GvFdx1_{rd}$ to GvFFTR or upon photoreduction, will be composed by the increase due to $GvFdx1_{rd}$ re-oxidation and the decrease due FAD band I reduction (Figure 8.9).

Similarly, at the neutral FAD_{sq} band (Figure 8.9 insets at 577 nm) absorption increases might be related to FAD_{sq} formation and/or $GvFdx1_{rd}$ re-oxidation, while decays can indicate $GvFdx1_{ox}$ reduction and/or FAD_{sq} transformation into FAD_{hq}. Altogether, this makes spectral evolution complex and difficult to deconvolute, but a careful analysis can bring some information. For the C-terminal tail variants and, but, particularly for GvFFTR_WT (Figure 8.9, compare panels A and D), it is evident that the 5-dRf/EDTA-irradiating environment promotes reduction of the flavin by GvFdx1 up to the FAD_{hq} state.

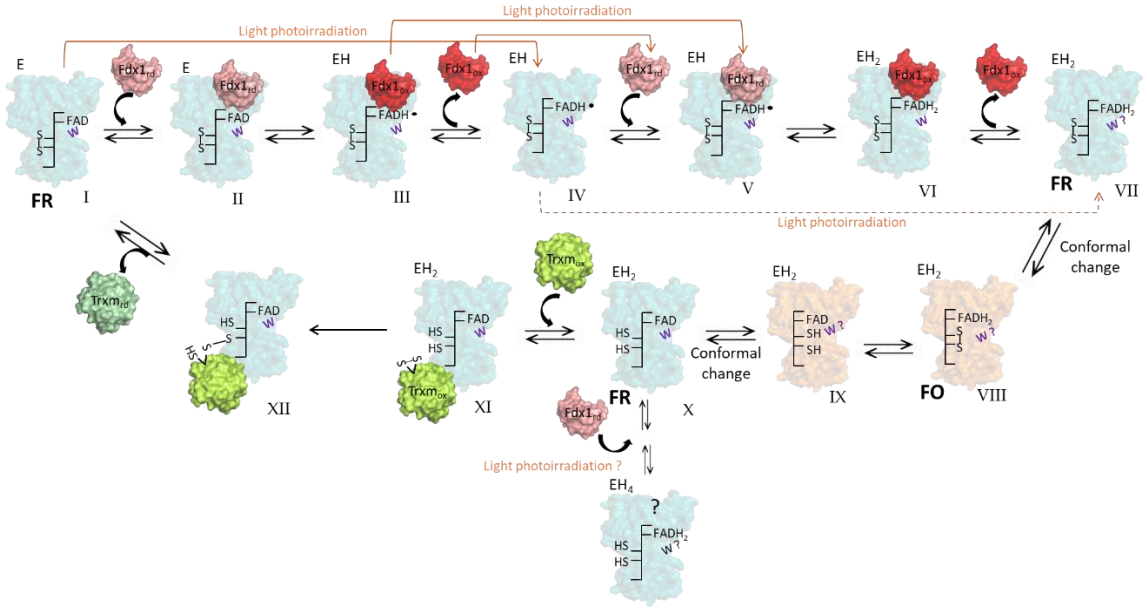

Figure 8.10. Working hypothesis for the mechanisms of GvFFTR. During the FAD reductive half reaction (I to VII) the GvFFTR maintains an unrotated open flavin reducing conformer (FR state) that allows its FAD_{ox} and the [2Fe2S] of $GvFdx1_{rd}$ being juxtaposed, so ET must occurs. Two $GvFdx1_{rd}$ molecules must sequentially access to the FAD cofactor of GvFFTR, the first one reducing it to FAD_{sq} and the second producing the FAD_{hq} state. To initiate the FAD oxidative reaction a rotation to a closed flavin oxidizing conformation (FO state) (VII to VIII) will be required to allow juxtaposition of the FAD_{hq} and the CxxC at the disulfide domain. Once the disulfide becomes reduced, a subsequent conformational change (probably reversion to the FR state) will allow $GvTrxm_{ox}$ coupling to the disulfide domain and dithiol exchange. Final release of $GvTrxm_{rd}$ will recover the starting GvFFTR FR state to initiate a new catalytic cycle. Apart from $GvFdx1_{rd}$, photoirradiation can also contribute to generate the reduced FAD states, particularly FAD_{sq}, as well as to regenerate $GvFdx1_{rd}$ from $GvFdx1_{ox}$. Photoirradiation processes more prone to produce GvFFTR_WT reduction, according to this study, are indicated by orange lines, while those potentially less probable are shown in orange dashed lines. Continuos photoirradiation and further supply of $GvFdx1_{rd}$ might also envisage formation of GvFFTR states where both FAD and the CxxC motive remain reduced. GvFFTR_W315 from the neighbor protomer stacking the FAD in FR conformations is indicated as a violet "W", while it is indicated as "W?" for FO conforms because its position is not clear.

Absorption decays at 422 nm and the flavin band I, correlating with FAD reduction for all these GvFFTR variants, indicate that this process occurs in at least two major kinetic phases separated by a lag period (insets Figure 8.9A-C), with the second phase achieving the full production of FAD_{hq} (insets Figure 8.9A-C). Noticeably, the absorption changes at 577 nm in both phases of the mutants show similar patterns, with initial increases suggesting FAD_{sq} formation followed by subsequent absorption decreases that correspond well with the transition to FAD_{hq} (Figure 8.9A-C, Figure 8.13D-F). Despite the spectroscopic complexity of the system, for the above mentioned variants we are able to fit phase 1 into a two-step process (Figure 8.13D-F). For the first step of phase 1 in the mutants, $k_{obsA \rightarrow B,1}$ values and their corresponding derived spectroscopic species match those of the controls in the absence of GvFdx1, suggesting a contribution of photoirradiation to this step despite the GvFdx1 presence.

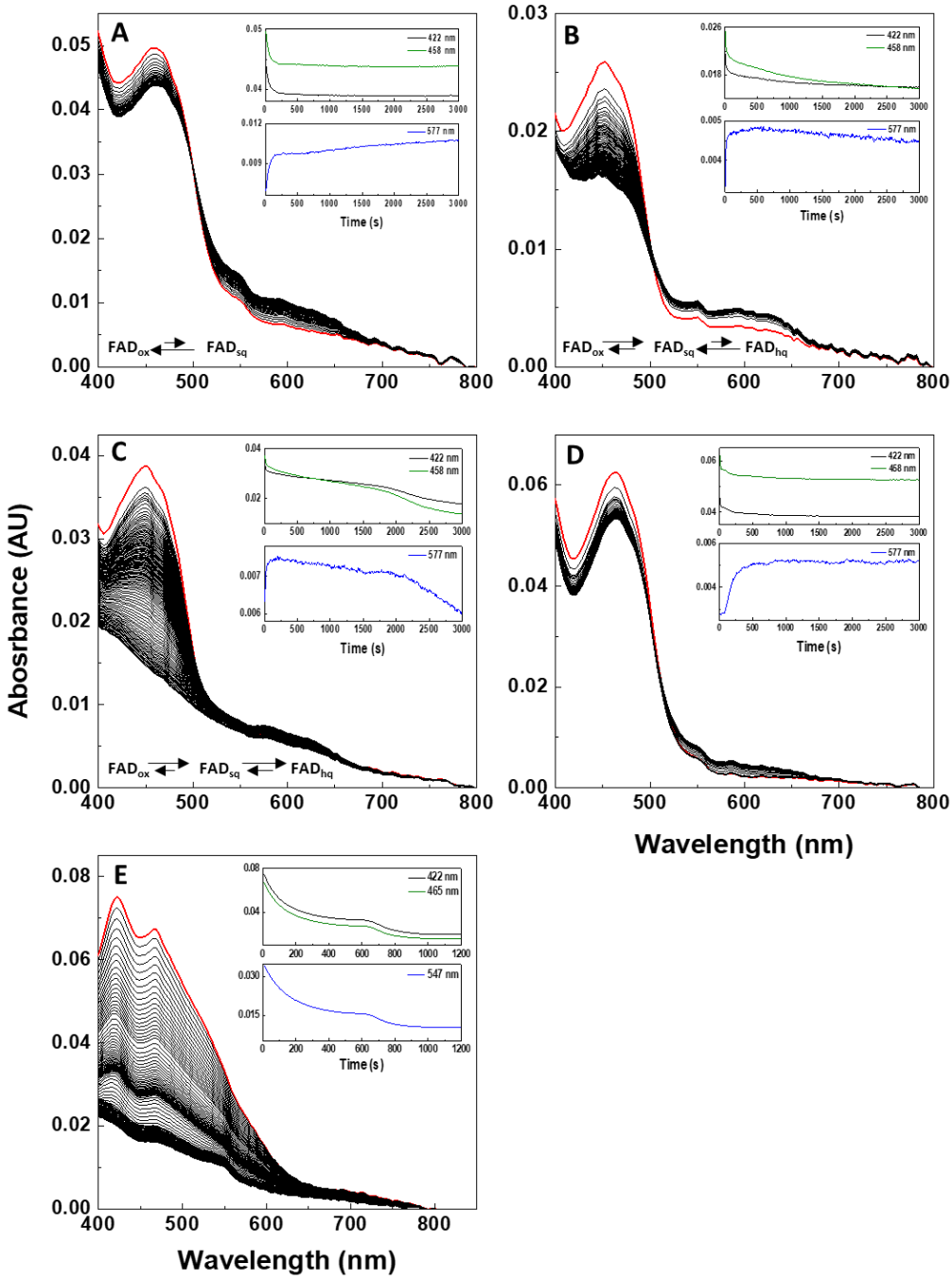

Figure 8.11. Spectral evolution for evaluation of the impact of photoirradiation by the light source of the stopped-flow equipment on GvFFTR reduction in the presence of the 5-dRf/EDTA system. Spectral evolution (3000 s) within the stopped-flow chamber of **(A)** GvFFTR_WT (~2.5 µM, considering homodimer), **(B)** GvFFTR_Δtail (~1.1 µM), **(C)** GvFFTR_W315A (~1.3 µM), **(D)** GvFFTR_C135S (~3.3 µM) and **(E)** GvFdx1 (~8.1 µM) upon mixing with buffer solution. Measurments carried out in 20 mM Tris/HCl, 150 mM KCl, pH 8.0 under anaerobic conditions at 25 °C, and containing 1.5 mM EDTA and 2 µM 5-dRf. Insets in panels A-B portray kinetic traces at 422 nm (black), 458 nm (green) and 577 nm (blue) nm, following respectively maximal absorption wavelengths for oxidized Fdx1, oxidized band I of the flavin and neutral semiquinone band of the flavin for GvFFTR_WT, GvFFTR_Δtail and GvFFTR_W315A, and at 422 nm (black), 465 nm (green) and 547 nm (blue) for GvFdx1. In all panels the first spectrum after mixing is shown in red line.

In GvFFTR_WT, the presence of GvFdx1 prevents the observation or stabilization of intermediate FAD_{sq}, but clearly enhances the rate of the process that initiates its reduction process (Figure 8.9A and 8.13A-D). In all cases, the second step of phase 1 despite showing faster FAD reduction ($k_{obsB\rightarrow C,1}$) compared to the absence of GvFdx1, indicates that full reduction of all flavin molecules within the GvFFTR homodimers is still far from being achieved, particularly in GvFFTR_WT. Phase 2 is complicated to deconvolute, but it is consistent with a first step involving the re-oxidation of $GvFdx1_{rd}$ (likely previously regenerated by photoirradiation) and the formation of FAD_{sq}, followed by a second reduction step to the FAD_{hq} state. The fact that FAD_{sq} is first formed and subsequently transformed to FAD_{hq} in both phases indicates that $GvFFTR_{sq}$ is more eager to accept an electron from the potential donating electron than $GvFFTR_{ox}$. Therefore, only a fraction of the total flavin cofactors in FFTR undergo reduction to the FAD_{hq} state. It is important to note that under the assay conditions, full formation of $GvFFTR\_WT_{hq}$ could not be achieved solely by photoirradiation in the absence of GvFdx1, while in the mutants it would require longer times (Figure 8.9D-F and 8.11A-C). Altogether, these observations lead us to propose that, under the assayed conditions: i) both EDTA/light and $GvFdx1_{rd}$ contribute to generate the FAD_{sq} state in GvFFTR_WT, and ii) FAD_{sq} does not accumulate in the presence of $GvFdx1_{rd}$ (Figure 8.9A and E) because GvFdx1 delivers a second electron to the flavin resulting in the formation of FAD_{hq}. Furthermore, the lower kinetic stability of FAD_{sq} in the C-terminal tail mutants suggests that upon photoirradiation it may readily capture electrons from $GvFdx1_{rd}$ without formation of a stable transient complex stabilized through specific interactions.

Spectroscopic changes of GvFFTR_C135S upon mixing with $GvFdx1_{rd}$ considerably differ from the rest of the variants. Spectral evolution shows a fast increase in the absorbance of the isoalloxazine band I, that is followed by its decrease (Figure 8.8). The overall process occurs without apparent stabilization of any transient FAD_{sq} and the final spectroscopic species only account by a small fraction of FAD molecules in the mixture achieving the FAD_{hq} state (Figure 8.8D and 8.9D). Noticeably, if we consider the maximum reached upon missing of the Flavin band I, the total amount of FAD_{hq} achieved might be close to what we were initially expected for all variants, given the amount of $GvFdx1_{rd}$ in the mixture would just provide one of the two electrons required for the full reduction of each FAD molecule within GvFFTR. Thus, as shown by the controls in the absence of GvFdx1, in this mutant the 5-dRf/EDTA-irradiating environment hardly contributes to promote reduction of the flavin of GvFFTR by GvFdx1.

Overall, these kinetic characterizations indicate that under our experimental conditions the reduction of the FAD of GvFFTR_WT is a relatively slow process where electrons are provided either by light irradiation or $GvFdx1_{rd}$. In addition, while removal of W315 and the C-terminal tail favours FAD reduction, replacement of Cys135 at the disulfide motif prevents reduction of FAD by both $GvFdx1_{rd}$ and photoirradiation.

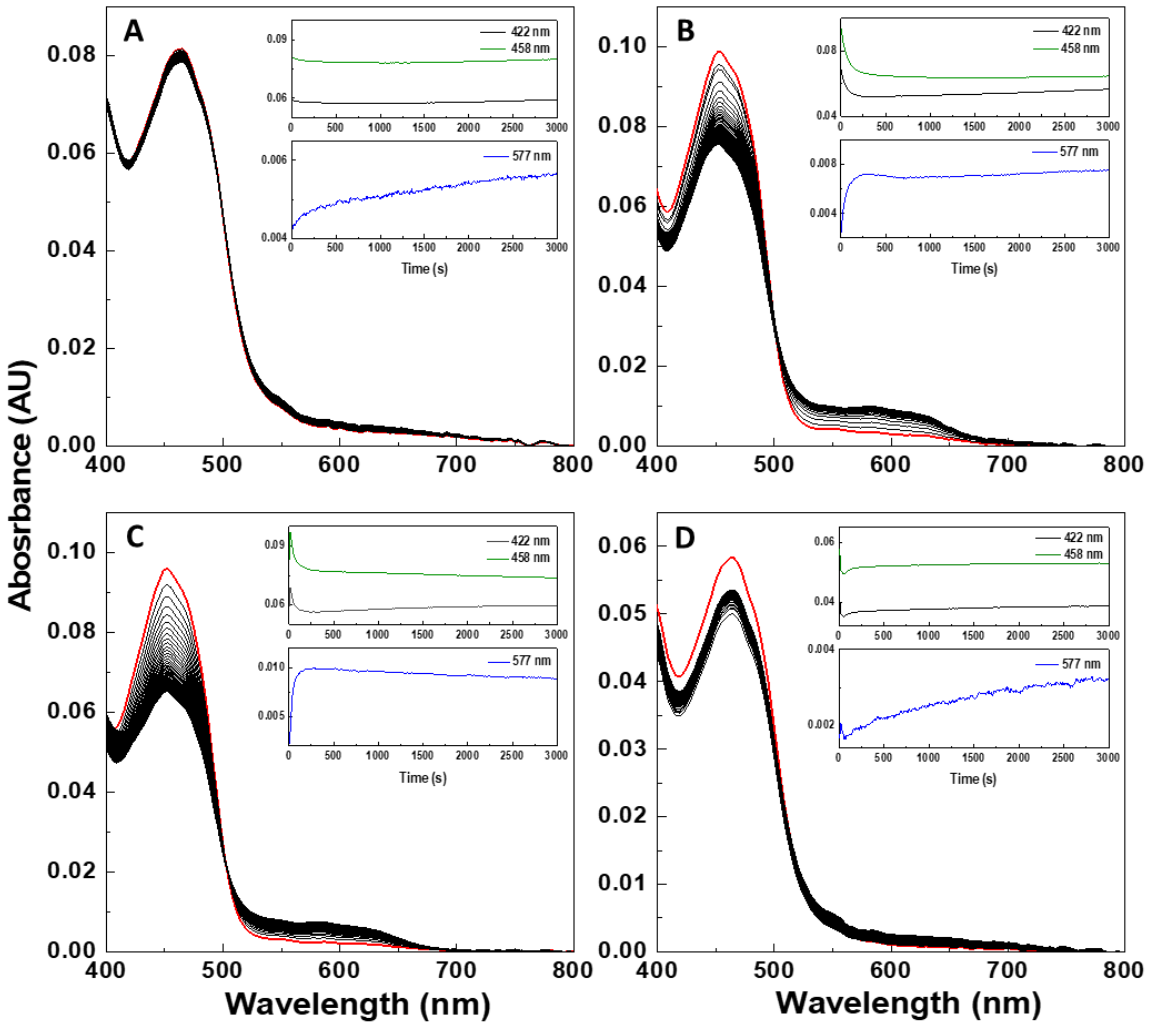

Figure 8.12. Spectral evolution for evaluation of the impact of photoirradiation by the light source of the stopped-flow equipment on GvFFTR reduction in the absence of the 5-dRf/EDTA system. Spectral evolution (3000 s) produced by the light source of the stopped-flow equipment within the chamber when mixing **(A)** GvFFTR_WT (~4.0 µM), **(B)** GvFFTR_Δtail (~3.8 µM), **(C)** GvFFTR_W315A (~3.6 µM) and **(D)** GvFFTR_C135S (~2.8 µM) with 20 mM Tris/HCl, 150 mM KCl, pH 8.0 under anaerobic conditions at 25 °C, and in the absence of 5-dRf/EDTA. Insets in panels portray kinetic traces at 422 nm (black), 458 nm (green) and 577 nm (blue). In all panels the first spectrum after mixing is shown in red line.

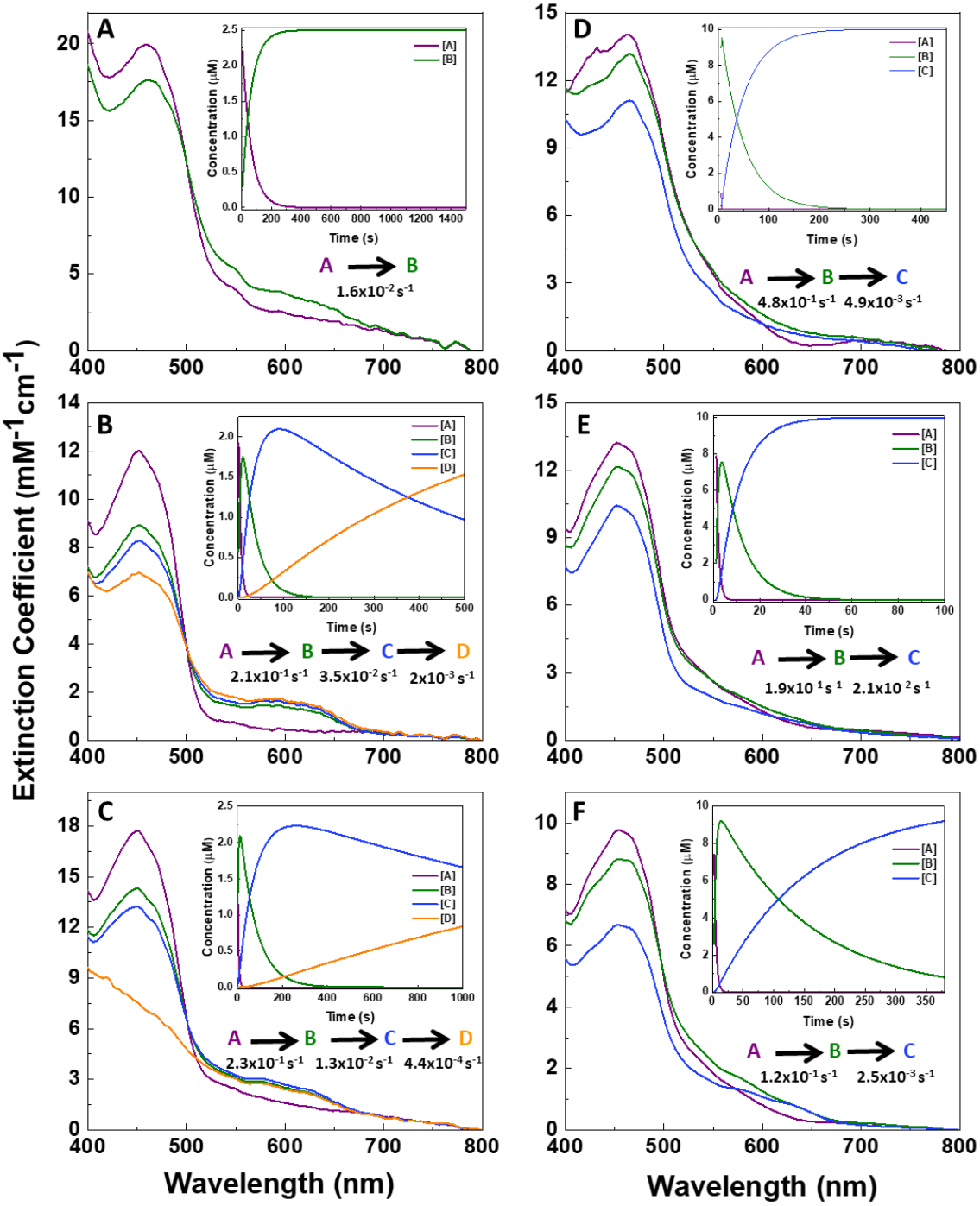

Figure 8.13. Deconvolution analysis for the reduction of FFTR homodimer on a stopped-flow equipment. Absorption spectra for the kinetically distinguishable spectroscopic species obtained by the global-fitting analysis of processes observed upon photoirradiation by the light source of the stopped-flow equipment in the presence of of 5-dRf/EDTA of **(A)** GvFFTR_WT, **(B)** GvFFTR_Δtail, and **(C)** GvFFTR_W315A. Absorption spectra for the kinetically distinguishable spectroscopic species obtained by the global-fitting analysis of overall phase 1 processes observed upon mixing **(D)** GvFFTR_WT, **(E)** GvFFTR_Δtail and **(F)** GvFFTR_W315A with GvFdx1$_{rd}$ within the stopped-flow equipment. Spectral deconvolutions were obtained by fitting to one-, two- or three-step models (A→B, A→B→C or A→B→C→D), showing for each panel the corresponding kinetic model as well as the observed kinetic constants for each step. In all cases insets show the corresponding evolution of A to D species along the time. Global-fit analysis correspond to data presented in Figure 8.6. Measurments carried out in 20 mM Tris/HCl, 150 mM KCl, pH 8.0 under anaerobic conditions at 25 °C, and containing 1.5 mM EDTA and 2 μM 5-dRf. Errors in given k_{obs} values are within 10% of the value.

8.3.4 Midpoint reduction potentials of FFTR variants

The above observations took us to determine the impact of the mutations in the FAD midpoint potential of GvFFTR. Figure 8.14 shows some examples of the spectral evolutions of the mixture of protein and dyes obtained in such determinations. The corresponding analysis yielded very negative $E_{ox/hq}$ values for GvFFTR_WT, -448 ± 8 mV, and GvFFTR_C135S, -420 ± 8 mV, while the corresponding values for GvFFTR_Δtail and GvFFTR_W315A mutants were -247 ± 4 mV and -242 ± 4 mV respectively. These data confirm that the C-tail, and, particularly, W315 are key elements to set the midpoint reduction potential of the FAD cofactor of GvFFTR_WT in very negative values, particularly by setting its $E_{sq/hq}$ redox-pair to relevant negative values that allow for FAD_{sq} stabilization. On the contrary, replacement by a Ser of the first Cys of the CxxC motif at the disulfide domain hardly impacts on the redox properties of the GvFFTR flavin cofactor. Similarly, the mid-point potential of the FAD_{ox}/FAD_{hq} pair in *E. coli* NTR has been shown to be hardly sensitive to replacement of any of the two Cys residues of its CxxC motif by Ser (Prongay & Williams, 1992).

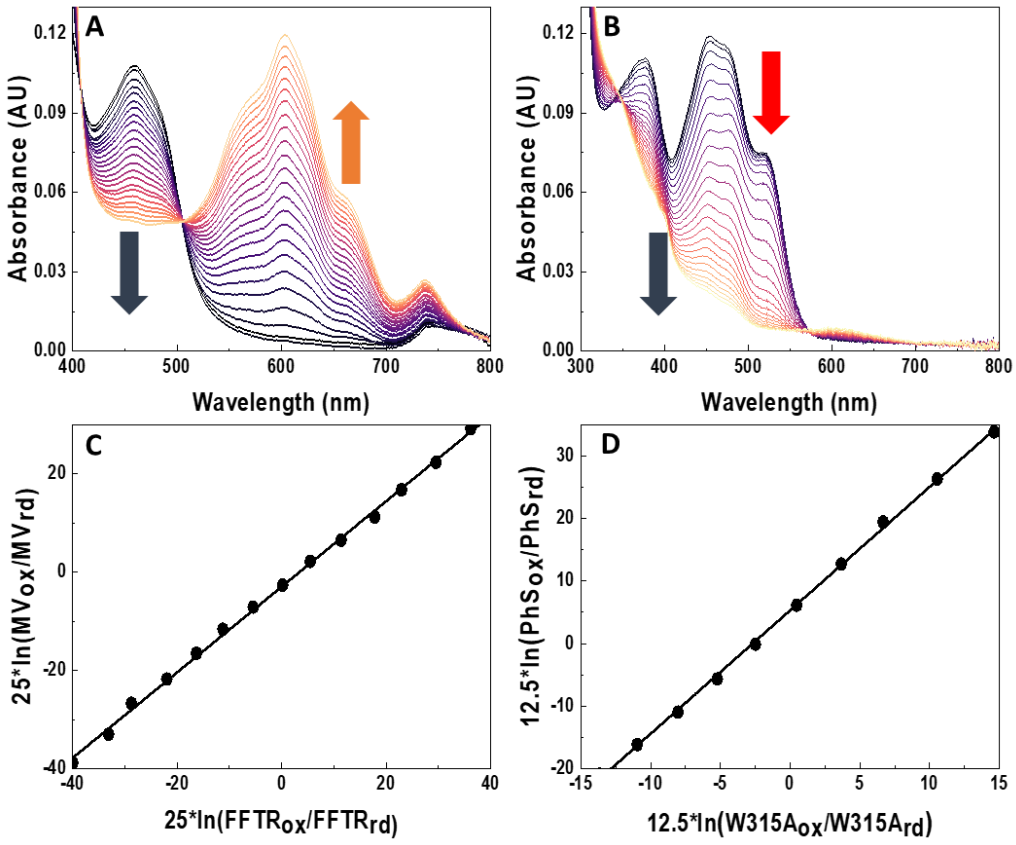

Figure 8.14. Midpoint reduction potential for GvFFTR_WT and GvFFTR_W315A. Spectral evolution upon midpoint reduction potential assessment for **(A)** GvFFTR_WT and **(B)** GvFFTR_W315A in samples containing respectively as dye methyl viologen and phenosafranine. Coloured visible absorption spectra in

dark blue to orange degradation correspond to different time points along protein/dye reduction. Samples were premixed with benzyl viologen (absent in (A)), xanthine and the dye of choice, made anaerobic by several cycles of vacuum application and bubbling with O2–free argon, and subsequently mixed with xanthine oxidase. Spectra were recorded every 3–5 min for up to 2 h, at 25 °C in 20 mM Tris/HCl pH 8.0, 150 mM NaCl. Blue, orange and red arrows represent changes at the flavin band I (~460 nm band), methyl viologen (600 broad band) and phenosafranine (512 nm band). **(C)** and **(D)** show the respective logarithm of the ratios of oxidized/reduced dye and oxidized/reduced protein at different time points of the reduction, which were calculated using equations 1 and 2 and using absorption data at 458 nm and 600 nm for the respectively flavin band I and methyl viologen in the GvFFTR_WT case and at 453 nm and 512 nm respectively flavin band I and phenosafranine.

8.4 DISCUSSION

The data here presented for GvFFTR_WT, GvFFTR_ Δtail and GvFFTR_W315A provide strong evidence that both the Trp315 side chain and the C-terminal tail play critical roles in setting the chemistry of the FAD cofactor within GvFFTR. Specifically, they show that despite removal of both elements does not produce a significant impact on the overall protein folding, they are crucial in conferring the significant low midpoint reduction potential value exhibited GvFFTR_WT. Moreover, the C-terminal tail is also a key element in stabilizing the neutral FAD_{sq}, a feature that is of particular relevance in GvFFTR when considering the single-electron exchanger GvFdx1 as its putative *in vivo* donor (Buey et al., 2021). This makes necessary two consecutive ET processes from two $GvFdx1_{rd}$ molecules to achieve GvFFTR reduction to the FAD_{hq} state that is necessary to reduce the CxxC motif at the redox-active disulfide domain. Stacking and hydrogen/ionic bonding of aromatic residues to the isoalloxazine usually contribute to shield it from the solvent, being also are recurrent strategies to set midpoint reduction potentials in very negative values for some flavoproteins (Frago et al., 2007; Hamdane et al., 2015; Lostao et al., 1997; Nogués et al., 2004). Thus, their removal generally produces variants less prone to stabilize semiquinone states and exhibiting considerably less negative midpoint reduction potentials, as here observed for GvFFTR. Such alterations usually have as a consequence the dysregulation of the redox processes in which the flavoprotein participates, but in many cases these residues and the regions containing them are also critical to allocate the substrate during catalysis and/or to release the product after completion of the ET (Frago et al., 2007; Hamdane et al., 2015; Lans et al., 2010, 2012; Lostao et al., 1997; Nogués et al., 2004).

The kinetic studies here presented for tracking the reduction of the FAD of GvFFTR by GvFdx1 have revealed intriguing insights. One of them is that this ET process appears relatively slow for GvFFTR_WT but becomes more efficient upon the removal of either the Trp315 residue or the C-terminal tail. This enhancement can be attributed to the very negative redox potential of the FAD within GvFFTR_WT, which not only affects ET from

GvFdx1 but also substantially retards its reduction by DTH or light irradiation. In agreement, the mutants with less negative midpoint potential and reduced FAD_{sq} stabilization exhibit greater propensity for complete reduction. Another intriguing finding from our kinetics experiments is the capability of the instrument observation light to trigger the reduction of the flavin in GvFFTR_WT, GvFFTR_ Δtail and GvFFTR_W315A as well as of the iron sulfur cluster of GvFdx1, even in the absence of 5-dRF/EDTA. This observation led to the finding of photoirradiation-induced reduction of GvFFTR and GvFdx1 samples within the stop-flow chamber, thereby augmenting the ability of GvFdx1 for ET to GvFFTR through the FAD_{sq} state. In this context, it is worth to note that a similar behavior was reported in the overall reduction of NTRs by NADPH upon photoirradiation (Zanetti et al., 1968), despite in this case FAD_{sq} does not participate in the catalytic reaction because all its electron donors/acceptors are obligatory two-electrons exchangers. In contrast, FAD_{sq} assumes a catalytically active role in GvFFTRs (as depicted in Figure 8.10) since its electron donor, $GvFdx1_{rd}$, can only donate a single-electron at a time. This requires the transient stabilization of FAD_{sq} before binding of a second $GvFdx1_{rd}$ for the subsequent transfer of the second electron to generate FAD_{hq}. Figure 8.10 summarizes a possible representation of the conformational changes and redox cofactor states expected during the GvFFTR_WT catalytic cycle for ET from $GvFdx1_{rd}$ to FAD and subsequently to Trx_{ox}. Figure 8.10 highlights several reaction steps where light irradiation might contribute to the photoreduction of GvFFTR and Fdx1. Overall, it suggests that both GvFFTR and GvFdx1 can acquire electrons through a combination of 5-dRf/EDTA and light. Additionally, the scheme highlights that FAD_{sq} could potentially accept electrons through photoirradiation within transient associations with $GvFdx1_{ox}$ and without the need for additional $GvFdx1_{rd}$ molecules. This complex interplay of ET pathways underscores the intricate mechanisms underlying the redox dynamics within the GvFFTR and GvFdx1 system in our experimental framework.

The information here presented confirms therefore the critical importance of Trp315 and the C-terminal tail in setting the FAD redox properties within the GvFFTR enzyme, but particularly provides unexpected observations that hold implications for a more comprehensive understanding of its physiological mechanism within the context of the oxygenic photosynthetic organism. Taken together, our results allow us to propose a reductive model specific for cyanobacterial-type FFTRs, distinguishing them from the functional mechanism employed by NTRs enzymes. Indeed, the distinctive two-ET

capability of Fdx observed in clostridial FFTR enzymes (Buey et al., 2018) provides a compelling explanation for the absence of the C-terminal tail structural component of the system. This structural variation likely reflects an evolved mechanism tailored to accommodate the unique ET requirements of these enzymes. Of particular intrigue is the revelation that light plays a role in the enzyme's reduction process, prompting avenues for future investigations. It is worth noting that our experiments highlight the inherent kinetic constraints of the reduction process and raise questions about its viability in a cellular context. The experimental results corroborate that the basal state of the protein, in the absence of Trx and specific targets, adopts a conformation poised for Fdx1 reduction. However, it appears that additional effectors might be required to achieve efficient reduction of the FAD cofactor.

The so far available experimental structural data do not envisage the need for displacement of the C-terminal tail to achieve ET from Fdx1 to GvFFTR_WT. However, such displacement is a requirement for stacking of the CxxC motif of the disulfide domain onto the reduced isoalloxazine, so ET from the second to the first would occur yielding its dithiol form. Displacement of the C-terminal tail in GvFFTR will then only transiently occur, and it might depend on its isoalloxazine being in a reduced state. Moreover, stabilization of the disulfide motif in the optimal closed conformation for the efficient ET from the isoalloxazine to the CxxC motif might be also influenced by the displaced C-terminal tail. In addition, once the ET has occurred the C-terminal tail might also favour displacement of the disulfide motif upon getting to its resting state position. Such hypotheses can be supported by our characterization of the GvFFTR_C135S mutant. Upon photoreduction of GvFFTR_C135S we observe spectral features that can be related to charge transfer interactions between the FAD_{sq}/FAD_{hq} and the hydroxyl or thiol, respectively, of the Ser and Cys residues at the SxxC motif that now are already reduced. Under such situation, no ET from the isoalloxazine to its natural CxxC acceptor might occur, but the charge transfer interaction might contribute to stabilize the closed flavin oxidizing conformation preventing subsequent flavin reduction processes. These observations are supported by studies on similar EcNTR mutants at the CxxC motif that are shown to be active for flavin reduction, while showing the ability of a Ser at the second Cys position of the mutant to even covalently bind to the flavin stabilizing the closed conformation (Prongay et al., 1989; Prongay & Williams, 1990). Full reduction of the C-terminal tail mutants being observed as faster than in GvFFTR_WT, also supports a dynamic and conformational role of Trp315 and of the C-

terminal tail. Here, we must remember that these two mutants have been shown unable to effectively reduce Trx and to specifically bind GvFdx1, observations that envisage observed kinetic processes potentially diverging for these variants. We might suspect that in GvFFTR_WT we are observing reduction all the way through from GvFdx1, to the FAD and from it to the CxxC motif at the disulfide domain. In this situation several conformational changes will be required to alternate conformations allowing flavin reduction and oxidation, and a number of reducing equivalents adding those of the flavin and the CxxC motif will be required to observe the FAD_{hq} state. On the contrary, flavin reduction processes when lacking Trp315 and/or the C-terminal tail could be favoured as a consequence of un-specific GvFdx1:GvFFTR interactions that facilitate reduction of the isoalloxazine from the thermodynamic point of view, while ET from FAD to the CxxC motif not being achieved because the C-terminal tail fails to promote its competent catalytic orientation regarding the flavin. In this case, the observed final reduction point in the mutants might only be flavin reduction, thus being observed as a faster process. In this context, the contribution of the disulfide bridge appears to be intricate, and the impact of conformational changes and potential alterations in the redox state of the disulfide within the enzyme warrant further exploration.

In summary, the multifaceted interplay between Trp315, the C-terminal tail, the disulfide domain and the redox dynamics of GvFFTR revealed by our study considerably enriches our understanding of the intricacies of the ET process in this enzyme. Nonetheless, these intriguing findings open avenues for future research aimed at deciphering the coordination of mechanistic and conformational details in FFTR, as well as of the physiological relevance of FFTR function in different biological contexts.

8.5 CONCLUSIONS

Both the side chain of Trp315 and the C-terminal tail play critical roles in setting the chemistry of the FAD cofactor within GvFFTR. Even though the removal of both elements does not significantly impact the overall protein folding, they are crucial for conferring the significantly low midpoint reduction potential value exhibited by GvFFTR_WT. The C-terminal tail is also a key element in stabilizing the neutral FAD_{sq}, a feature that is of particular relevance in GvFFTR when considering the single-electron exchanger GvFdx1 as its putative in vivo donor. This makes it necessary for two consecutive electron transfer processes from two $GvFdx1_{rd}$ molecules to achieve GvFFTR reduction to the FAD_{hq} state, which is necessary to reduce the CxxC motif at the redox-active disulfide domain.

Photoreduction of GvFFTR_WT results in a large amount of neutral semiquinone being stabilized, but this state is hardly populated upon photoreduction of GvFFTR_Δtail. This suggests an important role of the C-terminal tail in stabilizing the neutral semiquinone, significantly affecting flavin chemistry. The reduction rates of FAD in GvFFTR by GvFdx1 are more efficient in the GvFFTR_Δtail and GvFFTR_W315A variants compared to GvFFTR_WT. This enhancement can be attributed to the very negative redox potential of the FAD in GvFFTR_WT, which not only affects ET from GvFdx1 but also substantially retards its reduction by DTH or light irradiation. It has been observed that light triggers the reduction of the flavin in GvFFTR and the iron-sulfur clusters in GvFdx1, even in the absence of 5-dRF/EDTA. This suggests that light can contribute to the photoreduction of GvFFTR and GvFdx1 through the FAD_{sq} state, emphasizing the complexity of electron transfer mechanisms in the GvFFTR and GvFdx1 system in the experimental framework.

9. General Discussion

9. GENERAL DISCUSSION

9.1 Exploring the flavoproteome of *B. ovis*: unveiling potential targets for antimicrobials and biotechnological advancements

Flavoproteins, which contain flavins like FMN or FAD, play crucial roles in diverse biological processes. In the case of *B. ovis*, flavoproteins are expected to catalyze a significant number of reactions across metabolic pathways. They are implicated in electron transport to bacterial metabolism, primary and energy metabolism, oxidative stress response, tRNA methylation, and more, according to previous reports. Furthermore, some of these flavoproteins are suggested to play roles in microbial metabolism in different environments, xenobiotic metabolism for detoxification of aromatic compounds, bacterial virulence, or the activation of various metabolites. The presence of specific flavoproteins in *B. ovis* indicates a substantial dependence on these enzymes in *Brucella*'s metabolism. The results in this investigation also highlight that some of these flavoproteins belong to the core proteome of *Brucella*, emphasizing their fundamental importance in the bacterium's metabolism. However, it is noted that some of these proteins are degraded and likely non-functional, introducing variability in *B. ovis*'s metabolic abilities when compared to other *Brucella* species.

In the broader context of genomic research, the significance of identifying and understanding the biological function of proteins with undetermined or putative functions has been here also discussed. The importance of predicting and evaluating the functionality of flavoprotein candidates in specific organisms is emphasized. Additionally, some of these flavoproteins are suggested as potential targets for antimicrobial development, while others may have applications as novel biocatalysts.

9.2 Overall characterization of MurA, MurB and MurC from *B. ovis*

The analysis of MurA, MurB, and MurC sequences from various *Brucella* species highlights a high degree of similarity among them. Some species have two copies of the murA gene, contrary to the usual single gene in gram-negative bacteria. This study explores the evolutionary and functional implications of this observation, particularly in *Brucella* species isolated from different environments. Comparative analysis with other bacteria reveals that multiple copies of murA are not exclusive to *Brucella* and are also observed in gram-positive bacteria. In certain *Bacillus* strains, such as *B. cereus, B. thuringiensis* subp. *konkukian, B. anthracis,* and *B. thiaminolyticus,* two isoforms of murB are also expected. This genetic redundancy suggests possible differential regulation and adaptability in the first

steps of PG biosynthesis. Regarding genome organization, the murB and murC genes are present in most *Brucella* strains in an operon closely resembling that of *B. ovis*. A similar organization is observed in other bacteria, such as *B. licheniformis*, *B. quintana*, *C. aggregans*, *C. pelagibacter*, *G. oxydans*, *L. pneumophila*, *P. zucineum*, and *R. capsulatus*, while in other bacteria, such as those belonging to Verrucomicrobia and Methylacidiphilales, these genes are found in a single fusion ORF encoding a fused MurB/C protein. The formation of complexes and interaction between Mur enzymes is suggested, enhancing the biosynthesis of the cytoplasmic PG.

For functional and structural evaluation, the three enzymes were here cloned with a 6-His tag, enabling successful purification. Another variant of BoMurB was also generated without the tag (BoMurB). Spectroscopic analysis confirmed the folded states of each enzyme and revealed various structural properties. The thermal stability of all proteins was assessed using CD and fluorescence. BoHTMurA exhibited a multi-step development process indicative of two independent domains, with the presence of the substrate UNAG thermally stabilizing it. For BoHTMurB and BoMurB, it has been revealed that UNAGEP and a combination of UNAGEP and $NADP^+$ have a stabilizing effect on the secondary and tertiary structure of these proteins. In some cases, multiple transition states between the folded and unfolded structures were identified. BoHTMurC denaturation resulted in a two transition states.

The activity of BoHTMurA was not extensively measured, as the primary goal of this study was to find the optimal kinetic condition to produce appropriately UNAGEP, a relevant compound as it is the substrate for MurB. Based on the literature, we assumed that BoHTMurB/BoMurB oxidation tests required the presence of UNAGEP, as no spectral changes in the flavin band were observed when the enzyme was mixed with NADPH. However, reduction/oxidation tests with NADPH and UNAGEP substrates did not show the expected activity under any of the evaluated conditions. Although the reduction of the FAD cofactor was achieved with non-physiological electron donors, this unexpected result raises questions about the physiological redox activity of MurB in *B. ovis*, as well as of the possibility of other components being required for the reaction to occur. The product of the BoMurB reaction, the UNAM, was expected to be purified to proceed with kinetic assays involving BoHTMurC, as the involvement of UNAM is crucial for determining the enzyme's catalytic parameters, and unfortunately, it is not commercially available. Another point of interest in the study was the variability in reported kinetic parameters among the MurA,

MurB, and MurC enzymes from different bacterial species, suggestive of diverse capabilities in the PG synthesis among bacteria.

Crystal production was unequal successful for the three enzymes, with some noteworthy points. Although crystals were obtained for BoHTMurA, X-ray diffraction from them was insufficient to generate proper electron density maps. Consequently, protein modeling had to be performed using I-TASSER and AlphaFold. BoHTMurB did not form crystals unless the condition was enriched with previously produced and concentrated UNAGEP. The BoHTMurB crystals grew as thin needles on top of each other, making it challenging to separate monocrystals when placing them in loops to be send to the synchrotron. This was one of the reasons for deciding to clone the variant without the 6 His tag, which resulted in monocrystals that appeared within a few days. These crystals were successfully diffracted to 1.9 Å, revealing a monomeric structure of BoMurB with an incorporated FAD and UNAGEP at its active site, showing structural similarities with other type IIa MurBs. In the case of BoHTMurC, several conditions were identified that allowed the appearance of large protein crystals that diffracted poorly. Some efforts were carried out to optimize the crystallization conditions, leading to a density map at 3.2 Å. Two BoMurC molecules were found in the unit cell, but an analysis by PISA did not suggest a dimeric organization.

Sequence and structure analyses of Mur enzymes using ConSurf software reveal significant conservation in specific segments. Alignments among *Brucella* species show greater overall homogeneity, while comparative analysis with other bacterial species reveals a high degree of conservation in the active sites of each enzyme.

Additionally, it was proposed that BoMurB and BoMurC could form a complex during the catalytic reaction, based on studies conducted in other bacteria. There is even evidence of the presence of fused genes, where one portion encodes for MurB and another for MurC, giving rise to a hybrid protein with potential conformations that are not yet described. Therefore, a modeling with AlphaFold-Multimer of this potential complex was performed. Although the result did not meet our expectations, the model suggests an "open" conformation for the BoMurC monomer accommodating BoMurB. We propose that BoMurB should not be in that position but rather positioned in a way that the active sites of both proteins face each other. A docking analysis between these two proteins results in a strong affinity suggestive of a stable conformation. However, the need for additional validation through further experiments is emphasized.

9.3 The electron transfer mechanism in FFTR from *G. violaceus*

In the study of FFTR system from *G. violaceus*, the principal results show the critical roles of the Cys135 in the CxxC motif, Trp315 and the C-terminal tail in determining the FAD cofactor chemistry within this enzyme and its variants. Despite their removal not significantly impacting overall protein folding, these elements are crucial for conferring a significantly low midpoint reduction potential in GvFFTR_WT. The C-terminal tail is particularly important in stabilizing the neutral FAD_{sq}, a significance amplified when considering GvFdx1 as the *in vivo* donor. The need for two consecutive electron transfer processes from $GvFdx1_{rd}$ molecules is highlighted for GvFFTR reduction to the FAD_{hq} state, essential for reducing the CxxC motif at the redox-active disulfide domain. Kinetic studies indicate that the electron transfer process from GvFdx1 to GvFFTR is relatively slow in GvFFTR_WT, but surprisingly becomes more efficient upon the removal of either Trp315 or the C-terminal tail. This efficiency improvement is attributed to the very negative redox potential of FAD in GvFFTR_WT, affecting both GvFdx1 electron transfer and retarding its reduction by DTH or light irradiation. Notably, light is found to trigger the reduction of the flavin in GvFFTR and the iron-sulfur clusters in GvFdx1, even in the absence of 5-dRF/EDTA, suggesting a role for light in the photoreduction of GvFFTR and GvFdx1 through the FAD_{sq} state. The results envisage the possibility of photoirradiation-induced reduction and highlights the complex interplay of electron transfer pathways in the GvFFTR and GvFdx1 system. The findings lead to the proposal of a potential reductive model specific to cyanobacterial-type FFTRs, distinguishing them from the mechanism employed by NTRs enzymes. The absence of the C-terminal tail in clostridial FFTR enzymes is linked to their distinctive two-electron transfer capability of Fdx, indicating a tailored evolution to accommodate unique electron transfer requirements.

Overall, the study enriches the understanding of the intricate interplay between Trp315, the C-terminal tail, the CxxC motif and the redox dynamics of GvFFTR. The findings open avenues for future research to decipher the mechanistic and conformational details of FFTR and understand its physiological relevance in various biological contexts.

10. Conclusions

10. CONCLUSIONS

1. The *B. ovis* flavoproteome consists of 78 potential members, mostly enzymes, that utilize FMN and/or FAD (75% of them) as cofactors and participate in a wide range of physiological reactions.
2. 2.7% of the *B. ovis* proteome is comprised of flavoproteins, with 55% of them belonging to the core proteome of *Brucella*. These flavoproteins are found to be crucial for cell maintenance, survival, response to stress, virulence, and/or infectivity.
3. Some flavoproteins are divergent within the genus, suggesting modified catalytic activities or unidentified processes and indicating the need for further exploration into their functions. The lack of certain functional flavoenzymes in *B. ovis* might potentially contribute to its non-zoonotic nature.
4. The *B. ovis* flavoproteome can be a source of antimicrobial targets or biocatalysts.
5. The presence of multiple copies of murA and two isoforms of murB in certain *Brucella* species, along with similar observations in other bacteria, suggests certain genetic redundancy. This redundancy may indicate differential regulation and adaptability in the early stages of PG biosynthesis.
6. The organization of murB and murC genes in an operon in *Brucella* strains, including *B. ovis*, suggests a conserved genomic arrangement. This underscores the potential functional relationship between these genes in *Brucella* species and their importance in PG biosynthesis.
7. MurA, MurB, and MurC enzymes from *B. ovis* have been successful cloned, heterologously overexpressed and purified to homogeneity. This has allowed to initiate their functional and structural characterization.
8. The optimal conditions for the enzymatic production of UNAGEP by BoHTMurA involve pre-incubating the enzyme with 2 mM of UNAG at 37 °C for 10 min in a solution containing 50 mM Bis-Tris Propane at pH 7.0. Following this, 2 mM of PEP is added, and the reaction is allowed to proceed for an additional 30 min. V_{max} and apparent k_{cat} values are 1.6 µM min^{-1} and 32 min^{-1}, respectively.
9. The established conditions provide the foundation for further experimental developments, and are being used by other members of the team to use BoMurA as target for the screening of chemical molecules as potential antimicrobials.

10. Despite purified BoMurB is reduced by non-physiological reductants, reduction of its FAD cofactor by the NAD(P)H coenzyme was not detected *in vitro*. This challenged assumption about the mechanism for its physiological reaction, raising questions about the need for additional components in the reaction.
11. Crystallographic 3D structures solved include the BoMurB enzyme in complex with UNAGEP at 1.9 Å and BoMurC at 3.2 Å.
12. Potential models have been generated to evaluate potential interaction modes bewteen BoMurB and BoMurC that might facilitate the channeling of UNAM.
13. Trp315 and the C-terminal tail of GvFFTR highly contribute to modulate the spectroscopic properties and midpoint reduction potential of its FAD cofactor.
14. Removal of either Trp315 or the C-terminal tail enhances the efficiency of the FAD cofactor of GvFFTR to accept electrons by photo-irradiation, by non-physiological reductants as well as by GvFdx1.
15. Light triggers the reduction of the flavin in GvFFTR and the iron-sulfur clusters in GvFdx1, even in the absence of 5-dRF/EDTA. This might envisage a role for light in the photoreduction of GvFdx1 and GvFFTR (through the FAD_{sq} state), highlighting the complexity of electron transfer mechanisms in the system.
16. A reductive model might be envisaged specific to cyanobacterial-type FFTRs, distinguishing them from the mechanism employed by NTRs enzymes.
17. The Cys135Ser mutation at the disulfide motif of GvFFTR prevents competent binding of the GvFdx1 donor to initiate the electron transfer to FAD and might favour the “closed” conformation of the enzyme.

10. CONCLUSIONES:

1. El flavoproteoma de *B. ovis* consta de 78 componentes, en su mayoría enzimas, que utilizan FMN y/o FAD (el 75% de ellos) como cofactores y participan en una amplia gama de reacciones fisiológicas.
2. El 2.7% del proteoma de *B. ovis* está compuesto por flavoproteínas, siendo el 55% de ellas parte del proteoma central de *Brucella*. Estas flavoproteínas resultan ser cruciales para el mantenimiento celular, supervivencia, respuesta al estrés, virulencia y/o infectividad.
3. Algunas flavoproteínas son divergentes dentro del género, sugiriendo actividades catalíticas modificadas o procesos no identificados, lo que indica la necesidad de una mayor exploración de sus funciones. La ausencia de ciertas flavoenzimas funcionales en *B. ovis* podría contribuir potencialmente a su naturaleza no zoonótica.
4. El flavoproteoma de *B. ovis* puede ser una fuente de dianas de antimicrobianos o biocatalizadores.
5. La presencia de múltiples copias de murA y dos isoformas de murB en ciertas especies de *Brucella*, junto con observaciones similares en otras bacterias, sugiere cierta redundancia genética. Esta redundancia puede indicar una regulación diferencial y adaptabilidad en las primeras etapas de la biosíntesis de PG.
6. La organización de los genes murB y murC en un operón en distintas especies del género *Brucella*, incluida *B. ovis*, sugiere un arreglo genómico conservado. Esto subraya la potencial relación funcional entre estos genes en las especies de Brucella y su importancia en la biosíntesis de PG.
7. Las enzimas MurA, MurB y MurC de *B. ovis* han sido clonadas con éxito, sobre-expresadas heterólogamente y purificadas hasta la homogeneidad. Esto ha permitido iniciar su caracterización funcional y estructural.
8. Las condiciones óptimas para la producción enzimática de UNAGEP por BoHTMurA implican pre-incubar la enzima con 2 mM de UNAG a 37 °C durante 10 min en una solución que contiene 50 mM de Bis-Tris Propano a pH 7.0. Posteriormente, se añaden 2 mM de PEP y la reacción procede durante 30 min adicionales. Los valores de V_{max} y k_{cat} aparente son 1.6 µM min^{-1} y 32 min^{-1}, respectivamente.

9. Las condiciones establecidas sientan las bases para futuros desarrollos experimentales y están siendo utilizadas por otros miembros del equipo para utilizar BoMurA como diana en la búsqueda de moléculas químicas como posibles antimicrobianos.
10. A pesar de que BoMurB purificado es reducido por reductores no fisiológicos, no se detectó la reducción de su cofactor FAD por la coenzima NAD(P)H *in vitro*. Esto desafía la suposición sobre el mecanismo de su reacción fisiológica, planteando preguntas sobre la necesidad de componentes adicionales en la reacción.
11. Las estructuras cristalinas 3D resueltas incluyen la enzima BoMurB en complejo con UNAGEP a 1.9 Å y BoMurC a 3.2 Å.
12. Se generaron modelos potenciales para evaluar modos de interacción entre BoMurB y BoMurC que podrían facilitar el canalizado de UNAM.
13. Trp315 y el segmento C-terminal de GvFFTR contribuyen significativamente a modular las propiedades espectroscópicas y el potencial de reducción de su cofactor FAD.
14. La eliminación de Trp315 o el segmento C-terminal aumenta la eficiencia del cofactor FAD de GvFFTR para aceptar electrones mediante foto-irradiación, reductores no fisiológicos y GvFdx1.
15. La luz desencadena la reducción de la flavina en GvFFTR y los clústeres de hierro-azufre en GvFdx1, incluso en ausencia de 5-dRF/EDTA. Esto podría sugerir un papel de la luz en la fotorreducción de GvFdx1 y GvFFTR (a través del estado FAD_{sq}), resaltando la complejidad de los mecanismos de transferencia de electrones en el sistema.
16. Se podría concebir un modelo reductivo específico para las FFTR de tipo cianobacteria, distinguiéndolas del mecanismo utilizado por las enzimas NTRs.
17. La mutación Cys135Ser en el motivo de disulfuro de GvFFTR impide la unión competente del donador GvFdx1 para iniciar la transferencia de electrones al FAD y podría favorecer la conformación "cerrada" de la enzima.

11. Bibliography

11. BIBLIOGRAPHY

Abdou, E., Jiménez de Bagüés, M. P., Martínez-Abadía, I., Ouahrani-Bettache, S., Pantesco, V., Occhialini, A., Al Dahouk, S., Köhler, S., & Jubier-Maurin, V. (2017). RegA Plays a Key Role in Oxygen-Dependent Establishment of Persistence and in Isocitrate Lyase Activity, a Critical Determinant of In vivo Brucella suis Pathogenicity. *Frontiers in Cellular and Infection Microbiology*, *7*(MAY), 1–19. https://doi.org/10.3389/fcimb.2017.00186

Acebrón-García-de-Eulate, M., Mayol-Llinàs, J., Holland, M. T. O., Kim, S. Y., Brown, K. P., Marchetti, C., Hess, J., Di Pietro, O., Mendes, V., Abell, C., Floto, R. A., Coyne, A. G., & Blundell, T. L. (2022). Discovery of Novel Inhibitors of Uridine Diphosphate- N -Acetylenolpyruvylglucosamine Reductase (MurB) from Pseudomonas aeruginosa , an Opportunistic Infectious Agent Causing Death in Cystic Fibrosis Patients. *Journal of Medicinal Chemistry*, *65*(3), 2149–2173. https://doi.org/10.1021/acs.jmedchem.1c01684

Aguilera-Arreola, M. G., Ostria-Hernández, M. L., Albarrán-Fernández, E., Juárez-Enriquez, S. R., Majalca-Martínez, C., Rico-Verdín, B., Ruiz, E. A., Ruiz-Palma, M. del S., Morales-García, M. R., & Contreras-Rodríguez, A. (2018). Correct Identification of Ochrobactrum anthropi From Blood Culture Using 16rRNA Sequencing: A First Case Report in an Immunocompromised Patient in Mexico. *Frontiers in Medicine*, *5*(JUN), 1–6. https://doi.org/10.3389/fmed.2018.00205

Allerberger, F., & Klare, I. (1999). In-vitro activity of fosfomycin against vancomycin-resistant enterococci. *Journal of Antimicrobial Chemotherapy*, *43*(2), 211–217. https://doi.org/10.1093/jac/43.2.211

Alton, G. G., & Forsyth, J. R. L. (1996). *Brucella.* (S. Baron (ed.)).

Alton, G. G., Jones, L. M., Angus, R. D., & Verger, J. M. (1988). *Techniques for the brucellosis laboratory.* Institut National de la recherche Agronomique (INRA).

Alvarez, S., Jones, M., & Berk, S. L. (1985). In vitro activity of fosfomycin, alone and in combination, against methicillin-resistant Staphylococcus aureus. *Antimicrobial Agents and Chemotherapy*, *28*(5), 689–690. https://doi.org/10.1128/AAC.28.5.689

Amera, G. M., Khan, R. J., Pathak, A., Jha, R. K., Jain, M., Muthukumaran, J., & Singh, A. K. (2020). Structure based drug designing and discovery of promising lead molecules against UDP-N-acetylenolpyruvoylglucosamine reductase (MurB): A potential drug target in multi-drug resistant Acinetobacter baumannii. *Journal of Molecular Graphics and Modelling*, *100*, 107675. https://doi.org/10.1016/j.jmgm.2020.107675

Anast, J. M., Bobik, T. A., & Schmitz-Esser, S. (2020). The Cobalamin-Dependent Gene Cluster of Listeria monocytogenes: Implications for Virulence, Stress Response, and Food Safety. *Frontiers in Microbiology*, *11*(November), 1–9. https://doi.org/10.3389/fmicb.2020.601816

Anderson, J. D., & Smith, H. (1965). The Metabolism of Erythritol by Brucella abortus. *Journal of General Microbiology*, *38*(1), 109–124. https://doi.org/10.1099/00221287-38-1-109

Andres, C. J., Bronson, J. J., D'Andrea, S. V., Deshpande, M. S., Falk, P. J., Grant-Young, K. A., Harte, W. E., Ho, H. T., Misco, P. F., Robertson, J. G., Stock, D., Sun, Y., & Walsh, A. W. (2000). 4-Thiazolidinones: Novel inhibitors of the bacterial enzyme MurB. *Bioorganic and Medicinal Chemistry Letters*, *10*(8), 715–717. https://doi.org/10.1016/S0960-894X(00)00073-1

Ankisettypalli, K., Cheng, J. J.-Y., Baker, E. N., & Bashiri, G. (2016). PdxH proteins of mycobacteria are typical members of the classical pyridoxine/pyridoxamine 5′-phosphate oxidase family. *FEBS Letters*, *590*(4), 453–460. https://doi.org/10.1002/1873-3468.12080

Anoz-Carbonell, E., Timson, D. J., Pey, A. L., & Medina, M. (2020). The Catalytic Cycle of the Antioxidant and Cancer-Associated Human NQO1 Enzyme: Hydride Transfer, Conformational Dynamics and Functional Cooperativity. *Antioxidants*, *9*(9), 772. https://doi.org/10.3390/antiox9090772

Anoz-Carbonell, E., Rivero, M., Polo, V., Velázquez-Campoy, A., & Medina, M. (2020). Human riboflavin kinase: Species-specific traits in the biosynthesis of the FMN cofactor. *The FASEB Journal*, *34*(8), 10871–10886. https://doi.org/10.1096/fj.202000566R

Anwar, R. A., & Vlaovic, M. (1979). Purification of UDP- N -acetylenolpyruvoylglucosamine reductase from Escherichia coli by affinity chromatography, its subunit structure and the absence of flavin as the prosthetic group. *Canadian Journal of Biochemistry*, *57*(2), 188–196. https://doi.org/10.1139/o79-023

Arber, W. (2014). Horizontal gene transfer among bacteria and its role in biological evolution. *Life*, *4*(2), 217–224. https://doi.org/10.3390/life4020217

Arnér, E. S. J., & Holmgren, A. (2000). Physiological functions of thioredoxin and thioredoxin reductase. *European Journal of Biochemistry*, *267*(20), 6102–6109. https://doi.org/10.1046/j.1432-1327.2000.01701.x

Arscott, L. D., Gromer, S., Schirmer, R. H., Becker, K., & Williams, C. H. (1997). The mechanism of thioredoxin reductase from human placenta is similar to the mechanisms of lipoamide dehydrogenase

and glutathione reductase and is distinct from the mechanism of thioredoxin reductase from Escherichia coli. *Proceedings of the National Academy of Sciences*, *94*(8), 3621–3626. https://doi.org/10.1073/pnas.94.8.3621

Ashkenazy, H., Abadi, S., Martz, E., Chay, O., Mayrose, I., Pupko, T., & Ben-Tal, N. (2016). ConSurf 2016: an improved methodology to estimate and visualize evolutionary conservation in macromolecules. *Nucleic Acids Research*, *44*(W1), W344–W350. https://doi.org/10.1093/nar/gkw408

Audic, S., Lescot, M., Claverie, J.-M., & Scholz, H. C. (2009). Brucella microti: the genome sequence of an emerging pathogen. *BMC Genomics*, *10*(1), 352. https://doi.org/10.1186/1471-2164-10-352

Auldridge, M. E., Cao, H., Sen, S., Franz, L. P., Bingman, C. A., Yennamalli, R. M., Phillips, G. N., Mead, D., & Steinmetz, E. J. (2015). LucY: A Versatile New Fluorescent Reporter Protein. *PLOS ONE*, *10*(4), e0124272. https://doi.org/10.1371/journal.pone.0124272

Axley, M. J., Fairman, R., Yanchunas, J., Villafranca, J. J., & Robertson, J. G. (1997). Spectroscopic Properties of Escherichia coli UDP- N -Acetylenolpyruvylglucosamine Reductase. *Biochemistry*, *36*(4), 812–822. https://doi.org/10.1021/bi962260s

Babcock, G. T., & Wikström, M. (1992). Oxygen activation and the conservation of energy in cell respiration. *Nature*, *356*(6367), 301–309. https://doi.org/10.1038/356301a0

Balsera, M., & Buchanan, B. B. (2019). Evolution of the thioredoxin system as a step enabling adaptation to oxidative stress. *Free Radical Biology and Medicine*, *140*(March), 28–35. https://doi.org/10.1016/j.freeradbiomed.2019.03.003

Barbier, T., Collard, F., Zúñiga-Ripa, A., Moriyón, I., Godard, T., Becker, J., Wittmann, C., Van Schaftingen, E., & Letesson, J.-J. (2014). Erythritol feeds the pentose phosphate pathway via three new isomerases leading to D-erythrose-4-phosphate in Brucella. *Proceedings of the National Academy of Sciences*, *111*(50), 17815–17820. https://doi.org/10.1073/pnas.1414622111

Barreteau, H. (2008). *Cytoplasmic steps of peptidoglycan biosynthesis*. *32*, 168–207. https://doi.org/10.1111/j.1574-6976.2008.00104.x

Bartosik, D., Sochacka, M., & Baj, J. (2003). Identification and Characterization of Transposable Elements of Paracoccus pantotrophus. *Journal of Bacteriology*, *185*(13), 3753–3763. https://doi.org/10.1128/JB.185.13.3753-3763.2003

Basavannacharya, C., Robertson, G., Munshi, T., Keep, N. H., & Bhakta, S. (2010). ATP-dependent MurE ligase in Mycobacterium tuberculosis : Biochemical and structural characterisation. *Tuberculosis*, *90*(1), 16–24. https://doi.org/10.1016/j.tube.2009.10.007

Bateman, A., Martin, M.-J., Orchard, S., Magrane, M., Agivetova, R., Ahmad, S., Alpi, E., Bowler-Barnett, E. H., Britto, R., Bursteinas, B., Bye-A-Jee, H., Coetzee, R., Cukura, A., Da Silva, A., Denny, P., Dogan, T., Ebenezer, T., Fan, J., Castro, L. G., … Teodoro, D. (2021). UniProt: the universal protein knowledgebase in 2021. *Nucleic Acids Research*, *49*(D1), D480–D489. https://doi.org/10.1093/nar/gkaa1100

Baum, E. Z., Montenegro, D. A., Licata, L., Turchi, I., Webb, G. C., Foleno, B. D., & Bush, K. (2001). Identification and Characterization of New Inhibitors of the Escherichia coli MurA Enzyme. *Antimicrobial Agents and Chemotherapy*, *45*(11), 3182–3188. https://doi.org/10.1128/AAC.45.11.3182-3188.2001

Becana, M., Yruela, I., Sarath, G., Catalán, P., & Hargrove, M. S. (2020). Plant hemoglobins: a journey from unicellular green algae to vascular plants. *New Phytologist*, *227*(6), 1618–1635. https://doi.org/10.1111/nph.16444

Becker, D., & Natarajan. (2012). Role of apoptosis-inducing factor, proline dehydrogenase, and NADPH oxidase in apoptosis and oxidative stress. *Cell Health and Cytoskeleton*, *4*, 11. https://doi.org/10.2147/CHC.S4955

Bensen, D. S., Rodriguez, S., Nix, J., Cunningham, M. L., & Tari, L. W. (2012). Structure of MurA (UDP- N -acetylglucosamine enolpyruvyl transferase) from Vibrio fischeri in complex with substrate UDP- N -acetylglucosamine and the drug fosfomycin. *Acta Crystallographica Section F*, *F68*, 382–385. https://doi.org/10.1107/S1744309112006720

Benson, D. A., Cavanaugh, M., Clark, K., Karsch-Mizrachi, I., Lipman, D. J., Ostell, J., & Sayers, E. W. (2012). GenBank. *Nucleic Acids Research*, *41*(D1), D36–D42. https://doi.org/10.1093/nar/gks1195

Benson, T. E., Harris, M. S., Choi, G. H., Cialdella, J. I., Herberg, J. T., Martin, J. P., Baldwin, E. T., September, R. V, Re, V., Recei, M., & January, V. (2001). A Structural Variation for MurB : X-ray Crystal Structure of Staphylococcus aureus. *Biochemistry*, *40*(8), 2340–2350. https://doi.org/10.1021/bi002162d

Benson, T. E., Marquardt, J. L., Marquardt, A. C., Etzkorn, F. A., & Walsh, C. T. (1993). Overexpression , Purification , and Mechanistic Study of UDP-N-Acetylenolpyruvylglucosamine Reductase. *Biochemistry*, *32*(8), 2024–2030. https://doi.org/10.1021/bi00059a019

Benson, T. E., Walsh, C. T., & Hogle, J. M. (1994). Crystallization and preliminary X-ray crystallographic

studies of UDP-N-acetylenolpyruvylglucosamine reductase. *Protein Science*, *3*, 1125–1127.

Benson, T. E., Walsh, C. T., & Hogle, J. M. (1996). The structure of the substrate-free form of MurB, an essential enzyme for the synthesis of bacterial cell walls. *Structure*, *4*(1), 47–54. https://doi.org/10.1016/S0969-2126(96)00008-1

Benson, T. E., Walsh, C. T., Hogle, J. M., & August, R. V. (1997). X-ray Crystal Structures of the S229A Mutant and Wild-Type MurB in the Presence of the Substrate Enolpyruvyl-UDP- N -Acetylglucosamine at 1 . 8-Å. *Biochemistry*, *36*(4), 806–811. https://doi.org/10.1021/bi962221g

Benson, T. E., Walsh, C. T., & Massey, V. (1997). Kinetic Characterization of Wild-Type and S229A Mutant MurB: Evidence for the Role of Ser 229 as a General Acid. *Biochemistry*, *36*(4), 796–805. https://doi.org/10.1021/bi962220o

Bernofsky, C., & Wanda, S. Y. (1982). Formation of reduced nicotinamide adenine dinucleotide peroxide. *Journal of Biological Chemistry*, *257*(12), 6809–6817. https://doi.org/10.1016/S0021-9258(18)34502-2

Bertrand, J. A., Auger, G., Martin, L., Fanchon, E., Blanot, D., Le Beller, D., van Heijenoort, J., & Dideberg, O. (1999). Determination of the MurD mechanism through crystallographic analysis of enzyme complexes. *Journal of Molecular Biology*, *289*(3), 579–590. https://doi.org/10.1006/jmbi.1999.2800

Bi, S., Lv, Q.-Z., Wang, T.-T., Fuchs, B. B., Hu, D.-D., Anastassopoulou, C. G., Desalermos, A., Muhammed, M., Wu, C.-L., Jiang, Y.-Y., Mylonakis, E., & Wang, Y. (2018). SDH2 is involved in proper hypha formation and virulence in Candida albicans. *Future Microbiology*, *13*(10), 1141–1156. https://doi.org/10.2217/fmb-2018-0033

Biasini, M., Bienert, S., Waterhouse, A., Arnold, K., Studer, G., Schmidt, T., Kiefer, F., Cassarino, T. G., Bertoni, M., Bordoli, L., & Schwede, T. (2014). SWISS-MODEL: modelling protein tertiary and quaternary structure using evolutionary information. *Nucleic Acids Research*, *42*(W1), W252–W258. https://doi.org/10.1093/nar/gku340

Bijelic, A., & Rompel, A. (2018). Polyoxometalates: more than a phasing tool in protein crystallography. *ChemTexts*, *4*(3), 10. https://doi.org/10.1007/s40828-018-0064-1

Birnboim, H. C., & Doly, J. (1979). A rapid alkaline extraction procedure for screening recombinant plasmid DNA. *Nucleic Acids Research*, *7*(6), 1513–1523. https://doi.org/10.1093/nar/7.6.1513

Blacker, T. S., Mann, Z. F., Gale, J. E., Ziegler, M., Bain, A. J., Szabadkai, G., & Duchen, M. R. (2014). Separating NADH and NADPH fluorescence in live cells and tissues using FLIM. *Nature Communications*, *5*(May), 1–9. https://doi.org/10.1038/ncomms4936

Blake, K. L., Neill, A. J. O., Mengin-lecreulx, D., Henderson, P. J. F., Bostock, J. M., Dunsmore, C. J., Simmons, K. J., Fishwick, C. W. G., Leeds, J. A., & Chopra, I. (2009). The nature of Staphylococcus aureus MurA and MurZ and approaches for detection of peptidoglycan biosynthesis inhibitors. *Molecular Microbiology*, *72*(2), 335–343. https://doi.org/10.1111/j.1365-2958.2009.06648.x

Blötz, C., & Stülke, J. (2017). Glycerol metabolism and its implication in virulence in Mycoplasma. *FEMS Microbiology Reviews*, *41*(5), 640–652. https://doi.org/10.1093/femsre/fux033

Blyth, A. W. (1879). LVI.—The composition of cows' milk in health and disease. *J. Chem. Soc., Trans.*, *35*(2), 530–539. https://doi.org/10.1039/CT8793500530

Bornemann, S. (2002). Flavoenzymes that catalyse reactions with no net redox change. *Natural Product Reports*, *19*(6), 761–772. https://doi.org/10.1039/b108916c

Bouhss, A., Crouvoisier, M., Blanot, D., & Mengin-Lecreulx, D. (2004). Purification and characterization of the bacterial MraY translocase catalyzing the first membrane step of peptidoglycan biosynthesis. *Journal of Biological Chemistry*, *279*(29), 29974–29980. https://doi.org/10.1074/jbc.M314165200

Bouhss, A., Mengin-Lecreulx, D., Blanot, D., van Heijenoort, J., & Parquet, C. (1997). Invariant Amino Acids in the Mur Peptide Synthetases of Bacterial Peptidoglycan Synthesis and Their Modification by Site-Directed Mutagenesis in the UDP-MurNAc: <scp>l</scp> -Alanine Ligase from *Escherichia coli*. *Biochemistry*, *36*(39), 11556–11563. https://doi.org/10.1021/bi970797f

Briggs, W. R. (2007). The LOV domain: a chromophore module servicing multiple photoreceptors. *Journal of Biomedical Science*, *14*(4), 499–504. https://doi.org/10.1007/s11373-007-9162-6

Brodl, E., Winkler, A., & Macheroux, P. (2018). Molecular Mechanisms of Bacterial Bioluminescence. *Computational and Structural Biotechnology Journal*, *16*, 551–564. https://doi.org/10.1016/j.csbj.2018.11.003

Bronson, J. J., DenBleyker, K. L., Falk, P. J., Mate, R. A., Ho, H.-T., Pucci, M. J., & Snyder, L. B. (2003). Discovery of the first antibacterial small molecule inhibitors of MurB. *Bioorganic & Medicinal Chemistry Letters*, *13*(5), 873–875. https://doi.org/10.1016/S0960-894X(02)01076-4

Brown, E. D., Marquardt, J. L., Lee, J. P., Walsh, C. T., & Anderson, K. S. (1994). Detection and Characterization of a Phospholactoyl-Enzyme Adduct in the Reaction Catalyzed by UDP-N-acetylglucosamine Enolpyruvoyl Transferase, MurZ. *Biochemistry*, *33*(35), 10638–10645. https://doi.org/10.1021/bi00201a010

Brown, E. D., Vivas, E. I., Walsh, C. T., & Kolter, R. (1995). MurA (MurZ), the Enzyme That Catalyzes the First Committed Step in Peptidoglycan Biosynthesis, Is Essential in Escherichia coli. In *Journal of Bacteriology* (Vol. 177, Issue 14).

Brown, L., Wolf, J. M., Prados-Rosales, R., & Casadevall, A. (2015). Through the wall: extracellular vesicles in Gram-positive bacteria, mycobacteria and fungi. *Nature Reviews Microbiology*, *13*(10), 620–630. https://doi.org/10.1038/nrmicro3480

Brüggemann, H., Hagman, A., Jules, M., Sismeiro, O., Dillies, M. A., Gouyette, C., Kunst, F., Steinert, M., Heuner, K., Coppée, J. Y., & Buchrieser, C. (2006). Virulence strategies for infecting phagocytes deduced from the in vivo transcriptional program of Legionella pneumophila. *Cellular Microbiology*, *8*(8), 1228–1240. https://doi.org/10.1111/j.1462-5822.2006.00703.x

Bryskier, A. (2005). Anti-MRSA agents: Under investigation, in the exploratory phase and clinically available. *Expert Review of Anti-Infective Therapy*, *3*(4), 505–553. https://doi.org/10.1586/14787210.3.4.505

Bueno, P. S. A., Rodrigues-Vendramini, F. A. V., Toplak, M., Macheroux, P., Kioshima, É. S., & Seixas, F. A. V. (2019). New inhibitors of chorismate synthase present antifungal activity against Paracoccidioides brasiliensis. *Future Microbiology*, *14*(11), 969–980. https://doi.org/10.2217/fmb-2019-0052

Buey, R. M., Fernández-Justel, D., de Pereda, J. M., Revuelta, J. L., Schürmann, P., Buchanan, B. B., & Balsera, M. (2018). Ferredoxin-linked flavoenzyme defines a family of pyridine nucleotide-independent thioredoxin reductases. *Proceedings of the National Academy of Sciences*, *115*(51), 12967–12972. https://doi.org/10.1073/pnas.1812781115

Buey, R. M., Fernández-Justel, D., González-Holgado, G., Martínez-Júlvez, M., González-López, A., Velázquez-Campoy, A., Medina, M., Buchanan, B. B., & Balsera, M. (2021). Unexpected diversity of ferredoxin-dependent thioredoxin reductases in cyanobacteria. *Plant Physiology*, *186*(1), 285–296. https://doi.org/10.1093/plphys/kiab072

Buey, R. M., Galindo-Trigo, S., López-Maury, L., Velázquez-Campoy, A., Revuelta, J. L., Florencio, F. J., de Pereda, J. M., Schürmann, P., Buchanan, B. B., & Balsera, M. (2017). A New Member of the Thioredoxin Reductase Family from Early Oxygenic Photosynthetic Organisms. *Molecular Plant*, *10*(1), 212–215. https://doi.org/10.1016/j.molp.2016.06.019

Bugg, T. D. H., Braddick, D., Dowson, C. G., & Roper, D. I. (2011). Bacterial cell wall assembly : still an attractive antibacterial target. *Trends in Biotechnology*, *29*(4), 167–173. https://doi.org/10.1016/j.tibtech.2010.12.006

Campbell, G. R. O., Taga, M. E., Mistry, K., Lloret, J., Anderson, P. J., Roth, J. R., & Walker, G. C. (2006a). Sinorhizobium meliloti bluB is necessary for production of 5,6-dimethylbenzimidazole, the lower ligand of B 12. *Proceedings of the National Academy of Sciences*, *103*(12), 4634–4639. https://doi.org/10.1073/pnas.0509384103

Cao, X., Wu, L., Zhang, J., & Dolg, M. (2020). Density Functional Studies of Coenzyme NADPH and Its Oxidized Form NADP+: Structures, UV–Vis Spectra, and the Oxidation Mechanism of NADPH. *Journal of Computational Chemistry*, *41*(4), 305–316. https://doi.org/10.1002/jcc.26103

Capella-Gutierrez, S., Silla-Martinez, J. M., & Gabaldon, T. (2009). trimAl: a tool for automated alignment trimming in large-scale phylogenetic analyses. *Bioinformatics*, *25*(15), 1972–1973. https://doi.org/10.1093/bioinformatics/btp348

Castañeda-García, A., Blázquez, J., & Rodríguez-Rojas, A. (2013). Molecular mechanisms and clinical impact of acquired and intrinsic fosfomycin resistance. *Antibiotics*, *2*(2), 217–236. https://doi.org/10.3390/antibiotics2020217

Cersini, A., Salvia, A. M., & Bernardini, M. L. (1998). Intracellular Multiplication and Virulence of Shigella flexneri Auxotrophic Mutants. *Infection and Immunity*, *66*(2), 549–557. https://doi.org/10.1128/IAI.66.2.549-557.1998

Chakraborty, S., Ortiz-Maldonado, M., Entsch, B., & Ballou, D. P. (2010). Studies on the Mechanism of p-Hydroxyphenylacetate 3-Hydroxylase from Pseudomonas aeruginosa : A System Composed of a Small Flavin Reductase and a Large Flavin-Dependent Oxygenase. *Biochemistry*, *49*(2), 372–385. https://doi.org/10.1021/bi901454u

Chang, C. M., Chern, J., Chen, M. Y., Huang, K. F., Chen, C. H., Yang, Y. L., & Wu, S. H. (2015). Avenaciolides: Potential MurA-targeted inhibitors against peptidoglycan biosynthesis in methicillin-resistant staphylococcus aureus (MRSA). *Journal of the American Chemical Society*, *137*(1), 267–275. https://doi.org/10.1021/ja510375f

Chang, Y. C., Khanal Lamichhane, A., Bradley, J., Rodgers, L., Ngamskulrungroj, P., & Kwon-Chung, K. J. (2015). Differences between Cryptococcus neoformans and Cryptococcus gattii in the Molecular Mechanisms Governing Utilization of D-Amino Acids as the Sole Nitrogen Source. *PLOS ONE*, *10*(7), e0131865. https://doi.org/10.1371/journal.pone.0131865

Chapot-Charter, M. P., & Kulakauskas, S. (2014). *Cell wall structure and function in lactic acid bacteria*.

13(Suppl 1), 1–23.

Chen, M. W., Lohkamp, B., Schnell, R., Lescar, J., & Schneider, G. (2013). Substrate Channel Flexibility in Pseudomonas aeruginosa MurB Accommodates Two Distinct Substrates. *PLoS ONE*, *8*(6), 1–10. https://doi.org/10.1371/journal.pone.0066936

Cheng, Z., Zhang, J., Ballou, D. P., & Williams, C. H. (2011). Reactivity of Thioredoxin as a Protein Thiol-Disulfide Oxidoreductase. *Chemical Reviews*, *111*(9), 5768–5783. https://doi.org/10.1021/cr100006x

Cho, K. H., & Caparon, M. G. (2008). tRNA Modification by GidA/MnmE Is Necessary for Streptococcus pyogenes Virulence: a New Strategy To Make Live Attenuated Strains. *Infection and Immunity*, *76*(7), 3176–3186. https://doi.org/10.1128/IAI.01721-07

Christie, A. B. (1980). Infectious diseases: epidemiology and clinical practive. In *Infectious diseases: epidemiology and clinical practive* (p. 1033).

Christie, J. M., Blackwood, L., Petersen, J., & Sullivan, S. (2015). Plant flavoprotein photoreceptors. *Plant and Cell Physiology*, *56*(3), 401–413. https://doi.org/10.1093/pcp/pcu196

Christie, S. M. H., Kenner, G. W., & Todd, A. R. (1954). Nucleotides. Part XXV. A synthesis of flavin–adenine dinucleotide. *J. Chem. Soc.*, *34*, 46–52. https://doi.org/10.1039/JR9540000046

Constantine, K. L., Mueller, L., Goldfarb, V., Wittekind, M., Metzler, W. J., Jr, J. Y., Robertson, J. G., Malley, M. F., Friedrichs, M. S., & Ii, B. T. F. (1997). Characterization of NADP ‡ Binding to Perdeuterated MurB : Backbone Atom NMR Assignments and Chemical-shift Changes. *Journal of Molecular Biology*, *267*, 1223–1246.

Corbel, M. J. (2006). Brucellosis in humans and animals Brucellosis in humans and animals. *WHO Library Catalogue in Publication Data*, 1–88.

Crawford, N. M., Smith, M., Bellissimo, D., & Davis, R. W. (1988). Sequence and nitrate regulation of the Arabidopsis thaliana mRNA encoding nitrate reductase, a metalloflavoprotein with three functional domains. *Proceedings of the National Academy of Sciences of the United States of America*, *85*(14), 5006–5010. https://doi.org/10.1073/pnas.85.14.5006

Creasey, E. A., & Isberg, R. R. (2012). The protein SdhA maintains the integrity of the Legionella-containing vacuole. *Proceedings of the National Academy of Sciences of the United States of America*, *109*(9), 3481–3486. https://doi.org/10.1073/pnas.1121286109

Cremades, N., Velázquez-Campoy, A., Martínez-Júlvez, M., Neira, J. L., Pérez-Dorado, I., Hermoso, J., Jiménez, P., Lanas, A., Hoffman, P. S., & Sancho, J. (2009). Discovery of Specific Flavodoxin Inhibitors as Potential Therapeutic Agents against Helicobacter pylori Infection. *ACS Chemical Biology*, *4*(11), 928–938. https://doi.org/10.1021/cb900166q

Crooks, G. E., Hon, G., Chandonia, J.-M., & Brenner, S. E. (2004). WebLogo: A Sequence Logo Generator: Figure 1. *Genome Research*, *14*(6), 1188–1190. https://doi.org/10.1101/gr.849004

Cui, Z., Gorzelnik, K. V., Chang, J.-Y., Langlais, C., Jakana, J., Young, R., & Zhang, J. (2017). Structures of Qβ virions, virus-like particles, and the Qβ–MurA complex reveal internal coat proteins and the mechanism of host lysis. *Proceedings of the National Academy of Sciences*, *114*(44), 11697–11702. https://doi.org/10.1073/pnas.1707102114

Dai, H. J., Parker, C. N., & Bao, J. J. (2002). Characterization and inhibition study of MurA enzyme by capillary electrophoresis. *Journal of Chromatography B*, *766*(1), 123–132. https://doi.org/10.1016/S0378-4347(01)00461-3

Dai, S., Schwendtmayer, C., Johansson, K., Ramaswamy, S., Schürmann, P., & Eklund, H. (2000). How does light regulate chloroplast enzymes? Structure–function studies of the ferredoxin/thioredoxin system. *Quarterly Reviews of Biophysics*, *33*(1), 67–108. https://doi.org/10.1017/S0033583500003607

Daniels, J. B., Scoffield, J., Woolnough, J. L., & Silo-Suh, L. (2014). Impact of glycerol-3-phosphate dehydrogenase on virulence factor production by Pseudomonas aeruginosa. *Canadian Journal of Microbiology*, *60*(12), 857–863. https://doi.org/10.1139/cjm-2014-0485

Das, D., Hervé, M., Feuerhelm, J., Farr, C. L., Chiu, H.-J., Elsliger, M.-A., Knuth, M. W., Klock, H. E., Miller, M. D., Godzik, A., Lesley, S. A., Deacon, A. M., Mengin-Lecreulx, D., & Wilson, I. A. (2011). Structure and Function of the First Full-Length Murein Peptide Ligase (Mpl) Cell Wall Recycling Protein. *PLoS ONE*, *6*(3), e17624. https://doi.org/10.1371/journal.pone.0017624

Dayem, A. A., Hossain, M. K., Lee, S. Bin, Kim, K., Saha, S. K., Yang, G. M., Choi, H. Y., & Cho, S. G. (2017). The role of reactive oxygen species (ROS) in the biological activities of metallic nanoparticles. *International Journal of Molecular Sciences*, *18*(1), 1–21. https://doi.org/10.3390/ijms18010120

de Oliveira, M. V. D., Furtado, R. M., da Costa, K. S., Vakal, S., & Lima, A. H. (2022). Advances in UDP-N-Acetylglucosamine Enolpyruvyl Transferase (MurA) Covalent Inhibition. *Frontiers in Molecular Biosciences*, *9*(July), 1–9. https://doi.org/10.3389/fmolb.2022.889825

Deka, R. K., Deka, A., Liu, W. Z., Norgard, M. V., & Brautigam, C. A. (2022). Inhibition of bacterial <scp>FMN</scp> transferase: A potential avenue for countering antimicrobial resistance. *Protein*

Science, *31*(2), 545–551. https://doi.org/10.1002/pro.4241

DeLano, W. L. (2002). Pymol: An open-source molecular graphics tool. *CCP4, Newsletter On Protein Crystallography*, *40*, 82–92. http://www.ccp4.ac.uk/newsletters/newsletter40/11_pymol.pdf

Deng, G., Gu, R.-F., Marmor, S., Fisher, S. L., Jahic, H., & Sanyal, G. (2004). Development of an LC–MS based enzyme activity assay for MurC: application to evaluation of inhibitors and kinetic analysis. *Journal of Pharmaceutical and Biomedical Analysis*, *35*(4), 817–828. https://doi.org/10.1016/j.jpba.2004.02.029

Detilleux, P. G., Deyoe, B. L., & Cheville, N. F. (1990). Penetration and intracellular growth of Brucella abortus in nonphagocytic cells in vitro. *Infection and Immunity*, *58*(7), 2320–2328. https://doi.org/10.1128/iai.58.7.2320-2328.1990

Deva, T., Baker, E. N., & Squire, C. J. (2006). Structure of Escherichia coli UDP- N -acetylmuramoyl : L - alanine ligase (MurC). *Acta Crystallographica Section D*, *D62*, 1466–1474. https://doi.org/10.1107/S0907444906038376

Deva, T., Pryor, K. A. D., Leiting, B., Baker, E. N., & Smith, C. A. (2003). Purification, crystallization and preliminary X-ray analysis of Escherichia coli UDP-N-acetylmuramoyl:L-alanine ligase (MurC). *Acta Crystallographica - Section D Biological Crystallography*, *59*(8), 1510–1513. https://doi.org/10.1107/S090744490301285X

Dhalla, A. M., Yanchunas, J., Ho, H., & Robertson, J. G. (1995). Steady-State Kinetic Mechanism of Escherichia coli. *Biochemistry*, *34*(16), 5390–5402. https://doi.org/10.1021/bi00016a010

Dharmaraja, A. T. (2017). Role of Reactive Oxygen Species (ROS) in Therapeutics and Drug Resistance in Cancer and Bacteria. *Journal of Medicinal Chemistry*, *60*(8), 3221–3240. https://doi.org/10.1021/acs.jmedchem.6b01243

Di Salvo, M., Yang, E., Zhao, G., Winkler, M. E., & Schirch, V. (1998). Expression, Purification, and Characterization of RecombinantEscherichia coliPyridoxine 5′-Phosphate Oxidase. *Protein Expression and Purification*, *13*(3), 349–356. https://doi.org/10.1006/prep.1998.0904

Dijkman, W. P., & Fraaije, M. W. (2014). Discovery and Characterization of a 5-Hydroxymethylfurfural Oxidase from Methylovorus sp. Strain MP688. *Applied and Environmental Microbiology*, *80*(3), 1082–1090. https://doi.org/10.1128/AEM.03740-13

Dodhia, V. R., Sassone, C., Fantuzzi, A., Nardo, G. Di, Sadeghi, S. J., & Gilardi, G. (2008). Modulating the coupling efficiency of human cytochrome P450 CYP3A4 at electrode surfaces through protein engineering. *Electrochemistry Communications*, *10*(11), 1744–1747. https://doi.org/10.1016/j.elecom.2008.09.007

Donofrio, N. M., & Delaney, T. P. (2001). Abnormal Callose Response Phenotype and Hypersusceptibility to Peronospora parasitica in Defense-Compromised Arabidopsis nim1-1 and Salicylate Hydroxylase-Expressing Plants. *Molecular Plant-Microbe Interactions®*, *14*(4), 439–450. https://doi.org/10.1094/MPMI.2001.14.4.439

Dotreppe, D., Mullier, C., Letesson, J.-J., & De Bolle, X. (2011). The alkylation response protein AidB is localized at the new poles and constriction sites in Brucella abortus. *BMC Microbiology*, *11*(1), 257. https://doi.org/10.1186/1471-2180-11-257

Du, W., Brown, J. R., Sylvester, D. R., Huang, J., Chalker, A. F., So, C. Y., Holmes, D. J., Payne, D. J., & Wallis, N. G. (2000). Two Active Forms of UDP-N-Acetylglucosamine Enolpyruvyl Transferase in Gram-Positive Bacteria. In *JOURNAL OF BACTERIOLOGY* (Vol. 182, Issue 15).

Duan, H. D., Khan, S. A., & Miller, A.-F. (2021). Photogeneration and reactivity of flavin anionic semiquinone in a bifurcating electron transfer flavoprotein. *Biochimica et Biophysica Acta (BBA) - Bioenergetics*, *1862*(7), 148415. https://doi.org/10.1016/j.bbabio.2021.148415

Dube, S., Nanda, K., Rani, R., Kaur, N. J., Nagpal, J. K., Upadhyay, D. J., Cliffe, I. A., Saini, K. S., & Purnapatre, K. P. (2010a). UDP-N-acetylglucosamine enolpyruvyl transferase from Pseudomonas aeruginosa. *World Journal of Microbiology and Biotechnology*, *26*(9), 1623–1629. https://doi.org/10.1007/s11274-010-0338-2

Dunsmore, C. J., Miller, K., Blake, K. L., Patching, S. G., Henderson, P. J. F., Garnett, J. A., Stubbings, W. J., Phillips, S. E. V., Palestrant, D. J., Angeles, J. D. L., Leeds, J. A., Chopra, I., & Fishwick, C. W. G. (2008). 2-Aminotetralones: Novel inhibitors of MurA and MurZ. *Bioorganic and Medicinal Chemistry Letters*, *18*(5), 1730–1734. https://doi.org/10.1016/j.bmcl.2008.01.089

Dym, O., & Eisenberg, D. (2001a). Sequence-structure analysis of FAD-containing proteins. *Protein Science*, *10*(9), 1712–1728. https://doi.org/10.1110/ps.12801

Edmondson, D. E., & Tollin, G. (1983). Semiquinone formation in flavo- and metalloflavoproteins. *Topics in Current Chemistry*, *108*, 109–138. https://doi.org/10.1007/3-540-11846-2_4

Edwards, A. M. (2006). *Chapter 6. Light-Induced Flavin Toxicity* (pp. 115–130). https://doi.org/10.1039/9781847555397-00115

Edwards, A. M. (2014). *Chapter 1 Structure and General Properties of Flavins*. *1146*, 3–13. https://doi.org/10.1007/978-1-4939-0452-5

Efimov, I., Parkin, G., Millett, E. S., Glenday, J., Chan, C. K., Weedon, H., Randhawa, H., Basran, J., & Raven, E. L. (2014). A simple method for the determination of reduction potentials in heme proteins. *FEBS Letters*, *588*(5), 701–704. https://doi.org/10.1016/j.febslet.2013.12.030

Eggers, R., Jammer, A., Jha, S., Kerschbaumer, B., Lahham, M., Strandback, E., Toplak, M., Wallner, S., Winkler, A., & Macheroux, P. (2021). The scope of flavin-dependent reactions and processes in the model plant Arabidopsis thaliana. *Phytochemistry*, *189*(May), 112822. https://doi.org/10.1016/j.phytochem.2021.112822

Eisenberg, M. A., Prakash, O., & Hsiung, S. C. (1982). Purification and properties of the biotin repressor. A bifunctional protein. *Journal of Biological Chemistry*, *257*(24), 15167–15173. https://doi.org/10.1016/S0021-9258(18)33408-2

Eklund, H., Gleason, F. K., & Holmgren, A. (1991). Structural and functional relations among thioredoxins of different species. *Proteins: Structure, Function, and Genetics*, *11*(1), 13–28. https://doi.org/10.1002/prot.340110103

El-Gebali, S., Mistry, J., Bateman, A., Eddy, S. R., Luciani, A., Potter, S. C., Qureshi, M., Richardson, L. J., Salazar, G. A., Smart, A., Sonnhammer, E. L. L., Hirsh, L., Paladin, L., Piovesan, D., Tosatto, S. C. E., & Finn, R. D. (2019). The Pfam protein families database in 2019. *Nucleic Acids Research*, *47*(D1), D427–D432. https://doi.org/10.1093/nar/gky995

El Qaidi, S., Yang, J., Zhang, J.-R., Metzger, D. W., & Bai, G. (2013). The Vitamin B 6 Biosynthesis Pathway in Streptococcus pneumoniae Is Controlled by Pyridoxal 5′-Phosphate and the Transcription Factor PdxR and Has an Impact on Ear Infection. *Journal of Bacteriology*, *195*(10), 2187–2196. https://doi.org/10.1128/JB.00041-13

Emanuele, J. J., Jin, H., Jacobson, B. L., Chang, C. Y., Einspahr, H. M., & Villafranca, J. J. (1996). Kinetic and crystallographic studies of Escherichia coli UDP-N-acetylmuramate:L-alanine ligase. *Protein Science*, *5*(12), 2566–2574. https://doi.org/10.1002/pro.5560051219

Emsley, P., Lohkamp, B., Scott, W. G., & Cowtan, K. (2010). Features and development of Coot. *Acta Crystallographica Section D Biological Crystallography*, *66*(4), 486–501. https://doi.org/10.1107/S0907444910007493

Engel, H., Gutiérrez-fernández, J., Flückiger, C., Martínez-ripoll, M., & Mühlemann, K. (2013). Heteroresistance to Fosfomycin Is Predominant in Streptococcus pneumoniae and Depends on the murA1 Gene. *Antimicrobial Agents and Chemotherapy*, *57*(6), 2801–2808. https://doi.org/10.1128/AAC.00223-13

Eniyan, K., Dharavath, S., Vijayan, R., Bajpai, U., & Gourinath, S. (2018). Crystal structure of UDP-N-acetylglucosamine-enolpyruvate reductase (MurB) from Mycobacterium tuberculosis. *Biochimica et Biophysica Acta - Proteins and Proteomics*, *1866*(3), 397–406. https://doi.org/10.1016/j.bbapap.2017.11.013

Eniyan, K., Kumar, A., Rayasam, G. V., & Perdih, A. (2016). Development of a one-pot assay for screening and identification of Mur pathway inhibitors in Mycobacterium tuberculosis. *Scientific Reports*, *6*, 1–12. https://doi.org/10.1038/srep35134

Eschenburg, S., Kabsch, W., Healy, M. L., & Schönbrunn, E. (2003). A New View of the Mechanisms of UDP-N-Acetylglucosamine Enolpyruvyl Transferase (MurA) and 5-Enolpyruvylshikimate-3-phosphate Synthase (AroA) Derived from X-ray Structures of Their Tetrahedral Reaction Intermediate States. *Journal of Biological Chemistry*, *278*(49), 49215–49222. https://doi.org/10.1074/jbc.M309741200

Eschenburg, S., Priestman, M. A., Abdul-Latif, F. A., Delachaume, C., Fassy, F., & Schönbrunn, E. (2005). A Novel Inhibitor That Suspends the Induced Fit Mechanism of UDP-N-acetylglucosamine Enolpyruvyl Transferase (MurA). *Journal of Biological Chemistry*, *280*(14), 14070–14075. https://doi.org/10.1074/jbc.M414412200

Eschenburg, S., Priestman, M., & Schönbrunn, E. (2005). Evidence That the Fosfomycin Target Cys115 in UDP-N-acetylglucosamine Enolpyruvyl Transferase (MurA) Is Essential for Product Release. *Journal of Biological Chemistry*, *280*(5), 3757–3763. https://doi.org/10.1074/jbc.M411325200

Eschenburg, S., & Schönbrunn, E. (2000). Comparative X-ray analysis of the un-liganded fosfomycin-target MurA. *Proteins: Structure, Function, and Genetics*, *40*(2), 290–298. https://doi.org/10.1002/(SICI)1097-0134(20000801)40:2<290::AID-PROT90>3.0.CO;2-0

Espinosa-Ruiz, A., Bellés, J. M., Serrano, R., & Culiáñez-Macià, F. A. (1999). Arabidopsis thaliana AtHAL3: A flavoprotein related to salt and osmotic tolerance and plant growth. *Plant Journal*, *20*(5), 529–539. https://doi.org/10.1046/j.1365-313X.1999.00626.x

Esposito, D., Günster, R. A., Martino, L., El Omari, K., Wagner, A., Thurston, T. L. M., & Rittinger, K. (2018). Structural basis for the glycosyltransferase activity of the Salmonella effector SseK3. *Journal of*

Biological Chemistry, *293*(14), 5064–5078. https://doi.org/10.1074/jbc.RA118.001796

Evans, R., O'Neill, M., Pritzel, A., Antropova, N., Senior, A., Green, T., Žídek, A., Bates, R., Blackwell, S., Yim, J., Ronneberger, O., Bodenstein, S., Zielinski, M., Bridgland, A., Potapenko, A., Cowie, A., Tunyasuvunakool, K. ri., Jain, R., Clancy, E., … Jumper, J. (2021). Protein complex prediction with AlphaFold-Multimer. In *Methods in Molecular Biology* (Vol. 804, pp. 297–312). https://doi.org/10.1101/2021.10.04.463034

Ewing, T. A., Fraaije, M. W., Mattevi, A., & van Berkel, W. J. H. (2017). The VAO/PCMH flavoprotein family. *Archives of Biochemistry and Biophysics*, *632*, 104–117. https://doi.org/10.1016/j.abb.2017.06.022

Falagas, M. E., Athanasaki, F., Voulgaris, G. L., Triarides, N. A., & Vardakas, K. Z. (2019). Resistance to fosfomycin: Mechanisms, Frequency and Clinical Consequences. *International Journal of Antimicrobial Agents*, *53*(1), 22–28. https://doi.org/10.1016/j.ijantimicag.2018.09.013

Falagas, M. E., Vouloumanou, E. K., Samonis, G., & Vardakas, K. Z. (2016). *Fosfomycin*. *333*. https://doi.org/10.1128/CMR.00068-15.Address

Farfán-López, M., Espinoza-Culupú, A., García-de-la-Guarda, R., Serral, F., Sosa, E., Palomino, M. M., & Fernández Do Porto, D. A. (2020). Prioritisation of potential drug targets against Bartonella bacilliformis by an integrative in-silico approach. *Memórias Do Instituto Oswaldo Cruz*, *115*(7), 1–11. https://doi.org/10.1590/0074-02760200184

Farr Zuend, C., Nomellini, J. F., Smit, J., & Horwitz, M. S. (2019). A Caulobacter crescentus Microbicide Protects from Vaginal Infection with HIV-1 JR-CSF in Humanized Bone Marrow-Liver-Thymus Mice. *Journal of Virology*, *93*(18), 1–16. https://doi.org/10.1128/JVI.00614-19

Ferreira, P., & Medina, M. (2021). Anaerobic Stopped-Flow Spectrophotometry with Photodiode Array Detection in the Presteady State: An Application to Elucidate Oxidoreduction Mechanisms in Flavoproteins. In *Biochemical Society Transactions* (Vol. 5, Issue 2, pp. 135–155). https://doi.org/10.1007/978-1-0716-1286-6_9

Ferreira, P., Villanueva, R., Martínez-Júlvez, M., Herguedas, B., Marcuello, C., Fernandez-Silva, P., Cabon, L., Hermoso, J. A., Lostao, A., Susin, S. A., & Medina, M. (2014). Structural Insights into the Coenzyme Mediated Monomer–Dimer Transition of the Pro-Apoptotic Apoptosis Inducing Factor. *Biochemistry*, *53*(25), 4204–4215. https://doi.org/10.1021/bi500343r

Fillgrove, K. L., Pakhomova, S., Newcomer, M. E., & Armstrong, R. N. (2003). Mechanistic Diversity of Fosfomycin Resistance in Pathogenic Microorganisms. *Journal of the American Chemical Society*, *125*(51), 15730–15731. https://doi.org/10.1021/ja039307z

Fillgrove, K. L., Pakhomova, S., Schaab, M. R., Newcomer, M. E., & Armstrong, R. N. (2007). Structure and mechanism of the genomically encoded fosfomycin resistance protein, FosX, from Listeria monocytogenes. *Biochemistry*, *46*(27), 8110–8120. https://doi.org/10.1021/bi700625p

Fitzpatrick, T. B., Amrhein, N., & Macheroux, P. (2003). Characterization of YqjM, an Old Yellow Enzyme Homolog from Bacillus subtilis Involved in the Oxidative Stress Response. *Journal of Biological Chemistry*, *278*(22), 19891–19897. https://doi.org/10.1074/jbc.M211778200

Fiuza, M., Canova, M. J., Patin, D., Letek, M., Zanella-cle, I., Becchi, M., Mateos, L. M., Mengin-lecreulx, D., Molle, V., & Gil, A. (2008). The MurC Ligase Essential for Peptidoglycan Biosynthesis Is Regulated by the Serine / Threonine Protein Kinase PknA in Corynebacterium glutamicum *. *Journal of Biological Chemistry*, *283*(52), 36553–36563. https://doi.org/10.1074/jbc.M807175200

Foster, G., Osterman, B. S., Godfroid, J., Jacques, I., & Cloeckaert, A. (2007). Brucella ceti sp. nov. and Brucella pinnipedialis sp. nov. for Brucella strains with cetaceans and seals as their preferred hosts. *International Journal of Systematic and Evolutionary Microbiology*, *57*(11), 2688–2693. https://doi.org/10.1099/ijs.0.65269-0

Foulongne, V., Walravens, K., Bourg, G., Boschiroli, M. L., Godfroid, J., Ramuz, M., & O'Callaghan, D. (2001). Aromatic Compound-Dependent Brucella suis Is Attenuated in Both Cultured Cells and Mouse Models. *Infection and Immunity*, *69*(1), 547–550. https://doi.org/10.1128/IAI.69.1.547-550.2001

Foury, F. (1997). Human genetic diseases: a cross-talk between man and yeast. *Gene*, *195*(1), 1–10. https://doi.org/10.1016/S0378-1119(97)00140-6

Fraaije, M. W., & Mattevi, A. (2000). Flavoenzymes : diverse catalysts with recurrent features. *Reviews*, *0004*(1999), 126–132.

Frago, S., Goñi, G., Herguedas, B., Peregrina, J. R., Serrano, A., Perez-Dorado, I., Molina, R., Gómez-Moreno, C., Hermoso, J. A., Martínez-Júlvez, M., Mayhew, S. G., & Medina, M. (2007). Tuning of the FMN binding and oxido-reduction properties by neighboring side chains in Anabaena flavodoxin. *Archives of Biochemistry and Biophysics*, *467*(2), 206–217. https://doi.org/10.1016/j.abb.2007.08.024

Freer, E., Moreno, E., Moriyón, I., Pizarro-Cerdá, J., Weintraub, A., & Gorvel, J. P. (1996). Brucella-Salmonella lipopolysaccharide chimeras are less permeable to hydrophobic probes and more sensitive to

cationic peptides and EDTA than are their native Brucella sp. counterparts. *Journal of Bacteriology*, *178*(20), 5867–5876. https://doi.org/10.1128/jb.178.20.5867-5876.1996

Frenchick, P. J., Markham, R. J., & Cochrane, A. H. (1985). Inhibition of phagosome-lysosome fusion in macrophages by soluble extracts of virulent Brucella abortus. *American Journal of Veterinary Research*, *46*(2), 332–335.

Fridovich, I. (1983). Superoxide Radical: An Endogenous Toxicant. *Annual Review of Pharmacology and Toxicology*, *23*(1), 239–257. https://doi.org/10.1146/annurev.pa.23.040183.001323

Fuentes, D., Meneses, M., Nunes-Nesi, A., Araújo, W. L., Tapia, R., Gómez, I., Holuigue, L., Gutiérrez, R. A., Fernie, A. R., & Jordana, X. (2011). A deficiency in the flavoprotein of Arabidopsis mitochondrial complex ii results in elevated photosynthesis and better growth in nitrogen-limiting conditions. *Plant Physiology*, *157*(3), 1114–1127. https://doi.org/10.1104/pp.111.183939

Gallagher, L. A., & Manoil, C. (2001). Pseudomonas aeruginosa PAO1 Kills Caenorhabditis elegans by Cyanide Poisoning. *Journal of Bacteriology*, *183*(21), 6207–6214. https://doi.org/10.1128/JB.183.21.6207-6214.2001

Garg, A., & Gupta, D. (2008). VirulentPred: a SVM based prediction method for virulent proteins in bacterial pathogens. *BMC Bioinformatics*, *9*(1), 62. https://doi.org/10.1186/1471-2105-9-62

Gasteiger, E., Hoogland, C., Gattiker, A., Duvaud, S., Wilkins, M. R., Appel, R. D., & Bairoch, A. (2005). The Proteomics Protocols Handbook. In J. M. Walker (Ed.), *The Proteomics Protocols Handbook*. Humana Press. https://doi.org/10.1385/1592598900

Gennaris, A., Ezraty, B., Henry, C., Agrebi, R., Vergnes, A., Oheix, E., Bos, J., Leverrier, P., Espinosa, L., Szewczyk, J., Vertommen, D., Iranzo, O., Collet, J.-F., & Barras, F. (2015). Repairing oxidized proteins in the bacterial envelope using respiratory chain electrons. *Nature*, *528*(7582), 409–412. https://doi.org/10.1038/nature15764

Ghisla, S., & Massey, V. (1986). New flavins for old: artificial flavins as active site probes of flavoproteins. *Biochemical Journal*, *239*(1), 1–12. https://doi.org/10.1042/bj2390001

Ghisla, S., & Massey, V. (1989). Mechanisms of flavoprotein-catalyzed reactions. *European Journal of Biochemistry*, *181*(1), 1–17. https://doi.org/10.1111/j.1432-1033.1989.tb14688.x

Giancaspero, T. A., Colella, M., Brizio, C., Difonzo, G., Fiorino, G. M., Leone, P., Brandsch, R., Bonomi, F., Iametti, S., & Barile, M. (2015). Remaining challenges in cellular flavin cofactor homeostasis and flavoprotein biogenesis. *Frontiers in Chemistry*, *3*(April), 1–14. https://doi.org/10.3389/fchem.2015.00030

Gilbert, A. M., Failli, A., Shumsky, J., Yang, Y., Severin, A., Singh, G., Hu, W., Keeney, D., Petersen, P. J., & Katz, A. H. (2006). *Pyrazolidine-3 , 5-diones and 5-Hydroxy-1 H -pyrazol-3 (2 H) -ones , Inhibitors of UDP- N -acetylenolpyruvyl Glucosamine Reductase*. *3*(Scheme 2), 6027–6036.

Gish, W., & States, D. J. (1993). Identification of protein coding regions by database similarity search. *Nature Genetics*, *3*(3), 266–272. https://doi.org/10.1038/ng0393-266

Glaser, F., Pupko, T., Paz, I., Bell, R. E., Bechor-Shental, D., Martz, E., & Ben-Tal, N. (2003). ConSurf: Identification of Functional Regions in Proteins by Surface-Mapping of Phylogenetic Information. *Bioinformatics*, *19*(1), 163–164. https://doi.org/10.1093/bioinformatics/19.1.163

Goffin, C., & Ghuysen, J.-M. (2002). Biochemistry and Comparative Genomics of SxxK Superfamily Acyltransferases Offer a Clue to the Mycobacterial Paradox: Presence of Penicillin-Susceptible Target Proteins versus Lack of Efficiency of Penicillin as Therapeutic Agent. *Microbiology and Molecular Biology Reviews*, *66*(4), 702–738. https://doi.org/10.1128/mmbr.66.4.702-738.2002

Gomes, A. J., Lunardi, C. N., Rocha, F. S., & Patience, G. S. (2019). Experimental methods in chemical engineering: Fluorescence emission spectroscopy. *The Canadian Journal of Chemical Engineering*, *97*(8), 2168–2175. https://doi.org/10.1002/cjce.23506

Gordon, E., Flouret, B., Chantalat, L., Van Heijenoort, J., Mengin-Lecreulx, D., & Dideberg, O. (2001). Crystal Structure of UDP-N-acetylmuramoyl-L-alanyl-D-glutamate: meso-Diaminopimelate Ligase from Escherichia Coli. *Journal of Biological Chemistry*, *276*(14), 10999–11006. https://doi.org/10.1074/jbc.M009835200

Griffiths, E., & Gupta, R. S. (2006). Lateral transfers of serine hydroxymethyltransferase (glyA) and UDP-N-acetylglucosamine enolpyruvyl transferase (murA) genes from free-living actinobacteria to the parasitic chlamydiae. *Journal of Molecular Evolution*, *63*(2), 283–296. https://doi.org/10.1007/s00239-005-0286-x

Gross, E., Kastner, D. B., Kaiser, C. A., & Fass, D. (2004). Structure of Ero1p, Source of Disulfide Bonds for Oxidative Protein Folding in the Cell. *Cell*, *117*(5), 601–610. https://doi.org/10.1016/S0092-8674(04)00418-0

Gubler, M., Appoldt, Y., & Keck, W. (1996). Overexpression, purification, and characterization of UDP-N-acetylmuramyl:L-alanine ligase from Escherichia coli. *Journal of Bacteriology*, *178*(3), 906–910.

https://doi.org/10.1128/jb.178.3.906-910.1996

Gudipati, V., Koch, K., Lienhart, W.-D., & Macheroux, P. (2014). The flavoproteome of the yeast Saccharomyces cerevisiae. *Biochimica et Biophysica Acta (BBA) - Proteins and Proteomics*, *1844*(3), 535–544. https://doi.org/10.1016/j.bbapap.2013.12.015

Guo, Q., Wei, Y., Xia, B., Jin, Y., Liu, C., Pan, X., Shi, J., Zhu, F., Li, J., Qian, L., Liu, X., Cheng, Z., Jin, S., Lin, J., & Wu, W. (2016). Identification of a small molecule that simultaneously suppresses virulence and antibiotic resistance of Pseudomonas aeruginosa. *Scientific Reports*, *6*(1), 19141. https://doi.org/10.1038/srep19141

Guo, Y., Zhu, H., Wang, J., Huang, J., Khan, F., Zhang, J., Guo, A., & Chen, X. (2017). TrmFO, a Fibronectin-Binding Adhesin of Mycoplasma bovis. *International Journal of Molecular Sciences*, *18*(8), 1732. https://doi.org/10.3390/ijms18081732

Gupta, R., Gobble, T. R., & Schuster, M. (2009). GidA Posttranscriptionally Regulates rhl Quorum Sensing in Pseudomonas aeruginosa. *Journal of Bacteriology*, *191*(18), 5785–5792. https://doi.org/10.1128/JB.00335-09

Guzmán-Verri, C., González-Barrientos, R., Hernández-Mora, G., Morales, J.-A., Baquero-Calvo, E., Chaves-Olarte, E., & Moreno, E. (2012). Brucella ceti and Brucellosis in Cetaceans. *Frontiers in Cellular and Infection Microbiology*, *2*(February), 3. https://doi.org/10.3389/fcimb.2012.00003

Hajj Chehade, M., Loiseau, L., Lombard, M., Pecqueur, L., Ismail, A., Smadja, M., Golinelli-Pimpaneau, B., Mellot-Draznieks, C., Hamelin, O., Aussel, L., Kieffer-Jaquinod, S., Labessan, N., Barras, F., Fontecave, M., & Pierrel, F. (2013). ubiI, a New Gene in Escherichia coli Coenzyme Q Biosynthesis, Is Involved in Aerobic C5-hydroxylation. *Journal of Biological Chemistry*, *288*(27), 20085–20092. https://doi.org/10.1074/jbc.M113.480368

Hall, M. (2020). Flavoenzymes for biocatalysis. In *Enzymes* (Vol. 47, pp. 37–62). https://doi.org/10.1016/bs.enz.2020.05.001

Hamdane, D., Bou-Nader, C., Cornu, D., Hui-Bon-Hoa, G., & Fontecave, M. (2015). Flavin–Protein Complexes: Aromatic Stacking Assisted by a Hydrogen Bond. *Biochemistry*, *54*(28), 4354–4364. https://doi.org/10.1021/acs.biochem.5b00501

Hameed, P. S., Manjrekar, P., Chinnapattu, M., Humnabadkar, V., Shanbhag, G., Kedari, C., Mudugal, N. V., Ambady, A., De Jonge, B. L. M., Sadler, C., Paul, B., Sriram, S., Kaur, P., Guptha, S., Raichurkar, A., Fleming, P., Eyermann, C. J., McKinney, D. C., Sambandamurthy, V. K., … Ravishankar, S. (2014). Pyrazolopyrimidines establish MurC as a vulnerable target in Pseudomonas aeruginosa and Escherichia coli. *ACS Chemical Biology*, *9*(10), 2274–2282. https://doi.org/10.1021/cb500360c

Hammel, K. E., Cornwell, K. L., & Buchanan, B. B. (1983). Ferredoxin/flavoprotein-linked pathway for the reduction of thioredoxin. *Proceedings of the National Academy of Sciences*, *80*(12), 3681–3685. https://doi.org/10.1073/pnas.80.12.3681

Han, H., Yang, Y., Olesen, S. H., Becker, A., Betzi, S., & Schönbrunn, E. (2010). The Fungal Product Terreic Acid Is a Covalent Inhibitor of the Bacterial Cell Wall Biosynthetic Enzyme UDP- N -Acetylglucosamine 1-Carboxyvinyltransferase (MurA),. *Biochemistry*, *49*(19), 4276–4282. https://doi.org/10.1021/bi100365b

Han, S.-G., Jin, B.-S., Lee, W.-K., & Yu, Y.-G. (2011). Kinetic Properties of Wild-type and C117D Mutant UDP-N-Acetylglucosamine Enolpyruvyl Transferase (MurA) from Haemophilus influenzae. *Bulletin of the Korean Chemical Society*, *32*(8), 2549–2552. https://doi.org/10.5012/bkcs.2011.32.8.2549

Hayashi, M., & Nishimura, M. (2006). Arabidopsis thaliana-A model organism to study plant peroxisomes. *Biochimica et Biophysica Acta - Molecular Cell Research*, *1763*(12), 1382–1391. https://doi.org/10.1016/j.bbamcr.2006.08.014

He, Y., Wang, H., & Chen, L. (2015). Comparative secretomics reveals novel virulence-associated factors of Vibrio parahaemolyticus. *Frontiers in Microbiology*, *6*(JUN), 1–9. https://doi.org/10.3389/fmicb.2015.00707

Henriques, B., K. Olsen, R., Bross, P., & M. Gomes, C. (2010). Emerging Roles for Riboflavin in Functional Rescue of Mitochondrial β-Oxidation Flavoenzymes. *Current Medicinal Chemistry*, *17*(32), 3842–3854. https://doi.org/10.2174/092986710793205462

Hellmann, N., & Schneider, D. (2019). Hands On: Using Tryptophan Fluorescence Spectroscopy to Study Protein Structure. In *Methods in Molecular Biology* (Vol. 1958, pp. 379–401). https://doi.org/10.1007/978-1-4939-9161-7_20

Herrou, J., Czyż, D. M., Willett, J. W., Kim, H.-S., Chhor, G., Babnigg, G., Kim, Y., & Crosson, S. (2016a). WrpA Is an Atypical Flavodoxin Family Protein under Regulatory Control of the Brucella abortus General Stress Response System. *Journal of Bacteriology*, *198*(8), 1281–1293. https://doi.org/10.1128/JB.00982-15

Herrou, J., Czyż, D. M., Willett, J. W., Kim, H.-S., Chhor, G., Babnigg, G., Kim, Y., & Crosson, S. (2016b).

WrpA Is an Atypical Flavodoxin Family Protein under Regulatory Control of the Brucella abortus General Stress Response System. *Journal of Bacteriology*, *198*(8), 1281–1293. https://doi.org/10.1128/JB.00982-15

Hesse, L., Bostock, J., Dementin, S., Blanot, D., Mengin-lecreulx, D., Chopra, I., & Acteriol, J. B. (2003). Functional and Biochemical Analysis of Chlamydia trachomatis MurC , an Enzyme Displaying UDP- N -Acetylmuramate : Amino Acid Ligase Activity. *Journal of Bacteriology*, *185*(22), 6507–6512. https://doi.org/10.1128/JB.185.22.6507

Hill, S., Austin, S., Eydmann, T., Jones, T., & Dixon, R. (1996). Azotobacter vinelandii NIFL is a flavoprotein that modulates transcriptional activation of nitrogen-fixation genes via a redox-sensitive switch. *Proceedings of the National Academy of Sciences*, *93*(5), 2143–2148. https://doi.org/10.1073/pnas.93.5.2143

Holmgren, A., & Bjornstedt, M. (1995). Thioredoxin and thioredoxin reductase. In *Methods in Enzymology* (Vol. 252, Issue C, pp. 199–208). https://doi.org/10.1016/0076-6879(95)52023-6

Hong, P. C., Tsolis, R. M., & Ficht, T. A. (2000). Identification of Genes Required for Chronic Persistence of Brucella abortus in Mice. *Infection and Immunity*, *68*(7), 4102–4107. https://doi.org/10.1128/IAI.68.7.4102-4107.2000

Hördt, A., López, M. G., Meier-Kolthoff, J. P., Schleuning, M., Weinhold, L.-M., Tindall, B. J., Gronow, S., Kyrpides, N. C., Woyke, T., & Göker, M. (2020). Analysis of 1,000+ Type-Strain Genomes Substantially Improves Taxonomic Classification of Alphaproteobacteria. *Frontiers in Microbiology*, *11*(April). https://doi.org/10.3389/fmicb.2020.00468

Hrast, M., Jukič, M., Patin, D., Tod, J., Dowson, C. G., Roper, D. I., Barreteau, H., & Gobec, S. (2018). In silico identification, synthesis and biological evaluation of novel tetrazole inhibitors of MurB. *Chemical Biology and Drug Design*, *91*(6), 1101–1112. https://doi.org/10.1111/cbdd.13172

Hritz, J., Žoldák, G., & Sedlák, E. (2006). Cofactor assisted gating mechanism in the active site of NADH oxidase from Thermus thermophilus. *Proteins: Structure, Function, and Bioinformatics*, *64*(2), 465–476. https://doi.org/10.1002/prot.20990

Hudson, P., Gorton, T. S., Papazisi, L., Cecchini, K., Frasca, S., & Geary, S. J. (2006). Identification of a Virulence-Associated Determinant, Dihydrolipoamide Dehydrogenase (lpd), in Mycoplasma gallisepticum through In Vivo Screening of Transposon Mutants. *Infection and Immunity*, *74*(2), 931–939. https://doi.org/10.1128/IAI.74.2.931-939.2006

Hughes, V., Smith, S., Garcia-Sanchez, A., Sales, J., & Stevenson, K. (2007). Proteomic comparison of Mycobacterium avium subspecies paratuberculosis grown in vitro and isolated from clinical cases of ovine paratuberculosis. *Microbiology*, *153*(1), 196–206. https://doi.org/10.1099/mic.0.29129-0

Humljan, J., Kotnik, M., Contreras-Martel, C., Blanot, D., Urleb, U., Dessen, A., Šolmajer, T., & Gobec, S. (2008). Novel naphthalene-N-sulfonyl-D-glutamic acid derivatives as inhibitors of MurD, a key peptidoglycan biosynthesis enzyme. *Journal of Medicinal Chemistry*, *51*(23), 7486–7494. https://doi.org/10.1021/jm800762u

Imlay, J. A. (2013). The molecular mechanisms and physiological consequences of oxidative stress: lessons from a model bacterium. *Nature Reviews Microbiology*, *11*(7), 443–454. https://doi.org/10.1038/nrmicro3032

Iyanagi, T., Xia, C., & Kim, J.-J. P. (2012). NADPH–cytochrome P450 oxidoreductase: Prototypic member of the diflavin reductase family. *Archives of Biochemistry and Biophysics*, *528*(1), 72–89. https://doi.org/10.1016/j.abb.2012.09.002

Jackson, S. G., Zhang, F., Chindemi, P., Junop, M. S., & Berti, P. J. (2009). Evidence of Kinetic Control of Ligand Binding and Staged Product Release in MurA (Enolpyruvyl UDP-GlcNAc Synthase)-Catalyzed Reactions. *Biochemistry*, *48*(49), 11715–11723. https://doi.org/10.1021/bi901524q

Jeske, L., Placzek, S., Schomburg, I., Chang, A., & Schomburg, D. (2019). BRENDA in 2019: a European ELIXIR core data resource. *Nucleic Acids Research*, *47*(D1), D542–D549. https://doi.org/10.1093/nar/gky1048

Jiang, S., Gilpin, M. E., Attia, M., Ting, Y., & Berti, P. J. (2011). Lyme Disease Enolpyruvyl-UDP-GlcNAc Synthase : Fosfomycin-Resistant MurA from Borrelia burgdorferi,a Fosfomycin-Sensitive Mutant, and the Catalytic Role of the Active Site Asp. *Biochemistry*, *50*, 2205–2212.

Jiménez-García, B., Pons, C., & Fernández-Recio, J. (2013). pyDockWEB: A web server for rigid-body protein-protein docking using electrostatics and desolvation scoring. *Bioinformatics*, *29*(13), 1698–1699. https://doi.org/10.1093/bioinformatics/btt262

Jin, B.-S. (2009). Inhibitory Mechanism of Novel Inhibitors of UDP-N-Acetylglucosamine Enolpyruvyl Transferase from Haemophilus influenzae. *Journal of Microbiology and Biotechnology*, *19*(12), 1582–1589. https://doi.org/10.4014/jmb.0905.05036

Joosten, V., & Berkel, W. J. H. Van. (2007). Flavoenzymes. *Biocatalysis and Biotransformation*, *11*, 195–202.

https://doi.org/10.1016/j.cbpa.2007.01.010
Jortzik, E., Wang, L., Ma, J., & Becker, K. (2014a). Flavins and Flavoproteins: Applications in Medicine. In *Methods in Molecular Biology* (Vol. 1146, pp. 113–157). https://doi.org/10.1007/978-1-4939-0452-5_7
Jumper, J., Evans, R., Pritzel, A., Green, T., Figurnov, M., Ronneberger, O., Tunyasuvunakool, K., Bates, R., Žídek, A., Potapenko, A., Bridgland, A., Meyer, C., Kohl, S. A. A., Ballard, A. J., Cowie, A., Romera-Paredes, B., Nikolov, S., Jain, R., Adler, J., … Hassabis, D. (2021). Highly accurate protein structure prediction with AlphaFold. *Nature*, *596*(7873), 583–589. https://doi.org/10.1038/s41586-021-03819-2
Källberg, M., Wang, H., Wang, S., Peng, J., Wang, Z., Lu, H., & Xu, J. (2012). Template-based protein structure modeling using the RaptorX web server. *Nature Protocols*, *7*(8), 1511–1522. https://doi.org/10.1038/nprot.2012.085
Kämpfer, P., Huber, B., Busse, H.-J., Scholz, H. C., Tomaso, H., Hotzel, H., & Melzer, F. (2011). Ochrobactrum pecoris sp. nov., isolated from farm animals. *International Journal of Systematic and Evolutionary Microbiology*, *61*(9), 2278–2283. https://doi.org/10.1099/ijs.0.027631-0
Kao, Y.-T., Saxena, C., He, T.-F., Guo, L., Wang, L., Sancar, A., & Zhong, D. (2008). Ultrafast Dynamics of Flavins in Five Redox States. *Journal of the American Chemical Society*, *130*(39), 13132–13139. https://doi.org/10.1021/ja8045469
Kapoor, G., Saigal, S., & Elongavan, A. (2017). Action and resistance mechanisms of antibiotics: A guide for clinicians. *Journal of Anaesthesiology Clinical Pharmacology*, *33*(3), 300. https://doi.org/10.4103/joacp.JOACP_349_15
Karrer, P., Schöpp, K., Benz, F., & Pfaehler, K. (1935). Synthesen von Flavinen III. *Helvetica Chimica Acta*, *18*(1), 69–79. https://doi.org/10.1002/hlca.19350180111
Karsi, A., Gülsoy, N., Corb, E., Dumpala, P. R., & Lawrence, M. L. (2009). High-Throughput Bioluminescence-Based Mutant Screening Strategy for Identification of Bacterial Virulence Genes. *Applied and Environmental Microbiology*, *75*(7), 2166–2175. https://doi.org/10.1128/AEM.02449-08
Kawai, S., & Murata, K. (2008). Structure and function of NAD kinase and NADP phosphatase: Key enzymes that regulate the intracellular balance of NAD(H) and NADP(H). *Bioscience, Biotechnology and Biochemistry*, *72*(4), 919–930. https://doi.org/10.1271/bbb.70738
Keilin, D., & Hartree, E. F. (1946). Prosthetic Group of Glucose Oxidase (Notatin). *Nature*, *157*(3998), 801–801. https://doi.org/10.1038/157801a0
Kennedy, D. O. (2016). B vitamins and the brain: Mechanisms, dose and efficacy—A review. *Nutrients*, *8*(2). https://doi.org/10.3390/nu8020068
Khan, M., & Zahoor, M. (2018). An Overview of Brucellosis in Cattle and Humans, and its Serological and Molecular Diagnosis in Control Strategies. *Tropical Medicine and Infectious Disease*, *3*(2), 65. https://doi.org/10.3390/tropicalmed3020065
Khobragade, C. N., Bodade, R. G., Konda, S. G., Dawane, B. S., & Manwar, A. V. (2010). Synthesis and antimicrobial activity of novel pyrazolo[3,4-d]pyrimidin derivatives. *European Journal of Medicinal Chemistry*, *45*(4), 1635–1638. https://doi.org/10.1016/j.ejmech.2009.12.040
Kim, D. H., Lees, W. J., Kempsell, K. E., Lane, W. S., Duncan, K., & Walsh, C. T. (1996). Characterization of a Cys115 to Asp substitution in the Escherichia coli cell wall biosynthetic enzyme UDP-GlcNAc enolpyruvyl transferase (MurA) that confers resistance to inactivation by the antibiotic fosfomycin. *Biochemistry*, *35*(15), 4923–4928. https://doi.org/10.1021/bi952937w
Kim, M.-K., Cho, M. K., Song, H., Kim, D., Park, B., Lee, J. H., Kang, G. B., Kim, S. H., Im, Y. J., Lee, D., & Eom, S. H. (2006). Crystal structure of UDP-N-acetylenolpyruvylglucosamine reductase (MurB) from Thermus caldophilus. *Proteins: Structure, Function, and Bioinformatics*, *66*(3), 751–754. https://doi.org/10.1002/prot.21174
Kishino, H., & Hasegawa, M. (1989). Evaluation of the maximum likelihood estimate of the evolutionary tree topologies from DNA sequence data, and the branching order in hominoidea. *Journal of Molecular Evolution*, *29*(2), 170–179. https://doi.org/10.1007/BF02100115
Klein, C. D., & Bachelier, A. (2006). Molecular modeling and bioinformatical analysis of the antibacterial target enzyme MurA from a drug design perspective. *Journal of Computer-Aided Molecular Design*, *20*(10–11), 621–628. https://doi.org/10.1007/s10822-006-9062-2
Kodali, V. K., & Thorpe, C. (2010). Oxidative Protein Folding and the Quiescin – Sulfhydryl Oxidase Family of Flavoproteins. *Antioxidants & Redox Signaling*, *13*(8), 1217–1230.
König, B., Kümmel, S., Svobodová, E., & Cibulka, R. (2018). Flavin photocatalysis. *Physical Sciences Reviews*, *3*(8), 1–17. https://doi.org/10.1515/psr-2017-0168
Krapp, A. R., Rodriguez, R. E., Poli, H. O., Paladini, D. H., Palatnik, J. F., & Carrillo, N. (2002). The Flavoenzyme Ferredoxin (Flavodoxin)-NADP(H) Reductase Modulates NADP(H) Homeostasis during the soxRS Response of Escherichia coli. *Journal of Bacteriology*, *184*(5), 1474–1480. https://doi.org/10.1128/JB.184.5.1474-1480.2002

Krekel, F., Samland, A. K., Macheroux, P., Amrhein, N., & Evans, J. N. S. (2000). Determination of the p K a Value of C115 in MurA (UDP- N -Acetylglucosamine Enolpyruvyltransferase) from Enterobacter cloacae. *Biochemistry*, *39*(41), 12671–12677. https://doi.org/10.1021/bi001310x

Krissinel, E., & Henrick, K. (2005). *Detection of Protein Assemblies in Crystals* (pp. 163–174). https://doi.org/10.1007/11560500_15

Kuhn, R., Rudy, H., & Weygand, F. (1935). Über die zucker-ähnliche Seitenkette des Lactoflavins. *Berichte Der Deutschen Chemischen Gesellschaft (A and B Series)*, *68*(4), 625–634. https://doi.org/10.1002/cber.19350680413

Kumar, A., Saranathan, R., Prashanth, K., Tiwary, B. K., & Krishna, R. (2017). Inhibition of the MurA enzyme in Fusobacterium nucleatum by potential inhibitors identified through computational and in vitro approaches. *Molecular BioSystems*, *13*(5), 939–954. https://doi.org/10.1039/C7MB00074J

Kuo, C., Wang, S., Lin, C., Chiu, H., Huang, C., Lee, D., Chang, G., Chou, T., Chen, J.-W., & Chen, C. (2018). A multi-omic analysis reveals the role of fumarate in regulating the virulence of enterohemorrhagic Escherichia coli. *Cell Death & Disease*, *9*(3), 381. https://doi.org/10.1038/s41419-018-0423-2

Kyte, J. (1995). *Mechanism in protein chemistry* (Garland Publishing (ed.)).

Ladokhin, A. S. (2000). Fluorescence Spectroscopy in Peptide and Protein Analysis. In *Encyclopedia of Analytical Chemistry* (pp. 1–18). John Wiley & Sons, Ltd. https://doi.org/10.1002/9780470027318.a1611

Lamontagne, J., Forest, A., Marazzo, E., Denis, F., Butler, H., Michaud, J.-F., Boucher, L., Pedro, I., Villeneuve, A., Sitnikov, D., Trudel, K., Nassif, N., Boudjelti, D., Tomaki, F., Chaves-Olarte, E., Guzmán-Verri, C., Brunet, S., Côté-Martin, A., Hunter, J., … Paramithiotis, E. (2009). Intracellular Adaptation of Brucella abortus. *Journal of Proteome Research*, *8*(3), 1594–1609. https://doi.org/10.1021/pr800978p

Lan, C.-L., & Chen, S.-L. (2016). The Decarboxylation of α,β-Unsaturated Acid Catalyzed by Prenylated FMN-Dependent Ferulic Acid Decarboxylase and the Enzyme Inhibition. *The Journal of Organic Chemistry*, *81*(19), 9289–9295. https://doi.org/10.1021/acs.joc.6b01872

Landau, M., Mayrose, I., Rosenberg, Y., Glaser, F., Martz, E., Pupko, T., & Ben-Tal, N. (2005). ConSurf 2005: the projection of evolutionary conservation scores of residues on protein structures. *Nucleic Acids Research*, *33*(Web Server), W299–W302. https://doi.org/10.1093/nar/gki370

Lans, I., Anoz-Carbonell, E., Palacio-Rodríguez, K., Aínsa, J. A., Medina, M., & Cossio, P. (2020). In silico discovery and biological validation of ligands of FAD synthase, a promising new antimicrobial target. *PLOS Computational Biology*, *16*(8), e1007898. https://doi.org/10.1371/journal.pcbi.1007898

Lans, I., Medina, M., Rosta, E., Hummer, G., Garcia-Viloca, M., Lluch, J. M., & González-Lafont, À. (2012). Theoretical Study of the Mechanism of the Hydride Transfer between Ferredoxin–NADP + Reductase and NADP + : The Role of Tyr303. *Journal of the American Chemical Society*, *134*(50), 20544–20553. https://doi.org/10.1021/ja310331v

Lans, I., Peregrina, J. R., Medina, M., Garcia-Viloca, M., González-Lafont, À., & Lluch, J. M. (2010). Mechanism of the Hydride Transfer between Anabaena Tyr303Ser FNR rd /FNR ox and NADP + /H. A Combined Pre-Steady-State Kinetic/Ensemble-Averaged Transition-State Theory with Multidimensional Tunneling Study. *The Journal of Physical Chemistry B*, *114*(9), 3368–3379. https://doi.org/10.1021/jp912034m

Laskowski, R. A., Jabłońska, J., Pravda, L., Vařeková, R. S., & Thornton, J. M. (2018). PDBsum: Structural summaries of PDB entries. *Protein Science*, *27*(1), 129–134. https://doi.org/10.1002/pro.3289

Laskowski, R. A., MacArthur, M. W., Moss, D. S., & Thornton, J. M. (1993). PROCHECK: a program to check the stereochemical quality of protein structures. *Journal of Applied Crystallography*, *26*(2), 283–291. https://doi.org/10.1107/S0021889892009944

Lawrence, A. D., Deery, E., McLean, K. J., Munro, A. W., Pickersgill, R. W., Rigby, S. E. J., & Warren, M. J. (2008). Identification, Characterization, and Structure/Function Analysis of a Corrin Reductase Involved in Adenosylcobalamin Biosynthesis. *Journal of Biological Chemistry*, *283*(16), 10813–10821. https://doi.org/10.1074/jbc.M710431200

Lee, J. H., Choi, J. M., & Kim, H. J. (2017). Crystal structure of 5-enolpyruvylshikimate-3-phosphate synthase from a psychrophilic bacterium, Colwellia psychrerythraea 34H. *Biochemical and Biophysical Research Communications*, *492*(3), 500–506. https://doi.org/10.1016/j.bbrc.2017.08.063

Lee, M. N., Takawira, D., Nikolova, A. P., Ballou, D. P., Furtado, V. C., Phung, N. L., Still, B. R., Thorstad, M. K., Tanner, J. J., & Trimmer, E. E. (2009). Functional Role for the Conformationally Mobile Phenylalanine 223 in the Reaction of Methylenetetrahydrofolate Reductase from Escherichia coli. *Biochemistry*, *48*(32), 7673–7685. https://doi.org/10.1021/bi9007325

Lees, W. J., Benson, T. E., Hogle, J. M., & Walsh, C. T. (1996). (E)-Enolbutyryl-UDP- N -acetylglucosamine as a Mechanistic Probe of UDP- N -acetylenolpyruvylglucosamine Reductase (MurB) ,. *Biochemistry*,

35(5), 1342–1351. https://doi.org/10.1021/bi952287w

Lemieux, H., & Blier, P. U. (2022). Exploring Thermal Sensitivities and Adaptations of Oxidative Phosphorylation Pathways. *Metabolites*, *12*(4), 360. https://doi.org/10.3390/metabo12040360

Lemoine, F., Correia, D., Lefort, V., Doppelt-Azeroual, O., Mareuil, F., Cohen-Boulakia, S., & Gascuel, O. (2019). NGPhylogeny.fr: new generation phylogenetic services for non-specialists. *Nucleic Acids Research*, *47*(W1), W260–W265. https://doi.org/10.1093/nar/gkz303

Leone, P., Galluccio, M., Barbiroli, A., Eberini, I., Tolomeo, M., Vrenna, F., Gianazza, E., Iametti, S., Bonomi, F., Indiveri, C., & Barile, M. (2018). Bacterial Production, Characterization and Protein Modeling of a Novel Monofuctional Isoform of FAD Synthase in Humans: An Emergency Protein? *Molecules*, *23*(1), 116. https://doi.org/10.3390/molecules23010116

Leone, P., Galluccio, M., Quarta, S., Anoz-Carbonell, E., Medina, M., Indiveri, C., & Barile, M. (2019). Mutation of Aspartate 238 in FAD Synthase Isoform 6 Increases the Specific Activity by Weakening the FAD Binding. *International Journal of Molecular Sciences*, *20*(24), 6203. https://doi.org/10.3390/ijms20246203

Leys, D., & Scrutton, N. S. (2016). Sweating the assets of flavin cofactors: new insight of chemical versatility from knowledge of structure and mechanism. *Current Opinion in Structural Biology*, *41*, 19–26. https://doi.org/10.1016/j.sbi.2016.05.014

Li, H., Zhou, Y., Wang, N., Xin, Y., Tang, L., & Ma, Y. (2012). Identification and Characterization of a MurA, UDP-N-Acetylglucosamine Enolpyruvyl Transferase from Cariogenic Streptococcus Mutans. *Journal of Hard Tissue Biology*, *21*(1), 17–24. https://doi.org/10.2485/jhtb.21.17

Li, J., Pang, Z., Trivedi, P., Zhou, X., Ying, X., Jia, H., & Wang, N. (2017). ' Candidatus Liberibacter asiaticus' Encodes a Functional Salicylic Acid (SA) Hydroxylase That Degrades SA to Suppress Plant Defenses. *Molecular Plant-Microbe Interactions®*, *30*(8), 620–630. https://doi.org/10.1094/MPMI-12-16-0257-R

Li, L., Liu, X., Yang, W., Xu, F., Wang, W., Feng, L., Bartlam, M., Wang, L., & Rao, Z. (2008). Crystal Structure of Long-Chain Alkane Monooxygenase (LadA) in Complex with Coenzyme FMN: Unveiling the Long-Chain Alkane Hydroxylase. *Journal of Molecular Biology*, *376*(2), 453–465. https://doi.org/10.1016/j.jmb.2007.11.069

Li, Y., Zheng, X., Zhu, M., Chen, M., Zhang, S., He, F., Chen, X., Lv, J., Pei, M., Zhang, Y., Zhang, Y., Wang, W., Zhang, J., Wang, M., Wang, Z., Li, G., & Lu, G. (2019). MoIVD-Mediated Leucine Catabolism Is Required for Vegetative Growth, Conidiation and Full Virulence of the Rice Blast Fungus Magnaporthe oryzae. *Frontiers in Microbiology*, *10*(MAR), 1–13. https://doi.org/10.3389/fmicb.2019.00444

Lienhart, W. D., Gudipati, V., & MacHeroux, P. (2013). The human flavoproteome. *Archives of Biochemistry and Biophysics*, *535*(2), 150–162. https://doi.org/10.1016/j.abb.2013.02.015

Liger, D., Masson, A., Blanot, D., Van Heijenoort, J., & Parquet, C. (1995). Over-production, Purification and Properties of the Uridine-diphosphate- N -Acetylmuramate: l -alanine Ligase from Escherichia coli. *European Journal of Biochemistry*, *230*(1), 80–87. https://doi.org/10.1111/j.1432-1033.1995.0080i.x

Lipton, S. A., & Bossy-Wetzel, E. (2002). Dueling Activities of AIF in Cell Death versus Survival. *Cell*, *111*(2), 147–150. https://doi.org/10.1016/S0092-8674(02)01046-2

Liu, B., Hou, W., Li, K., Chen, Q., Liu, Y., & Yue, T. (2021). Specific gene SEN1393 contributes to higher survivability of Salmonella Enteritidis in egg white by regulating sulfate assimilation pathway. *International Journal of Food Microbiology*, *337*, 108927. https://doi.org/10.1016/j.ijfoodmicro.2020.108927

Liu, B., Liu, H., Zhong, D., & Lin, C. (2010). Searching for a photocycle of the cryptochrome photoreceptors. *Current Opinion in Plant Biology*, *13*(5), 578–586. https://doi.org/10.1016/j.pbi.2010.09.005

Liu, L.-K., Abdelwahab, H., Martin Del Campo, J. S., Mehra-Chaudhary, R., Sobrado, P., & Tanner, J. J. (2016). The Structure of the Antibiotic Deactivating, N-hydroxylating Rifampicin Monooxygenase. *Journal of Biological Chemistry*, *291*(41), 21553–21562. https://doi.org/10.1074/jbc.M116.745315

Lostao, A., Gómez-Moreno, C., Mayhew, S. G., & Sancho, J. (1997). Differential stabilization of the three FMN redox forms by tyrosine 94 and tryptophan 57 in flavodoxin from Anabaena and its influence on the redox potentials. *Biochemistry*, *36*(47), 14334–14344. https://doi.org/10.1021/bi971384h

Lowe, H. J., & Clark, W. M. (1956). Studies on Oxidation-Reduction. *Journal of Biological Chemistry*, *221*(2), 983–992. https://doi.org/10.1016/s0021-9258(18)65211-1

Lu, G., Lindqvist, Y., Schneider, G., Dwivedi, U., & Campbell, W. (1995). Structural Studies on Corn Nitrate Reductase: Refined Structure of the CytochromebReductase Fragment at 2.5 Å, its ADP Complex and an Active-site Mutant and Modeling of the CytochromebDomain. *Journal of Molecular Biology*, *248*(5), 931–948. https://doi.org/10.1006/jmbi.1995.0273

Lu, J., & Holmgren, A. (2014). The thioredoxin antioxidant system. *Free Radical Biology and Medicine*, *66*, 75–87. https://doi.org/10.1016/j.freeradbiomed.2013.07.036

Luo, X., Tian, T., Tan, X., Zheng, Y., Xie, C., Xu, Y., & Yang, X. (2020). VdNPS, a Nonribosomal Peptide

Synthetase, Is Involved in Regulating Virulence in Verticillium dahliae. *Phytopathology®*, *110*(8), 1398–1409. https://doi.org/10.1094/PHYTO-02-20-0031-R

Macheroux, P. (1999). UV-Visible Spectroscopy as a Tool to Study Flavoproteins. In *Flavoprotein Protocols* (Vol. 131, pp. 1–8). Humana Press. https://doi.org/10.1385/1-59259-266-X:1

Macheroux, P., Kappes, B., & Ealick, S. E. (2011). Flavogenomics - A genomic and structural view of flavin-dependent proteins. *FEBS Journal*, *278*(15), 2625–2634. https://doi.org/10.1111/j.1742-4658.2011.08202.x

Maddila, S., Gorle, S., & Jonnalagadda, S. B. (2020). Drug screening of rhodanine derivatives for antibacterial activity. *Expert Opinion on Drug Discovery*, *15*(2), 203–229. https://doi.org/10.1080/17460441.2020.1696768

Makarov, M. V., Trammell, S. A. J., & Migaud, M. E. (2018). The chemistry of the vitamin B3 metabolome. *Biochemical Society Transactions*, *47*(1), 131–147. https://doi.org/10.1042/BST20180420

Maklashina, E., & Cecchini, G. (2020). Determination of Flavin Potential in Proteins by Xanthine/Xanthine Oxidase Method. *BIO-PROTOCOL*, *10*(7), 1–13. https://doi.org/10.21769/BioProtoc.3571

Mansoorabadi, S. O., Thibodeaux, C. J., & Liu, H. (2007). The Diverse Roles of Flavin CoenzymesNature's Most Versatile Thespians. *The Journal of Organic Chemistry*, *72*(17), 6329–6342. https://doi.org/10.1021/jo0703092

Marcuello, C., Frempong, G. A., Balsera, M., Medina, M., & Lostao, A. (2021). Atomic Force Microscopy to Elicit Conformational Transitions of Ferredoxin-Dependent Flavin Thioredoxin Reductases. *Antioxidants*, *10*(9), 1437. https://doi.org/10.3390/antiox10091437

Marmor, S., Petersen, C. P., Reck, F., Yang, W., Gao, N., & Fisher, S. L. (2001). Biochemical characterization of a phosphinate inhibitor of Escherichia coli MurC. *Biochemistry*, *40*(40), 12207–12214. https://doi.org/10.1021/bi015567m

Marquardt, J. L., Brown, E. D., Lane, W. S., Haley, T. M., Ichikawa, Y., Wong, C., & Walsh, C. T. (1994). Kinetics, Stoichiometry, and Identification of the Reactive Thiolate in the Inactivation of UDP-GlcNAc Enolpyruvoyl Transferase by the Antibiotic Fosfomycin. *Biochemistry*, *33*(35), 10646–10651. https://doi.org/10.1021/bi00201a011

Marquardt, J. L., Siegele, D. A., Kolter, R., & Walsh, C. T. (1992). Cloning and Sequencing of Escherichia coli murZ and Purification of Its Product , a UDP-N-Acetylglucosamine Enolpyruvyl Transferase. *Journal of Bacteriology*, *174*(17), 5748–5752.

Martin, C., Trajkovic, M., & Fraaije, M. W. (2020). Production of Hydroxy Acids: Selective Double Oxidation of Diols by Flavoprotein Alcohol Oxidase. *Angewandte Chemie International Edition*, *59*(12), 4869–4872. https://doi.org/10.1002/anie.201914877

Martínez-Júlvez, M., Goñi, G., Pérez-Amigot, D., Laplaza, R., Ionescu, I., Petrocelli, S., Tondo, M., Sancho, J., Orellano, E., & Medina, M. (2017). Identification of Inhibitors Targeting Ferredoxin-NADP+ Reductase from the Xanthomonas citri subsp. citri Phytopathogenic Bacteria. *Molecules*, *23*(1), 29. https://doi.org/10.3390/molecules23010029

Maskar, A. U., & Meshram, R. J. (2013). Homology Modeling of Chorismate Synthase from Brucella melitensis : A Novel Target. *Research and Reviews: Journal of Microbiology and Biotechnology*, *2*(3), 7–18.

Massey, V. (2000). The Chemical and Biological Versatility of Riboflavin. *Biochemical Society Transactions*, *28*(4), 283. https://doi.org/10.1042/0300-5127:0280283

Massey, V., & Palmer, G. (1966). On the Existence of Spectrally Distinct Classes of Flavoprotein Semiquinones. A New Method for the Quantitative Production of Flavoprotein Semiquinones *. *Biochemistry*, *5*(10), 3181–3189. https://doi.org/10.1021/bi00874a016

Matope, G., Bhebhe, E., Muma, J. B., Oloya, J., Madekurozwa, R. L., Lund, A., & Skjerve, E. (2011). Seroprevalence of brucellosis and its associated risk factors in cattle from smallholder dairy farms in Zimbabwe. *Tropical Animal Health and Production*, *43*(5), 975–982. https://doi.org/10.1007/s11250-011-9794-4

Mattevi, A. (2006). To be or not to be an oxidase: challenging the oxygen reactivity of flavoenzymes. *Trends in Biochemical Sciences*, *31*(5), 276–283. https://doi.org/10.1016/j.tibs.2006.03.003

Mayer, C. (2017). X-Ray Diffraction in Biology: How Can We See DNA and Proteins in Three Dimensions? In *X-ray Scattering*. InTech. https://doi.org/10.5772/64999

Mayhew, S. G. (1999). The effects of pH and semiquinone formation on the oxidation-reduction potentials of flavin mononucleotide. A reappraisal. *European Journal of Biochemistry*, *265*(2), 698–702. https://doi.org/10.1046/j.1432-1327.1999.00767.x

Mayhew, S. G., & Massey, V. (1969). Purification and Characterization of Flavodoxin from Peptostreptococcus elsdenii. *Journal of Biological Chemistry*, *244*(4), 794–802. https://doi.org/10.1016/S0021-9258(18)91858-2

Mayrose, I., Graur, D., Ben-Tal, N., & Pupko, T. (2004). Comparison of Site-Specific Rate-Inference Methods for Protein Sequences: Empirical Bayesian Methods Are Superior. *Molecular Biology and Evolution*, *21*(9), 1781–1791. https://doi.org/10.1093/molbev/msh194

McCoy, A. J., & Maurelli, A. T. (2005). Characterization of Chlamydia MurC-Ddl, a fusion protein exhibiting D-alanyl-D-alanine ligase activity involved in peptidoglycan synthesis and D-cycloserine sensitivity. *Molecular Microbiology*, *57*(1), 41–52. https://doi.org/10.1111/j.1365-2958.2005.04661.x

McCoy, A. J., Sandlin, R. C., & Maurelli, A. T. (2003). In vitro and in vivo functional activity of Chlamydia MurA, a UDP-N-acetylglucosamine enolpyruvyl transferase involved in peptidoglycan synthesis and fosfomycin resistance. *Journal of Bacteriology*, *185*(4), 1218–1228. https://doi.org/10.1128/JB.185.4.1218-1228.2003

McDevitt, D., Payne, D. J., Holmes, D. J., & Rosenberg, M. (2002). Novel targets for the future development of antibacterial agents. *Journal of Applied Microbiology*, *92*, 28S-34S. https://doi.org/10.1046/j.1365-2672.92.5s1.16.x

McNeil, M. B., Hampton, H. G., Hards, K. J., Watson, B. N. J., Cook, G. M., & Fineran, P. C. (2014). The succinate dehydrogenase assembly factor, SdhE, is required for the flavinylation and activation of fumarate reductase in bacteria. *FEBS Letters*, *588*(3), 414–421. https://doi.org/10.1016/J.FEBSLET.2013.12.019

Meinke, D. W., Cherry, J. M., Dean, C., Rounsley, S. D., & Koornneef, M. (1998). Arabidopsis thaliana: A model plant for genome analysis. *Science*, *282*(5389). https://doi.org/10.1126/science.282.5389.662

Mendgen, T., Scholz, T., & Klein, C. D. (2010). Structure–activity relationships of tulipalines, tuliposides, and related compounds as inhibitors of MurA. *Bioorganic & Medicinal Chemistry Letters*, *20*(19), 5757–5762. https://doi.org/10.1016/j.bmcl.2010.07.139

Mengin-Lecreulx, D., Flouret, B., & van Heijenoort, J. (1983). Pool levels of UDP N-acetylglucosamine and UDP N-acetylglucosamine-enolpyruvate in Escherichia coli and correlation with peptidoglycan synthesis. *Journal of Bacteriology*, *154*(3), 1284–1290. https://doi.org/10.1128/jb.154.3.1284-1290.1983

Menino, J. F., Saraiva, M., Gomes-Rezende, J., Sturme, M., Pedrosa, J., Castro, A. G., Ludovico, P., Goldman, G. H., & Rodrigues, F. (2013). P. brasiliensis Virulence Is Affected by SconC, the Negative Regulator of Inorganic Sulfur Assimilation. *PLoS ONE*, *8*(9), e74725. https://doi.org/10.1371/journal.pone.0074725

Merrill, A. H., & McCormick, D. B. (2020). Riboflavin. In *Present Knowledge in Nutrition* (Vol. 1, pp. 189–207). Elsevier. https://doi.org/10.1016/B978-0-323-66162-1.00011-1

Metzler, D., Metzler, C., & Sauke, D. (2003). *Biochemistry* (2nd ed.). Harcourt, Academic Press.

Meyer, M. E. (1967). Metabolic Characterization of the Genus Brucella VI. Growth Stimulation by i -Erythritol Compared with Strain Virulence for Guinea Pigs. *Journal of Bacteriology*, *93*(3), 996–1000. https://doi.org/10.1128/jb.93.3.996-1000.1967

Michalopoulos, A. S., Livaditis, I. G., & Gougoutas, V. (2011). The revival of fosfomycin. *International Journal of Infectious Diseases*, *15*(11), e732–e739. https://doi.org/10.1016/j.ijid.2011.07.007

Mingorance, J., Tamames, J., & Vicente, M. (2004). Genomic channeling in bacterial cell division. *Journal of Molecular Recognition*, *17*(5), 481–487. https://doi.org/10.1002/jmr.718

Mirdita, M., Schütze, K., Moriwaki, Y., Heo, L., Ovchinnikov, S., & Steinegger, M. (2022). ColabFold: making protein folding accessible to all. *Nature Methods*, *19*(6), 679–682. https://doi.org/10.1038/s41592-022-01488-1

Mirnejad, R., Jazi, F. M., Mostafaei, S., & Sedighi, M. (2017). Molecular investigation of virulence factors of Brucella melitensis and Brucella abortus strains isolated from clinical and non-clinical samples. *Microbial Pathogenesis*, *109*, 8–14. https://doi.org/10.1016/j.micpath.2017.05.019

Miyachiro, M. M., Granato, D., Trindade, D. M., Ebel, C., Paes Leme, A. F., & Dessen, A. (2019). Complex Formation between Mur Enzymes from Streptococcus pneumoniae. *Biochemistry*, *58*(30), 3314–3324. https://doi.org/10.1021/acs.biochem.9b00277

Mizuno, Y., Yaegashi, M., & Ito, E. (1973). Purification and Properties of Uridine Diphosphate N-Acetylmuramate : L-Alanine Ligase*. *The Journal of Biochemistry*, *74*(3), 525–538. https://doi.org/10.1093/oxfordjournals.jbchem.a130273

Mol, C. D., Brooun, A., Dougan, D. R., Hilgers, M. T., Tari, L. W., Wijnands, R. A., Knuth, M. W., McRee, D. E., & Swanson, R. V. (2003). Crystal structures of active fully assembled substrate- and product-bound complexes of UDP-N-acetylmuramic acid:L-alanine ligase (MurC) from Haemophilus influenzae. *Journal of Bacteriology*, *185*(14), 4152–4162. https://doi.org/10.1128/JB.185.14.4152-4162.2003

Montoya-Peleaz, P. J., Riley, J. G., Szarek, W. A., Valvano, M. A., Schutzbach, J. S., & Brockhausen, I. (2005). Identification of a UDP-Gal: GlcNAc-R galactosyltransferase activity in Escherichia coli VW187. *Bioorganic & Medicinal Chemistry Letters*, *15*(4), 1205–1211.

https://doi.org/10.1016/j.bmcl.2004.11.077

Moraes, G. L., Gomes, G. C., Monteiro De Sousa, P. R., Alves, C. N., Govender, T., Kruger, H. G., Maguire, G. E. M., Lamichhane, G., & Lameira, J. (2015). Structural and functional features of enzymes of Mycobacterium tuberculosis peptidoglycan biosynthesis as targets for drug development. *Tuberculosis*, *95*(2), 95–111. https://doi.org/10.1016/j.tube.2015.01.006

Moran, G. R. (2019). Anaerobic methods for the transient-state study of flavoproteins: The use of specialized glassware to define the concentration of dioxygen. In *Methods in Enzymology* (1st ed., Vol. 620, pp. 27–49). Elsevier Inc. https://doi.org/10.1016/bs.mie.2019.03.005

Moreno, A., Martinez-Julvez, M., & Medina, M. (2023). Searching for potential drugs to inhibit the activity of the enzyme MurA involved in the cell wall biosynthesis in Brucella ovis. *45º Congreso de La Sociedad Española de Bioquímica y Biología Molecular. Póster. Zaragoza, España*.

Moreno, A., Taleb, V., Sebastián, M., Anoz-Carbonell, E., Martínez-Júlvez, M., & Medina, M. (2022). Cofactors and pathogens: Flavin mononucleotide and flavin adenine dinucleotide (FAD) biosynthesis by the FAD synthase from Brucella ovis. *IUBMB Life*, *74*(7), 655–671. https://doi.org/10.1002/iub.2576

Morozov, G. I., Porat, N., Kushnir, T., Najmuldeen, H., Adawi, A., Chalifa-Caspi, V., Benisty, R., Ohayon, A., Liron, O., Azriel, S., Malka, I., Dotan, S., Portnoi, M., Piotrowski, A. A., Kafka, D., Hajaj, B., Fishilevich, T., Shagan, M., Tal, M., … Nebenzahl, Y. M. (2018). Flavin Reductase Contributes to Pneumococcal Virulence by Protecting from Oxidative Stress and Mediating Adhesion and Elicits Protection Against Pneumococcal Challenge. *Scientific Reports*, *8*(1), 314. https://doi.org/10.1038/s41598-017-18645-8

Mulo, P., & Medina, M. (2017). Interaction and electron transfer between ferredoxin–NADP+ oxidoreductase and its partners: structural, functional, and physiological implications. *Photosynthesis Research*, *134*(3), 265–280. https://doi.org/10.1007/s11120-017-0372-0

Munro, A. W., & Noble, M. A. (1999). Fluorescence Analysis of Flavoproteins. In *Flavoprotein Protocols* (Vol. 131, Issue 3, pp. 25–48). Humana Press. https://doi.org/10.1385/1-59259-266-X:25

Munshi, T., Gupta, A., Evangelopoulos, D., Guzman, J. D., Gibbons, S., Keep, N. H., & Bhakta, S. (2013). Characterisation of ATP-Dependent Mur Ligases Involved in the Biogenesis of Cell Wall Peptidoglycan in Mycobacterium tuberculosis. *PLoS ONE*, *8*(3), e60143. https://doi.org/10.1371/journal.pone.0060143

Murshudov, G. N., Vagin, A. A., & Dodson, E. J. (1997). Refinement of Macromolecular Structures by the Maximum-Likelihood Method. *Acta Crystallographica Section D Biological Crystallography*, *53*(3), 240–255. https://doi.org/10.1107/S0907444996012255

Murthy, Y. V. S. N., & Massey, V. (1997). *Syntheses and applications of flavin analogs as active site probes for flavoproteins* (Vol. 280, Issue 1986, pp. 436–460). https://doi.org/10.1016/S0076-6879(97)80135-8

Murty, C. V. R., & Adiga, P. R. (1982). Pregnancy Suppression by Active Immunization Against Gestation-Specific Riboflavin Carrier Protein. *Science*, *216*(4542), 191–193. https://doi.org/10.1126/science.7063879

Murzin, A. G. (1996). Structural classification of proteins: new superfamilies. *Current Opinion in Structural Biology*, *6*(3), 386–394. https://doi.org/10.1016/S0959-440X(96)80059-5

Myllykallio, H., Lipowski, G., Leduc, D., Filee, J., Forterre, P., & Liebl, U. (2002). An Alternative Flavin-Dependent Mechanism for Thymidylate Synthesis. *Science*, *297*(5578), 105–107. https://doi.org/10.1126/science.1072113

Naqvi, K. F., Patin, D., Wheatley, M. S., Savka, M. A., Dobson, R. C., Ming-Gan, H., Barreteau, H., Blanot, D., Mengin-lecreulx, D., & Hudson, A. O. (2016). Identification and Partial Characterization of a Novel UDP- N - Acetylenolpyruvoylglucosamine Reductase / UDP- N - Acetylmuramate : L -Alanine Ligase Fusion Enzyme from Verrucomicrobium spinosum DSM 4136T. *Frontiers in Microbilogy*, *7*(362), 1–13. https://doi.org/10.3389/fmicb.2016.00362

Natan, E., Wells, J. N., Teichmann, S. A., & Marsh, J. A. (2017). Regulation, evolution and consequences of cotranslational protein complex assembly. *Current Opinion in Structural Biology*, *42*, 90–97. https://doi.org/10.1016/j.sbi.2016.11.023

Nirwan, S., Chahal, V., & Kakkar, R. (2019). Thiazolidinones: Synthesis, Reactivity, and Their Biological Applications. *Journal of Heterocyclic Chemistry*, *56*(4), 1239–1253. https://doi.org/10.1002/jhet.3514

Nishida, S., Kurokawa, K., Matsuo, M., Sakamoto, K., Ueno, K., Kita, K., & Sekimizu, K. (2006). Identification and Characterization of Amino Acid Residues Essential for the Active Site of UDP- N - acetylenolpyruvylglucosamine Reductase (MurB) from Staphylococcus aureus *. *Journal of Biological Chemistry*, *281*(3), 1714–1724. https://doi.org/10.1074/jbc.M509277200

Nishimasu, H., Ishitani, R., Yamashita, K., Iwashita, C., Hirata, A., Hori, H., & Nureki, O. (2009). Atomic structure of a folate/FAD-dependent tRNA T54 methyltransferase. *Proceedings of the National Academy of Sciences*, *106*(20), 8180–8185. https://doi.org/10.1073/pnas.0901330106

Nivière, V., Vanoni, M. A., Zanetti, G., & Fontecave, M. (1998). Reaction of the NAD(P)H:flavin

oxidoreductase from Escherichia coli with NADPH and riboflavin: Identification of intermediates. *Biochemistry*, *37*(34), 11879–11887. https://doi.org/10.1021/bi980396f

Nogués, I., Tejero, J., Hurley, J. K., Paladini, D., Frago, S., Tollin, G., Mayhew, S. G., Gómez-Moreno, C., Ceccarelli, E. A., Carrillo, N., & Medina, M. (2004). Role of the C-Terminal Tyrosine of Ferredoxin-Nicotinamide Adenine Dinucleotide Phosphate Reductase in the Electron Transfer Processes with Its Protein Partners Ferredoxin and Flavodoxin. *Biochemistry*, *43*(20), 6127–6137. https://doi.org/10.1021/bi049858h

Nöldeke, E. R., Muckenfuss, L. M., Niemann, V., Müller, A., Störk, E., Zocher, G., Schneider, T., & Stehle, T. (2018). Structural basis of cell wall peptidoglycan amidation by the GatD/MurT complex of Staphylococcus aureus. *Scientific Reports*, *8*(1), 12953. https://doi.org/10.1038/s41598-018-31098-x

Novo, N., Ferreira, P., & Medina, M. (2021). The apoptosis-inducing factor family: Moonlighting proteins in the crosstalk between mitochondria and nuclei. *IUBMB Life*, *73*(3), 568–581. https://doi.org/10.1002/iub.2390

O'Loughlin, J., Napolitano, S., Alkhathami, F., O'Beirne, C., Marhöfer, D., O'Shaughnessy, M., Howe, O., Tacke, M., & Rubini, M. (2021). The Antibacterial Drug Candidate SBC3 is a Potent Inhibitor of Bacterial Thioredoxin Reductase. *ChemBioChem*, *22*(6), 1093–1098. https://doi.org/10.1002/cbic.202000707

Oliver, K. E., & Silo-Suh, L. (2013). Impact of <scp>d</scp> -amino acid dehydrogenase on virulence factor production by a *Pseudomonas aeruginosa*. *Canadian Journal of Microbiology*, *59*(9), 598–603. https://doi.org/10.1139/cjm-2013-0289

Onyenwoke, R., Brill, J., Farahi, K., & Wiegel, J. (2004). Sporulation genes in members of the low G+C Gram-type-positive phylogenetic branch (Firmicutes). *Archives of Microbiology*, *182*(2–3), 182–192. https://doi.org/10.1007/s00203-004-0696-y

Oren, A., & Garrity, G. (2020). List of new names and new combinations previously effectively, but not validly, published. *International Journal of Systematic and Evolutionary Microbiology*, *70*(7), 4043–4049. https://doi.org/10.1099/ijsem.0.004244

Pace, C. N., Vajdos, F., Fee, L., Grimsley, G., & Gray, T. (1995). How to measure and predict the molar absorption coefficient of a protein. *Protein Science*, *4*(11), 2411–2423. https://doi.org/10.1002/pro.5560041120

Palfey, B. A., & McDonald, C. A. (2010). Control of catalysis in flavin-dependent monooxygenases. *Archives of Biochemistry and Biophysics*, *493*(1), 26–36. https://doi.org/10.1016/j.abb.2009.11.028

Pandey, A., Ray, S. K., Sonti, R. V., & Rajeshwari, R. (2014). gltB/D Mutants of Xanthomonas oryzae pv. oryzae are Virulence Deficient. *Current Microbiology*, *68*(1), 105–112. https://doi.org/10.1007/s00284-013-0444-0

Parsons, H. G., & Dias, V. C. (1991). Intramitochondrial fatty acid metabolism: riboflavin deficiency and energy production. *Biochemistry and Cell Biology*, *69*(7), 490–497. https://doi.org/10.1139/o91-073

Patin, D., Boniface, A., Kovač, A., Hervé, M., Dementin, S., Barreteau, H., Mengin-Lecreulx, D., & Blanot, D. (2010). Purification and biochemical characterization of Mur ligases from Staphylococcus aureus. *Enfermedades Infecciosas y Microbiologia Clinica*, *28*(SUPPL. 3), 1793–1800. https://doi.org/10.1016/j.biochi.2010.07.009

Paul, P. E. V., Sangeetha, V., & Deepika, R. G. (2019). Emerging Trends in the Industrial Production of Chemical Products by Microorganisms. In *Recent Developments in Applied Microbiology and Biochemistry* (pp. 107–125). Elsevier. https://doi.org/10.1016/B978-0-12-816328-3.00009-X

Pavlovska, T., & Cibulka, R. (2021). Structure and Properties of Flavins. In *Flavin-Based Catalysis* (pp. 1–27). Wiley. https://doi.org/10.1002/9783527830138.ch1

Pazos, M., & Peters, K. (2019). *Bacterial Cell Walls and Membranes* (A. Kuhn (ed.); Vol. 92). Springer International Publishing. https://doi.org/10.1007/978-3-030-18768-2

Perdih, A., Hrast, M., Barreteau, H., Gobec, S., Wolber, G., & Solmajer, T. (2014). Benzene-1,3-dicarboxylic acid 2,5-dimethylpyrrole derivatives as multiple inhibitors of bacterial Mur ligases (MurC-MurF). *Bioorganic and Medicinal Chemistry*, *22*(15), 4124–4134. https://doi.org/10.1016/j.bmc.2014.05.058

Pérez-Amigot, D., Taleb, V., Boneta, S., Anoz-Carbonell, E., Sebastián, M., Velázquez-Campoy, A., Polo, V., Martínez-Júlvez, M., & Medina, M. (2019). Towards the competent conformation for catalysis in the ferredoxin-NADP+ reductase from the Brucella ovis pathogen. *Biochimica et Biophysica Acta (BBA) - Bioenergetics*, *1860*(10), 148058. https://doi.org/10.1016/j.bbabio.2019.148058

Petersen, E., Rajashekara, G., Sanakkayala, N., Eskra, L., Harms, J., & Splitter, G. (2013). Erythritol triggers expression of virulence traits in Brucella melitensis. *Microbes and Infection*, *15*(6–7), 440–449. https://doi.org/10.1016/j.micinf.2013.02.002

Picard-Hagen, N., Berthelot, X., Champion, J. L., Eon, L., Lyazrhi, F., Marois, M., Peglion, M., Schuster, A., Trouche, C., & Garin-Bastuji, B. (2015). Contagious epididymitis due to Brucella ovis: relationship

between sexual function, serology and bacterial shedding in semen. *BMC Veterinary Research*, *11*(1), 125. https://doi.org/10.1186/s12917-015-0440-7

Pimviriyakul, P., & Chaiyen, P. (2020). Overview of flavin-dependent enzymes. In *Enzymes* (1st ed., Vol. 47). Elsevier Inc. https://doi.org/10.1016/bs.enz.2020.06.006

Pinto, J. T., & Cooper, A. J. L. (2014). From Cholesterogenesis to Steroidogenesis: Role of Riboflavin and Flavoenzymes in the Biosynthesis of Vitamin D. *Advances in Nutrition*, *5*(2), 144–163. https://doi.org/10.3945/an.113.005181

Prongay, A. J., Engelke, D. R., & Williams, C. H. (1989). Characterization of two active site mutations of thioredoxin reductase from Escherichia coli. *Journal of Biological Chemistry*, *264*(5), 2656–2664. https://doi.org/10.1016/S0021-9258(19)81664-2

Prongay, A. J., & Williams, C. H. (1990). Evidence for direct interaction between cysteine 138 and the flavin in thioredoxin reductase. A study using flavin analogs. *Journal of Biological Chemistry*, *265*(31), 18968–18975. https://doi.org/10.1016/S0021-9258(17)30610-5

Prongay, A. J., & Williams, C. H. (1992). Oxidation-reduction properties of Escherichia coli thioredoxin reductase altered at each active site cysteine residue. *Journal of Biological Chemistry*, *267*(35), 25181–25188. https://doi.org/10.1016/S0021-9258(19)74022-8

Pueyo, J. J., & Gómez-Moreno, C. (1991). Purification of Ferredoxin-NADP + Reductase, Flavodoxin and Ferredoxin from a Single Batch of the Cyanobacterium Anabaena PCC 7119. *Preparative Biochemistry*, *21*(4), 191–204. https://doi.org/10.1080/10826069108018571

Pupko, T., Bell, R. E., Mayrose, I., Glaser, F., & Ben-Tal, N. (2002). Rate4Site: an algorithmic tool for the identification of functional regions in proteins by surface mapping of evolutionary determinants within their homologues. *Bioinformatics*, *18*(suppl_1), S71–S77. https://doi.org/10.1093/bioinformatics/18.suppl_1.S71

Rabe, F., Ajami-Rashidi, Z., Doehlemann, G., Kahmann, R., & Djamei, A. (2013). Degradation of the plant defence hormone salicylic acid by the biotrophic fungus Ustilago maydis. *Molecular Microbiology*, *89*(1), 179–188. https://doi.org/10.1111/mmi.12269

Ragunathan, A., Malathi, K., & Anbarasu, A. (2018). MurB as a target in an alternative approach to tackle the Vibrio cholerae resistance using molecular docking and simulation study. *Journal of Cellular Biochemistry*, *119*(2), 1726–1732. https://doi.org/10.1002/jcb.26333

Rajashankar, K. R., Bryk, R., Kniewel, R., Buglino, J. A., Nathan, C. F., & Lima, C. D. (2005). Crystal Structure and Functional Analysis of Lipoamide Dehydrogenase from Mycobacterium tuberculosis. *Journal of Biological Chemistry*, *280*(40), 33977–33983. https://doi.org/10.1074/jbc.M507466200

Rausch, S., Hänchen, A., Denisiuk, A., Lçhken, M., & Schneider, T. (2011). Feglymycin is an Inhibitor of the Enzymes MurA and MurC of the Peptidoglycan Biosynthesis Pathway. *Chem Bio Chem*, *12*, 1171–1173. https://doi.org/10.1002/cbic.201100120

Raymond, J. B., Price, N. P., & Pavelka, M. S. (2003). A method for the enzymatic synthesis and HPLC purification of the peptidoglycan precursor UDP- N -acetylmuramic acid. *FEMS Microbiology Letters*, *229*(1), 83–89. https://doi.org/10.1016/S0378-1097(03)00793-6

Rhodes, D. L. V., Crump, K. E., Makhlynets, O., Snyder, M., Ge, X., Xu, P., Stubbe, J. A., & Kitten, T. (2014). Genetic characterization and role in virulence of the ribonucleotide reductases of Streptococcus sanguinis. *Journal of Biological Chemistry*, *289*(9), 6273–6287. https://doi.org/10.1074/jbc.M113.533620

Rinaldi, J., Arrar, M., Sycz, G., Cerutti, M. L., Berguer, P. M., Paris, G., Estrín, D. A., Martí, M. A., Klinke, S., & Goldbaum, F. A. (2016). Structural Insights into the HWE Histidine Kinase Family: The Brucella Blue Light-Activated Histidine Kinase Domain. *Journal of Molecular Biology*, *428*(6), 1165–1179. https://doi.org/10.1016/j.jmb.2016.01.026

Rinaldi, J., Fernández, I., Shin, H., Sycz, G., Gunawardana, S., Kumarapperuma, I., Paz, J. M., Otero, L. H., Cerutti, M. L., Zorreguieta, Á., Ren, Z., Klinke, S., Yang, X., & Goldbaum, F. A. (2021). Dimer Asymmetry and Light Activation Mechanism in Brucella Blue-Light Sensor Histidine Kinase. *MBio*, *12*(2), 1–18. https://doi.org/10.1128/mBio.00264-21

Rodríguez, M. C., Viadas, C., Seoane, A., Sangari, F. J., López-Goñi, I., & García-Lobo, J. M. (2012). Evaluation of the Effects of Erythritol on Gene Expression in Brucella abortus. *PLoS ONE*, *7*(12), e50876. https://doi.org/10.1371/journal.pone.0050876

Romero, E., & Gadda, G. (2014). Alcohol oxidation by flavoenzymes. *Biomolecular Concepts*, *5*(4), 299–318. https://doi.org/10.1515/bmc-2014-0016

Romero, E., Gómez Castellanos, J. R., Gadda, G., Fraaije, M. W., & Mattevi, A. (2018). Same Substrate, Many Reactions: Oxygen Activation in Flavoenzymes. *Chemical Reviews*, *118*(4), 1742–1769. https://doi.org/10.1021/acs.chemrev.7b00650

Ronneau, S., Moussa, S., Barbier, T., Conde-Álvarez, R., Zuniga-Ripa, A., Moriyon, I., & Letesson, J.-J.

(2016). Brucella , nitrogen and virulence. *Critical Reviews in Microbiology*, *42*(4), 507–525. https://doi.org/10.3109/1040841X.2014.962480

Sadeghian, H., Sadeghian, A., Pordel, M., Rahimizadeh, M., Jahandari, P., Orafaie, A., & Bakavoli, M. (2010). Design, synthesis, and structure-activity relationship study of 5-amido-1-(2,4-dinitrophenyl)-1H-4-pyrazolecarbonitrils as DD-carboxypeptidase/ penicillin-binding protein inhibitors with Gram-positive antibacterial activity. *Medicinal Chemistry Research*, *19*(2), 103–119. https://doi.org/10.1007/s00044-009-9175-y

Samland, A. K., Amrhein, N., & Macheroux, P. (1999). Lysine 22 in UDP- N -Acetylglucosamine Enolpyruvyl Transferase from Enterobacter cloacae Is Crucial for Enzymatic Activity and the Formation of Covalent Adducts with the Substrate Phosphoenolpyruvate and the Antibiotic Fosfomycin. *Biochemistry*, *38*(40), 13162–13169. https://doi.org/10.1021/bi991041e

Sangari, F. J., Agüero, J., & García-Lobo, J. M. (2000). The genes for erythritol catabolism are organized as an inducible operon in Brucella abortus The GenBank accession number for the sequence reported in this paper is U57100. *Microbiology*, *146*(2), 487–495. https://doi.org/10.1099/00221287-146-2-487

Sasindran, S. J., Saikolappan, S., & Dhandayuthapani, S. (2007). Methionine sulfoxide reductases and virulence of bacterial pathogens. *Future Microbiology*, *2*(6), 619–630.

Sauvage, E., Kerff, F., Terrak, M., Ayala, J. A., & Charlier, P. (2008). The penicillin-binding proteins: Structure and role in peptidoglycan biosynthesis. *FEMS Microbiology Reviews*, *32*(2), 234–258. https://doi.org/10.1111/j.1574-6976.2008.00105.x

Sbriglio, J. L., Sbriglio, H., & Sainz, S. (2007). Brucelosis Una patología generalmente subdiagnosticada en Humanos y que impacta negativamente en la producción pecuaria y desarrollo de nuestros países. *Revista Bianálisis*, *1*, 18, 19,. http://www.revistabioanalisis.com/images/flippingbook/Rev13 n/Nota3.pdf

Schall, P., Marutschke, L., & Grimm, B. (2020). The flavoproteome of the model plant arabidopsis thaliana. *International Journal of Molecular Sciences*, *21*(15), 1–18. https://doi.org/10.3390/ijms21155371

Scheffers, D., & Pinho, M. G. (2005). Bacterial Cell Wall Synthesis : New Insights from Localization Studies. *Microbiology and Molecular Biology Reviews*, *69*(4), 585–607. https://doi.org/10.1128/MMBR.69.4.585

Scholz, A., Stahl, J., de Berardinis, V., Müller, V., & Averhoff, B. (2016). Osmotic stress response in Acinetobacter baylyi : identification of a glycine-betaine biosynthesis pathway and regulation of osmoadaptive choline uptake and glycine-betaine synthesis through a choline-responsive BetI repressor. *Environmental Microbiology Reports*, *8*(2), 316–322. https://doi.org/10.1111/1758-2229.12382

Scholz, H. C., Hubalek, Z., Sedlacek, I., Vergnaud, G., Tomaso, H., Al Dahouk, S., Melzer, F., Kampfer, P., Neubauer, H., Cloeckaert, A., Maquart, M., Zygmunt, M. S., Whatmore, A. M., Falsen, E., Bahn, P., Gollner, C., Pfeffer, M., Huber, B., Busse, H.-J., & Nockler, K. (2008). Brucella microti sp. nov., isolated from the common vole Microtus arvalis. *INTERNATIONAL JOURNAL OF SYSTEMATIC AND EVOLUTIONARY MICROBIOLOGY*, *58*(2), 375–382. https://doi.org/10.1099/ijs.0.65356-0

Schönbrunn, E., Eschenburg, S., Krekel, F., Luger, K., & Amrhein, N. (2000). Role of the Loop Containing Residue 115 in the Induced-Fit Mechanism of the Bacterial Cell Wall Biosynthetic Enzyme MurA. *Biochemistry*, *39*(9), 2164–2173. https://doi.org/10.1021/bi991091j

Schönbrunn, E., Eschenburg, S., Luger, K., Kabsch, W., & Amrhein, N. (2000). Structural basis for the interaction of the fluorescence probe 8-anilino-1-naphthalene sulfonate (ANS) with the antibiotic target MurA. *Proceedings of the National Academy of Sciences*, *97*(12), 6345–6349. https://doi.org/10.1073/pnas.120120397

Schönbrunn, E., Sack, S., Eschenburg, S., Perrakis, A., Krekel, F., Amrhein, N., & Mandelkow, E. (1996). Crystal structure of UDP-N-acetylglucosamine enolpyruvyltransferase, the target of the antibiotic fosfomycin. *Structure*, *4*(9), 1065–1075. https://doi.org/10.1016/S0969-2126(96)00113-X

Schulte, M., Frick, K., Gnandt, E., Jurkovic, S., Burschel, S., Labatzke, R., Aierstock, K., Fiegen, D., Wohlwend, D., Gerhardt, S., Einsle, O., & Friedrich, T. (2019). A mechanism to prevent production of reactive oxygen species by Escherichia coli respiratory complex I. *Nature Communications*, *10*(1), 2551. https://doi.org/10.1038/s41467-019-10429-0

Schweizer, T., Kubach, H., & Koch, T. (2021). Investigations to characterize the interactions of light radiation, engine operating media and fluorescence tracers for the use of qualitative light-induced fluorescence in engine systems. *Automotive and Engine Technology*, *6*(3–4), 275–287. https://doi.org/10.1007/s41104-021-00092-3

Sebastián, M., Anoz-Carbonell, E., Gracia, B., Cossio, P., Aínsa, J. A., Lans, I., & Medina, M. (2018). Discovery of antimicrobial compounds targeting bacterial type FAD synthetases. *Journal of Enzyme Inhibition and Medicinal Chemistry*, *33*(1), 241–254. https://doi.org/10.1080/14756366.2017.1411910

Seo, P.-W., Park, S.-Y., Hofmann, A., & Kim, J.-S. (2021). Crystal structures of UDP- N -acetylmuramic acid L -alanine ligase (MurC) from Mycobacterium bovis with and without UDP- N -acetylglucosamine. *Acta Crystallographica Section D Structural Biology*, *77*(5), 618–627.

https://doi.org/10.1107/S2059798321002199

Serer, M. I., Carrica, M. del C., Trappe, J., López Romero, S., Bonomi, H. R., Klinke, S., Cerutti, M. L., & Goldbaum, F. A. (2019). A high-throughput screening for inhibitors of riboflavin synthase identifies novel antimicrobial compounds to treat brucellosis. *The FEBS Journal*, *286*(13), 2522–2535. https://doi.org/10.1111/febs.14829

Serrano, A., Ferreira, P., Martinez-Julvez, M., & Medina, M. (2013). The Prokaryotic FAD Synthetase Family: A Potential Drug Target. *Current Pharmaceutical Design*, *19*(14), 2637–2648. https://doi.org/10.2174/1381612811319140013

Serrano, A., Frago, S., Velázquez-Campoy, A., & Medina, M. (2012). Role of Key Residues at the Flavin Mononucleotide (FMN):Adenylyltransferase Catalytic Site of the Bifunctional Riboflavin Kinase/Flavin Adenine Dinucleotide (FAD) Synthetase from Corynebacterium ammoniagenes. *International Journal of Molecular Sciences*, *13*(12), 14492–14517. https://doi.org/10.3390/ijms131114492

Shahab, M., Verma, M., Pathak, M., Mitra, K., & Misra-Bhattacharya, S. (2014). Cloning, expression and characterization of UDP-N-acetylglucosamine enolpyruvyl transferase (MurA) from Wolbachia endosymbiont of human lymphatic filarial parasite Brugia malayi. *PLoS ONE*, *9*(6), 1–14. https://doi.org/10.1371/journal.pone.0099884

Sham, L.-T., Butler, E. K., Lebar, M. D., Kahne, D., Bernhardt, T. G., & Ruiz, N. (2015). MurJ is the flippase of lipid-linked precursors for peptidoglycan biogenesis. *HHS Public Acces*, *345*(6193), 220–222. https://doi.org/10.1126/science.1254522.MurJ

Sharma, A., Sharma, D., & Verma, S. K. (2017). Proteome wide identification of iron binding proteins of Xanthomonas translucens pv. undulosa: focus on secretory virulent proteins. *BioMetals*, *30*(1), 127–141. https://doi.org/10.1007/s10534-017-9991-3

Sherwood, A. R., Paasch, B. C., Worby, C. A., & Gentry, M. S. (2014). A Malachite Green-Based Assay to Assess Glucan Phosphatase Activity. *NIH Public Access*, *435*(1), 54–56. https://doi.org/10.1016/j.ab.2012.10.044.A

Shim, S., Im, Y. Bin, Jung, M., Park, W. Bin, & Yoo, H. S. (2018). Genes Related to Intracellular Survival of Brucella abortus in THP-1 Macrophage Cells. *Journal of Microbiology and Biotechnology*, *28*(10), 1736–1748. https://doi.org/10.4014/jmb.1805.05068

Shippy, D. C., Heintz, J. A., Albrecht, R. M., Eakley, N. M., & Fadl, A. A. (2012). Deletion of glucose-inhibited division (gidA) gene alters the morphological and replication characteristics of Salmonella enterica Serovar typhimurium. *Archives of Microbiology*, *194*(6), 405–412. https://doi.org/10.1007/s00203-011-0769-7

Shirakawa, K. T., Sala, F. A., Miyachiro, M. M., Job, V., Trindade, D. M., & Dessen, A. (2023). Architecture and genomic arrangement of the MurE–MurF bacterial cell wall biosynthesis complex. *Proceedings of the National Academy of Sciences*, *120*(21), 2017. https://doi.org/10.1073/pnas.2219540120

Sievers, F., Wilm, A., Dineen, D., Gibson, T. J., Karplus, K., Li, W., Lopez, R., McWilliam, H., Remmert, M., Söding, J., Thompson, J. D., & Higgins, D. G. (2011). Fast, scalable generation of high-quality protein multiple sequence alignments using Clustal Omega. *Molecular Systems Biology*, *7*(1), 539. https://doi.org/10.1038/msb.2011.75

Sikorska, E., Khmelinskii, I. V., Prukała, W., Williams, S. L., Patel, M., Worrall, D. R., Bourdelande, J. L., Koput, J., & Sikorski, M. (2004). Spectroscopy and Photophysics of Lumiflavins and Lumichromes. *The Journal of Physical Chemistry A*, *108*(9), 1501–1508. https://doi.org/10.1021/jp037048u

Silhavy, T. J., Kahne, D., & Walker, S. (2010). The Bacterial Cell Envelope1 T. J. Silhavy, D. Kahne and S. Walker, . *Cold Spring Harb Perspect Biol*, *2*, 1–16. https://www.ncbi.nlm.nih.gov/pmc/articles/PMC2857177/pdf/cshperspect-PRK-a000414.pdf

Sim, M. M., Ng, S. B., Buss, A. D., Crasta, S. C., Goh, K. L., & Lee, S. K. (2002). Benzylidene rhodanines as novel inhibitors of UDP-N-acetylmuramate/L-alanine ligase. *Bioorganic and Medicinal Chemistry Letters*, *12*(4), 697–699. https://doi.org/10.1016/S0960-894X(01)00832-0

Šink, R., Kovač, A., Tomašić, T., Rupnik, V., Boniface, A., Bostock, J., Chopra, I., Blanot, D., Mašič, L. P., Gobec, S., & Zega, A. (2008). Synthesis and biological evaluation of N-acylhydrazones as inhibitors of MurC and MurD ligases. *ChemMedChem*, *3*(9), 1362–1370. https://doi.org/10.1002/cmdc.200800087

Skarzynski, T., Kim, D. H., Lees, W. J., Walsh, C. T., & Duncan, K. (1998). Stereochemical course of enzymatic enolpyruvyl transfer and catalytic conformation of the active site revealed by the crystal structure of the fluorinated analogue of the reaction tetrahedral intermediate bound to the active site of the C115A mutant of Mu. *Biochemistry*, *37*(8), 2572–2577. https://doi.org/10.1021/bi9722608

Skarzynski, T., Mistry, A., Wonacott, A., Hutchinson, S. E., Kelly, V. A., & Duncan, K. (1996). Structure of UDP-N-acetylglucosamine enolpyruvyl transferase, an enzyme essential for the synthesis of bacterial peptidoglycan, complexed with substrate UDP-N-acetylglucosamine and the drug fosfomycin. *Structure*, *4*(12), 1465–1474. https://doi.org/10.1016/S0969-2126(96)00153-0

Song, E.-S., Park, Y.-J., Noh, T.-H., Kim, Y.-T., Kim, J.-G., Cho, H., & Lee, B.-M. (2012). Functional analysis of the aroC gene encoding chorismate synthase from Xanthomonas oryzae pathovar oryzae. *Microbiological Research*, *167*(6), 326–331. https://doi.org/10.1016/j.micres.2011.11.002

Sonkar, A., Shukla, H., Shukla, R., Kalita, J., Pandey, T., & Tripathi, T. (2017). UDP-N-Acetylglucosamine enolpyruvyl transferase (MurA) of Acinetobacter baumanii (AbMurA): Structural and functional properties. *International Journal of Biological Macromolecules*, *97*, 106–114.

Spaans, S. K., Weusthuis, R. A., van der Oost, J., & Kengen, S. W. M. (2015). NADPH-generating systems in bacteria and archaea. *Frontiers in Microbiology*, *6*(JUL), 1–27. https://doi.org/10.3389/fmicb.2015.00742

Spellerberg, B., Cundell, D. R., Sandros, J., Pearce, B. J., Idänpään-Heikkilä, I., Rosenow, C., & Masure, H. R. (1996). Pyruvate oxidase, as a determinant of virulence in Streptococcus pneumoniae. *Molecular Microbiology*, *19*(4), 803–813. https://doi.org/10.1046/j.1365-2958.1996.425954.x

Spraggon, G., Schwarzenbacher, R., Kreusch, A., Lee, C. C., Abdubek, P., Ambing, E., Biorac, T., Brinen, L. S., Canaves, J. M., Cambell, J., Chiu, H.-J., Dai, X., Deacon, A. M., DiDonato, M., Elsliger, M.-A., Eshagi, S., Floyd, R., Godzik, A., Grittini, C., … Wilson, I. A. (2004). Crystal structure of an Udp-n-acetylmuramate-alanine ligase MurC (TM0231) from Thermotoga maritima at 2.3 Å resolution. *Proteins: Structure, Function, and Bioinformatics*, *55*(4), 1078–1081. https://doi.org/10.1002/prot.20034

Srilunchang, T., Proungvitaya, T., Wongratanacheewin, S., Strugnell, R., & Homchampa, P. (2009). Construction and characterization of an unmarked aroC deletion mutant of Burkholderia pseudomallei strain A2. *The Southeast Asian Journal of Tropical Medicine and Public Health*, *40*(1), 123–130. http://www.ncbi.nlm.nih.gov/pubmed/19323044

Stietz, M. S., Lopez, C., Osifo, O., Tolmasky, M. E., & Cardona, S. T. (2017). Evaluation of the electron transfer flavoprotein as an antibacterial target in Burkholderia cenocepacia. *Canadian Journal of Microbiology*, *63*(10), 857–863. https://doi.org/10.1139/cjm-2017-0350

Štrancar, K., Blanot, D., & Gobec, S. (2006). Design, synthesis and structure-activity relationships of new phosphinate inhibitors of MurD. *Bioorganic and Medicinal Chemistry Letters*, *16*(2), 343–348. https://doi.org/10.1016/j.bmcl.2005.09.086

Štrancar, K., Boniface, A., Blanot, D., & Gobec, S. (2007). Phosphinate inhibitors of UDP-N-acetylmuramoyl-L-alanyl-D-glutamate: L-lysine ligase (MurE). *Archiv Der Pharmazie*, *340*(3), 127–134. https://doi.org/10.1002/ardp.200600191

Straub, F. B. (1939). Isolation and properties of a flavoprotein from heart muscle tissue. *Biochemical Journal*, *33*(5), 787–792. https://doi.org/10.1042/bj0330787

Strauss, E., Kinsland, C., Ge, Y., McLafferty, F. W., & Begley, T. P. (2001). Phosphopantothenoylcysteine Synthetase from Escherichia coli. *Journal of Biological Chemistry*, *276*(17), 13513–13516. https://doi.org/10.1074/jbc.C100033200

Subramoni, S., Nguyen, D. T., & Sokol, P. A. (2011). Burkholderia cenocepacia ShvR-Regulated Genes That Influence Colony Morphology, Biofilm Formation, and Virulence. *Infection and Immunity*, *79*(8), 2984–2997. https://doi.org/10.1128/IAI.00170-11

Sun, M., Moore, T. A., & Song, P.-S. (1972). Molecular luminescence studies of flavines. I. Excited states of flavines. *Journal of the American Chemical Society*, *94*(5), 1730–1740. https://doi.org/10.1021/ja00760a052

Susanti, D., Loganathan, U., & Mukhopadhyay, B. (2016). A Novel F420-dependent Thioredoxin Reductase Gated by Low Potential FAD. *Journal of Biological Chemistry*, *291*(44), 23084–23100. https://doi.org/10.1074/jbc.M116.750208

Susin, S. A., Lorenzo, H. K., Zamzami, N., Marzo, I., Snow, B. E., Brothers, G. M., Mangion, J., Jacotot, E., Costantini, P., Loeffler, M., Larochette, N., Goodlett, D. R., Aebersold, R., Siderovski, D. P., Penninger, J. M., & Kroemer, G. (1999). Molecular characterization of mitochondrial apoptosis-inducing factor. *Nature*, *397*(6718), 441–446. https://doi.org/10.1038/17135

Sützl, L., Foley, G., Gillam, E. M. J., Bodén, M., & Haltrich, D. (2019). The GMC superfamily of oxidoreductases revisited: analysis and evolution of fungal GMC oxidoreductases. *Biotechnology for Biofuels*, *12*(1), 118. https://doi.org/10.1186/s13068-019-1457-0

Swartz, T. E., Corchnoy, S. B., Christie, J. M., Lewis, J. W., Szundi, I., Briggs, W. R., & Bogomolni, R. A. (2001). The Photocycle of a Flavin-binding Domain of the Blue Light Photoreceptor Phototropin. *Journal of Biological Chemistry*, *276*(39), 36493–36500. https://doi.org/10.1074/jbc.M103114200

Swartz, T. E., Tseng, T., Frederickson, M. A., Paris, G., Comerci, D. J., Rajashekara, G., Kim, J., Mudgett, M. B., Splitter, G. A., Ugalde, R. A., Goldbaum, F. A., Briggs, W. R., & Bogomolni, R. A. (2007). Blue-Light-Activated Histidine Kinases: Two-Component Sensors in Bacteria. *Science*, *317*(5841), 1090–1093. https://doi.org/10.1126/science.1144306

Sylvester, D. R., Alvarez, E., Patel, A., Ratnam, K., Kallender, H., & Wallis, N. G. (2001). Identification and

characterization of UDP-N-acetylenolpyruvylglucosamine reductase (MurB) from the Gram-positive pathogen Streptococcus pneumoniae. *Biochemistry*, *355*, 431–435.

Taga, M. E., Larsen, N. A., Howard-Jones, A. R., Walsh, C. T., & Walker, G. C. (2007). BluB cannibalizes flavin to form the lower ligand of vitamin B12. *Nature*, *446*(7134), 449–453. https://doi.org/10.1038/nature05611

Tamura, K., Stecher, G., & Kumar, S. (2021). MEGA11: Molecular Evolutionary Genetics Analysis Version 11. *Molecular Biology and Evolution*, *38*(7), 3022–3027. https://doi.org/10.1093/molbev/msab120

Tan, W., Jiang, P., Zhang, W., Hu, Z., Lin, S., Chen, L., Li, Y., Peng, C., Li, Z., Sun, A., Chen, Y., Zhu, W., Xue, Y., Yao, Y., Li, X., Song, Q., He, F., Qin, W., & Pei, H. (2021). Posttranscriptional regulation of de novo lipogenesis by glucose-induced O-GlcNAcylation. *Molecular Cell*, *81*(9), 1890-1904.e7. https://doi.org/10.1016/j.molcel.2021.02.009

Tang, G., Li, N., Liu, Y., Yu, L., Yan, J., & Luo, L. (2018). Sinorhizobium meliloti Glutathione Reductase Is Required for both Redox Homeostasis and Symbiosis. *Applied and Environmental Microbiology*, *84*(3), 1–10. https://doi.org/10.1128/AEM.01937-17

Theorell, H. (1935). Purification of the active group of the yellow enzyme. *Biochem. Z.*, *275*, 344–346.

Torres-Guzman, J. C., Padilla-Guerrero, I. E., Cervantes-Quintero, K. Y., Martinez-Vazquez, A., Ibarra-Guzman, M., & Gonzalez-Hernandez, G. A. (2021). Peculiarities of nitronate monooxygenases and perspectives for in vivo and in vitro applications. *Applied Microbiology and Biotechnology*, *105*(21–22), 8019–8032. https://doi.org/10.1007/s00253-021-11623-1

Torres, A., Kasturiarachi, N., DuPont, M., Cooper, V. S., Bomberger, J., & Zemke, A. (2019). NADH Dehydrogenases in Pseudomonas aeruginosa Growth and Virulence. *Frontiers in Microbiology*, *10*(FEB), 1–10. https://doi.org/10.3389/fmicb.2019.00075

Trefzer, C., Škovierová, H., Buroni, S., Bobovská, A., Nenci, S., Molteni, E., Pojer, F., Pasca, M. R., Makarov, V., Cole, S. T., Riccardi, G., Mikušová, K., & Johnsson, K. (2012). Benzothiazinones Are Suicide Inhibitors of Mycobacterial Decaprenylphosphoryl-β- <scp>d</scp> -ribofuranose 2′-Oxidase DprE1. *Journal of the American Chemical Society*, *134*(2), 912–915. https://doi.org/10.1021/ja211042r

Trujillo, M. E., Willems, A., Abril, A., Planchuelo, A.-M., Rivas, R., Ludeña, D., Mateos, P. F., Martínez-Molina, E., & Velázquez, E. (2005). Nodulation of Lupinus albus by Strains of Ochrobactrum lupini sp. nov. *Applied and Environmental Microbiology*, *71*(3), 1318–1327. https://doi.org/10.1128/AEM.71.3.1318-1327.2005

Tsolis, R. M., Seshadri, R., Santos, R. L., Sangari, F. J., Lobo, J. M. G., de Jong, M. F., Ren, Q., Myers, G., Brinkac, L. M., Nelson, W. C., DeBoy, R. T., Angiuoli, S., Khouri, H., Dimitrov, G., Robinson, J. R., Mulligan, S., Walker, R. L., Elzer, P. E., Hassan, K. A., & Paulsen, I. T. (2009). Genome Degradation in Brucella ovis Corresponds with Narrowing of Its Host Range and Tissue Tropism. *PLoS ONE*, *4*(5), e5519. https://doi.org/10.1371/journal.pone.0005519

Typas, A., Banzhaf, M., Gross, C. A., & Vollmer, W. (2011). From the regulation of peptidoglycan synthesis to bacterial growth and morphology. *Nature Publishing Group*, *10*(2), 123–136. https://doi.org/10.1038/nrmicro2677

Vagin, A., & Teplyakov, A. (1997). MOLREP : an Automated Program for Molecular Replacement. *Journal of Applied Crystallography*, *30*(6), 1022–1025. https://doi.org/10.1107/S0021889897006766

van den Berg, P. A. W., Feenstra, K. A., Mark, A. E., Berendsen, H. J. C., & Visser, A. J. W. G. (2002). Dynamic Conformations of Flavin Adenine Dinucleotide: Simulated Molecular Dynamics of the Flavin Cofactor Related to the Time-Resolved Fluorescence Characteristics. *The Journal of Physical Chemistry B*, *106*(34), 8858–8869. https://doi.org/10.1021/jp020356s

van Pée, K.-H., & Unversucht, S. (2003). Biological dehalogenation and halogenation reactions. *Chemosphere*, *52*(2), 299–312. https://doi.org/10.1016/S0045-6535(03)00204-2

van Schie, M. M. C. H., Younes, S. H. H., Rauch, M. C. R., Pesic, M., Paul, C. E., Arends, I. W. C. E., & Hollmann, F. (2018). Deazaflavins as photocatalysts for the direct reductive regeneration of flavoenzymes. *Molecular Catalysis*, *452*, 277–283. https://doi.org/10.1016/j.mcat.2018.04.015

Varesio, L. M., Fiebig, A., & Crosson, S. (2021). Brucella ovis Cysteine Biosynthesis Contributes to Peroxide Stress Survival and Fitness in the Intracellular Niche. *Infection and Immunity*, *89*(6), 1–12. https://doi.org/10.1128/IAI.00808-20

Velasco, J., Romero, C., Lopez-Goni, I., Leiva, J., Diaz, R., & Moriyon, I. (1998). Evaluation of the relatedness of Brucella spp. and Ochrobactrum anthropi and description of Ochrobactrum intermedium sp. nov., a new species with a closer relationship to Brucella spp. *International Journal of Systematic Bacteriology*, *48*(3), 759–768. https://doi.org/10.1099/00207713-48-3-759

Viadas, C., Rodríguez, M. C., Sangari, F. J., Gorvel, J.-P., García-Lobo, J. M., & López-Goñi, I. (2010). Transcriptome Analysis of the Brucella abortus BvrR/BvrS Two-Component Regulatory System. *PLoS ONE*, *5*(4), e10216. https://doi.org/10.1371/journal.pone.0010216

Villanueva, R., Romero-Tamayo, S., Laplaza, R., Martínez-Olivan, J., Velázquez-Campoy, A., Sancho, J., Ferreira, P., & Medina, M. (2019). Redox- and Ligand Binding-Dependent Conformational Ensembles in the Human Apoptosis-Inducing Factor Regulate Its Pro-Life and Cell Death Functions. *Antioxidants & Redox Signaling*, *30*(18), ars.2018.7658. https://doi.org/10.1089/ars.2018.7658

Vollmer, W., Blanot, D., & De Pedro, M. A. (2008). Peptidoglycan structure and architecture. *FEMS Microbiology Reviews*, *32*(2), 149–167. https://doi.org/10.1111/j.1574-6976.2007.00094.x

Walsh, C., Fisher, J., Spencer, R., Graham, D. W., Ashton, W. T., Brown, J. E., Brown, R. D., & Rogers, E. F. (1978). Chemical and enzymic properties of riboflavin analogs. *Biochemistry*, *17*(10), 1942–1951. https://doi.org/10.1021/bi00603a022

Walsh, C. T., & Chen, Y.-C. J. (1988). Enzymic Baeyer-Villiger Oxidations by Flavin-Dependent Monooxygenases. *Angewandte Chemie International Edition in English*, *27*(3), 333–343. https://doi.org/10.1002/anie.198803331

Walsh, C. T., & Wencewicz, T. A. (2013). Flavoenzymes: Versatile catalysts in biosynthetic pathways. *Nat. Prod. Rep.*, *30*(1), 175–200. https://doi.org/10.1039/C2NP20069D

Wang, Y., Tang, C., Yu, X., Xia, M., & Yue, H. (2010). Distribution of serotypes and virulence-associated genes in pathogenic Escherichia coli isolated from ducks. *Avian Pathology*, *39*(4), 297–302. https://doi.org/10.1080/03079457.2010.495742

Wanke, C., Falchettob, R., & Amrhein, N. (1992). *Molecular cloning, sequencing of the gene and overexpression of the enzyme* (Vol. 301, Issue 3). European Biochemical Societies.

Warburg, O., & Christian, W. (1933). Über das gelbe Ferment und seine Wirkungen. *Biochem. Z.*, *266*, 377–411.

Wargo, M. J. (2013). Choline Catabolism to Glycine Betaine Contributes to Pseudomonas aeruginosa Survival during Murine Lung Infection. *PLoS ONE*, *8*(2), e56850. https://doi.org/10.1371/journal.pone.0056850

Waseem, H., Williams, M. R., Stedtfeld, T., Chai, B., Stedtfeld, R. D., Cole, J. R., Tiedje, J. M., & Hashsham, S. A. (2017). Virulence Factor Activity Relationships (VFARs): A Bioinformatics Perspective. *Royal Society of Chemistry*, *19*, 247–260. https://doi.org/10.1039/C6EM00689B

Weber, G. (1950). Fluorescence of riboflavin and flavin-adenine dinucleotide. *Biochemical Journal*, *47*(1), 114–121. https://doi.org/10.1042/bj0470114

Wegrzyn, A. B., Stolle, S., Rienksma, R. A., Martins dos Santos, V. A. P., Bakker, B. M., & Suarez-Diez, M. (2019). Cofactors revisited – Predicting the impact of flavoprotein-related diseases on a genome scale. *Biochimica et Biophysica Acta (BBA) - Molecular Basis of Disease*, *1865*(2), 360–370. https://doi.org/10.1016/j.bbadis.2018.10.021

Westphal, A. H., Tischler, D., Heinke, F., Hofmann, S., Gröning, J. A. D., Labudde, D., & van Berkel, W. J. H. (2018). Pyridine Nucleotide Coenzyme Specificity of p-Hydroxybenzoate Hydroxylase and Related Flavoprotein Monooxygenases. *Frontiers in Microbiology*, *9*(December), 1–17. https://doi.org/10.3389/fmicb.2018.03050

Whatmore, A. M., Davison, N., Cloeckaert, A., Al Dahouk, S., Zygmunt, M. S., Brew, S. D., Perrett, L. L., Koylass, M. S., Vergnaud, G., Quance, C., Scholz, H. C., Dick, E. J., Hubbard, G., & Schlabritz-Loutsevitch, N. E. (2014). Brucella papionis sp. nov., isolated from baboons (Papio spp.). *International Journal of Systematic and Evolutionary Microbiology*, *64*(Pt_12), 4120–4128. https://doi.org/10.1099/ijs.0.065482-0

Williams, C. H., Arscott, L. D., Müller, S., Lennon, B. W., Ludwig, M. L., Wang, P.-F., Veine, D. M., Becker, K., & Schirmer, R. H. (2000). Thioredoxin reductase. *European Journal of Biochemistry*, *267*(20), 6110–6117. https://doi.org/10.1046/j.1432-1327.2000.01702.x

Williams, K. P., Sobral, B. W., & Dickerman, A. W. (2007). A Robust Species Tree for the Alphaproteobacteria. *Journal of Bacteriology*, *189*(13), 4578–4586. https://doi.org/10.1128/JB.00269-07

Wingfield, P. (1998). Protein Precipitation Using Ammonium Sulfate. In *Current Protocols in Protein Science* (p. A.3F.1-A.3F.8). John Wiley & Sons, Inc. https://doi.org/10.1002/0471140864.psa03fs13

Winn, M. D., Ballard, C. C., Cowtan, K. D., Dodson, E. J., Emsley, P., Evans, P. R., Keegan, R. M., Krissinel, E. B., Leslie, A. G. W., McCoy, A., McNicholas, S. J., Murshudov, G. N., Pannu, N. S., Potterton, E. A., Powell, H. R., Read, R. J., Vagin, A., & Wilson, K. S. (2011). Overview of the CCP 4 suite and current developments. *Acta Crystallographica Section D Biological Crystallography*, *67*(4), 235–242. https://doi.org/10.1107/S0907444910045749

Winterbourn, C. C. (2008). Reconciling the chemistry and biology of reactive oxygen species. *Nature Chemical Biology*, *4*(5), 278–286. https://doi.org/10.1038/nchembio.85

Wong, C. M., Dilworth, M. J., & Glenn, A. R. (1994). Cloning and sequencing show that 4-hydroxybenzoate hydroxylase (PobA) is required for uptake of 4-hydroxybenzoate in Rhizobium leguminosarum. *Microbiology*, *140*(10), 2775–2786. https://doi.org/10.1099/00221287-140-10-2775

Wunsch, P., & Zumft, W. G. (2005). Functional Domains of NosR, a Novel Transmembrane Iron-Sulfur Flavoprotein Necessary for Nitrous Oxide Respiration. *Journal of Bacteriology*, *187*(6), 1992–2001. https://doi.org/10.1128/JB.187.6.1992-2001.2005

Xiang, Z., Tian, Y., & He, Y. (2007). PHIDIAS: a pathogen-host interaction data integration and analysis system. *Genome Biology*, *8*(7), R150. https://doi.org/10.1186/gb-2007-8-7-r150

Xiang, Z., Zheng, W., & He, Y. (2006). BBP: Brucella genome annotation with literature mining and curation. *BMC Bioinformatics*, *7*(1), 347. https://doi.org/10.1186/1471-2105-7-347

Xu, L., Wu, D., Liu, L., Zheng, Q., Song, Y., Ye, L., Sha, S., Kang, J., Xin, Y., & Ma, Y. (2014). Characterization of mycobacterial UDP-N-acetylglucosamine enolpyruvyle transferase (MurA). *Research in Microbiology*, *165*(2), 91–101. https://doi.org/10.1016/j.resmic.2014.01.004

Yang, J., & Zhang, Y. (2015). I-TASSER server: new development for protein structure and function predictions. *Nucleic Acids Research*, *43*(W1), W174–W181. https://doi.org/10.1093/nar/gkv342

Yang, M., Lu, R., Guja, K. E., Wipperman, M. F., St. Clair, J. R., Bonds, A. C., Garcia-Diaz, M., & Sampson, N. S. (2015). Unraveling Cholesterol Catabolism in Mycobacterium tuberculosis : ChsE4-ChsE5 α 2 β 2 Acyl-CoA Dehydrogenase Initiates β-Oxidation of 3-Oxo-cholest-4-en-26-oyl CoA. *ACS Infectious Diseases*, *1*(2), 110–125. https://doi.org/10.1021/id500033m

Yang, Y., Severin, A., Chopra, R., Krishnamurthy, G., Singh, G., Hu, W., Keeney, D., Svenson, K., Petersen, P. J., Labthavikul, P., Shlaes, D. M., Rasmussen, B. A., Failli, A. A., Shumsky, J. S., Kutterer, K. M. K., Gilbert, A., & Mansour, T. S. (2006). 3 , 5-Dioxopyrazolidines , Novel Inhibitors of UDP- N - Acetylenolpyruvylglucosamine Reductase (MurB) with Activity against Gram-Positive Bacteria. *Antimicrobial Agents and Chemotherapy*, *50*(2), 556–564. https://doi.org/10.1128/AAC.50.2.556

Yeh, J. I., Chinte, U., & Du, S. (2008). Structure of glycerol-3-phosphate dehydrogenase, an essential monotopic membrane enzyme involved in respiration and metabolism. *Proceedings of the National Academy of Sciences*, *105*(9), 3280–3285. https://doi.org/10.1073/pnas.0712331105

Yoo, M., Bestel-Corre, G., Croux, C., Riviere, A., Meynial-Salles, I., & Soucaille, P. (2015). A Quantitative System-Scale Characterization of the Metabolism of Clostridium acetobutylicum. *MBio*, *6*(6), 1–12. https://doi.org/10.1128/mBio.01808-15

Yoon, H., Lee, S. J., Mikami, B., Park, H., Yoo, J., & Suh, S. W. (2008). Crystal structure of UDP-Nacetylglucosamine enolpyruvyl transferase from Haemophilus influenzae in complex with UDP-N-acetylglucosamine and fosfomycin. *PROTEINS: Structure, Function and Bioinformatics*, 1032–1037. https://doi.org/10.1002/prot.21959

Young, I. G., Stroobant, P., Macdonald, C. G., & Gibson, F. (1973). Pathway for Ubiquinone Biosynthesis in Escherichia coli K-12: Gene-Enzyme Relationships and Intermediates. *Journal of Bacteriology*, *114*(1), 42–52. https://doi.org/10.1128/jb.114.1.42-52.1973

Yruela, I., Moreno-Yruela, C., & Olsen, C. A. (2021). Zn2+-Dependent Histone Deacetylases in Plants: Structure and Evolution. *Trends in Plant Science*, *26*(7), 741–757. https://doi.org/10.1016/j.tplants.2020.12.011

Zanetti, G., Williams, C. H., & Massey, V. (1968). Influence of Photoirradiation on the Oxidation-Reduction State of Thioredoxin Reductase. *Journal of Biological Chemistry*, *243*(15), 4013–4019. https://doi.org/10.1016/S0021-9258(18)93272-2

Zhang, L., Trncik, C., Andrade, S. L. A., & Einsle, O. (2017). The flavinyl transferase ApbE of Pseudomonas stutzeri matures the NosR protein required for nitrous oxide reduction. *Biochimica et Biophysica Acta (BBA) - Bioenergetics*, *1858*(2), 95–102. https://doi.org/10.1016/j.bbabio.2016.11.008

Zhang, M., Wang, L., & Zhong, D. (2017). Photolyase: Dynamics and electron-transfer mechanisms of DNA repair. *Archives of Biochemistry and Biophysics*, *632*, 158–174. https://doi.org/10.1016/j.abb.2017.08.007

Zhang, Y.-J., Li, J., Zhao, W., & Zhou, M.-G. (2010). A single amino acid substitution in the SdhB protein of succinate dehydrogenase determines resistance to amicarthiazol in Xanthomonas oryzae pv. oryzae. *Pest Management Science*, *66*(6), 627–633. https://doi.org/10.1002/ps.1919

Zhang, Y., & Skolnick, J. (2005). TM-align: a protein structure alignment algorithm based on the TM-score. *Nucleic Acids Research*, *33*(7), 2302–2309. https://doi.org/10.1093/nar/gki524

Zheng, H., Lu, L., Wang, B., Pu, S., Zhang, X., Zhu, G., Shi, W., Zhang, L., Wang, H., Wang, S., Zhao, G., & Zhang, Y. (2008). Genetic Basis of Virulence Attenuation Revealed by Comparative Genomic Analysis of Mycobacterium tuberculosis Strain H37Ra versus H37Rv. *PLoS ONE*, *3*(6), e2375. https://doi.org/10.1371/journal.pone.0002375

Zheng, W., Zhang, C., Li, Y., Pearce, R., Bell, E. W., & Zhang, Y. (2021). Folding non-homologous proteins by coupling deep-learning contact maps with I-TASSER assembly simulations. *Cell Reports Methods*, *1*(3), 100014. https://doi.org/10.1016/j.crmeth.2021.100014

Zhou, X., Zheng, W., Li, Y., Pearce, R., Zhang, C., Bell, E. W., Zhang, G., & Zhang, Y. (2022). I-TASSER-

MTD: a deep-learning-based platform for multi-domain protein structure and function prediction. *Nature Protocols*, *17*(10), 2326–2353. https://doi.org/10.1038/s41596-022-00728-0

Zhu, J., Yang, Y., Han, H., Betzi, S., Olesen, S. H., Marsilio, F., & Schönbrunn, E. (2012). Functional Consequence of Covalent Reaction of Phosphoenolpyruvate with UDP-N-acetylglucosamine 1-Carboxyvinyltransferase (MurA). *Journal of Biological Chemistry*, *287*(16), 12657–12667. https://doi.org/10.1074/jbc.M112.342725

Zhu, M., & Dai, X. (2018). On the intrinsic constraint of bacterial growth rate: M. tuberculosis 's view of the protein translation capacity. *Critical Reviews in Microbiology*, *44*(4), 455–464. https://doi.org/10.1080/1040841X.2018.1425672

Zoeiby, A. El, Beaumont, M., Dubuc, E., Sanschagrin, F., Voyer, N., & Levesque, R. C. (2003). Combinatorial enzymatic assay for the screening of a new class of bacterial cell wall inhibitors. *Bioorganic and Medicinal Chemistry*, *11*(7), 1583–1592. https://doi.org/10.1016/S0968-0896(02)00447-9

Zurdo-Piñeiro, J. L., Rivas, R., Trujillo, M. E., Vizcaíno, N., Carrasco, J. A., Chamber, M., Palomares, A., Mateos, P. F., Martínez-Molina, E., & Velázquez, E. (2007). Ochrobactrum cytisi sp. nov., isolated from nodules of Cytisus scoparius in Spain. *International Journal of Systematic and Evolutionary Microbiology*, *57*(4), 784–788. https://doi.org/10.1099/ijs.0.64613-0

Zurfluh, K., Treier, A., Schmitt, K., & Stephan, R. (2020). Mobile fosfomycin resistance genes in Enterobacteriaceae—An increasing threat. *MicrobiologyOpen*, *9*(12), 1–13. https://doi.org/10.1002/mbo3.1135